# Visual Impairment in the absence of ON-pathway signal

*Dennis Manuel Fritsch*

A dissertation submitted in partial fulfillment

of the requirements for the degree of

**Doctor of Philosophy**

of

**University College London**.

UCL Great Ormond Street Institute of Child Health

University College London

May 11, 2018

I, Dennis Manuel Fritsch, confirm that the work presented in this thesis is my own. Where information has been derived from other sources, I confirm that this has been indicated in the work. Where part of the work was performed collaboratively with others, this is also indicated in the the work.

# Abstract

Congenital retinal diseases are a major cause of childhood and lifelong visual impairment. Such conditions can manifest a variable array of severe and subtle effects on vision. Assessment of visual function in children can be challenging; yet, knowledge about phenotype, genotype and impact of these disorders is crucial for providing appropriate support, tailored diagnostics and for developing treatments.

ON-and OFF-pathways are separately transmitting information on brightness and darkness from the retina to the cortex, where their interplay is crucial in visual perception. This project investigated the effects of retinal ON-pathway dysfunction on vision.

A cohort of 109 patients with ON-pathway dysfunction was examined from four subgroups of visual electrophysiological phenotypes (incomplete and complete Congenital Stationary Night Blindness - CSNB, Duchenne Muscular Dystrophy - DMD, and congenital disorders of N-glycosylation - PMM2-CDG). Using specialised visual evoked potential stimuli, designed to distinguish the ON-and OFF-pathway signal arrival at the striate cortex, marked ON system delays were revealed in patients with subtypes of CSNB, *DMD* mutations post exon 30 and PMM2-CDG. A child-friendly psychophysical software called $LumiTrack^{Tm}$ was developed to assess motion and contrast perception, two important qualities conveyed by ON-and OFF-pathways. Patients with subtypes of CSNB and PMM2-CDG showed abnormalities in motion perception and subnormal contrast sensitivity, while patients with DMD performed at the level of healthy volunteers. These impairments may occur due to a delay of signal transmission through the retina, resulting in an ON/OFF signal asymmetry within the visual system. A genotype-phenotype comparison sug-

gested a trend of increasing ON/OFF asymmetry associated with genetic defects affecting proteins placed later within the photoreceptor / ON bipolar cell signalling cascade.

This systematic study of cortical and behavioural visual function in patients with ON-pathway dysfunction highlights the impairments encountered by patients in visual qualities important for everyday life.

# Acknowledgements

First and foremost I would like to thank my supervisors Professor Jane Sowden and Dr Dorothy Thompson for giving me the opportunity to carry out this exciting PhD project under their supervision. Their advice and guidance have been invaluable over the last three years. With their support, I was allowed an insight into the world of clinical ophthalmological research.

I am infinitely grateful for the help and engagement of all the patients, their families and the volunteers taking part in this research study. Patient recruitment help came from Kate Maresh, Katie Groves and Joana Pisco Domingos from the Neuromuscular department and Professor Stephanie Grünewald from the Metabolic Medicine department. Further, I would like to express my sincere gratitude to Coram's Fields Out of School Club and Brentwood Preparatory School for providing support in the recruitment of volunteers.

I also want to acknowledge my collaborators who supported me in various aspects of this project. I would like to thank Dr Jane Hayward for her help with the Oculome NGS. Also, Lighta Godino and the team at GOSH clinical genetics always provided easy and swift support obtaining patient DNA samples. A special thanks goes out to Maximilian Kerz for help with the programming of $LumiTrack^{Tm}$.

Further, I would like to thank the Ulverscroft Vision Research Group, as well as the GOSH Children's Charity and the NIHR Biomedical Research Centres at GOSH and the UCL GOS Institute of Child Health for funding this project.

I also thank all my current and past lab members from the UCL GOS Institute of Child Health, as well as the ophthalmology and electrophysiology teams at GOSH for making my last three years an enjoyable journey and for a providing an

always friendly and gratifying working environment.

Ultimately, I am grateful for the support and encouragement from my friends and family in London, Germany and France. A special thanks goes to my grandparents, who provided a quiet and calm place for me to write a big part of this thesis.

# Abbrevations

The following abbreviations were used in this thesis:

2AFC: Two Alternative Forced Choice

AD: Amplitude Difference

A/D: Analog-to-Digital converter

AMD: Age-related Macular Degeneration

APB: 2-amino-4-phosphobutyric acid

AVV: Adeno-associated Viral Vector

BEO: Both Eyes Open

bp: base pairs

BWA: Burrows Wheeler Aligner

CACNA1f: Calcium Voltage-Gated Channel Subunit Alpha1 F

CC: Correlation Coefficient

CI: Confidence Interval

cm: centimetres

CNV: Copy number variation

CNS: Central Nervous System

CSF: Contrast Sensitivity Function

CSNB: Congenital Stationary Night Blindness

cCSNB/CSNB1: complete Congenital Stationary Night Blindness

iCSNB/CSNB2: incomplete Congenital Stationary Night Blindness

deg: degrees

ddNTPs: 2',3' dideoxynucleotides

DMD: Duchenne Muscular Dystrophy

DMSO: Dimethyl Sulfoxide

DNA: Deoxyribonucleic acid

cDNA: complementary DNA

DTL: Dawson, Trick, and Litzkow (electrode)

EEG: Electroencephalogram

EDTA: Ethylene Diamine Tetraacetic Acid

ERG: Electroretinogram

ETDRS: Early Treatment Diabetic Retinopathy Study

ExoSAP: Exol Shrimp Alkaline Phosphatase

fMRI: functional Magnetic Resonance Imaging

GB: Gigabyte

GCL: Ganglion Cell Layer

GNB3: Guanine Nucleotide-Binding Protein 3

GOSH: Great Ormond Street Hospital

GPR179: G Protein-Coupled Receptor 179

GRM6: Glutamate Metabotropic Receptor 6

Hz: Hertz

ICH: Institute of Child Health

ILM: Inner Limiting Membrane

INL: Inner Nuclear Layer

IPL: Inner Plexiform Layer

ISCEV: International Society for Clinical Electrophysiology of Vision

ISI: Inter Stimulus Interval

KO: Knock-out

LCD: Liquid Crystal Display

LRIT3: Leucine-rich Repeat, Immunoglobin-like and Transmembrane Domain-containing Protein 3

MAR: Minimum Angle of Resolution

mM: millimolar

ms: milliseconds

$\mu$V: micro Volts

$\mu$M: micromolar

nM: nanomolar

NGS: Next Generation Sequencing

nob: no b-wave

NYX: Nyctalopin

OLM: Outer Limiting Membrane

ONL: Outer Nuclear Layer

OPL: Outer Plexiform Layer

PCR: Polymerase Chain Reaction

PET: Positron Emission Tomography

PI: Prediction Interval

PMM2-CDG: Phosphomannomutase 2 deficiency

RNA: Ribo-Nucleic Acid

cRNA: Complementary Ribo-Nucleic Acid

RPE: Retinal Pigment Epithelium

RP: Retinitis pigmentosa

RT: Room temperature

SNP: Single Nucleotide Polymorphism

TAE: Tris Acetate Ethylene Diamine Tetraacetic Acid

TE: Tris-Ethylene Diamine Tetraacetic Acid

TD: Time Difference

td: Troland

TRPM1: Transient Receptor Potential Cation Channel Subfamily M Member 1

TTX: Tetrodotoxin

V1: Primary visual cortex / striate cortex

V4: Visual area 4

V5: Visual area 5

VA: Visual Acuity

VEP: Visual Evoked Potential

WES: Whole Exome Sequencing

WGS: Whole Genome Sequencing

WHO: World Health Organisation

# Contents

# List of Figures

# List of Tables

Chapter 1

# Introduction

# 1.1 The human visual system from eye to cortex

## 1.1.1 The human eye

Vision depends crucially on the functionality of the eye and its structure. The human eye is made up of several different parts and layers (Figure 1.1), which enable it to detect and channel light information from the environment, in order to translate and relay it for processing in the visual centres of the brain. While visual processing begins with the *retina*, the light sensitive tissue at the back of the eye, the anterior parts of the eye are concerned with contributing to optimal capturing of light from the environment. In order to enter the eye, light is channeled through the *pupil*, a ”window”, the size of which is controlled by the *iris*. This muscular ring contracts the pupil - making the window smaller - in response to high ambient light levels in the environment, and expands it when ambient light levels are low. It also contains distinct pigmentation and therefore presents what is commonly referred to as ”eye-colour”. Both, the pupil and the iris are covered by two exterior layers. The *sclera* is the opaque outermost layer of the eyeball and provides protection and structural support [1], while the *cornea* is the transparent cover, which plays a major role in focusing light on the retina. The crystalline *lens*, which is situated behind the pupil, further contributes to the refractive properties of the eye. The retina - the light sensitive tissue at the posterior end of the eye - stands at the beginning of the visual signalling pathways. Overlying the retina is the *retinal pigment epithelium (RPE)* which supports retinal and optical function by absorbing scattered light, as well as carrying out a nutrient and ion exchange function for photoreceptors [2, 3]. Firmly attached to the RPE is the vascular layer of the eye, called the *choroid*. It supplies the outer retina with oxygen and nutrients, such as glucose and retinal, which plays a role in the process of absorption of photons by visual pigments [1].

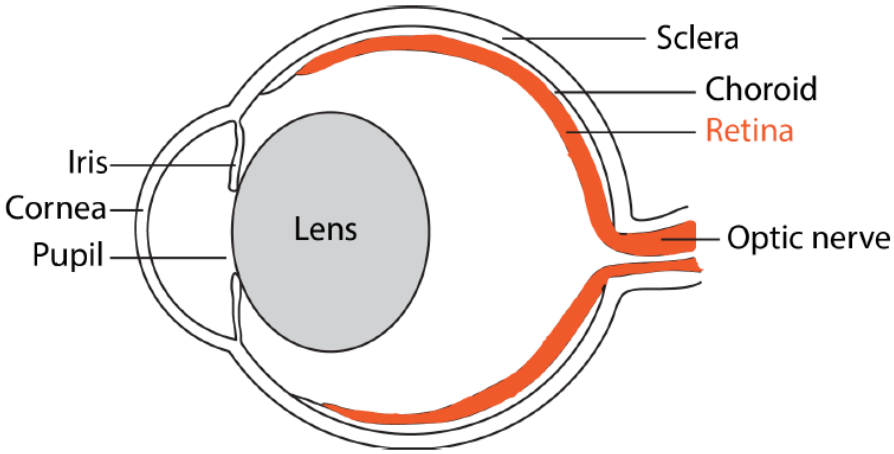


**Figure 1.1:** A simple schematic of the main structures and layers of the mammalian eye. Highlighted in orange is the retina. Used with permission of [4].

The anatomy of the retina was first highlighted in ground-breaking work by Spanish neuroscientist and pathologist Ramon y Cajal (1894). His detailed drawings of cells from retina and brain, made at the beginning of the twentieth century, are still used for educational purposes today. He found the retina was highly complex neural tissue, comprising in excess of sixty different cell types [5] arranged in three different layers [1]. A simple schematic of the major retinal cell types and layers is given in Figure 1.2.

The light-sensitive cells are the photoreceptor cells in the outer retina. Humans have two distinct types of photoreceptor cells: rods, responsible for vision in dim light and peripheral vision, and cones, responsible for the ability to visualise fine detail and colour. The light information is converted into an electrical current via the phototransduction cascade, involving conformation changes of several molecules, and passed on to subsequent retinal cell types via chemical or electrical synapses. Photoreceptors capture photons via specialised molecules, opsins, which triggers an intracellular cascade, provoking a change of their membrane potential, causing the cells to hyperpolarise.

The cell bodies of both cell types constitute the Outer Nuclear Layer (ONL) of the retina. Rods and cones continuously release the neurotransmitter L-glutamate in the dark which inhibits (hyperpolarises) ON bipolar cells and excites (depolarises) OFF bipolar cells in the Inner Nuclear Layer (INL). The synaptic release of L-glutamate is inhibited under light stimulation when the photoreceptor cells hyperpolarise [6]. This reduction of L-glutamate in the OPL causes the bipolar cells to either depolarise or hyperpolarise depending on their unique receptors [7, 8]. Human ON bipolar cells have a metabotropic mGluR6 receptor [9] and OFF bipolar cells ionotropic glutamate receptors [10].

Bipolar cells alert the ganglion cells located in the Ganglion Cell Layer (GCL) of increases (ON) and decreases (OFF) of light, either directly or indirectly via amacrine cells. This opposite polarity response introduced at the bipolar cell level creates a first dichotomy in the processing of light signals. Therefore, organization at the level of the retina begins for two parallel pathways: the ON-pathway, which

responds to an increase in brightness and the OFF-pathway, which responds to a decrease in brightness[1] [11].

In addition to bipolar cells, the INL also contains horizontal cells, which further regulate the photoreceptor output by lateral integration and inhibition across several photoreceptors, as well as amacrine and Müller cells. Amacrine cells build a network of interneurons connecting bipolar cells with ganglion cells and are thought to mostly integrate and modulate signals from other cell types, introducing a temporal domain to the visual message presented to the ganglion cells. This temporal domain later becomes crucial in the perception of motion[2]. Müller cells mainly have a supportive function for photoreceptors and other inner retinal cell types, being important mediators of neurotransmitters, such as glutamate [12].

The ONL, INL and GCL are separated by two synaptic layers, the Outer Plexiform Layer (OPL) and Inner Plexiform Layer (IPL) [1]. The OPL comprises photoreceptor cell axons connecting to the dendritic tips of bipolar and horizontal cells, while the IPL is the synaptic area where information from the bipolar cells is transmitted to the ganglion cells, either directly or indirectly via amacrine cells. In order to activate the visual processes, light has to travel across all retinal layers to reach the photoreceptors. The mammalian retina is therefore referred to as an inverse retina.

[1] A more detailed account of ON-and OFF-pathways is given in Section 1.1.3

[2] A more detailed account of the perception of contrast, as well as different domains of motion is presented in Chapter 4 - $LumiTrack^{Tm}$

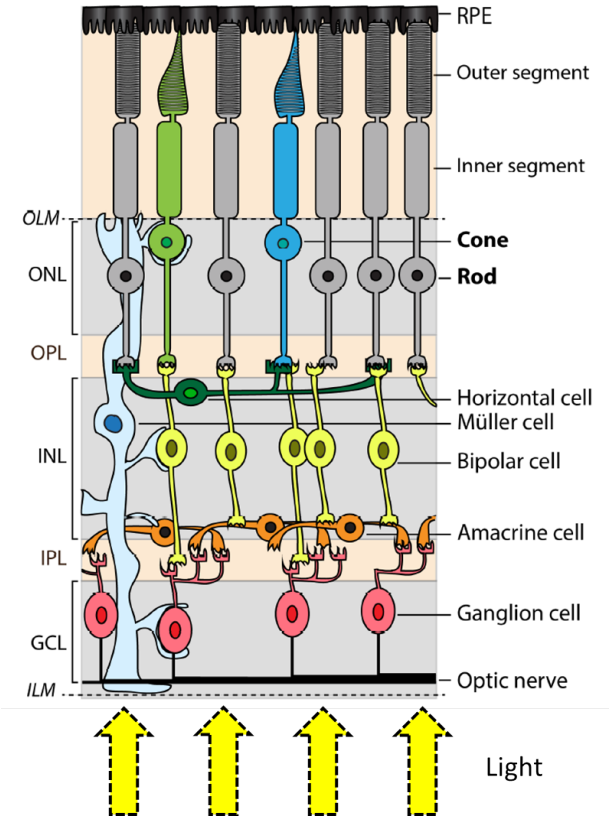


**Figure 1.2:** A simple schematic cross-section of the retinal layers and main cell types (cones, rods, horizontal, amacrine, bipolar, Müller, and ganglion cells) organised in three different cell layers (ONL, INL and GCL). RPE: retinal pigment epithelium. OLM: outer limiting membrane. ONL: outer nuclear layer. OPL: outer plexiform layer. INL: inner plexiform layer. IPL: inner plexiform layer. GCL: ganglion cell layer. ILM: inner limiting membrane. Light has to travel all layers of the retina, before initiating light detection at the photoreceptors. Adapted from [4].

### 1.1.2 From Retina to visual cortex

Once the light signal reaches the ganglion cells, it leaves the retina via the optic nerve, a bundle of retinal ganglion cell axons exiting the eyeball towards the brain. In this area of the posterior eye, no light-sensitive photoreceptor cells are present[3] and the so-called optic disc (the optic nerve head) creates a small blind spot in the visual field. Around 55% of ganglion cell axons making up the optic nerves of each eye cross over to the contralateral hemisphere at the optic chiasm and make synapses with cells in the lateral geniculate bodies (LGN). The LGN represent the first synapse of ganglion cell axons after leaving the retina. Here, their signals are segregated into six layers, depending on the type of information they carry.

Ganglion cells carrying non-chromatic information connect to M-cells in the magnocellular layers 1 and 2 of the LGN. Chromatic information from cones is relayed through ganglion cells to the parvocellular cells (P-cells) in LGN layers 3-6 [14, 15]. The information from short-wavelength S-cones is relayed via koniocellular cells (K-cells), located between M and P layers. These pathways differ in their functional characteristics and provide a further separation of light signals depending on the luminance contrast and properties of the light stimulus [16, 17, 18]: While the magnocellular system responds well under low contrast conditions, most cells in the parvocellular system do not respond well to contrasts lower than 20% [19].

From these specialised layers, axons project via the optic radiations to the visual cortex (Figure 1.3). Here, signals from both eyes are integrated first in layer 4C - also called the striate cortex. Signal integration within the striate cortex is thought to result in considerable cross-talk between different visual subsystems, such as the ON-and OFF-pathways, as well as the magnocellular, parvocellular and koniocellular systems, presenting their first point of interaction and signal integration [20, 21]. It is important to note, that the connections projecting from the retina to the LGN and from there to the striate cortex are topographically organized. This means that neighbouring spots on the retina are represented by neighbouring neurons in the LGN.

[3] Although some light-sensitive retinal ganglion cells were reported to exist [13].

At the striate cortex, the signals which originated and were separated at the retinal level, are pooled in cortical cells of differing complexity. They are characterised according to their receptive field structures and response behaviours, which are increasingly complex and selective to specific stimulation. The concept of receptive fields is a recurring theme in the visual system, as it has extensive influence on the way the visual system encodes the signal input it receives from the environment via ON-and OFF-pathways.

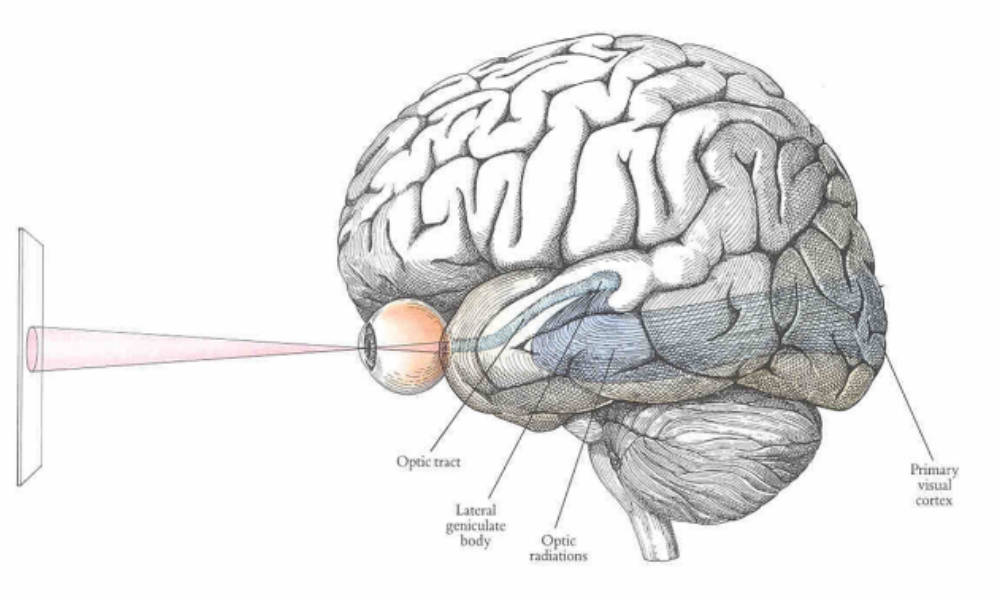


**Figure 1.3:** A schematic drawing displaying the visual pathway from optic nerve (here called the optic tract) to LGN, and via the optic radiations to the visual cortex. Taken from [22].

### 1.1.3 The ON-and OFF-pathways of the visual system - Receptive fields and increasing complexity

After the transduction of light by the photoreceptor cells, the separation of bright and dark parts of an image is crucial in order to build up contrast [23]. This step happens in the retina at the level of the bipolar cells, where sign-inverting or sign-conserving glutamate receptors determine whether the cells depolarise (ON) or hyperpolarise (OFF) to light, initiating ON-and OFF-pathways which transmit the perceptions brightness and darkness to the visual cortex. The way information is relayed from photoreceptor cells to ganglion cells varies depending on ambient light levels and at least six distinct pathways of signal transmission from rods and cones to bipolar and ganglion cells have been shown to exist in the mouse retina [24]. Of these, four pathways have been thoroughly described and are thought to be active in the scotopic light spectrum, their activity determined by different light levels. The work by Bloomfield and Dacheux gives a comprehensive overview [25]:

1. Rods → ON bipolar cells → AII amacrine cells → ON cone bipolar cells → ON ganglion cells [26]

   Cones → ON/OFF bipolar cells → ON/OFF ganglion cells[4]

2. Rods → cones (via gap junctions or electrical synapses) → ON cone bipolar cells → ON ganglion cells [27]

3. Rods → ON/OFF cone bipolar cells → ON/OFF ganglion cells [28]

4. Direction-sensitive ON/OFF ganglion cells, which receive direct input from cones only via both, ON and OFF bipolar cells, were reported to exist in rabbit and mouse retina [29, 30].

Figure 1.4 shows a schematic drawing of these different paths light signals can take through the retina[5].

[4] This pathway is only active once the cone threshold is reached, at light luminance of approximately 0.2 trolands.

[5] Under mesopic light conditions, considerable interaction of rod and cone systems is suggested [31].

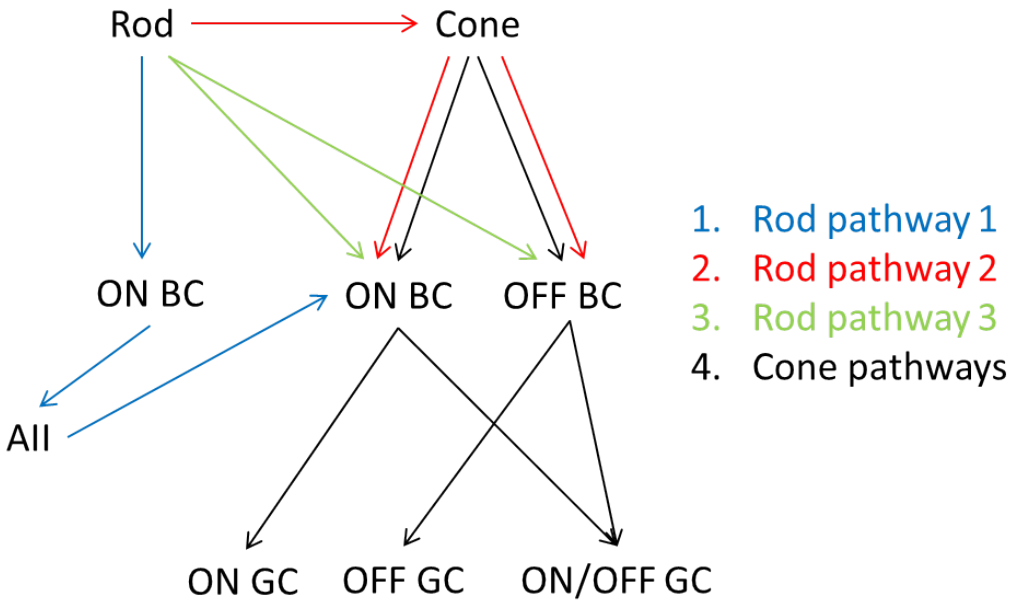


**Figure 1.4:** A schematic drawing displaying the four major signal pathways through the retina from photoreceptor cells to retinal ganglion cells. The different pathways are indicated by a colour scheme and the following abbreviations used for retinal cells: BC - bipolar cell, GC - ganglion cell, AII - AII amacrine cell.

The subdivision of the light signal into ON and OFF signals at the level of the bipolar cells is thought to be maintained until at least the striate cortex with the help of receptive fields. The interaction of these signals in higher cortical areas contribute to the perceptions of contrast differences, as well as motion (for example [32, 33]). A receptive field can generally be defined as the region in sensory space where changes in the stimulus influence the neuron's behaviour and output. The total area occupied by photoreceptors in the ONL that subsequently feed one ganglion cell in the INL, directly or indirectly, represents the receptive field of the ganglion cell: This is the region of the retina over which the cell's firing behaviour can be influenced by light stimulation (Figure 1.5). Receptive field structures were first detected in retinal ganglion cells [34] but were subsequently suggested to already be present at the level of bipolar cells in the primate [35].

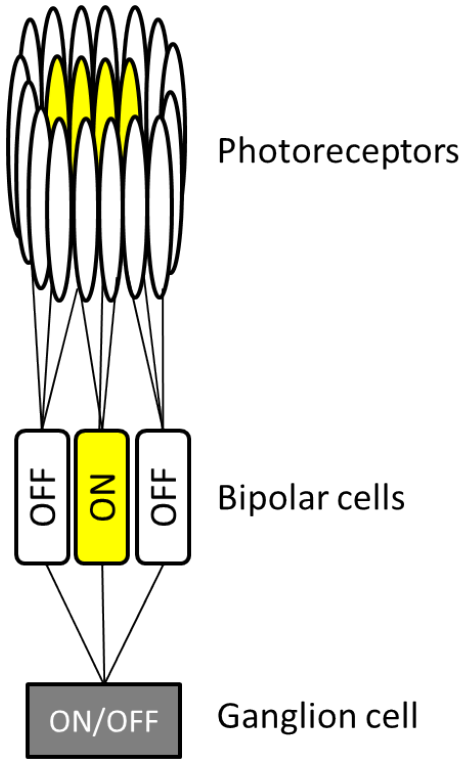


**Figure 1.5:** A simplified schematic of the inputs to an ON/OFF ganglion cell's receptive field. The cells making up the ON-centre are highlighted in yellow, while the cells lying in the OFF-surround are shown in white. Several photoreceptor cell outputs converge on some bipolar cells and these, in turn, connect to one ganglion cell. At the fovea, a 1:1:1 connection is achieved.

The way in which bipolar and ganglion cells maintain the ON and OFF polarity of their output is via an antagonistic centre-surround structure of their receptive fields. Here, either the central region of the receptive field reacts to light increment and the surround to light decrement, called ON centre, or vice versa, called OFF centre [34]. Further, the centre and surround regions react in an antagonistic way: the effect of a spot of light shone on the centre of an ON centre cell will be diminished by shining a second spot onto its surround [36], or by increasing the spot size until it also covers part of the receptive field surround. Depending on the ratio of light falling onto the excitatory receptive field centre and/or the inhibitory surround, the cell's output firing rate is altered, which enables the visual system to not only respond to the temporal presence or absence of light, but also to convey information about its spatial distribution. Neighbouring ganglion cells can receive their inputs from overlapping and different arrays of receptors. This can also lead to one receptor exciting some cells and inhibiting others, depending on their structure and the receptor's location on their centre or surround[6]. A schematic displaying the centre-surround antagonism of an ON centre cell is shown in Figure 1.6.

At the level of the LGN, cells within the magnocellular and parvocellular layers respond to light in much the same way as retinal ganglion cells, having similar ON-centre and OFF-centre circular-surround receptive fields, maintaining the ON-and OFF-pathway dichotomy. An exception is the koniocellular system, which primarily receives input from ON-ganglion cells [41]. Continuing along the visual pathway, simple cells in the cortex integrate the signals of neurons projecting from the LGN. Instead of having a centre-surround structure, most simple cells show rather elongated receptive fields [42].

The majority of cells found in V1, however, are complex cells. While they share the quality of responding only over a limited region of the visual field with simple cells, they also respond to shapes in a certain orientation or even movement in a certain direction [43]. Unlike simple cells, complex cells do not seem to have a

[6]It is thought that an interplay of excitatory and inhibitory inputs from cell networks are at the base of the direction selectivity of some ganglion cell types [30, 37, 38]. These were found to respond preferably to motion into different directions in rabbit and mouse [39, 29] or are specialised in detecting object motion [40].

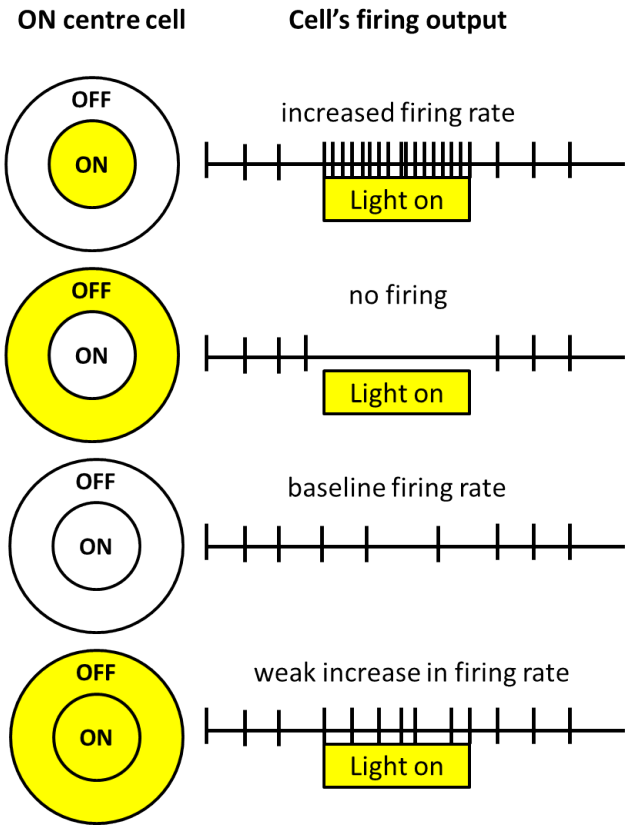


**Figure 1.6:** A simplified schematic of the centre-sourround antagonism of an ON centre cell (an OFF centre cell will react in the opposite manner to light stimulation). If light is shone on its receptive field centre only (indicated by yellow colouring), the cell's firing rate increases.

fine separation of their receptive fields into excitatory and inhibitory regions[7].

The post-striate cortex processing of visual signals involves many different areas of the brain, depending on the specific visual input. At this point in visual processing, ON-and OFF-pathways are expected to be heavily interconnected and estimates about their outputs are more difficult to attribute. Ungerleider and Mishkin (1982) proposed a model of two functionally specialised pathways of visual processing originating in the striate cortex, called the ventral and dorsal streams, due to their trajectories from the occipital cortex along the ventral cortical surface to the temporal cortex and dorsally into the parietal cortex, respectively [47]. The ventral stream is believed to mainly subserve recognition and discrimination of visual

[7] A sub-population of those cortical cells exhibit a further complexity in response selectivity, by only responding to specific stimuli of a certain length or size [44]. Such cells are referred to as "end-stopped" and are sensitive to corners, curvatures or sudden breaks in lines [45, 46].

shapes and objects, whereas the dorsal stream has been primarily associated with the analysis of the spatial location, shape, and orientation of objects[8].

Such a functional difference between both streams is supported by physiological studies of cortical cells in the primate, which highlight selective responses to geometric shapes in cells within the ventral stream (for example in primate V4 [49]) and a selectivity to object motion direction and speed in cells within the dorsal stream (for example in primate area MT [50]). While the knowledge about which cortical areas were involved in the higher processing of visual stimuli in humans initially came from studies of individuals with cortical lesions and their associated clinical visual impairments (for example [51]), the advent of functional brain imaging made it possible to investigate the organisation of the human visual pathways with more precision. Haxby and colleagues (1994) were able to distinguish a functional difference between ventral and dorsal streams by using positron emission tomography (PET), supporting the initial theory by Ungerleider and Mishkin [52]. While this "Two-Streams-Hypothesis" certainly presents an oversimplification of the complex relationships in visual processing, for example omitting that both streams are heavily interconnected (for example [53, 54]), it highlights two functionally distinct passageways for visual signals originating in the striate cortex[9].

In summary, the visual pathway seems to be hierarchically structured with an increasing complexity of cellular outputs and selectivity. At the same time, parallel subsystems exist in the visual system, such as ON-and OFF-pathways. Photoreceptor cells in the retina are the first component of the visual pathway and are influenced by light. Next, bipolar cells introduce a first stage of discrimination, separating increments (ON) and decrements (OFF) of light. Ganglion cells, LGN cells, as well as some cortical cells display a centre-surround receptive field organisation, making them more likely to be influenced by the contours of a stimulus falling into their

[8]This theory was subsequently slightly modified by Goodale and Milner (1992), emphasizing "perception" vs. "action" for ventral and dorsal streams, respectively [48]

[9]A more detailed account and discussion of the theories of visual perception can be found in Joel Norman's review "Two visual systems and two theories of perception: An attempt to reconcile the constructivist and ecological approaches" [55]

receptive fields. The ON and OFF centre-surround spatial organization is one of the core features of receptive field structure in visual neurons and this arrangement enables bipolar and ganglion cells, and subsequently the visual system, to signal changes in local contrast and even moving stimuli.

While a preference for direction stimuli was discovered at the retinal level in some species [30, 37, 38], complex cells in the cortex show an increased specificity and selectivity for incoming stimulation. They might not only be selective for stimulus contour, but also for its orientation or motion into one direction. This mechanism of increasingly specific requirements for a cell's activation, the higher it is placed in the visual pathway, results in a high efficiency. This way, an object in the visual field stimulates only a small fraction of the cortical cells on whose receptive fields it falls. Moreover, the increasing complexity of receptive field responses, as well as the receptive field sizes and stimulus selectivity along the visual pathway allows higher order cells to be more robust to small changes of spatial stimulus placement in the visual fieldn. This hierarchy continues as signals are transmitted to higher cortical areas involved in vision and perception, such as V5, which is involved in global motion processing, or V4, which contributes to the processing of simple shapes.

In summary, the interplay of ON-and OFF-pathway signals transmitted through the retinal layers is critical in building receptive fields of cells throughout the visual pathways until the cortical structures. A disruption of their interaction caused by signalling abnormalities in the visual pathways is therefore expected to affect visual performance under scotopic and photopic lighting conditions. To what extent this is the case in human observers with ON-or OFF-pathway dysfunction has never been systematically investigated.

## 1.2 Clinical measures of vision

Vision encompasses the physical and cognitive processing of light stimuli. It depends on the functionality of various different parts of the eye and the subsequent structures of the brain. Different approaches, assessing structure and function of the visual system, have been developed in order to judge an individual's visual capabilities as accurately as possible. In clinical practice, these assessments are crucial for diagnostics and the patient management designed to improve visual outcome. The outcome of a vision assessment helps define what may be considered a signature of abnormality in visual phenotypes of a specific condition.

### 1.2.1 Structural measures

Observation and knowledge of the structure and appearance of the retina can give valuable information on the state of the visual system. In the past, morphological information on the structure of the retina was usually obtained post-mortem via biopsies; however, advancements in technology have improved the way morphological information on the retina is obtained in clinical practice.

An impression of the ocular fundus can be obtained, in a non-invasive manner, through the pupil, using an ophthalmoscope [56] or more specialised fundus photography techniques [57, 58]. In order to get an idea of the integrity of the retinal architecture, a cross-section through the retinal layers can be retrieved using Optical Coherence Tomography (OCT)[10]. Both, fundus photography and OCT, rely on the reflective properties of the retinal layers [61, 62] and are useful in detecting and monitoring ocular disease affecting retinal cell populations [63, 64].

[10] A comprehensive review of the OCT and its influence on biomedical imaging is provided by Fujimoto and colleagues [59]. Digital ocular fundus imaging was reviewed by Bernardes and colleagues [60].

### 1.2.2 Physiological measures - Visual Electrophysiology

While knowing about the structure and appearance of the retina and the eye is useful for staging, consequence and prognosis of ocular disease, further important information comes from looking at the functional integrity of the parts of the visual pathway. Physiological measures of visual function allow an insight into the actual changes of electrical currents within the visual structures which are associated with visual processes. In particular, the clinical electrophysiology of vision can be suggestive of the functionality of visual processes in the retina and the optic pathways. A big part of this thesis was to investigate the ON-and OFF-pathways at the level of the visual cortex and hence, the electrophysiological methods appropriate for their examination are described in more detail below.

#### 1.2.2.1 The electroretinogram (ERG)

The electroretinogram (ERG) describes a recording of the summed electrical signal produced by the retina when stimulated with a flash of light. More precisely, it measures the electrical responses of retinal cells, resulting from membrane potentials generated by light-induced changes in the flux of trans-retinal ions[11]. The conditions under which an ERG is recorded, determine the shape of the waveform and the cells contributing to it. In addition, the duration of the stimulus, the interval between the different stimuli, the age of the individual [66] and, of course, different retinal diseases can affect the ERG notably.

The ERG is usually recorded to an ascending array of light flashes with increasing strength (which is given in candelas per second and square metre, cd*s*$m^{-2}$; the luminous intensity of a light flash per square metre per second), usually with the help of corneal electrodes (for example DTL thread electrodes [67]), however, skin electrodes can be advantageous in some situations, especially when recording from young children. When the ERG response to a dim flash (for example 0.01 cd*s*$m^{-2}$) is recorded from a dark-adapted eye, the response will be derived from the rod system. In return, if the same stimulus is presented to a light-adapted eye, the response will be driven by the activity of the cones.

[11] For a comprehensive review, see for example [65].

The classic ERG waveform recorded from a dark-adapted subject (DA 3.0 cd*s*m$^{-2}$) usually consists of three major distinct curves called a-, b-, and d-waves[12]. The a-wave describes an initial negative deflection shortly after stimulus onset. It is derived from the photoreceptor cells and represents their hyperpolarisation following a light stimulus. The a-wave is, in the dark adapted human ERG, followed by a positive b-wave. This positive peak is derived from the inner retina, mostly generated by the depolarisation of ON bipolar cells. In addition to the ON bipolar cells, this peak receives its descending limb from the subsequently depolarised Müller cells. The ratio of b:a wave when recorded to a "standard" flash of 3.0 cd*s*m$^{-2}$ under dark adapted conditions is approximately 2:1. In cases where a normal a-wave can be recorded but the b-wave is diminished, leading to a ratio of 1:1 or less, the term "negative ERG" is used. Such a dark adapted negative ERG indicates a signalling abnormality at the synapse between photoreceptors and ON-bipolar cells and is a hallmark of ON-pathway dysfunction [68, 69][13]. Ultimately, an additional positive wave, which is more rarely recorded at the end of a light stimulus, is the d-wave (OFF response). Under conventional repeated flash stimulation conditions, this component merges within the b-wave and is therefore rendered invisible. In order to isolate this d-wave, prolonged on-off stimulation is required. This prolonged ON/OFF ERG can be useful in determining ON-or OFF-pathway defects, separating light onset and offset components.

When removing these low frequency components from the ERG waveform with the help of band pass filters, the high frequency components of the light and dark adapted ERG can be extracted, the oscillatory potentials (OPs) [72, 73]. The exact cellular generators of the OPs are still unknown but is has been suggested that inner retinal potentials generated by amacrine, bipolar and/or ganglion cells

[12]Another component, the c-wave, usually peaks 2 to 10 seconds after a visual stimulus is presented, with a latency depending on the flash intensity and duration. Due to this long latency, the c-wave response is prone to influences from blinks and eye movements and therefore difficult to observe. Its occurrence results from a change in the trans-epithelial potential after the hyperpolarisation of the apical RPE membrane cells and distal Müller cells.

[13]This type of ERG, where the a-wave amplitude is normal or only slightly subnormal is referred to as a "Schubert-Bornschein-type ERG", compared to the "Riggs-type ERG" which can show a reduced b:a-wave ratio but is characterised by a decreased a-wave amplitude [70, 71].

are most probably responsible [74, 75, 76]. Alongside the conventional ERG, they can give information on the functional integrity of dark and light adapted inhibitory feedback circuits, initiated by the amacrine cell network. In certain retinal conditions the absence of OPs aids clinical diagnosis, and for example patients with the complete form of Congenital Stationary Night Blindness (CSNB) show a characteristic lack of the first two major dark adapted OPs [77, 78], while reduced amplitude dark adapted OPs can be observed in individuals with the incomplete form [79]. The absence of specific OP peaks can hint at dysfunction in different parts of the neuronal circuitry of the inner retina. While absence of the earlier dark adapted OPs seems to be related to the ON-pathway, later OPs are thought to represent signalling within the OFF-pathway [80, 81, 82].

The standards of ERG testing are set by the International Society for the Clinical Electrophysiology of Vision (ISCEV)[14]. These comprise a set of ERG stimulation parameters leading to at least six different ERG protocols aiding the clinical diagnosis of retinal disorders. These standard protocols[15] are listed below. The parameters are named according to the stimulus flash strength and the state of adaptation of the subject.:

1. Dark-adapted 0.01 ERG (a rod-system response dependent upon ON bipolar cells)

2. Dark-adapted 3.0 ERG (combined responses arising from photoreceptors and bipolar cells of both the rod and cone systems; rod dominated)

3. Dark-adapted 10.0 ERG (combined response with enhanced a-waves to reflect photoreceptor function unambiguously)

4. Dark-adapted oscillatory potentials (responses primarily from amacrine cells)

5. Light-adapted 3.0 ERG (responses of the cone system; a-waves arise from cone photoreceptors and cone OFF bipolar cells; the b-wave comes from ON and OFF cone bipolar cells)

[14] www.iscev.org
[15] Taken from the most recent ISCEV standard 2015 [83]

6. Light-adapted 30 Hz flicker ERG (reflects cone system sensitivity)

An overview over the six basic ERG waveforms defined by the ISCEV standard and further waveforms is displayed in Figure 1.7.

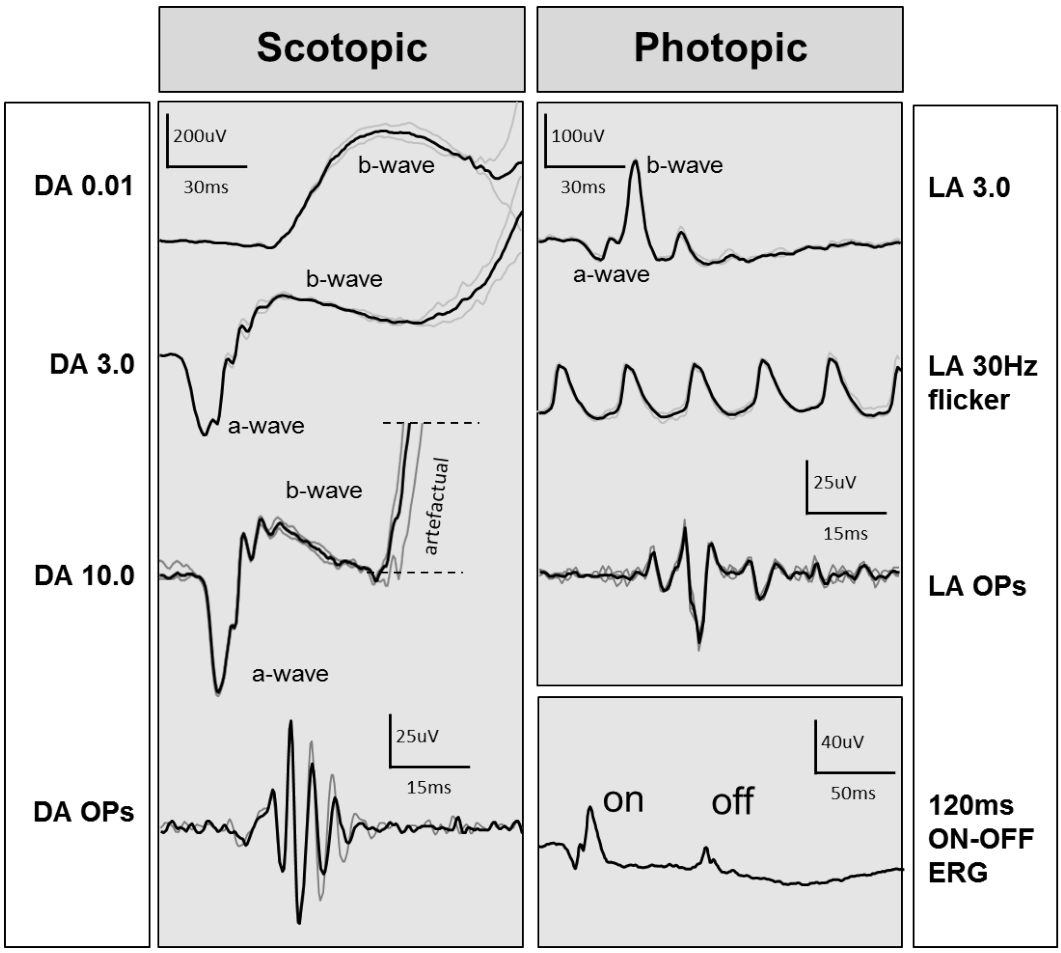


**Figure 1.7:** An array of exemplary ERG waveforms obtained from a healthy subject to all six ISCEV standard protocols, as well as light adapted OPs and the waveform obtained to prolonged (120ms) ON-OFF ERG stimulation. A-and b-waves are indicated. The OFF-peak in the ON-OFF ERG represents the d-wave. A blink/eye roll artefact can be seen in the DA 10 trace.

#### 1.2.2.2 Pattern ERG

The contribution of the macula to the full field ERG is negligible. To localise the retinal area stimulated, pattern ERGs are used. In order to record a PERG, the subject is conventionally presented with a phase reversing checkerboard stimulus[16]. It can be used to complement the ERG, as well as cortical recordings, as it reflects, at least partly, monocular retinal ganglion cell integrity [84, 85].

The conventional PERG consists of two major components, a positivity at around 50ms post-stimulus (P50) and a negativity occurring after approximately 95ms (N95). Sometimes, an early negative component (N35) can be observed before the P50 (Figure 1.8). The precise cellular origins of these components are a matter of debate. Groneberg and Teping (1980) were the first to ascribe an inner retinal origin to the PERG by recording an abnormal waveform from an individual with optic nerve section [86]. These findings of abnormal PERGs upon ganglion cell injury were later replicated in the cat [87, 88] and primate [89]. Subsequently, it was shown that the retinal origin of the P50 component differs from the one of the N95 [90], with the negative component probably reflecting ganglion cell activity. Because the P50 was still recordable in patients with optic nerve transsection [91], a predominantly ganglion cell retinal origin for this component was excluded.

Luo and Frishman found that the PERG in macaque monkeys is driven approximately equally by ON-and OFF-pathways, with P50 elicited by spiking and non-spiking activity in both pathways, while N95 originates from only spiking activity in both pathways [92]. When blocking retinal spiking activity in macque monkeys using Tetrodotoxin (TTX), they observed an early and reduced P50 and and a complete absence of the N95 component, indicating that ganglion cells contribute to both components. Moreover, Berninger and Schuurmans proved that both components display different spatial tuning characteristics [84, 85]. These findings suggest that the P50 component is at least partly generated distal to the retinal ganglion cells. Thus, potential candidates for P50 generation include ganglion cells but also macular photoreceptors or amacrine cells [93, 94].

[16]The same stimulus can be used to record the conventional pattern VEP, described in Subsection 1.3.2.3

In the literature, an influence of ganglion cell integrity on the waveform of the PERG is evident and thus, the PERG can expand the value of the ERG by adding the possibility of investigating monocular retinal ganglion cell function driven by ON-and OFF-pathway activity. In cases where the ERG is normal and an abnormality suspected in the subsequent structures of the visual pathway, the PERG can give valuable information about whether a pathology is located in the anterior or posterior optic pathways, when combined with the cortical VEP.

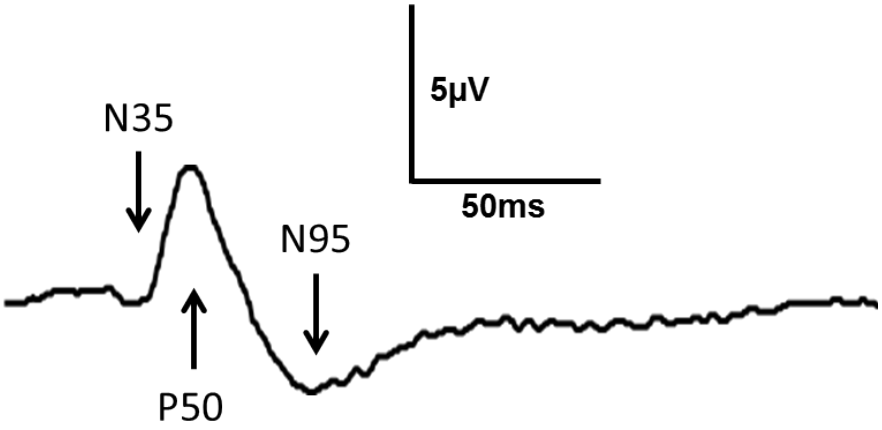


**Figure 1.8:** An example of a standard PERG waveform elicited from a healthy subject to a checkerboard which phase reversed three times per second. Arrows indicate the main components.

### 1.2.2.3 Visual Evoked Potential - VEP

The visual evoked potential (VEP) is frequently used to assess optic nerve function in clinical practice as it is thought to reflect ganglion cell firing, although it is generated in the cortical layers [95]. The VEP is part of the electroencephalogram (EEG), which can deliver temporal and spatial information about the signal processing along the visual pathway, beginning with the cells of the retina and leading to the higher visual areas of the primary visual cortex (V1 or striate cortex). Further, as only cortical electrodes are required for its recording, it is relatively easy to record in paediatric patients when compared to the ERG.

It is important to note that the VEP represents only the central macular area of the visual field (10° or less). The macula, carrying the fovea in its centre, is the retinal region responsible for high acuity vision and is retinotopically mapped to the occipital pole of each hemisphere. Additionally, the cortical area representing the macula is expanded resulting in a cortical magnification of the macula signal.

In clinical electrophysiological practice, the most common stimulus to be used in order to elicit a cortical response of macula function is a black and white checkerboard pattern that phase reverses once to three times per second, recording the pattern reversal VEP (pVEP); the same stimulus used to record a PERG. The pVEP is usually characterised by three main components (Figure 1.9).

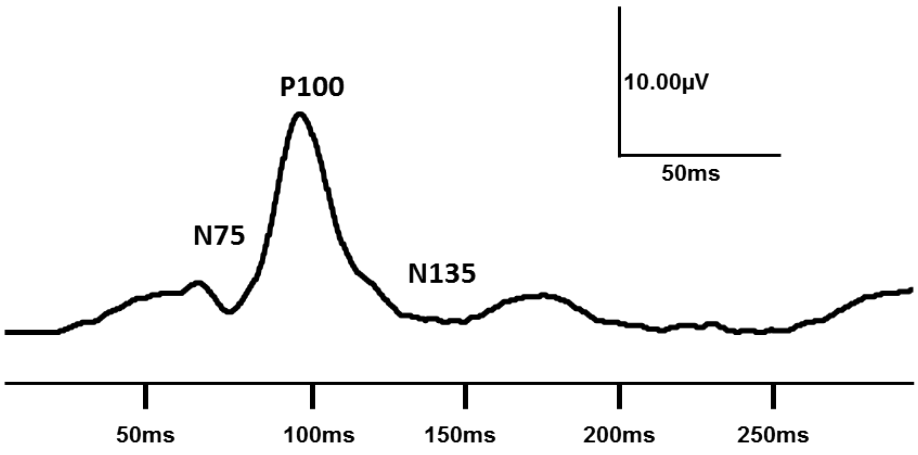


**Figure 1.9:** A typical pattern reversal VEP of a healthy volunteer elicited to 50'checks reversing at a rate of 3/s with main components indicated.

The first negative component appears at about 75ms after stimulus onset and is therefore referred to as N75. A larger positive peak appears at about 100ms, called P100 and a more variable negative component at 135ms (N135) [96]. In general, the VEP waveform amplitudes and peak latencies depend largely on the parameters of the stimulus, for example the size of each unit in the pattern, stimulus luminance, contrast and size of the visual field [97, 98]. It is therefore crucial to only compare responses which were recorded using the same parameters.

The pattern reversal stimulus delivers a well recognizable waveform across different subjects of a wide age-range, exhibiting a high inter-subject reliability.This is beneficial when assessing visual function of the macula in a clinical setting, where patients present with a variety of visual conditions. The P100 component is very reliable in its latency between individuals and stable from about seven months of age [99, 100]. The P100 latency is therefore frequently referred to as a standard value in electrophysiological testing and clinical diagnostics. VEP responses evoked by flashes of light (flash VEP) and pattern onset (onset VEP) are other means of evoking a physiological visual response from the cortex of human subjects. In contrast to the pVEP, they are reproducible in their form within an individual but vary considerably between subjects [66] and with age [101].

As a diagnostic tool, VEPs can deliver information about the functional state of the visual pathway and processing to the striate cortex. Generally, a low VEP amplitude implies a lack of functioning or firing neuronal fibres [102]. A delayed, broad or degraded waveform usually suggests dysfunctional fibres or alternatively, that not all fibres are firing synchronously [103]. A delay of the P100 peak is generally interpreted as a delay of signal processing or slow conduction speed along the visual pathway, as observed for example in conditions causing demyelination such as optic neuritis [103].

### 1.2.3 Psychophysical measures

With the complexity of the visual system and a lot of unknowns within the processes that lead to vision, deriving functional conclusions about how someone can see, from structural and physiological information, can be challenging. While the electrophysiological methods described can localise the site of dysfunction along the visual pathway and objectively assess function, the assessment of what influence conditions affecting the visual pathways can have on perceived vision, important for daily tasks, is difficult in a clinical context. Hence, psychophysical testing, which is the scientific study of the relationship between the physical properties of sensory stimuli and the behavioral perceptions that are elicited by these stimuli in human observers, has a special case in the assessment of the visual phenotype and the impact of disease on an individual.

In order to obtain a psychophysical result, the subject is presented with a stimulus and by careful adjustment of its intensity (or any other parameter of interest), the subject's threshold of perception is defined[17]. If care is taken when designing a psychophysical test, such tasks can be of great value as they allow an insight into the visual performance and perception of an individual. Further, they can elucidate which measurable physiological processes along the visual pathways are linked to which visual percepts.

[17] A more detailed account on how to obtain a threshold value in visual psychophysical testing is given in Chapter 4.

#### 1.2.3.1 Visual acuity and contrast sensitivity

Psychophysical eyesight testing is by no means a modern invention and was supposedly already practised by ancient peoples, using the stars. In the Persian army for example, elite warriors were tested for their visual spatial resolution (i.e. visual acuity) by having to distinguish the separation of the two stars Mizar and Alcor in the constellation of the Big Bear [104][18].

Visual acuity is crucial for many visual tasks, such as reading or face recognition, and the first standardised visual acuity tests were developed as early as 1843, when German ophthalmologist Heinrich Küchler invented the first symbol eye chart. An evolution of this early chart is the conventional Snellen Visual Acuity chart from 1892 [106], which has a single, large, high-contrast letter at the top and with each successive row, the letters become more numerous and progressively smaller. The more rows of letters one is able to read, the better his / her performance in this test. However, the test-retest variability with such charts is relatively high (up to a 2-line discrepancy) [107]. A clinical need for standardisation in visual testing led by the Early Treatment Diabetic Retinopathy Study (ETDRS) resulted in the creation of the ETDRS eye charts [108]. By using the same chart design but making the letters used equally legible, as well as providing a standardised protocol for visual acuity testing, the ETDRS charts became the gold standard for most clinical trials [109]. This logarithmic (logMAR) system was introduced in order to accommodate a wider range of letter sizes and achieve a more standardised measure of the Minimum Angle of Resolution (MAR). While Snellen and logMAR methods are used in clinical practice, the logMAR chart is considered most accurate, as it displays the same amount of letters per row with defined inter-letter and inter-row spacing, as well as being considered more sensitive to abnormality, because it allows a letter per letter scoring [110, 111]. Further, results obtained using a logMAR chart show a high reproducibility [112].

The assessment of VA is usually quick and easy to carry out in patients across

[18] Although this assessment was developed centuries years ago, it still holds validity, as being able to see the separation between the two stars is approximately equivalent to a 20/20 Snellen visual acuity [105].

a wide age range. The development of visual acuity, when assessed by psychophysical methods, such as preferential looking or lettermatching tasks, has been shown to develop rapidly during the first few years of life and to reach adult levels from the third and fourth years of life [113, 114, 115]; however, some studies found a slower trajectory with adult performance only achieved at around six years of age [116]. Commonly, foveal visual acuity is tested in clinical practice, as visual spatial resolution is highest here due to the 1:1:1 connection of retinal cells, with one cone photoreceptor cell connecting to one bipolar cell connecting to one ganglion cell.

A draw-back to visual acuity testing is that it only assesses visual spatial resolution at high contrast. In order to gain insight into an individual's performance under different (and more "life-like") contrast conditions, contrast sensitivity is sometimes tested in clinical practice using grating patterns of black and white bars with different spatial frequencies, or cycles (one black bar + one white bar). Here, the amount of cycles of the grating subtending one degree at the eye represents the coarseness of the grating. At a given spatial frequency, the contrast of the grating is altered until the subject cannot perceive it anymore, representing his / her contrast threshold. As mentioned earlier and discussed in more detail in Chapter 4, the perception of contrast is linked to the interplay of ON-and OFF-pathways originating in the retina. A loss of contrast sensitivity is a sign of many ocular conditions affecting one or both of these pathways, such as glaucoma [117]. Knowing about a loss of contrast sensitivity of a patient is important for monitoring of disease progression and for advice about appropriate adjustments facilitating everyday life, such as increasing the contrast of steps and stairs.

#### 1.2.3.2 Visual field testing

The assessments of visual acuity and contrast sensitivity are not very specific in locating disorders within the visual system, as disorders affecting the eye or visual pathways can produce similar visual acuity impairments and, by default, only central visual performance is tested. In order to obtain a spatial dimension of visual performance, the assessment of visual fields can be of benefit, locating dysfunction in central and peripheral vision of an individual. Visual field testing is generally

carried out by using a perimeter, displaying light targets mapped to specific positions of the subject's visual field. The subject is required to indicate if a target was seen or not seen. Hence, a systematic assessment of the light sensitivity of a subject at different positions of his / her visual field is achieved and can be mapped.

While peripheral vision occupies more than 99% of the total field of view and is highly sensitive for the detection of motion [118], many patients are unaware of a loss of visual function if it occurs in the periphery [119]. However, many disorders of the visual pathways produce initial deficits in the peripheral visual field and early detection of such disturbances can aid successful treatment. Examples of conditions with visual field defects include retinal dystrophies, like retinitis pigmentosa, or glaucoma [120], where ”the nasal step” - a scotomata occuring above and below the fixation point, producing a horizontal step-like defect in the nasal visual field - can be an early characteristic of field loss [121, 122].

### 1.2.4 Current limitations of clinical measures of vision

A difficulty for the progress of treatment options for congenital retinal diseases is that their pathophysiology is often not sufficiently described [123]. Current clinical vision assessments allow an insight into retinal and ocular structure (via the OCT and fundus photography) and physiology (via the ERG and PERG), as well as a general insight into the spatial and temporal physiology of culminated cortical visual signals (via the VEP and other cortical imaging methods). A link of these tests to visual perceptual performance is achieved by additional psychophysical assessment, for example of visual acuity, contrast sensitivity and visual fields.

All these tests deliver crucial diagnostic information but many can be challenging to perform in children, who show the earliest signs of visual impairment and in whom therapies may have the greatest chance of success. Structural and physiological assessments require good cooperation of the subject and are usually carried out with the help of precise but delicate and immobile technical equipment, an example being retinal electrophysiological assessments. These often rely on the use of fragile and irritating corneal electrodes as well as steady fixation of the visual target for optimal precision. While using sticker electrodes for the ERG can prove to be ad-

vantageous for an initial assessment in infants or uncooperative children [124, 125], the presence of nystagmus or frequent eye and head movements can quickly degrade such delicate recordings. VEP waveforms are usually more robust and easier to record, as they only require scalp electrode placement, but muscle artefacts and lack of cooperation might still pose an obstacle in young or restless children. Clinical visual tests which are easy and quick to carry out can provide the opportunity to improve the testing experience of patients and clinical teams. If these tests are also mobile and fun for patients to carry out, their overall cooperation and attention, and therefore quality of clinical data acquisition can be enhanced.

Obtaining structural and physiological information about the visual pathways is obtained with the ultimate aim to explain and define a patient's visual performance. However, the interpretation of such observational results is not trivial. Cortical imaging methods give insight into the collective visual signal originating in the retina. However, several major visual pathways, such as the ON-and OFF-pathways, first come together at the cortical level and significant interplay is thought to be present here. More specific tests, selectively assessing the functionality of these different visual pathways can be of great benefit in order to probe their contributions to visual perception. In the case of ON-pathway dysfunction, a retinal dystrophy which displays a high variability in visual impairments across individuals, more sensitive tests would be beneficial in order to identify the physiological patterns associated with best visual outcome.

In adult clinical practice, patient accounts can also be of help in order to learn about the perceptual signs and symptoms an individual is experiencing. In children, such direct reports are more difficult to acquire and are often obtained with the help of a patient's parents. Therefore, behavioural measures of visual perceptual performance, like psychophysical tasks, are an important factor complementing clinical diagnostics. While psychophysical testing is widely used in clinical practice, standardised assessments of many perceptual functions used in everyday situations are lacking. In vision research, psychophysical tasks assessing different kinds of motion perception, an important visual feature transmitted through ON-and OFF-

pathways, have been applied in a variety of studies (for example [126, 127, 128]). However, standardised tests for application in a clinical paediatric setting do not exist. Being able to better link patients' visual behaviour to their clinical test results, by means of more specialised and realistic complementary psychophysical tasks, would provide a more complete clinical phenotypic picture to clinical teams and hence inform on the best possible interventions and care.

## 1.3 What is visual impairment?

A defect or abnormality in any of the structures and processes described in the first section can lead to an impairment of visual function and perception in an individual. The types and underlying causes of visual impairment can be manifold and the impact such an impairment can have on life varies from an individual to the next. Further, the cumulative years lived with a visual impairment can vary from congenital conditions to visual impairments only occurring during later life.

Many visual conditions are currently not treatable, most of which are congenital disorders. Congenital retinal disease is one of the two major causes of childhood blindness in the UK, the other one being Cortical Visual Impairment (CVI) [123]. Anomalies such as coloboma, nystagmus and inherited severe early onset retinal dystrophy are examples of impairments present at birth. Inherited retinal dystrophies present a genetic diversity which is yet unparalleled in human diseases with Mendelian inheritance, with over 185 genetic loci related to such retinal degenerations having been identified[19].

However, it is estimated that these loci only harbour approximately half of the genetic defects present in patients with the other half still unknown [129]. Additionally, congenital retinal dystrophies can have multiple inheritance patterns (autosomal dominant, autosomal recessive, X-linked, digenic and mitochondrial), and clinical symptoms can often overlap, making accurate diagnosis difficult. In view of such challenges and a multitude of disease causing genes to be discovered, clinical diagnostics, alongside the development of possible treatments for these conditions, heavily rely on accurate genetic testing of patients with inherited retinal defects.

[19] A database of genetic loci related to retinal dystrophies can be found via RetNet: www.sph.uth.edu/retnet.

### 1.3.1 The value of genetic testing for clinical care of patients with retinal dystrophies

DNA screening was initially introduced by Sanger and colleagues [130], enabling the investigation of genetic material and culminating in the first complete sequencing of a human genome in 2004 [131]. While Sanger sequencing is still carried out conventionally in laboratories for verification of individual variants, more recent, high-throughput sequencing methods are referred to as "Next Generation Sequencing" (NGS). The major advantage of NGS methods over "first generation sequencing" methods is that they are able to process millions of sequence reads in parallel, allowing to collate vast amounts of genetic data rapidly, in contrast to a maximum of 96 reads achieved simultaneously during Sanger sequencing [132]. NGS methods have evolved considerably over the last years, becoming faster and more affordable[20] [134].

Examples of NGS methods are Whole Exome Sequencing (WES) and Whole Genome Sequencing (WGS), enabling the analysis of all coding regions of a gene (the exome, roughly 30 million base pairs [135]) or the complete genome of a patient (around 3.2 billion base pairs per haploid genome [136]), respectively. More recently, the use of targeted gene panel sequencing approaches has increased, for example allowing the rapid investigation of known genetic risk variants in patients with breast cancer [137] and the detection of disease causing variants in known disease genes in patient with inherited peripheral neuropathies [138]. NGS approaches using gene panels can be useful in cases where a rapid confirmation of a clinical diagnosis is crucial and the disease causing genes are (at least partly) known. If such gene panel approaches do not deliver a disease causing mutation in a patient with a congenital disorder, the more extensive WES or WGS approaches give the potential to carry out an exome-or genome-wide analysis of the DNA[21].

From a patient care standpoint, genetic testing can be greatly beneficial in supporting diagnostics. In many cases, clinical diagnostic testing by assessing pheno-

[20] A review of commercially available sequencers is given in [133].

[21] This study benefited from Sanger Sequencing, WES, as well as targeted gene panel NGS approaches. This will be further described in Chapter 3.

typical attributes helps to narrow down the amount of possible conditions likely to explain a patient's signs and symptoms. However, genetic testing can aid diagnostic accuracy in situations where the diagnosis is not completely clear. An example of this is the differentiation between the two congenital retinal disorders Congenital Stationary Night Blindness and Retinitis pigmentosa. Both conditions can cause similar symptoms in patients, but have very different disease progression and visual implications [139]. Thus, distinction between them can be challenging, especially in cases where visual testing conditions and results might not be of ideal quality, for example due to the age or cooperation of the patient. Monitoring of disease progression aids in determining whether a condition is progressive or stationary, however, early correct diagnosis is always paramount. In such situations, genetic testing can assist in giving the correct diagnosis, which, in this example, results in drastically different patient care and follow-up depending on which condition the patient has.

Additionally, knowing about the genetic reason for the occurrence of a certain condition gives insight into its heredity, having implications for the patient and his / her family. Often, knowing the chance of passing on a genetic defect to one's children or the knowledge of whether or not one is a carrier for a recessive mutation, has great impact on family planning. A genetic counselling appointment is therefore often useful for patients and families who want to know more about certain genetic disorders and the risks associated with them. This can also happen in view of the prediction of disease progression and therefore is useful in anticipation of future care required [140].

From a medical and research standpoint, genetic testing of congenital retinal disorders, combined with the detailed assessment of visual phenotypes, has the potential to narrowing the gap between knowledge obtained from visual testing and the actual process of vision. An understanding of the key molecules and interactions at any stage of the visual process is of tremendous importance in view of targeted pharmacological treatments, as well as for potential future gene-therapies. Such developments go hand in hand with the appreciation that every human has a slightly different genetic make-up and therefore a ”personalised medicine” approach could

lead to a higher efficiency in medical treatments.

The notion of treating congenital retinal conditions by replacing mutated genes with functional ones led to a surge in studies attempting to rescue visual phenotypes in animal models. Several of these approaches showed promise in model organisms, such as mice and canines [141, 142]. However, recent studies of the genetic repair of the retina, for example in patients with choroideremia [143] or Leber congenital amaurosis [144], delivered mixed results[22]. In order for potential gene-therapies to work, the knowledge of an individual's genetic make-up is crucial for a targeted approach which can increase the likelihood of success. Further, information on which molecules are affected in a certain disease context, fosters the understanding of molecular processes necessary within the visual system for best visual outcome, highlighting the value of genetic testing for the advancement of medical research.

[22]While some patients indeed seem to show an improvement in visual performance following gene-therapy treatment, the success-rate of these treatments is still relatively low and potential adverse effects require further study [145].

### 1.3.2 Legal framework in the UK

The primary aim of clinical ophthalmology is to assess and describe visual function in individuals with visual impairments. In order to ensure successful detection of abnormalities, a clear definition of a ”visual impairment” is crucial. In 1972, a study group on the *Prevention of Blindness* was convened by the WHO in order to provide a standardised definition of visual function to answer the question ”What is visual impairment?”. Despite the seemingly straightforward general understanding of ”visual impairment” as a decreased ability to see, a definition of the term has been subject to many revisions and changes in the past due to the variability of impacts different visual conditions can have. A standardised classification was anticipated to facilitate a comparative study of the prevalence of vision impairment and blindness in patient populations[23].

In the UK, the recognition of the variability of visual function across the population has resulted in a relatively recent amendment of the Certificate of Vision Impairment, which has been used to register impaired vision as a legal disability since 1990. The most recent legal document from 2005 refers to the definition of *severe sight impairment* from the National Assistance Act (1948): in order to be considered severely sight impaired, a person needs to be ”so blind as to be unable to perform any work for which eye sight is essential”. This vague definition is expanded by the recognition of different categories, into which people fall depending on the severity of their visual impairment, relying mostly on the measure of best corrected (monocular or binocular) visual acuity and visual fields[24]. In contrast, there is no legal definition of slight *sight impairment* in the UK and ophthalmologists rely on several guidelines when assessing sight impairment[25].

Individuals who are certified as *sight impaired* are entitled to the same help from their local social services as those who are certified as *severely sight impaired.* However, when it comes to certain social security and tax benefits, people with a

[23]The levels of visual function are described in [146].

[24]These categories can be found on the website of the UK government: www.gov.uk/government/publications/guidance-published-on-registering-a-vision-impairment-as-a-disability

[25]The VA measures of the patients investigated in this study is shown in Chapter 2, Section 2.3.3.1.

slight visual impairment might not be eligible.

Of course, a legal framework for judging and classifying visual impairment relating to disability is highly important; nonetheless, visual acuity and visual fields alone are not always a good predictor of the degree of problems a person may have, as someone with the slightest visual impairment can experience challenges in his / her daily activities, as well as social life. Therefore, precise, quantifiable and robust measures of visual function are crucial in providing information on an individual's visual abilities.

### 1.3.3 ON-pathway dysfunction

Twenty-five thousand blind or sight impaired children and young people under 16 years are estimated to live in the UK [147]. Congenital disorders of the retina are diverse and their impact on patients variable [123]. When acknowledging the time living with a visual impairment, it becomes clear that early age onset visual impairments can have a drastic impact on the development of children and young people. Most children with a congenital visual impairment will require life long support and resources. Early diagnosis and support of children and young people with visual impairments are crucial in ensuring their best possible development, as they are also prone to show developmental delays and are at greater risk to experience social communication, attention and behavioural difficulties [148, 149].

While aids alongside educational and financial disability support are beneficial for people with visual impairments, they do not improve their actual visual abilities. Unfortunately, treatment options for inherited damage to the retina are limited, although recent studies of gene-therapies and stem-cell replacements are showing some promise [150, 151]. The success of such therapies crucially relies on restoring structural functionality to the retina, allowing "normal" cellular signalling along the visual pathways. Two major pathways signalling from retina to visual cortex are the ON-and OFF-pathways. While the significance of their interplay in cortical areas and a potential influence on perceived vision in general are not very well understood at present, the knowledge of their role in the visual system can be improved by the study of visual impairments present in patients with a dysfunction of either pathway.

While selective OFF-pathway dysfunction is uncommon and accounts are rare in the literature [152], retinal ON-pathway dysfunction is relatively more prevalent, as it is part of several different conditions. An retinal ON-pathway dysfunction is generally reflected by a disruption of signal transmission at the synapse between photoreceptors and bipolar cells [69]. ON-pathway dysfunction can be a part of several different conditions and is not treatable at present. Individuals affected can present with a variety of signs and symptoms ranging from night blindness over

nystagmus to subnormal visual acuity and photo-aversion[26]. Due to the insufficient understanding of this retinal dysfunction and its variable visual phenotypes, encompassing a range from slight to moderate sight impairment, it has been difficult to give appropriate advice to patients and their parents and carers.

[26]Chapter 2 gives a detailed overview over the clinical presentation of patients with ON-pathway dysfunction.

## 1.4 Aims of this study

The study of conditions which selectively affect the retinal ON-or OFF-pathways can provide useful insight into their role and importance for human vision, potentially informing studies of novel therapies for congenital retinal dystrophies involving these pathways. Thus, the improvement of knowledge on visual phenotypes caused by such a retinal abnormality by means of applying specific visual tests, alongside the investigation of the underlying genetic make-up of such congenital retinal conditions, are crucial in the advancement of care provided by clinical teams to patients, their families and carers. Hence, the aim of this study was to get a better idea of what effect a dysfunctional ON-pathway has on vision, by systematically investigating and comparing phenotypes and genotypes encountered in patients with ON-pathway dysfunction.

Conventional clinical tests are difficult to carry out in children and are not specific enough to highlight the impact of an ON-pathway dysfunction on visual function. Hence, most information on how individuals with ON-pathway dysfunction see, comes from patient accounts. While these provide an invaluable (subjective) insight into the patients' visual experience, in order to obtain a full clinical picture of this retinal dysfunction, a quantifiable assessment of visual function and behaviour would be beneficial.

This thesis sought to elucidate the ways in which a disruption of the ON-pathway at the level of the retina might affect higher order visual signalling. Further, potential asymmetries between positive and negative contrast situations, thought to bias ON-and OFF-pathway contributions to the visual processes, were investigated. The effects of ON-pathway dysfunction were expected to be detectable via electrophysiological testing and psychophysical detection tasks.

Temporal and spatial firing patterns of retinal ganglion cells are thought to be crucial in the transmission of visual information from the ganglion cells to the cells of the striate cortex [153, 154, 155]. A selective disruption of ganglion cell firing through the ON-and OFF-pathways may alter the symmetry of the visual signal arriving at the striate cortex and this, in return, affect perceived vision. It was

anticipated that such a selective disturbance of ganglion cell firing would change the timing and size of the VEP waveform. There is some evidence from animal models of ON-pathway dysfunction indicating that ganglion cell firing is disturbed [156, 157, 158, 159]. Whether an ON-pathway dysfunction has a similar impact in human visual processing is not known. As ON-pathway signalling plays an important role in the perception of motion and contrast, these processes were predicted to be especially affected.

In order to test the hypothesis, the following objectives were set:

- Develop a child-friendly ON-pathway toolkit from novel and conventional stimuli to probe and distinguish different visual networks that the ON-pathway contributes to via electrophysiological and psychophysical methods;
- Use these new stimuli to elicit responses in a control group and optimise to get a robust response;
- Apply the ON-pathway toolkit in patients with ON-pathway dysfunction and compare their results to those of the control group to find out how ON-pathway dysfunction affects vision;
- Identify and correlate the genotype of these patients with their visual phenotypes to improve understanding of the interactions along the visual pathway that are associated with better visual outcome.

By providing novel and more specific visual tests for retinal disease, which are easy to carry out and child-friendly, such a toolkit could have the potential to increase the knowledge about the visual functions and percepts which are conveyed by ON-and OFF-pathways. Further, the tests could provide a tool to investigate and interpret better the patterns of visual loss which occur in children with visual impairment, where testing was previously difficult. The knowledge gained is aimed at supporting and informing patients, as well as parents and carers of the most appropriate intervention in order to improve the life of individuals affected. Moreover, correlating genotype and visual phenotype of patients has the potential to give an insight into the molecular key-players involved in signal transmission at the photoreceptor / ON-bipolar cell synapse.

In order to obtain a good overview of the range of visual impairments encountered in individuals with ON-pathway dysfunction, three different genetic conditions were selected on the base of showing a dysfunctional ON-pathway and their prevalence in clinical paediatric care:

- **Congenital Stationary Night Blindness (CSNB)**: stationary retinal dystrophy
- **Congenital disorders of N-glycosylation (PMM2-CDG)**: progressive metabolic condition
- **Duchenne Muscular Dystrophy (DMD)**: progressive neuromuscular condition with almost no visual symptoms reported in patients

This study was multidisciplinary and encompassed the investigation of clinical, physiological and psychophysical phenotypes, alongside the genotypes of patient subgroups with ON-pathway dysfunction. For ease of presentation, each part of the study will be described in a separate chapter. An overview on how patients with ON-pathway dysfunction present clinically is given in the following chapter (**Chapter 2**), while **Chapter 3** deals with the genetic analysis of patients within the ON-pathway dysfunction cohort. The clinical electrophysiological VEP data reviewed and obtained applying novel and conventional stimuli is explored in **Chapter 4**. **Chapter 5** is dedicated to the development, implementation and application of a novel clinical psychophysical software, $LumiTrack^{Tm}$, which was designed to measure the behavioural impact an ON-pathway function has on vision. Ultimately, **Chapter 6** integrates all the results described in earlier chapters for a genotype-phenotype correlation and the thesis concludes with **Chapter 7**, the final discussion of the findings.

Chapter 2

# Clinical presentation of patients with ON-pathway dysfunction

## 2.1 Clinical phenotype database

The first step for this study of the effects of ON-pathway dysfunction on vision was to obtain ethical approval from the Research and Development offices of Great Ormond Street Hospital (GOSH) and the UCL GOS Institute of Child Health, as well as the NHS Research Ethics Committee (REC). Ethical approval was obtained using the Integrated Research Application System (IRAS, study number 158971) and the study subsequently included on the UKCRN study database (UKCRN ID: 18348).

Patients seen in the Ophthalmology Department at GOSH, who exhibited an ON-pathway dysfunction were identified from electrophysiological records. By compiling clinical information on visual phenotypes encountered in these patients and the extent to which these vary across conditions, I aimed to obtain an overview of the extent and range of visual impairments caused by ON-pathway dysfunction. This information was then subsequently exploited during the design and development stages of the ON-pathway toolkit of novel visual tests described in Chapters 4 and 5.

### 2.1.1 Selection criteria

Retinal ON-pathway dysfunction can manifest in several conditions, where a signalling defect at the level of the photoreceptor / ON-bipolar cell synapse is present. The foremost clinical diagnostic method to evaluate the integrity of retinal function in patients is the ERG. As discussed in the introduction, the so-called ”negative ERG”, or a small b:a-wave ratio, is a hallmark of ON-pathway dysfunction [71]. The b-wave reflects the depolarization of ON bipolar cells upon light stimulation of the photoreceptor cells. A lack or small size of the representative b-wave with preserved a-wave results in a small b:a-wave ratio or even a negative ERG, and indicates an abnormality of signal transmission between these two successive cell types [160]. This ERG signature is most often noticed under dark adapted conditions because rods predominantly use the ON-pathway. A b-wave abnormality in the light adapted ERG further indicates an effect on cone ON-bipolar cell signalling [69].

Another indication of a dysfunctional ON-pathway can be an abnormal cone-

driven ON system response in the non-standard light adapted ON/OFF ERG [161] and therefore, whenever available, results from such stimulation were also considered. Thus, the initial criterion for selection of a condition for investigation was for the patients to display altered ON-pathway function in the full field ERG. Additional inclusion and exclusion criteria for this study are displayed in Table 2.1.

| Inclusion criteria | Exclusion criteria |
|---|---|
| Male and female participants between 4 weeks and 70 years of age with: | Patients with Cortical Visual Impairment who are unable to sustain looking performance and who have seizures |
| Duchenne Muscular Dystrophy | Patients treated at GOSH who are taking a combination of drugs that have known visual side effects |
| Congenital Stationary Night Blindness | |
| Congenital disorders of N-glycosylation | |
| Healthy control group of adults and children | |

**Table 2.1:** Tabular overview over the study inclusion and exclusion criteria

I identified patients with altered ON-pathway function from clinical records comprising all patients seen at the Tony Kriss Visual Electrophysiology Unit of GOSH since 2008. Also, several cases previous to 2008 were reviewed and analysed. Based on their clinical electrophysiological responses, 109 patients showing signs of ON-pathway dysfunction were selected. This cohort was then further subdivided by condition into subgroups of patients with Congenital Stationary Night Blindness (CSNB), disorders of N-glycosylation (PMM2-CDG) and Duchenne Muscular Dystrophy (DMD), depending on their electrophysiological responses and previous diagnosis derived from clinical letters[1]. Subsequently, all patients seen at the Tony Kriss Electrophysiology Unit at GOSH diagnosed with one of these conditions were included in the final database, which pooled several of the patients' clinical visual results, such as electrophysiological results (ERG, PERG, VEP), prevalence of nystagmus, visual acuity, age and gender.

It quickly became clear that, although a negative ERG or low b:a-wave ratio

[1]While individuals with X-linked retinoschisis can sometimes show a negative ERG waveform [162], patients with this condition were not included in the database as individuals usually show variable ERG waveforms and not always have a b:a-wave ratio smaller than 1.

was common in all subgroups, each condition showed slightly different waveform characteristics, possibly owing to slightly different molecular disruptions responsible for their ON-pathway dysfunction. For example, some patients with DMD did not exhibit a severely electro-negative ERG in response to dark adapted ISCEV standard flash stimulation of 3.0 cd*s*m$^{-2}$. A recent study by Ricotti and colleagues showed that the severity of the ON-pathway dysfunction in DMD seems to be linked to their genetic make-up [163]. Hence, the DMD subgroup was further subdivided into patients showing a mutation pre exon 30 of the DMD gene and those with a mutation post exon 30, affecting different isoforms of the dystrophin protein[2]. An overview over the patient subgroups investigated in this study is given in Table 2.2. Representative full field ERG responses for each of the subgroups are shown in Figure 2.1. The following section provides a more detailed review of the phenotypical and genotypical characteristics of the conditions investigated in this study.

[2]In fact, none of the patients with *DMD* mutations pre exon 30 showed a severely negative ERG waveform at 3.0 cd*s*m$^{-2}$. The division into two subgroups was only carried out once all patients with DMD were added to the database. Patients with DMD were nonetheless included, as some individuals show a negative ERG at this flash strength. A more comprehensive analysis of ERG responses in the patient subgroups is given in Section 2.3.2 of this chapter.

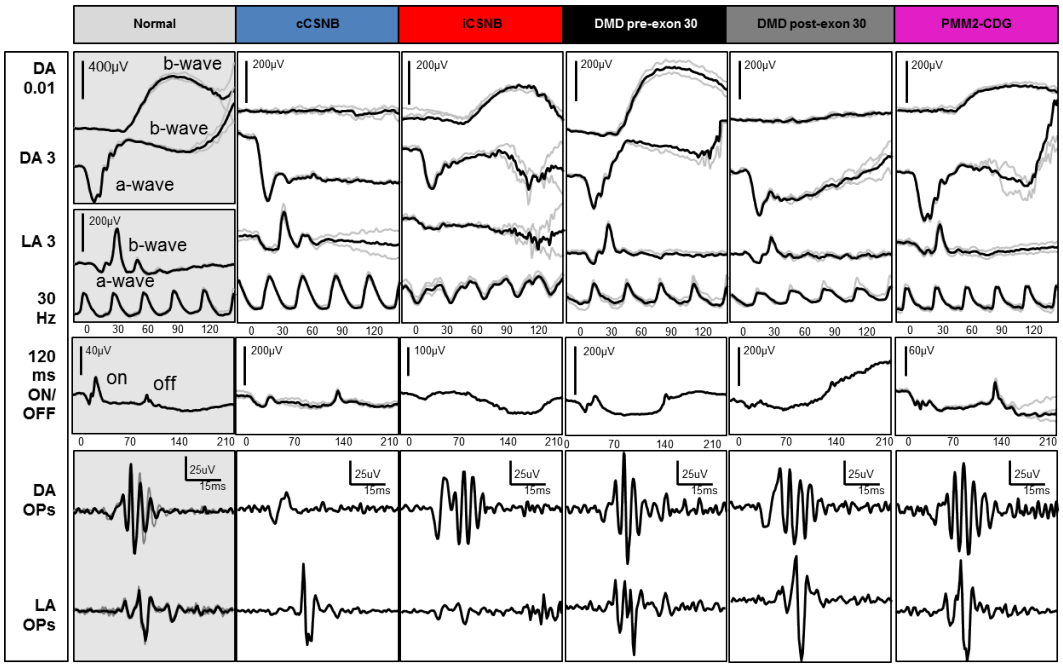


**Figure 2.1:** Overview of ERG waveforms encountered in different subgroups of patients with ON-pathway dysfunction to different dark adapted (DA) and light adapted (LA). ERG stimulation. Each column represents one study subgroup and the individual waveforms were taken from one representative subject of each subgroup.

| Condition | Median age + range [years] | n |
|---|---|---|
| **cCSNB** (OMIM: 310500, 613216, 257270, 614565, 615058, 617024) | 15 (3-43) | 33 |
| **iCSNB** (OMIM: 300071, 610427) | 11 (5-26) | 42 |
| **DMD pre exon 30** (OMIM: 310200) | 16 (9-21) | 8 |
| **DMD post exon 30** (OMIM: 310200) | 16 (7-20) | 11 |
| **PMM2-CDG** (OMIM: 212065) | 15 (5-26) | 15 |
| Total | 3-43 | 109 |

**Table 2.2:** Tabulated overview over the patient subgroups investigated in this study, including the OMIM identifiers attached to the conditions (taken from www.omim.org). The number presented in this table represent the total amount of patients assigned to each subgroup. In order to carry out the novel vision tests described in chapters 4 and 5, as many patients as possible from this initial pool were recruited.

## 2.2 ON-pathway dysfunction in different conditions

### 2.2.1 Congenital Stationary Night Blindness (CSNB)

CSNB refers to a group of clinically and genetically heterogeneous retinal disorders[3]. Depending on the specific pathways and underlying genes affected, CSNB can be subdivided into the incomplete form (ON-and OFF-pathway dysfunction) and the complete form (selective ON-pathway dysfunction) [69]. Patients with CSNB generally have difficulty adapting to low light situations as they mostly show a reduced activity of the rod pathway, which depends on ON-bipolar cell signals [164]. However, the cone ON-pathway is also reported to be affected [165]. Other signs may include reduced visual acuity, nystagmus or photo-aversion. An overview of the current classification based on inheritance patterns, as well as ocular phenotypes is displayed in Figure 2.2[4].

Incomplete CSNB (iCSNB) manifests itself through impaired rod and cone system function which is due to presynaptic defects at the synapse of photoreceptor cells and ON- and OFF-bipolar cells. Complete CSNB (cCSNB), on the other hand, reveals a complete loss of rod pathway function due to postsynaptic defects affecting the same synaptic link between photoreceptors and ON bipolar cells. Several genes have been found to be implicated in these CSNB subtypes[5] and a schematic drawing of the molecular interactions of these genes' protein products at the photoreceptor cell - ON bipolar cell synapse is shown in Figure 2.3.

At the initiation of the ON-pathway, the ON bipolar cells, the first ”point of contact” for glutamate released from photoreceptors upon light stimulation is mGluR6, a metabotropic glutamate receptor. It is located at the dendritic tips of rod and cone ON bipolar cells and glutamate binding to mGluR6, which happens in the dark, activates an intracellular trimetric G-protein complex, leading to the closure

[3]As mentioned previously, in this thesis, I focus on the Schubert-Bornschein types of CSNB, as these show a dysfunction at the level of the photoreceptor - bipolar cell synapse, whereas the Riggs-type of CSNB is characterised by photoreceptor dysfunction.

[4]The gene nomenclature used in this thesis is according to the HUGO Gene Nomenclature Committee for human gene names, and according to the International Committee on Standardized Genetic Nomenclature for Mice for mouse gene names. These guidelines can be found on www.genenames.org (human) and http://www.informatics.jax.org (mouse), respectively.

[5]For a comprehensive review see [166].

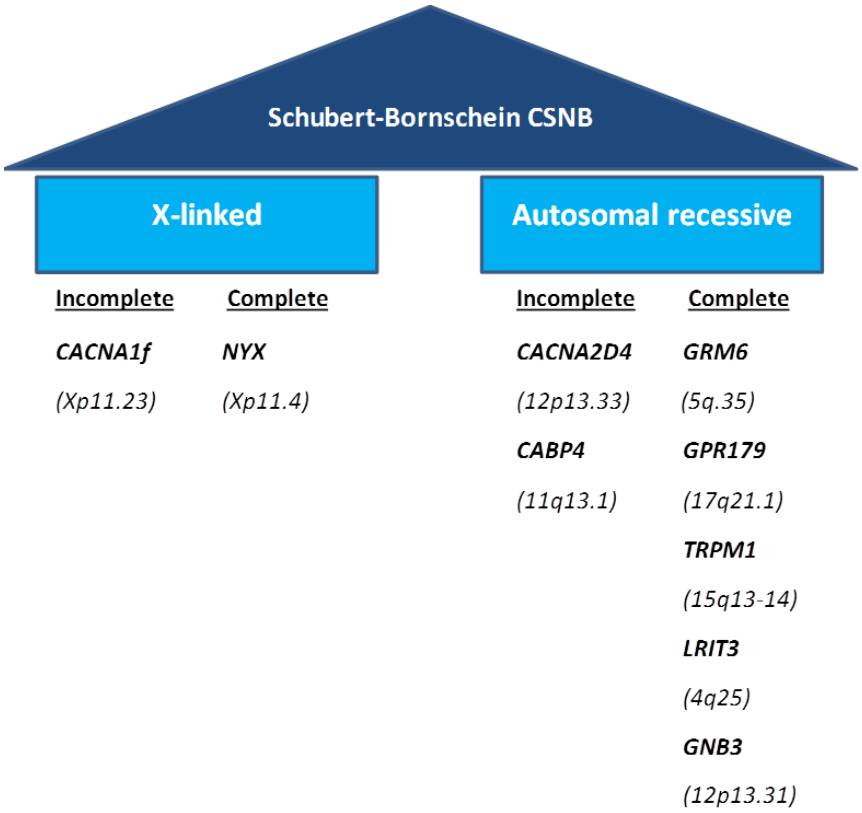


**Figure 2.2:** Overview of the current classification of the Schubert-Bornschein ERG types of CSNB according to inheritance patterns. The genes associated with the individual types are listed including their chromosomal location. Adapted from [166]

of the cation channel at the end of the ON-bipolar cell signalling cascade (TRPM1) [167, 168]. The gene encoding mGluR6 is *GRM6*, which is located on chromosome 5 at position q35 [169]. Dryja and colleagues first linked this gene to the autosomal recessive type of complete CSNB. Mutations in the *GRM6* gene can lead to a loss of function of the receptor due to a disruption in glutamate recruitment and protein truncation [170].

The endpoint of the signalling cascade starting with mGluR6 is the non-selective cation channel TRPM1 (Transient Receptor Potential Melastatin 1). In its open configuration, TRPM1 allows a cation influx into the cell environment which leads to the depolarization of the bipolar cell upon light stimulation [167]. It was first linked to night blindness in Appaloosa Horses as this protein is responsible for their coat spotting pattern, being involved in the pigmentation of the skin in these

horses [171]. In recent years, mutations in the *TRPM1* gene, located on chromosome 15 at position q13.3, have also frequently been linked to CSNB in humans [172, 173, 174]. A mutation can lead to the complete lack of *TRPM1* mRNA and therefore lack of functional TRPM1 protein on the cell surface of ON bipolar cells [175]. Further, patients with Melanoma Associated Retinopathy (MAR) also showing signs of night blindness and a reduced b-wave ERG were found to produce antibodies against TRPM1 which can be detected in their serum [176], highlighting the important role TRPM1 plays in ON-pathway signalling.

The seven trans-membrane G-protein coupled receptor 179 (GPR179) is also attributed an important role in supporting the signalling processes in ON bipolar cells [177]. It is not yet fully known if this protein carries out a structural or functional role, however, it is thought to be involved in the correct localisation of protein regulators RGS7 and RGS11, which control the ability of mGluR6 to gate TRPM1 [178]. Mutations of the *GPR179* gene - located on chromosome 17 - can result in complete absence of the protein and lead to the mislocalisation of the RGS7/11 complex and ultimately in the loss or closure of the TRPM1 channel at the cell membrane [179].

Similar to GPR179, Nyctalopin is involved in the ON bipolar cell signalling cascade, however, it is thought to play only a structural role in assembling and maintaining the signal protein complex in ON-bipolar cells [180]. In vitro, it was shown to interact with mGluR6 and both proteins are indispensable for correct localization of the TRPM1 cation channel in mice [181]. This small leucine-rich proteoglycan is encoded by the gene *NYX*, located at position p11.4 on the X-chromosome. Mutations in this gene are responsible for complete CSNB with X-linked inheritance [182].

Ultimately, the last known gene to be implicated in the complete form of CSNB is *LRIT3* [183]. It is located at chromosomal position 4q25 and encodes for a protein with a leucine-rich repeat domain, an immunoglobulin-like domain and transmembrane domains. The protein is expressed at the dendritic tips of ON bipolar cells [184]. Its function is as of yet, unknown; however, patients with a defect in LRIT3

show the classical cCSNB phenotype, making this protein a good candidate for the missing links within the retinal ON bipolar cell signalling cascade.

The protein mostly associated with the incomplete form of X-linked CSNB is CACNA1f. This voltage gated L-type calcium channel $\alpha 1$ sub-unit, found at the synaptic terminal of photoreceptor cells, is involved in the signal transmission process from photoreceptors to subsequent ON- and OFF-bipolar cells. It is vital for the functional assembly and maintenance, as well as synaptic functions of photoreceptor ribbon synapses [185]. It is encoded by a gene of the same name, found on the X chromosome at position p11.23. Reported mutations in this gene lead to alterations in the calcium mediated neurotransmitter release from photoreceptor cells due to loss-of-function and missense mutations [186, 187].

The very rare autosomal recessive form of incomplete CSNB is associated with mutations in the genes *CABP4* [188] and possibly *CACNA2D4* [189]. CABP4 encodes a $Ca^{2+}$ binding protein located in the synaptic terminal of photoreceptors. The CACNA2D4 protein, similar to CACNA1f, is a subunit of the $Ca^{2+}$ channel in photoreceptors, the $\alpha 2$ $\delta$-subunit. In the mouse, mutations in either gene result in dysfunctional $Ca^{2+}$ channel activity, similar to what is seen in patients with X-linked iCSNB due to *CACNA1f* mutations [190].

Recently, an unusual form of CSNB with reduced cone sensitivity observed in four patients was attributed to homozygous or compound heterozygous mutations in *GNB3* [191], which encodes the $\beta$ subunit of G-protein heterotrimer G$\alpha\beta\gamma$ and is expressed in ON-bipolar cells of mice [192]. The G$\beta 3$ subunit is specifically involved in modulating cone and rod bipolar cell signalling, as well as cone transducin function [191]. Biallelic mutations of *GNB3* are therefore likely to cause a dysfunction of the G protein in rod and cone ON bipolar cells (G$\alpha$o$\beta 3\gamma 13$), as well as in cones (G$\alpha$t2$\beta 3\gamma$t2). This unusual type of CSNB, linked to a partial or severe degree of ON bipolar cell dysfunction and variably reduced cone sensitivity presents a combination of the phenotypes commonly observed in complete and incomplete CSNB.

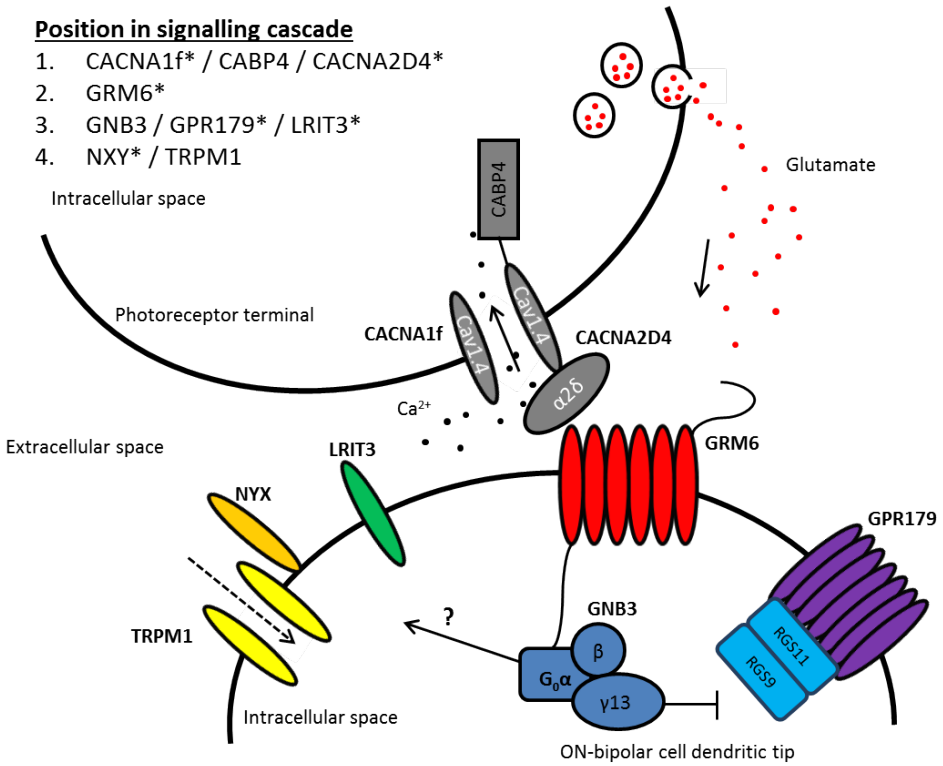


**Figure 2.3:** Schematic drawing of the molecular interactions of the proteins involved in CSNB at the photoreceptor - ON bipolar cell synapse. Gene names are located next to their protein products in bold. The order and position of the gene products in the photoreceptor - ON bipolar cell synaptic signalling cascade, according to current knowledge, is indicated on the right. N-glycosylated proteins are indicated by an asterisk.

In a nutshell, the molecular cascade taking place in ON bipolar cells upon light stimulation begins with the detection of low glutamate levels by the receptor mGluR6. This leads to the deactivation of the intracellular $G\alpha o\beta 3\gamma 13$ G-protein complex, which is regulated by protein regulators RGS7 and RGS11, as well as by GPR179. In turn, this results in the opening of the cation channel TRPM1, likely involving interplay by nyctalopin and LRIT3, allowing the influx of cations into the cell and resulting in its depolarisation.

Knowledge of the signalling cascade leading to ON bipolar cell depolarisation and hence signal transmission is not complete and there are several missing links yet to be discovered. Often these are first identified by means of exploring retinal signalling in model organisms and subsequent candidate gene approaches in patient

genetic sequencing. Further, visual phenotypical research using intracellular signal recordings in model organisms can aid the understanding of signalling networks and processes in the human disease context.

#### 2.2.1.1 Model organisms for CSNB

Mouse models are by far the most common organisms used in research on the genetics and molecular signalling of CSNB, as mutations in implicated genes lead to a ERG signature in mice, which is comparable to that of human patients with CSNB. Therefore, only these will be discussed briefly in this section[6]. The major mouse lines used in CSNB research are listed in Tables 2.3 and 2.4.

[6]For a comprehensive overview of mouse models and other model organisms for CSNB (for example horse, zebrafish or rat), the review by Zeitz and colleagues is recommended [166].

| Mouse name | Gene affected | Mutation location | Abnormality |
|---|---|---|---|
| nob | *Nyx* | exon 4, 171bp deletion | DA and LA ERG: absent b-waves |
| *Grm6*$^{tm1Nak}$ | *Grm6* | exon 8, knock out | DA and LA ERG: absent b-waves + delayed ON system response in RGC and SC cells |
| nob3 | *Grm6* | intron 2, splice site | DA and LA ERG: absent b-waves + delayed ON system response in RGC and SC cells |
| nob4 | *Grm6* | exon 3, missense | DA and LA ERG: absent b-waves + delayed ON system response in RGC and SC cells |
| nob7 | *Grm6* | exon 8, missense | DA and LA ERG: absent b-waves |
| nob8 | *Grm6* | exon 2, missense | reduced but not abolished DA and LA ERG b-waves + slightly delayed ON system response in RGC |
| *Trpm1*$^{tm1Lex}$ | *Trpm1* | exon 4-6, knock out | DA and LA ERG: absent b-waves |
| *Trpm1*$^{tvrm27/tvrm27}$ | *Trpm1* | exon 23, missense | negative DA ERG + het mice show b-wave reduction |
| nob5 | *Gpr179* | intron 1, transposon insertion | DA ERG: absent b-waves + LA ERG: reduced or missing b-waves |
| nob6 | *Lrit3* | exon 3+4, knock out | DA ERG: absent b-waves + LA ERG: reduced or missing b-waves + thinning of INL |
| GNB3 KO | *Gnb3* | total gene knock out | DA and LA ERG: narrow a-waves, reduced b-waves |

**Table 2.3:** CSNB mouse models

| Mouse name | Gene affected | Mutation location | Abnormality |
|---|---|---|---|
| nob2 | *Cacna1f* | exon 2, incomplete knock out | DA ERG: normal or slightly reduced a-waves, absent b-waves and OPs + reduced LA ERG b-waves + slight OPL thinning |
| Cacna1f KO a | *Cacna1f* | exon 7, knock out | reduced a-wave, absent b-wave + LA ERG: absent cone responses + slight OPL thinning |
| Cacna1f KO b | *Cacna1f* | exon 14-17, knock out | DA ERG: normal or slightly reduced a-waves, absent b-waves and OPs + reduced LA ERG b-waves |
| Cacna1f KI | *Cacna1f* | exon 17, knock in | DA ERG: absent b-waves and OPs + reduced LA ERG + slight OPL and ONL thinning |
| Cabp4 KO | *Cabp4* | exon 1+2, knock out | DA ERG: a-wave reduction, lack of b-wave + LA ERG: slight a-wave reduction, severe b-wave reduction + OPL thinning |
| C57BL/10 | *Cacna2D4* | exon 25, 15bp frameshift | DA ERG a-and b-wave reduction + no detectable LA ERG + OPL thinning and rod degeneration |

**Table 2.4:** CSNB mouse models - continuation

The first mouse line to be introduced, carrying a naturally occurring deletion in exon 4 of the *Nyx* gene, was also the one to determine the nomenclature of most mouse models. Due to the lack of a dark adapted b-wave, these mice were called *nob* for "no b-wave" [193]. Like human patients with cCSNB, these mice show normal retinal cellular structure but a decreased light sensitivity paired with a negative ERG signature under light[7] and dark adapted conditions [69]. Alongside the nob mouse, several other mouse models carrying defects in other genes implicated in the incomplete and complete forms of CSNB were discovered or created for research purposes (*Grm6* [194, 157, 156, 195, 196], *Gpr179* [197], *Lrit3* [198], *Gnb3* [192], *Cacna1f* [187, 199, 185, 200, 201, 202]). The establishment of some models even led to candidate gene approaches in human patients confirming the involvement of certain genes in CSNB (for example *Trpm1* [172, 203, 204], *Cabp4* [205, 188] and *Cacna2D4* [206, 189, 207]).

Apart from valuable information on the genetic make-up underlying the types of CSNB in humans, mouse models can also give indications on the visual phenotypes resulting from specific mutations. Despite showing some slight differences in the ERG (see Table 2.4) [202, 160, 187, 185], all iCSNB murine models show some ocular similarities: a mislocalisation or absence of the Cav1.4 channel subunit (normally localizing in the OPL), alongside general thinning of the OPL have been observed in most cases [205, 208, 201]. The cCSNB mouse lines show no great phenotypic variability in any of the cCSNB mouse lines with all showing an absent or severely reduced ERG b-wave under dark and light adapted conditions [187]. Further, the majority of cCSNB mouse models do not display any obvious morphological abnormalities, apart from one report of INL thinning in the nob6 mouse (*Lrit3* knock out) [198].

An exception within these mouse models might present those carrying a defect in mGluR6 function due to mutations in *Grm6*. These mice were linked to abnormal inner retinal cell firing with delayed or absent ON system responses in

[7]The light adapted ERG with undetectable b-wave amplitude in almost all mouse lines stands in some contrast to the ERG of human patients with cCSNB, where the light adapted b-wave is present, albeit showing an abnormal shape[193].

ganglion cells [156, 157], as well as Superior colliculus cells [158]. Such findings support my hypothesis that a dysfunctional ON-pathway could lead to altered signal arrival at the visual cortex in humans with ON-pathway dysfunction. To the author's knowledge, ON system responses in other mouse models for CSNB have yet to be investigated.

Thanks to phenotypical and genetic studies in human and mouse, an idea of how signal transmission between photoreceptor cells and ON-bipolar cells functions has emerged. However, many key players within these signalling cascades and complexes are still unknown and further studies investigating genotype and phenotype of individuals with ON-pathway dysfunction are required in order to elucidate these.

### 2.2.2 Congenital disorders of N-glycosylation (PMM2-CDG)

ERG phenotypes similar to patients with CSNB are observed when examining individuals with PMM2-CDG, also known as phosphomannomutase 2 deficiency. With a prevalence of approximately 1 in 20,000 globally [209], it is a rare metabolic disease which is inherited in an autosomal recessive pattern. PMM2-CDG typically reveals itself during infancy, where characteristic signs are developmental delay, hypotonia, an abnormal distribution of fat, strabismus and failure to thrive [210]. Due to multiple organ failure, about 20% of affected infants do not survive the first year of life [211, 212].

The affected gene is *PMM2* (chr16p13) encoding the 246-amino acid protein phosphomannomutase 2, an enzyme required for the biosynthesis of N-glycoproteins [213]. Mutations in the *PMM2* gene lead to the production of abnormal phosphomannomutase with reduced activity, resulting in incorrect oligosaccharide synthesis. The wide variety of signs and symptoms in PMM2-CDG are likely due to the abnormal production of phosphomannomutase 2 in many organs and tissues [214].

There have been several reports of retinal effects in PMM2-CDG in recent years, starting with Retinits pigmentosa [210]. Others linked the disorder to abnormal development of the lens or the retina [215], alongside signs of ON-pathway dysfunction with preserved oscillatory potentials of the ERG [216]. This finding is supported by the fact that a variety of key proteins involved in ON bipolar cell signalling are N-glycosylated (for example Nyctalopin and mGluR6, see Figure 2.3) [217]. A disruption in the glycosylation of these proteins is expected to disturb the protein function and hence, affect retinal signalling in a similar fashion as seen in patients with CSNB. In contrast to CSNB however, the visual phenotype in PMM2-CDG is progressive and photoreceptors can also be affected [216].

### 2.2.3 Duchenne Muscular Dystrophy (DMD)

The visual experience of patients with Duchenne muscular dystrophy (DMD) stands in stark contrast to both aforementioned conditions, as individuals do not usually complain of any visual problems and generally exhibit normal visual acuity. DMD is a form of muscular dystrophy affecting around 1 in 3600 boys [218]. This X-linked disease is generally associated with muscle weakness linked to a loss of muscle mass. Hence, loss of movement occurs, eventually leading to paralysis. The average life expectancy for individuals with DMD is around 25 years [219].

DMD is caused by mutations in the *DMD* gene which is located on the short arm of the X chromosome (Xp21.2-p21.1). Its protein product, dystrophin, is responsible for connecting the cytoskeleton of each muscle fiber to the underlying basal lamina through a protein complex.

Protein isoforms of dystrophin are present in a variety of CNS regions, as well as the human retina, and their expression is required for normal retinal function [220]. Figure 2.4 gives an overview of the different isoforms of the protein which are produced via distinct promoters, alternative splicing or use of different polyA-addition signals.

At least three different dystrophin variants are present in photoreceptor synaptic complexes (Dp427, Dp260 and Dp140) [222]. These isoforms were recently found to be expressed in inner retinal neurons of mice with the shortest dystrophin isoform (Dp71) being expressed in Müller cells [223]. Supporting these findings, some individuals with DMD were found to present with a reduced b-wave electroretinogram (ERG), indicating inner retinal dysfunction [224]. A recent study by Ricotti and colleagues linked specific sites of mutation in DMD with differential retinal function. Patients with DMD and mutations downstream of exon 30 were found to show negative dark adapted ERGs. They further discovered that neurodevelopmental disturbances were most severe when the shorter isoforms of dystrophin were affected by mutation, as boys with Dp71 disruption presented the most severe phenotypes. The authors suggested the use of ERG recordings as biomarker for dystrophin function in the CNS due to the strong correlation between the pa-

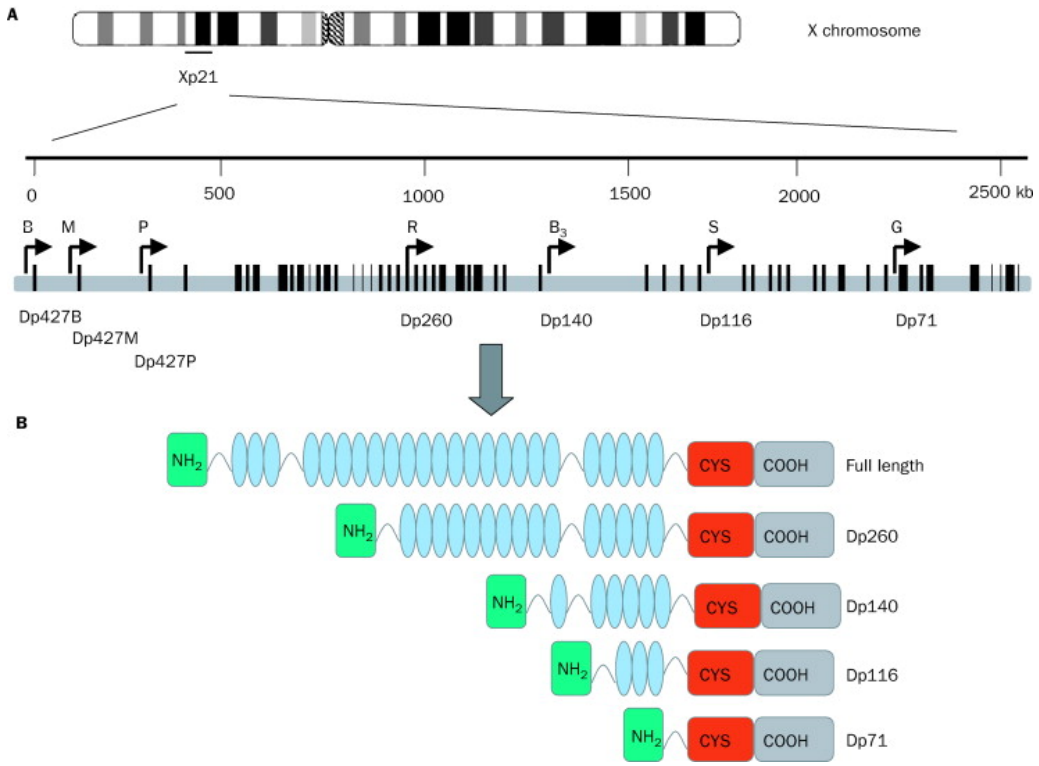


**Figure 2.4:** A: Schematic of the genomic organisation of the dystrophin gene. Black vertical lines represent the 79 exons of the dystrophin gene distributed over around 2.5 million bases. Arrows indicate the promoters: brain (B), muscle (M), and Purkinje (P); R, B3, S, and G represent the Dp260 (retinal), Dp140 (brain3), Dp116 (Schwann cells), and Dp71 (general) promoters. B: Domain composition of the different dystrophin isoforms. The amino-terminal domain is followed by the spectrin like domain, the cysteine rich, and the carboxy-terminal domain. Taken from [221].

tients' dark adapted ERG responses and their genetic make-up. This study and others suggest a role of dystrophin isoforms in retinal signalling and neurotransmission, however, their specific roles remain unknown [225, 226, 227].

### 2.2.4 Summary of ON-pathway dysfunction cohort selection

By comparing the visual phenotypes of these distinct conditions, I aimed to get an insight into the workings and importance of ON-pathway signalling on physiological and behavioural visual outcome. CSNB presents an interesting case as its investigation allows an insight into visual impairment caused by a pre-synaptic signalling defect (iCSNB) and a post-synaptic signalling defect (cCSNB). Hence, the patient subgroups with CSNB provided the main work of this study. While incomplete and complete CSNB present a set of mostly stationary disorders of the ON-pathway[8], PMM2-CDG is known to be progressive. A curiosity presents itself in the case of DMD. While patients with this condition do not usually suffer from any visual problems, some patients do display clinical electrophysiological evidence of a dysfunctional ON-pathway and the severity of this dysfunction seems to be linked to their underlying genotype.[9]

[8] In some patients with a CACNA1f gene defect, leading to iCSNB (which also affects OFF-pathway signalling), a slight progressive retinal dysfunction can be observed later in life [228].

[9] It is noteworthy, that cCSNB presents the only condition under investigation in this study where dysfunction is thought to be solely confined to the ON-pathway. Current knowledge shows, that the incomplete form of CSNB affects both ON-and OFF-pathway, whereas the situation in DMD is not fully clear. Further PMM2-CDG may involve a progressive degeneration of visual structures not confined to those in the ON-pathway only.

## 2.3 Phenotypical cohort presentation

*"I feel like I am a part of both worlds - the sighted and the blind. Summer is the best part of the year when it is light out longer and I can see better, but during winter I have very little vision and am almost completely reliant on others."*
- anonymous

*"I am registered as blind and when it is dark only see black. In bright light I lose all contrast and for want of a better description see a white haze. In dull conditions I can see enough to get around and read large print."*
- anonymous

These two quotes, taken from an online support forum for individuals with CSNB[10], give a small insight into the variable visual impairments which patients with ON-pathway dysfunction can exhibit[11]. In order to obtain a clinical picture of the visual and ocular phenotypes of patients with ON-pathway dysfunction, available results of vision tests conventionally carried out at GOSH were reviewed and, whenever possible, were compared to reports from the literature.

[10] http://www.visionaware.org

[11] A captivating first-hand account of a life with visual impairment due to CSNB is described in [229].

### 2.3.1 Structural measures

From a total of 75 CSNB patients, reports about fundus appearance were available for 34 (14 cCSNB, 20 iCSNB). Some patients with cCSNB and iCSNB showed myopic changes (n= 8/34), as well as tilted optic discs (n= 7/34). Slight temporal pallor of the optic discs was detected in three patients, one with cCSNB and two with iCSNB. The remaining patients showed normal fundi, which were usually described as ”healthy” or ”unremarkable”.

Thinning of the central retinal nerve fibre layer, evaluated by OCT imaging, was reported in one patient with clinically diagnosed iCSNB in the patient cohort (Pat120)[12]. Figure 2.5 displays representative fundus and OCT images of patients with iCSNB (Pat46) and cCSNB (Pat26), as well as representative OCT images of the same patients. The retinal layers are indicated in white on the OCT image of Pat46, representative of a healthy retinal architecture.

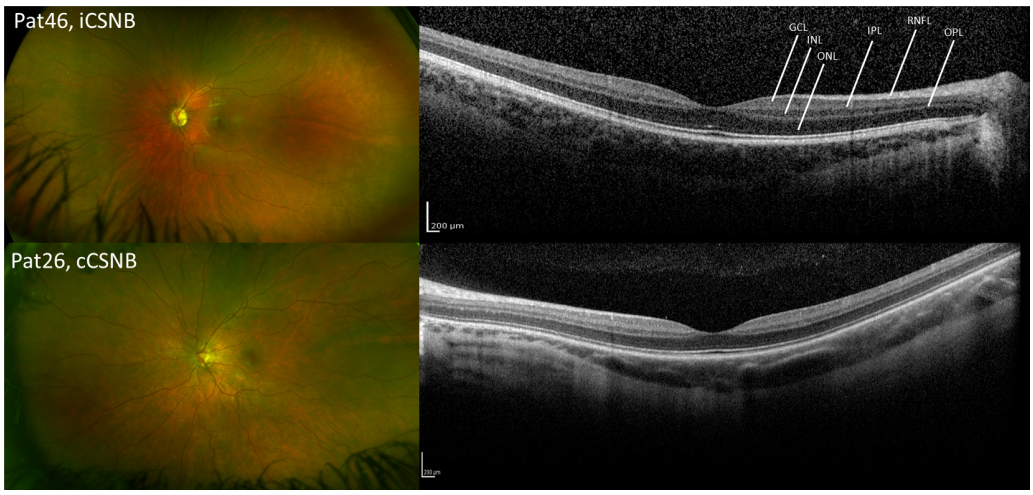


**Figure 2.5:** Exemplary fundus photographs of a patient with iCSNB (Top: Pat46, left eye) and a patient with cCSNB (Bottom: Pat26, left eye). The OCTs display transsections through the foveal area. The representative retinal layers discussed in the introduction of this thesis are indicated in white on the OCT image of Pat46. ONL: Outer Nuclear Layer, OPL: Outer Plexiform Layer, INL: Inner Nuclear Layer, IPL: Inner Plexiform Layer, GCL: Ganglion Cell Layer, RNFL: Retinal Nerve Fibre Layer

[12]OCT images were analysed where available.

In the literature, patients with CSNB generally are not reported to show any fundus abnormalities, apart from myopic changes in some patients [166]. However, myopic maculopathy [230], tilted disc and disc pallor [77] have been reported and are likely linked to the occurrence of myopia in these patients [231]. Further, no changes of anatomic structure and normal photoreceptor density are generally observed [232, 233]. Nonetheless, some (rare) reports of retinal thinning do exist. Godara and colleagues reported retinal thinning in the parafoveal region (including the ganglion cell layer but sparing the outer retina) in three patients with cCSNB (due to mutations in *GRM6*) [234]. Also, one report from Sustar and colleagues mentions a cCSNB patient with abnormality at the level of the IPL [235], they specifically suggest a possible lack of the sub-layer containing ON bipolar cell terminals. Non-progressive thinning of the GCL, IPL and INL, as well as the RPE, in five cases of iCSNB (with confirmed *CACNA1f* mutations) when compared to myopic controls, was also reported in the same year, although retinal architecture was reported as ”qualitatively normal” [236]. These findings in patients with iCSNB agree with the retinal thinning observed in most mouse models with *Cacna1f* mutations (see Table 2.4). Structural alterations caused by a reduction in ganglion cell axonal projections could potentially explain the thinning of the retinal nerve fibre layer in the iCSNB patient. However, Chen and colleagues reported normal retinal nerve fibre layer thickness in their iCSNB patients. Thus, a more detailed examination of retinal architecture in Pat120 would be beneficial in determining the significance of this finding[13].

[13]Pat120 was clinically diagnosed with iCSNB, however his DNA was not available for genetic analysis.

Similar to the majority of patients with CSNB, in boys with DMD, normal fundi are usually observed [224][14]. Along with reports of unremarkable ocular presentation, Ricotti and colleagues also reported normal retinal layer thickness and architecture in DMD boys with mutations pre and post exon 30 [163]. Of the 19 boys with DMD, only two had an OCT carried out, accompanied by infrared fundus images. Both patients showed normal retinal architecture and the images are displayed in Figure 2.6.

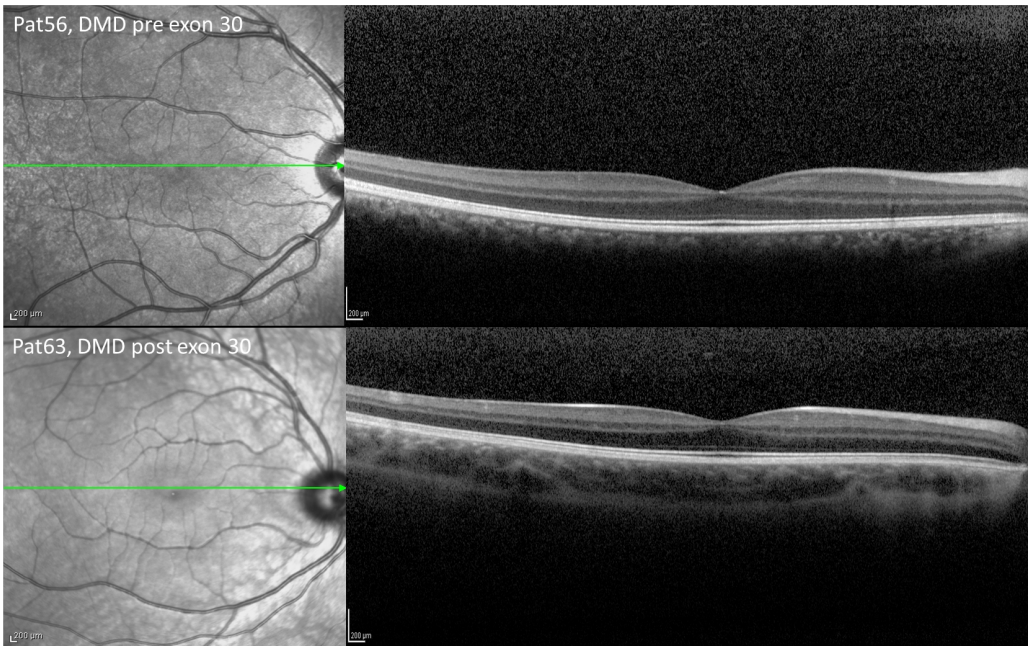


**Figure 2.6:** Exemplary infrared fundus photographs of a patient with DMD mutation pre exon 30 (Top: Pat56, right eye) and a patient with DMD mutation post exon 30 (Bottom: Pat63, right eye). The OCTs display transsections through the foveal area.

[14]However, there is one report of slightly increased macular pigmentation with otherwise normal ocular examination [220].

Patients with PMM2-CDG do not only manifest an ON-pathway dysfunction, but can also suffer from other metabolic and visual phenotypes [237]. Hence, an association of any fundus and structural changes solely due to ON-pathway dysfunction is difficult in these individuals. The description of fundus changes in the literature on PMM2-CDG is rare but Thompson and colleagues reported ”fine yellow dots” in the parafoveal region at the level of the RPE [238]. Further, Messenger and colleagues reported hypopigmentation in some patients [239].

Out of the 12 PMM2-CDG patients part of this study cohort, OCT and fundus images were only available for two (Pat73 and Pat74). Pat73 showed some white pigmentation, similar to the phenotype described by Messenger and colleagues. Structurally, Pat73 showed a normal fovea in the OCT but a loss of the photoreceptor layer immediately outside the parafoveal area, alongside some RPE changes in peripheral retina. Pigment in the retina can indicate the death of photoreceptors and the parafoveal thinning of the outer retina in this patient likely reflects the progressive photoreceptor loss which is associated with PMM2-CDG [240]. In contrast, Pat 74 showed no major structural abnormalities. Figure 2.7 compares the images obtained from both patients with PMM2-CDG.

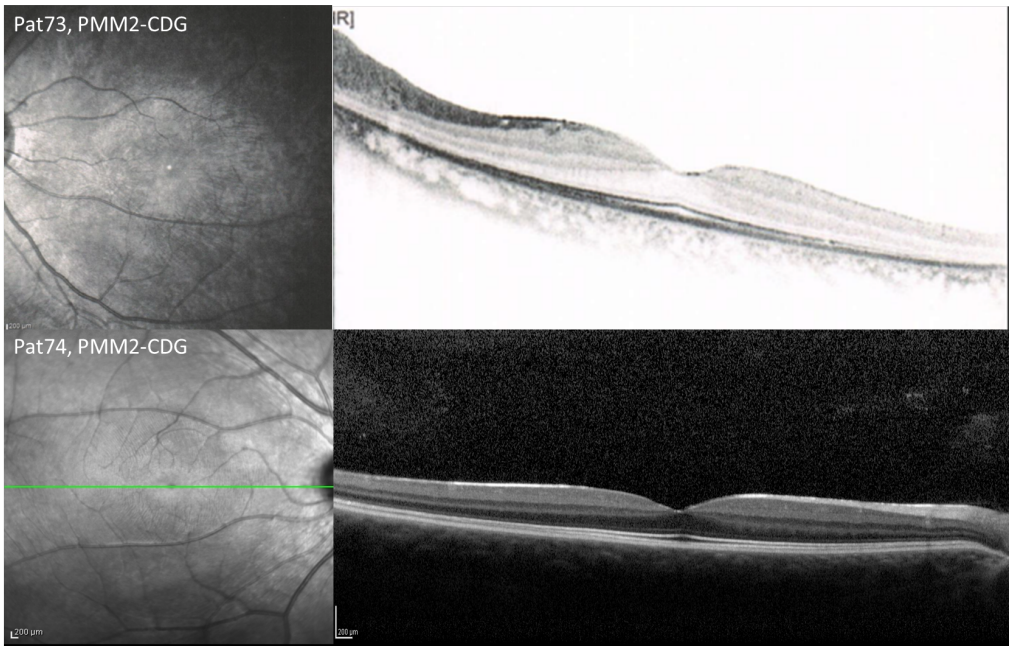


**Figure 2.7:** Exemplary infrared fundus photographs of two patients with PMM2-CDG (Top: Pat73, left eye; Bottom: Pat 74, right eye). The OCTs display transsections through the foveal area.

### 2.3.2 Electrophysiology

The signalling defect in patients with ON-pathway dysfunction is localised to the level of the photoreceptor / ON-bipolar cell synapse in the retina by the means of the ERG [69]. Hence, individual ERG results were crucial in the selection of patients for the cohort investigated in this study. While a negative or low b:a-wave ratio ERG, as well as an abnormal ON system response in the prolonged ON/OFF ERG, were most indicative of an ON-pathway dysfunction in general, the different subgroups of patients showed slight differences in their responses to different light stimuli.

In order to reveal these differences, a thorough analysis of the patients' ERG waveforms to ISCEV standard flash arrays was carried out[15]. Also, the PERG and VEP responses available, reflecting ganglion cell and optic pathway integrity, were analysed by means of component analysis across all patient subgroups. Dark adapted and light adapted ERG responses are displayed in Section 2.3.2.1, while an analysis of OPs is shown in Section 2.3.2.3[16]. PERG responses are shown in Section 2.3.2.4 and the VEP results are discussed in more detail in Chapter 4. Component size measurements for all electrophysiological data was carried out following the guidelines published by ISCEV [83, 241, 242].

#### 2.3.2.1 ERG

The dark adapted a-wave is thought to reflect rod photoreceptor hyperpolarisation upon light stimulation at low flash luminances. A mixed response from rod and cone systems is expected when using flash strengths of 3.0 cd*s*$m^{-2}$ and above, where the ISCEV standard first mentions the appearance of an a-wave [83]. In general, subgroups followed the trajectory of the normative data range for dark adapted a-wave amplitudes (Figure 2.8). Mean a-wave amplitudes of the cCSNB, iCSNB and DMD post exon 30 subgroups fell within the normal range for all flash

[15] 38/109 patients had an ISCEV ERG recorded. These recordings were carried out using a Colour-Dome Binocular Flash Simulator from Diagnosys LLC. Filters were set as follows: Frequency band-width 0.15 - 300 Hz, notch filters were not used. The values presented in the following subsections were always obtained by measuring responses from the better eye.

[16] For exemplary waveforms for each condition, the reader is referred to Section 2.1 of this chapter, Figure 2.1

strengths. While patients with cCSNB generally followed the lower margin of the normative data range, PMM2-CDG and DMD pre exon 30 subgroup average amplitudes turned out slightly lower than this at flash strengths above 3.0 cd*s*m$^{-2}$. A low a-wave amplitude could be indicative of a photoreceptor dysfunction. Several clinical studies recorded attenuated dark adapted a-wave amplitudes from patients with PMM2-CDG [240, 216], likely indicative of the progressive photoreceptor dystrophy present in these patients. Thus, a-wave amplitudes were investigated in more detail across subgroups for the ISCEV standard flash strengths of 3.0 and 10.0 cd*s*m$^{-2}$, alongside a high intensity flash of 200.0 cd*s*m$^{-2}$, and compared to clinical normative data from GOSH. These results are displayed in Figure 2.9.

From this analysis of dark adapted a-wave amplitudes elicited in each subgroup, it became clear that patients with ON-pathway dysfunction mostly showed dark adapted a-wave amplitudes lower than the normative data median value for each flash strength. However, none of the subgroups showed mean dark adapted a-wave amplitudes which were significantly lower than those in healthy observers (One-way ANOVA and post hoc Tukey means comparison)[17].

[17]It is important to note that the a-wave is also thought to contain some post-receptoral contributions from rod and cone systems at the light intensity of 3.0 cd*s*m$^{-2}$ [243, 83], which can impact on its size and timing. Therefore models suggest to consider only the middle slope for measurements [244]. This was taken into account when a-wave amplitudes and times to peak were measured in this cohort.

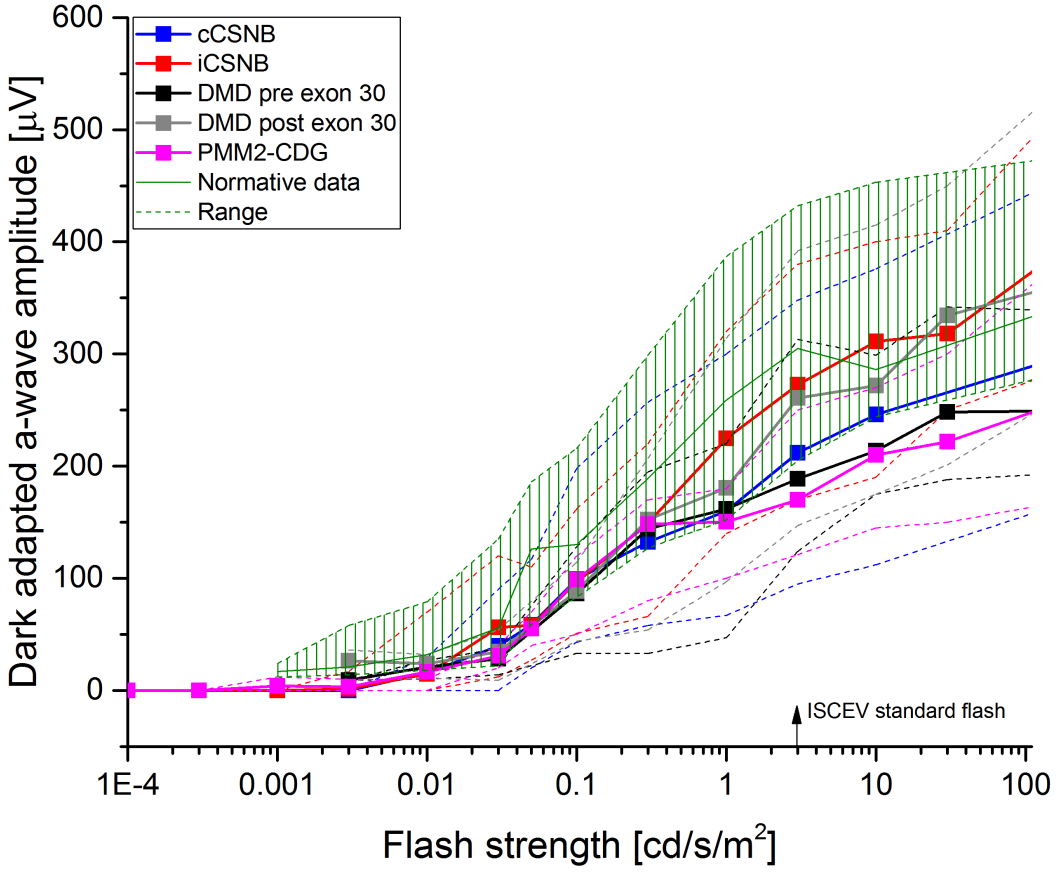


**Figure 2.8:** Average subgroup a-wave amplitudes elicited under dark adapted conditions are displayed over a range of flash strengths and compared to clinical normative data from GOSH (green striped area). All data are shown including range (dashed lines). Flash strengths are displayed on a logarithmic scale.

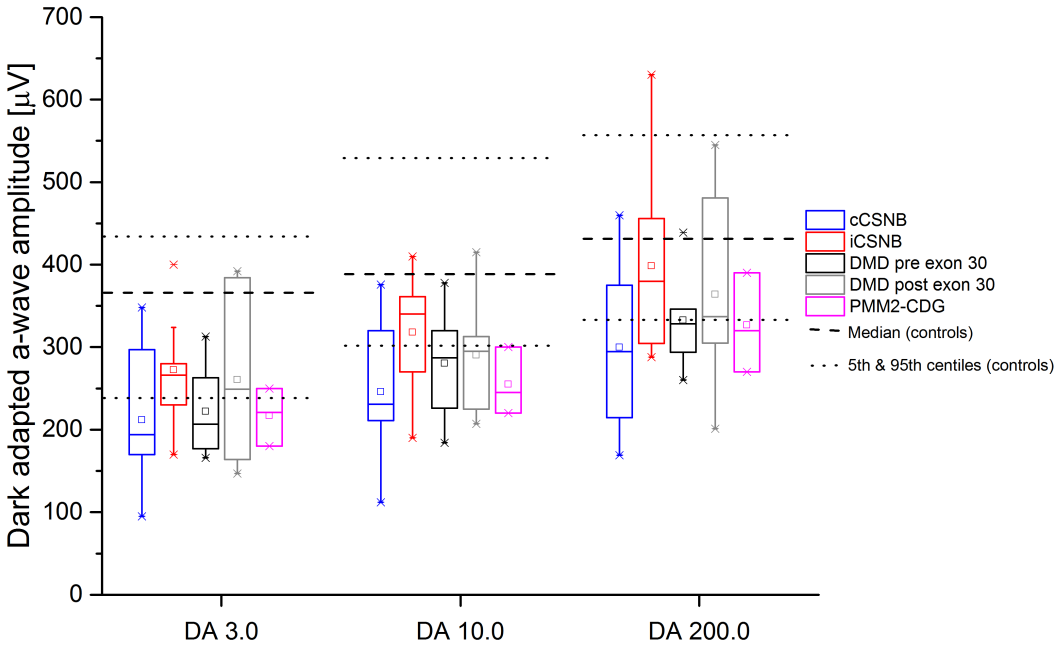


**Figure 2.9:** Subgroup a-wave amplitudes elicited under dark adapted conditions are displayed for the ISCEV standard flash strengths of 3.0 and 10.0, including a high intensity flash of 200.0 cd*s*m$^{-2}$ and compared to clinical normative data from GOSH (dashed line: median, dotted lines: 5th and 95th percentiles). Boxes give Max and Min (-), Mean (square), Median (line inside the boxes), 99% and 1% (x), as well as 75% and 25% (margins of the boxes) percentiles.

When regarding the dark adapted a-wave times to peak, patient responses generally followed the trajectory of the normative data range and times to peak were becoming shorter with increasing flash intensities (Figure 2.10). All of the subgroups fell within the normal range for the ISCEV standard flash of 3.0 cd*s*m$^{-2}$ and above.

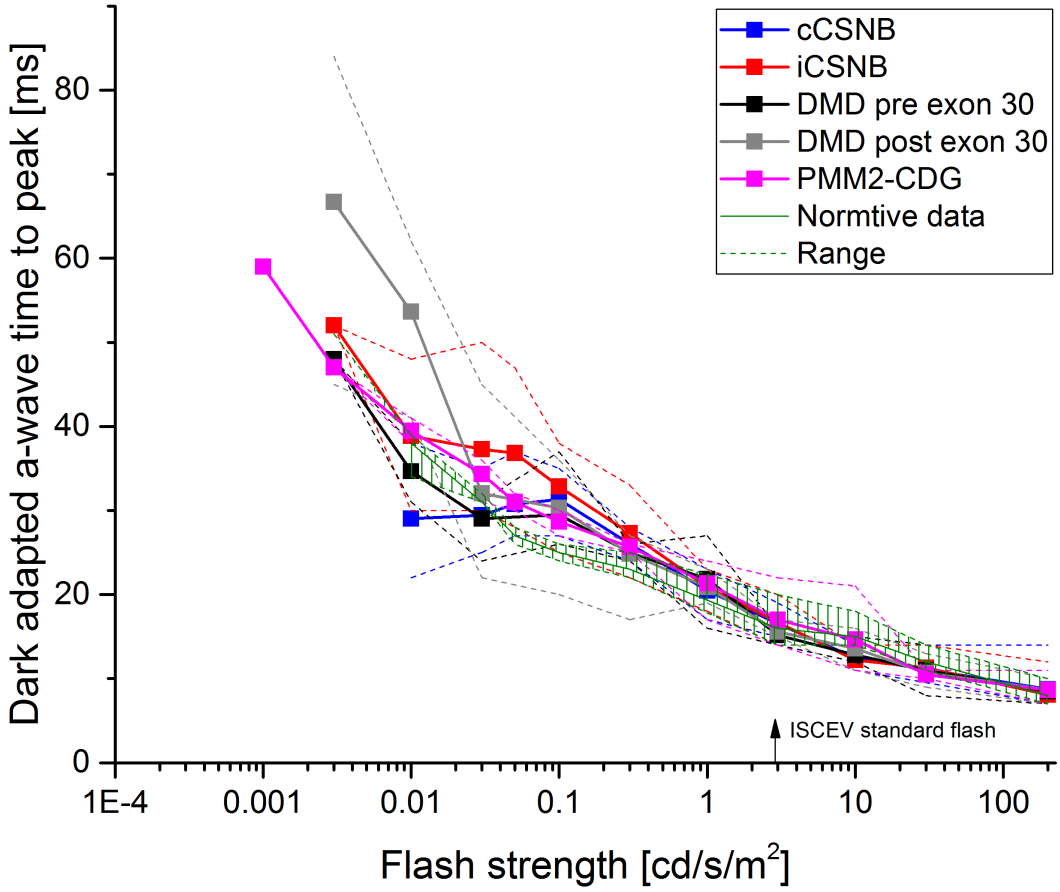


**Figure 2.10:** Average subgroup a-wave times to peak elicited under dark adapted conditions are displayed over a range of flash strengths and compared to clinical normative data from GOSH (green striped area). All data are shown including range (dashed lines). Flash strengths are displayed on a logarithmic scale.

The cardinal component in the diagnosis of ON-pathway dysfunction is the dark adapted b-wave amplitude, reflecting ON-pathway initiation at the level of the bipolar cells. While following a similar trajectory to the normative data, increasing in component size with flash strength, all subgroups fell below the normative range across the spectrum of flash strengths (Figure 2.11). Interestingly, there was a distinction in severity, or size of the b-wave, between subgroups. Patients with DMD pre exon 30 displayed overall highest dark-adapted b-waves, followed by patients with PMM2-CDG. While patients in the iCSNB and DMD post exon 30 subgroups showed smaller but approximately similar b-wave amplitudes across the range of flash strengths, patients with cCSNB generally exhibited the smallest amplitudes.

Apart from a dysfunctional ON-pathway affecting dark adapted b-wave amplitudes, axial length of the eyeball is thought to affect ERG amplitudes [245, 246]. As mentioned in Section 2.3.1, eight CSNB patients in this cohort showed myopic fundus changes. Chia and colleagues, as well as Westall and colleagues report slightly lower b-wave amplitudes in eyes with higher axial length and link this finding to a relative thinning of the retina. Hence, the small b-wave amplitudes observed in some patients in this cohort might also be, partly, caused by myopia and/or thin retinae present in some patients.

Further, differences in the minimum light strength necessary to elicit a b-wave were noted between groups. Boys with DMD, as well as patients with iCSNB showed detectable b-waves at flash strengths comparable to controls (DMD/iCSNB: from 0.0003 cd*s*$m^{-2}$ vs. controls: from 0.0001 cd*s*$m^{-2}$). In contrast, patients with cCSNB and PMM2-CDG showed a decreased sensitivity, requiring a ten-fold increase in flash strength to elicit a b-wave (cCSNB/PMM2-CDG: from 0.001 cd*s*$m^{-2}$).

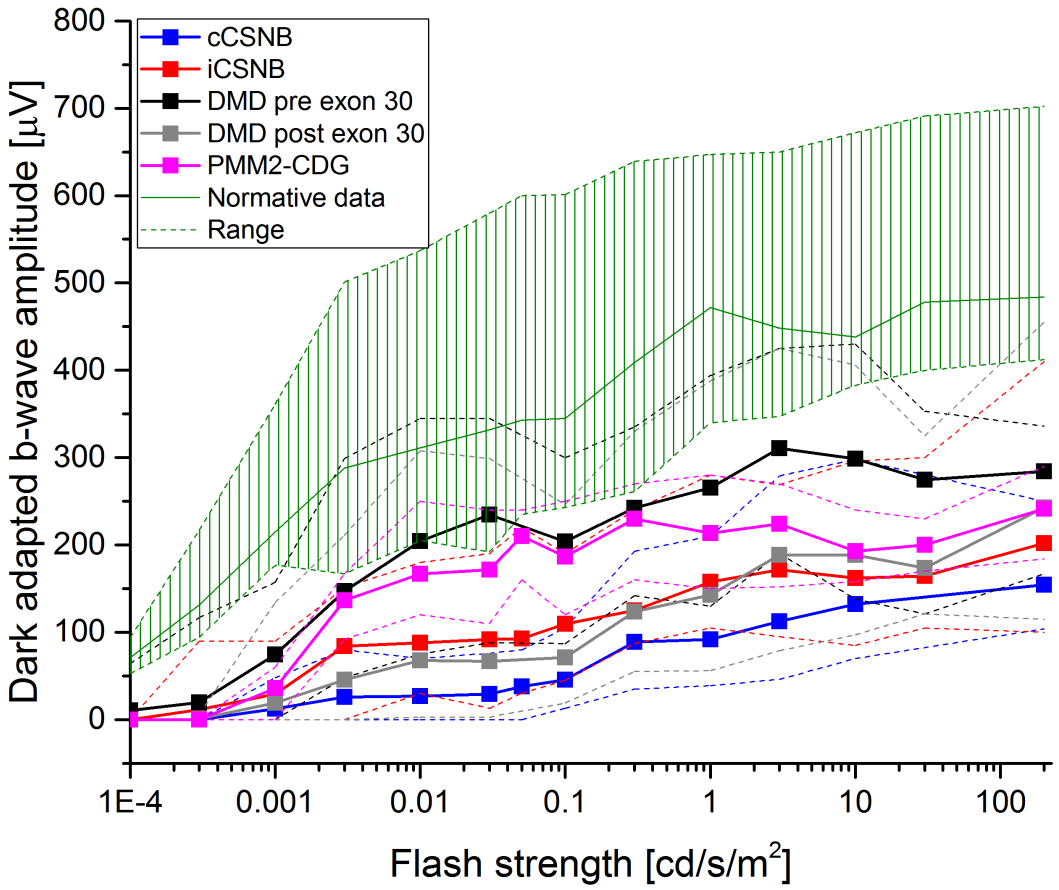


**Figure 2.11:** Average subgroup b-wave amplitudes elicited under dark adapted conditions are displayed over a range of flash strengths and compared to clinical normative data from GOSH (green striped area). All data are shown including range (dashed lines). Flash strengths are displayed on a logarithmic scale.

B-wave times to peak generally shortened with increasing flash strength and fell within the normative range for PMM2-CDG, iCSNB and DMD pre exon 30 subgroups, above a flash strength of 0.1 cd*s*$m^{-2}$ and until the highest strength of 200.0 cd*s*$m^{-2}$ (Figure 2.12). At this point, patients with iCSNB showed a shortened timing of the b-wave. Also, patients with DMD mutations post exon 30 and those with cCSNB showed generally shorter dark adapted b-wave times to peak falling below the normative data range for higher flash strengths over 10.0 cd*s*$m^{-2}$.

The observed slight shortening of b-wave times to peak in the subgroups might be due to the lack or relatively small size of the b-waves of patients[18]. This was especially prevalent in patients with cCSNB who showed the smallest b-wave amplitudes (Figure 2.11), alongside the shortest b-wave peak times to peak (Figure 2.12) across subgroups. Apart from the filter settings chosen having an effect on waveform shape and components, there are other explanations for an occurrence of a small and early b-wave in patients with ON-pathway dysfunction.

As mentioned above, the size of the b-wave can be influenced by axial length of the eye. However, in the case of ON-pathway dysfunction, the fact that a dark adapted b-wave is detectable to a certain extent is interesting, as it is thought to mainly reflect ON bipolar cell activity. The dark adapted a-wave is known to contain not only photoreceptor components but also post-receptoral contributions [243, 83]. The recovery of the visible negativity thought to reflect photoreceptor cell hyperpolarisation is usually overlaid by the positive b-wave and could be revealed by its absence [247, 248]. Hence, this a-wave recovery, which is thought to appear earlier with higher flash strengths [248], might mimic a small b-wave in combination with OPs, which are usually observed on the ascending limb of the b-wave [83]. Under dark adapted conditions, these are almost abolished in patients with cCSNB (see Section 2.3.2.2) but relatively preserved in the other patient subgroups. A combination of late a-wave component and OPs could thus represent the small positive going peak, following the a-wave trough observed in the patient cohort.

[18]The component time to peak was always measured from stimulus onset to the first peak after the a-wave trough.

This theory does not yet explain a shortened b-wave time to peak in patients with cCSNB, however, where the dark adapted OPs are nearly absent. Alternatively, the small positivity could represent the normally obscured d-wave, driven by OFF bipolar cell activity [249]. For short flash durations, this component is usually obscured by the b-wave and it is only distinguished when using long duration flashes separating the light onset and offset responses. With increasing flash intensity, the contribution of cone circuit activity to the ERG waveform increases and hence the question arises, whether a small positivity with a short time to peak, observed under bright flash stimulation (over 10.0 cd*s*$m^{-2}$), might reflect such a (cone driven) OFF component.

Furthermore, there is some evidence that the occurrence of such an early recovery of the positive-going component, even in patients with cCSNB, might stem from current flows in the outer nuclear layer [248].

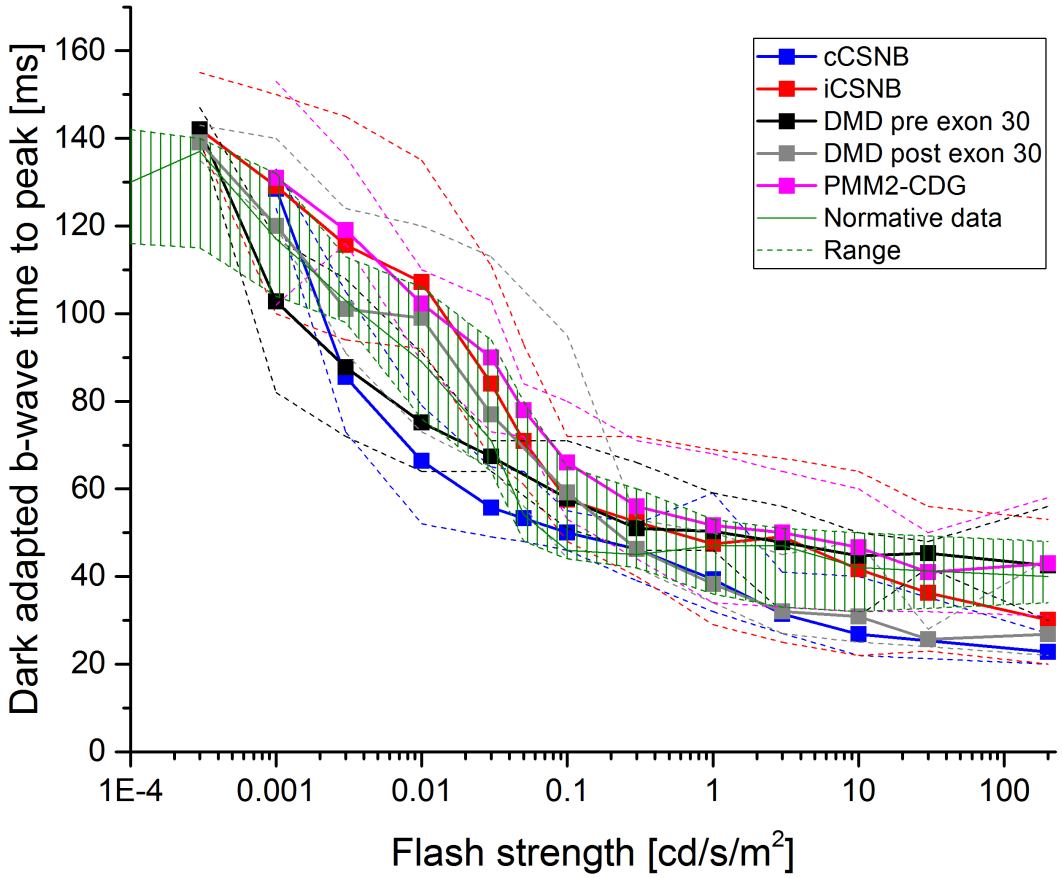


**Figure 2.12:** Average subgroup b-wave times to peak elicited under dark adapted conditions are displayed over a range of flash strengths and compared to clinical normative data from GOSH (green striped area). All data are shown including range (dashed lines). Flash strengths are displayed on a logarithmic scale.

Figures 2.13 and 2.14 display the a-wave amplitudes and times to peak for an ERG luminance response series recorded under light adapted conditions. Here, the a-wave mainly reflects cone photoreceptor hyperpolarisation, as well as post receptoral contributions. The amplitude of this component increased similarly with increasing flash intensities in patient subgroups (Figure 2.13). Patients with iCSNB showed the lowest amplitudes across the board, falling below the lower margin of the normative data range for flash strengths of 0.3 and 1.0 cd*s*$m^{-2}$. This can be explained by the fact that in iCSNB, signalling from photoreceptors to ON- and OFF-bipolar cells is impaired. OFF-bipolar cells contribute a large part to the light-adapted a-wave and therefore a signalling impairment is expected to affect the shape of this component [244]. The remaining data points for all subgroups fell within the normative data range.

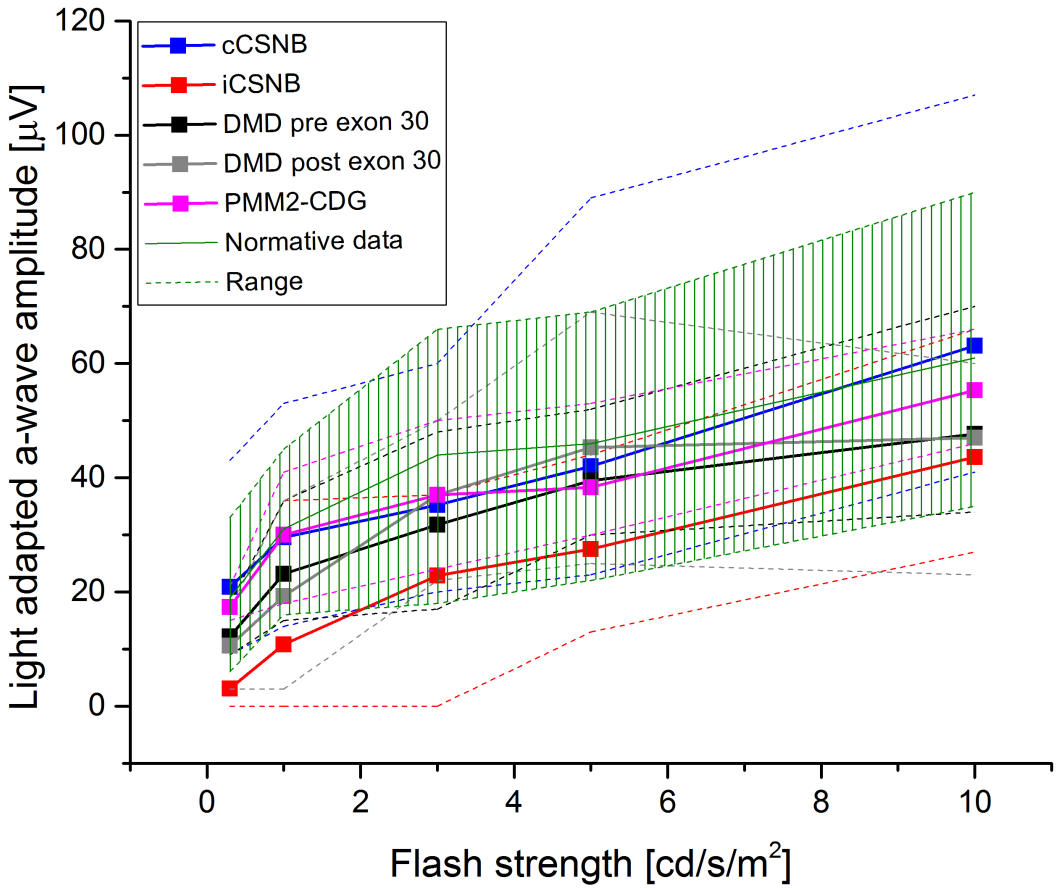


**Figure 2.13:** Average subgroup a-wave amplitudes elicited under light adapted conditions are displayed over a range of flash strengths and compared to clinical normative data from GOSH (green striped area). All data are shown including range (dashed lines). Flash strengths are displayed on a logarithmic scale.

The analysis of light adapted a-wave times to peak produced a slightly different picture (Figure 2.14). While patient values of the DMD and PMM2-CDG subgroups were predominantly normal, subtypes of CSNB produced prolonged a-wave timing compared to healthy observers. This was true for patients with iCSNB for flash strengths above 5.0 cd*s*m$^{-2}$ and for patients with cCSNB even earlier, for flash strengths above 0.3 cd*s*m$^{-2}$. The delay in a-wave peak timing observed here is likely due to the broad a-wave shape present in patients with cCSNB under light adapted conditions [250]. In cases where a-waves were broad with no obvious minimum, times to peak were always measured mid-trough and therefore a broad a-wave could influence the value measured.

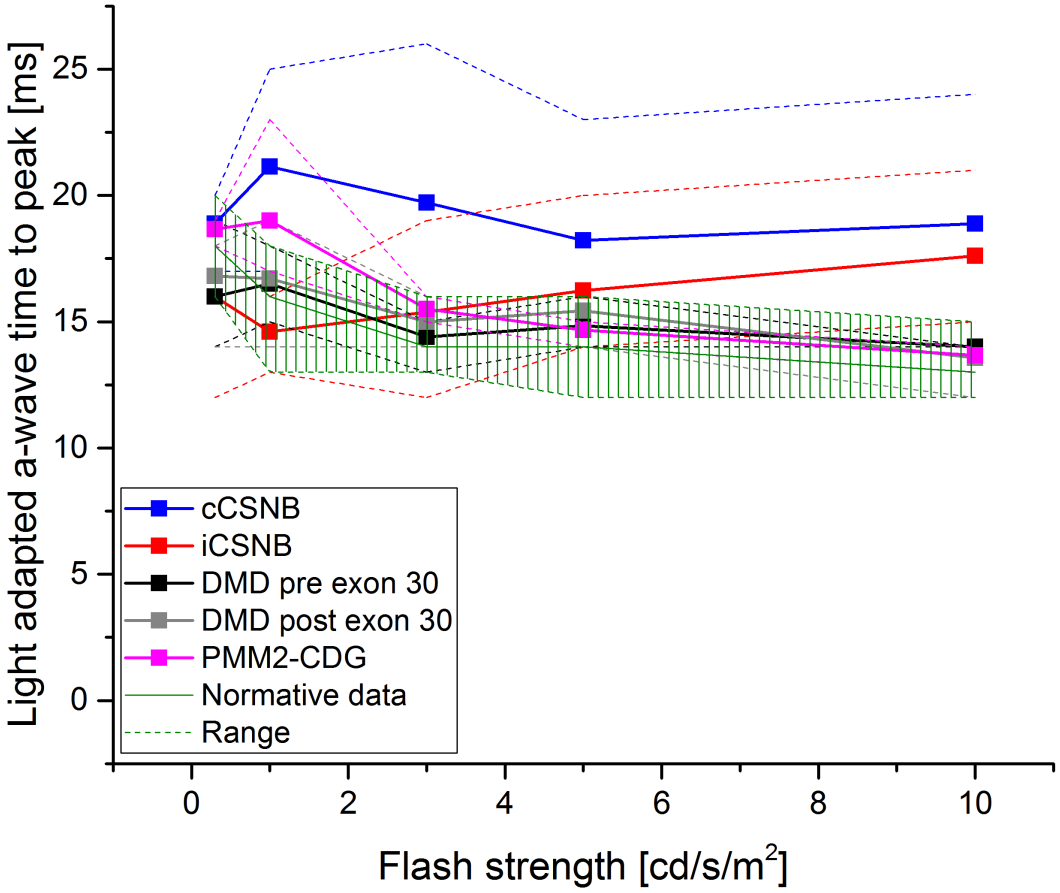


**Figure 2.14:** Average subgroup a-wave times to peak elicited under light adapted conditions are displayed over a range of flash strengths and compared to clinical normative data from GOSH (green striped area). All data are shown including range (dashed lines). Flash strengths are displayed on a logarithmic scale.

The analysis of light adapted b-wave amplitudes highlighted the difference in the localisation of the signalling defect between iCSNB and the other subgroups. While the initial disruption in iCSNB is pre-synaptic, located within the calcium channels of the photoreceptor terminals, the defects encountered in cCSNB, PMM2-CDG, as well as DMD are thought to occur post-synaptically. Hence, in iCSNB, signal transmission onto ON and OFF bipolar cells, which both contribute to the light adapted b-wave, is impaired [251][19]. Such an affected cone ERG can be observed in Figure 2.15, where the light-adapted b-wave amplitudes of patients with iCSNB remained at a very low level across all flash strengths, never reaching normal levels. In stark contrast, light adapted b-wave amplitudes for all other subgroups followed the trajectory of the normative data range, albeit at its lower margin, indicating a preserved cone OFF-pathway.

Light adapted b-wave time to peak was unremarkable in DMD and PMM2-CDG patient subgroups (Figure 2.16). Patients with cCSNB, however, showed a slightly elevated b-wave timing until flash strengths of 3.0 cd*s*$m^{-2}$ were reached and remained at the upper margin of the normative data range for higher flash luminances. While values for the iCSNB subgroup remained ”normal” until 5.0 cd*s*$m^{-2}$, an increase in peak timing was observed for the highest flash strength of 10.0 cd*s*$m^{-2}$, where light adapted b-waves are expected to be smallest.

These results can be explained by regarding the unusual luminance-response function encountered when recording b-waves under light adapted conditions. In healthy observers, light adapted b-wave amplitudes are known to experience a ”photopic hill”, where the light adapted b-wave amplitude increases with progressively brighter stimulation until a maximum is reached after which they decrease to finally reach a plateau. This phenomenon was first described by Wali and colleagues [252], and was absent in all patient subgroups with ON-pathway dysfunction. Instead, only a plateau of b-wave amplitudes at higher flash intensities was observed.

This lack of a photopic hill in my patient cohort can be explained by tak-

[19]ON bipolar cells are thought to contribute a positive component to the light adapted b-wave, while OFF bipolar cells contribute a negative component [251], as they hyperpolarise in response to a light stimulus.

ing into account the nature of overlapping post-receptoral ON-and OFF-pathway components contributing to the light adapted b-wave. Hamilton and colleagues developed a mathematical model suggesting that the contributions of ON-and OFF-pathways to this component can be represented by a logistic and a Gaussian curve, respectively [253]. Following this model, in case of an impaired ON-pathway, the contribution of the logistic function should be small (or even abolished), resulting in a b-wave which is shaped mainly by the OFF-pathway driven Gaussian function. Recently, Garon and colleagues confirmed this by showing that patients with cCSNB display a greater contribution of the Gaussian function when compared to healthy observers, indicating that the ON-pathway contribution to the light adapted b-wave is abnormal in these patients [254]. A smaller and broader (or absent) ON-pathway driven peak to a light onset, combined with a later OFF-pathway driven peak to light offset would thus result in a small and late light-adapted b-wave peak, as observed in my patient cohort. In the case of iCSNB, where both pathways are affected, a more severe reduction of the light adapted b-wave was observed.

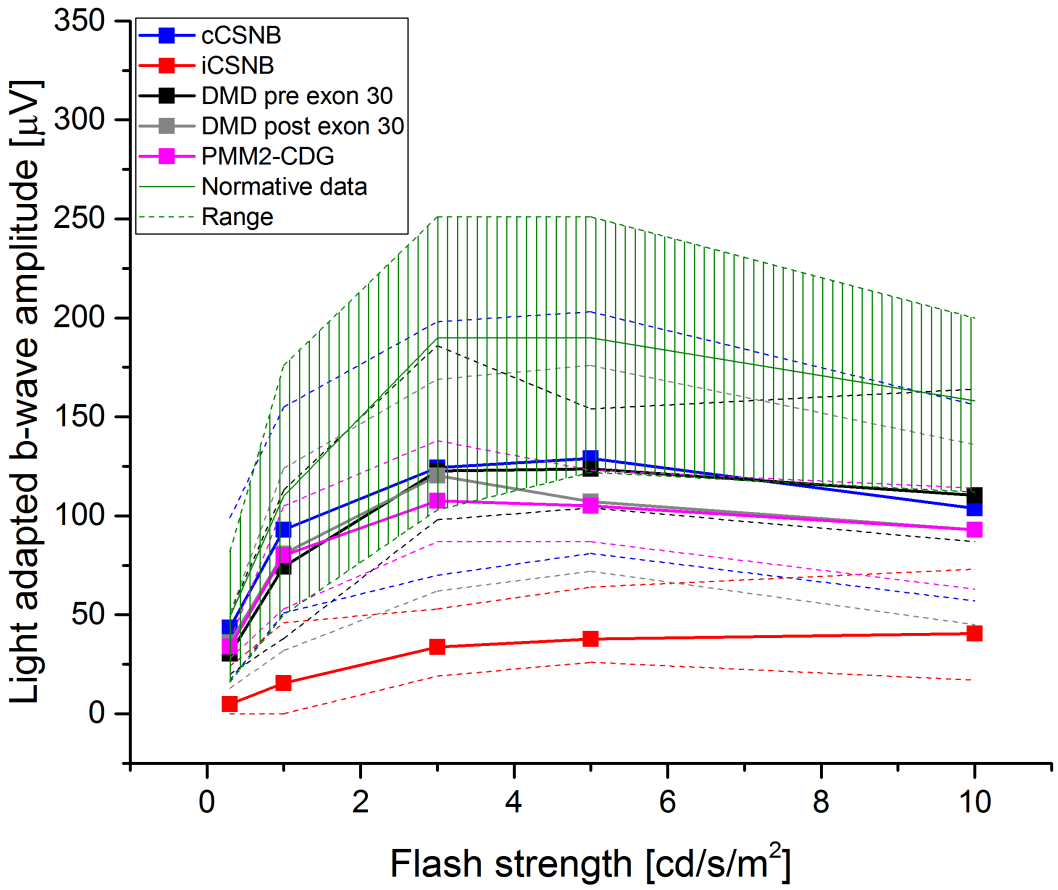


**Figure 2.15:** Average subgroup b-wave amplitudes elicited under light adapted conditions are displayed over a range of flash strengths and compared to clinical normative data from GOSH (green striped area). All data are shown including range (dashed lines). Flash strengths are displayed on a logarithmic scale.

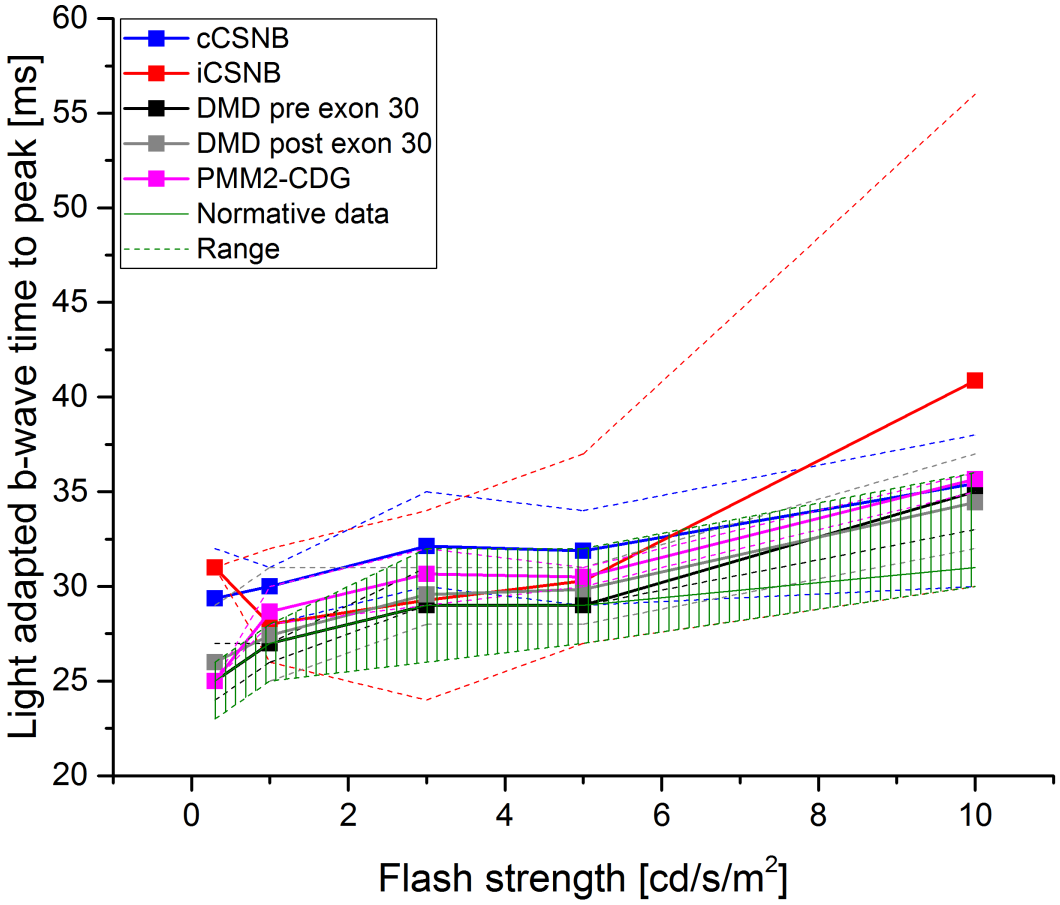


**Figure 2.16:** Average subgroup b-wave times to peak elicited under light adapted conditions are displayed over a range of flash strengths and compared to clinical normative data from GOSH (green striped area). All data are shown including range (dashed lines). Flash strengths are displayed on a logarithmic scale.

#### 2.3.2.2 Oscillatory Potentials

Oscillatory potentials[20] reflect spiking cell activity of the retina and are thought to be mainly driven by the amacrine cell circuits with potential inner retinal contributions from bipolar and/or ganglion cells. Under dark adapted conditions, contributions from the post-receptoral rod amacrine network are highlighted (but a cone driven contribution cannot be completely excluded) [255]. Patients with PMM2-CDG, DMD and iCSNB generally showed a presence of all four OPs, with patients within the DMD pre exon 30 subgroup exhibiting the highest amplitudes in OP2 and OP3. In contrast, individuals with cCSNB displayed a severe reduction or absence of three OPs under dark adapted conditions.

Those patients also showed slightly prolonged timing for OP2 and OP3, when compared to the results from the remaining subgroups, which revealed approximately matching timings. These data are presented in Figure 2.18, while the times to peak of the individual OPs are shown in Figure 2.19. An overview over representative dark adapted OPs is given in Figure 2.17.

[20]The filter settings of the Espion Visual Electrophysiology System (Diagnosys, LLC) were set at a band-pass ranging from 100 Hz to 300Hz, in order to obtain high-frequency oscillatory potentials.

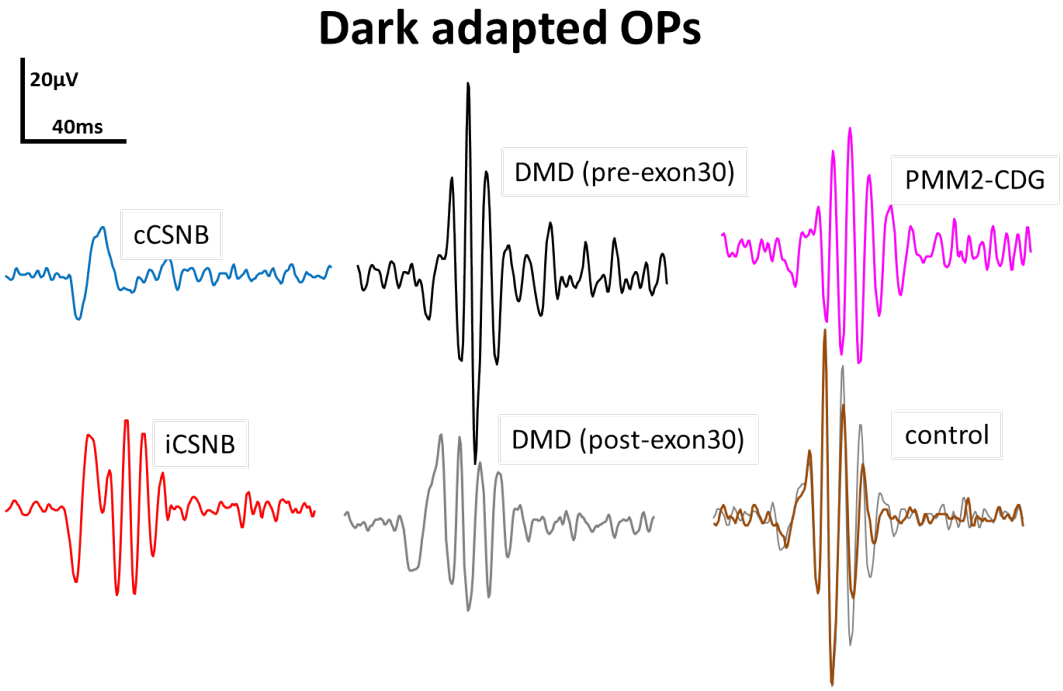


**Figure 2.17:** Representative OPs elicited under dark adapted conditions for each patient subgroup. A trace from a healthy observer is displayed for comparison.

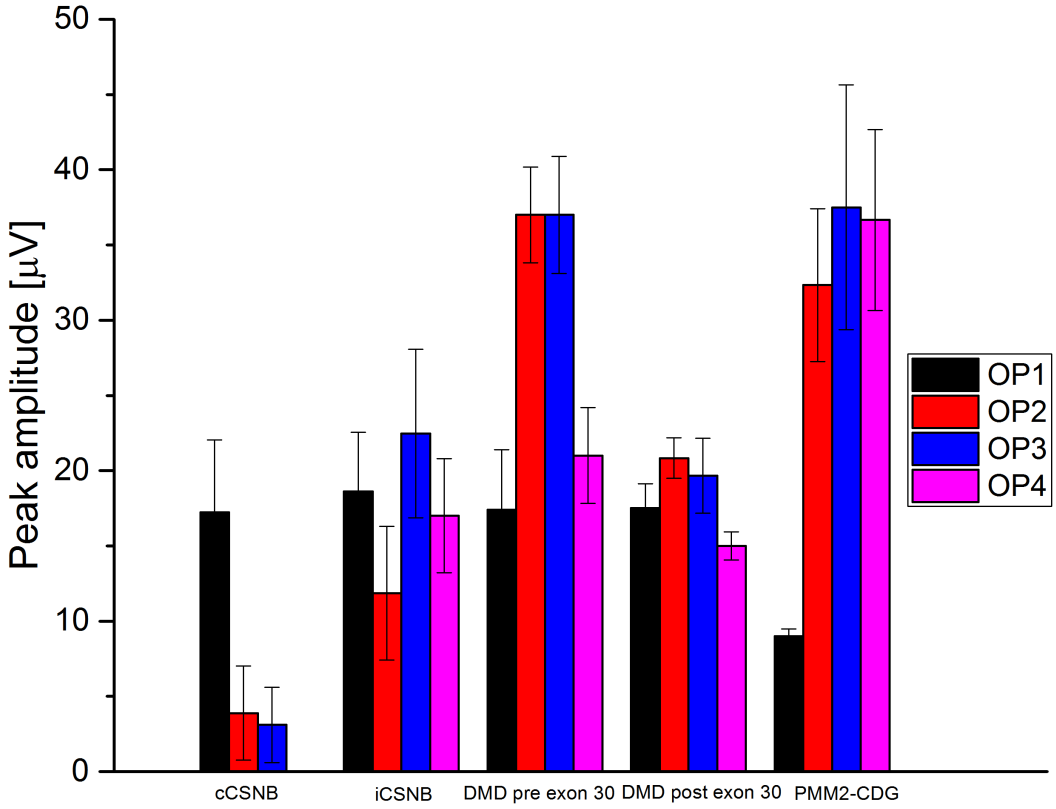


**Figure 2.18:** Displayed are group mean peak amplitudes for all four OPs obtained under dark adapted conditions across patient subgroups. Standard errors are indicated for each bar.

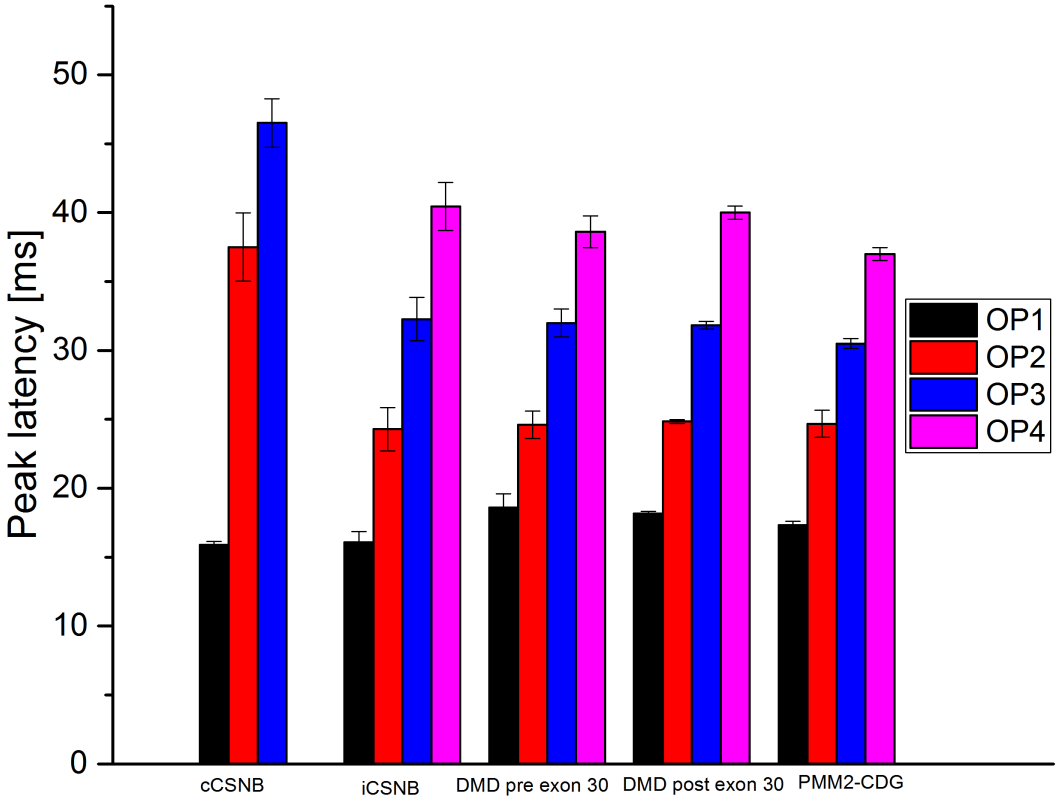


**Figure 2.19:** Displayed are group mean peak latencies for all four OPs obtained under dark adapted conditions across patient subgroups. Standard errors are indicated for each bar.

Under light adapted conditions, where cone circuits are expected to be predominantly active [255], patients with cCSNB showed all four OPs, however, OP3 and OP4 were relatively small (Figure 2.21). Patients with PMM2-CDG, as well as patients from the DMD post exon 30 subgroup, showed waveforms akin to those observed in cCSNB. Patients with DMD and mutations pre exon 30 revealed intermediate amplitudes of all four OPs. In stark contrast to dark adapted conditions, patients with iCSNB revealed a striking decrease in amplitude of all four OPs, almost down to noise levels. When analysing OP times to peak, a similar picture as under dark adapted conditions emerged (Figure 2.22). Patients with cCSNB showed slightly prolonged times to peak when compared to the remaining subgroups. These, again, showed almost identical timings for all four OPs. An overview over light adapted OP waveform shape across patient subgroups is shown in Figure 2.20.

In conclusion, altered inner retinal signalling, was evident in the OP analysis of patients with ON-pathway dysfunction. Especially striking was the almost opposite behaviour of OPs from patients with cCSNB and iCSNB under different light conditions. Whereas under dark adapted conditions, OPs were almost completely abolished in patients with cCSNB and normal in patients with iCSNB, this picture was reversed under light adapted conditions where OPs were abolished in patients with iCSNB. In contrast, OPs were relatively preserved in patients with DMD and mutations pre exon 30 and patients with PMM2-CDG. Patients with DMD and mutations post exon 30 showed slight abnormalities in the amplitudes of their light adapted OPs. The significance of these OP results is discussed in the final chapter of this thesis (Chapter 7, Section 7.2.2.2).

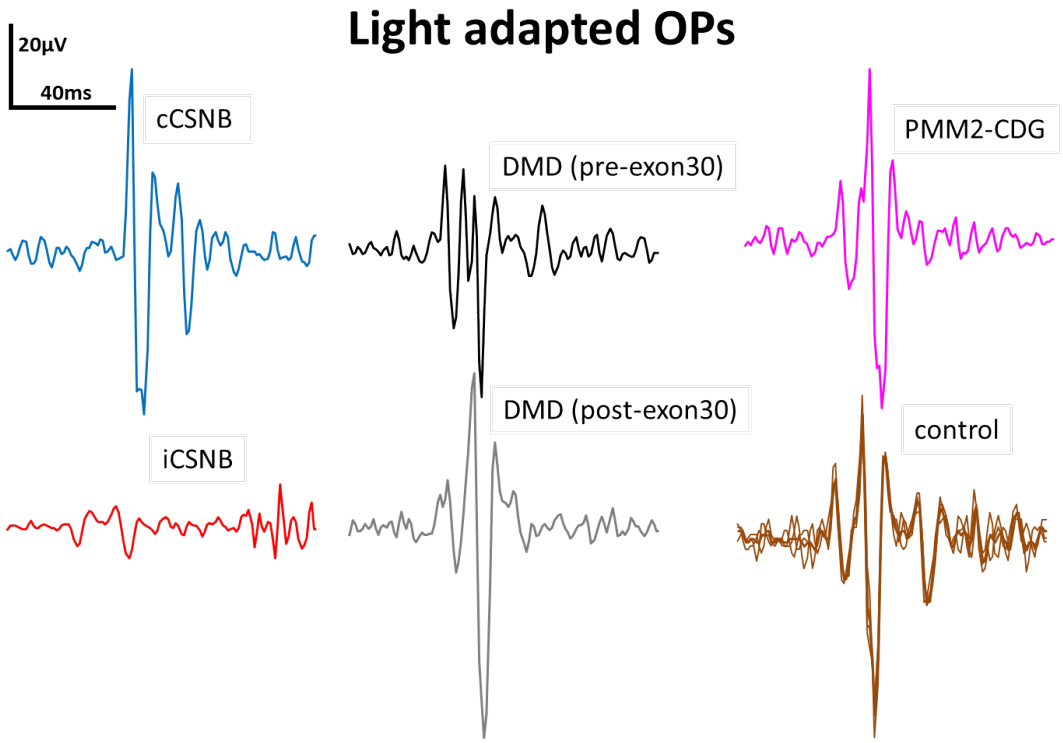


**Figure 2.20:** Representative OPs elicited under light adapted conditions for each patient subgroup. A trace from a healthy observer is displayed for comparison.

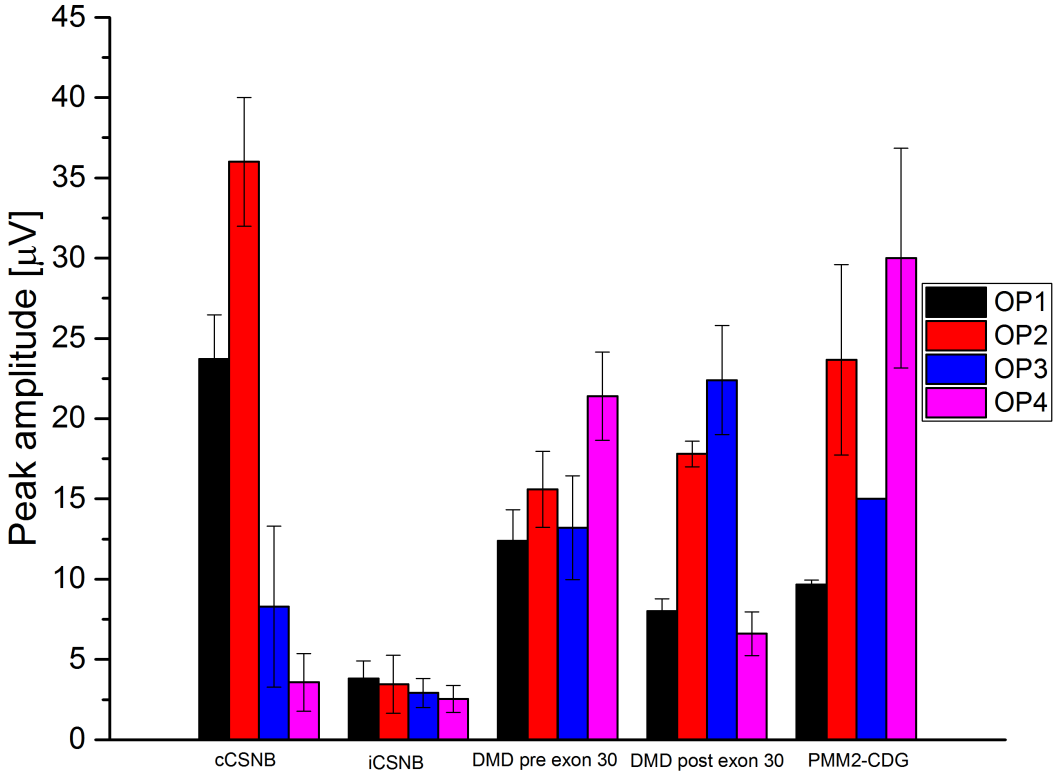


**Figure 2.21:** Displayed are group mean peak amplitudes for all four OPs obtained under light adapted conditions across patient subgroups. Standard errors are indicated for each bar.

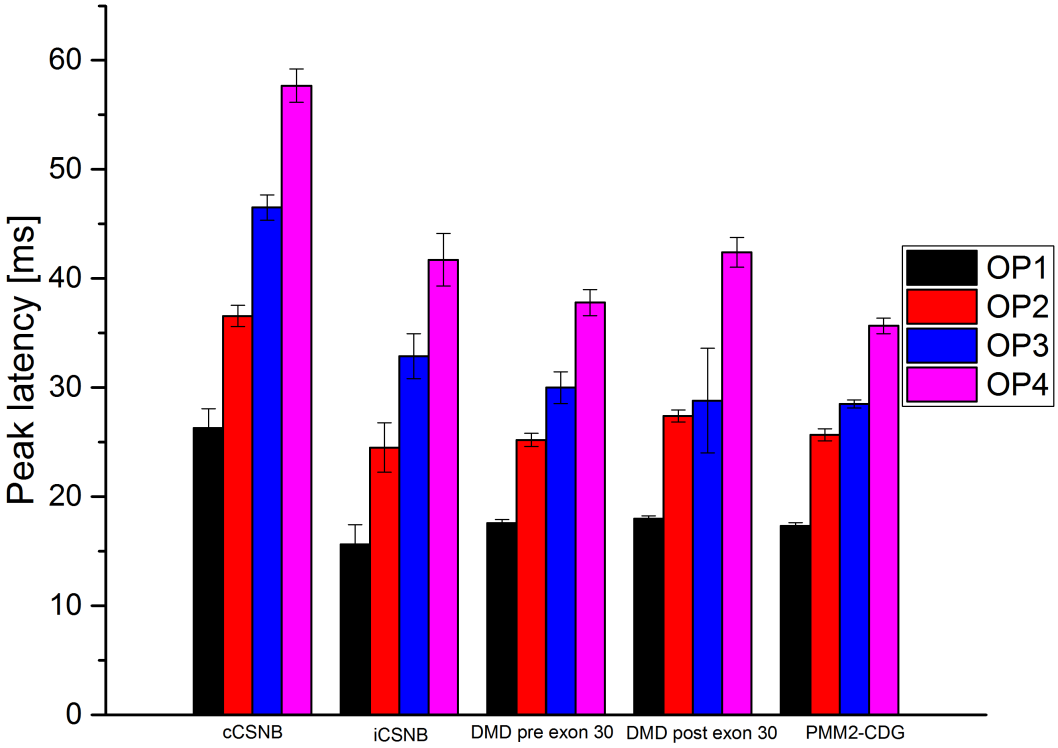


**Figure 2.22:** Displayed are group mean peak latencies for all four OPs obtained under light adapted conditions across patient subgroups. Standard errors are indicated for each bar.

#### 2.3.2.3 Diagnosing ON-pathway dysfunction by means of the ERG

Electrodiagnostic testing using the ERG is an invaluable tool in order to clinically diagnose a disruption of the ON-pathway at the retinal level. The patient subgroups investigated in this study all showed slightly different ERG waveforms to light stimulation, highlighting the diverse impacts such a dysfunction can have on different signalling pathways. While any one ERG stimulation on its own is far from being pathognomonic in patients with ON-pathway dysfunction, compiling responses to a whole set of stimuli can reveal an ERG signature, which is fairly specific to the individual conditions. In the following the patient subgroups are compared according to their ERG signature.

- **cCSNB:**
  - DA ERG
    - normal photoreceptor components (a-wave)
    - lowest b-wave amplitudes among all patient subgroups with values never exceeding 300$\mu$V even at highest flash strengths
    - b-wave was only measurable from stimulus luminances of 0.001 cd*s*m$^{-2}$ and above, requiring a ten times stronger light stimulus to elicit a b-wave compared to healthy observers
    - b-wave times to peak were shorter than normal, probably owing to small b-wave amplitudes. However, these small peaks could also be showing the recovery of the a-wave or a light offset component.
    - DA OPs almost completely missing, implying further inner retinal abnormalities
  - LA ERG
    - broad photoreceptor trough with normal amplitude (a-wave)
    - b-wave times to peak just around the upper margin of normal across all flash strengths and b-waves abnormally low at the highest flash strength (LA 10.0 cd*s*m$^{-2}$)
    - LA OPs displayed small amplitudes for OP3 and OP4, implying further inner retinal abnormalities

- **iCSNB:**
  - DA ERG
    - normal photoreceptor component size and timing
    - ON bipolar cell signalling disruption was evident across all flash strengths (low b-wave amplitude with normal timing)
    - DA OPs of intermediate amplitude
  - LA ERG
    - a-waves were prolonged and amplitudes low, but within normal limits
    - b-wave times to peak were prolonged and b-wave amplitudes severely reduced and never reached a size above 75$\mu$V across flash strengths
    - almost complete abolishing of all light adapted OPs, implying further inner retinal abnormalities
- **DMD pre exon 30:**
  - DA ERG
    - normal photoreceptor component timing and slightly subnormal size which was not significantly lower than normal
    - subnormal b-wave amplitudes (with normal timing) but overall highest DA b-wave amplitudes among all subgroups
    - normal OPs
  - LA ERG
    - normal a-wave timing and amplitudes
    - b-wave amplitudes at lower margin of normal but with normal timing
    - OPs of intermediate size
- **DMD post exon 30:**
  - DA ERG
    - normal photoreceptor components (a-wave)

    - subnormal b-wave amplitudes across all flash strengths with slightly shortened b-wave times to peak for mixed rod-cone stimulation
    - DA OPs of intermediate size
  - LA ERG
    - normal photoreceptor components (a-wave)
    - subnormal b-wave amplitudes at higher flash luminances with normal b-wave timing
    - small OP1 and OP4 peaks, implying further inner retinal abnormalities

- **PMM2-CDG:**
  - DA ERG
    - normal a-wave timing but slightly decreased amplitudes from flash strengths of 3.0 cd*s*$m^{-2}$ onward. These were not significantly lower than normal but could be indicative of the progressive photoreceptor dysfunction these patients are known to experience.
    - slightly prolonged b-wave timing with subnormal b-wave amplitudes across all flash strengths
    - decreased sensitivity of the dark adapted rod driven circuits, similar to patients with cCSNB
    - DA OPs similar to those of patients with DMD mutations post exon 30
  - LA ERG
    - broad a-wave with normal size (similar to patients with cCSNB), sometimes showing a double a-wave trough
    - normal b-wave timing but subnormal b-wave amplitudes for high flash strengths of 5.0 cd*s*$m^{-2}$ and above
    - LA OPs akin to those observed in DMD boys with mutations pre exon 30

#### 2.3.2.4 Pattern Reversal ERG - PERG

Additional information on the impact of ON-pathway dysfunction on the visual pathways subsequent to the bipolar cells can be obtained using the clinical pattern reversal ERG (PERG). The PERG allows an insight into retinal cell function and can be recorded simultaneously to the pattern VEP, applying the same stimulus. In order to probe whether an ON-pathway dysfunction leads to altered ganglion cell firing in human subjects, PERGs of patients from the patient subgroups were reviewed and analysed. Due to the difficulties one can encounter when recording such responses, especially from young children and patients with nystagmus, only a total number of 30/109 individuals from the patient cohort had ISCEV reversal PERGs recorded simultaneous to pattern VEP recordings. The cohort breakdown into subgroups was as follows:

- 9x cCSNB
- 7x iCSNB
- 6x DMD pre exon 30
- 6x DMD post exon 30
- 2x PMM2-CDG

Tables 2.5 and 2.6 give an overview over the individual P50 and N95 component amplitudes and times to peak across subgroups.

| Patient ID | Subgroup | P50 [$\mu$V] | N95 [$\mu$V] |
|---|---|---|---|
| Pat23 | cCSNB | 6 | 9 |
| Pat26 | cCSNB | 2.5 | 3 |
| Pat116 | cCSNB | 1.5 | 2 |
| Pat101 | cCSNB | 7 | 5 |
| Pat18 | cCSNB | nm | nm |
| Pat16 | cCSNB | nm | nm |
| Pat27 | cCSNB | nm | nm |
| Pat117 | cCSNB | nm | nm |
| Pat3 | cCSNB | 5 | 7 |
| Pat32 | iCSNB | 3 | 6 |
| Pat31 | iCSNB | 2.5 | 4.5 |
| Pat39 | iCSNB | 8 | 18 |
| Pat15 | iCSNB | 3 | 3 |
| Pat4 | iCSNB | 4 | 9 |
| Pat107 | iCSNB | 4 | 7 |
| Pat109 | iCSNB | 4 | 7 |
| Pat119 | DMD pre exon 30 | 4.3 | 11 |
| Pat56 | DMD pre exon 30 | 20 | 12 |
| Pat57 | DMD pre exon 30 | 10 | 11 |
| Pat58 | DMD pre exon 30 | 10 | 13 |
| Pat59 | DMD pre exon 30 | 6 | 10 |
| Pat60 | DMD pre exon 30 | 8 | 9 |
| Pat61 | DMD post exon 30 | 15 | 18 |
| Pat62 | DMD post exon 30 | 12 | 14 |
| Pat63 | DMD post exon 30 | 11 | 16 |
| Pat64 | DMD post exon 30 | 8 | 15 |
| Pat65 | DMD post exon 30 | 4 | 8 |
| Pat66 | DMD post exon 30 | 8 | 13 |
| Pat74 | PMM2-CDG | 6 | 9 |
| Pat77 | PMM2-CDG | 6 | 7 |
| GOSH | normative data range | 4-18 | 10-25 |

**Table 2.5:** Overview table of PERG component amplitude to a pattern reversing checkerboard stimulus with 50' check size in a 30° stimulus field. Measured PERG waveforms were averaged responses over 2x200 sweeps, ensuring reliability and repeatability of the data. Rows marked as ”nm” represent components which were not measurable (at noise level or flat). The clinical normative data range is taken from GOSH.

| Patient ID | Subgroup | P50 [ms] | N95 [ms] |
|---|---|---|---|
| Pat23 | cCSNB | 45 | 90 |
| Pat26 | cCSNB | 58 | 113 |
| Pat116 | cCSNB | 65 | 124 |
| Pat101 | cCSNB | 50 | 85 |
| Pat18 | cCSNB | nm | nm |
| Pat16 | cCSNB | nm | nm |
| Pat27 | cCSNB | nm | nm |
| Pat117 | cCSNB | nm | nm |
| Pat3 | cCSNB | 53 | 97 |
| Pat32 | iCSNB | 53 | 97 |
| Pat31 | iCSNB | 61 | 100 |
| Pat39 | iCSNB | 48 | 108 |
| Pat15 | iCSNB | 47 | 88 |
| Pat4 | iCSNB | 54 | 110 |
| Pat107 | iCSNB | 51 | 96 |
| Pat109 | iCSNB | 59 | 111 |
| Pat119 | DMD pre exon 30 | 52 | 96 |
| Pat56 | DMD pre exon 30 | 50 | 93 |
| Pat57 | DMD pre exon 30 | 46 | 99 |
| Pat58 | DMD pre exon 30 | 49 | 107 |
| Pat59 | DMD pre exon 30 | 43 | 97 |
| Pat60 | DMD pre exon 30 | 49 | 95 |
| Pat61 | DMD post exon 30 | 52 | 96 |
| Pat62 | DMD post exon 30 | 53 | 87 |
| Pat63 | DMD post exon 30 | 47 | 99 |
| Pat64 | DMD post exon 30 | 44 | 96 |
| Pat65 | DMD post exon 30 | 49 | 91 |
| Pat66 | DMD post exon 30 | 50 | 96 |
| Pat74 | PMM2-CDG | 47 | 108 |
| Pat77 | PMM2-CDG | 47 | 106 |
| GOSH | normative data range | 43-52 | 87-111 |

**Table 2.6:** Overview table of PERG component time to peak to a pattern reversing checkerboard stimulus with 50' check size in a 30° stimulus field. Measured PERG waveforms were averaged responses over 2x200 sweeps, ensuring reliability and repeatability of the data. Rows marked as ”nm” represent components which were not measurable (at noise level or flat). The clincial normative data range is taken from GOSH.

PERGs were reviewed from subjects with ON-pathway dysfunction, except for four patients with cCSNB whose responses were at noise level and therefore not measurable. Only one of these had nystagmus (Pat117). Nonetheless, it was possible to obtain reliable waveforms from several patients who had nystagmus, excluding this as an explanation for abnormal PERG waveforms or absent responses. Thus, a not measurable response could suggest an abnormality at the level of the macular ganglion cells in these patients.

While there was no significant difference observed when comparing the times to peak across conditions and to the normative data range given by GOSH (One-way ANOVA and post-hoc Tukey means comparison), patients with cCSNB showed a trend of later P50 and N95 peak time (Figure 2.23). Further, N95 was slightly (but not-significantly) delayed in patients with iCSNB. When regarding individual patient results, a P50 delay was observed for two patients with cCSNB, three patients with iCSNB and one patient within the DMD post exon 30 subgroup. N95 was delayed for two cCSNB patients, as well as one patient with iCSNB. Such delays could suggest a delay of signalling through macular amacrine cells and/or ganglion cells [90, 93, 94].

In size, the P50 component was not significantly different from the GOSH clinical normative data range, however, the amplitude of this component differed greatly across the patient subgroups and statistical differences were observed (Figure 2.24). P50 was smallest in the cCSNB and iCSNB subgroups and biggest in boys with DMD, while patients affected by PMM2-CDG exhibited intermediate amplitudes. However, only cCSNB and iCSNB subgroups showed significantly smaller P50 components compared to boys with DMD and mutations post exon 30 (One-way ANOVA and post-hoc Tukey means comparison: cCSNB: $p=0.02$; iCSNB: $p=0.01$). Two patients with cCSNB, as well as two with iCSNB showed a P50 amplitude lower than the GOSH normative data range. Additionally, several patients showed P50 amplitudes just at the lower margin of the GOSH clinical normative data range (iCSNB n=3; DMD pre exon 30 n=1; DMD post exon n=1).

A similar picture emerged when looking at the ganglion cell evoked N95 com-

ponent across subgroups. For this component, all patients with cCSNB and PMM2-CDG, all but one with iCSNB, as well as one from each DMD subgroup fell below the GOSH clinical normative range. The smallest amplitudes were found in the cCSNB and iCSNB subgroups. The largest N95 negativity was obtained recording from boys with DMD and components of intermediate size from PMM2-CDG patients. These differences were statistically significant between patients with DMD and post exon 30 mutations and patients from all other subgroups except other DMD boys (cCSNB: $p<0.0001$, iCSNB: $p=0.008$, PMM2-CDG: $p=0.05$ ). Further, significantly smaller N95 amplitudes were observed in patients with cCSNB, when compared to boys with DMD pre exon 30 mutations ($p=0.001$).

In addition, it is useful to regard amplitudes in electrophysiological recordings as relative (not absolute), due to possible inter-subject differences in amplitudes. Hence, the N95:P50 ratio in patients was of interest. An abnormally low ratio (under 1.25 according to Holder [90]) could be suggest retinal ganglion cell or optic nerve dysfunction. Figure 2.25 shows the ratios obtained across patient subgroups. While patients with cCSNB generally showed the lowest N95:P50 ratios, no subgroup showed an abnormally low average ratio when compared to normative data [90]. However, several patients across the patient cohort showed individually abnormally low ratios. Of these, two (out of five) had cCSNB, one (out of seven) had iCSNB, three (out of six) were from either DMD subgroup and one patient (out of 2) had PMM2-CDG.

In summary, these findings indicate a differential effect of ON-pathway dysfunction on retinal circuitry in the different subgroups. Retinal signalling in patients with cCSNB and iCSNB seemed to be affected more severely than in boys with DMD and patients with PMM2-CDG. However, abnormal N95:P50 size ratios were observed for individuals across all patient subgroups, indicating ganglion cell signalling irregularities[21]. These abnormalities could be explained by altered or asymmetrical retinal ganglion cell firing caused by an ON system signalling dis-

[21]It is noteworthy that ISCEV does not provide normative ranges for such ratios, nor do they provide normative N95 amplitude ranges due to high amplitude and timing variability in this component[256].

turbance at the level of the photoreceptor / ON bipolar cell synapse. Due to the relatively small number of patients with a recorded clinical PERG[22], in order to investigate this possibility further, the analysis of retinal signal arrival at the striate cortex was of interest and a signalling abnormality at the cortical level would lend further support to my hypothesis. Cortical visual signalling and the integrity of the optic pathways are assessed clinically via the pVEP.

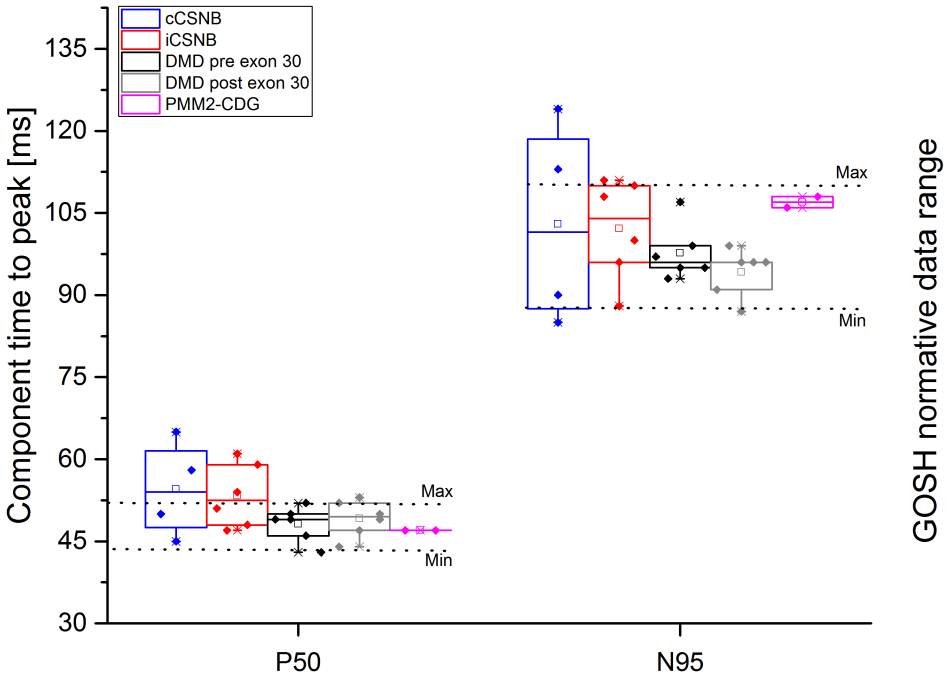


**Figure 2.23:** Overview of the times to peak of the conventional PERG main components. Asterisks show statistically significant differences between the values and the normative data ranges (One-way ANOVA and post-hoc Tukey means comparison). Measured PERG waveforms were averaged responses over 2x200 sweeps, ensuring reliability and repeatability of the data. Diamond symbols represent individual subjects. Boxes give Max and Min (-), Mean (square), Median (line inside the boxes), 99% and 1% (x), as well as 75% and 25% (margins of the boxes) percentiles. The normative data was taken from GOSH.

[22]Clinical appointments are usually made for diagnostic purposes and after full field ERG recordings, time constraints, as well as tolerance of the patients for corneal electrodes meant that a clinical PERG recording may not be included.

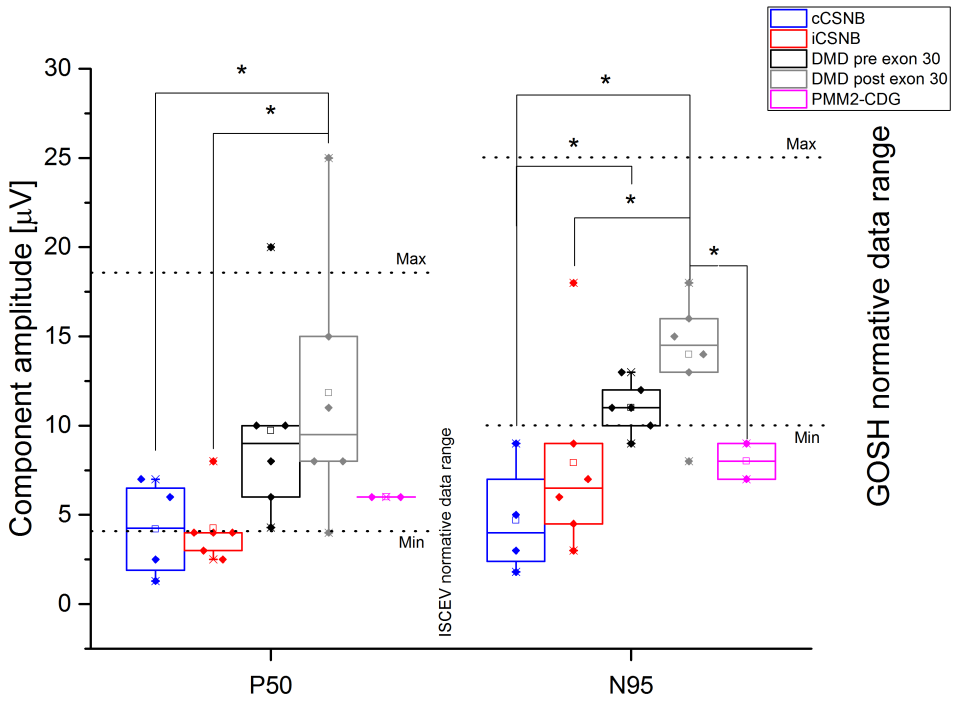


**Figure 2.24:** Overview of the amplitudes of the conventional PERG main components. Asterisks show statistically significant differences between the patient subgroups (One-way ANOVA and post-hoc Tukey means comparison). Measured PERG waveforms were averaged responses over 2x200 sweeps, ensuring reliability and repeatability of the data. Diamond symbols represent individual subjects. Boxes give Max and Min (-), Mean (square), Median (line inside the boxes), 99% and 1% (x), as well as 75% and 25% (margins of the boxes) percentiles. Normative data was taken from GOSH.

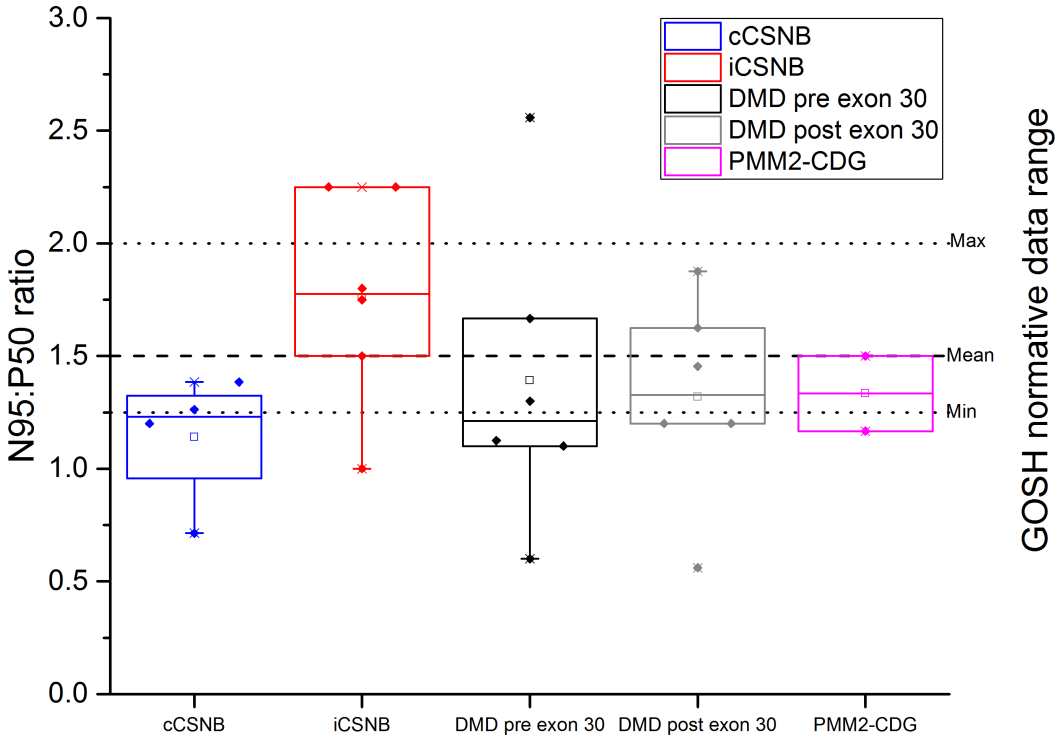


**Figure 2.25:** Overview of the N95:P50 amplitudes ratios obtained across patient subgroups. Asterisks show statistically significant differences between the values and the normative data range (One-way ANOVA and post-hoc Tukey means comparison). Measured PERG waveforms were averaged responses over 2x200 sweeps, ensuring reliability and repeatability of the data. Diamond symbols represent individual subjects. Boxes give Max and Min (-), Mean (square), Median (line inside the boxes), 99% and 1% (x), as well as 75% and 25% (margins of the boxes) percentiles. The clinical normative data was taken from GOSH.

#### 2.3.2.5 Pattern Reversal VEP - PVEP

Abnormal ganglion cell firing was reported in several mouse models of ON-pathway dysfunction at the level of the retinal ganglion cells and the LGN [158, 156, 157]. In humans, it is not clear whether an ON-pathway dysfunction alters ganglion cell firing patterns and subsequently affects signalling at the level of the striate cortex. Abnormally low amplitudes and delayed timing of the N95 component in a part of the cohort of patients with ON-pathway dysfunction gave a first hint into this direction. In order to assess this possibility in a large group of patients with retinal ON-pathway dysfunction, a retrospective analysis of conventional clinical pattern reversal VEP results was carried out. This analysis is described in detail in Chapter 4, Section 4.1, as it served as an important preliminary step in the development of the novel electrophysiological ON-pathway test battery.

### 2.3.3 Behavioural vision assessments

Structural malformations of the eye or functional disruptions of visual signalling often cause impairment of perceived vision. Clinically, certain perceptual qualities are assessed in patients with visual impairments alongside the previously discussed assessments, in order to allow an association of physiology and structure with behavioural visual function. Such behavioural assessment results obtained from clinical records of patients within the ON-pathway dysfunction subgroups are reviewed in the following sections[23].

#### 2.3.3.1 Visual acuity

Decreased visual acuity is sometimes associated with a dysfunctional ON-pathway [164]. Hence, it was important to get an understanding of how this measure of spatial visual resolution was distributed across the patient subgroups as it would give a first idea of how visual function can be affected by a disturbed ON-pathway. An overview of VA values obtained from the patient cohort is shown in Figure 2.26. VA measurements shown were always obtained with both eyes viewing (BEO = "both eyes open") and under best-corrected circumstances[24].

[23] Clinical assessments of contrast sensitivity were not available for the patients this was subsequently assessed using the novel LumiTrack$^{Tm}$ software.

[24] Focusing on binocular VA was in view of the subsequent electrophysiological and psychophysical test batteries being carried out with both eyes viewing and under best-corrected conditions. Further, VA obtained with both eyes viewing provides a more realistic measure of spatial visual resolution

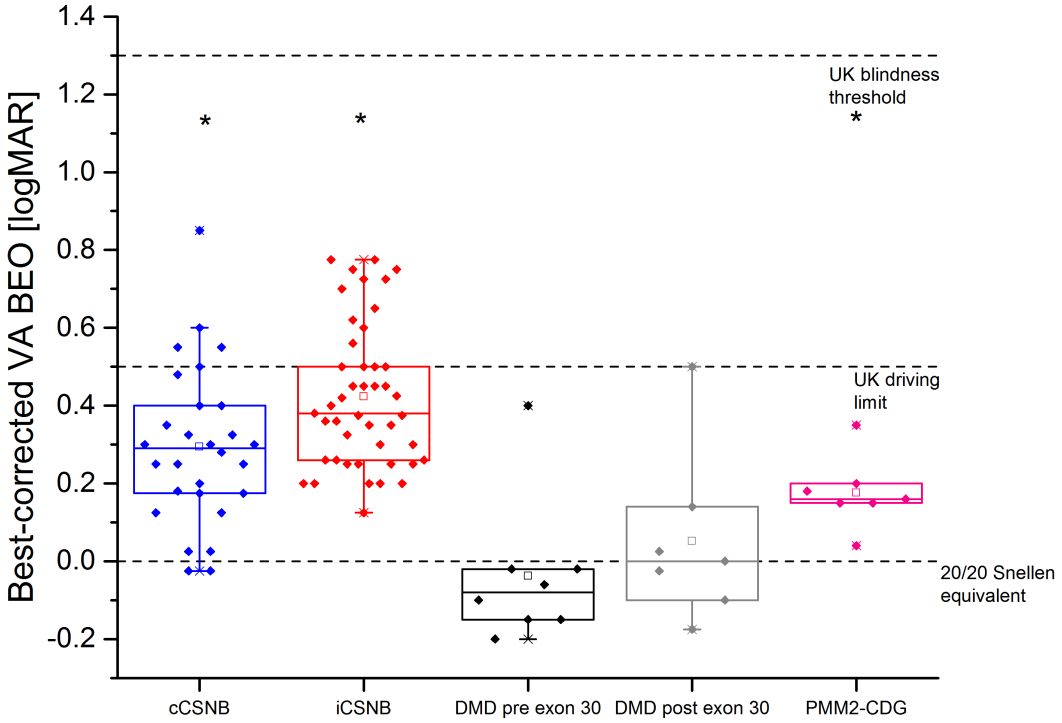


**Figure 2.26:** The graph displays the distribution of best-corrected visual acuities across the patient subgroups, measured with both eyes viewing. Asterisks show statistically significant differences to the control cohort (One-way ANOVA and post-hoc Tukey means comparison). Diamond symbols represent individual subjects. Boxes give Max and Min (-), Mean (square), Median (line inside the boxes), 99% 1% (x), as well as 75% 25% (margins of the boxes) percentiles.

When looking at the distribution of VA values across the patient subgroups, it became clear that the CSNB patients displayed the highest prevalence of subnormal VA values. Particularly the iCSNB subgroup contained no patient with a VA better than 0.1 logMAR. The cCSNB subgroup displayed a wider range with values from -0.025 to a maximum of 0.85 logMAR. Both subgroups showed individuals with a best-corrected VA poorer than the UK driving limit of 0.5 logMAR, but also patients with normal VA were part of these subgroups. Moreover, 33 out of 109 (cCSNB n=8, iCSNB n=23, DMD pre exon 30 n=1, DMD post exon 30 n=1) patients within this cohort fell under the "low vision" definition according to the WHO[25] [146]. Individuals affected by PMM2-CDG seemed to exhibit decreased visual acuity, as this patient subgroup, together with both CSNB subgroups, displayed a significantly higher group average VA when compared to a cohort of 150 healthy volunteers[26] (cCSNB: $p<0.0001$, iCSNB: $p<0.0001$, PMM2-CDG: $p<0.0001$). Ultimately, the majority of patients with DMD showed normal visual acuity values, with only one subject having a VA of 0.5 logMAR at the UK driving limit.

Letter recognition VA is thought to change rapidly within the first years of life and adult levels can be reached already between the third and fourth year of life in healthy observers (see for example [113, 99]). Hence, a great improvement of VA with age in the patient cohort, where the youngest patients carrying out comparable visual acuity assessments were five years old, was not anticipated. In order to get empirical evidence for this in the patient cohort, the patients' binocular VA values were plotted against their age. This data is shown in Figure 2.27 which shows a wide spread of VA values across the CSNB and PMM2-CDG subgroups, but there is no evidence of a striking developmental trajectory of the data.

[25] A VA of lower than 0.4 logMAR

[26] These healthy volunteers comprised the control cohort who carried out the electrophysiological and psychophysical test batteries discussed in subsequent chapters.

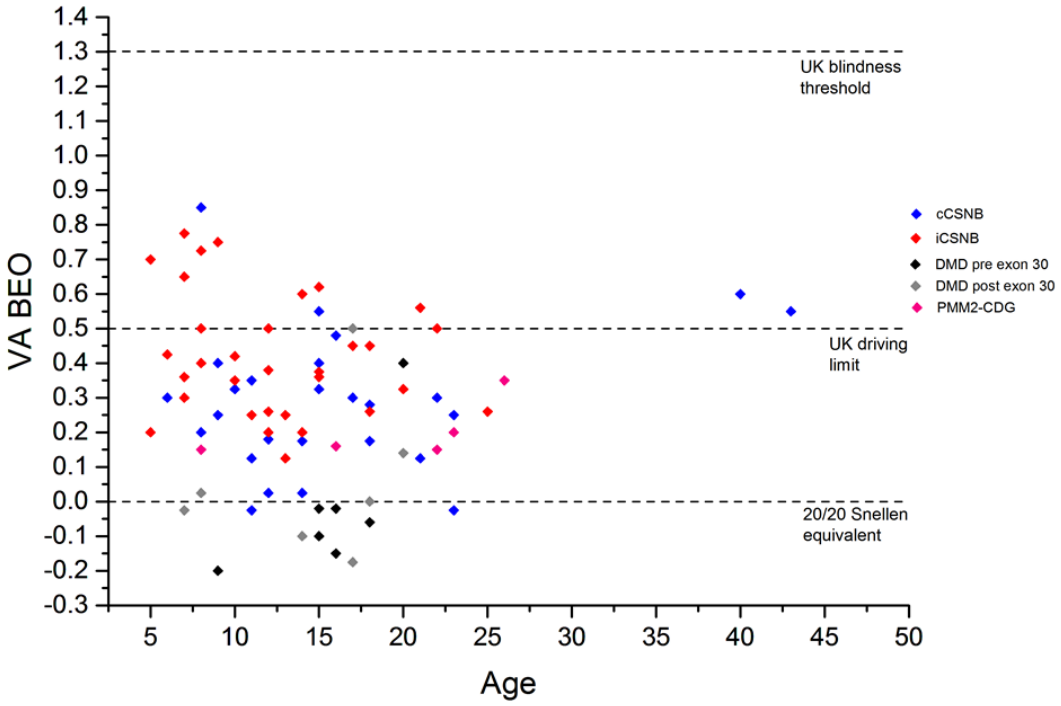


**Figure 2.27:** The graph displays the distribution of best-corrected visual acuities across the patient subgroups and across ages, measured with both eyes viewing. Diamond symbols represent individual subjects.

#### 2.3.3.2 Visual Fields

In the literature, visual field testing in patients with ON-pathway dysfunction generally presents no abnormal findings in patients with CSNB [174, 257, 78, 203, 164] and DMD [258]. While normal visual fields can be detected in patients with PMM2-CDG, two reports mention constricted peripheral visual fields, likely due to progressive rod/cone photoreceptor loss, in such patients [215, 240]. Mostly, however, it is challenging to obtain such data due to the intellectual disability often present in these patients [240].

In accordance with these reports, there were no visual field defects observed in the CSNB subgroups, except for one patient with cCSNB who showed a large blind spot in the left eye within the central 20°. Such central blind spots can be caused by diseases of the macula [259] and as such decrease the amplitude of the pVEP [260]. The patient's pVEP amplitudes and times to peak to a reversing checkerboard stimulus of 50' check size, however, were within normal limits[27], making macula degeneration an unlikely reason for this blind spot[28]. Blind spots can also be caused by a high refractive error, which is not uncommon in patients with CSNB and could explain the visual field defect reported here [261].

Moreover, only one patient within the PMM2-CDG subgroup was able to carry out visual field testing (Pat74). He displayed a slightly constricted visual field compared to the ones obtained from patients with CSNB. An exemplary field test result for the iCSNB subgroup, as well as the visual field plots of the discussed cCSNB and PMM2-CDG patients, are shown in Figure 2.28. No patient with DMD had carried out a visual field assessment and hence, no data was available for the DMD pre and post exon 30 subgroups. However, as mentioned by Jensen and colleagues, visual fields in patients with DMD appear to be normal [258].

[27] Amplitude: 42$\mu$V, Time to peak: 113ms

[28] This patient did not subsequently carry out any of the novel electrophysiological and psychophysical assessments, presented in Chapters 4 and 5.

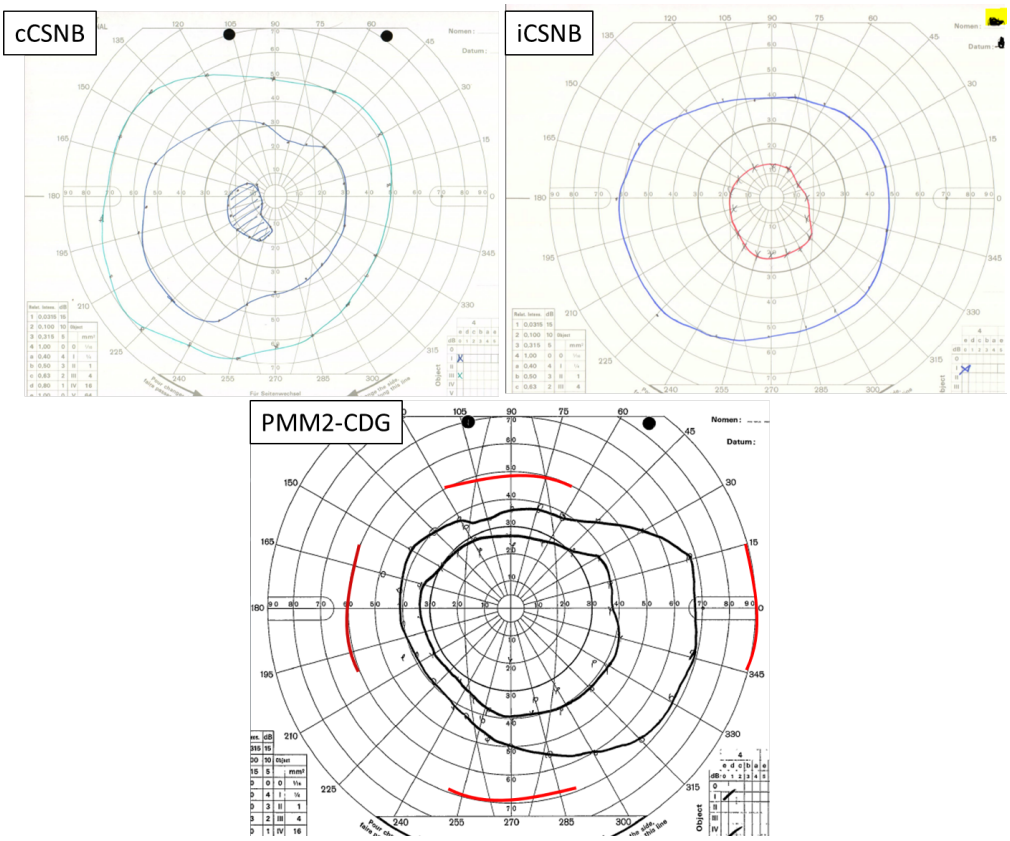


**Figure 2.28:** Exemplary visual field assessment results for different patient subgroups: cCSNB (Pat18, left eye), iCSNB (Pat46, left eye), PMM2-CDG (Pat74, right eye). No visual field measures for patients with DMD were available. An approximation of the margins for a normal (monocular) visual field are shown in red on the plot representing the patient with PMM2-CDG. It extends from approximately 60 degrees nasally to 90 - 110 degrees temporally from the vertical meridian, and from approximately 50-70 degrees above to 70-80 below the horizontal meridian [262, 263].

### 2.3.4 Other measures and reports

Apart from the clinical measures of vision described above, other signs and symptoms encountered in patients within the cohort were added to the ON-pathway database, some by means of reviewing clinical letter or reports, others by personal patient accounts. These complete the clinical picture gained from the retrospective analysis of patient data and are laid out in the following.

#### 2.3.4.1 Incidence of nystagmus in patients with retinal ON-pathway dysfunction

A contributor to the difficulties encountered during visual testing is the occurrence of nystagmus in patients with ON-pathway dysfunction. Nystagmus can have a degrading effect on pattern reversal stimulation during electrophysiological recordings, such as the PERG [230] and the pVEP [264]. Hence, the presence of nystagmus in patients with retinal ON-pathway dysfunction was an important factor to consider during the design and development stages of the novel ON-pathway toolkit aiming to evaluate the physiological and perceptual impact of this retinal dystrophy on vision. Figure 2.29 shows the relative incidence of nystagmus across the patient cohort, highlighting the differences between subgroups. The highest incidence existed within the iCSNB subgroup, where 68% (28/42) of patients exhibited nystagmus. This number decreased slightly to 57% (19/33) for patients with cCSNB and to 50% (7/14) in the PMM2-CDG subgroup[29]. Patients with DMD did not show nystagmus at all (0/8 and 0/11).

As nystagmus is thought to result in a constant motion of the retinal image [264], it was of interest to investigate whether the presence of nystagmus in patients influences visual spatial resolution. Thus, the VA BEO values of patients with and without nystagmus were compared (Figure 2.30). No statistical significance between VA scores was detected, indicating no influence of nystagmus on visual spatial resolution in this cohort.

[29]Only 14 out of 15 patients with PMM2-CDG had a VA assessment carried out and reported in the clinical notes.

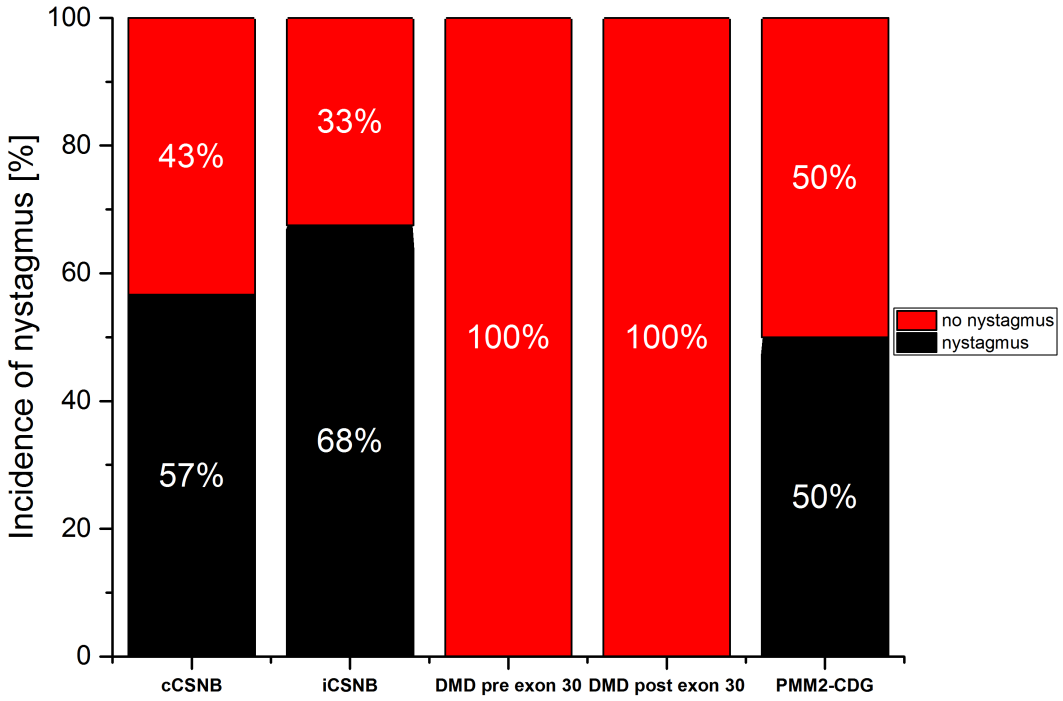


**Figure 2.29:** Relative incidence of nystagmus across the patient subgroups. Black bars signify the presence of nystagmus, red bars the absence of nystagmus. Numbers might not add up to 100% due to rounding.

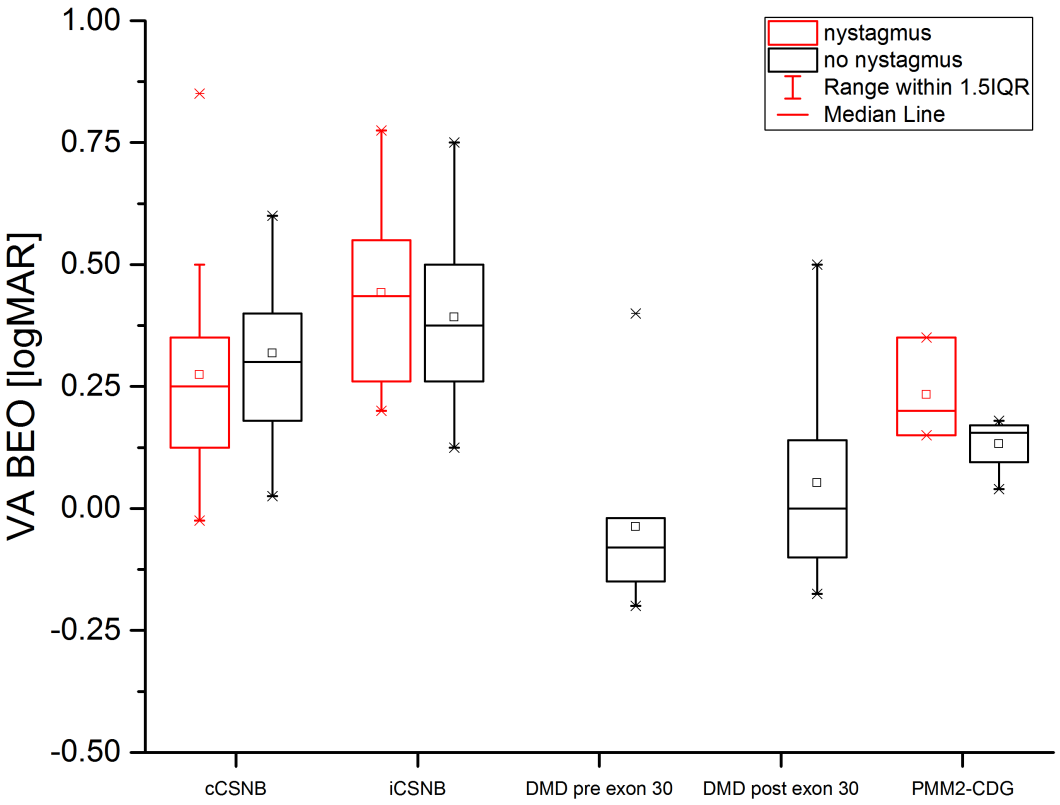


**Figure 2.30:** VA BEO values of patients with and without nystagmus were compared across subgroups. Black boxes signify the presence of nystagmus, red boxes the absence of nystagmus.

#### 2.3.4.2 Patient accounts

A range of visual problems were described by patients within the ON-pathway dysfunction subgroups. The most frequent visual impairment articulated by patients with subtypes of CSNB was night blindness. This is readily understood, as a selective ON-pathway dysfunction is expected to especially disrupt rod pathways. The signal relay under low ambient light (scotopic) conditions relies exclusively on the direct connection between rod photoreceptors and ON bipolar cells, whereas no OFF bipolar cells connect to rod photoreceptors. In contrast, cone signals can be relayed through ON-and OFF-pathways [1].

Of course, a retrospective analysis of clinical notes and reports is limited by the completeness of description of the visual impairments experienced by patients within the reports. Hence, night blindness might not always have been explicitly mentioned in reports of patients with ON-pathway dysfunction, making an estimate of the incidence of such impairment challenging. Nonetheless, the majority of patients with cCSNB (30 out of 33) reported having problems under low lighting conditions, either describing these personally during an appointment or it was explicitly noted in the patient's clinical notes. Similarly, of the 22 patients with iCSNB who attended the author's clinical appointments for this study, 15 explicitly stated to experience difficulties at low ambient light levels[30]. Many patients described this as ”difficulties seeing in the dark” and expressed problems such as ”not finding the seat in the cinema” or were not able to see ”stars in the night sky”, when unaffected siblings could. The majority of these, mostly young patients, also slept with room or bedside lighting switched on.

One recent study by Bijveld and colleagues specifically assessed night vision problems in patients with iCSNB and cCSNB and also found this visual disability to be more prevalent in patients with cCSNB than patients with iCSNB [164]. A more confident estimate could be given for patients with DMD who did not report to experience any night vision problems at all. Further, none of the seven PMM2-CDG patients seen by the author at GOSH during the course of the study reported

[30]This was upon the author asking whether the patients experienced any apparent difficulties in low light situations or at night, when compared to other children or unaffected siblings.

any noticeable night vision problems[31].

Not only did many patients report problems seeing under low light conditions, some (though considerably fewer) patients with CSNB also reported some photoaversion. Seven patients with iCSNB and one patient with cCSNB had slight difficulties in very bright light. Further, more sporadic accounts of difficulties seeing low contrast (for example noticing a ”dark chair standing in the shade” (Pat8, iCSNB)) or motion (for example Pat4 (iCSNB) who enjoyed playing tennis but did not pursue the sport as he ”had trouble seeing the ball, when it was going fast”) were also frequent. Such impairments can be great limitations in everyday situations. However, the depth of such visual problems was not captured by conventional clinical tests, making it difficult to estimate a complete picture of visual impairment due to ON-pathway dysfunction.

[31] Whenever the patients were not able to answer independently, their parents were asked.

## 2.4 Summary and conclusion

### 2.4.1 Summary

- Structural measures of the ocular phenotypes of patients revealed no major abnormalities in patient subgroups, although some myopic fundus changes and retinal thinning were observed in a few patients.
- Patients within all subgroups showed signs of ON-pathway dysfunction in the ERG. However, slight differences in dark adapted and light adapted ERG waveform signatures were present. The main findings are listed below:

  - *Dark adapted*: All subgroups showed abnormal components under dark adapted conditions. Patients with cCSNB and PMM2-CDG showed a b-wave only to flashes of 0.001 cd*s*$m^{-2}$ and above. Patients with cCSNB showed the smallest b-wave amplitudes across subgroups, never exceeding 150$\mu$V.
  - *Light adapted*: Patients with iCSNB showed the most severe disruption of light adapted retinal signalling. Patients with DMD mutations pre exon 30 showed almost normal light adapted responses, whereas patients with cCSNB, PMM2-CDG and DMD mutations post exon 30 showed subnormal b-wave amplitudes at high light adapted flash luminances.
  - *OPs*: Most striking were the almost complete absence of dark adapted OPs in cCSNB, and of light adapted OPs in patients with iCSNB. In contrast, OPs were mostly preserved in patients with PMM2-CDG.
  - *Clinical PERGs*: The smallest P50 and N95 components were detected in patients with complete CSNB, while patients with DMD showed the biggest amplitudes, with components of intermediate size in PMM2-CDG, independent of nystagmus. Subnormal N95:P50 amplitude ratios, indicative of retinal ganglion cell or optic nerve dysfunction, were observed in individual patients of all patient subgroups.

- Subnormal visual acuity was frequent across subgroups with a majority of pa-

tients with incomplete CSNB showing decreased VA values. VA was mostly better than the UK driving limit in boys with DMD and patients with PMM2-CDG.

- Visual field assessments were normal in the majority of patients with subtypes of CSNB, while one patient with PMM2-CDG showed a slightly constricted visual field. Visual fields have been reported to be normal in patients with DMD.
- Nystagmus was prevalent in three out of five subgroups of patients with ON-pathway dysfunction. These were cCSNB, iCSNB and PMM2-CDG.
- Other visual signs and symptoms, such as photo-aversion, night blindness and problems seeing contrast and motion were recovered from patient accounts, which were not captured by clinical measures of vision.

### 2.4.2 Conclusion

This chapter gave an overview of the clinically reported structural and physiological visual phenotypes encountered in patients with ON-pathway dysfunction. The function of the retina crucially depends on the structural integrity of its components. The review of clinical notes and reports and the subsequent analysis of these data revealed that a majority of patients did not display any observable defects of ocular and retinal structure. Most patients with subtypes of CSNB and DMD showed normal fundi and retinal layer architecture, whereas some abnormalities were present in patients with PMM2-CDG and a minority of patients with subtypes of CSNB associated with myopia. The literature on CSNB, DMD and PMM2-CDG also reveals limited impact of these ON-pathway dysfunctions on the structure of the eye or retinal layers, which is observable using OCT or fundus photography.

Due to the unremarkable structural phenotypes of most patients within the cohort, it is possible that a visual abnormality is only picked up upon assessing the physiological and functional integrity of the visual system via electrophysiological and psychophysical methods. Evidence of a disrupted ON-pathway across all patient subgroups was revealed analysing full field ERG responses and upon more detailed analysis, slight waveform differences and signatures associated with the individual conditions were observed.

Upon analysing clinical behavioural measures, a profound impact of ON-pathway dysfunction on visual acuity was observable in many patients with cCSNB and iCSNB. Surprisingly, most patients with DMD and PMM2-CDG did not show any such decrease in VA, despite showing ERG evidence for retinal ON-pathway dysfunction. The relative preservation of OPs in individuals with DMD and PMM2-CD could suggest a role of spiking neuron integrity for intact VA.

In contrast to central visual spatial resolution, visual field measurements did not reveal abnormalities in the majority patients with CSNB. Similarly, no visual field defects were reported in the literature on DMD. One patient with PMM2-CDG showed a slightly constricted visual field, likely caused by the progressive photoreceptor loss often present in such patients. The incidence of nystagmus across the

patient subgroups was at least 50% in patients with cCSNB, iCSNB and PMM2-CDG. In contrast, patients with DMD did not show nystagmus.

In conclusion, there is a whole range of visual phenotypes present in patients within the study cohort, despite all of them showing electrophysiological evidence of a retinal ON-pathway dysfunction. Additionally, as ON-pathway dysfunction manifests as a part of different conditions, the interpretation of clinical results is challenging and the presence of other ocular conditions alongside retinal ON-pathway dysfunction makes it difficult to attribute some visual signs and symptoms to ON-pathway dysfunction alone. This makes the acquisition of a complete clinical picture of a patient's visual phenotype even more important, in order to compare which of those signs and symptoms occur frequently within a patient subgroup. While such reports of visual phenotypes are often found in the literature on patients with subtypes of CSNB, information on patients with DMD and PMM2-CDG is scarce.

Functional vision levels of patients with ON-pathway dysfunction have rarely been assessed systematically. One study from Bijveld and colleagues (2013) specifically investigated night vision problems in patients with CSNB and found them to be ”not conspicuous and generally not disabling” [164, 265]. However, a variability of different visual abilities was evident in this study of patients with retinal ON-pathway dysfunction. Several subjects reported night blindness, in addition to photo-aversion and problems seeing contrast and motion. Apart from such patient accounts and the study carried out by Bijveld and colleagues, not much is known about the functional deficits in different visual domains these patients may have. An explanation of why patients with ON-pathway dysfunction can exhibit a whole range of visual impairments could be given by investigating the molecular differences between these conditions.

Conventional clinical vision tests do not necessarily capture these visual impairments specifically, making the objective judgment of possible impairments of certain visual qualities, such as motion perception, difficult. Furthermore, as mentioned in Chapter 1, such vision tests are sometimes challenging to carry out in

younger patients, where early detection of abnormality has the potential to improve quality of life considerably, by tailoring patient care to individual needs from an early stage. There is therefore an opportunity of further insight of visual performance by developing novel or more specific visual tests and correlating these with known physiological and genetic information. Being able to draw a more complete picture of the visual abilities of patients with ON-pathway dysfunction has the potential to subsequently benefit clinicians in informing parents and carers of the most appropriate intervention in order to improve quality of life of patients.

The following chapter will investigate the genotypes present in the subgroups of patients with ON-pathway dysfunction.

Chapter 3

# Genetic analysis of patients with ON-pathway dysfunction

## 3.1 Introduction

Hereditary retinal diseases are the major cause of childhood blindness in the UK [266]. The majority of these currently are not treatable, although recent studies of gene-therapies and stem-cell replacements are showing promise [151, 150]. Most retinal diseases are not described sufficiently and visual testing is challenging in children, who show the earliest signs and in whom therapies may have the greatest chance of success. Knowledge about the genetic make-up underlying congenital retinal conditions can aid the understanding of the biological processes implicated in the visual signs and symptoms observed in patients. Further, it can provide key information on expected disease progression and heredity, making it a crucial diagnostic tool.

The retina uses separate signaling pathways for bright (ON) and dark (OFF) parts of an image. This underpins edge detection, a basic requirement for vision. A number of retinal disorders appear to preferentially disturb the ON-pathway. As a result a child may experience night blindness, photo-aversion, nystagmus and subnormal visual acuity. These visual phenotypes observed in individuals with ON-pathway dysfunction, discussed in the previous chapter, are thought to be due to a retinal signalling defect which affects signal transmission between photoreceptor cells and ON bipolar cells [69]. However, knowledge of cell interactions (and molecular key players) at the photoreceptor / ON bipolar cell synapse of the human retina is incomplete [166]. I aim to provide an analysis of the genotypes present in the patient cohort, in order to gain an insight into how these translate into visual outcome at the cortex and behaviourally. Genotype-phenotype correlations are crucial for establishing what role affected genes play in the retina, alongside having the potential to inform future efforts in treatments for retinal disease.

To ultimately conduct genotype-phenotype correlations, I aimed to assemble and identify the genetic variants causing ON-pathway dysfunction for the entire study cohort. The genotypes of the DMD and PMM2-CDG subgroups were partly described in previous studies [238, 216, 163] and were provided by the collaboration of these research teams. These genotypes are listed in Tables 3.6 and 3.7.

Patients with suspected CSNB (based on their clinical electrophysiological data) were without genetic diagnosis and a range of approaches were used to identify the genetic variants causing ON-pathway dysfunction in these individuals.

Those CSNB patients without a genetic diagnosis, who were approached to take part in the study, were informed of the possibility to take part in the genetic research part of the study[1]. Patients and their families provided DNA samples if there was interest.

For these samples, mutation screening for potential disease causing variants was performed for all known CSNB genes using a targeted gene panel sequencing approaches. Further, exome-wide analysis was used to identify potential novel CSNB in a part of the CSNB cohort. From these approaches, potentially pathogenic variants were identified and classified and subsequently confirmed via Sanger sequencing. Whenever possible, segregation analysis via Sanger sequencing was carried out, using parental DNA and DNA of siblings. Any clinically relevant findings from this analysis were fed back to the lead clinician.

The complete procedure of genetic analysis is described in the following section.

[1] An example of a Participant Information Sheet used is provided in the Appendix.

## 3.2 Methods

### 3.2.1 DNA extraction

#### 3.2.1.1 DNA extraction from blood and saliva samples

The majority of patient DNA samples were obtained by means of the patients - as well as any members of their families - giving blood samples via the phlebotomy service at GOSH. DNA was extracted from these samples by the Clinical Genetics and Diagnostic laboratory at GOSH.

It was not always possible to obtain blood samples from affected individuals. In these cases, genetic samples were obtained from patient saliva samples using Oragene OG-500 DNA Self-collection Kits. In order to extract the DNA from these samples, they were incubated at 50°C for two hours (or over night) using an oven. The samples were then transferred into autoclaved 1.5mL Eppendorf tubes (Eppendorf UK Limited). Oragene Purifier (which was provided with the OG-500 Self-collection kits, DNA Genotek Inc.) was then added to the tubes at a volume of 1/25 and this was then mixed by inversion. The samples were then incubated on ice for 10min and subsequently centrifuged at 13,000g for 3min at room temperature (RT).

The clear supernatant was then carefully taken off with a pipette and transferred into a new 1.5ml Eppendorf tube. To this, an equal amount of 95% Ethanol was added and the contents mixed by inverting multiple times. Afterwards, DNA precipitation was allowed by incubation at RT for 10min, followed by centrifuging at 13,000g for 5 min. Following this, the pellet was air dried.

When completely dry, the DNA pellet was dissolved in TE buffer (made up of 10mM Tris and 1mM EDTA). The amount of TE buffer corresponded to 1/10th of the initial amount of saliva present in the tube[2]. Ultimately, the tubes were incubated at 4°C overnight to allow proper dissolving. DNA from the same individual was combined in one tube and the concentration of the DNA sample was measured using a NanoDrop Microvolume Spectrophotometer (Thermo Fisher Scientific UK) and then stored for further processing at -20°C.

[2]If the tube had an initial amount of 600$\mu$l, 500$\mu$l, or 400$\mu$l, the pellet was dissolved in 60$\mu$l, 50$\mu$l or 40$\mu$l TE buffer, respectively.

### 3.2.2 Targeted gene panel - The Oculome

To detect mutations in the clinically diagnosed CSNB patients without known genotype, a newly developed targeted panel Next Generation Sequencing (NGS) approach was used. This gene panel approach was developed in the Sowden laboratory by Dr Jane Hayward in collaboration with the North East Thames Regional Genetics Laboratory. The Oculome panel-gene test applies the SureSelect target enrichment technique using RNA baits designed to target the coding exons (including 25 intronic flanking bases upstream and downstream of these) of 436 known genes linked to eye function and development. The large panel is subdivided into 5 virtual subpanels of overlapping genes for retinal conditions (212), anterior segment dysgenesis and glaucoma (47), microphthalmia-anophthalmia-coloboma (MAC) (86), congenital cataracts and lens-associated conditions (84) and albinism (16). All the genes selected are described on OMIM and had previously been reported to contain a pathogenic mutation in at least one human family with an inherited eye disease.

The subpanel covering retinal conditions contains 212 genes, out of whom nine were previously associated to a subtype of CSNB[3]. The genes were chosen using RetNet, OMIM and with the advice of ophthalmic experts, and reflect the diverse genetic and clinical heterogeneity for retinal dystrophies [267].

The SureSelect Target Enrichment System Capture Process is initiated by an enzymatic shearing step which simultaneously fragments the DNA and ligates adapter tags. The genomic sample is then hybridized with 120mer cRNA library capture baits specific for the regions of interest. Subsequently, target regions were selected using magnetic streptavidin beads and these then amplified via PCR. The PCR additionally adds sample specific indices. The amplified fragments (*libraries*) were then sequenced using the Illumina HiSeq2000 flow cell with 2x100 bp reads. The sequencing reads are aligned to the reference genome and detected variants subsequently annotated[4].

For the analysis of the data from the HiSeq sequencing instruments, an in-

[3]For all genes included in the Oculome panel, see Appendix, for CSNB genes included see Chapter 2, Figure 2.2.

[4]A schematic of the SureSelect Target Enrichment System Capture Process can be found in the Appendix.

house developed pipeline using open-source tools was used. These provided read alignment (BWA; Burrows Wheeler Aligner v0.6.1-r104[5]), pileup (SamTools; Samtools v0.1.18[6]), variant calling (VarScan2; VarScan2 v2.3.6[7]) and variant annotation (Variant effect predictor v73: [8]).

Following the sequencing steps, a first automatic variant filtering pipeline was applied. Variants had to be present in 20% of at least 30 reads to be called. Further, all variants with a Minor Allelle Frequency of $>2\%$ were automatically filtered out (Class I variants). The next filtering step was to distill the results even further by removing variants with non-coding mutation types (Intronic, 3'-UTR, 5'-UTR, upstream, downstream and synonymous coding variants). Frameshift, stop-gained, stop-lost, missense, as well as splice site mutations were retained. These filtering steps extracted rare coding variants from the initial large set of variant calls. Copy number variation (CNV) analysis was performed using ExomeDepth for individual samples without a predicted class 4 or 5 mutation [268]. The ensuing analysis and classification of variants was manual.

### 3.2.3 Whole exome sequencing - GOSgene

A set of CSNB cases (n= 9) were analysed in collaboration with the in-house gene discovery service GOSgene[9], using a Whole Exome Sequencing (WES) approach. These DNA samples were selected for exome-wide analysis as the majority of these patients were female and therefore provided an opportunity to discover novel genes associated with the rare autosomal recessive form of CSNB.

The samples for WES were prepared using the Agilent SureSelect v4 (51Mb) chemistry and were run on Illumina Hiseq2500 sequencers to give at least 100X coverage. The resulting raw data was aligned to the reference genome (hg19)[10] using the Burrows Wheeler Aligner. Finally, GATK haplotype caller software was used to call variants and Ingenuity Variant Analysis software for data interpretation.

[5] www.bio-bwa.sourceforge.net
[6] www.samtools.sourceforge.net
[7] www.varscan.sourceforge.net
[8] www.ensembl.org/info/docs/tools/vep/index.html
[9] www.ucl.ac.uk/ich/research/genetics-genomic-medicine/gosgene
[10] www.genome.ucsc.edu

### 3.2.4 Analysis pipeline

Genetic data were manually analysed following a pipeline and classification system for the variants detected [269]. For this, the variants were assigned classes, according to their probability of being disease-causing:

**Class II** unlikely pathogenic, previously reported as benign

**Class III** Variant of uncertain clinical significance

**Class IV** likely pathogenic, not previously reported

**Class V** previously reported pathogenic mutation

The output received for manual analysis was a list of variants set in excel, including information such as gene name, zygosity, mutation type, location and pathogenicity analysis. The classification was based on impact of the mutation and mutation type (for example frameshift, splice-site, stop gain, missense), phenotype(s) previously associated with mutations in the same gene and phenotype observed in the patient, zygosity of the variant and inheritance pattern previously reported for mutations in the same gene. Further, the predicted pathogenicity of the mutation based on in-silico tools like SIFT[11] and Polyphen[12] was taken into consideration. Variants in patient samples which were assigned Classes IV and V, were followed up for confirmation analysis via Sanger sequencing. Only variants within Classes IV and V were suitable for reporting to the lead clinician.

### 3.2.5 Sanger sequencing

To confirm the presence of the predicted pathogenic variants identified from the NGS apporaches, Sanger Sequencing was carried out on all Class IV and V variants. This included sequencing in affected and unaffected family members (where possible) to confirm co-segregation of predicted mutations with disease. Sanger sequencing is a method that uses DNA polymerase inhibiting dideoxynucleotide triphosphates (ddNTPs) for chain termination. The termination happens because

[11] www.sift.jcvi.org
[12] www.genetics.bwh.harvard.edu/pph2

ddNTPs lack a 3'-OH group which is required for polymerisation to continue. Each of the four types of ddNTPs is fluorescently labelled by dyes which absorb light of different wavelengths, hereby making determination of the exact base at which the sequence is terminated possible. Primers for template annealing were designed for the individual samples. Sanger Sequencing was performed following the protocol below.

#### 3.2.5.1 Primer design

First, the UCSC genome browser[13] was used to find the exact sequence of interest for each individual variant detected by NGS. The DNA sequence was used to find matching primers amplifying the region of interest using Primer3[14]. When using primers for Sanger sequencing, it is important to leave at least 50bp from the start and end of the sequence of interest. This allows for a sufficient amount of "buffer-zone" bases on each side of the position of the variant call, while keeping the resulting size of the sequence at around 500bp. However, this size could vary due to single nucleotide polymorphisms (SNPs) falling into the desired primer sequence. Following this, the primers with the best properties were chosen using the guidelines below:

- Try to choose a primer with 18-30 oligo nucleotides in length. The longer end of this range allows higher specificity.
- Make sure the melting temperature of the primers are not more than 5°C different from each other.
- The GC content of each primer should be in the range of 40-60% for optimum PCR efficiency.
- Try to have uniform distribution of G and C nucleotides, as clusters of G's or C's can cause non-specific priming.
- Avoid long runs of the same nucleotide.
- Primers should not be self-complementary or complementary to the other primer in the reaction mixture. This could result in the formation of hairpins and primer dimers.

Once suitable primers were found, it was ensured that the primer pair had different binding sites within the genome by conducting an in-silico PCR on the UCSC website[15]. Further, it was ensured (whenever possible) to keep the amount of SNPs to a minimum, preferably zero. To check for the presence of SNPs in the predicted

[13] www.genome.ucsc.edu
[14] www.primer3.ut.ee
[15] www.genome.ucsc.edu

primer binding sites, SNPcheck3 was used[16]. Unless otherwise stated, all reagents used in this study, including the primers, were purchased from Thermo Fisher Scientific[17].

Primers were re-suspended to give 100$\mu$mol solutions by adding MilliQ $H_2O$ and the primers then stored at -20°C until further processing. A list of the primers used in this study can be found in the appendix.

#### 3.2.5.2 Polymerase Chain Reaction - PCR

Initially, the stock genomic DNA was diluted (1:10, using MilliQ $H_2O$). A mastermix for the PCR reaction was made in a 0.5 or 1.5ml Eppendorf tube (depending on the amount of mastermix required):

| Ingredient | 1x [$\mu l$] |
|---|---|
| 10X Buffer | 2.0 |
| 2nM ddNTPs | 2.0 |
| DMSO | 2.0 |
| 50mM $MgCl_2$ | 0.6 |
| 100$\mu$M F Primer | 0.1 |
| 100$\mu$M R Primer | 0.1 |
| MilliQ $H_2O$ | 12.1 |
| Taq Polymerase (Qiagen 201203) | 0.1 |
| DNA (1:10) | 1.0 |
| Total | 20.0 |

**Table 3.1:** PCR Mastermix

When finished, the mastermix was vortexed to ensure proper mixing. Then the samples were run using the following PCR protocol on a Thermal Cycler[18]:

1. 95°C - 2min
2. 95°C - 20s
3. (Annealing temp)°C - 20s
4. 72°C - 30s

[16] www.secure.ngrl.org.uk/SNPCheck
[17] www.thermofisher.com
[18] Applied Biosystems: www.thermofisher.com/uk/en/home/brands/applied-biosystems.html

Following this, the samples were run on a 1% agarose gel[19] containing 10$\mu$l of Sybrsafe DNA gel stain. For this, 5$\mu$l of PCR product was mixed with 1$\mu$l of loading dye and loaded into the wells. The gel was run for about 50 min at 150mV.

#### 3.2.5.3 ExoSAP treatment

Following the initial PCR reaction, an enzymatic clean-up step of PCR products eliminating unincorporated primers and ddNTPs via ExoSAP-treatment was necessary. For this, an ExoSAP mastermix was made, composed of:

| Ingredient | 1x [$\mu l$] |
|---|---|
| Exol | 0.3 |
| Shrimp Alkaline Phosphatase | 1.0 |
| Dilution Buffer | 0.9 |
| MilliQ H2O | 0.3 |
| Total | 2.5 |

**Table 3.2:** ExoSAP Mastermix

Then, 2.5$\mu$l of ExoSAP mix was added into each PCR well with the left over PCR product. Then the following program was run on the thermocycler:

1. 37°C - 30min
2. 80°C - 5min

Following this, the samples were stored at -20°C.

#### 3.2.5.4 BigDye Terminator

To sequence the samples, the Big Dye Terminator v.1.1 was used. As forward and reverse strands of the region of interest are sequenced separately in this reaction, two reactions were needed for each sample.

| Ingredient | 1x [$\mu l$] |
|---|---|
| BigDye Terminator | 1.0 |
| Buffer | 1.5 |
| 5M Betaine | 2.0 |
| Total | 4.5 |

**Table 3.3:** BigDye Mastermix

[19] For a 100ml gel, 100ml 1xTAE + 1g Agarose were used.

Now, 1$\mu$l of 5$\mu$M primer (1:20 dilution of the original stock) was added to 4.5$\mu$l of mastermix and 5$\mu$l of the PCR product into a new 96-well plate (i.e. for one sample two tubes for forward and reverse primer were needed). Then, the plate was run on the thermocycler:

1. 96°C - 2min
2. 96°C - 15sec
3. 55°C - 10sec
4. 60°C - 4min

#### 3.2.5.5 Ethanol Precipitation

The final step was the Ethanol precipitation, required for the purification of the samples. For this, Ethanol precipitation solution was prepared (50ml 100% Ethanol + 2ml 3M Na-Acetate) and 50$\mu$l of this solution added to each well of the 96-well plate. This was left at RT for 20 minutes. Now, the plate was spun at maximum speed (3000xg) for 45 minutes in order to make the DNA pellet accumulate at the bottom of each well. Following this, the contents of each tube were tipped out onto a tissue paper without disturbing the pellet. Then, 50$\mu$l of 70% Ethanol were added and this spun again at maximum speed for 15 minutes. Again, the contents were tipped out afterwards. To remove any remaining Ethanol from the wells, the plate was spun upside down on a tissue paper for 30 seconds at 300xg. Sequentially, the wells were air-dried for 5min and 15$\mu$l of 0.1xTE Buffer were added to the wells and the plate covered with a sticky plastic cover. Ultimately, plates were run on the ABI 3730xl DNA Analyzer by staff in the Regional Diagnostic Laboratories at GOSH using BigDye Terminator v1.1 Cycle Sequencing.

#### 3.2.5.6 Sequencher software

Sequencing data files were analysed using the Sequencher software 5.2.4. As Sequencher does not recognise errors in the sequence or missing base pairs, these had to be detected and changed manually with the recognition threshold being set at

45% certainty. Following this, the reference sequences matching the obtained forward and reverse sequences were imported into the software and these aligned. Reference sequences were retrieved by running in-silico PCRs on the UCSC website[20]. Once aligned, changes in the sequences were detectable. An exemplary output of the Sanger sequencing traces of the family of Pat10 and Pat11 is displayed in Figure 3.1.

[20] www.genome.ucsc.edu/cgi-bin/hgPcr

## 3.3 Results

The genotypes of the DMD and PMM2-CDG subgroups were already known in part from published studies [238, 216, 163]. A further set of CSNB patients, who consented to genetic analysis, was analysed via NGS sequencing, either by Whole Exome Sequencing in collaboration with GOSgene or by a targeted gene panel approach (The Oculome). In some cases a genetic diagnosis was provided by external clinical diagnostic services/teams. Predicted pathogenic variants were subsequently verified using Sanger Sequencing.

An example of a segregation analysis of one family where both siblings were affected, alongside the sequence output received from the analysis software is shown in Figure 3.1. In such cases where more than one child in a family was affected, only one patient was run on the NGS panel and all DNA samples of the family subsequently analysed for segregation of the variant via Sanger Sequencing. Hence, Figures 3.4 - 3.8 contain more than the amount of patients with genotype mentioned below and display the genetic results in detail. Figures 3.9 and 3.10 include the genetic information on patients from the DMD and PMM2-CDG subgroups.

From a total of 75 patients with a subtype of CSNB included in this study, a proportion of 64% (n=48) had genetic testing carried out[21], either via GOSgene (n=9), the Oculome (n=28), or externally (n=6). In cases where an affected sibling of a patient, who had genetic testing carried out, also provided a DNA sample, the variant detected was subsequently confirmed via Sanger sequencing only (n=5). Of all these patients, 92% (n=44) received a genetic diagnosis from genetic testing.

While 100% of patients with a mutation in a known gene from the iCSNB cohort showed variants in *CACNA1f* (n=24), there was a greater variety in the cCSNB subgroup. Here, 35% of patients showed bi-allelic mutations in *TRPM1* (n=7) and another 35% showed hemizygous variants in *NYX* (n=7), whereas 15% patients had bi-allelic variants in *GRM6* (n=3) and another 15% in *GPR179* (n=3) (see Figure 3.2)[22]. Further, patients with cCSNB also showed the greatest variety of mutation

[21] The remaining 27 patients without a genotype did not provide DNA samples for analysis.

[22] Four patients in the cCSNB subgroup only showed a single heterozygous change in a known

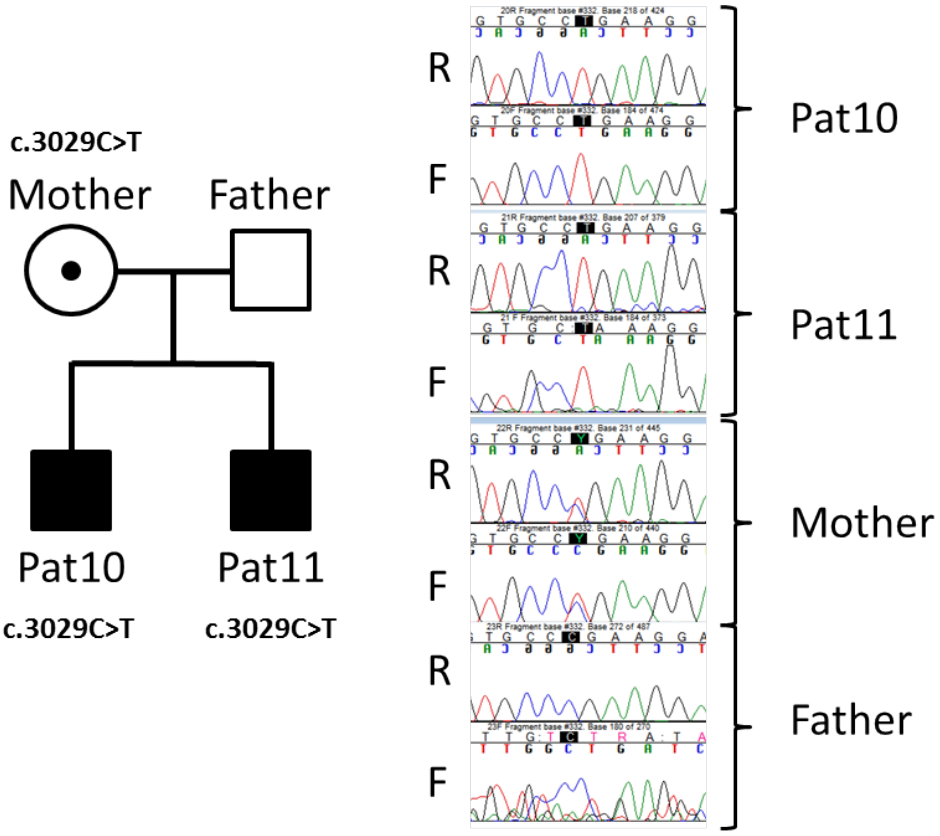


**Figure 3.1:** Exemplary output of Sequencher software for X-linked iCSNB cases Pat10 and Pat11, as well as both parental samples. Two labeled sequences per individual are the forward (F) and reverse (R) strands of the region of interest harboring the variant call. The highlighted base shows the predicted homozygous change in both patients, as well as in the mother, however, not in the father. The pedigree schematic on the left shows the segregation of the variant within the family. Both male children are affected (black squares) and showed variants p.Leu1010Pro and p.Arg508Gln in the *CACNA1f* gene. The mother is a carrier of these X-linked variants (white circle with black centre) and the father unaffected (white square).

types, with six different mutation types leading to complete CSNB (Figure 3.3). While missense mutations were the major mutation type detected in patients with cCSNB, iCSNB and PMM2-CDG, patients with DMD mostly showed deletions of

cCSNB gene (GPR179, TRPM1). These would technically be classified as Class III variants, as no pathogenic heterozygous variant was previously associated with these mutations and the genes are generally considered to lead to autosomal recessive cCSNB. Nonetheless, these changes were included in Figures 3.4 and 3.5, as the occurrence of another heterozygous hit in these genes would have rendered these variants as bi-allelic Class IV or V. The targeted gene panel approach is subject to some shortcomings, such as that it, for example, does not detect the absence of whole exons or the occurrence of copy number variants (CNVs). The inclusion of the single heterozygous variants encountered in these patients is further discussed in the conclusion of this chapter, Section 3.4.2.

whole exons in the *DMD* gene.

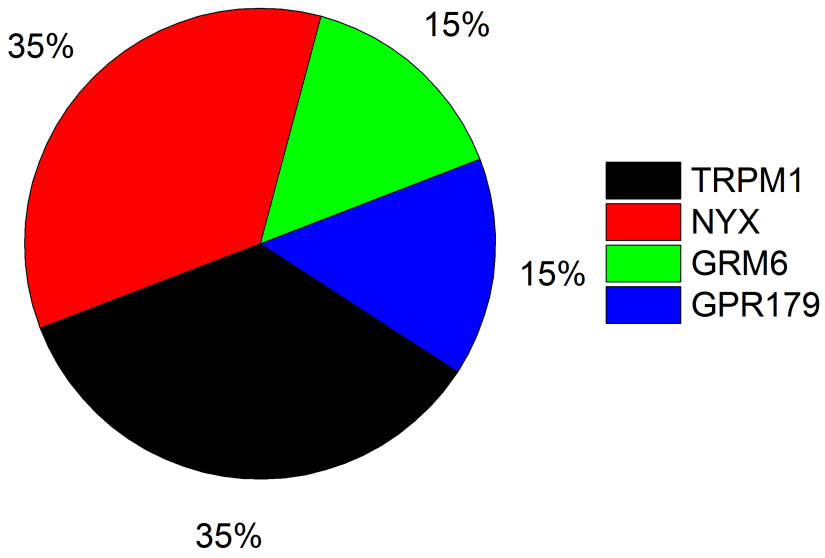


**Figure 3.2:** Piechart showing the prevalence of different genes affected in the cCSNB cohort.

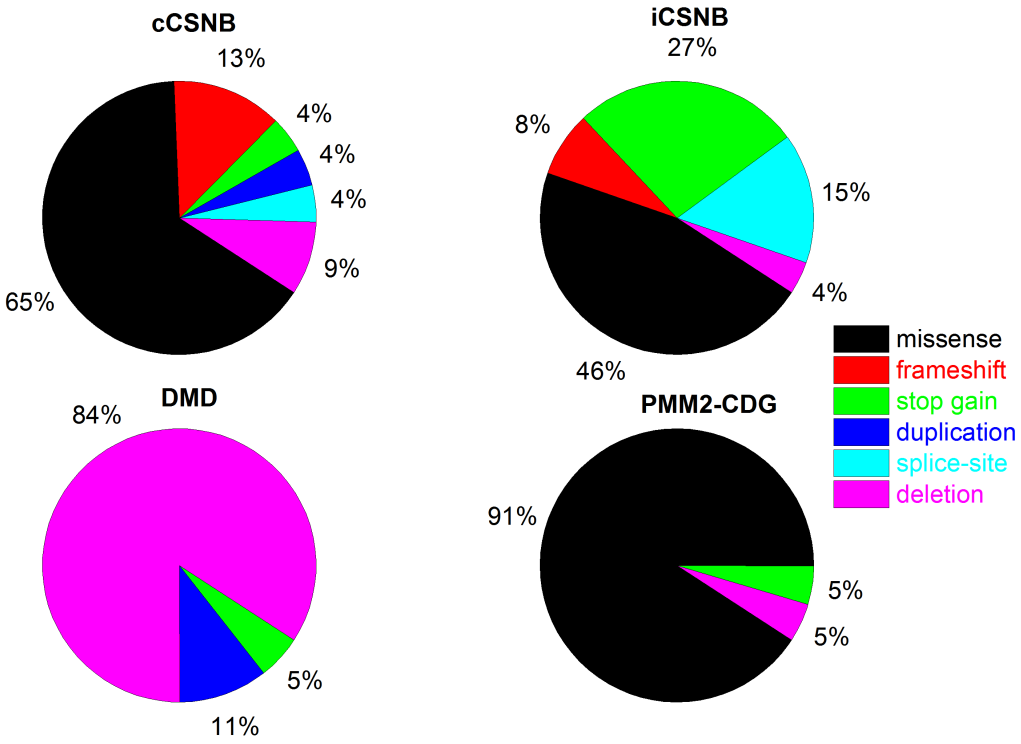


**Figure 3.3:** Piechart showing the prevalence of different gene mutations types in the ON-pathway dysfunction cohort.

| Patient ID | Gender | Relatives | Gene | Inheritance mode | OMIM number | Amino acid change | Nucleotide change | Zygosity | Mutation type | Segregation analysis | Sample type | NGS | Novel variant? | Mutation class |
|---|---|---|---|---|---|---|---|---|---|---|---|---|---|---|
| Pat3 | f | - | *GPR179* | autosomal recessive | 614565 | p.Thr620del | c.1891-11_1891-9delACT | het | deletion | not found in mother or unaffected sister | blood | Oculome | yes | III |
| Pat7 | m | - | *NYX* | X-linked | 310500 | p.Ser372Arg | c.1122C>G | hem | missense | yes | blood | Oculome | yes | IV |
| Pat16 | m | brother Pat29 | *TRPM1* | autosomal recessive | 613216 | p.Tyr111Cys | c.332A>G | het | missense | yes | saliva | - | yes | III |
| Pat17 | f | - | *TRPM1* | autosomal recessive | 613216 | p.Glu1281Lys, p.Leu682Pro | c.3841G>A, c.1928T>C | hom, hom | 2x missense | both het in mother, no paternal DNA available | blood | WES | yes, yes | IV, IV |
| Pat18 | f | - | *TRPM1*, *GPR179* | autosomal recessive | 613216, 614565 | p.Ile1011Asn, p.Gly1630Gln | c.2915T>A, c.4888G>C | hom, hom | 2x missense | both het in mother and father | blood | WES | yes, yes | IV, IV |
| Pat19 | f | - | *GRM6* | autosomal recessive | 257270 | p.Ala738fs*81, p.Cys522Tyr | c.2219GGAGACCdel ,c.1565G>A | het, het | deletion, missense | yes, compound het | blood | WES | yes, yes | IV, IV |
| Pat20 | f | - | *GRM6* | autosomal recessive | 257270 | p.Val243fs*21, p.Thr177Ile | c.727Gdel, c.530C>T | het, het | deletion, missense | yes, compound het | blood | WES | yes, yes | IV, IV |
| Pat21 | f | - | *GPR179* | autosomal recessive | 614565 | p.Ser329fs*4 | c.984Cdel | hom | deletion | found in father, no maternal DNA available | blood | WES | no [215] | V |
| Pat22 | f | - | *GRM6* | autosomal recessive | 257270 | p.Arg621* | c.1861C>T | hom | missense stop gain | het in father and mother | blood | Oculome | no [168] | V |
| Pat24 | m | brother Pat25 | *NYX* | X-linked | 310500 | p.Arg29_Ala36 del | c.85_108del | hem | deletion | found in mother and affected brother, not in father | saliva | Oculome | no [180] | V |
| Pat25 | m | brother Pat24 | *NYX* | X-linked | 310500 | p.Arg29_Ala36 del | c.85_108del | hem | deletion | found in mother and affected brother, not in father | blood | WES | no [180] | V |
| Pat26 | m | - | *NYX* | X-linked | 310500 | p.Arg124_Leu1 26dup | c.371_379dup | hem | duplication | found in mother, not in father | blood | Oculome | yes | IV |
| Pat27 | m | - | *TRPM1* | autosomal recessive | 613216 | p.Arg941His, p.Cys954Tyr | c.2822G>A, c.2795G>A | het, het | 2x missense | yes, compound het | blood | WES | yes | IV |
| Pat29 | m | brother Pat16 | *TRPM1* | autosomal recessive | 613216 | p.Tyr111Cys | c.332A>G | het | missense | yes | blood | Oculome | yes | III |
| Pat30 | m | - | *TRPM1* | autosomal recessive | 613216 | p.Ala1049Thr | c.3145G>A | hom | missense | het in father, no maternal DNA available | blood | WES | yes | IV |

**Figure 3.4:** Overview over genetic results within the cCSNB subgroup. Zygosity is given as abbreviations: hom - homozygous; het - heterozygous, hem - hemizygous. Results displayed fell within Classes III, IV or V.

| Patient ID | Gender | Relatives | Gene | Inheritance mode | OMIM number | Amino acid change | Nucleotide change | Zygosity | Mutation type | Segregation analysis | Sample type | NGS | Novel variant? | Mutation class |
|---|---|---|---|---|---|---|---|---|---|---|---|---|---|---|
| Pat85 | m | - | *TRPM1* | autosomal recessive | 613216 | p.Ile1041Phe | c.3121A>T | het | missense | found in father, no maternal DNA available | blood | Oculome | yes | III |
| Pat101 | m | - | *NYX* | X-linked | 310500 | p.Leu69Pro | c.206T>C | hem | missense | found in mother, not in father | blood | Oculome | yes | IV |
| Pat116 | m | brother Pat117 | *NYX* | X-linked | 310500 | p.His222_Ser334del | c.1122_1457del | hem | deletion | found in affected brother and affected nephew | blood | external | yes | IV |
| Pat117 | m | brother Pat116 | *NYX* | X-linked | 310500 | p.His222_Ser334del | c.1122_1457del | hem | deletion | found in affected brother and affected nephew | blood | external | yes | IV |
| Pat118 | m | nephew Pat117 & 118 | *NYX* | X-linked | 310500 | p.His222_Ser334del | c.1122_1457del | hem | deletion | found in affected uncles | blood | external | yes | IV |

**Figure 3.5:** Overview over genetic results within the cCSNB subgroup. Zygosity is given as abbreviations: hom - homozygous; het - heterozygous, hem - hemizygous. Results displayed fell within Classes III, IV or V.

| Patient ID | Gender | Relatives | Gene | Inheritance mode | OMIM number | Amino acid change | Nucleotide change | Zygosity | Mutation type | Segregation analysis | Sample type | NGS | Novel variant? | Mutation class |
|---|---|---|---|---|---|---|---|---|---|---|---|---|---|---|
| Pat4 | m | - | *CACNA1f* | X-linked | 300071 | p.Phe582Leufs*5 | c.1742dup | hem | duplication | found in mother, not in father | blood | Oculome | yes | IV |
| Pat6 | m | - | *CACNA1f* | X-linked | 300071 | p.Thr1515Lys | c.4544C>A | hem | missense | found in mother, not in father | blood | Oculome | yes | IV |
| Pat9 | m | - | *CACNA1f* | X-linked | 300071 | p.Arg290Cys | c.868C>T | hem | missense | found in mother, no paternal DNA available | blood | Oculome | yes | IV |
| Pat10 | m | brother Pat11 | *CACNA1f* | X-linked | 300071 | p.Leu1010Pro | c.3029C>T | hem | missense | found in mother and affected brother, not in father | blood | Oculome | yes | IV |
| Pat11 | m | brother Pat10 | *CACNA1f* | X-linked | 300071 | p.Leu1010Pro | c.3029C>T | hem | missense | found in mother and affected brother, not in father | blood | - | yes | IV |
| Pat12 | m | brother Pat13 | *CACNA1f* | X-linked | 300071 | p.Arg625* | c.1876C>T | hem | missense stop gain | found in mother and affected brother, not in father | blood | Oculome | yes | IV |
| Pat13 | m | brother Pat12 | *CACNA1f* | X-linked | 300071 | p.Arg625* | c.1876C>T | hem | missense stop gain | found in mother and affected brother, not in father | blood | Oculome | yes | IV |

**Figure 3.6:** Overview over genetic results within the iCSNB subgroup. Zygosity is given as abbreviations: hom - homozygous; het - heterozygous, hem - hemizygous. Results displayed fell within Classes III, IV or V.

| Patient ID | Gender | Relatives | Gene | Inheritance mode | OMIM number | Amino acid change | Nucleotide change | Zygosity | Mutation type | Segregation analysis | Sample type | NGS | Novel variant? | Mutation class |
|---|---|---|---|---|---|---|---|---|---|---|---|---|---|---|
| Pat14 | m | - | *CACNA1f* | X-linked | 300071 | p.Arg62Gln | c.245G>A | hem | missense | found in mother, no paternal DNA available | blood | Oculome | yes | IV |
| Pat31 | m | - | *CACNA1f* | X-linked | 300071 | p.Glu891Lys | c.2733+1G>A | hem | missense | found in mother, no paternal DNA available | blood | Oculome | yes | IV |
| Pat32 | m | brother Pat33 | *CACNA1f* | X-linked | 300071 | p.Arg961* | c.2881C>T | hem | missense stop gain | found in affected brother, no parental DNA available | blood | Oculome | yes | IV |
| Pat33 | m | brother Pat32 | *CACNA1f* | X-linked | 300071 | p.Arg961* | c.2881C>T | hem | missense stop gain | found in affected brother, no parental DNA available | blood | - | yes | IV |
| Pat34 | m | - | *CACNA1f* | X-linked | 300071 | p.Gly552Trp | c.1715+1G>T | hem | missense | found in mother and unaffected sister, not in father | blood | WES | yes | IV |
| Pat39 | m | - | *CACNA1f* | X-linked | 300071 | p.Asp1031fs*4 | c.3089+2_3089+7delGACG | hem | deletion | found in mother, no paternal DNA available | blood | Oculome | yes | IV |
| Pat42 | m | - | *CACNA1f* | X-linked | 300071 | p.Pro1491Leu | c.4472C>T | hem | missense | - | - | external | yes | IV |

**Figure 3.7:** Overview over genetic results within the iCSNB subgroup. Zygosity is given as abbreviations: hom - homozygous; het - heterozygous, hem - hemizygous. Results displayed fell within Classes III, IV or V.

| Patient ID | Gender | Relatives | Gene | Inheritance mode | OMIM number | Amino acid change | Nucleotide change | Zygosity | Mutation type | Segregation analysis | Sample type | NGS | Novel variant? | Mutation class |
|---|---|---|---|---|---|---|---|---|---|---|---|---|---|---|
| Pat44 | m | - | *CACNA1f* | X-linked | 300071 | p.Ser285_Ala291del | c.854_874del | hem | deletion | found in mother, not in unaffected brother and father | saliva | Oculome | yes | IV |
| Pat45 | m | brother Pat46 | *CACNA1f* | X-linked | 300071 | p.Ile1377Lys | c.4130T>A | hem | missense | found in mother and affected brother, not in brother | blood | Oculome | yes | IV |
| Pat46 | m | brother Pat45 | *CACNA1f* | X-linked | 300071 | p.Ile1377Lys | c.4130T>A | hem | missense | found in mother and affected brother, not in brother | blood | - | yes | IV |
| Pat47 | m | - | *CACNA1f* | X-linked | 300071 | p.Arg447fs | c.1338_1339insT | hem | insertion | - | blood | external | yes | IV |
| Pat48 | m | - | *CACNA1f* | X-linked | 300071 | p.Arg1296Cys | c.3886C>T | hem | missense | - | blood | external | yes | IV |
| Pat54 | m | - | *CACNA1f* | X-linked | 300071 | p.Arg82* | c.244C>T | hem | missense stop gain | found in mother, not in father | blood | Oculome | yes | IV |
| Pat90 | m | brother Pat91 | *CACNA1f* | X-linked | 300071 | p.Arg614* | c.1873C>T | hem | missense stop gain | found in mother and affected brother, not in father | blood | Oculome | yes | IV |
| Pat91 | m | brother Pat90 | *CACNA1f* | X-linked | 300071 | p.Arg614* | c.1873C>T | hem | missense stop gain | found in mother and affected brother, not in father | blood | - | yes | IV |
| Pat102 | m | - | *CACNA1f* | X-linked | 300071 | p.Cys292Tyr | c.875G>A | hem | missense | found in mother, not in father | blood | Oculome | yes | IV |
| Pat109 | m | - | *CACNA1f* | X-linked | 300071 | p.His688Glu | c.2086-1G>C | hem | missense | found in mother, not in father | blood | Oculome | yes | IV |

**Figure 3.8:** Overview over genetic results within the iCSNB subgroup. Zygosity is given as abbreviations: hom - homozygous; het - heterozygous, hem - hemizygous. Results displayed fell within Classes III, IV or V.

| Patient ID | Gender | Gene | Inheritance mode | OMIM number | Exons affected | Zygosity | Mutation type |
|---|---|---|---|---|---|---|---|
| Pat55 | m | *DMD* | X-linked | 310200 | 3-7 | hom | deletion |
| Pat56 | m | *DMD* | X-linked | 310200 | 3-7 | hom | deletion |
| Pat57 | m | *DMD* | X-linked | 310200 | 5-7 | hom | deletion |
| Pat58 | m | *DMD* | X-linked | 310200 | 8-13 | hom | deletion |
| Pat59 | m | *DMD* | X-linked | 310200 | 3-11 | hom | deletion |
| Pat60 | m | *DMD* | X-linked | 310200 | 8-13 | hom | deletion |
| Pat61 | m | *DMD* | X-linked | 310200 | 56-57 | hom | duplication |
| Pat62 | m | *DMD* | X-linked | 310200 | 56-57 | hom | duplication |
| Pat63 | m | *DMD* | X-linked | 310200 | 51-54 | hom | deletion |
| Pat64 | m | *DMD* | X-linked | 310200 | 48-50 | hom | deletion |
| Pat65 | m | *DMD* | X-linked | 310200 | 44 | hom | deletion |
| Pat66 | m | *DMD* | X-linked | 310200 | 51 | hom | deletion |
| Pat67 | m | *DMD* | X-linked | 310200 | 70 | hom | deletion |
| Pat68 | m | *DMD* | X-linked | 310200 | 70 | hom | deletion |
| Pat69 | m | *DMD* | X-linked | 310200 | 70 | hom | nonsense |
| Pat99 | m | *DMD* | X-linked | 310200 | 10-11 | hom | deletion |
| Pat105 | m | *DMD* | X-linked | 310200 | 45 & 52 | hom | deletion |
| Pat119 | m | *DMD* | X-linked | 310200 | 8-21 | hom | deletion |
| Pat121 | m | *DMD* | X-linked | 310200 | 45-50 | hom | deletion |

**Figure 3.9:** Overview over genetic results within the DMD subgroups. Zygosity is given as abbreviations: hom - homozygous; het - heterozygous, hem - hemizygous. These genotypes were previously published in [163].

| Patient ID | Gender | Gene | Inheritance mode | OMIM number | Amino acid change | Nucleotide change | Zygosity | Mutation type |
|---|---|---|---|---|---|---|---|---|
| Pat70 | m | *PMM2* | autosomal recesive | 212065 | p.Pro69Ser, p.Arg141His | c.205C>G, c.422G>A | compound het | 2x missense |
| Pat71 | f | *PMM2* | autosomal recesive | 212065 | p.Pro69Ser, p.Phe157Ser | c.205C>G, c.470T>C | compound het | 2x missense |
| Pat72 | f | *PMM2* | autosomal recesive | 212065 | p.Phe119Leu, p.Arg141His | c.357C>A, c.422G>A | compound het | 2x missense |
| Pat73 | m | *PMM2* | autosomal recesive | 212065 | p.Pro20fs*1, p.Thr237Met | c.124delC, c.710C>T | compound het | deletion, missense |
| Pat74 | m | *PMM2* | autosomal recesive | 212065 | p.Pro69Ser, p.Arg141His | c.205C>G, c.422G>A | compound het | 2x missense |
| Pat75 | m | *PMM2* | autosomal recesive | 212065 | p.Val129Met, p.Thr211Pro | c.385G>A, c.640-9T>G | compound het | 2x missense |
| Pat76 | m | *PMM2* | autosomal recesive | 212065 | p.Arg41His, p.Val231Met | c.422G>A, c.691G>A | compound het | 2x missense |
| Pat77 | m | *PMM2* | autosomal recesive | 212065 | p.Ala108Val, p.Asp48Asn | c.323C>T, c.442G>A | compound het | 2x missense |
| Pat78 | f | *PMM2* | autosomal recesive | 212065 | p.Phe144Leu, p.Gly186Arg | c.430T>C, c.556G>A | compound het | 2x missense |
| Pat79 | m | *PMM2* | autosomal recesive | 212065 | p.Phe144Leu, p.Gly186Arg | c.430T>C, c.556G>A | compound het | 2x missense |
| Pat81 | m | *PMM2* | autosomal recesive | 212065 | p.Phe119Leu, p.Arg141His | c.357C>A, c.422G>A | compound het | 2x missense |
| Pat84 | m | *PMM2* | autosomal recesive | 212065 | p.Val108Met, p.Arg141His | c.691G>A, c.442G>A | compound het | 2x missense |
| Pat93 | m | *PMM2* | autosomal recesive | 212065 | p.Ala108Val, p.Arg123Gln | c.323_324CG>TA, c.368G>A | compound het | 2x missense |
| Pat96 | f | *PMM2* | autosomal recesive | 212065 | p.Ala108Val, p.Arg141His | c.323_324CG>TA, c.442G>A | compound het | 2x missense |
| Pat97 | f | *PMM2* | autosomal recesive | 212065 | p.Ala108Val, p.Arg141His | c.323_324CG>TA, c.442G>A | compound het | 2x missense |

**Figure 3.10:** Overview over genetic results within the PMM2-CDG subgroup. Zygosity is given as abbreviations: hom - homozygous; het - heterozygous, hem - hemizygous. These genotypes were previously published in [238, 216].

#### 3.3.0.1 False positive - *CAPN5*

One cCSNB case analysed by WES did not show a Class IV or V variant in a known CSNB gene. However, two heterozygous missense changes in the gene *CAPN5* - which is located at chromosomal position 11q14 and encodes for the protein calpain 5 - were detected in this patients (Pat24). These variants, resulting in p.Phe32Ser and p.Asp66Gly amino acid changes, were predicted to lead to a compound heterozygous mutation with pathogenicity scores of "probably damaging" and "possibly damaging", respectively[23]. The CAPN5 protein is an intracellular cysteine protease, found in inner and outer segments of photoreceptor cells, with a yet unknown physiological function. Previously, photoreceptor degeneration was found to be associated with excess calpain activity [270]. A mutation in *CAPN5* had not been linked to CSNB before, however, a negative ERG phenotype was reported [271]. Hence, *CAPN5* was suggested as a potential novel gene implicated in cCSNB.

However, the mutations detected by WES could not be validated by Sanger sequencing. Following this, the original raw data files were revisited and re-analysed and indeed this was found to be a false positive result originating from low quality variant calls creating an artefact. Following this, a further potential variant was detected in the patient after analysing the DNA of the patients affected brother (Pat25) via the Oculome. The brother showed a previously described deletion of 34 base pairs in the *NYX* gene, encoding for nyctalopin (c.85_108del). The *NYX* mutations in both brothers were subsequently confirmed by Sanger Sequencing.

### 3.3.1 Unsolved cases

Despite the WES and gene panel approaches, for some of the patient samples sequenced no phenotype causing variant could be detected in any known CSNB gene or any other retinal disease gene[24]. These unsolved cases are listed in Table 3.4 and are candidates for future genetic analysis.

[23] These scores were obtained using PolyPhen: www.genetics.bwh.harvard.edu/pph2

[24] The gene panel also took into account the most recent findings of patients with CSNB showing bi-allelic mutations in the gene GNB3 [191]. Apart from Pat8, none of these patients showed any Class III variants in a retinal gene.

In Pat8, a possible novel heterozygous missense mutation in *PDE6B* was detected, leading to AD CSNB. The patient's a-wave was preserved to standard and maximal flashes and only slightly reduced under light-adapted conditions, resulting in an overall electronegative ERG waveform, not necessarily indicating the Riggs-type ERG usually observed in patients with PDE6B mutations. However, his ERG recordings were heavily affected by muscle artifacts and hence, Sanger sequencing was carried out on this sample, in order to assess whether this proposed disease-causing mutation was present in the patient. The variant could be detected and validated in the patient but not in the mother, making a de-novo mutation of this gene a possibility. No genetic or phenotypical information on the father was available. The patient was the only affected individual in the family.

Future analysis is needed to identify new candidate disease causing genes via Whole Exome Sequencing or by submission to Genomics England (GEL) for Whole Genome Sequencing (WGS) as part of the 100,000 Genomes Project[25]. These steps will optimistically lead to a genetic diagnosis for these patients and give a clearer picture of their conditions and inheritability.

| Study ID | Gender | Clinical diagnosis | Possible variants detected |
|---|---|---|---|
| Pat5 | m | ?CSNB | ? |
| Pat111 | f | ?CSNB | ? |
| Pat15 | m | iCSNB | ? |
| Pat8 | m | iCSNB | *PDE6B* (AD CSNB, Class III): p.Asn15Thr, c.44A<C |

**Table 3.4:** Overview over genetic results of unsolved cases. All patients were investigated using the targeted gene panel approach (The Oculome).

[25] www.genomicsengland.co.uk

## 3.4 Summary and Conclusion

### 3.4.1 Summary

- Of 75 individuals with a subtype of CSNB in the patient cohort, 48 had genetic testing carried out. Class IV and V variants identified were verified by Sanger Sequencing (n= 28 Oculome, n= 9 GOSgene, n= 6 externally, n=5 affected siblings with only Sanger sequencing verification). Of these, 44 now have a genetic diagnosis (92%) and the results were reported to their clinical care team:
  - 20 patients with cCSNB (genes: *GRM6, GPR179, TRPM1, NYX*)
  - 24 patients with iCSNB (gene: *CACNA1f*)
  - Four patient samples from the CSNB subgroup did not yield a result from sequencing. These are considered for future WES with GOSgene or WGS with Genomics England.
- Patients from the DMD (n= 19) and PMM2-CDG (n= 15) subgroups already had published genotypes [238, 216, 163].

| Subgroup | Patients in subgroup | Patients sequenced in this study | Genotype confirmed |
|---|---|---|---|
| cCSNB | 33 | 22 | 20 |
| iCSNB | 42 | 26 | 24 |
| DMD pre exon 30 | 8 | - | 8 |
| DMD post exon 30 | 11 | - | 11 |
| PMM2-CDG | 15 | - | 15 |

**Table 3.5:** Summary of patient numbers with genetic analysis carried out across subgroups. Genotypes were confirmed by Sanger sequencing verification of predicted variants from NGS, or were taken from previously published data.

### 3.4.2 Conclusion

The patient cohorts investigated in this study comprise a varied overview of the impact a dysfunctional ON-pathway can have in different rare diseases involving the visual system. Getting a full correlation of genetic makeup and clinical visual phenotype of patients with ON-pathway dysfunction gives a more complete understanding of the proteins and processes involved in retinal signal transmission. Whereas all individuals within the iCSNB group were found to have underlying mutations in *CACNA1f*, the genetic results in the cCSNB group were more diverse. Here, mutations in four different genes previously linked to the autosomal recessive and X-linked forms of cCSNB were detected (*TRPM1, GRM6, GPR179* and *NYX*). The ratios of gene mutation prevalence in cCSNB agree with those reported by Zeitz and colleagues, with *NYX* and *TRPM1* variants being more frequently detected in individuals with cCSNB than *GRM6* or *GPR179*, and mutations in *CACNA1f* being the main cause for iCSNB [166]. These genetic data correlated well with the clinical diagnoses of patients with cCSNB and iCSNB.

Four patients with a clinical diagnosis of cCSNB only showed a single heterozygous change in *TRPM1* (Pat19, 26 and 85) or *GPR179* (Pat3). The Oculome targeted gene panel approach is not sensitive to detect intronic or long range changes in genes, such as copy number variations (CNV). Hence, such a CNV in the other allele of the affected gene could account for the phenotypes encountered in these patients. Although CNV analysis was performed for those patients, no such structural variations were detected in these samples. While there is no literature on a heterozygous mutation in *GPR179* causing autosomal dominant cCSNB, there is one report suggesting autosomal dominant cCSNB in one family due to a heterozygous mutation in *TRPM1* [217]. Supporting these findings is the heterozygous *TRPM1* mouse model Trpm1$^{+/tvrm27}$ which shows reduced ERG b-wave amplitudes in dark-adapted conditions [197]. Autosomal dominant cCSNB due to single heterozygous variants can therefore not be excluded and requires further investigation of the genotypes of family members. Until such future investigation has been carried out, these patients are without a clear genetic diagnosis.

Genotype analysis was performed covering all known genes in all patients who carried out a conventional electrophysiological test or at least one of the novel ON-pathway vision assessments, apart from cases where DNA samples were not available. By using an efficient genotyping approach, a success rate of 92% solved cases was achieved, i.e. 44 out of 48 patients in the CSNB cohort received a genetic diagnosis which was confirmed using Sanger sequencing. Out of the pathogenic variants detected, a majority was not previously described, with only 18% of variants (9 out of 49) found being already published.

Genetic testing of patients with an ON-pathway deficit is vital for further clinical investigation of individual patients and the care provided to affected families. Being able to differentiate ON-pathway dysfunction from progressive retinal dystrophies with similar phenotypic features - for example, retinitis pigmentosa which can cause night blindness and may initially manifest with normal or near-normal fundus appearance - can exclude the possibility of significant disease progression and therefore impact greatly on the management of the patient. Furthermore, molecular diagnosis of the underlying genetic defect in many cases facilitates counselling by informing patients and their families of the inheritability of the condition. From a clinical research standpoint, in the case of ON-pathway dysfunction, several key players associated with best visual outcome are still unknown. This is evident by not having been able to detect any viable pathogenic variant in a small part of the patient cohort.

A further insight into the functional consequences of genetic mutations affecting vision can be acquired through the linkage of genetic make-up of a patient with his / her clinical visual phenotype[26]. For this, informative and accurate visual testing is indispensable. One way of acquiring information on the physiological integrity of the visual pathways is by electrophysiological testing, which is discussed in the following chapter.

[26] A genotype-phenotype correlation of the patient data acquired in this study is given in Chapter 6 and further discussed in Chapter 7.

Chapter 4

# Electrophysiological test battery

## 4.1 Systematic review of clinical pVEPs

The pVEP is a conventional electrophysiological test which is carried out routinely in patients with visual symptoms to assess visual pathway integrity. Despite their value in clinical diagnostics, there is little literature on VEP recordings in patients with ON-pathway dysfunction. If a dysfunctional ON-pathway led to abnormal ganglion cell firing and subsequent altered arrival of retinal signals at the visual cortex, could such abnormalities already affect the conventional pVEP? As the pVEP is the most commonly used electrophysiological stimulus in the clinical setting [272], the majority of patients in the ON-pathway dysfunction cohort had a pVEP recorded at 50' check size. Thus, it was decided to investigate whether the pVEP could provide an objective measure of ON-pathway dysfunction, by giving an initial insight into the signal arrival at the visual cortex in these patients.

The rationale for this analysis stemmed from previous reports of abnormal signalling on the level of the retinal ganglion cells and the LGN in mouse models of ON-pathway dysfunction [158, 156, 157]. If such abnormal signalling at the level of the thalamus was caused by a retinal ON-pathway dysfunction in humans, this might be detectable in the cortical VEP. Indeed, there are three reports of altered VEP waveforms in patients with a dysfunctional ON-pathway, mentioning but not detailing prolonged P100/C1 components to pattern VEP stimulation [273, 79, 274] in patients with CSNB. Only one of these studies mentions pattern reversal VEP times to peak around the 125ms mark in three patients with (a not further defined type of) CSNB [274]. For DMD and PMM2-CDG, there was even less conclusive evidence to be found in the literature. The only accounts are describing ”reduced VEP responses” but lack any presentation of the actual VEP data (PMM2-CDG [211, 275]) or a ”trend of increasing VEP latency” (DMD [276]). None of these studies comprehensively and systematically investigated the effects of ON-pathway dysfunction on the pVEP waveform. In order to investigate this, the clinical pVEP P100 component was retrospectively analysed in a cohort of 109 patients with ON-pathway dysfunction.

### 4.1.1 Results

All pattern reversal VEP waveforms of patients in the ON-pathway dysfunction cohort from the visual electrophysiology database of GOSH (n=109) were probed and their P100 components analysed. Figures 4.1 and 4.2 show the P100 times to peak and amplitudes for individual patients across the clinical subgroups, previously identified by the ERG to have a dysfunctional ON-pathway at the retinal level. In view of P100 time to peak being a more robust measure when comparing across individuals, the definition of ”abnormality” was applied if a subject's P100 time to peak fell outside of the 95th percentile of the clinical reference range or if the patients showed a non-measurable response at a checksize of 50'.

Both, the cCSNB and iCSNB groups showed markedly delayed times to peak when compared to the other conditions, with some data points falling well outside of the 95th percentile of the clinical reference range. The group mean of patients with iCSNB even proved to be significantly delayed when compared to the clinical reference range (One-way ANOVA with post-hoc Tukey means comparison: $p= 0.002$). This can be indicative of an affected signal transmission along the optic nerve and disrupted post-retinal visual processing. Further, one patient with PMM2-CDG fell outside the clinical normative data range for P100 time to peak. The overall amplitude differences were less distinct but all subgroups showed a marginally lowered amplitude when compared to healthy controls. However, most of the patients still fell within the clinical reference range.

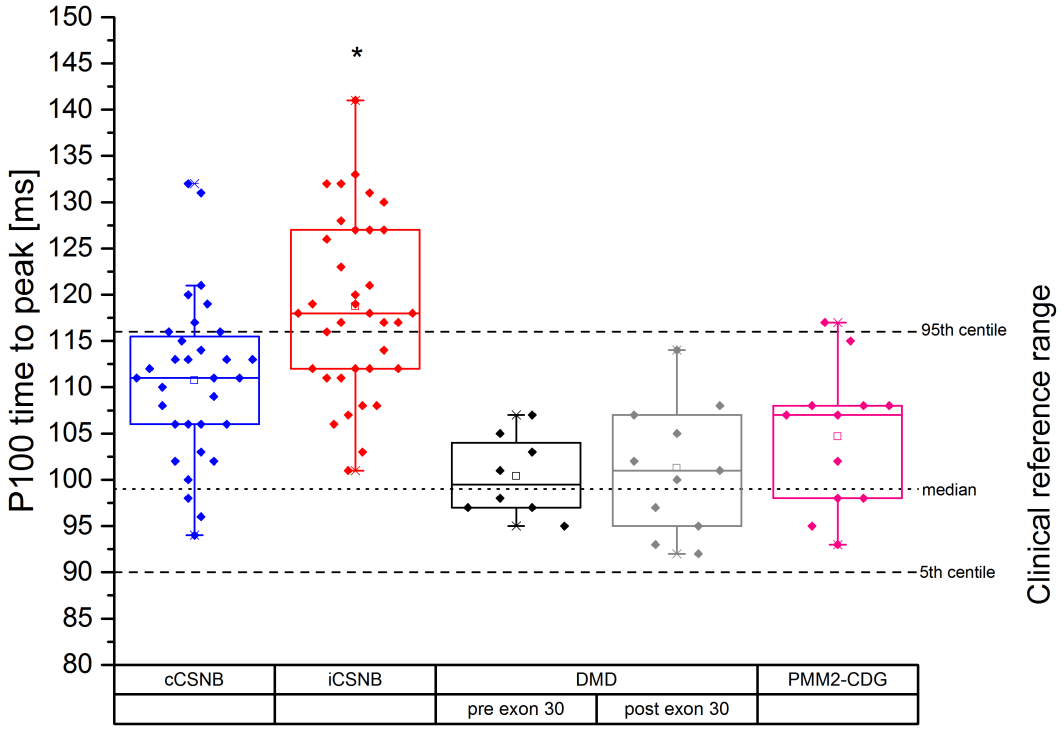


**Figure 4.1:** The P100 time to peak of individual patients is plotted across all clinical subgroups. The 5th and 95th centile, as well as the median of the GOSH laboratory clinical reference range are indicated by black bars. Diamond symbols indicate individual patients (blue = cCSNB, red = iCSNB, black = DMD pre exon 30, grey = DMD post exon 30, pink = PMM2-CDG). Boxes give Max and Min (-), Mean (square), Median (border inside the boxes), 99% and 1% (x), as well as 75% and 25% (margins of the boxes) percentiles. Statistical significance is indicated by an asterisk (One-way ANOVA with post-hoc Tukey means comparison: p= 0.002).

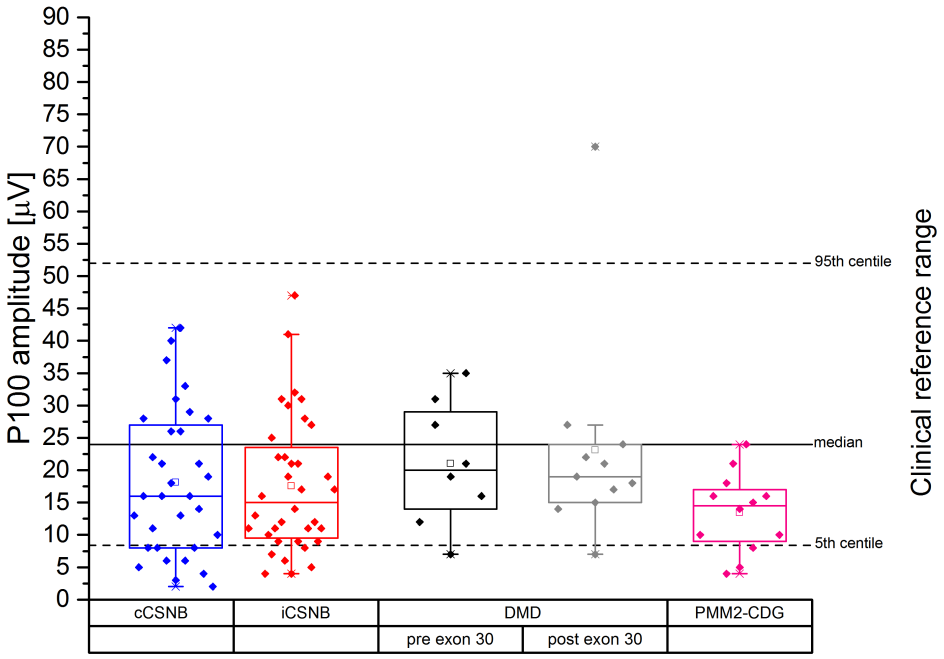


**Figure 4.2:** The P100 amplitude of individual patients is plotted across all clinical subgroups. The 5th and 95th centile, as well as the median of the GOSH laboratory clinical reference range are indicated by black bars. Diamond symbols indicate individual patients (blue = cCSNB, red = iCSNB, black = DMD pre exon 30, grey = DMD post exon 30, pink = PMM2-CDG). Boxes give Max and Min (-), Mean (square), Median (border inside the boxes), 99% and 1% (x), as well as 75% and 25% (margins of the boxes) percentiles.

The number of individuals in each subgroup with an abnormal pVEP response to a checksize of 50' is displayed in Table 4.1. The highest fraction of individuals with abnormal pVEP was observed in the iCSNB subgroup (29/42 = 69%), followed by the cCSNB subgroup (9/33 = 27%). The remaining clinical subgroups did either not show any individual with an abnormal pVEP time to peak to 50' checks (DMD) or only one (PMM2-CDG).

| Subgroup | n | delayed P100 time to peak | small P100 amplitude | response not measurable |
|---|---|---|---|---|
| cCSNB | 33 | 8 | 9 | 1 |
| iCSNB | 42 | 24 | 6 | 5 |
| DMD pre-exon 30 | 8 | 0 | 1 | 0 |
| DMD post-exon 30 | 11 | 0 | 1 | 0 |
| PMM2-CDG | 15 | 1 | 3 | 0 |
| total | 109 | 33 | 20 | 6 |

**Table 4.1:** Number of subjects with abnormal pattern reversal VEP responses (including abnormal amplitude) to 50' checks across study groups.

#### 4.1.1.1 Potential limitations

A potential limitation of the pVEP data shown is the presence of nystagmus in some patients. Nystagmus has been linked to degraded pVEP waveforms in the past, mostly explained by a blurring of the retinal image affecting the waveform. In order to investigate this possible influence, Hoffman and colleagues induced retinal image motion mechanically by using a mirror and observed degrading effects on pVEP amplitude but not time to peak of this induced nystagmus [264]. Arlt and colleagues also reported a reduction of pVEP amplitude associated with nystagmus; likewise, they did not observe a significant shift in peak time to peak [277]. The only account of a potential influence of nystagmus on VEP peak time to peak comes from Saunders and colleagues (1997). The authors observed slightly prolonged onset peaks in patients with nystagmus, however, these were overall not significant [278].

Despite a line of evidence suggesting a degrading effect of nystagmus on the pVEP amplitude, the peak time to peak of the P100 component does not seem to be affected. Additionally, data acquired with colleagues at GOSH confirm normal pVEP responses in children with retinal dysfunction and nystagmus [279]. For this evaluation, the pVEP results of 287 patients presenting with nystagmus at the GOSH Ophthalmology Department were audited, of whom 29% had chiasmal defects, 23% a type of retinal dystrophy (like CSNB or cone dystrophy), 24% no recognised sensory visual pathway defect (congenital idiopathic nystagmus), 9% were born prematurely, 4% had Trisomy 21, and the remaining 11% showed other ocular abnormalities. Of these patients, 38% (n=108) produced completely normal pVEP waveforms to 50' checks[1]. These findings support the data reported here in the patient subgroups with ON-pathway dysfunction, showing that it is possible to reliably record pVEP responses even in the presence of nystagmus. Hence, a delayed P100 component can indicate an effect of signalling dysfunction on the pVEP, independent of nystagmus.

[1]Of these, n= 44 (41%) were diagnosed with congenital idiopathic nystagmus. In total, this resulted in 64% of patients with nystagmus but without a recognised sensory visual pathway defect showing normal VEP times to peak.

### 4.1.2 Conclusion

Abnormalities in the time to peak and amplitude of the conventional pattern reversal VEP to 50' checks, consistent with disorganised ganglion cell firing, were found in patients with retinal ON-pathway disruption, specifically in patients with the incomplete and complete types of CSNB. As anticipated, the data indicate an effect of ON-pathway signal transmission dysfunction on the VEP waveform obtained from the scalp overlaying the visual cortex. This effect was observed in patients independent of nystagmus.

Sixty-eight percent of patients with iCSNB showed abnormal pVEP responses to 50' checks. The apparent link of an abnormal VEP time to peak to this subtype of CSNB has not been reported before. In iCSNB, both, the rod and the cone systems are affected presynaptically. As the pVEP is macula dominated, and this area of the retina is rich in cones, an effect of such a disruption on ON and OFF ganglion cell firing could be expected. Notably, this disorder is not described as a selective ON-pathway dysfunction by some authors, but rather a dysfunction of both, the ON-and OFF-pathways[2]. Pattern reversal VEP abnormalities were also observed in the cCSNB subgroup: 27% of subjects with cCSNB showed abnormal P100 times to peak. In contrast, individuals with DMD did not show such VEP abnormalities and only one PMM2-CDG patient displayed a slightly delayed P100.

Despite the fact that all individuals in the patient cohort displayed an ON-pathway dysfunction at the retinal level (as initially detected via the ERG), major differences in VEP waveforms between the subgroups were detected and not all patients with a dysfunctional ON-pathway showed abnormal P100 timing. In total, the conventional pVEP test only shows a sensitivity of 37%, i.e. abnormal pVEP waveforms in 39/109 patients with ON-pathway dysfunction[3]. Presuming that an ON-pathway dysfunction causes abnormal retinal signalling, in order to reduce the amount of false-negative results encountered when using the conventional clinical

[2]A recent study on the effects of CSNB on visual performance in dim light conditions even suggested the use of a different nomenclature for iCSNB ("photoreceptor synapse deficiency") [164].

[3]This number excludes any patients with amplitude abnormalities, as this could potentially be influenced by the prevalence of nystagmus in the patient cohort, as well as due to a generally higher inter-subject variability of P100 amplitudes in pVEP recordings.

pVEP tests in patients, more sensitive clinical electrophysiological tests were required. These were designed to selectively stimulate the ON-and OFF-pathways and hence be able to pick up and further delineate cortical signalling abnormalities in the patient subgroups.

## 4.2 Novel electrophysiological test battery

The analysis of pattern reversal VEPs in a cohort of patients with ON-pathway dysfunction primarily revealed abnormalities in subgroups of patients with CSNB. In order to further expand these findings, VEP stimuli were designed to selectively probe and distinguish contributions of ON-and OFF-pathways in order to achieve a physiological measure with a potentially higher sensitivity of detecting abnormalities in visual cortical processing due to retinal ON-pathway dysfunction.

Nystagmus is frequently seen in patients with a dysfunctional ON-pathway, which can make the electrophysiological recording to pattern reversal stimuli challenging. Although a pVEP with normal time to peak can be recorded even in the presence of nystagmus [279, 277], it would be advantageous to exclude nystagmus as a possible confounding factor for VEP recordings. In such cases, pattern onset stimulation can give an insight into visual pathway function [278, 264].

ON-and OFF-pathways in the visual system convey the perceptions of light increment and decrement to the visual cortex [32]. In primates, a pharmacological blockade of the ON-pathway using APB, results in impairment of light increment perception, as well as loss of contrast sensitivity [280]. Hence, the potential of incremental and decremental "pedestal" pattern onset stimulation was explored, in view of investigating and functionally distinguishing ON-and OFF-pathway contributions to optic pathway function in healthy controls. These raised pedestal checkerboard stimuli represent the most robust, largest luminance change from a black or white background. They were included to investigate the reports from primates that a block of the ON-pathway affects perception of light increment whilst perception of light decrement is unaffected [281].

Similarly, an impairment in the perception of positive contrast stimuli due a pharmacological block of the ON-pathway was previously reported in non-human primates [280]. Positive and negative contrast are processed independently and differentially in the visual system [282, 283] via ON-and OFF-pathways [284]. Isolated check VEP stimulation offers a method of graded contrast change from a grey background to distinguish ON-and OFF-pathways [285], and such stimuli have been

applied clinically in patients with Retinitis Pigmentosa (RP) [286] and as a diagnostic tool for glaucoma [287]. Additionally, there are three clinical case reports of abnormal isolated check onset VEPs in patients with suspected ON-pathway dysfunction, one due to an atypical type of CSNB and two due to Melanoma Associated Retinopathy (MAR) [288, 289].

Hence, a novel set of two electrophysiological pattern onset stimuli was designed with the aim of emphasising responses from ON-and OFF-pathways selectively. One set consisted of a pedestal onset VEP stimulation introducing light increment and decrement to checkerboard pattern stimulation by using black and white backgrounds. The other aimed to bias cortical ON-and OFF-pathway responses by using positive and negative contrast isolated check stimuli[4].

By introducing opposing stimulation in order to highlight contributions to the VEP from ON and OFF systems, I was aiming at investigating a possible asymmetry in ON-and OFF-pathway signalling from retina to the visual cortex in patients. Ultimately, these specialised electrophysiological tests may present a viable and more sensitive alternative in patients with ON-pathway dysfunction who also have nystagmus. In order to validate this novel electrophysiological test battery, the stimuli were first probed in a cohort of healthy volunteers.

[4] An overview of the test stimuli used with the testing protocol is given in Figures 4.4 and 4.5 and a summary at the end of Section 4.2.1.

### 4.2.1 Methods

PARTICIPANTS. Pattern onset VEP responses were recorded from 50 healthy subjects (median age 24.5 years, range: 6 to 72 years, VA range with both eyes viewing: -0.275 to + 0.25 logMAR). For the recordings subjects were refracted as needed for best corrected vision outcome. The research followed the tenets of the Declaration of Helsinki. Informed consent was obtained from the subjects after explanation of the nature and possible consequences of the study. The research was approved by the Research Ethics Committee, NRES Committee London South East (REC number 14/LO/2136).

ELECTRODE PLACEMENT. Pattern onset and reversal VEPs were recorded from an occipital array referred to Fz. An EEG was recorded from the scalp overlaying the visual cortex (active electrode positions: O2, Oz, O1, P3, Pz, P4, Inion, reference: Fz, ground: T3) following the international 10-20 EEG electrode placement system. Responses were recorded with both eyes viewing.

SPECIFICATIONS. Visual evoked potentials were recorded as continuous EEG files using Neuroscan 4.2 software (Compumedics Ltd. Victoria, Australia). Amplifiers were set to an A/D rate of 1000 and had a band pass filter of 0.5 to 100Hz. For stimulus generation, the Stim2 software was used (Compumedics Ltd. Victoria, Australia). The stimulus generation software sent out a trigger every time the stimulus was displayed to allow subsequent offline analysis of the continuous EEG file via epoching and averaging. One epoch was defined as the time range from 15ms pre-stimulus/trigger until 500ms post-stimulus/trigger in order to capture all relevant components of VEP waveforms. An online artifact rejection was enabled for all responses outside of +-150 $\mu$V amplitude, responses with amplitudes falling outside of this range were rejected automatically. For each subject 150 accepted sweeps were recorded for each VEP testing condition. In order to distinguish the small recordings from noise, the mean noise level encountered in all subjects was retrieved by measuring the waveforms' mean deflection from zero over a period of 10ms pre-stimulus. Subsequently, the 95% Confidence Interval (CI) was calculated for these values. For the VEP recordings, the mean noise level was 0.93 $\mu$V

with a 95% CI ranging from 0.55 $\mu$V to 1.29 $\mu$V; however, to obtain more robust values, the cut-off limit was doubled achieving a supra-threshold level. The VEP components therefore needed to have an amplitude of at least 2.58 $\mu$V.

STIMULI. The clinical pattern reversal VEP stimulus consisted of a simple checkerboard pattern which phase-reversed with a frequency of 3 Hz. The display contained an equal number of black and white checks with a check side length of 50'. An example of the stimulus is shown in Figure 4.3.

Light increment and decrement stimuli were black and white checks of side length 60' and 88% Michelson spatial contrast appearing in a stimulus field within a bright 110 cd/m$^2$ surround of 87x62°. In the light increment/decrement condition, each subject was presented with one of three backgrounds: (1) White background (mean luminance 110 cd/m$^2$); (2) Grey background (mean luminance 48 cd/m$^2$); (3) Black background (mean luminance 7 cd/m$^2$) for 1000ms after which a checkerboard stimulus of the same size covered the same area for 200ms. An example of the stimuli used is given in Figure 4.4. Isolated check stimuli were isolated squares with either positive or negative contrast of different magnitudes (either 50% or 20% Michelson temporal contrast) relative to the mean grey background and surround (mean luminance 48 cd/m$^2$). In this study, a maximum contrast stimulus at 50% Michelson contrast was used, alongside stimuli with a 20% Michelson contrast, because it was reported that at this level, the conventional pVEP amplitude is reduced significantly [290, 291] and the influence of temporal stimulus contrast on ON-and OFF-pathway responses was of interest.

The inter-check spacing was kept constant corresponding to the width of a check. The isolated check VEPs were recorded by presenting interleaved positive (white: 110 cd/m$^2$) and negative (black: 7 cd/m$^2$) contrast checks of side length 60' for 200ms after which the stimulus disappeared into a mean grey background of 48 cd/m$^2$ for 1000ms. The checks of 20% Michelson contrast produced a luminance of 75 cd/m$^2$ (positive) and 31 cd/m$^2$ (negative), respectively. An example of the stimuli used is given in Figure 4.5.

All stimuli were arranged in a square 16° field, presented on a plasma display

panel and viewed at 1m. The inter-stimulus-interval (ISI) for all stimuli was chosen based on removing any potential visual adaptation processes affecting subsequent waveform size after repeated stimulation [154]. The resulting onset VEP waveforms were evaluated and the amplitude and time to peak of the main peaks and troughs measured. In cases where C1-C2-C3 morphology of the onset VEP waveform was not evident, the first main positive peak was taken as C1. In cases where C1 was not identified but a major negative C2 was prominent, the time point at the beginning of the C2 descent from baseline was taken as C1 time to peak with an amplitude of zero.

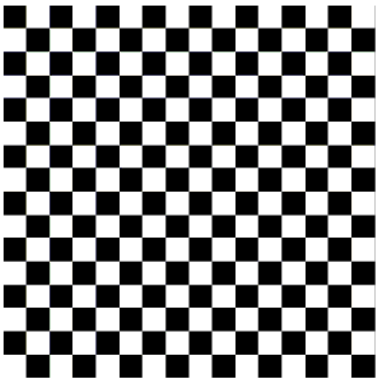

**Figure 4.3:** Example of the pattern reversal VEP stimulus: A black and white checkerboard that reverses its contrast three times per second. The check side length was 50'.

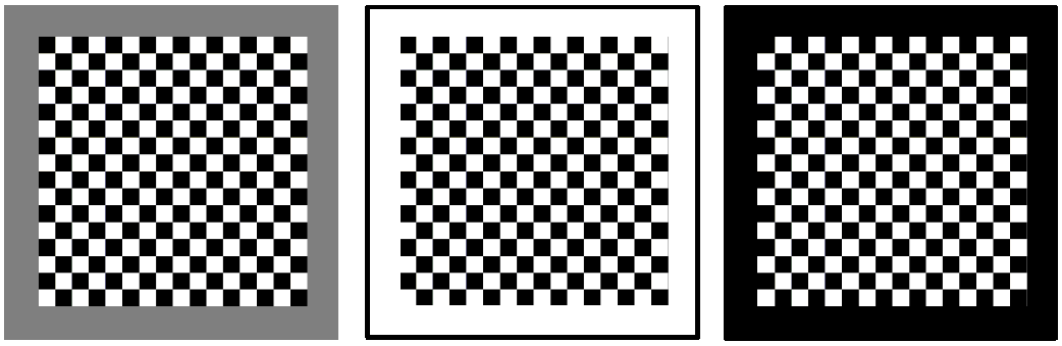

**Figure 4.4:** Examples of the Onset VEP test stimuli: Checkerboard pattern on grey background (clinical equivalent), on white background (negative contrast) and on black background (positive contrast). All stimuli are applied with a check side length of 60' presented at a viewing distance of 1m. These are displayed for 200ms followed by 1000ms of background.

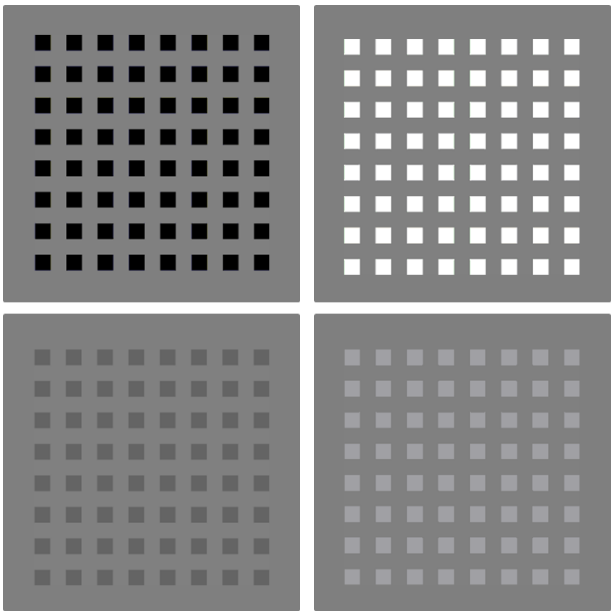

**Figure 4.5:** Examples of the Isolated check stimuli: Pictures on the left display an overview over the negative contrast stimuli for 50% and 20% contrast, while the ones on the right display the positive contrast stimuli. The stimuli consist of a 8x8° field of squares of 60' side length presented at a viewing distance of 1m. The stimuli were displayed for 200ms followed by 1000ms of a mid-grey background. Positive and negative contrast stimuli of the same contrast level were interleaved during the isolated check test.

In summary, the electrophysiological test battery included:

- Pattern reversal stimulation (clinical test equivalent)
- Pedestal pattern onset stimulation
    1. Checkerboard appearing from black background (light increment)
    2. Checkerboard appearing from white background (light decrement)
    3. Checkerboard appearing from grey background (clinical test equivalent)
- Isolated checks as a function of contrast
    1. Isolated checks of 50% positive and negative contrast
    2. Isolated checks of 20% positive and negative contrast

The protocol used during a recording session is shown in Figure 4.6.

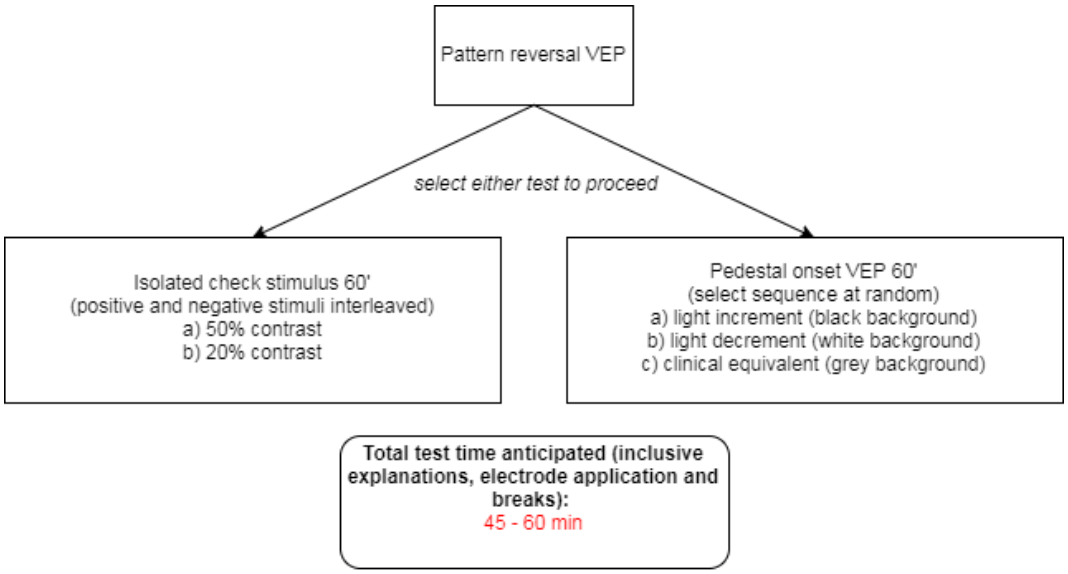


**Figure 4.6:** The testing protocol followed for VEP recordings.

## 4.3 Results

### 4.3.1 Healthy volunteers show similar VEP waveforms to ON- and OFF-pathway stimulation

In order to functionally distinguish ON-and OFF-pathways, pattern onset VEPs were recorded to stimuli arising from a black background (light increment) and a white background (light decrement), respectively; as well as to positive and negative contrast isolated check stimulation. The stimuli were initially validated in ten participants as a proof of concept. Reliable pattern onset VEP waveforms were recorded from all subjects to all conditions. Although the VEP waveforms varied across subjects and with age, within a healthy individual there was good concordance between waveforms produced by patterns appearing due to light increment and decrement (Figure 4.7), as well as to positive and negative contrast stimulation (Figure 4.8). In view of this, it was initially decided to analyse the waveform shape and timing by calculating the Correlation Coefficient (CC) for each subject. This would allow to capture a more appropriate reflection of waveform shape and similarity compared to a conventional single component analysis. For this, the waveform behaviour and shape was correlated over a time period of 400ms by comparing two corresponding points from the light increment and decrement (or positive and negative contrast) conditions per millisecond. Hence, the similarity of both responses was calculated with a resolution of 400 points (1 point/ms). Resulting from this, the overall group mean CC for the light increment/decrement stimuli was 87% (Table 4.2). For the isolated check VEPs, the CC was even higher at 91% for the 50% Michelson contrast condition and 90% for the 20% Michelson contrast condition (Table 4.3).

Upon exploring the results in more detail, it seemed that in children, the CC was higher than in adults, however, following statistical analysis, this was neither significant for the light increment/decrement condition, nor for the isolated check VEPs (One-way ANOVA and post-hoc Tukey means comparison: 50%: p= 0.306, 20%: p=0.177, Pedestal onset: p=0.088) at either contrast (Figure 4.9).

Overall, the waveforms obtained from children were less variable than in

adults, with all of them showing a big positive first peak followed by a negativity. The waveform of the pattern onset VEP matures and becomes more complex with age and continues to eventually differentiate into the three clear components C1:C2:C3 by around 45years [101]. Some young adult subjects showed similar looking waveforms to children, others displayed more complex responses. The early peaks (C1) were the most similar when produced by light increment and decrement, as well as positive and negative contrast stimulation. This was supported by the finding that a higher group CC (90% for light increment/decrement stimulation, as well as 95% and 93% for isolated check stimulation to 50% and 20% Michelson contrast, respectively) was achieved when only analysing a duration of 200ms from stimulus onset focusing on the timing of the first positive peak.

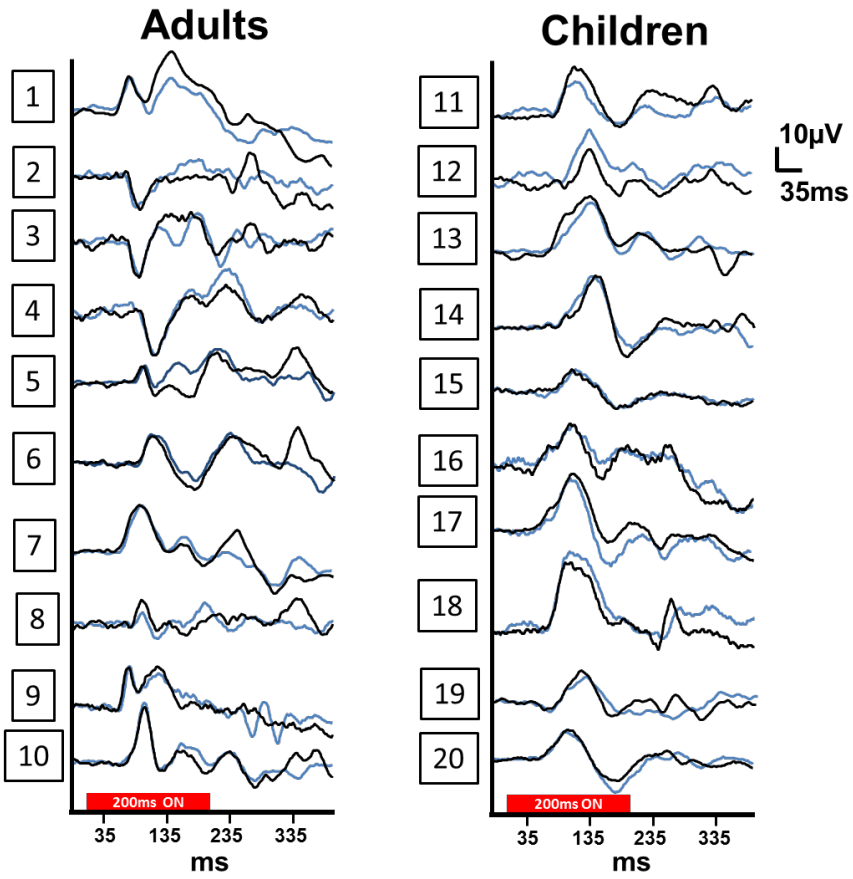


**Figure 4.7:** Pedestal Pattern Onset VEPs elicited with light increment (blue) and light decrement (black) stimulation are overlaid for comparison. Each trace is an average of 150 sweeps recorded from Pz.

| Subject | Correlation Coefficient [%] including 95% CI | Subject | Correlation Coefficient [%] including 95% CI |
|---|---|---|---|
| 1 | 75 (66-82) | 11 | 96 (95-97) |
| 2 | 96 (95-98) | 12 | 94 (91-96) |
| 3 | 60 (47-70) | 13 | 98 (97-99) |
| 4 | 88 (83-91) | 14 | 98 (97-99) |
| 5 | 42 (26-56) | 15 | 84 (78-87) |
| 6 | 89 (85-93) | 16 | 87 (82-91) |
| 7 | 92 (88-94) | 17 | 98 (97-99) |
| 8 | 99 (98-99) | 18 | 99 (98-99) |
| 9 | 80 (73-86) | 19 | 77 (69-84) |
| 10 | 86 (80-90) | 20 | 96 (93-97) |
| Mean CC (range) | 81 (42-99) | Mean CC (range) | 93 (77-99) |

**Table 4.2:** Correlation coefficients (CC) of pedestal Pattern Onset VEP waveforms over 400ms are shown for individual subjects. Values represent the percentage of correlation for waveforms obtained to light increment and decrement, as well as the 95% confidence interval (CC). The closer this value is to 100, the more similar are the two waveforms.

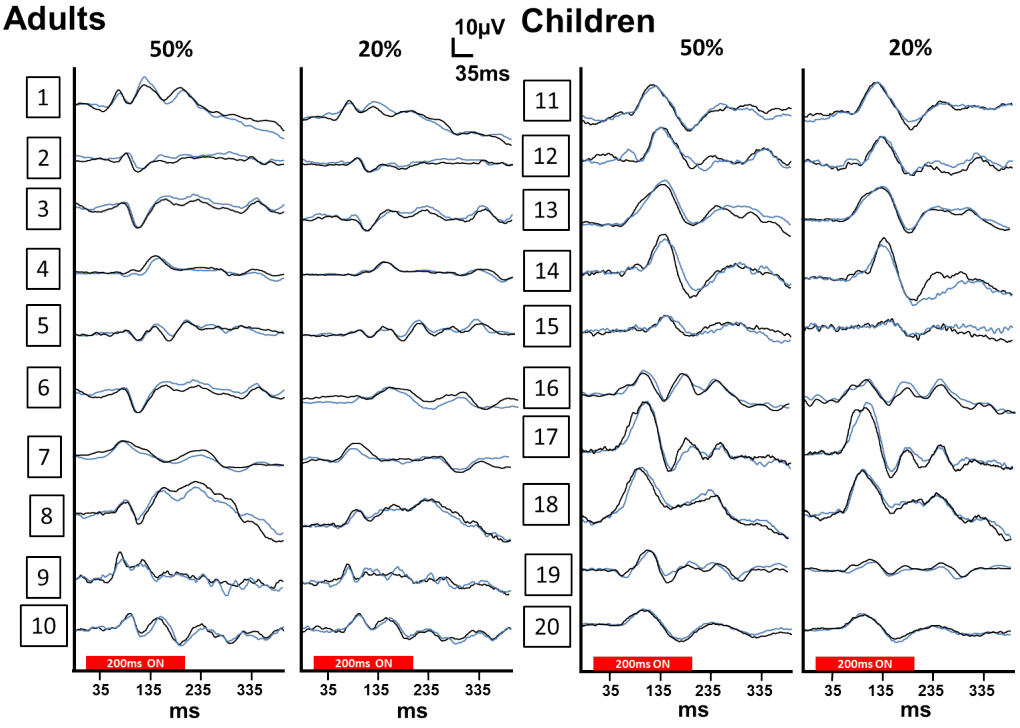


**Figure 4.8:** Isolated check VEPs elicited with positive (blue) and negative (black) contrast stimulation are overlaid for comparison to 50% and 20% Michelson contrast. Each trace is an average of 150 sweeps recorded from Pz.

| Subject | Correlation Coefficient [%] including 95% CI | | Subject | Correlation Coefficient [%] including 95% CI | |
|---|---|---|---|---|---|
| Adults | 50% | 20% | Children | 50% | 20% |
| 1 | 94 (93-96) | 92 (90-94) | 11 | 96 (95-97) | 96 (94-97) |
| 2 | 94 (91-96) | 72 (62-80) | 12 | 95 (92-96) | 97 (96-98) |
| 3 | 99 (98-99) | 90 (87-93) | 13 | 93 (90-95) | 97 (96-98) |
| 4 | 85 (79-89) | 97 (95-98) | 14 | 94 (92-96) | 99 (98-99) |
| 5 | 81 (75-87) | 81 (73-87) | 15 | 85 (80-90) | 95 (93-97) |
| 6 | 81 (74-87) | 75 (67-82) | 16 | 90 (86-93) | 91 (87-93) |
| 7 | 95 (91-96) | 93 (86-94) | 17 | 96 (95-97) | 93 (90-95) |
| 8 | 92 (89-95) | 78 (69-84) | 18 | 92 (89-95) | 92 (89-95) |
| 9 | 86 (80-90) | 76 (69-83) | 19 | 85 (80-90) | 97 (96-98) |
| 10 | 90 (86-93) | 94 (91-96) | 20 | 96 (94-97) | 97 (96-98) |
| Mean CC (range) | 90 (81-99) | 85 (72-97) | Mean CC (range) | 92 (85-96) | 94 (91-99) |

**Table 4.3:** Correlation coefficients (CC) of Isolated check VEP waveforms at 50% and 20% Michelson contrast over 400ms are shown for individual subjects. Values represent the percentage of correlation for waveforms obtained to light increment and decrement, as well as the 95% confidence interval (CC). The closer this value is to 100, the more similar are the two waveforms.

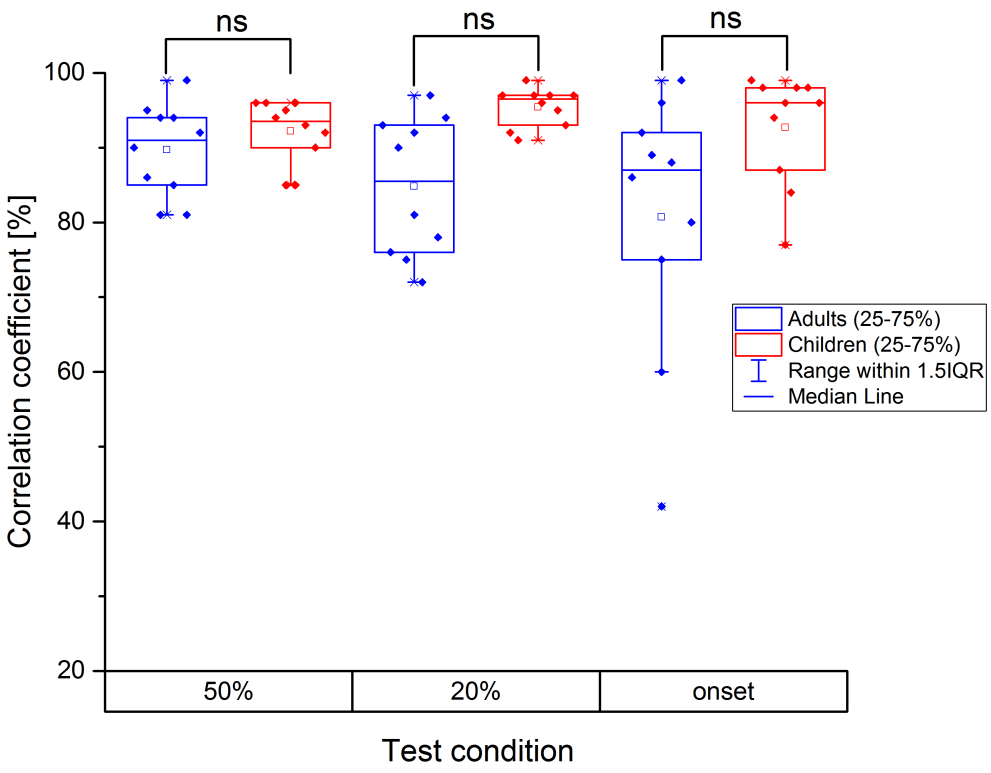


**Figure 4.9:** Comparison of the Correlation Coefficients obtained for each group from light increment and decrement, as well as isolated check VEP recordings. Diamonds represent the individual subjects with the boxes displaying the median 50% of the values. Blue boxes represent values of adult subjects, red boxes the values of the children group. The children group displays an overall higher mean and median CC between the two conditions (light increment/decrement, positive/negative contrast, as well as a narrower range of values. However, statistical analysis did not find a significant difference between the two groups (One-way ANOVA and post-hoc Tukey means comparison: 50% p= 0.306, 20% p=0.177, onset p=0.088).

In view of ON and OFF responses being highly similar within a subject, contrasting the large variety of waveform shapes encountered across individuals and with age, it was necessary to determine what waveform components to expect when recording from subjects of different ages, as well as the most appropriate and robust analysis method for waveforms obtained from patients. Hence, the cortical origins and main components of the pattern onset VEP will be discussed below.

### 4.3.2 Components of the onset VEP

The ISCEV standard for the pattern onset VEP mentions a well-defined waveform with an initial positive peak (C1), followed by a negativity (C2) and another positivity (C3) [242]. Compared to the conventional clinical pattern reversal VEP, which is highly reproducible across individuals of different ages [100, 292], the onset VEP waveform shape displays a high inter-subject variability [242] and changes with maturation [101, 293].

Although VEP waveform maturation is usually rapid within the first months of life, the onset and pattern reversal VEP waveforms differ in their subsequent maturation patterns. Early landmark studies found a rapid change in onset VEP waveform shape between birth and eight months of age followed by a slower phase of maturation ending at puberty with C1-C2-C3 morphology apparent in subjects as early as at 16 years [294]. A similar trajectory is observed in the pattern reversal VEP, however, the major positive peak (P100) does not change greatly after seven months post-term [295], remaining at around 100ms post stimulus onset in healthy individuals into adulthood. In very young children (around six months of age), the first major onset VEP component (C1) was observed to appear at around 120ms post-stimulus onset and develops to occur within a wide range of 75-155ms in children of around six years [99]. A recent study carried out in our laboratory at GOSH found a similar range for C1 timing in 16 young children at seven months after birth (76-134ms) [101]. Peak times for C1 derived from adult data usually appear earlier after stimulus onset and show a narrower value range (65-80ms [293], 80-110m [294] and 69-109ms [101]).

The major negative component (C2) is also subject to developmental changes. DeVries and Spekreijse reported C2 becoming recognisable from around 20 months after birth in 40% of their subjects, whereas it was found in all children of eight years [296]. In children and teenagers, however, the onset VEP waveform is sometimes dominated by a late big positivity (around 130-138ms), rather than a C1-C2-C3 complex which can mask the C2 and C3 components [101]. The C3 component is seldom described in the literature and was reported by Kriss and colleagues to

occur between 150 - 200ms post-stimulus in adult subjects [297].

The main components of the onset VEP waveform seem to originate from an interplay and summation of activity from different cortical origins. The majority of studies sees the C1 originating from the primary visual cortex (Broadmann's area 17, striate cortex) [298, 297, 299, 300]. This view is based on evidence from experiments showing that the polarity of the C1 reverses when comparing upper and lower visual-field stimulation [298, 301, 299]. The upper and lower banks of the calcarine fissure - situated in the striate cortex - are mapping the upper and lower visual hemifields, respectively[5]. Nonetheless, the striate cortex origin of the C1 component of the onset VEP was challenged by Spekreijse and van der Tweel, who suggested that the C1 originates from local luminance changes in extra-striate area 18 [302]. Also Edwards and Drasdo linked C1 to activity in area 18 [303]. Discussion and controversy about the exact cortical generators of these components continues even in the 21st century [304, 305].

In contrast to C1, C2 does not show a polarity reversal for upper compared with lower visual-field stimulation [299, 306], suggesting an extra-striate origin for this negativity, although no clear consensus has yet been reached regarding the exact location of its sources. Several studies have suggested the C2 to be sensitive to contrast, defocus [302], as well as spatial characteristics of the stimulus [302, 101]. The cortical origins of the C3 component were only rarely investigated but Vanni and colleagues found it to have posterior parietal cortex contributions in fMRI recordings [307].

In summary, the components of the onset VEP probably originate from a multitude of visual cortical areas and most likely present an interaction of activity from striate and extra-striate areas. C1 shows inputs from various visual areas but has predominant contribution from V1, whereas C2 reflects activity in dorsal and ventral extra-striate areas. C3, in addition, has some posterior parietal cortex contributions [308, 307]. These varied contributions change with age, likely influencing the mat-

[5]Jeffreys and Axford suggested that potentials of opposite polarity are elicited when stimulating above and below the horizontal meridian of the visual field by activating neural populations with geometrically opposite orientations [298].

uration of the onset VEP waveforms. Whilst extra-striate (C2) activity dominates in later life, the ON-pathway dysfunction cohort in this study mainly consisted of young children, in whom striate cortex (C1) activity dominates [309]. Furthermore, a study by Apkaria and Tijssen found the most consistent and reliable component of the pattern onset VEP to be C1 in children with ocular albinism [310], consistent with the results obtained from healthy subjects in this study (Section 4.3.1). In view of these findings and with the aspiration to highlight robust differences between ON-and OFF-pathway signalling in the patient cohort, it was thought most appropriate to focus on the activity of the striate cortex by emphasizing the C1 component / first main positive peak in the analysis of VEP waveforms elicited to ON-and OFF-pathway stimulation.

The hypothesis that ON-pathway dysfunction impacts on ganglion cell firing patterns and therefore alters signal arrival at the visual cortex implies a possible asymmetry between responses recorded from ON-and OFF-pathways in patients with disrupted ON-pathway signalling. The calculation of a CC - intended to capture the similarities of ON and OFF system responses in healthy individuals, while allowing for great inter-subject variability - was not considered sensitive enough for a thorough analysis of such an outcome.

Instead, analysing the differences of components of the waveform data was considered to be more appropriate, allowing a robust comparison of the characteristics in component time to peak and amplitude. In addition, the fact that the timing and size of the first positive peak was observed to be so highly variable depending on the age of the subject, supported the use of this analysis method, as comparing the differences between ON-and OFF-pathway signals allows for an evaluation independent of the subjects' ages.

Hence, the VEP data of all healthy individuals (n=50) were analysed by component difference analysis, focusing on the most similar component observed in healthy volunteers (C1). These results provided a reference range for the comparison of the findings in the ON-pathway dysfunction cohort with those of healthy volunteers, which is displayed in Table 4.4.

### 4.3.3 Differences between ON-and OFF-pathway responses

In order to further highlight the similarities of ON-and OFF-pathway signals in the control cohort, the data obtained from healthy volunteers was subsequently analysed calculating the difference in response time (TD, Figure 4.10) and amplitude (AD, Figure 4.11). As previously evident in the analysis of the CC, ON and OFF responses did not differ significantly for either TD or AD across both stimulation conditions, highlighting the similarities between both responses in healthy individuals[6].

When analysing the time to peak for subjects in the control cohort, the data showed a clear division in individuals who had waveforms with a timing of under 100ms and some with a timing of over 100ms. It was found that this was linked to the age of the subjects. Comparing the differences of ON-and OFF-pathway signals for specific components had the advantage that it allowed to investigate the similarities and differences in ON-and OFF-pathway signals independent of the subjects' age. Therefore it was possible to obtain a common normative data range for all subjects (Table 4.4).

[6]For TD a slight shift of the data towards an ON-delay was observed, however this was on average 1ms only.

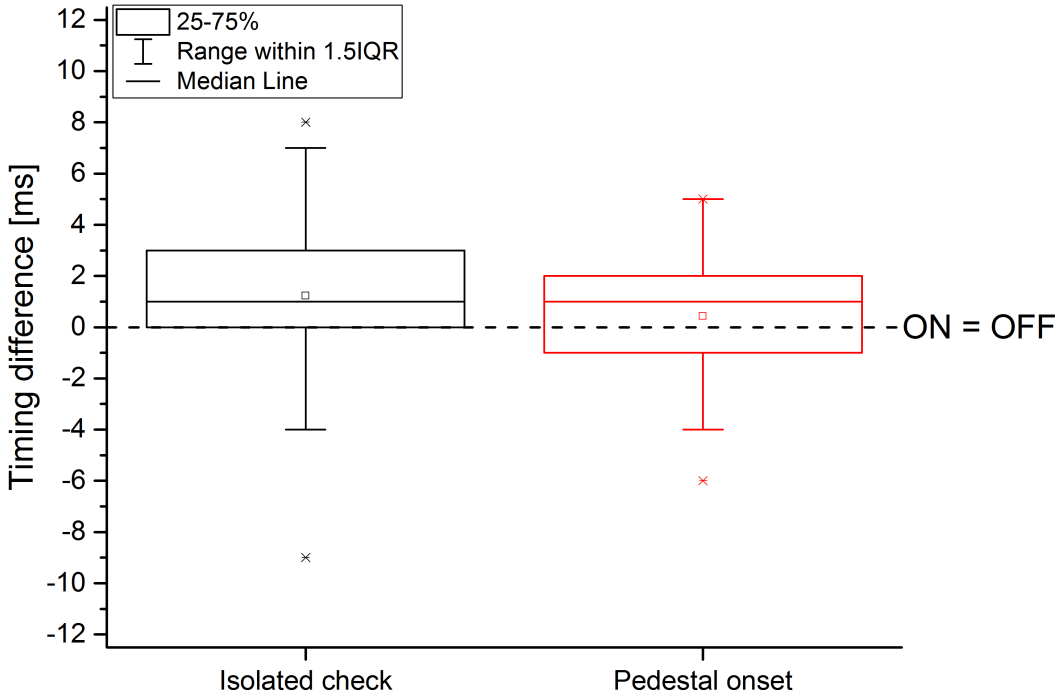


**Figure 4.10:** The difference in time to peak (TD) between ON-and OFF-pathway signals was calculated by subtracting the ON-pathway from the OFF-pathway response time. The resulting value was plotted for each test condition (Isolated check = black, Pedestal onset = red). If the resulting value = 0, ON-and OFF-pathway signals had the same timing. A positive value represents a timing delay of the ON-pathway and a negative value a delay of the OFF-pathway signal, respectively. Diamond symbols represent individual subjects. Boxes give Max and Min (-), Mean (square), Median (border inside the boxes), 99% and 1% (x), as well as 75% and 25% (margins of the boxes) percentiles.

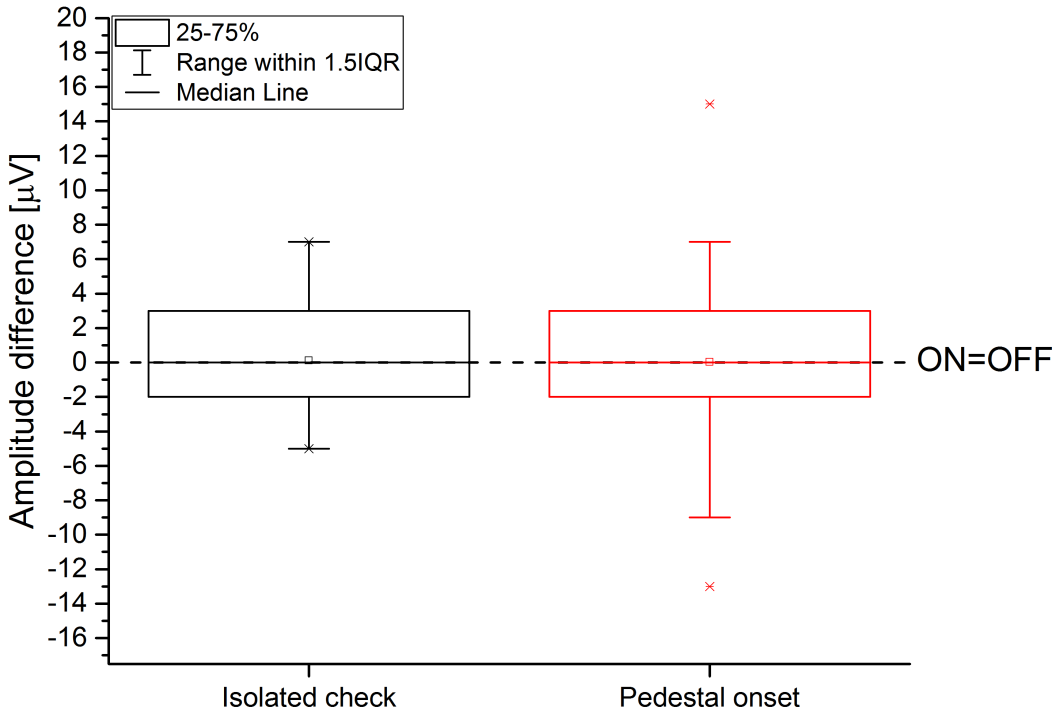


**Figure 4.11:** The difference in peak amplitude (AD) between ON-and OFF-pathway signals was calculated by subtracting the ON-pathway from the OFF-pathway response amplitude. The resulting value was plotted for each test condition (Isolated check = black, Pedestal onset = red). If the resulting value = 0, ON- and OFF-pathway signals had the same size. A positive value represents a bigger ON-pathway component and a negative value a bigger OFF-pathway signal, respectively. Diamond symbols represent individual subjects. Boxes give Max and Min (-), Mean (square), Median (border inside the boxes), 99% and 1% (x), as well as 75% and 25% (margins of the boxes) percentiles.

| | **Isolated checks** | | | **Pedestal onset** | | |
|---|---|---|---|---|---|---|
| | Median | Min | Max | median | Min | Max |
| TD | +1ms | -9ms | +8ms | +1ms | -6ms | +5ms |
| AD | 0$\mu$V | -13$\mu$V | +7$\mu$V | 0$\mu$V | -13$\mu$V | +15$\mu$V |
| TD 20% | +1ms | -18ms | +15ms | | | |
| AD 20% | 0$\mu$V | -7$\mu$V | +7$\mu$V | | | |

**Table 4.4:** The normative data ranges for both tests (isolated check and pedestal onset VEP) were calculated for the timing (TD) and amplitude difference (AD) of the first positive peak occurring after stimulus onset (C1). The median, as well as Miniumum and Maximum of the values obtained from the cohort of healthy volunteers is displayed.

### 4.3.4 Conclusion

I have applied a set of electrophysiological tests assessing visual pathway function separately in the ON-and OFF-pathways of the visual system of healthy volunteers. This was achieved by utilising conventional pattern onset stimulation and introducing a pedestal light increment and decrement component by presenting checkerboards arising from a black or white background, as well as by introducing a positive and negative contrast stimulation via isolated check VEPs. It was possible to show that pattern onset VEPs are similar to ON-and OFF-pathway stimulation in healthy observers across all testing conditions by analysing the Correlation Coefficients (CC). Although there was waveform variation across the subject cohort, a good concordance within individual subjects was observed[7]. Generally, the first positive peak (C1) seemed to be the most robust and comparable component when produced by light increment and decrement, as well as by positive and negative contrast.

In conclusion, the results presented in this section show that pedestal pattern onset stimulation can be useful to assess ganglion cell, as well as visual pathway integrity selectively in ON-and OFF-pathways. VEPs recorded from healthy volunteers showed a high correlation when waveforms elicited to light incremental and decremental, as well as positive and negative contrast stimulation were compared. Subsequently, these stimuli were applied in patients with retinal ON-pathway dysfunction in order to investigate the effect of a dysfunctional ON-pathway on ON and OFF signal arrival at the striate cortex. Due to the high inter-subject variability of the visual cortical responses encountered in healthy volunteers, it was decided to focus on the difference between ON-and OFF-pathway responses by calculating their timing (TD) and amplitude difference (AD) within a subject. This allowed the robust comparison of the main waveform characteristic (C1) across subjects and ages, as well as conditions. The results obtained from patients were compared to the normative data range established.

[7]Part of these data, specifically those obtained from increment and decrement onset VEP stimuli, were included in a manuscript accepted for publication in IOVS in December 2017: Fritsch, DM, Sowden, JC and Thompson, DA: "Pattern onset ERGs and VEPs produced by patterns arising from light increment and decrement", 2018. The manuscript can be found in the appendix.

## 4.4 Cortical ON-and OFF-pathway signals in ON-pathway dysfunction

Separate and comparative probing of ON-and OFF-pathways was carried out with the aim of increasing the sensitivity of electrophysiological tests to pick up abnormalities in cortical signalling due to retinal ON-pathway dysfunction. As highlighted in the previous section, the ON-and OFF-pathway responses obtained in healthy subjects were highly similar in timing and amplitude, especially the C1 component. In contrast, the responses acquired from individuals with ON-pathway dysfunction showed some marked abnormalities between ON-and OFF-pathway responses. The most prominent one was the timing delay encountered in the ON-pathway response. An exemplary trace of a subject with cCSNB displayed next to a trace obtained from a healthy volunteer for comparison can be found in Figure 4.12, highlighting this timing difference. For the representative ON-pathway dysfunction patient (Pat20), the amplitude difference was negligible, while the difference in timing amounted to 11ms at C1. This delay continued to the C2 and C3 components.

This initial finding suggested that the novel electrophysiological test battery was, in fact, sensitive to detecting patients with ON-pathway dysfunction as abnormal. This preliminary result required confirmation across all patient subgroups, including a total of 53 patients, using the pedestal onset, as well as the isolated check VEP conditions, in order to determine if and to what extent both tests were sensitive to detect imbalances in ON-and OFF-pathway signalling.

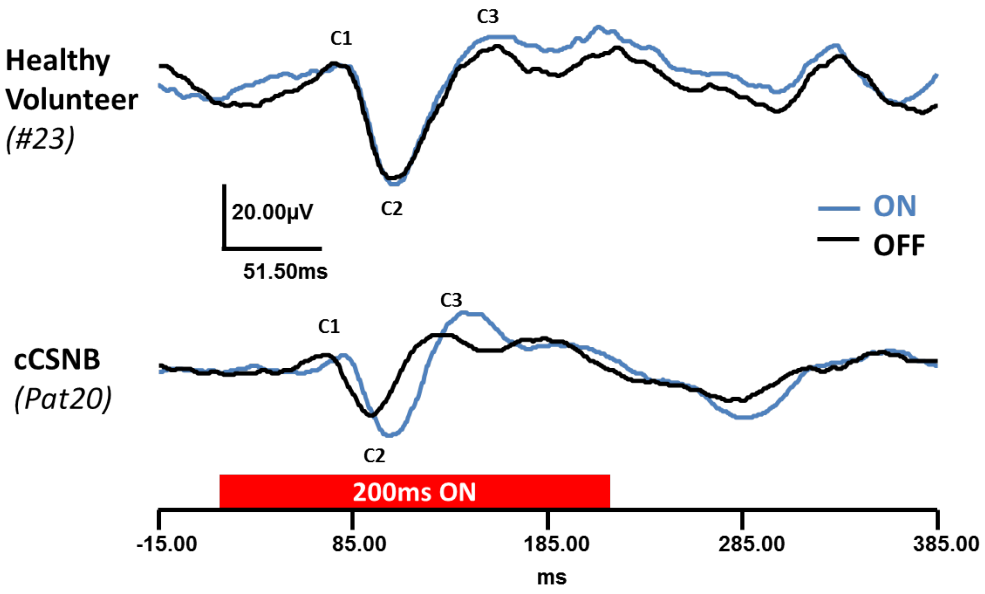


**Figure 4.12:** Exemplary traces to show the difference between VEP waveforms elicited from a patient with ON-pathway dysfunction and a healthy subject. This example shows the waveform recorded from isolated check stimulation to 50% Michelson contrast; however, the difference observed in the other stimulation conditions was highly similar. Blue traces represent the responses recorded from the ON-pathway (positive contrast) and black traces the responses from the OFF-pathway (negative contrast), respectively. A visible difference between ON-and OFF-pathway responses is apparent in the patient traces, while ON and OFF traces of the healthy individual are highly similar (especially for components C1 and C2).

### 4.4.1 Isolated check VEPs

Isolated check stimulation to positive and negative contrast of 50% proved to be highly sensitive in detecting abnormalities of ON-pathway signalling, eliminating false negatives all together in the cCSNB subgroup with 100% of patients falling outside the normative data range ($p<0.0001$), with these having an average ON delay of 18ms and ranging from 10-30ms.

The cCSNB subgroup was not the only one with markedly abnormal TD results: The iCSNB, DMD post exon 30 and PMM2-CDG subgroups displayed significantly different TD values from the normative data range (iCSNB: $p=0.01$, DMD post exon 30: $p<0.0001$ and PMM2-CDG: $p=0.009$), respectively). While patients with iCSNB displayed both, individual ON and OFF delays with a slightly elevated group mean ON delay, all patients with PMM2-CDG showed ON delays, save for Pat70 with a TD of zero. DMD boys displayed highly variable TDs across individuals with ON, as well as OFF delays in both subgroups. However, while the DMD patients with a mutation post exon 30 - affecting the shorter dystrophin isoforms - showed a significant difference when compared to healthy volunteers, the DMD pre exon 30 subgroup did not.

Upon analysing AD across subgroups, only four patients fell outside of the normative data range (1x DMD pre exon 30, 1x DMD post exon 30 and 2x PMM2-CDG). No asymmetry pattern between ON-and OFF-pathway responses was apparent in these individuals with two patients showing ON delays and two showing OFF delays. Both subgroups of patients with CSNB showed an approximately symmetrical distribution of AD values around zero with no individual falling outside the normative data range.

What effect does a lower temporal contrast have on TD and AD values in the isolated check condition? As observed in the 50% isolated check condition, the cCSNB subgroup showed an overall significant difference when compared to healthy controls in its distribution of TD values (with an average ON delay of 15ms), which showed not a single patient with a $TD<0$ ($p<0.0001$). Only two other patients (Pat8, iCSNB and Pat60, DMD pre exon 30) displayed abnormal TD values at 20%

contrast stimulation. All remaining patients fell within the normative data range and therefore displayed no abnormal TD between ON-and OFF-pathway responses at C1. Curiously, patients with iCSNB seemed to show a slight tendency towards an OFF delay (negative TD) at this lower contrast stimulation condition. This was, however, still within the normative data range. Even less abnormal responses were evident across the patient subgroups when comparing AD for 20% contrast stimulation. Only Pat10 (cCSNB) fell outside the normative data range with an AD of +9$\mu$V (bigger ON system response). The differences of ON-and OFF-pathway responses to 50% positive and negative contrast stimulation are displayed in Figures 4.13 (TD) and 4.14 (AD). The responses resulting from a positive and negative contrast stimulation of 20% can be found in Figures 4.15 (TD) and 4.16 (AD). All data was probed for statistical significance using a One-way ANOVA plus post-hoc Tukey means comparison.

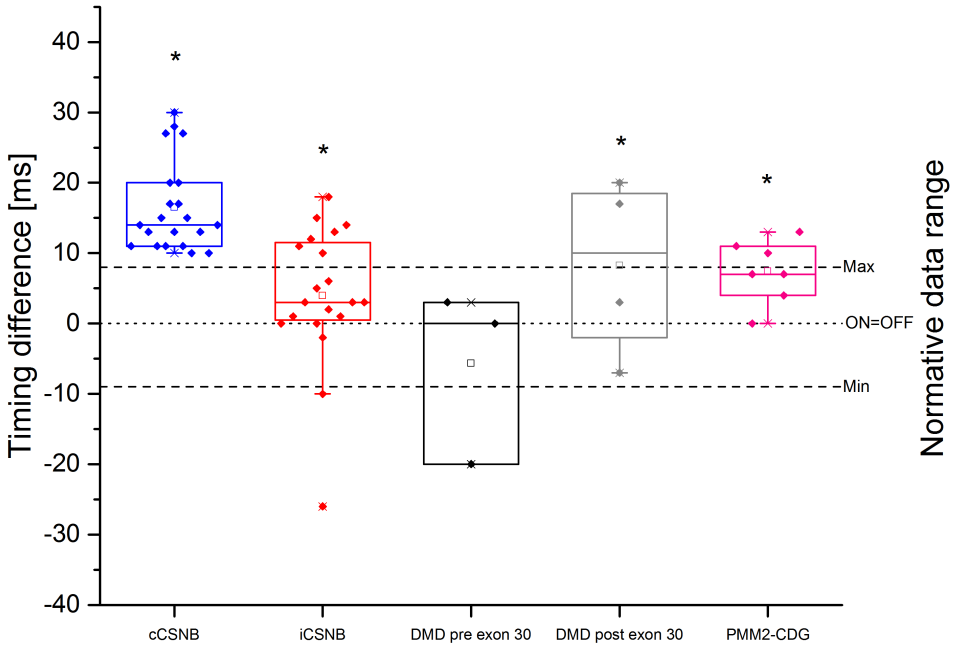


**Figure 4.13:** The times to peak for positive and negative contrast stimulation at a level of 50% Michelson contrast are plotted against the normative data range of healthy volunteers. Where subgroups showed a statistically significant difference from the normative data range this is indicated by an asterisk. Diamond symbols represent individual subjects. Boxes give Max and Min (-), Mean (square), Median (border inside the boxes), 99% and 1% (x), as well as 75% and 25% (margins of the boxes) percentiles.

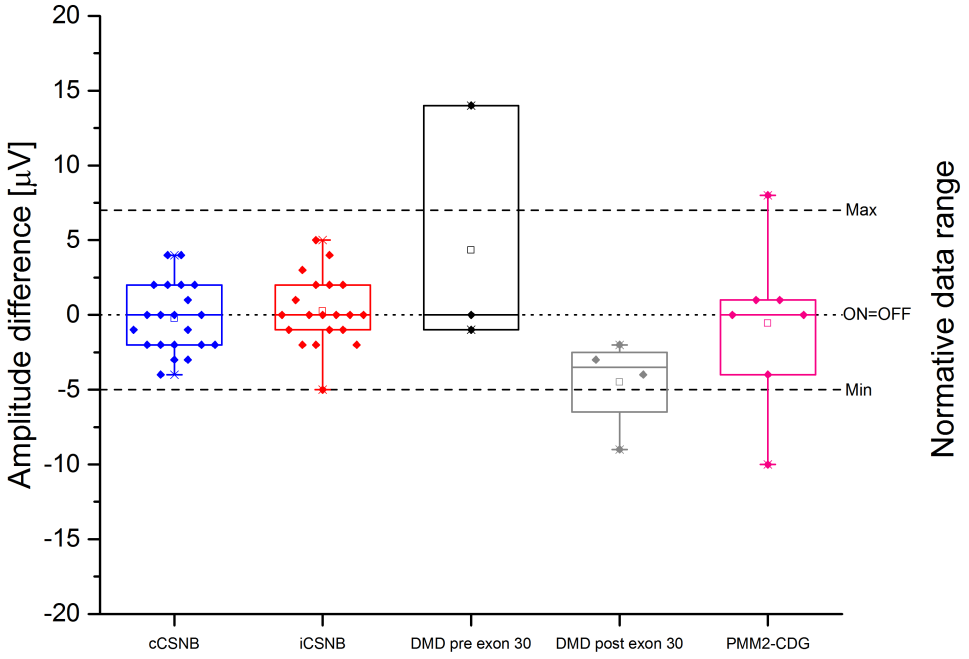


**Figure 4.14:** The amplitudes for positive and negative contrast stimulation at a level of 50% Michelson contrast are plotted against the normative data range of healthy volunteers. Diamond symbols represent individual subjects. Boxes give Max and Min (-), Mean (square), Median (border inside the boxes), 99% and 1% (x), as well as 75% and 25% (margins of the boxes) percentiles.

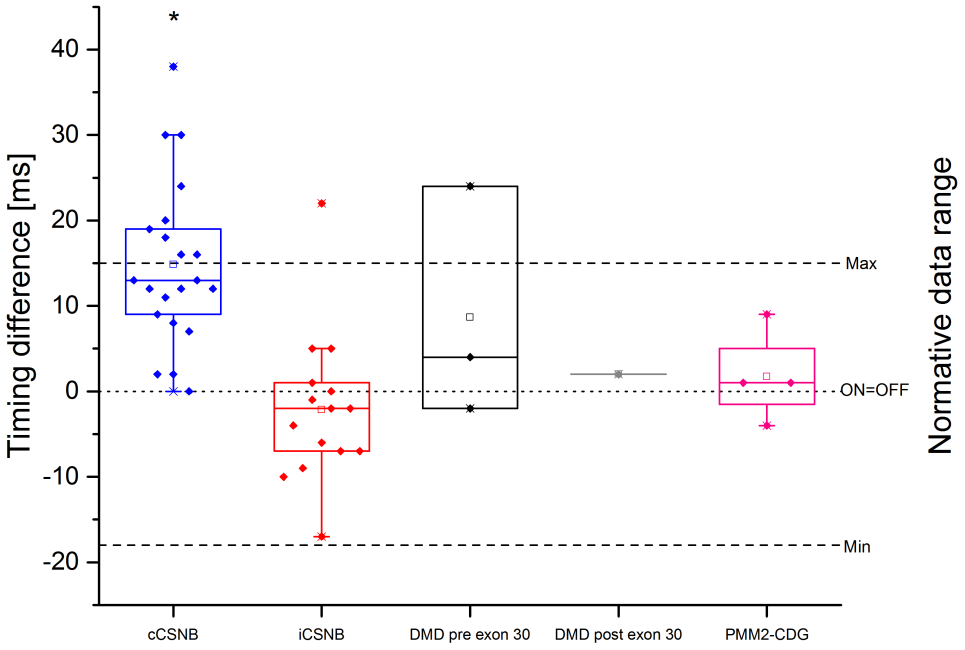


**Figure 4.15:** The times to peak for positive and negative contrast stimulation at a level of 20% Michelson contrast are plotted against the normative data range of healthy volunteers. Where subgroups showed a statistically significant difference from the normative data range this is indicated by an asterisk. Diamond symbols represent individual subjects. Boxes give Max and Min (-), Mean (square), Median (border inside the boxes), 99% and 1% (x), as well as 75% and 25% (margins of the boxes) percentiles.

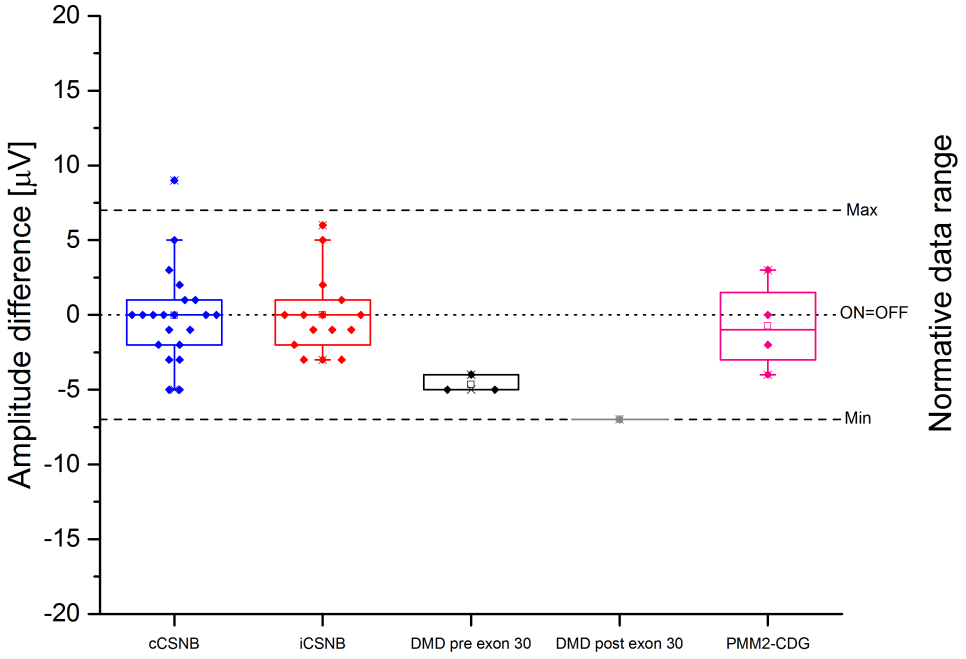


**Figure 4.16:** The amplitudes for positive and negative contrast stimulation at a level of 20% Michelson contrast are plotted against the normative data range of healthy volunteers. Diamond symbols represent individual subjects. Boxes give Max and Min (-), Mean (square), Median (border inside the boxes), 99% and 1% (x), as well as 75% and 25% (margins of the boxes) percentiles.

### 4.4.2 Pedestal onset VEPs

While increment/decrement stimulation yielded abnormal TD results in four out of five patient subgroups, only the cCSNB and DMD post exon 30 subgroups showed an overall ON-pathway signalling delay which was significantly different to the normative data range (cCSNB: $p<0.0001$ and DMD post exon 30: $p=0.04$). Again, patients with cCSNB showed a positive TD value (with an average ON delay of 10ms). The DMD boys with a mutation post exon 30 in the dystrophin gene had a more wide spread distribution of TD values. The biggest individual timing difference of +39ms (ON delay) was encountered in this subgroup (Pat67). Six patients with iCSNB showed timing differences which fell grossly out of the normative data range of healthy volunteers with two subjects having a timing difference of -20ms (OFF delay) or more (Pat8 and Pat45). Nonetheless, the iCSNB group mean did not differ significantly from healthy controls as the distribution of values was fairly equal around zero. Similarly, DMD boys with a mutation pre exon 30 did not show any TD between ON-and OFF-pathway responses rendering their group mean TD at zero. In the PMM2-CDG subgroup, three patients showed abnormal timing differences (ON delays) and an overall elevated group mean compared to healthy volunteers (however, this was not significantly different).

When investigating the ON-and OFF-signal amplitude differences, a wide range of values across subgroups was evident. However, an also highly variable normative data range ruled out significant differences between any of the patient subgroups and healthy volunteers.

The differences of ON-and OFF-pathway responses to light increment and decrement stimulation are displayed in Figures 4.17 (TD) and 4.18 (AD). All data was probed for statistical significance using a One-way ANOVA plus post-hoc Tukey means comparison.

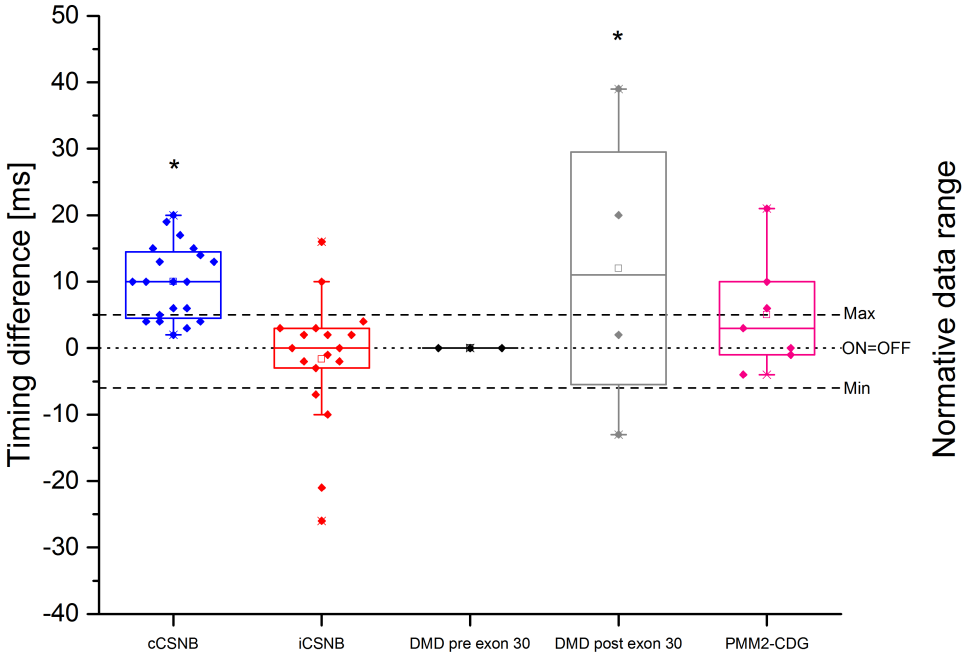


**Figure 4.17:** The times to peak for light increment/decrement stimulation are plotted against the normative data range of healthy volunteers. Where subgroups showed a statistically significant difference from the normative data range this is indicated by an asterisk. Diamond symbols represent individual subjects. Boxes give Max and Min (-), Mean (square), Median (border inside the boxes), 99% and 1% (x), as well as 75% and 25% (margins of the boxes) percentiles.

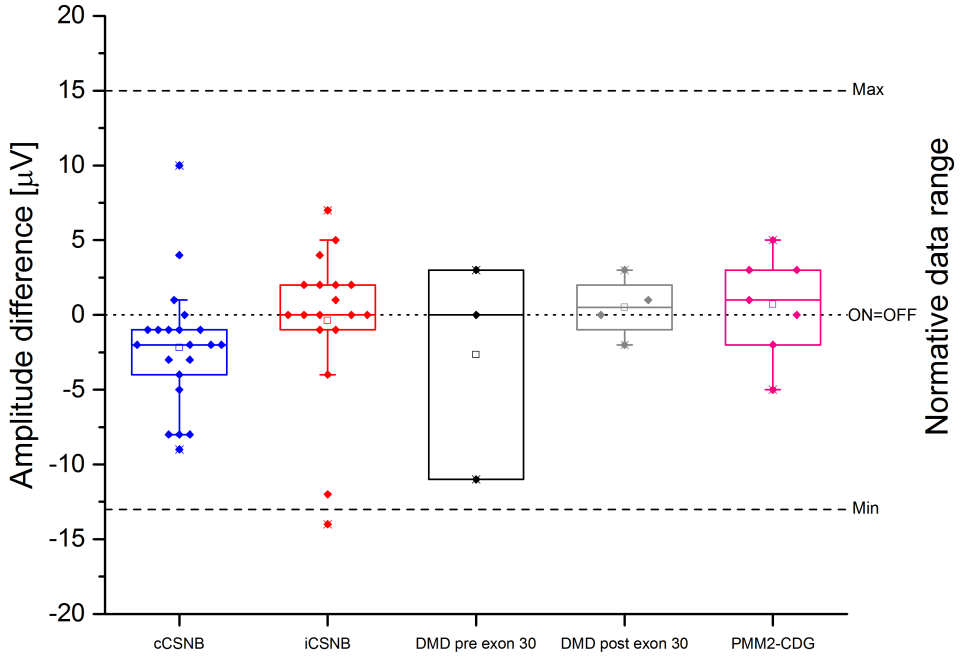


**Figure 4.18:** The amplitudes for light increment/decrement stimulation are plotted against the normative data range of healthy volunteers. Diamond symbols represent individual subjects. Boxes give Max and Min (-), Mean (square), Median (border inside the boxes), 99% and 1% (x), as well as 75% and 25% (margins of the boxes) percentiles.

## 4.5 Summary and Conclusion

### 4.5.1 Summary

- A novel set of electrophysiological pattern onset tests was established to decrease the number of false negative results encountered in conventional pVEP testing in patients with ON-pathway dysfunction
- These tests enabled the separate and comparative investigation of signals from ON-and OFF-pathways at the level of the striate cortex.
  - Pedestal Onset VEP: light increment/decrement stimulation
  - Isolated check VEP: positive and negative contrast stimulation
- The tests were validated in n=50 volunteers. Despite a high variability in waveform shape across subjects and with age, within a healthy volunteer, ON-and OFF-pathway responses were highly similar.
- Analysing the difference between ON-and OFF-pathway responses was considered the most appropriate analysis method of the data as it allowed assessment of ON-and OFF-pathway waveform differences independent of age and inter-subject variability. A normative data range emerged from this.
- In patients (n=53), clear temporal differences between ON-and OFF-pathway responses were observed in the cCSNB, iCSNB, DMD post exon30, as well as PMM2-CDG subgroups. The difference was most prominent in patients with cCSNB, showing an average ON system delay of 18ms in the isolated check condition.
- Isolated check VEP (positive/negative contrast) stimulation seemed to increase the sensitivity in picking up cortical signalling abnormalities in patients more than pedestal onset (light increment/decrement) stimulation. Compared to conventional pattern reversal stimulation, isolated check VEPs increased sensitivity to 83% and pedestal onset VEPs to 58% (both from 37% for the pVEP). An overview is shown in Figure 4.19.

| Test | cCSNB | iCSNB | DMD pre-exon30 | DMD post-exon30 | PMM2-CDG |
|---|---|---|---|---|---|
| Onset VEP 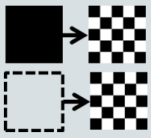 | 12/21 **57%** ↑ | 12/17 **71%** ↑ | 1/3 **33%** ↑ | 3/4 **75%** ↑ | 2/7 **29%** ↑ |
| Isolated checks 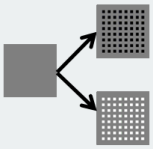 | 21/21 **100%** ↑ | 14/18 **78%** ↑ | 2/3 **66%** ↑ | 3/4 **75%** ↑ | 4/7 **57%** ↑ |
| Conventional clinical PR VEP  | 9/33 **27%** | 29/42 **69%** | 0/8 **0%** | 0/11 **0%** | 1/12 **8%** |

**Figure 4.19:** Sensitivity of the novel electrophysiological test battery compared to the conventional pattern reversal stimulus used in clinical practise. Green arrows indicate an increase in sensitivity (i.e. less false negative results) compared to the pattern reversal VEP. The amount of abnormal waveforms obtained out of total patients tested are displayed including the subsequent percentage of abnormalities picked up.

### 4.5.2 Conclusion

A novel set of electrophysiological tests was designed in order to improve the sensitivity of such tests in picking up cortical signalling abnormalities due to a disrupted retinal ON-pathway. The set of tests comprised the introduction of a light increment/decrement, as well as positive/negative contrast components into pattern onset stimulation. This was in view of previous studies reporting an ON-pathway disruption affecting light increment and positive contrast processing. Additionally, the incidence of nystagmus in the patient cohort, as well as the low sensitivity of the conventional pattern reversal VEP in detecting abnormalities in these patients, favoured the use of pattern onset stimulation in order to probe visual pathway integrity.

While ON-and OFF-pathway responses were highly similar in healthy volunteers, they differed significantly in patient subgroups across stimulation conditions, especially in patients with cCSNB. These findings suggest that a disruption of the ON-pathway originating in the retina can have an effect which is still measurable at the striate cortex. While a clear asymmetry in ON and OFF signals was exposed in patients, the detection of ON-responses reaching the visual cortex despite an ON-pathway dysfunction initially came as a surprise. If all ON system responses were abolished in patients, as seen at the retinal level in the light and dark adapted ERG, one could expect that no signals were transmitted via the ON-pathway and thus no VEP would be recordable to ON-pathway stimulation. Although Alexander and colleagues observed a similar result with positive and negative contrast stimulation in one individual with an unusual type of suspected CSNB, the occurrence of an ON-response, despite presumed complete ON-pathway blockade in the patient, was never questioned [289]. My finding that a response could be recorded from the ON-pathway to light increment and positive contrast stimulation in subgroups of patients with a retinal ON-pathway dysfunction signifies that the visual system could potentially have an alternative route of transmitting ON signals from retina to visual cortex. The possibility of such an ”alternative ON-pathway route” will be discussed further in Chapter 7.

Another finding, when investigating the sensitivity of the novel electrophysiological test set, was the observation that positive/negative contrast stimulation using isolated check VEPs was more sensitive to abnormal ON-signalling than light increment/decrement stimulation, detecting significant ON/OFF timing asymmetries in four out of five patient subgroups. This disparity in sensitivity when comparing the two stimulation conditions could originate from the different temporal contrasts displayed in the testing conditions. While the pedestal onset VEP test exhibited a 100% relative temporal and spatial contrast, the isolated check test produced a maximum of 50% relative contrast. Hence, is it possible that either test was primarily eliciting responses from a certain subsystem?

The contrast sensitivity for M cells, part of the magnocellular pathway, is thought to be nearly 10 times greater than that of P cells of the parvocellular pathway [311]. Additionally, magnocellular responses are thought to saturate at moderate contrasts, whereas the responses of P cells increase approximately linearly with increasing contrast [312]. Zemon and colleagues used VEP stimulation to emphasise either pathways' influence on cortical responses by applying a high contrast pedestal stimulus to accentuate the parvocellular, and lower contrast stimulation to highlight magnocellular contributions [312]. It is therefore possible that the stimuli applied in this study biased either the magnocellular or the parvocellular subsystems. If so, the greater amount of abnormality observed in patients using the (relatively lower contrast) isolated check VEP test would agree with a greater impact of a dysfunctional ON-pathway on the magnocelluar system. However, as abnormalities were also detected when using the (high contrast) pedestal onset VEP test, an - albeit lesser - impact of a retinal ON-pathway dysfunction on the parvocellular system cannot be excluded.

#### 4.5.2.1 Limitations

In the cohort of healthy volunteers, either test - pedestal onset and isolated check VEP - were equally as successful in obtaining similar responses from ON-and OFF-pathways. In contrast, the isolated check VEP stimulation was more successful in detecting ON-pathway delays in patients.

Van der Tweel and colleagues showed that responses to short appearance (such as encountered in the onset VEP) obey the contrast equivalent of Bloch's law [313]. According to this law, the detectability of otherwise identical visual stimuli depends only on their energy [314]. Using the onset VEP as an example, the response to a pattern with 20% contrast presented for 20ms would be similar in amplitude to the response to a pattern with 40% contrast presented for 10ms. Spekreijse and colleagues linked this phenomenon to the adaptation of the visual system to high contrast stimulation. According to their theory, contrast sensitive cortical cells lose their excitation gradually at the offset of a high spatial contrast. If a too-short inter-stimulus-interval (ISI) is applied, the system's representation of the contrast might not have reached the zero position at the moment of another stimulus onset [290], resulting in the succeeding response to not fully develop upon subsequent stimulation.

While care was taken when designing the electrophysiological stimuli, it is possible that the occurrence of abnormal adaptation in the patients could have influenced the responses obtained. In patients with CSNB, it was previously shown that dark-adaptation can be abnormal [315, 164]. While dark-adaptation deficits are usually measured over a time span of several minutes, abnormalities in the retinal adaptation system could also influence contrast adaptation in these patients. If abnormality in contrast adaptation in patients would result in a slower recovery of the retinal and cortical systems generating the VEP response, this could affect successive waveform recordings to high contrast stimulation. This, in turn, might explain the slight disparity in sensitivity encountered between pedestal onset VEP and isolated check VEP conditions.

In summary, my findings indicate an influence of selective retinal ON-pathway dysfunction on post-retinal visual processing, which results in asymmetrical signal arrival at the striate cortex. Surprisingly, ON system responses were not completely abolished at the cortical level. However, an impact of a disrupted ON-pathway was suggested on the magnocellular and parvocellular systems with a slight disadvantage for the magnocellular pathway. What influence such an asymmetry has on higher order visual functions conveyed by ON-and OFF-pathways like motion and contrast was investigated via a psychophysical software called *LumiTrack*$^{Tm}$ and the results discussed in the next chapter.

**Chapter 5**

# *LumiTrack*$^{Tm}$ - A novel and child-friendly psychophysical software for the assessment of vision

## 5.1 Introduction

As described in the previous chapter, there appears to be an asymmetrical arrival of ON-and OFF-pathway signals at the striate cortex, evident in a delay of the VEP waveform to stimuli emphasising ON-pathway contributions in all patient groups. In order to investigate the impact of this cortical signal pattern asymmetry on higher visual functions and perception, a psychophysical assessment of individuals in the patient subgroups was deemed most appropriate.

While the applied VEP recordings can give an insight into temporal domain visual signalling, psychophysical tasks are often used to investigate visual perception in human subjects. When working with young children specifically, a psychophysical task can be advantageous in obtaining a scalable evaluation of a child's visual capabilities in a playful and easy manner, for example using Random Dot Displays. Moreover, if designed with care, such tests are able to provide insights into a patient's performance in everyday situations. Hence, a psychophysical test battery - complementing the previously described electrophysiological tests set - was developed to assess the effect of a dysfunctional ON-pathway on visual perception.

In order to develop psychophysical stimuli, fundamental visual percepts, for which ON-and OFF-pathway signalling would appear crucial, were considered. Motion and contrast perception are two major visual functions which are required regularly in everyday situations. An impairment in the perception of either visual percept can have severe effects on the quality of life of individuals affected [316, 317, 123]. Importantly, both are transmitted via the interplay of ON-and OFF-pathways [318, 319, 320, 321] and therefore present ideal candidates for the investigation of the impact of a retinal ON-pathway dysfunction, and subsequent cortical signal asymmetry, on higher order visual function. Studies in primates support the selection of motion and contrast perception as targets for the design of the psychophysical test battery: a selective pharmacological block of the ON-pathway, using the metabotropic glutamate antagonist 2-amino-4-phosphonobutyric acid (APB), was noted to impair measures of motion perception and contrast sensitivity, especially under positive contrast conditions (when bright stimuli were pre-

sented on a dark background) [322]. Further, psychophysical tests assessing motion perception were frequently and successfully used in patient populations with visual impairments (for example in children and adults with bilateral and unilateral amblyopia [127, 323, 324]). Therefore motion and contrast vision were selected as perceptual targets for the psychophysical test battery. In order to adequately design this psychophysical test battery, it was important to understand the way the precepts of motion and contrast are processed along the visual pathway and which cortical areas are involved.

## 5.2 Contrast perception

Contrast discrimination is one of the first steps in vision. It is the separation of ”brightness” and ”darkness” as two distinct qualities, from which edges and boundaries of an object or a letter are formed. Contrast describes the difference in luminance or brightness (or colour) between different objects in the same field of view. This disparity makes the object distinguishable from its background and other objects.

In the inner retina, ON and OFF bipolar cells represent the starting points of the ON-and OFF-pathways of the visual system which separately convey these qualities from eye to visual cortex. The contrasting power of retinal bipolar cells is enhanced by horizontal and likely amacrine cell contribution to the receptive field centre-surround antagonism of bipolar cells. Depending on the excitatory input received from photoreceptor cells, horizontal cells laterally inhibit neighboring bipolar cells [325]. Through this, a difference in luminance of two adjoining regions in the visual field is enhanced at the bipolar cell level and encoded by subsequent differential retinal ganglion cell activity. By means of this retinal ”contrast gain” mechanism, contrast and sharpness of a visual image are built up [326].

The signalling of brightness and darkness is kept separate with ON-and OFF-pathways until the visual cortex [327, 322]. While local (small scale) contrast is discerned at the level of retinal ganglion cells, no physiological correlate of area contrast of a complete visual scene has been denoted in either retina or the LGN.

Following the hierarchy of the visual system, it is possible that area contrast is processed by cortical mechanisms, where signals are pooled and the task of contrast discrimination is thought to be executed across several different cortical areas, such as V1, V2d, V3d and V3A [328, 329, 330].

Different hypotheses have been suggested, trying to explain how contrast perception is actually mediated and elicited in these areas. While Morrone and Burr (1988) proposed that the perception of contrast depends on the symmetry of receptive field shapes of cortical cells and how their outputs are subsequently added up and correlated [331], Fiorentini and colleagues (1990) argued that the percept of area contrast could arise from specific oriented cortical neurons. These might not only encode orientation, disparity and size of a stimulus but may also be selective for bright and dark parts of an image [332, 333]. By encoding a spatial change of darkness and brightness occurring across their receptive fields, possibly by means of comparing information from their borders, area contrast of the whole scene could be computed. In the simple example of a white bar on dark ground, only cells with receptive fields falling directly onto the borders of this bar would be required to fire, signalling a contrast change or gradient. Cells with receptive fields falling into areas of homogeneous luminance would not exhibit a change in their firing patterns. Such an arrangement would allow to signal contrast, as well as the perceptions of darkness and brightness, involving a minimal amount of active cells.

While highly energy efficient, complexity is added to such a system through specific cell types with different response behaviours linked to their receptive fields and preferences. Shapley and Perry (1986) highlighted that neurons with a sustained or transient type of response, or neurons with different contrast sensitivity and contrast gain, might contribute differently to produce contrast effects [334]. Further, different visual pathways like the M-and P-pathways exhibit different contrast sensitivities [335], adding a further level of complexity.

Although many cortical areas involved in contrast perception are known, how and where exactly the perceptions of brightness and darkness are elicited in the cortex remains unclear. Nonetheless, contrast sensitivity is an important visual function

and the involvement of ON-and OFF-pathways in its generation is clear. Hence, an impact of retinal ON-pathway dysfunction on contrast sensitivity was considered a possibility.

## 5.3 Motion perception

The ability to detect motion is ubiquitous in the animal kingdom, as it is highly important for any sighted animal and its interaction with the environment. In the visual world motion is breaking camouflage and for example enables prey to perceive a predator rapidly, therefore increasing the chances for its survival. Similarly for humans, the perception of motion is vital. Dynamic visual cues extracted from a visual scene are key for interaction with our environment; evident, for example, in the simple process of throwing and catching of a ball or, judging the motion of one's own body. In addition, motion perception contributes to a range of cognitive functions such as understanding and interpreting the actions and intentions of living beings[1]. But how exactly do we perceive motion?

The brain integrates several different motion cues (not only from the visual, but also from vestibular and proprioreceptive systems), but the early stages of visual motion processing are thought to take place in the retina. In order to efficiently integrate cues received from the visual field via the retina, a linear transmission of signals is not possible. The information from millions of retinal cells has to be integrated and interpreted over a matter of milliseconds. While bright and dark parts of the visual image are separately processed from the level of the ON and OFF bipolar cells until the cortex, retinal ganglion cells were found to be the first cells to respond to motion stimulation specifically in rabbits [30, 337]. These cells respond maximally to stimuli moving in a particular (preferred) direction and minimally to stimuli moving in the opposite (or null) direction. Further research has revealed different subsets of retinal ganglion cells responding selectively to different kinds of motion, such as approaching motion in frogs and mouse [338, 339], acceleration in the turtle [340], motion in a preferred direction in the rabbit [341] and motion

[1]The first suggestion that humans may possess mechanisms which are tuned to perceive motion specifically linked to biological movements came from early fMRI studies (for example [336]).

relative to background in salamander and rabbit [342].

Several computational models on how motion perception could be encoded along the visual pathway have been developed over the years. In an early model introduced by Reichardt and Hassenstein, the outputs of specific ON and OFF cells (i.e. the firing rates of their centre vs. surround) were combined by retinal ”lightening” and ”darkening” cells [343]. At the heart of this model is a delay-and-compare mechanism. Using again the simple example of a bright bar moving on a dark background, the brightness signal as measured by one photoreceptor cell is subsequently delayed and compared to the signal derived from an immediate neighbouring location. The comparison of the time difference of both signals results in a directionally tuned output. Figure 5.1 displays a schematic of such a system.

More recent research in the cat and rabbit suggests that such a signal time-delay could be already introduced at the bipolar cell level by relaying signals to special starburst amacrine cells in a motion direction-dependent manner [344, 345]. Further evidence that bipolar cells and their successive amacrine cells could be contributing to the receptive field of direction specific ganglion cells comes from work on the salamander retina, highlighting that interacting local populations of amacrine and bipolar cells form the receptive fields of motion-sensitive ganglion cells [346]. In flies, temporal delays in synaptic convergence establish the first set of visual neurons that encode directional motion [347, 348], supporting the classic model first proposed by Hassenstein and Reichardt. In the primate, temporal information transmitted from retinal ganglion cells to the cortex also seems to be crucial for the signalling of motion [349].

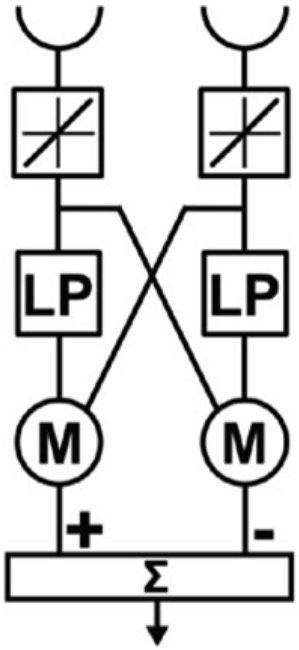


**Figure 5.1:** A schematic displaying the classic motion perception model proposed by Reichardt and Hassenstein. Inputs from the two photoreceptors are asymmetrically delayed by low-pass filtering (LP) and multiplied (M) leading to a direction-selective output signal. Taken from [350].

After ON and OFF signals are separated in the retina, this separation is maintained at the level of the LGN, where motion information from ganglion cells is relayed in the magnocellular layers 1 and 2. These layers exclusively receive input from parasol ganglion cells, which are able to detect high temporal frequencies and thus can detect quick changes in position of an object [351, 352]. Further, they exhibit important contrast and edge detection properties [181, 353] and convey achromatic information about the orientation and location of objects to the cortex [354, 355] while also directing attention and guiding saccadic eye movements in conjunction with the Superior colliculus (SC).

Following the retinal signal computation proposed by Hassenstein and Reichardt, a lightening unit in the LGN would be excited by the ON cells in its receptive field centre and the OFF cells in its surround and inhibited by the OFF cells in its centre and the ON cells in its surround. The outputs from these ”lightening” and ”darkening” cells are thought to activate short-range filters that pool evidence for motion in a given direction in direction-selective cortical cells [356, 357, 343]. As described in the introduction[2], most of the cells in the striate cortex (V1) are motion or direction sensitive. At this level, the separation into ON-and OFF-pathways is maintained in the simple cells, the first point of contact for LGN neurons, which are pooling signals from both pathways in different lamina [335]. However, a first interaction of ON and OFF signalling happens as receptive field structures change from strictly separated excitatory and inhibitory regions in the retina and LGN, reacting to light increment and decrement, to complex cells responding to more specialised stimulation such as stimuli of a specific orientation or movement into a certain direction [43].

Cortically, not only V1 but also other areas such as V3 and MT/V5 seem to be specialised for motion processing in humans [358, 359]. Tootell and colleagues provided experimental proof of this using fMRI to locate areas of cortical activity subject to a motion aftereffect caused by the waterfall illusion [359]. Additionally, the processing of motion is tightly linked with different perceptual qualities, like

[2]Section 1.1.3

the processing of shapes. Julesz (1971) highlighted motion as an important cue for identifying shape boundaries by using random dot streograms to elicit the perception of stereoscopic depth [360]. Moreover, shape-from-motion-stimuli, in which the perception of a shape is induced by motion in different directions at its borders, can be used to demonstrate that motion information alone can give the perception of two and three dimensional shapes [361, 362, 363].

Common motion of a group of otherwise unrecognizable dots is a very powerful cue for the visual system. It enables the visual system to realize that it is dealing with a single object. The perception of biological motion relies on this ability to perceive form from motion [364, 365]. Here, the camouflage of a static object is broken by the correlated motion of its parts. A striking example of such an effect is the perception of biological motion by detecting ”point-light-walkers”. In these displays, no single dot conveys information about the figure or event being depicted - individual dots merely undergo translational and/or elliptical motions. The perception of a biological organism engaged in an activity must therefore entail global integration of these motion signals over space and time.

Such displays were first introduced by Johansson (1973), who filmed actors dressed in black with white reflective dots attached to their joints against a black background. When watching the recordings, only the light points at the actors' joints were visible to the observer. Nonetheless, test subjects were immediately able to recognize a human being shaped by these light dots and their relative motion. Further, they could easily recognize the action the actor executed (for example walking or dancing). When shown the individual frames of the videos as static pictures, such a recognition was significantly more difficult or even impossible [366][3].

Specialised cortical areas subsequent to area MT/V5, such as the Superior Temporal Sulcus (STS) seem to be involved in the processing of biological motion stimuli [336, 369, 370, 371]. Also, the temporal polysensory area (STP) in primates, which receives input from dorsal and ventral visual pathways, seems to

[3]Since Johansson's pioneering work, a variety of different studies have shown different aspects of biological motion perception, such as the ability to infer gender from the walking gait of point-light-walkers [367], or the robustness of such displays to masking with random dots [368].

contain cells that are selectively tuned in their response to precise primate forms and movements [372], as well as to point-light-walkers [364]. Knowledge about cortical areas involved in the processing of such motion stimuli in humans was greatly aided by studies using fMRI [336, 370, 371] or psychophysical assessments [369].

It is possible to assess the functionality of processes in higher cortical areas indirectly by using different psychophysical tasks, as done by Vaina and colleagues (1990) in a patient with with bilateral cortical lesions involving the posterior visual pathways [369]. Here, the authors used random dot and point-light-walker displays to assess "earlier and later aspects of image-motion processing". When assessing the percept of motion, one can take advantage of the relatively hierarchical properties of the visual system. Therefore, in order to probe the functionality of different cortical target areas in patients in an easy and child-friendly manner, a psychophysical test battery aiming to assess the perception of motion displays of increasing complexity, as well as the contrast sensitivity of these was designed. This approach aimed to further delineate the scope a retinal ON-pathway dysfunction has on the visual perception. A hierarchical perceptual test battery allowed the assessment of the cortical levels on which the visual system was impacted by this retinal signalling disruption.

Choosing the cortical targets was the first step in the design and development of the psychophysical software named $LumiTrack^{Tm}$. Subsequently, a thorough review of literature on psychophysical tasks was carried out. Comparing different studies applying psychophysical motion tasks was challenging due to the fact that few studies used comparable stimulus parameters. This variability resulted in a wide range of different values obtained by the individual studies, revealing the importance of parameter choice and constancy for the reliability and comparability of such tests. These parameters considered during the design stage were:

- How to obtain a threshold value of motion perception
- Dot size
- Dot density
- Dot lifetime
- Stimulus display time
- Dot speed
- Stimulus field size and shape

The next section describes the rationale behind designing and developing the

*LumiTrack*$^{Tm}$ psychophysical test battery from the ground up. A summary of the parameters finally applied in *LumiTrack*$^{Tm}$ is given in Section 5.5.7.

## 5.4 *LumiTrack*$^{Tm}$ test choice and rationale

In the previous chapter it was shown that ON signalling is altered at the level of the striate cortex in patients with a dysfunctional ON-pathway. The aim was to target the visual functions motion perception and contrast sensitivity, as these are likely to be affected by a dysfunctional ON-pathway. In addition, these tests were designed to assess positive (ON-pathway) and negative (OFF-pathway) contrast stimulation conditions. The aim was for the psychophysical tests to complement the electrophysiological recordings, described in the previous chapter, by tapping into higher cortical function, providing a non-invasive way of elucidating any effect an ON-pathway disruption might have on visual qualities processed in higher cortical areas.

The tests needed to provide independent control of positive and negative contrast, alongside other stimulus parameters, in order to explore the relative contributions of ON-and OFF-pathways to motion[4] perception and contrast sensitivity of motion in the variable ON-pathway dysfunction patient cohort. A psychophysical software with this level of flexibility was not available as a commercial package. Therefore *LumiTrack*$^{Tm}$ was designed and programmed using an open source programming language called "Processing"[5][6]. Developing a software from the ground up maximised the flexibility of stimulus choice, design, and control of important parameters. Further, having a mobile psychophysical assessment, which could be presented on a laptop, improved the ease of data acquisition. The individual tests and the rationale for parameter choice are described in more detail in the following section.

[4]Due to the circumstance of displaying the psychophysical test battery on a computer screen, where a moving stimulus is presented by showing as a succession of illuminated pixels, strictly speaking, the subjects were shown stimuli exhibiting "apparent" motion. Here, a sense of motion is evoked by the rapid succession of illuminated pixels of the screen, even though there is no physical motion involved. The perceptions of physical and apparent motion are considered the same in the cortex [373, 374] and are not perceptually different. Hence, the perception of "apparent motion" and "physical motion" are considered interchangeable and termed simply "motion perception" in this study.

[5]www.processing.org

[6]The design, parameter choice, as well as biological background research for *LumiTrack*$^{Tm}$ was carried out by the author, while the majority of the programming work was done by collaborator Maximilian Kerz.

## 5.5 Methods

The following sections describe the individual tests compiled in the *LumiTrack*$^{Tm}$ software, as well as giving an insight into the design and development process before implementation.

### 5.5.1 Test 1 - Coherent Motion

To assess global coherent motion perception, a random dot setup was used[375]. The subjects were shown dots which were randomly moving over the screen (noise dots) with a fraction of them moving coherently in one direction (signal dots). A stimulus based on Brownian motion was initially chosen as it is fairly robust to changes in contrast, speed, aperture size, as well as spatial displacement and temporal displacement of dots [376]. This robustness makes it ideal for testing in a paediatric setting where ideal testing conditions might not always be guaranteed.

The task for the subjects was to indicate (via key-press, by pointing or saying) in which direction the signal dots were moving. This was a Two-alternative-forced-choice (2AFC) scenario[377]. The difficulty of the task increased and decreased, depending on the subject's answers by changing the signal/noise ratio. The test subsequently continued following the underlying staircase algorithm until ten reversals were reached[7]. The resulting value (threshold) was directly translatable into an absolute measure of the amount or the percentage of signal dots required to perceive a global coherent motion into one direction.

As no shape cues were given, this assessment aimed at testing simple global motion coherence, thought to be processed in the middle temporal visual area (MT or V5) [378]. An exemplary screenshot of the Coherent motion tests is shown in Figure 5.2.

[7]How a threshold value was obtained is explained in Section 5.5.5.1

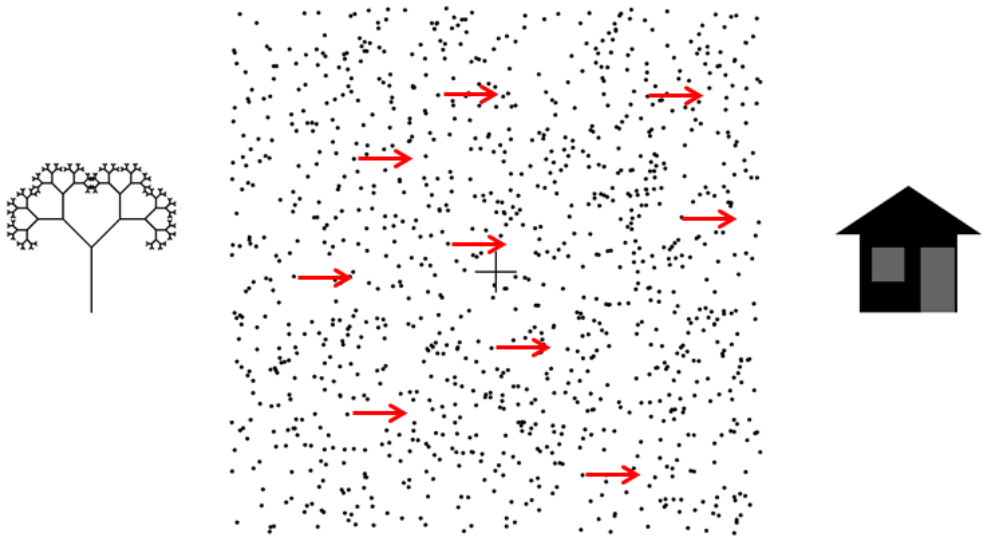

**Figure 5.2:** A field of dots was displayed with a fraction of them moving in one direction (up, down, left, right) (signal dots) and the remaining dots moving randomly across the stimulus field (noise dots). The subject was asked to tell the direction of the coherent motion via key press or verbally (”Do the dots go to the tree or to the house?”). Red arrows were not visible during the test and are displayed for illustration purposes only.

### 5.5.2 Test 2 - Shape From Motion

This test consisted of two equal panels of moving dots. All dot parameters (dot speed, size, density, motion type etc.) were the same as for the coherent motion test. Here, however, the signal dots were confined to a shape placed in the centre of each dot-panel. A fixed number of signal dots inside this ”signal-shape” were moving in the opposite direction compared to the noise dots [369]. Having opposing dot motion directions in a restricted area for the signal dots created a shape (in this case a square and a diamond) visible to the subjects, although no contour was actually given. The extraction of such motion-induced boundaries is likely to be mediated by a short-range mechanism that matches corresponding local pattern elements of the same luminance polarity in successive time frames according to previous work by Braddick [379]. The two shapes ”square” and ”diamond” were chosen as they could be designed using the same amount of signal dots, occupying the same space, resulting in the same dot density within the signal fields. This removed any impact of disparate dot densities between the two shapes aiding a subject's decision.

How high does the fraction of coherently moving dots have to be for the subjects to distinguish the two shapes? By increasing and decreasing the signal/noise ratio of the stimulus, it became more or less difficult for the subjects to distinguish the two shapes, culminating in a final threshold value. This was subsequently directly translatable into an absolute measure of the amount or the percentage of signal dots required to distinguish two shapes.

This test served as an intermediate step between the coherent global motion detection task, thought to be processed in area MT/V5 [380], and the biological motion detection task, thought to involve higher cortical processing in the STS [381]. Shape from motion processing is thought to involve the dorsal (”where”) and the ventral (”what”) pathways [378]. An exemplary screenshot of the Shape from motion tests is shown in Figure 5.3.

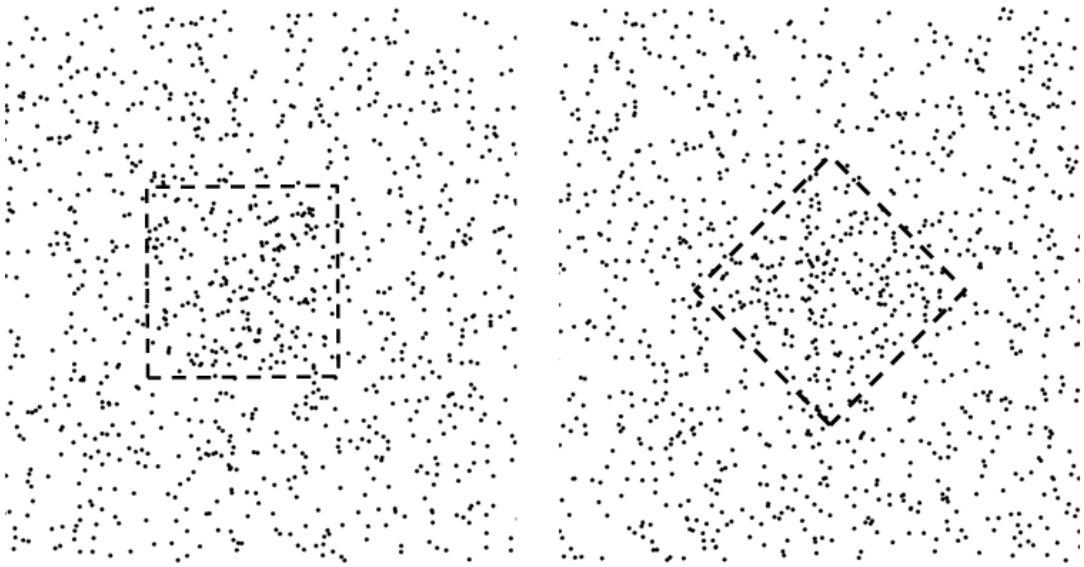

**Figure 5.3:** Two fields of dots were displayed with the dots moving in one direction. Some of the dots were moving in the opposite direction but only in a field confined to a central square or diamond (as indicated by the dashed lines). The opposing motion direction of the dots created the perception of two distinct shapes in the centre of each stimulus field. When the dots were viewed statically, the shapes completely blend into the background. The subject was asked to tell which field contains the square via key press and verbally. Dashed lines indicating the shapes were not visible during the test and are displayed for illustration purposes only.

### 5.5.3 Test 3 - Biological Motion

This task assessed the subject's ability to detect a Johansson point-light-walker presented within a mask made from spatially random noise dots. A ”dot walker”, either facing left (toward a tree) or right (towards a house), was presented in the centre of the screen. This walker was made up of eleven dots with single dots representing the head, one shoulder, one hip, as well as each of the two elbows, wrists, knees, and ankles. The walker was shown walking in place, as if on a treadmill in order to give the percept of a walking motion without any spatial dislocation of the figure. If not animated, the walker was completely invisible among the static noise dots.

The primary task for subjects was to indicate (via a key-press) in which direction the walker was facing. In this case, the test difficulty was altered by increasing or decreasing the amount of noise dots obscuring the walker. The resulting threshold comprised the amount of noise dots a subject was able to tolerate while maintaining the ability to successfully locate the walker and decide which direction it was facing. It was not considered sufficient for the subject to locate the walker on the screen as this could be achieved by locating an area of slight higher dot density (in low-noise situations). Hence, it was necessary to also perceive the direction which the walker was facing. To be able to successfully complete this task, subjects needed to be able to:

1. Perceive the dots as moving
2. Perceive them as a human figure, facing into one direction

Cortically, biological motion is thought to be processed in the STS (Superior temporal sulcus) [382, 370, 371], located in the temporal lobe, and requires some social cognition processing. Two exemplary screenshots of the Biological motion tests are shown in Figure 5.4 (without noise dots) and 5.5 (with noise dots).

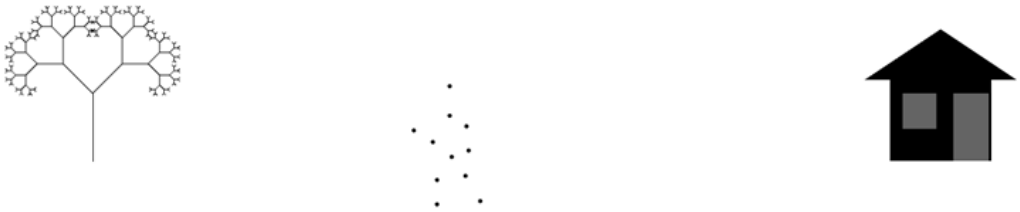

**Figure 5.4:** The point light walker is displayed without any noise dots. Subjects were shown this during their practice trials with an animated point light walker to familiarise themselves with the task before the actual test commenced.

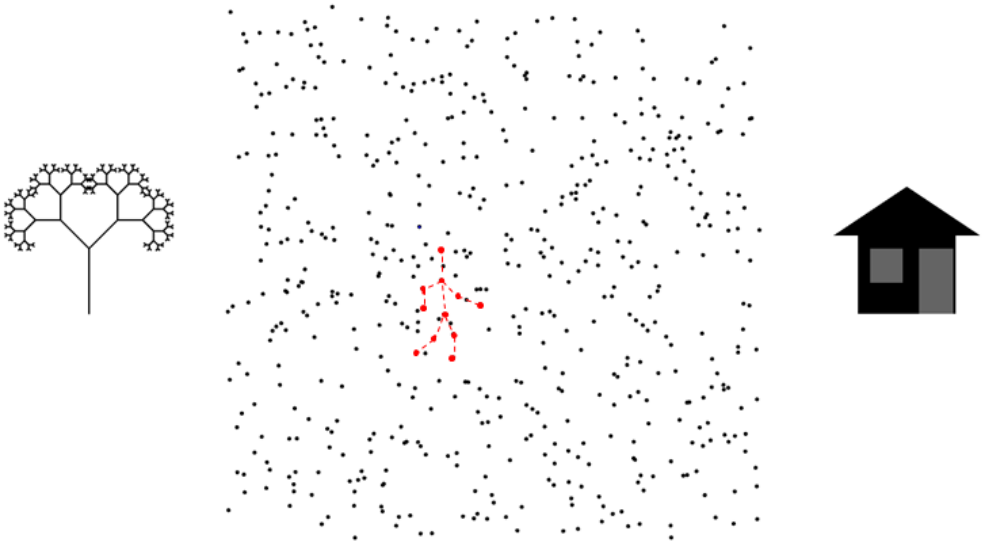

**Figure 5.5:** Within the mask of randomly moving dots, the point light walker was ”hidden” (here shown in red and connected with dashed lines for illustration purposes). When viewed statically, the point light walker was only dots among dots, only when animated a perception of a walking person was achieved. The subject was asked to tell which direction (”towards the tree or towards the house”) the point light walker was facing (”walking”) via key press or verbally. Dashed lines indicating the figure were not visible during the test and are displayed for illustration purposes only. Also, red dots highlighting the figure were the same as the noise dots during the test.

### 5.5.4 Addition: Contrast sensitivity of motion

The three motion tests of increasing complexity were designed to be carried out with either 100% positive (white dots on black background) or negative (black dots on white background) contrast in order to allow a more specific assessment of ON-and OFF-pathway processing. In addition, another test was included in the *LumiTrack*$^{Tm}$ software. It was aimed at delineating the impact of asymmetrical ON and OFF system signalling further by allowing a more precise assessment of an individual's sensitivity to positive and negative contrast.

For this, the motion stimuli were displayed at a fixed "difficulty-level"[8], while the contrast of the dots was altered across trials compared to a mid-grey background. This fixed difficulty level was chosen so that no subject would have a problem in correctly carrying out the test. The rate of change from trial to trial followed a cubic function ($y=x^3$). This allowed a finer assessment of performance at contrast values close to zero, while testing high contrast values time-efficiently. The displayed dots changed from black (RGB: 0) to white (RGB: 255) in an ascending or descending manner. This way it was possible to assess the influence of positive contrast (brighter than the background) and negative contrast (darker than the background) using one single test and by doing so, to evaluate a range of small contrast steps in a relatively short time.

The subjects were given the same instructions as before but were alerted to the contrast change happening across trials. If a subject could not reliably detect the specific motion due to the contrast being too low, he / she was required to press the "space-bar" which produced a negative result. In order to ensure a robustness, subjects were required to answer (unknowingly) twice at each contrast level. This provided a more secure way of assessing whether a subject was not able to see the stimulus due to low contrast - as intended - or was just guessing. A schematic illustrating the logic behind the contrast sensitivity assessment applied in *LumiTrack*$^{Tm}$ is shown in Figure 5.6.

This novel contrast sensitivity of motion assessment resulted in a range of con-

[8]Coherent motion: 75% signal to noise dots, Shape from motion: 75% signal to noise dots, Biological motion: 25%: noise dots

trast values (from positive to negative contrast) which were too low for the subject to perceive. If the contrast of the stimulus compared with the background was increased and fell outside of this range (in either direction), the subject was able to perceive the stimulus. Using this setup, the contrast sensitivity of motion, as well as the symmetry of this contrast sensitivity in positive and negative contrast domains could be assessed.

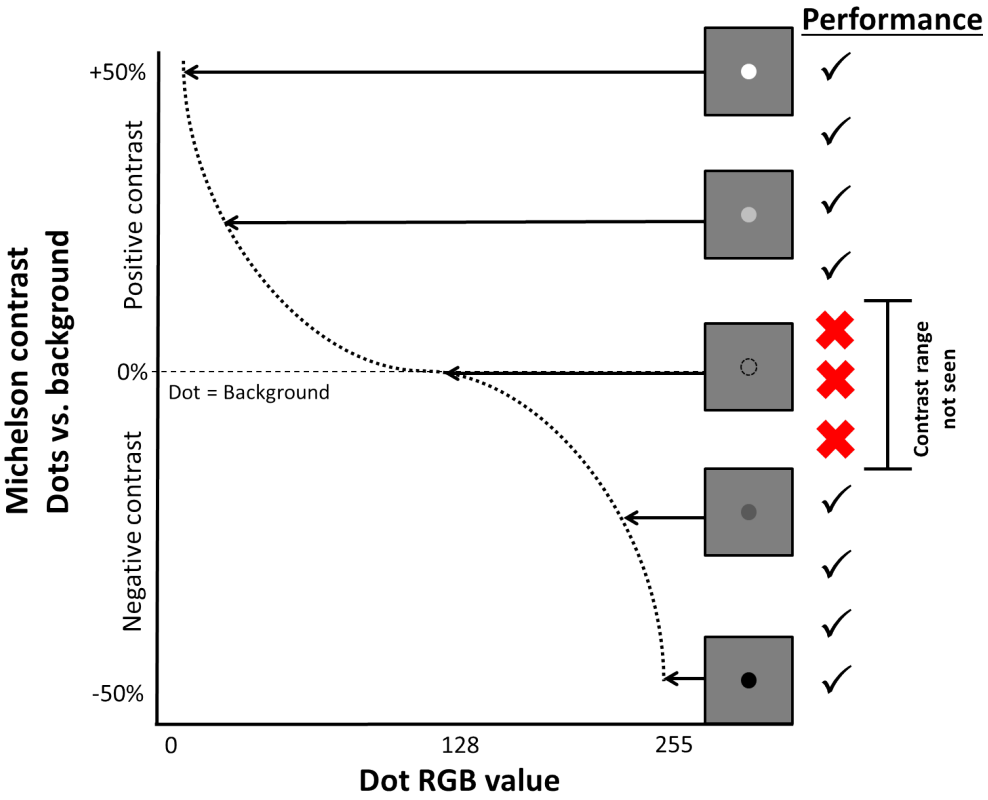


**Figure 5.6:** This schematic explains the contrast sensitivity assessment of *LumiTrack*$^{Tm}$. Michelson contrast of dots compared to background is compared to the actual RGB value of the individual dots. The change in contrast follows a cubic function from positive to negative contrast, here indicated by a dotted line. Examples of how the dots look on the background at several steps are given on the right. At 0% Michelson contrast, the signal dots are of the same grey as the background and therefore invisible (dot is indicated by a dashed border which is not present in the actual stimulus). An exemplary performance of one subject is given on the right. Tick marks indicate a correct response, whereas red crosses indicate wrong responses. As a result, the range of contrast values between the first and last incorrect answer are taken. The subject was not able to perceive this range of contrasts and needed a higher dot vs. background contrast in order to perceive the stimulus. This way, contrast sensitivity of motion, as well as the symmetry of this contrast sensitivity in positive and negative contrast domains could be assessed.

These four different tests were combined in the *LumiTrack*$^{Tm}$ software, anticipated to assess several levels of motion and contrast processing with different cortical targets. The coherent motion task required the integration of local motion cues into global motion, while the performance in the shape from motion task required both, local motion integration and processing of implied form information [383]. In addition to this, the processing of biological motion required bottom-up integration from basic visual motion perception along with top-down social cognition [384].

### 5.5.5 Stimulus parameters

The stimulus parameters were carefully chosen with the aim to extract the most robust testing conditions. Robustness was crucial as it was anticipated to carry out this test battery in subjects of different ages, as well as exhibiting a big range of visual performances. In the following sections, the different parameters considered during the design process of $LumiTrack^{Tm}$ are discussed.

#### 5.5.5.1 How to obtain a threshold value

The first parameter which needed to be chosen was the algorithm behind the testing procedure, or, how to obtain robust and meaningful data from the test. It was crucial that the test was flexible (due to a high variability in visual abilities in the cohort), had a high efficiency (being able to obtain a threshold value as quickly as possible is advantageous when working with young children especially), as well as great confidence that the obtained value is a good representation of the subject's actual visual performance. Many different testing procedures are being applied in psychophysical testing with adaptive testing procedures used most often due to high efficiency, flexibility and little bias [385]. The advantage of being able to reach a reliable threshold value easily and in short time was key in selecting an adaptive staircase method for my test battery.

There are several different types of adaptive staircase methods for a psychophysical task. The simplest one used in the literature to assess motion perception is a 1up/1down method (for example [386, 387], for which a schematic is shown in Figure 5.7.

Here, one correct answer results in a lowering of the independent variable by one step and an incorrect answer results in its elevation. The target value this method converges at is 50%, meaning that it returns the threshold value where 50% or more of the answers given by the subject were correct. However, the 1up/1down method has several disadvantages and was therefore not selected here; for example when choosing too small or too big step sizes relative to the threshold level, the data will be badly placed around the target value [385]. Further, a precision of only 50% results in a relatively low confidence in the data obtained using this method.

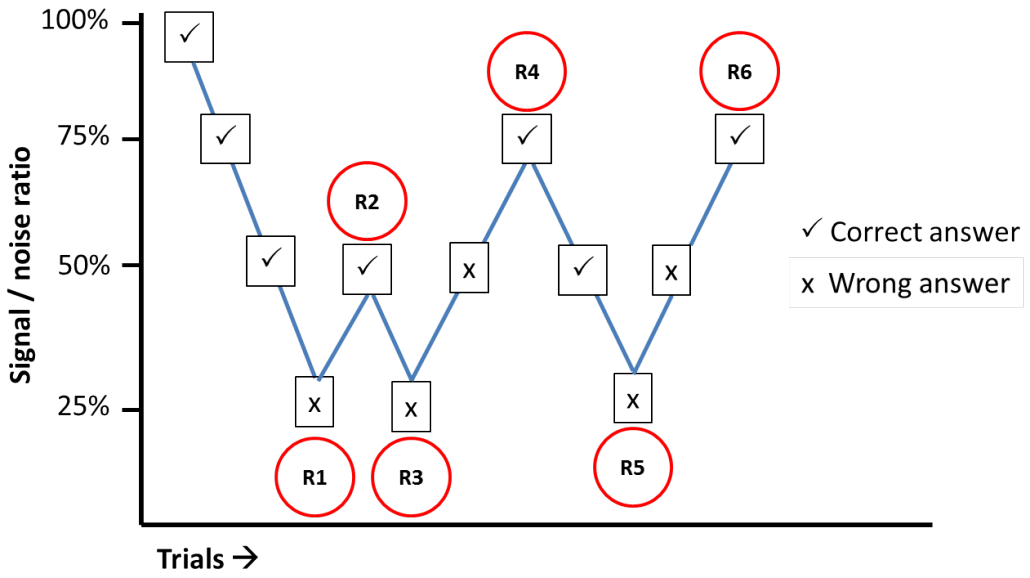


**Figure 5.7:** A simple schematic of a 1up/1down adaptive staircase method. One correct answer results in a lowering of the signal to noise ratio, making it more difficult to perceive the stimulus. One false response is followed by an increase of the signal to noise ratio of the stimulus, facilitating perception. Across a predetermined number of trials, the reversal values model the subject's threshold performance value, which is obtained by calculating the average of the reversal values.

Another option is the use of transformed staircase procedures like the 2up/1down staircase method (for example [126, 127]). The value of the independent variable tested is elevated by one step size after one incorrect response; however, two correct responses are needed for decreasing this value. This method results in a precision level of 70.4%. However, it is not advised to use this method with less than 20 reversals, as this results in a decrease in precision of the estimate [388]. Hence, this method was also not considered adequate for use in the *LumiTrack*$^{Tm}$ test battery, as I was aiming for a staircase returning a threshold value as robust and reliable as possible while minimising test duration.

Such a higher efficiency with a target value of 79.4% is achieved when using a 3down/1up method, requiring a sequence of three correct answers for a lowering of the tested variable value. Its advantages over the previous 2down/1up method are an increase in efficiency [389] and a smaller standard error (SE) of the resulting threshold [390]. Of course, a 4down/1up staircase would result in an even higher

efficiency; however, both strategies have been shown to be of comparable efficiency and precision, while the 4down/1up method results in longer trial duration [391, 388]. **Therefore, a 3down/1up adaptive staircase method was chosen for the *LumiTrack*$^{Tm}$ test battery.**

While acknowledging that an increase in reversal number increases the robustness of the estimated threshold, care has to be taken when choosing this number, as a short trial duration is preferred. Previous studies testing motion coherence used a total of eight reversals [126, 392, 127], or ten reversals [387, 386] with calculating the threshold value by taking the mean of the last six or eight reversal values, respectively. **Based on these findings, the duration of one staircase was set to ten reversals with the threshold calculated by taking the mean of the last eight reversal values.** This was to ensure to get a robust threshold value, while reducing test duration to a minimum.

To account for a robust threshold level, choosing the right step size within the staircase was also important. Comparing fixed step 1down/1up, 2down/1up, 3down/1up and 4down/1up staircase methods, Schlauch and Rose (1990) suggested that an increase in step size results in an increased SE of the resulting threshold value and therefore advised to use small step sizes [391]. However, this suggestion was based on the observation that small step sizes resulted in a smaller difference of results across all four staircase methods which does not necessarily represent the robustness of an individual method. Hence, Levitt (1971) suggested gradually reducing the step size over the course of the staircase to increase precision and decrease SE [385]. A gradual reduction of the step size was also suggested to reduce bias of the staircase [393, 390]. Contrary to these suggestions, Garcia-Perez (1998) links equal step sizes for steps up and down to an inappropriate sampling of the psychometric function. Therefore, he advises to use larger steps up than down in a ratio of Down/Up = 0.7393 for staircases of the 3down/1up rule. This way, the author suggested, the exact step size would not matter.

From the literature a consensus is not obtained. It seems, however, that most studies favoured methods of reducing step size across the staircase (for example

[126, 392, 127, 378, 394, 395]. Further, all six of these studies tested motion perception in children or infants. **In view of a potential comparability of results from this thesis with those obtained from experiments carried out with similar thresholding methods, it was decided to apply the method suggested by Levitt (1971), while still acknowledging the suggestion of Garcia-Perez (1998) of using large step sizes, at least for the initial part of the staircase until the first reversal.**

In conclusion, the staircase parameters selected for *LumiTrack*$^{Tm}$ were:

1. A 3down/1up adaptive staircase method was selected as it is time efficient while having a high reliability with a 79.4% convergence value.

2. The staircase is terminated after 10 reversals and the resulting threshold value is calculated by taking the average of the last eight reversal values. This was expected to be a good compromise of robust results but relatively short testing duration for each subject.

3. Following the suggestion by Levitt and colleagues (1971), as well as Edwards and Wakefield (1988) and Green and colleagues (1989), a gradual reduction in step-sizes was used: The starting value was chosen as 100% signal dots (and 0% noise dots) and upon each correct answer until the first reversal, the value of the independent variable was decreased by one octave (to 50%, 25% and so forth) per step. Upon the first reversal, the step-size decreased to a third of an octave (for example from from 50% to 67%) and was kept constant. From this point onward, the 3down/1up rule was initiated until termination of the staircase.

After deciding on the method of data acquisition via an adaptive staircase, it was important to decide on crucial parameters of the visual stimuli.

#### 5.5.5.2 Dot size and visibility

The patients of the ON-pathway dysfunction cohort exhibited a wide range of visual abilities. The patients' visual acuity scores were reviewed (see Chapter 2) and the resulting Minimum Angle of Resolution (MAR) was calculated in order to get an idea of how big a single dot in the stimulus display would need to be, in order to be visible for every patient. Visual acuity across the study cohort ranged from 0.85 to -0.2 logMAR (mean: 0.38logMAR) and thus the minimum angle of resolution (MAR) ranged from 7.15' to 0.63' (mean: 2.59'). In order for the patient with the most subnormal VA to see one individual dot in the motion test battery, its size needed to be at least 7.15'. The resulting minimum dot size for the stimulus was calculated:

2cm on screen = 100 px

1 px = 0.02cm = 0.02° (at 57cm distance) = 1.2'MAR

For a MAR of 7.15', the **individual dots would have to be at least 6 px (= 0.1° / 6')** as a 5 px dot size only caters a MAR of 6'.

In order to make sure that a subject was able to see a single dot of a certain size, an additional "pre-test" dot size assessment was used. Here, the subject was shown a black and a white dot of 2.5 px (equivalent of a MAR of 3') each appearing on a grey background (resulting in a 50% Michelson contrast). The dot was randomly displaced on the display each second. The dot size was doubled until the subject could detect the dots successfully. Once the subject was able to detect each of the dots successfully at a certain dot size, this size was doubled to achieve a supra-threshold dot size for the subsequent psychophysical tests. For example, if the black and the white dot were located successfully at a dot size of 2.5 px, the $LumiTrack^{Tm}$ tests were subsequently carried out with dots of 5 px. If the subject was only able to detect both dots successfully with a 5 px dot size, the psychophysical tasks were carried out with a dot size of 10 px and so forth. Using **supra-threshold values for dot size** ensured that the subject was able to perceive a single dot in the motion displays, independent of their visual acuity.

#### 5.5.5.3 Influence of nystagmus on motion perception

As discussed in the previous chapter on VEP stimulation, nystagmus (and therefore retinal image blurring) can be a confounding factor in the assessment of visual function. It has a direct impact on vision through a constant motion of the retinal image and individuals with nystagmus often show subnormal visual acuity. In the literature, motion coherence thresholds are not correlated with contrast sensitivity or visual acuity in 4.5-year-old children with normal vision [231]. Also, visual acuity does not show a link to motion perception thresholds in children [324, 127] and adults [323] with amblyopia (uni-and bilateral).

These findings suggest that motion processing is largely independent of visual acuity. A proportion of patients (n= 31/75) in the iCSNB and cCSNB subgroups showed manifest clinical nystagmus that was mainly horizontal:

- 28x horizontal
- 2x fine rotary
- 1x fine vertical

Most people with nystagmus have a particular head position that results in the slowest movement of their eyes and therefore better contrast sensitivity - the ”null point”. While it seems intuitive that a reduction in nystagmus in this position would in turn favour visual function, minimising the amplitude of the nystagmus waveform does not necessarily mean an improvement in visual acuity [396]. Further, results presented in this thesis in Section 2.3.4.1 showed no influence of the presence of nystagmus on visual spatial resolution in patients with ON-pathway dysfunction. Visual performance, in fact, seems rather to depend on the alignment and duration of foveation periods present in an individual's nystagmus waveform [397]. Even though visual acuity does not seem to be linked to performance in motion perception tasks, subjects with nystagmus were allowed to watch the stimulus in their naturally preferred ”null position”. Further, by including the possibility to change dot-size

in the software and by using supra-threshold dot sizes, it was ensured that the dot visibility was excluded as a confounding factor.

In the case of motion perception, one could argue further that a constant involuntary retinal image motion might ”adapt” the visual system of an individual with nystagmus to this particular motion direction. For example, if the subject has a horizontal nystagmus, and a stimulus with horizontal motion is used for the psychophysical assessment, the threshold obtained from this individual could be affected by the nystagmus-related adaptation of his/her visual system. Considering this, Lappin and colleagues (2009) found subjects with congenital nystagmus to perform as well as healthy volunteers in motion perception tasks, as long as the speed of the dots was above 1 deg/s [398]. **Even so, in order to exclude any possibility of such a confounding ”pre-adaptation” of the visual system in patients with nystagmus, the option of varying the dot motion direction from left / right to up / down was included in the coherent motion perception test (Test 1) - where the detection of dot motion direction was crucial. This allowed some flexibility in cases where a patient might have nystagmus.**

#### 5.5.5.4 Dot density

The density of dots in the stimulus display is an important factor to consider when creating a random dot display as it influences performance. A value of **32 dots/deg**$^2$ was previously reported to result in adult-like motion coherence threshold values in three year-old children [399]. In order to maintain testing parameters which are as robust as possible to the variation in age and visual performance encountered in clinical paediatric care, an equivalent density was used for stimulus presentation in *LumiTrack*$^{Tm}$. Further, it was anticipated that children should be able to carry out the *LumiTrack*$^{Tm}$ tasks from a young age.

Whereas the authors used dots of 1 px in size [399], it was necessary to use a display of bigger dots for this study in view of very variable visual performance exhibited by patients with ON-pathway dysfunction. Hence, in order to match the testing conditions used by Parrish and colleagues [399], the relative dot density was kept constant when changing dot sizes. This resulted in different dot amounts being

displayed depending on dot size in order to maintain the ideal dot density:

| Dot size [pixel] | Amount of dots required to maintain relative density |
|---|---|
| 5 | 1081 |
| 10 | 541 |
| 15 | 361 |
| 20 | 270 |

#### 5.5.5.5 Dot lifetime

In order to eliminate the possibility for the subject to track an individual dot over time and therefore use local motion cues to guess the overall direction of the coherent motion used in *LumiTrack*$^{Tm}$, it was important to limit the time any one dot was displayed on the screen (its "lifetime") [400]. In such a situation, the visual system is facing a temporal correspondence problem [379] and resulting from this, the perception of coherent motion is extracted by temporal and spatial integration of local motion signals [401, 402]. During animation, **a new set of signal dots were randomly chosen to move in the signal direction every 200ms**. The noise dots exhibited the same lifetime but were randomly relocated (similar to the parameter used previously in dyslexic adults [387] or in autistic children [386]). In order to avoid all dots disappearing at the same time and thereby interrupting the perception of coherent motion, the "renewal moment" for signal and noise dots was temporally shifted.

#### 5.5.5.6 Stimulus display time

As *LumiTrack*$^{Tm}$ was designed to be mainly used in children, the maturation of the obtained threshold values was of importance in selecting the stimulus display time for the tests. The stimulus display time represents the time a subject has, in order to respond to the stimulus by pressing a key (or verbally). Generally, studies with limited stimulus display time found a later maturation of motion perception thresholds than studies using an unlimited display time.

Parrish and colleagues (2005) stated adult-like coherence thresholds from an age of three to four years using unlimited dot life-time, whereas Atkinson and colleagues (2003), as well as Ellemberg and colleagues (2002), using limited dot life-

times, only confirmed adult-like thresholds in children of five years and older or six years, respectively [399, 403, 127]. In view of this study's patient cohort age range, an unlimited stimulus presentation time was chosen[9] for *LumiTrack*$^{Tm}$. A limited presentation time was considered to be quite difficult to handle for young children, especially at low signal to noise ratios. I aimed for *LumiTrack*$^{Tm}$ to be useful across a wide age range and an unlimited stimulus presentation and response time allowed the tests to be carried out in children from around four years. Making the test easier to carry out, on the other hand, could have the potential to mask any deficit in patients to some extent. However, two of the ON-pathway cohort subgroups consisted of boys with DMD who can have neuromuscular issues and therefore might not be able to respond quickly. This could introduce abnormalities into the dataset which would not solely be due to visual impairment.

Ultimately, three different motion domains were targeted with this software, which required three very distinct visual tasks. While Test 1, detecting coherent motion direction, might be quickly responded to, especially Test 3 - the biological motion task - required the subjects to find the point-light-walker in a mask of noise dots (which can take time, especially in young children) and then making a decision of the figure's facing direction. In support of this, previous work highlighted the improvement in performance with increased display duration [376]. It was considered most important to allow all subjects to perform at their best and therefore obtain a true representation of their visual perception through the resulting threshold values. Hence, **stimulus presentation was terminated upon key-press by the subject** [10].

[9]The software gives the opportunity to switch to a limited presentation time if required. This feature was not used to obtain the data in this study

[10]While the reaction time of each response was recorded by the software, it was not taken into account during the data analysis due to the fluctuation of neuromuscular abilities and ages across the cohort subgroups.

#### 5.5.5.7 Dot speed

While there is generally little agreement in the literature on which dot speeds favour early maturation, some valuable conclusions can be derived from work where several different dot speeds were compared within the same study. In such studies, higher thresholds and larger age-related changes were reported for slower speeds compared to faster ones (for example [404]: 1.5 deg/s vs. 6 and 9 deg/s). This suggests that higher dot speeds (over 1.5 deg/s) seem to allow for adult-like motion coherence threshold levels from a younger age and therefore were considered favourable when testing children.

When taking nystagmus into account, as mentioned earlier, dot speeds under 2 deg/s were associated with elevated global motion coherence thresholds in observers with congenital nystagmus. Motion thresholds obtained with dot speeds exceeding this velocity were normal in subjects with nystagmus [398]. As it was the aim to minimise any influence of nystagmus on motion perception in the patient cohort, a minimum speed of 2 deg/s was anticipated for the test battery. In order to maintain a constant set of parameters across the different tests in the $LumiTrack^{Tm}$ software and to minimise developmental effects and potential effects of nystagmus on motion coherence thresholds, **dot speed was kept constant at 5 deg/s**.

#### 5.5.5.8 Stimulus field size and shape

The stimulus field was chosen to be a **central square of 13 deg**$^2$ containing all noise and signal dots[11]. An exception was the stimulus field for the shape from motion task (Test 2), where it was necessary to display two of these stimulus fields in order to display two different shapes. In this case, both stimulus fields were squares of 13 deg$^2$.

The size of the field was chosen as it was the biggest field size possible to be displayed on the laptop screen while maintaining equal field side lengths. The information of stimulus field size and shape is not always given in the literature but studies which mention this parameter used field sizes between 7 deg$^2$ and 30 deg$^2$ [386, 378]. The deciding factor for these sizes seemed to be mostly the available screen size, similar to the situation in this study.

Equal side length for the stimulus field was selected because of the ease of calculating dot density, as well as having a symmetric stimulation across the visual field of a subject[12].

[11] When viewed at a distance of 57cm.

[12] This means, the same visual field area is stimulated in all directions when fixating the centre of the stimulus display.

### 5.5.6 Laptop specifications

#### 5.5.6.1 Dell Latitude E7240

Resolution: 1366x768px

Screen size: Width 28cm, Height 15.6cm, Diagonal 31.75cm

Screen type: LCD

Screen refresh rate: 60Hz

sRGB gamma: 1.0 (factory default)

Processor: Intel core i7-4600U vPro

Memory: 8GB

Hard Drive: 256 Solid State Drive

Video Card: Intel HD Graphics 4400

#### 5.5.6.2 Output luminance and stimulus contrast

The output luminance was linked to the absolute RGB values used when programming the stimuli. The following values are the minima and maxima of the laptop output luminances with screen brightness at the highest level. Care was taken to remove or disable any in-built adaptive brightness processes which could have an influence on output luminance.

Stimulus luminance range:

12.1 cd/m$^2$ (black, RGB value 0) - 169.8 cd/m$^2$ (white, RGB value 255)

Stimulus background luminance for contrast sensitivity tasks:

56.6 cd/m$^2$ (mid grey, RGB value 128)

The resulting maximum Michelson contrast values for the stimulus display were:

| Stimulus | Michelson contrast |
|---|---|
| Black stimulus + white background<br>White stimulus + black background | 86.7% |
| Black stimulus + grey background | 64.7% |
| White stimulus + grey background | 50.0% |

### 5.5.7 Summary

The psychophysical tests were designed to keep parameters constant across all test conditions as far as possible. This was considered critical, as published studies applying motion psychophysical tasks vary considerably in parameter choice both within and across studies which causes a great variation in absolute threshold values obtained. Constancy of key parameters facilitates subsequent comparison across the test battery and allows a hierarchical assessment of motion and contrast sensitivity of motion within a subject.

$LumiTrack^{Tm}$ aimed at assessing different domains of motion and contrast vision in a manner of increasing complexity of the stimulus and cortical target. Four different domains of visual processing were incorporated in the test battery. These are listed below in increasing complexity. Figure 5.8 shows a schematic of the cortical targets of each individual test.

- The **coherent motion task** requires the integration of local motion cues into global motion (Figure 5.2)
- The **shape from motion task** requires both local motion integration and processing of implied form information (Figure 5.3).
- The **biological motion task** additionally requires integration from basic visual motion perception along with top-down social cognition (Figures 5.4 and 5.5).
- The assessment of the **contrast sensitivity** of these three motion tasks was a novelty in the approach. To the author's knowledge, this had not been evaluated previously and was anticipated to assess the impact of ON-pathway dysfunction on vision more selectively.

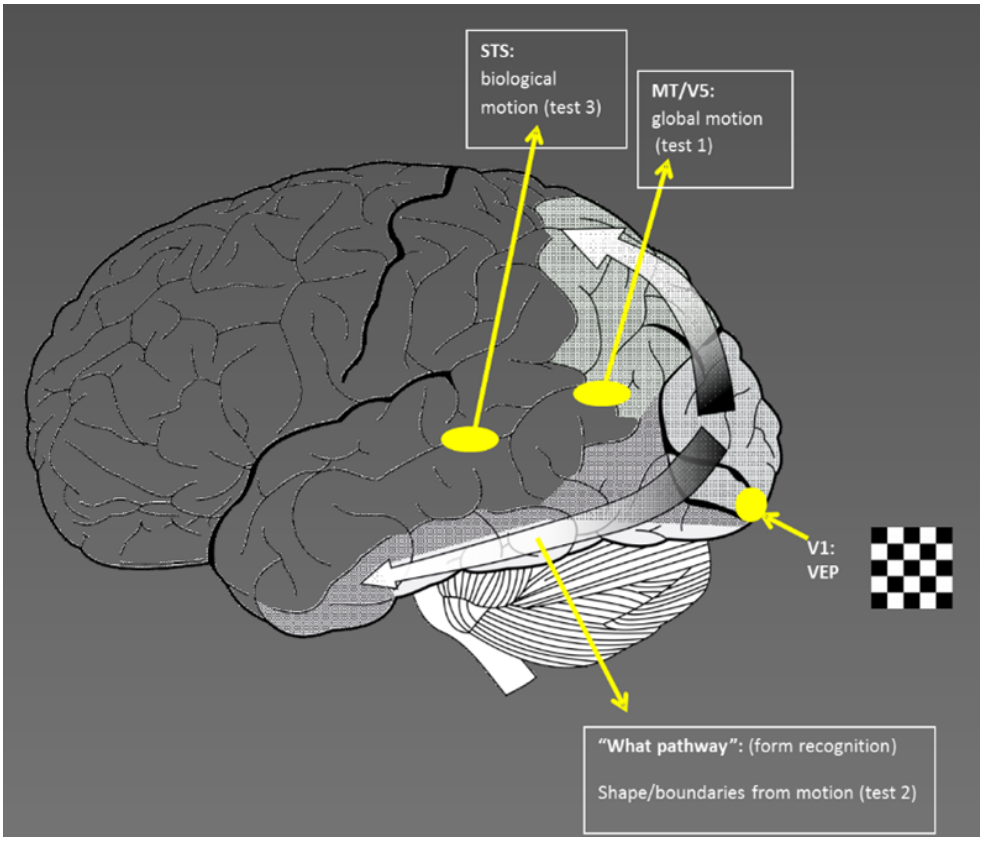


**Figure 5.8:** The cortical targets of the *LumiTrack*$^{Tm}$ test battery are indicated. Taken from [22] and altered.

A short summary of the parameters applied in the *LumiTrack*$^{Tm}$ psychophysical test battery is given below. The protocol that was followed for testing is displayed in Figure 5.9[13].

- Adaptive 3down/1up staircase with decreasing step-size over 10 reversals
- Changeable dot size according to individual needs of the subject
- Dot density relative to 32 dots/deg$^2$
- Dot lifetime of 200ms after which each dot gets randomly replaced
- Stimulus display time until key-press
- Dot speed of 5 deg/s
- Square stimulus field of 13deg$^2$ viewed from 57cm distance

[13]While the pre-test dot detection task was always carried out before the actual testing began, the order of Tests 1, 2 and 3 was always kept random.

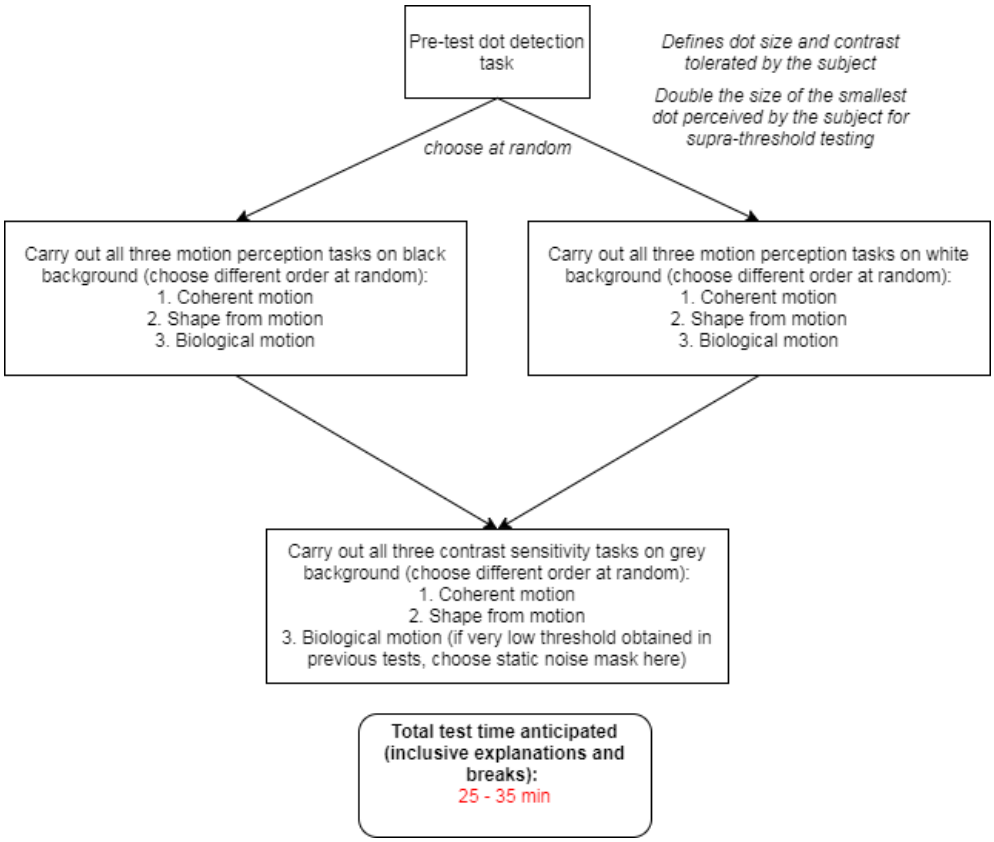


**Figure 5.9:** The protocol utilised for psychophysical testing with *LumiTrack*$^{Tm}$.

This unique battery of perceptual tasks of increasing complexity aimed to delineate motion perception and contrast sensitivity impairments that result from retinal ON-pathway dysfunction. A novelty in this approach was the addition of a contrast sensitivity assessment in moving stimuli, as well as keeping a constant set of parameters across the assessment of different motion and contrast vision domains. The motion tasks were similar to those previously used by others in the field with the advantage of consistent integrated parameters across all the tests in $LumiTrack^{Tm}$. This allowed a cohort-wide comparison of motion and contrast vision in patients with retinal ON-pathway dysfunction. The next step after design and development of the $LumiTrack^{Tm}$ software was to validate its functionality in healthy volunteers of all ages, which is discussed in the next section (5.6.1).

## 5.6 Results

### 5.6.1 Healthy volunteers

After design and implementation of a psychophysical test, the validation of its functionality is a crucial step. *LumiTrack*$^{Tm}$ was trialled in a cohort of 150 healthy volunteers[14] (median age: 10 years, range: 4 - 50 years) who were recruited mostly from local schools via Coram's Fields Playground in London[15], as well as Brentwood Preparatory School in Essex[16]. A detailed analysis of the results obtained from this cohort is outlined in the following sections.

[14] This number represents the total amount of healthy volunteers who carried out at least one of the *LumiTrack*$^{Tm}$ tests. Detailed subject participation numbers for each individual test are mentioned in the corresponding sections.

[15] www.coramsfields.org.uk

[16] www.brentwoodschool.co.uk

#### 5.6.1.1 A guide to data presentation

Before presenting the results obtained from healthy volunteers and their analysis, I want to explain how these data were derived and treated before graphical representation:

- **Motion perception** was always assessed at a 100% contrast, either positive (white dots on black ground) or negative (black dots on white ground). In order to obtain a value representing the motion perception performance of each subject, the adaptive staircase method discussed in section 5.5.5.1 was used. The resulting value from the average of the last eight reversals, represented the individual motion threshold of a subject. In the case of Tests 1 (Coherent motion) and 2 (Shape from motion), the lower this threshold value was, the better was the performance. This meant for Test 1, requiring less signal dots (a lower signal / noise ratio) in order to correctly perceive coherent motion of dots in one direction. For Test 2, a lower threshold value signified requiring less signal dots to make up a shape, but still being able to distinguish the square and the diamond. The inverse was true for Test 3 (Biological motion), where a higher threshold translated into tolerating a higher amount of noise.
- The outcome of the **contrast sensitivity** assessment was a range of values for each subject[17], which represented the dot vs. background contrasts, which were too low for the subject to perceive (in positive and negative contrast spectra). If the contrast was increased so much as to lie outside this range, the individual was able to reliably perceive the stimulus again.
- The following sections provide empirical validation of the parameter choice discussed earlier, as well as giving an overview over the actual motion and contrast sensitivity values obtained from healthy volunteers.

[17] The way this was obtained is explained in more detail in section 5.5.4.

#### 5.6.1.2 Visual acuity does not influence motion threshold

Although parametrically it was ensured that visual acuity (VA) and dot size should not be a barrier or influence thresholds, it was subsequently empirically demonstrated in the study cohort of healthy controls. This was important as patients with ON-pathway dysfunction can display a great range of visual acuities and exclusion of VA as having an effect on these visual functions would make the results obtained with the *LumiTrack*$^{Tm}$ software more reliable[18].

The visual acuity of all subjects in the control cohort was assessed by using a 3m Keeler LogMAR Crowded Test (Keeler Ltd. Windsor, England) prior to the psychophysical tasks and each subject had a best corrected visual acuity with both eyes viewing appropriate for their age (median VA BEO: -0.075logMAR , range: -0.275 - +0.35logMAR). Figure 5.10 displays the motion threshold values of all subjects linked with their respective visual acuity. The regression analysis of the data showed very low adjusted $R^2$ values for all three tests and additionally very similar values for 100% positive and negative contrast stimulation (Test 1: positive contrast = 0.19, negative contrast = 0.24; Test 2: positive contrast = 0.02, negative contrast 0.05; Test 3: positive contrast = 0.28, negative contrast = 0.27). This indicates a large spread in the threshold data. In addition, no influence of contrast (positive or negative contrast) was observed, giving a very similar data point distribution for both conditions[19].

As expected from parameter choice, no influence of visual acuity on threshold values could be observed when comparing the correlations across tests. The reason for this is most likely the relatively big spread of the data. This analysis does not include the age of the participants and hence possibly influences the data spread. Visual acuity is known to mature until up to six years of age (see for example [116]) but can be adult-like already earlier in life (for example [113, 99]). While the control cohort sampled many children from the age of around six to seven years onward, fewer children of the ages four to five were tested with *LumiTrack*$^{Tm}$. Additionally,

[18]Further, in Section 2.3.4.1 of this thesis, an influence of nystagmus on VA in patients was not observed.

[19]The effect of the different contrast conditions will be discussed in section 5.6.1.5

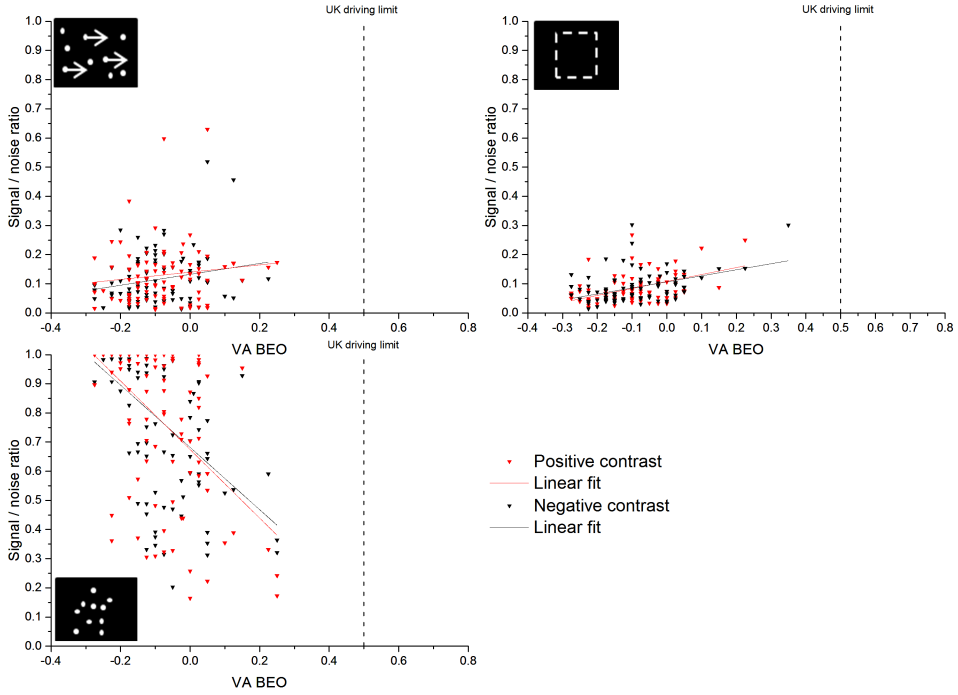


**Figure 5.10:** Scatter plot of motion perception thresholds for all three *LumiTrack*$^{Tm}$ tasks for positive (red symbols) and negative (black symbols) contrast conditions across binocular visual acuities. Linear fits were added to the data.

motion perception is expected to be subject to a developmental improvement in threshold levels in the first years of life (see for example [399]). The data obtained in this study cohort confirms such a maturation in young children. It is possible that the few subjects displaying a lower visual acuity (but still well within expected limits), as well as a poorer motion threshold value are younger children and thus the relationship of age and VA, as well as age and motion threshold skews the data slightly. Nonetheless, this skewing is not enough to derive a good coefficient of determination (adjusted $R^2$), and therefore a causative relationship, between VA and motion perception from these data. This finding is in line with previous reports suggesting no correlation for VA values and motion thresholds in human subjects (for example [231]).

### 5.6.1.3 Dot size does not influence motion threshold

During the design stage of *LumiTrack*$^{Tm}$, care was taken to be aware of the minimum dot size required for visibility after taking into account the visual acuity values in the patient cohort. Moreover, the software included a pre-test assessment of dot visibility and the dot size used during the psychophysical tasks could be changed accordingly. Hence, it was important to know whether the use of different dot sizes influenced the thresholds obtained. In order to investigate this, several subjects agreed to carry out the *LumiTrack*$^{Tm}$ tests using dot sizes ranging from 1 px to 20 px. Figures 5.11 and 5.12 present the results of this investigation.

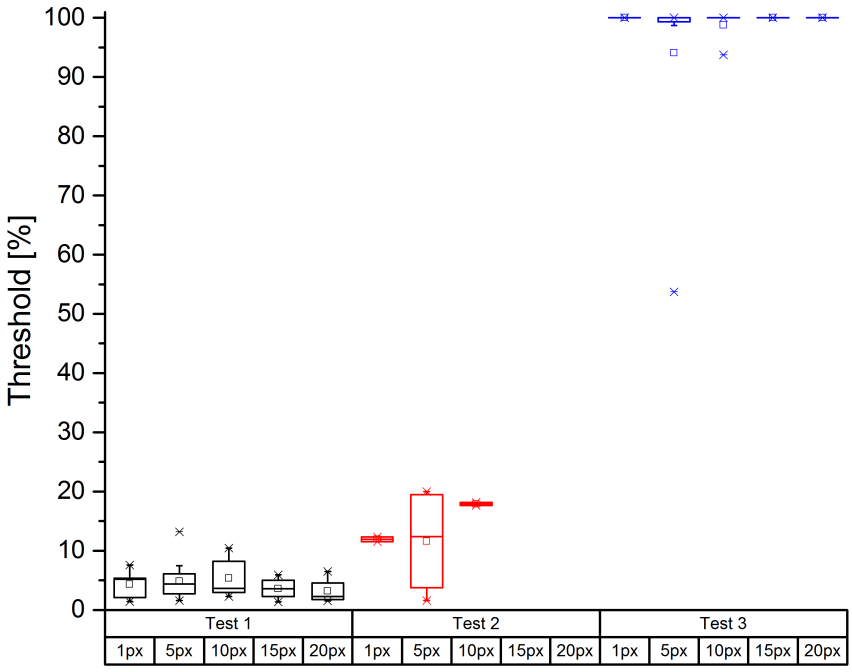


**Figure 5.11:** All three motion perception tests were carried out by healthy volunteers with dot sizes ranging from 1 px to 20 px (Test 1/coherent motion task: n= 14, Test 2/shape from motion task: n= 7, Test 3/biological motion task: n= 8). No data was obtained for dot sizes 15 px and 20 px for Test 2. Boxes give Max and Min (-), Mean (square), Median (line inside the boxes), 99% and 1% (x), as well as 75% and 25% (margins of the boxes) percentiles.

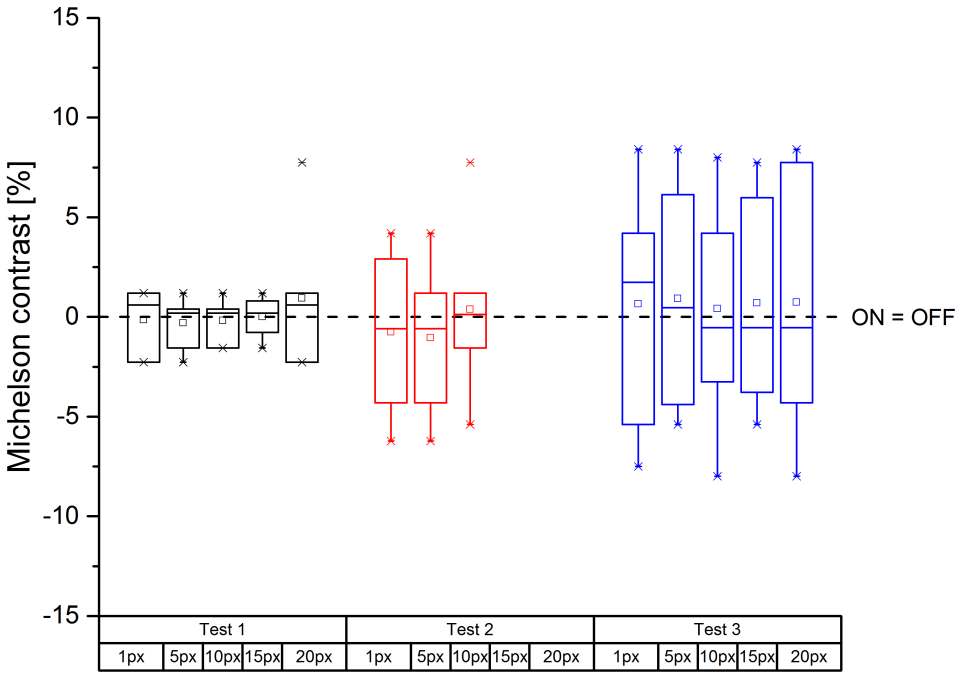


**Figure 5.12:** All three contrast sensitivity of motion perception tests were carried out by healthy volunteers with dot sizes ranging from 1 px to 20 px (Test 1/coherent motion task: n= 6, Test 2/shape from motion task: n= 6, Test 3/biological motion task: n= 10). No data was obtained for dot sizes 15 px and 20 px for Test 2. Boxes give Max and Min (-), Mean (square), Median (line inside the boxes), 99% and 1% (x), as well as 75% and 25% (margins of the boxes) percentiles.

No significant difference in motion threshold values was obtained when using dots of different sizes (One-way ANOVA with Tukey means comparison: Test 1: $p>0.1$ for all conditions; Test 2: $p>0.2$ for all conditions; Test 3: $p>0.5$ for all conditions). Neither an analysis of the contrast sensitivity ranges across all three tests delivered a significant influence of dot size (One-way ANOVA with Tukey means comparison: Test 1: $p>0.05$ for all conditions; Test 2: $p>0.4$ for all conditions; Test 3: $p>0.1$ for all conditions). This supports a comparability of threshold values obtained from subjects who required the use of different dot sizes in their assessments.

#### 5.6.1.4 No influence of dot motion direction

It was possible to change the dot motion direction between horizontal and vertical in the coherent motion task (Test 1), in order to be flexible in cases where patients with nystagmus were assessed[20]. Being able to discriminate coherent motion direction was crucial for successful performance of this task. As the effect of a retinal ON-pathway dysfunction on coherent motion perception was intended to be subsequently assessed in the patient subgroups, it was important to exclude any effects inflicted by dot motion direction on threshold values. Figure 5.13 shows a comparison of threshold values of different dot motion directions across the whole healthy volunteer cohort ($n^{horizontal}$ = 65, $n^{vertical}$= 75).

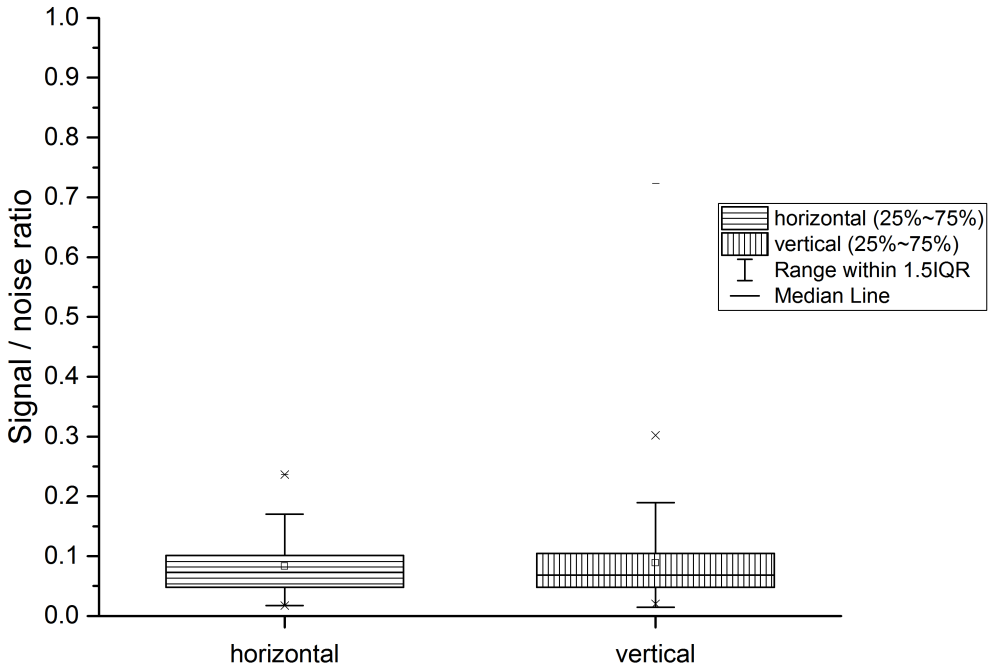


**Figure 5.13:** Coherent motion thresholds were obtained to horizontal and vertical dot motion direction and then compared. Boxes give Max and Min (-), Mean (square), Median (line inside the boxes), 99% and 1% (x), as well as 75% and 25% (margins of the boxes) percentiles.

[20] As discussed in the Methods (Section 5.5.5.3), nystagmus can be a confounding factor in vision testing but is not thought to influence motion perception assessed using random dot displays for dot speeds above 2 deg/s.

Statistical analysis of the data revealed no difference between the two conditions, confirming no influence on dot motion direction on coherent motion perception in healthy observers (Two sample t-test: p= 0.55). This allowed subsequent pooling of results obtained from Test 1 to either dot motion direction for healthy controls. Further, a comparison of results obtained from patients to different dot motion options was supported by this empirical evidence that dot motion direction does not influence thresholds obtained.

#### 5.6.1.5 Different contrast conditions do not influence motion threshold and contrast sensitivity

The *LumiTrack*$^{Tm}$ software was developed to assess motion perception and contrast sensitivity in children with ON-pathway dysfunction. An important feature included for this reason was the ability to test perception for positive and negative contrast conditions separately. In order to be able to analyse and compare ON and OFF systems in the patient cohort, it was important to assess their relationship in healthy volunteers. This gave an insight into the contributions of ON-and OFF-pathways to the perception of these visual functions. For this purpose, the results from positive contrast stimulation for motion and contrast sensitivity tests were compared to the results obtained from negative contrast stimulation. The results are presented in Figures 5.14 and 5.15.

Results across all three tests were remarkably similar (One-way ANOVA and Tukey means comparison: Test 1: p= 0.54, Test 2: p= 0.45, Test 3: p= 0.48), suggesting a comparable perception of positive and negative contrast displays in healthy observers (Figure 5.14). When comparing the contrast sensitivity of the ON and OFF systems (see Figure 5.15) a similar picture emerged (One-way ANOVA and Tukey means comparison: Test 1: p= 0.27, Test 2: p= 0.27, Test 3: p= 0.22). This highlights that these qualities conveyed via ON-and OFF-pathways are thought to be perceived equally.

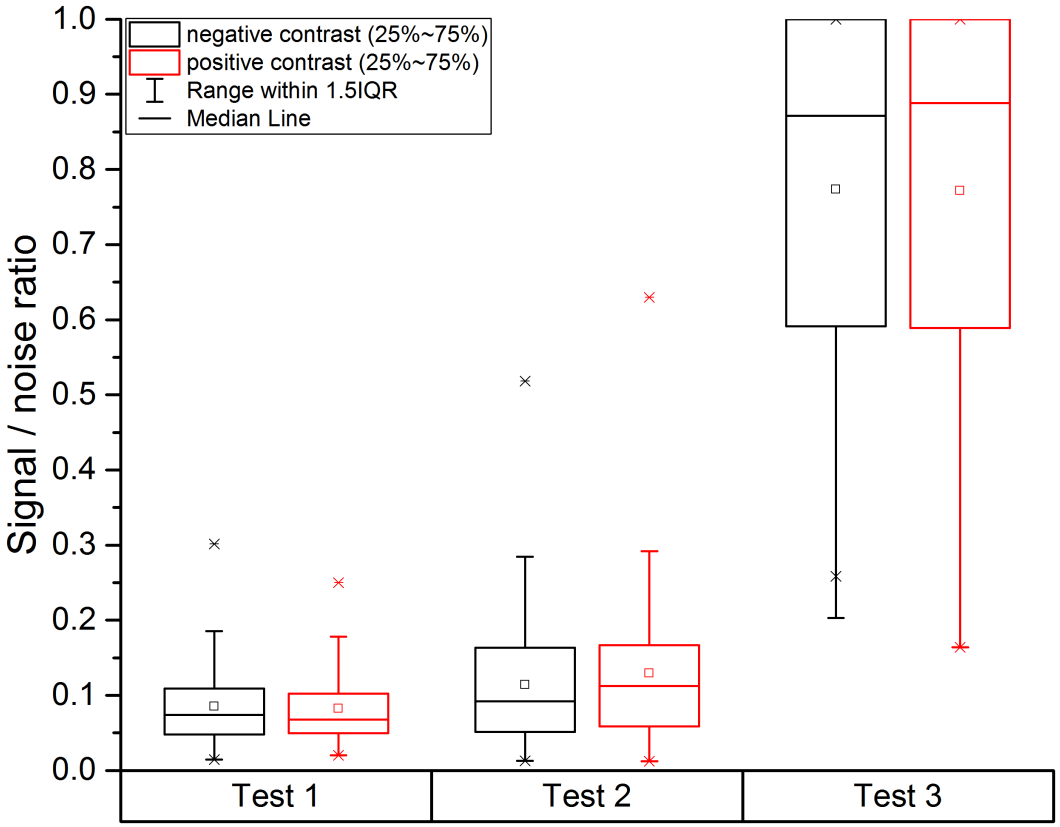


**Figure 5.14:** The motion threshold values for all three tests are shown (Test1: coherent motion task, Test 2: shape from motion task, Test 3: biological motion task). The values obtained from negative (black boxes) and positive (red boxes) contrast conditions are compared. Boxes give Max and Min (-), Mean (square), Median (line inside the boxes), 99% and 1% (x), as well as 75% and 25% (margins of the boxes) percentiles.Boxes give Max and Min (-), Mean (square), Median (line inside the boxes), 99% and 1% (x), as well as 75% and 25% (margins of the boxes) percentiles. Test 3 displays higher threshold values, as in this case, a higher threshold translated into a higher tolerance to noise in the biological motion display.

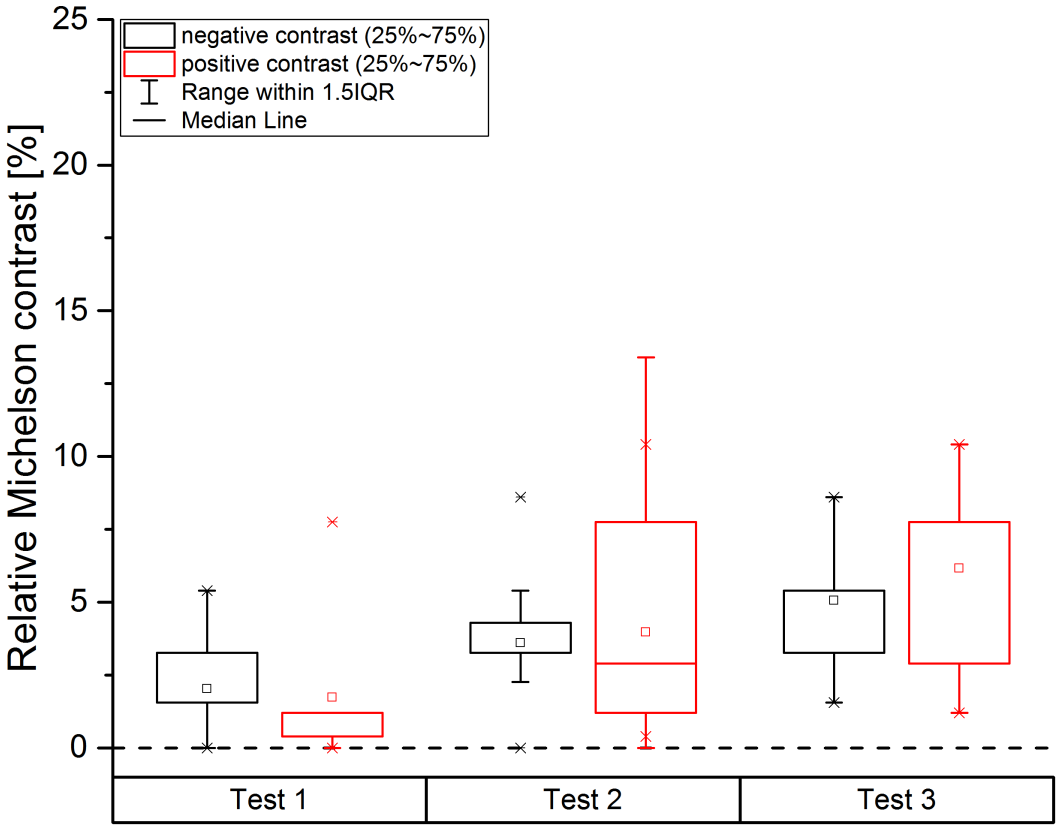


**Figure 5.15:** The relative contrast sensitivity ranges for all three tests are shown (Test 1/coherent motion task: n= 106; Test 2/shape from motion task: n= 111, Test 3/biological motion task: n= 102). The ranges of Michelson contrast required to successfully execute the tasks in negative (black boxes) and positive (red boxes) contrast conditions are compared. Boxes give Max and Min (-), Mean (square), Median (line inside the boxes), 99% and 1% (x), as well as 75% and 25% (margins of the boxes) percentiles.

#### 5.6.1.6 No training effect

An influence on results in psychophysical testing and the relationship between positive and negative contrast stimulation could come from the subjects displaying a change in performance over time due to a training effect. A training effect describes an improvement in performance as a result of repeated carrying out of the tests or due to carrying out the tests in a specific order which has a beneficial effect on performance. In order to investigate this possibility, the data obtained from healthy volunteers were analysed taking into account whether the positive or negative contrast condition was carried out first[21]. The results from this are shown in Figure 5.16. From this analysis, no statistically significant difference was observed (One-way ANOVA with Tukey means comparison: Test 1: $p>0.1$ for both conditions; Test 2: $p>0.3$ for both conditions; Test 3: $p>0.05$ for both conditions). This suggests that the results obtained from the *LumiTrack*$^{Tm}$ test battery are not influenced by a training effect or by the presentation order of contrast condition.

[21] During data acquisition, positive and negative contrast conditions were always assessed in a random order.

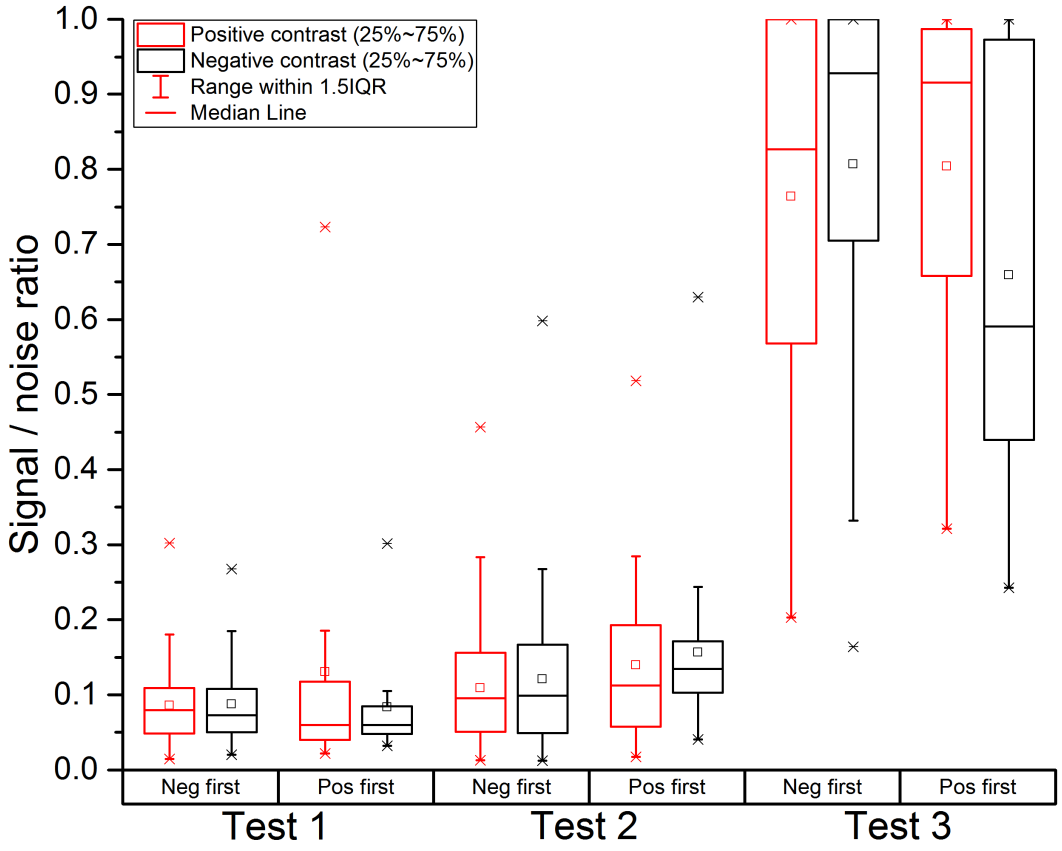


**Figure 5.16:** All three tests were compared taking into account the testing order with either the negative contrast condition first or the positive contrast condition first (Test1: coherent motion task, Test 2: shape from motion task, Test 3: biological motion task). Boxes give Max and Min (-), Mean (square), Median (line inside the boxes), 99% and 1% (x), as well as 75% and 25% (margins of the boxes) percentiles. Test 3 displays higher threshold values, as in this case, a higher threshold translated into a higher tolerance to noise in the biological motion display.

#### 5.6.1.7 Age-dependent improvement in performance - motion

After not finding any significant effects of several parameters on motion threshold and contrast sensitivity values obtained by using the *LumiTrack*$^{Tm}$ in healthy volunteers, the maturation of performance was investigated. In the literature, motion perception is suggested to change considerably with age, as the visual system is subject to maturation. This is also evident in other measures of visual function, such as visual acuity or the waveform of the VEP. For this reason, when recruiting healthy individuals for the validation of *LumiTrack*$^{Tm}$, care was taken to collect data from subjects across a wide age range (from 4 to 50 years of age). The threshold values of these subjects were plotted against their ages and the results are shown in Figures 5.17 - 5.19. In each graph, the results to positive and negative contrast, representing ON-and OFF-pathway processing, are shown next to each other for comparison. The amount of subjects who carried out the individual tests is included in the figure captions. This analysis gave an indication of the influence of age and the symmetry of ON and OFF processing in healthy individuals.

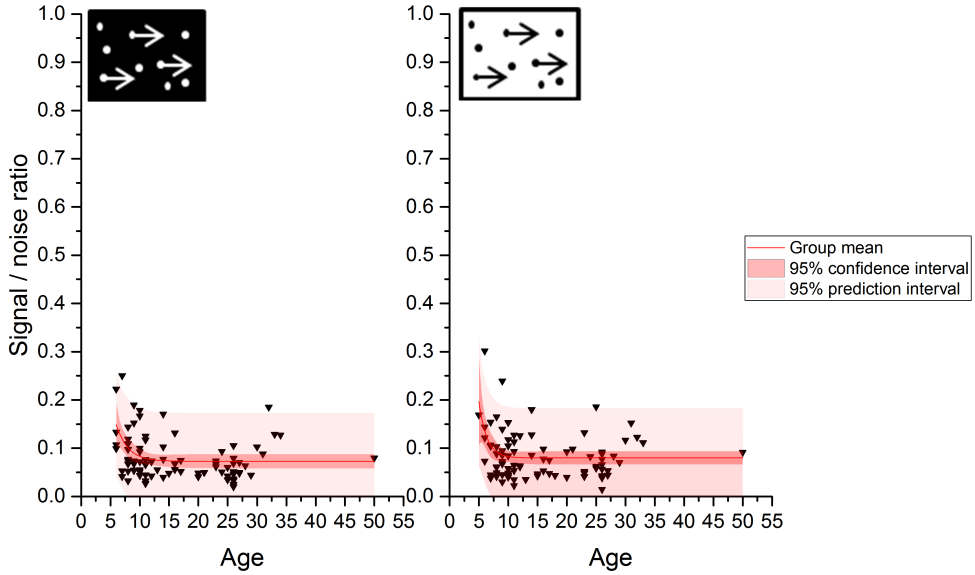


**Figure 5.17:** The two graphs display the development of coherent motion threshold values with age in the cohort of healthy volunteers. Thresholds were obtained to either horizontal or vertical dot motion. Each individual subject is indicated by a black, upside-down triangle. Also shown are the group mean (straight red line), 95% confidence interval (CI, dark red band) and 95% prediction interval (PI, light red band). The 95% CI indicates how well the group mean is chosen to represent the data, the 95% PI predicts the spread of 95% of the data. The results for positive contrast stimuli are given on the left (n= 101), the negative contrast results on the right (n= 101). The lower the value, the better the performance in this task (i.e. the fewer dots are needed to perceive a coherent motion in one direction).

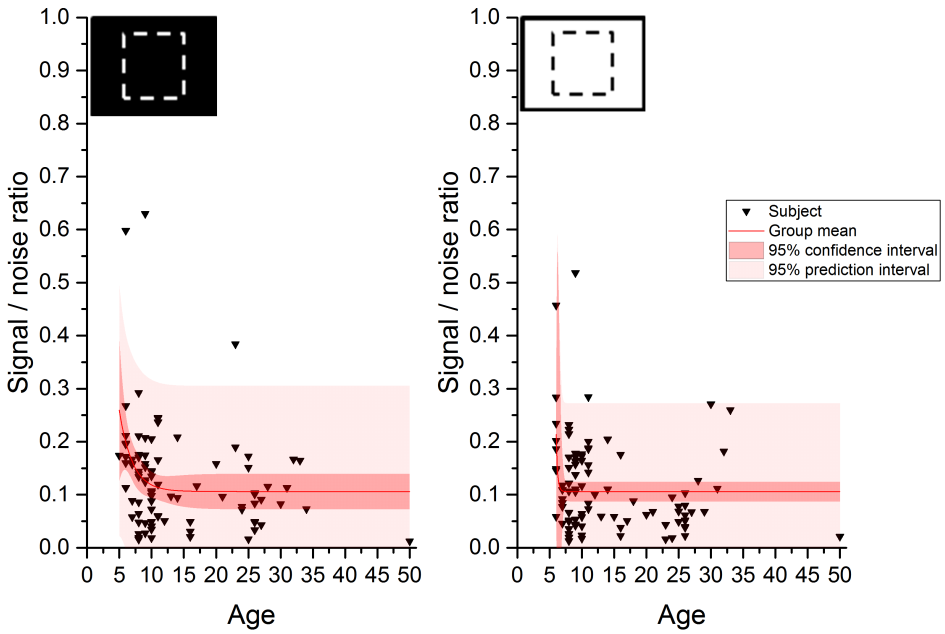


**Figure 5.18:** The two graphs display the development of shape from motion threshold values with age in the cohort of healthy volunteers. Each individual subject is indicated by a black, upside-down triangle. Also shown are the group mean (straight red line), 95% confidence interval (CI, dark red band) and 95% prediction interval (PI, light red band). The 95% CI indicates how well the group mean is chosen to represent the data, the 95% PI predicts the spread of 95% of the data. The results for positive contrast stimuli are given on the left (n= 93), the negative contrast results on the right (n= 99). The lower the value, the better the performance in this task (i.e. the fewer dots are needed to make up a shape, while still being able to distinguish the shapes reliably).

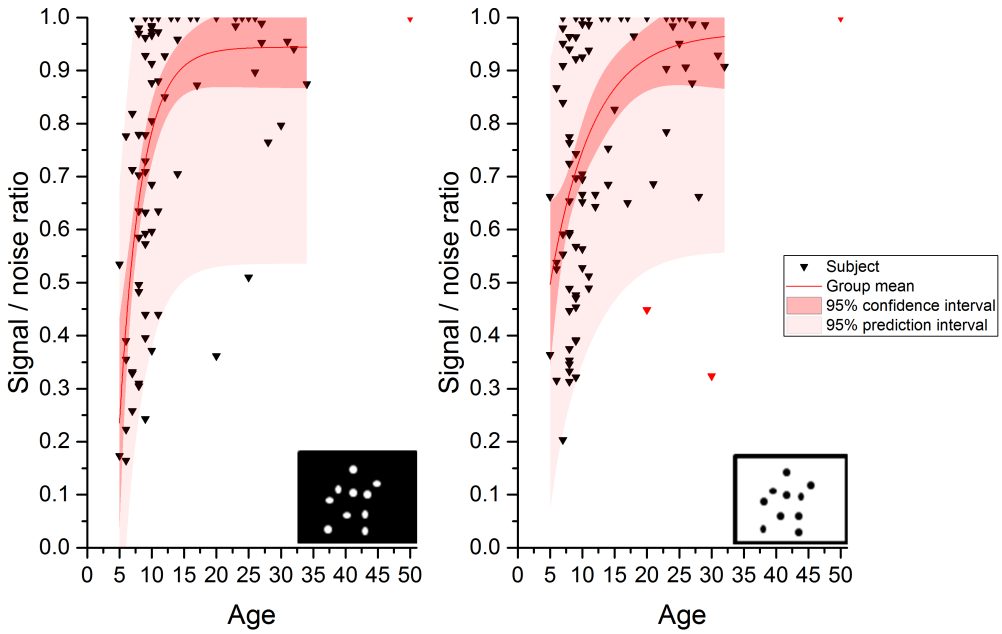


**Figure 5.19:** The two graphs display the development of biological motion threshold values with age in the cohort of healthy volunteers. Each individual subject is indicated by a black, upside-down triangle. Also shown are the group mean (straight red line), 95% confidence interval (CI, dark red band) and 95% prediction interval (PI, light red band). The 95% CI indicates how well the group mean is chosen to represent the data, the 95% PI predicts the spread of 95% of the data. The results for positive contrast stimuli are given on the left (n= 97), the negative contrast results on the right (n= 106). The higher the value, the better the performance in this task (i.e. the more noise dots are tolerated).

There was a clear effect of age on the motion thresholds obtained in this control group. In all three tests, an improvement of performance with age was seen. This was true for positive, as well as negative contrast conditions. According to the data obtained in Test 1, an adult-like motion coherence threshold of 7% can be obtained from the age of 7 - 9 years (Figure 5.17). The data ranges from a minimum of 2% to a maximum of 27% with the "cut-off" for the 95% prediction interval (PI) being at a threshold of around 18%. Figure 5.18 displays the thresholds of subjects from the shape from motion task plotted against age. These data show wider ranges (for example: Min: 2% to Max: 63% in a 7 year old subject) until around 8 years of age, where the data spread narrows and an adult-like threshold of around 10% between the ages of 9 - 10 years is reached. According to these results, the upper limit of the 95% PI lies at around 28 - 30%. The data displayed in Figure 5.19 represents the biological motion threshold values for each subject plotted against age. Adult-like threshold levels here are reached slightly later than for the previous two tests and begin from around 10 - 12 years of age. However, for this test, the data generally show a much wider range from 15% (for children of 5-6 years) to 100% noise dots tolerated. This spread narrows somewhat as subject get older, with adult threshold values only varying from 30% to 100%. The lower limit of the 95% PI for Test 3 lay at around 53 - 55%.

Several studies have assessed motion coherence thresholds in the past but there is a high variation of parameters across studies, making absolute threshold value comparison difficult. Examples for this variability are dot speed - Taylor and colleagues (2009) applied a dot speed of 18 deg/s, while Cornelissen and colleagues (1995) applied 2.5 deg/s, or dot density - Parrish and colleagues (2005) used a density of 32 dots/deg$^2$, whereas Spencer and colleagues (2000) used a mere 4 dots/deg$^2$ [395, 126, 399]. This diversity in parameter choice resulted in very different motion thresholds obtained from subjects. Moreover, studies employing more than one motion test (for example motion coherence alongside biological motion) mostly failed to keep comparable parameters across the different tests. Nonetheless, the maturation of threshold values is comparable across studies. The majority

of studies comparing different age groups found an improvement of thresholds with age, with adults performing best. In order to compare the findings in the cohort of healthy volunteers with maturation curves suggested in the literature, Figures 5.20 - 5.22 show the data collected in this study compared to existing findings from different studies employing similar motion threshold assessments. For ease of presentation, only the results for positive contrast stimuli were compared, as threshold values and maturation were comparable between positive and negative contrast conditions for *LumiTrack*$^{Tm}$.

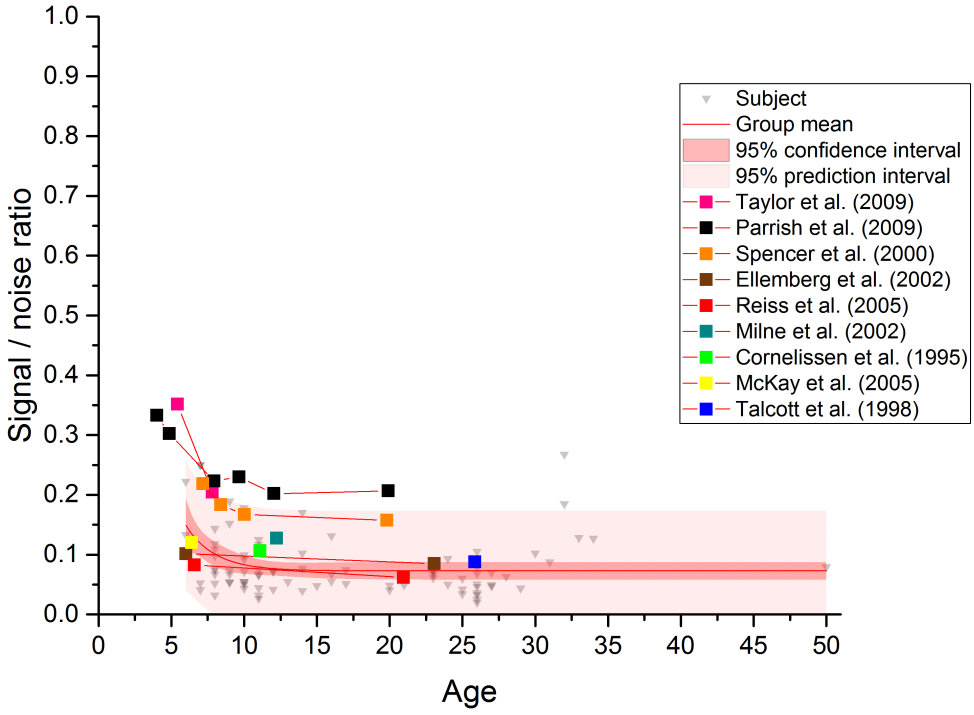


**Figure 5.20:** The graph displays the development of coherent motion threshold values with age in the cohort of healthy volunteers overlaid with values from the literature. Values obtained from the literature are squares of different colours, values obtained in this study are faded. Also shown are the group mean (straight red line), 95% confidence interval (CI, dark red band) and 95% prediction interval (PI, light red band) obtained from the results in this study.

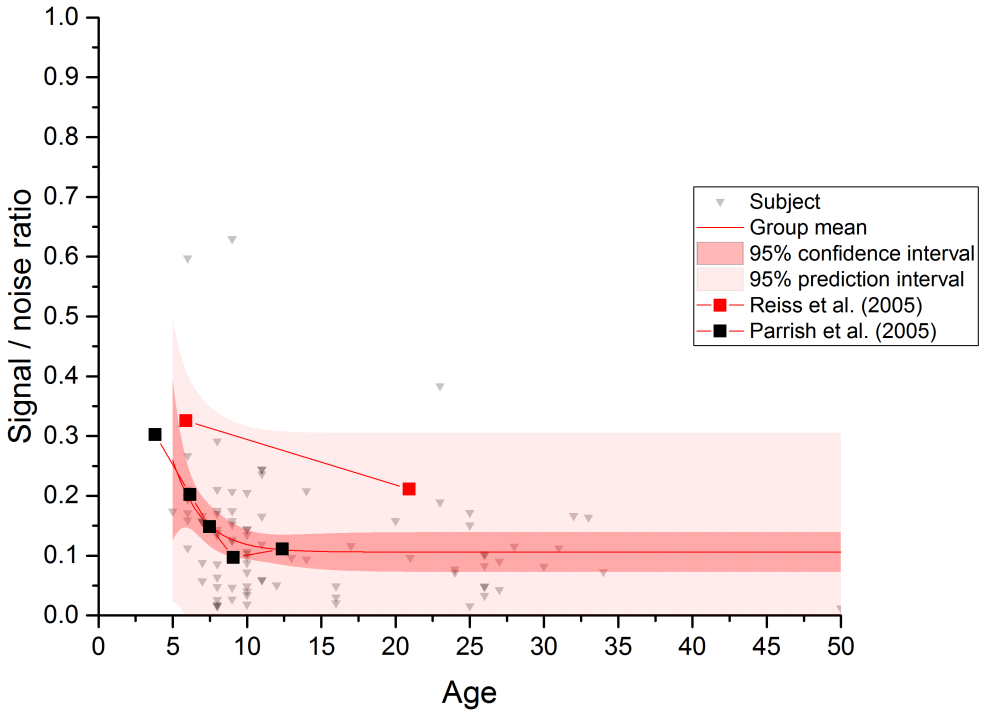


**Figure 5.21:** The graph displays the development of shape from motion threshold values with age in the cohort of healthy volunteers overlaid with values from the literature. Values obtained from the literature are squares of different colours, values obtained in this study are faded. Also shown are the group mean (straight red line), 95% confidence interval (CI, dark red band) and 95% prediction interval (PI, light red band) obtained from the results in this study.

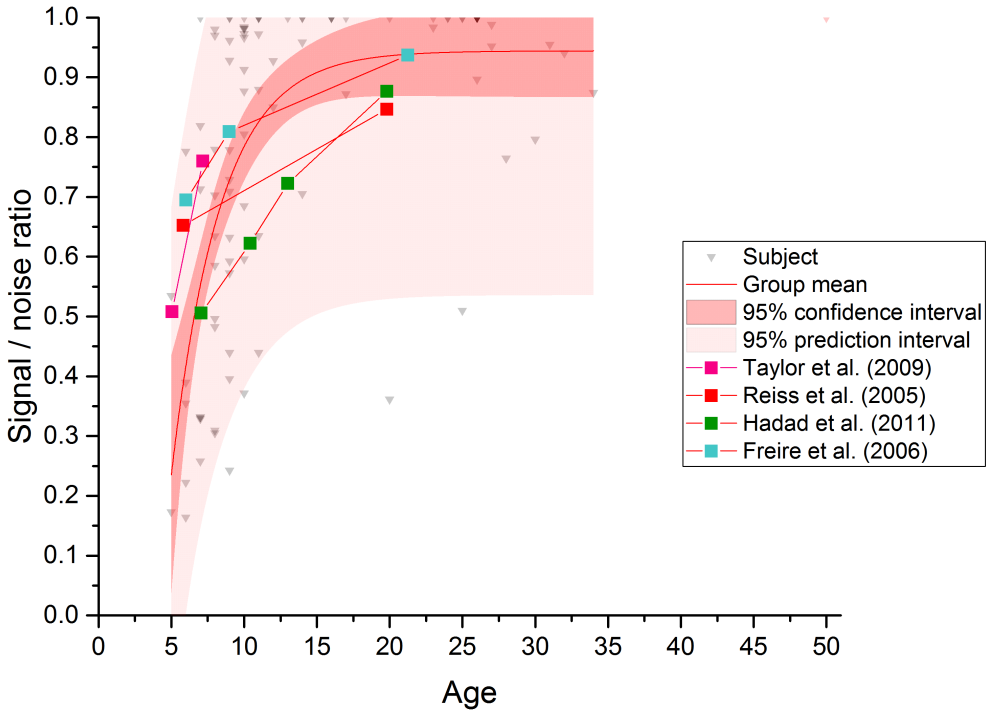


**Figure 5.22:** The graph displays the development of biological motion threshold values with age in the cohort of healthy volunteers overlaid with values from the literature. Values obtained from the literature are squares of different colours, values obtained in this study are faded. Also shown are the group mean (straight red line), 95% confidence interval (CI, dark red band) and 95% prediction interval (PI, light red band) obtained from the results in this study.

The motion threshold maturation observed in this study agrees well with the trajectories described in the literature. For Test 1, adult-like motion coherence thresholds are observed in subjects from 8 - 9 years (Figure 5.20). This is in agreement with other studies that even show overall more elevated motion coherence thresholds (for example [399, 378]), where adult-like threshold values are reached at around 9 - 10 years of age. Previous work studying shape from motion thresholds in healthy subjects is scarce; however, there are two studies who applied a shape from motion stimulus, showing a similar trend of a decreasing of the threshold with age (Figure 5.21) [405, 399]. All reported values fall within the range of values obtained in this study and show a similar trend of maturation. Most already existing data for biological motion tests point at a rather long developmental trajectory (for example [406]). The previously published data fall into a similar range as the control data collected in this study (Figure 5.22).

Overall, the threshold values obtained with $LumiTrack^{Tm}$ from a cohort of healthy volunteers improved with age and agree well with the trajectories reported in previous studies using similar psychophysical tasks. The difference in absolute threshold values across studies is most likely due to the application of different testing parameters. $LumiTrack^{Tm}$, however, is the first software to employ three assessments of different motion qualities of increasing complexity, while keeping the stimulus parameters constant.

#### 5.6.1.8 Task-dependent changes in performance - contrast sensitivity

The value ranges for the contrast sensitivity of motion perception did not fluctuate much with age. A slight narrowing of the range (i.e. needing a lower stimulus to background contrast in order to correctly perform the test) with increasing age was seen in Test 2, but the difference was minimal. However, it appeared that subjects required the stimulus to have different Michelson contrasts, depending on which test was carried out. The subjects required least contrast for correct execution of Test 1 and most for Test 3, with Test 2 requiring an intermediate contrast. Figure 5.26 highlights these findings, while Figures 5.23 - 5.25 show the obtained contrast sensitivity ranges for each task.

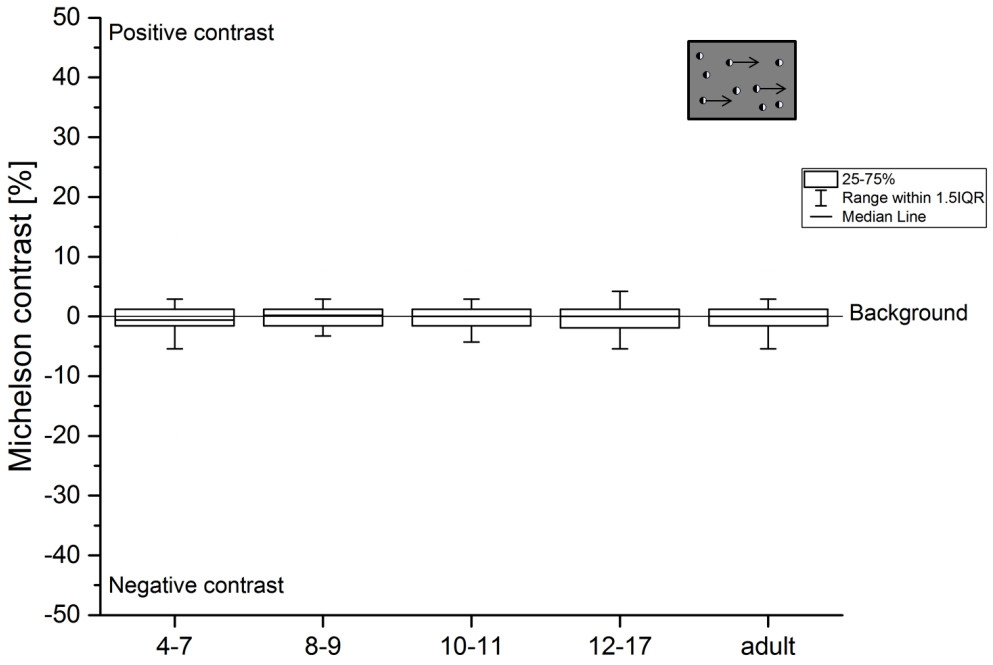


**Figure 5.23:** The graph shows the maturation of contrast sensitivity of coherent motion perception. Subjects (n= 99) were pooled by age. Displayed is the Michelson contrast range (positive and negative) for which the subjects could not perceive the stimulus. When using a higher (positive or negative) contrast value for the stimuli, the subjects were able to reliably give the correct answer. Boxes give Max and Min (-), Mean (square), Median (line inside the boxes), 99% and 1% (x), as well as 75% and 25% (margins of the boxes) percentiles.

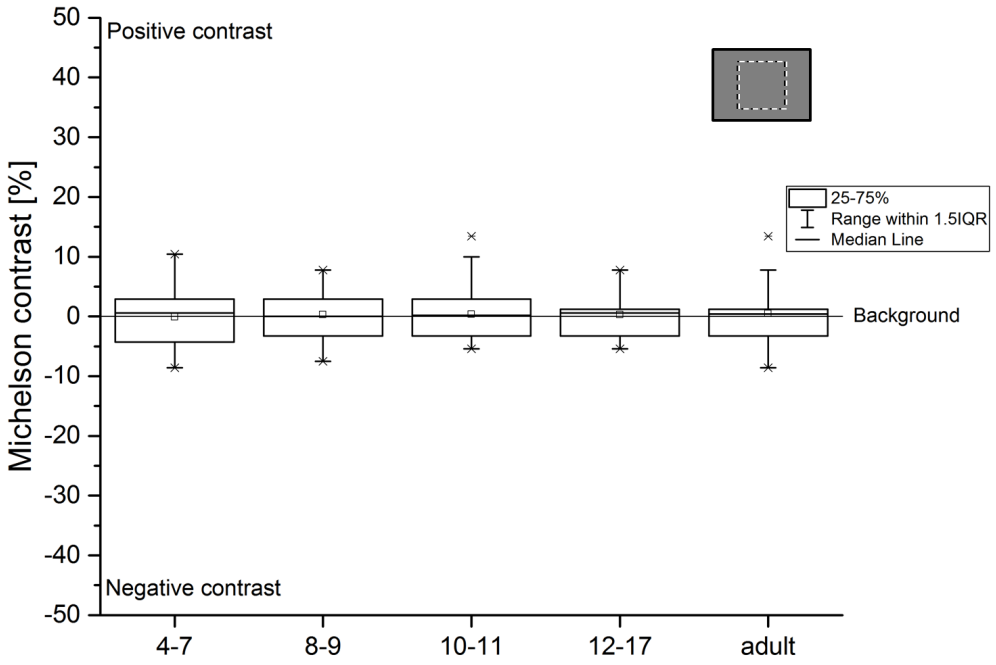


**Figure 5.24:** The graph shows the maturation of contrast sensitivity of shape from motion perception. Subjects (n= 101) were pooled by age. Displayed is the Michelson contrast range (positive and negative) for which the subjects could not perceive the stimulus. When using a higher (positive or negative) contrast value for the stimuli, the subjects were able to reliably give the correct answer. Boxes give Max and Min (-), Mean (square), Median (line inside the boxes), 99% and 1% (x), as well as 75% and 25% (margins of the boxes) percentiles.

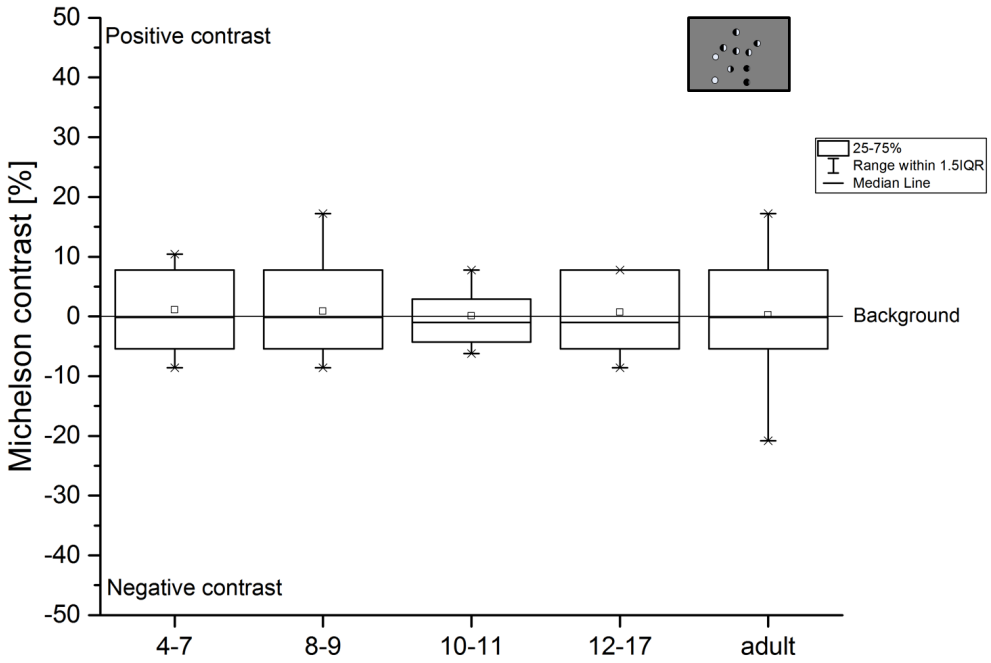


**Figure 5.25:** The graph shows the maturation of contrast sensitivity of biological motion perception. Subjects (n= 91) were pooled by age. Displayed is the Michelson contrast range (positive and negative) for which the subjects could not perceive the stimulus. When using a higher (positive or negative) contrast value for the stimuli, the subjects were able to reliably give the correct answer. Boxes give Max and Min (-), Mean (square), Median (line inside the boxes), 99% and 1% (x), as well as 75% and 25% (margins of the boxes) percentiles.

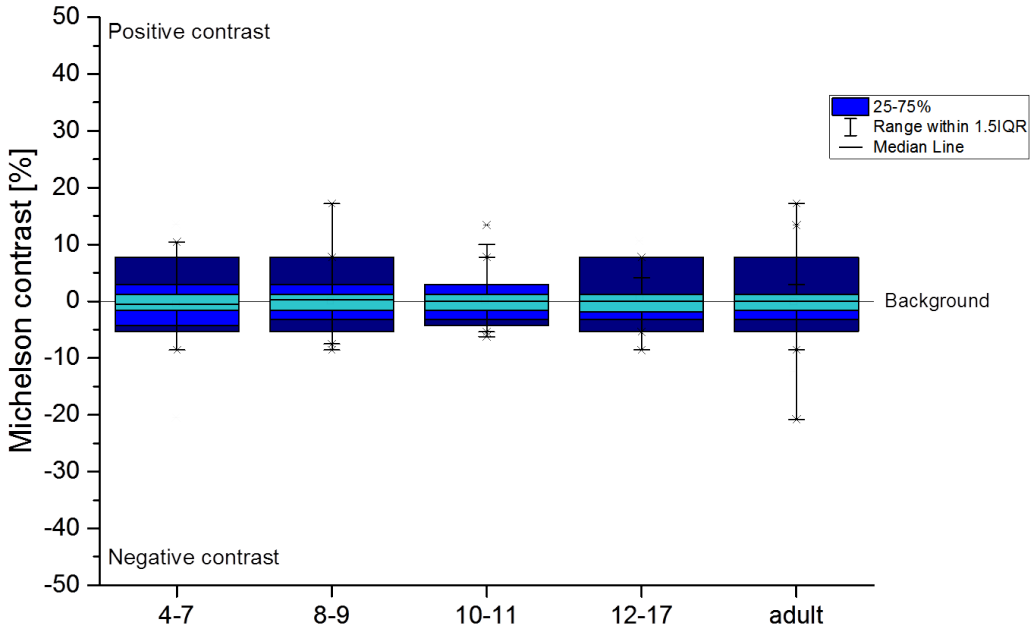


**Figure 5.26:** This summary graph shows the maturation of contrast sensitivity of coherent, shape from motion, as well as biological motion perception. Ranges for all tests are overlaid for comparison (Test 1: light blue; Test 2: mid-blue; Test 3: dark blue). Subjects were pooled by age. Displayed are the Michelson contrast ranges (positive and negative) for which the subjects could not perceive the stimulus. When using a higher (positive or negative) contrast value for the stimuli, the subjects were able to reliably give the correct answer. Boxes give Max and Min (-), Mean (square), Median (line inside the boxes), 99% and 1% (x), as well as 75% and 25% (margins of the boxes) percentiles.

#### 5.6.1.9 Summary

After validation of the software in a large cohort of healthy volunteers and a thorough analysis of the influence of different parameters on the results, age was found to impact motion perception greatly. When comparing the maturation trajectory of values from this study to other publications assessing similar visual functions, a good agreement of the development of performance was observed. From these results, normative data ranges for each test were derived. The results obtained from patients with ON-pathway dysfunction were subsequently compared to these ranges for positive and negative contrast conditions separately.

### 5.6.2 Clinical outcome - patient cohorts

After successfully trialling and validating the *LumiTrack*$^{Tm}$ psychophysical test battery in healthy volunteers and obtaining an reference data set covering a wide age-range, the impact of a retinal ON-pathway dysfunction on visual perception was assessed in the clinical cohort. Upon attendance of a patient in clinic for VEP recordings, the option of carrying out the *LumiTrack*$^{Tm}$ test battery was mentioned and the results of the assessments of those patients who agreed to participate are described below[22].

#### 5.6.2.1 Abnormal motion perception in patients

The investigation of a potential impact on higher cortical processing and perception of the asymmetry of ON and OFF signalling at the visual cortex described in the previous chapter, was assessed using a psychophysical test battery. Motion perception was one visual function hypothesised to be affected by such an imbalance in human subjects with retinal ON-pathway dysfunction. How patients from the clinical cohort performed in the newly designed *LumiTrack*$^{Tm}$ hierarchical motion tasks is laid out in Figures 5.27 - 5.29.

[22]In order to avoid an ascertainment bias in the selection of patients carrying out the novel tests, all patients over an age of 3yrs who agreed to take part in the study were approached to carry out the psychophysical tests.

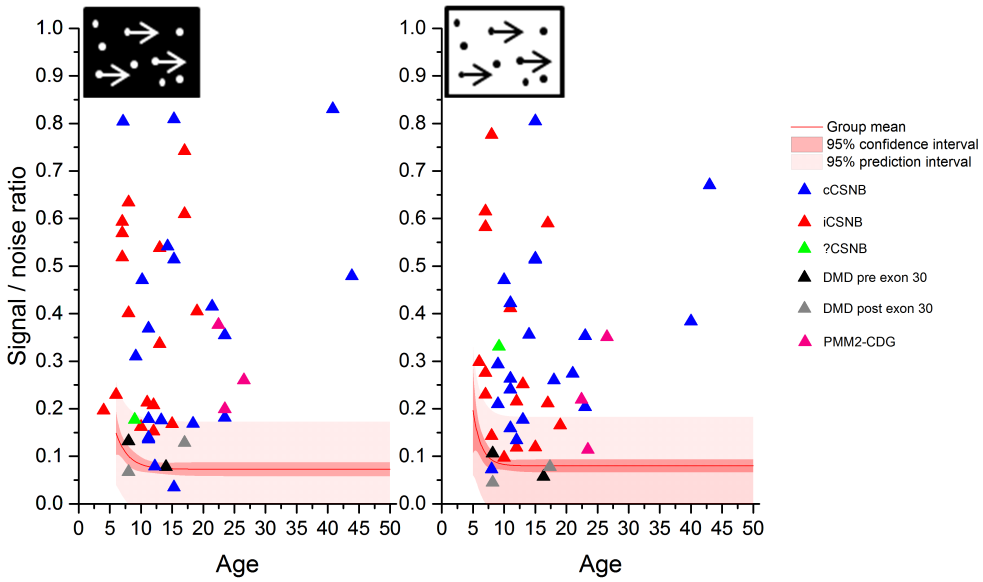


**Figure 5.27:** The normative data ranges for positive and negative contrast conditions obtained from healthy volunteers in the coherent motion task (Test 1) are overlaid by individual data points derived from patients (positive contrast: n= 42, negative contrast: n= 42). Triangles represent individual patients (blue = cCSNB, red = iCSNB, green = ?CSNB, black = DMD pre exon 30, grey = post exon 30, pink = PMM2-CDG). The normative data ranges comprise group mean (straight red line), 95% confidence interval (CI, dark red band) and 95% prediction interval (PI, light red band). The lower the value, the better the performance in this task (i.e. the fewer dots were needed to perceive a coherent motion in one direction). As mentioned in Section 5.6.1.4, dot motion direction was always selected to be orthogonal to a patient's nystagmus waveform. As dot motion direction was not shown to influence the coherent motion threshold, these data were pooled for display.

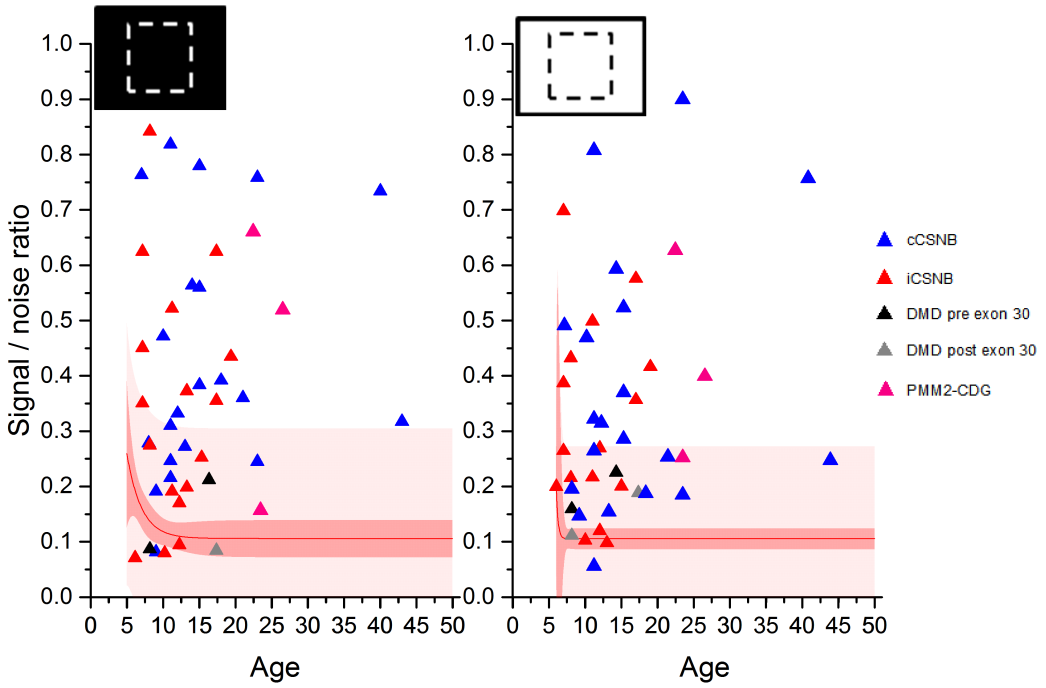


**Figure 5.28:** The normative data ranges for positive and negative contrast conditions obtained from healthy volunteers in the shape from motion task (Test 2) are overlaid by individual data points derived from patients (positive contrast: n= 41; negative contrast: n= 43) Triangles represent patients (blue = cCSNB, red = iCSNB, green = ?CSNB, black = DMD pre exon 30, grey = post exon 30, pink = PMM2-CDG). The normative data ranges comprise group mean (straight red line), 95% confidence interval (CI, dark red band) and 95% prediction interval (PI, light red band). The lower the value, the better the performance in this task (i.e. the fewer dots were needed to make up a shape, while still being able to distinguish the shapes reliably).

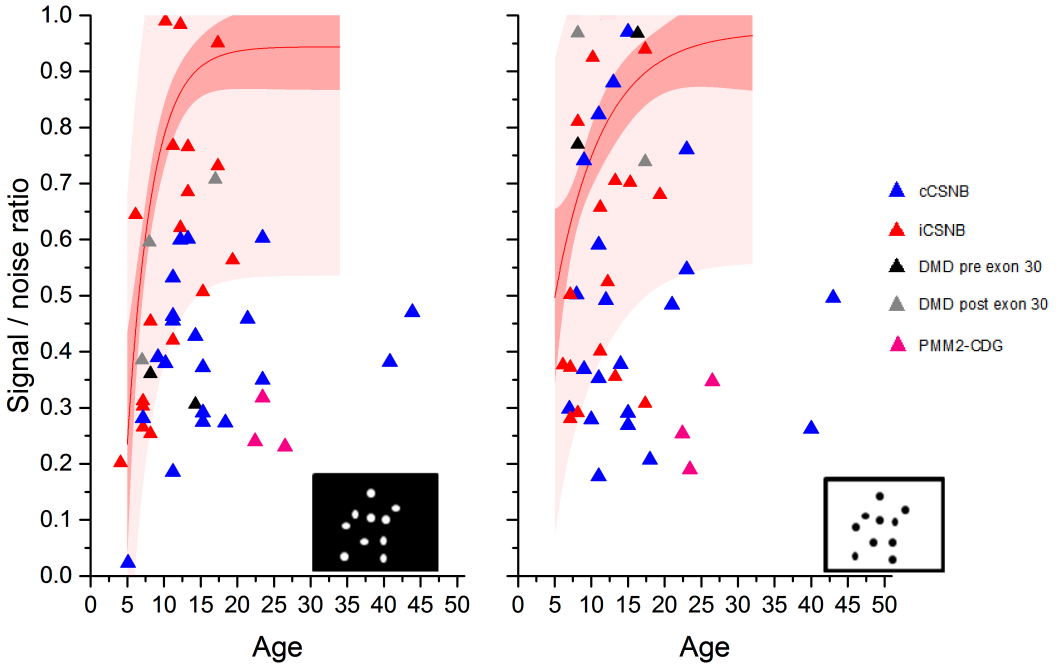


**Figure 5.29:** The normative data ranges for positive and negative contrast conditions obtained from healthy volunteers in the biological motion task (Test 3) are overlaid by individual data points derived from patients (positive contrast: n= 46; negative contrast: n= 45). Triangles represent patients (blue = cCSNB, red = iCSNB, green = ?CSNB, black = DMD pre exon 30, grey = post exon 30, pink = PMM2-CDG). The normative data ranges comprise group mean (straight red line), 95% confidence interval (CI, dark red band) and 95% prediction interval (PI, light red band). The higher the value, the better the performance in this task (i.e. the more noise dots were tolerated).

Patients with ON-pathway dysfunction showed an overall poorer motion perception compared to healthy volunteers of the same age. This became clear when acknowledging how many of the patients' data points fell out of the normative data range. When assessing coherent motion perception, most patients displayed severe difficulties to correctly complete the task when the signal to noise ratio was below 0.2 (or 20% coherence). Seventy-six percent of patients showed an abnormal motion perception threshold in the positive contrast condition (32 out of 42), while the negative contrast condition yielded 71% (30 out of 42) with values lying outside the normative 95% prediction interval[23]. A wider normative data range resulted in lower percentage values obtained from the shape from motion task. When shapes

[23]Patients who displayed nystagmus were shown the stimulus with a dot motion direction orthogonal to their nystagmus waveform wherever possible. For example, a patient with a horizontal nystagmus was shown the dots moving vertically across the screen.

were displayed with white dots on black ground (positive contrast), 54% of patients (22 out of 41) showed an abnormal performance, while for the opposite condition (negative contrast) this value rose slightly to 58% (25 out of 43). Following the hierarchy of motion testing, an even wider normative data range led to the lowest amount of patients with an abnormal result in the biological motion task. In the positive contrast condition only 33% (15 out of 46) of patients showed an atypical threshold value, while only 27% (12 out of 45) did so in the negative contrast condition.

While these results suggest that a retinal ON-pathway dysfunction can have an impact on motion perception and that this impact varies with the motion domain assessed, a more detailed picture of clinical impact could be obtained by separating these results into the patient subgroups. An overview of how these results translated into the patient subgroups is shown in Table 5.1.

| Test | cCSNB | iCSNB | DMD pre exon 30 | DMD post exon 30 | PMM2-CDG |
|---|---|---|---|---|---|
| 1 positive | 73% (14/19) | 88% (15/17) | 0% (0/2) | 0% (0/2) | 100% (3/3) |
| 1 negative | 80% (16/20) | 63% (10/16) | 0% (0/2) | 0% (0/2) | 67% (2/3) |
| 2 positive | 55% (11/20) | 53% (8/15) | 0% (0/2) | 0% (0/2) | 100% (3/3) |
| 2 negative | 62% (13/21) | 63% (10/16) | 0% (0/2) | 0% (0/1) | 67% (2/3) |
| 3 positive | 55% (11/20) | 6% (1/17) | 50% (1/2) | 0% (0/3) | 100% (3/3) |
| 3 negative | 33% (7/21) | 12% (2/17) | 0% (0/2) | 0% (0/3) | 100% (3/3) |

**Table 5.1:** The table gives an overview of how sensitive the *LumiTrack*$^{Tm}$ motion tests were in picking up abnormalities. An abnormality was defined as a threshold value which fell outside the normative data range 95% prediction interval. Not all patients carried out all tests, therefore the absolute amount of abnormal results is given alongside the percentage.

While the overall picture remained the same when analysing the results of the ON-pathway dysfunction subgroups in more detail, coherent motion perception (Test 1) provided the most problems in almost all subgroups, big differences between the subgroups emerged. These were akin to the differences between subgroups observed in electrophysiological VEP responses. Both CSNB subgroups contained the most patients with abnormal threshold values, suggesting a more significant impact on motion perception in these patients. Also, patients with PMM2-CDG showed severely abnormal threshold values. Most boys with DMD, in contrast, displayed completely normal motion perception performances across all three tests and both contrast conditions. Only one DMD patient (Pat99) with a mutation pre exon 30 obtained an abnormal threshold to the biological motion task when carried out with positive contrast.

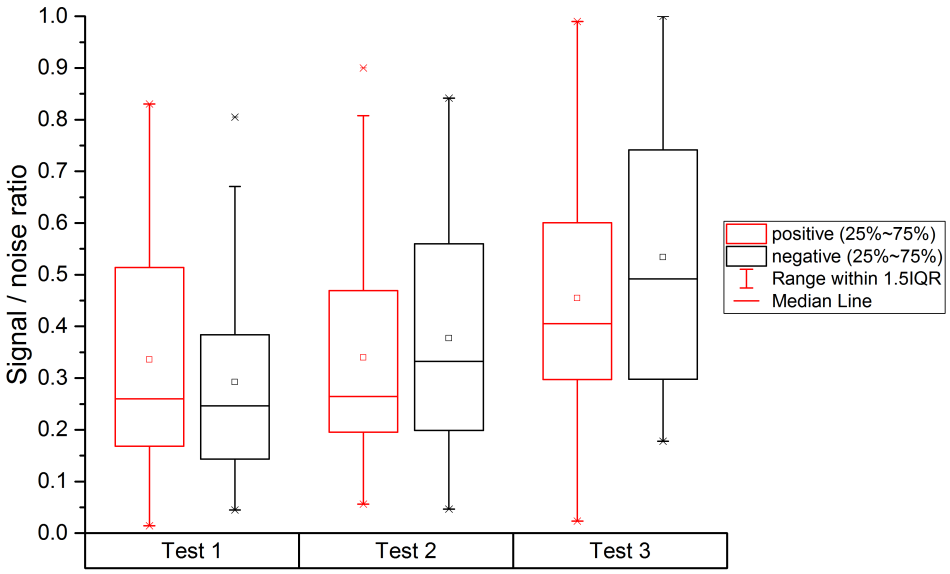


**Figure 5.30:** The motion threshold values of all patients of the ON-pathway dysfunction cohort for all three tests are shown. The values obtained from negative (black boxes) and positive (red boxes) contrast conditions are compared. Boxes give Max and Min (-), Mean (square), Median (line inside the boxes), 99% and 1% (x), as well as 75% and 25% (margins of the boxes) percentiles. Boxes give Max and Min (-), Mean (square), Median (line inside the boxes), 99% and 1% (x), as well as 75% and 25% (margins of the boxes) percentiles.

When comparing the influences of ON and OFF systems on motion perception in the patients, surprisingly, no contrast condition seemed to be primarily affected with the abnormality values fluctuating across tests and clinical subgroups (see Figure 5.30). Upon matching threshold values of all patients from positive and negative contrast conditions - as done previously for the healthy volunteers - no significant difference was found (One-way ANOVA and Tukey means comparison: Test 1: $p>0.9$; Test 2: $p>0.8$; Test 3: $p>0.08$)[24]. Even when removing data obtained from boys with DMD from the analysis, as they showed a performance on par with healthy controls, no significance was reached[25]. Comparing these results with those of healthy volunteers, one could observe that group thresholds increased for Tests 1 and 2, and decreased for Test 3, illustrating the hierarchical decline in motion perception performance due to ON-pathway dysfunction. Further, the data were more spread with patients showing a greater range of motion perception thresholds in all tests.

[24] Scatter plots of the patients' motion thresholds comparing performance of positive and negative contrast conditions within individual patients can be found in the appendix. No obvious influence of either contrast condition on the data could be found, as data points were fairly spread.

[25] These data can be found in the appendix.

#### 5.6.2.2 Abnormal contrast sensitivity of motion processing in patients

After abnormal ON and OFF signalling at the level of the visual cortex was shown to affect motion perception, it was investigated whether a retinal ON-pathway dysfunction was also associated with an impaired contrast sensitivity of motion. Figures 5.31 - 5.33 show the ranges of Michelson contrast needed by patients, in order to perceive the stimuli during the *LumiTrack*$^{Tm}$ contrast sensitivity assessments. For representation purposes, the ranges of individual patients are displayed as a dot for the negative contrast and one for the positive contrast value. If these fell outside the value ranges obtained from healthy volunteers (black boxes), they were considered "abnormal" and the patient regarded as having an abnormal contrast sensitivity of motion. An overview over the the prevalence of abnormal contrast sensitivity performance across the three tests is given in Table 5.2.

| Test | cCSNB | iCSNB | DMD pre exon 30 | DMD post exon 30 | PMM2-CDG |
|---|---|---|---|---|---|
| 1 positive | 67% (14/21) | 58% (11/19) | 0% (0/3) | 0% (0/2) | 100% (3/3) |
| 1 negative | 76% (16/21) | 63% (12/19) | 0% (0/3) | 0% (0/2) | 67% (2/3) |
| 2 positive | 86% (18/21) | 65% (11/17) | 0% (0/3) | 0% (0/2) | 100% (3/3) |
| 2 negative | 100% (21/21) | 71% (12/17) | 33% (1/3) | 0% (0/2) | 100% (3/3) |
| 3 positive | 95% (20/21) | 84% (16/19) | 0% (0/3) | 0% (0/3) | 100% (3/3) |
| 3 negative | 81% (17/21) | 68% (13/19) | 33% (1/3) | 0% (0/3) | 100% (3/3) |

**Table 5.2:** The table gives an overview of how sensitive the *LumiTrack*$^{Tm}$ contrast sensitivity measures were in picking up abnormalities. An abnormality was defined as a contrast value which fell outside the normative data range 95% prediction interval (i.e. where a patient required more contrast in order to perceive a stimulus and correctly complete the task). Not all patients carried out all tests, therefore the absolute amount of abnormal results is given alongside the percentage.

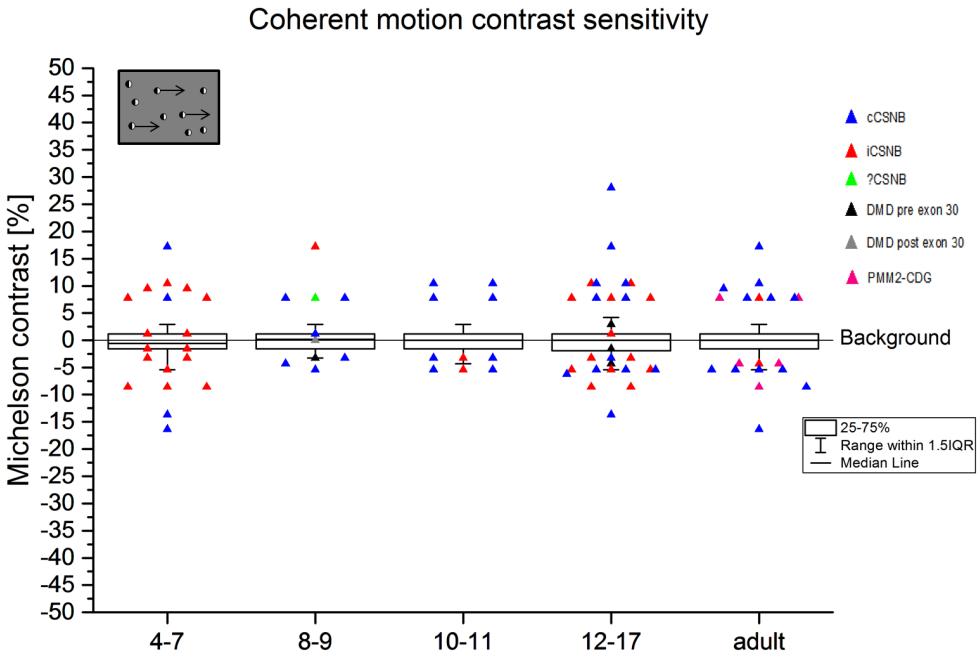


**Figure 5.31:** The graph shows the ranges of contrast for stimulus vs background which the patients could not see. Triangle symbols indicate individual patient's ranges (n= 48) with all values in between two symbols representing the range of values not seen. Blue = cCSNB, red = iCSNB, green = ?CSNB, black = DMD pre exon 30, grey = post exon 30, pink = PMM2-CDG. Black boxes represent give Max and Min (-), Mean (square), Median (border inside the boxes), 99% and 1% (x), as well as 75% and 25% (margins of the boxes) percentiles or control results.

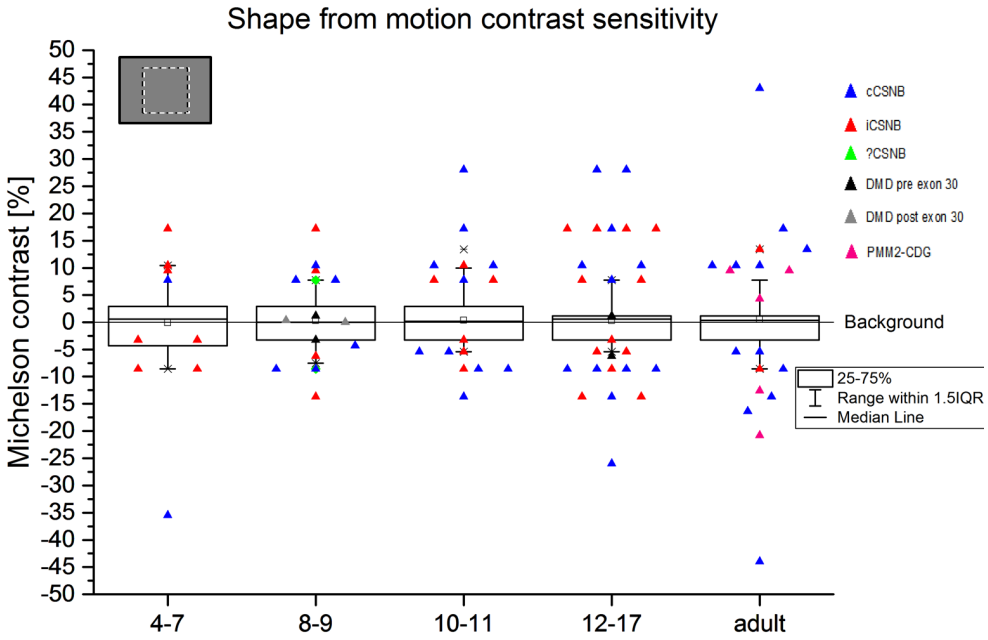


**Figure 5.32:** The graph shows the ranges of contrast for stimulus vs background which the patients could not see. Triangle symbols indicate individual patient's ranges (n= 44) with all values in between two symbols representing the range of values not seen. Blue = cCSNB, red = iCSNB, green = ?CSNB, black = DMD pre exon 30, grey = post exon 30, pink = PMM2-CDG. Black boxes represent give Max and Min (-), Mean (square), Median (border inside the boxes), 99% and 1% (x), as well as 75% and 25% (margins of the boxes) percentiles or control results.

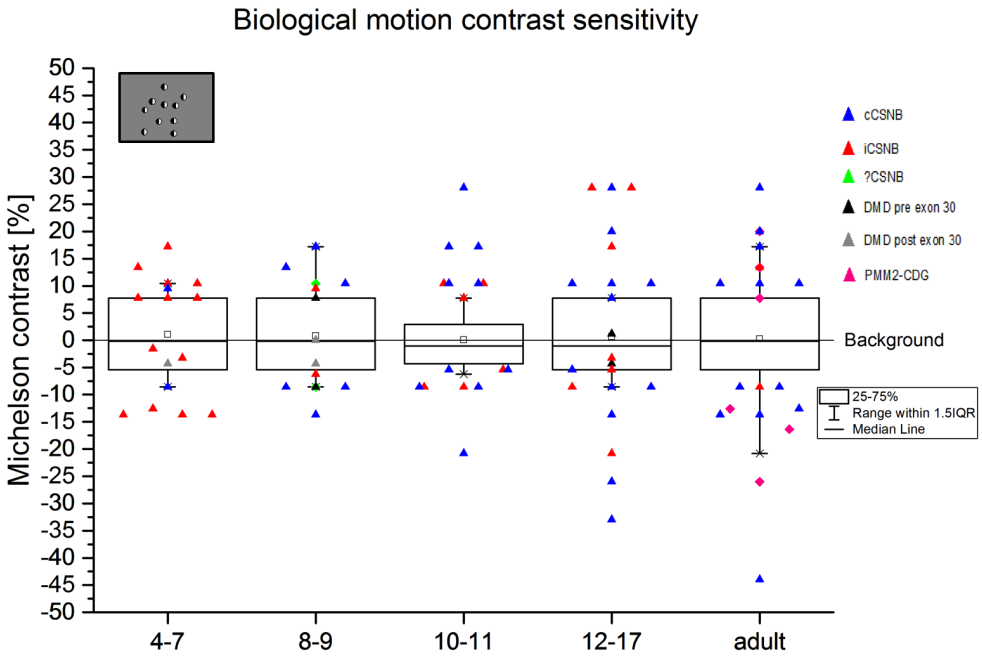


**Figure 5.33:** The graph shows the ranges of contrast for stimulus vs background which the patients could not see. Triangle symbols indicate individual patient's ranges (n= 47) with all values in between two symbols representing the range of values not seen. Blue = cCSNB, red = iCSNB, green = ?CSNB, black = DMD pre exon 30, grey = post exon 30, pink = PMM2-CDG. Black boxes represent give Max and Min (-), Mean (square), Median (border inside the boxes), 99% and 1% (x), as well as 75% and 25% (margins of the boxes) percentiles or control results.

When regarding the graphical presentation of the data, a loss of contrast sensitivity in patients with ON-pathway dysfunction became apparent. The majority of patient values fell well outside the normative data ranges on the positive, as well as the negative contrast sides. Fifty-eight percent of patients showed an abnormal contrast sensitivity value in the positive contrast condition (28 out of 48), while 63% (30 out of 48) of patients were showing abnormal contrast perception to negative contrast stimulation. In contrast to the motion perception analysis, where the anomalies decreased across patients with increasing test complexity, contrast sensitivity seemed to be sequentially more affected when ascending the hierarchy of tests. Following from this, and despite wider normative data ranges, 70% (32 out of 46) of patients exhibited an abnormal positive contrast sensitivity value in the shape from motion task. This percentage increased to 80% (37 out of 46) in the negative contrast condition. Although healthy volunteers showed even wider contrast sensitivity ranges in the biological motion task, the positive contrast sensitivity abnormality score in patients increased to 80% (39 out of 49) for the positive contrast stimulation and slightly decreased to 69% (34 out of 40) when dots were darker than the background (negative contrast).

As seen in the previously described electrophysiological and psychophysical assessments, patients showed great differences in their contrast perception performance (see Table 5.2). Patients in cCSNB, iCSNB and PMM2-CDG subgroups experienced severe problems perceiving the stimuli at low contrasts. This impairment was most extreme in the cCSNB and PMM2-CDG subgroups who showed abnormalities in up to 100% of the patients. Again, the visual function of patients with DMD seemed largely unaffected by their retinal ON-pathway dysfunction. From these boys only one (Pat119) showed an abnormal result in his negative contrast sensitivity in Tests 2 and 3.

As with the motion perception tasks, it was of particular interest whether there was a difference in performance between ON and OFF systems. When comparing relative contrast sensitivities for positive and negative contrast stimulation (Figure 5.34), patients displayed a better contrast sensitivity of the OFF system across all three tests. This disparity was significant in the coherent motion task (One-way ANOVA with Tukey means comparison: Test 1: p= 0.04; Test 2: p= 0.15, Test 3: p= 0.53). Hence, individuals with ON-pathway dysfunction required a higher Michelson contrast in order to perceive the stimuli under positive contrast conditions (i.e. when dots were brighter than the background). Upon a more detailed analysis of ON and OFF contrast sensitivity within the individual subgroups, it became clear that this overall trend of a disadvantage of the ON system was most prevalent in patients with cCSNB and iCSNB, whereas patients with DMD and PMM2-CDG showed no such tendency. The results of this more specific analysis are displayed in Figure 5.35.

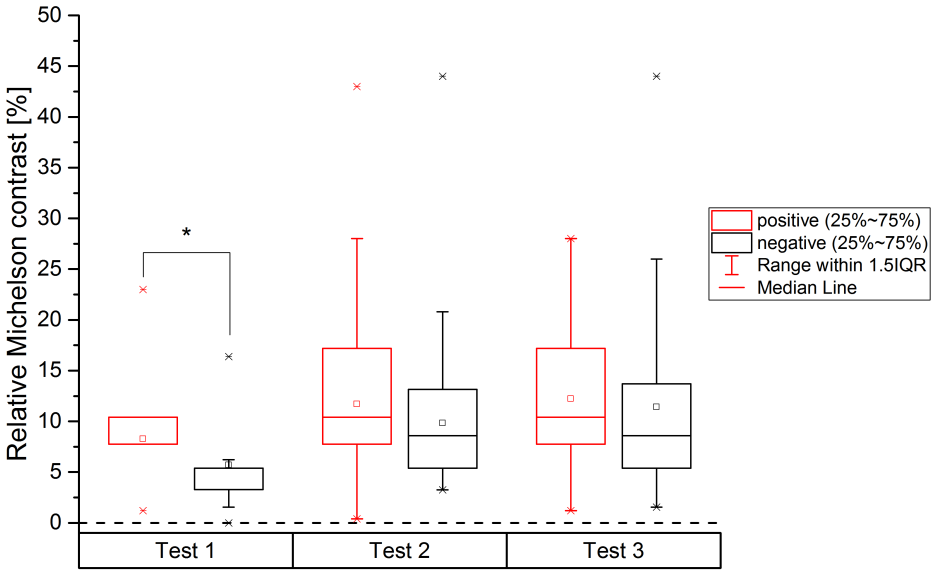


**Figure 5.34:** The relative contrast sensitivity ranges of all patients of the ON-pathway dysfunction cohort for all three tests are shown. The values obtained from negative (black boxes) and positive (red boxes) contrast conditions are compared. Boxes give Max and Min (-), Mean (square), Median (line inside the boxes), 99% and 1% (x), as well as 75% and 25% (margins of the boxes) percentiles. Boxes give Max and Min (-), Mean (square), Median (line inside the boxes), 99% and 1% (x), as well as 75% and 25% (margins of the boxes) percentiles. Statistically significant differences are market by an asterisk.

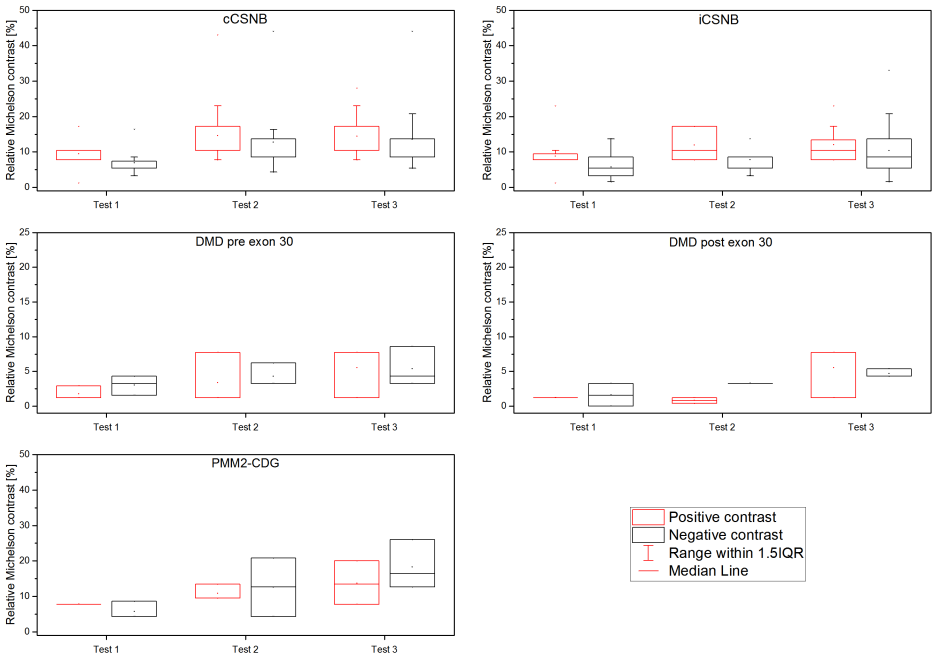


**Figure 5.35:** The relative contrast sensitivity ranges of all patients of the ON-pathway dysfunction cohort for all three tests are shown. The results are divided into the respective subgroups. The values obtained from negative (black boxes) and positive (red boxes) contrast conditions are compared. Boxes give Max and Min (-), Mean (square), Median (line inside the boxes), 99% and 1% (x), as well as 75% and 25% (margins of the boxes) percentiles. Boxes give Max and Min (-), Mean (square), Median (line inside the boxes), 99% and 1% (x), as well as 75% and 25% (margins of the boxes) percentiles. Note a halving of the vertical scale (x-axis) in the DMD subgroups in order to improve presentation.

### 5.6.2.3 How sensitive to abnormality is *LumiTrack*$^{Tm}$?

As with the novel electrophysiological tests presented in the previous chapter, after proving their functionality and their ability to detect abnormalities in patients with retinal ON-pathway dysfunction, it was important to determine how sensitive these tests were to detect abnormalities in patients. While the electrophysiological test battery was compared to the sensitivity of the conventional pattern reversal VEP, no standard clinical assessment for motion perception existed previous to *LumiTrack*$^{Tm}$. Therefore, the sensitivity of the different tasks across the test battery was analysed.

The sensitivity of *LumiTrack*$^{Tm}$ to abnormality of the whole patient cohort are listed in Table 5.3. While cohort abnormality levels fall with increasing test complexity for motion perception, the opposite behaviour is observed when looking at contrast sensitivity where more patients show an abnormal result with increasing test complexity.

| Condition | Test 1 | Test 2 | Test 3 |
|---|---|---|---|
| Motion positive | 76% (32/42) | 54% (22/42) | 33% (15/46) |
| Motion negative | 71% (30/42) | 58% (25/43) | 27% (12/45) |
| Contrast positive | 58% (28/48) | 70% (32/46) | 80% (39/49) |
| Contrast negative | 63% (30/48) | 80% (37/46) | 69% (34/40) |

**Table 5.3:** The table gives an overview of how sensitive the *LumiTrack*$^{Tm}$ psychophysical tests were in picking up abnormalities in all patient groups. An abnormality was defined as a value which fell outside the normative data ranges. Not all patients carried out all tests, therefore the absolute amount of abnormal results is given alongside the percentage.

Figure 5.36 shows a detailed overview of the sensitivity across patient subgroups, across tests and for both contrast conditions. Each data point represents the grouped data of one patient subgroup and its behaviour across the different conditions. It emerged that in the majority of patient subgroups at least 50% of the patients showed abnormalities (with DMD being the exception) in Tests 1 and 2. For Test 3, these values dropped below the 50% mark (until 6% for iCSNB) and were generally more spread. Overall, motion perception performance of patients with CSNB improved with increasing motion task complexity, and declined in the

contrast sensitivity tasks. For the PMM2-CDG subgroup, positive contrast stimulation resulted in consistent abnormality in all patients, while a lower abnormality score was reached for negative contrast stimulation. This difference evened when assessing the contrast sensitivity of shape from motion, as well as the perception of biological motion and contrast, where all patients with PMM2-CDG exhibited abnormal values. Some abnormalities were also detected in patients with DMD and mutations pre exon 30, but only in the shape from motion and biological motion tasks. The only patients who showed no abnormalities at all were DMD patients with a mutation post exon 30 in the DMD gene.

In summary, the sensitivity of $LumiTrack^{Tm}$ seemed to depend on the complexity of the test, as well as the clinical subgroup assessed. A consistent pattern relating to contrast condition across patient subgroups did not emerge. This reflects the picture observed in cortical electrophysiological testing, as well as in the variability of visual impairment encountered in these patients.

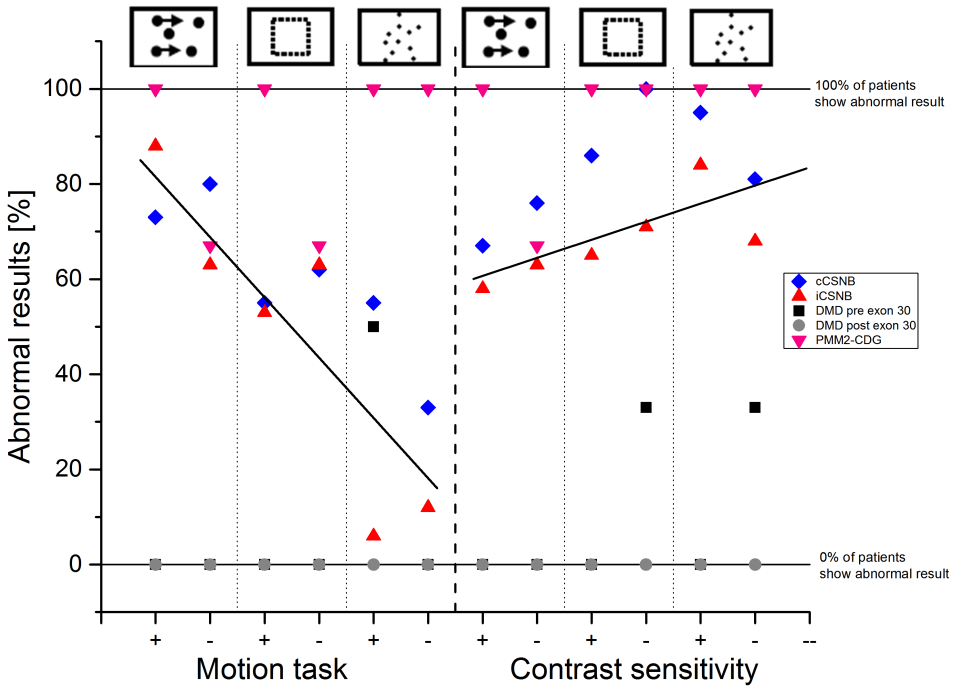


**Figure 5.36:** The graph shows the percentage of abnormal results encountered in each patient subgroup across all *LumiTrack*$^{Tm}$ tasks (motion perception and contrast sensitivity). Each symbol represents grouped threshold data for one patient subgroup (blue diamond = cCSNB; red triangle = iCSNB; black square = DMD pre exon 30; grey circle = DMD post exon 30; pink upside-down triangle = PMM2-CDG). The data are further separated into results from positive (+) and negative (-) contrast conditions. A linear fit through the data is indicated.

## 5.7 Summary and conclusion

### 5.7.1 Summary

- A novel set of psychophysical tasks assessing the perception of motion in a hierarchical manner, as well as assessing contrast sensitivity of motion, was designed and developed from the ground up. This psychophysical software, called *LumiTrack*$^{Tm}$, allowed for a reliable, flexible and easy evaluation of functional vision in subjects of a wide age range. Testing parameters were kept constant, ensuring important comparability across and within subjects, as well as allowing the evaluation of any differential effect of positive and negative contrast stimulation, relating to ON-and OFF-pathway signalling, respectively.
- *LumiTrack*$^{Tm}$ was validated in a large cohort of healthy volunteers (n= 150), delivering robust and comparable results. These served as the basis for an normative data set for subsequent comparison to performance in patient subgroups. Motion perception experienced a clear maturation across the first ten years of age, whereas for contrast sensitivity this effect was not as severe. Instead, contrast sensitivity varie depending on the task and decreased with increasing complexity of the motion tasks.
- When assessing individuals with ON-pathway dysfunction, it became clear that most patients with subtypes of CSNB, as well as patients with PMM2-CDG showed **abnormal motion perception** across all tests. This was most severe in the coherent motion task and sequentially less so in the shape from motion and biological motion tasks. Almost all boys with DMD performed on a normal level.
- Patients with ON-pathway dysfunction also displayed considerably **poorer contrast sensitivities** across the board when compared to healthy volunteers. This impairment appeared to increase with higher complexity of the task. Again, most boys with DMD exhibited contrast sensitivities on the level of healthy observers.
- The investigation of patient performance comparing positive (ON-pathway)

and negative contrast (OFF-pathway) conditions revealed some curious and unexpected results:

- No clear differences were observed when comparing motion perception performance between positive and negative contrast conditions in healthy observers, or patients with ON-pathway dysfunction.
- In patients with a disrupted ON-pathway, a better group contrast sensitivity was always achieved under negative contrast conditions. This trend agrees with an affected ON-pathway and was significant in the coherent motion task. Upon more detailed analysis of the subgroups it emerged that this trend was most prevalent in the patients within either CSNB subgroup.

## 5.7.2 Conclusion

### 5.7.2.1 Healthy volunteers

Overall, the *LumiTrack*$^{Tm}$ psychophysical test battery delivered satisfactory results in healthy volunteers and thus enabled me to proceed to carrying out the tests in subgroups of patients with retinal ON-pathway dysfunction. The test battery was arranged in a hierarchical fashion with increasing test complexity. First, the perception of coherent motion was assessed, requiring motion direction discrimination, and values exhibited an improvement with age until around 8 - 9 years, where adult-like threshold values were obtained. The second task, distinguishing two shapes which are elicited by dots moving in opposite directions, showed a similar trajectory with mature threshold values first obtained in children of 9 - 10 years. The ability to perceive biological motion was adult-like from an age of 10 - 12 years. These results agreed well with previously published data (for example [407, 408, 409]). The age ranges at which motion perception stabilises, coincides with the age at which synaptic density in the visual cortex is thought to stabilise (around 10 years of age [410]). Further, the finding that adult-like performance occurs slightly later in healthy observers (depending on complexity of the motion percept) supports the assumption that the three *LumiTrack*$^{Tm}$ motion tasks are, in fact, targeting different

cortical areas. Brain areas associated with more basic motor and sensory functions are thought to mature first, followed by brain regions related to higher cognitive function (for example [411]). The finding that contrast sensitivity ranges expanded with increasing test complexity, supports the notion that the tasks increase in processing difficulty. Contrast sensitivity is reported to fully mature across a large age range of 7 - 19 years, depending on the study [412, 413, 414]. This wide range of ages at which adult-like performance can be achieved is most likely the reason why there was no obvious improvement of contrast sensitivity with age in this study. In addition to the successful validation, some interesting findings arose when analysing the data of healthy observers.

While Tests 1 and 2 proved to be very robust, Test 3 - assessing biological motion perception - was subject to some irregularities. As shown in Figure 5.19, some of the threshold values obtained from healthy volunteers exhibited a ceiling effect, i.e. some subjects managed to correctly identify the point-light-walker and its facing direction, tolerating 100% noise. The maximum level of 100% noise corresponded to the 32 dots/deg$^2$ dot density decided upon in the design stage of *LumiTrack*$^{Tm}$, aiming to keep parameters constant across tests. For most healthy subjects, this maximum noise level was appropriately placed and they already failed to answer correctly at lower noise levels; however, 14 subjects managed to reach the maximum level without making any mistakes[26].

As previously established, the perception of biological motion requires not only the integration of motion and form, but also some social cognition with respect to associating the animated point-light-walker with a human walking. For this reason, its results could be more prone to external factors like attention or motivation to complete the test. These are variable factors which are difficult to control. Of course, the question of attention of a subject is always an important one in psychophysical testing and care was taken to ensure participants were performing attentively and to remove any possible distractions. Mostly, children were very attentive and motivated to carry out the tests, as they required their active partici-

[26]In such cases, the subjects were required to make 15 subsequent correct responses at the maximum noise level before the test was terminated, in order to ensure reliability in the performance.

pation. Only results obtained from individuals who satisfactorily[27] carried out the tests were included in the analysis.

In order to solve this issue in healthy volunteers, some of the subjects carried out Test 3 with a higher maximum noise dot amount of 5000 dots[28] (and hence, a higher maximum dot density). The resulting threshold values ranged from 115% to 330% when compared to the original signal noise ratio (where 32 dots/deg$^2$ accounted for 100% under normal circumstances). For future application of this test, such an increase in maximum noise level can be advantageous when encountering a subject who reaches the ceiling level easily. While a comparison across different individuals is more difficult when changing a parameter, valuable information on the visual function of such subjects can still be derived from the test. Hence, the ability to change dot amount / dot density easily in the *LumiTrack*$^{Tm}$ software was a beneficial feature and increased flexibility.

Another possibility to overcome the ceiling effect could be to limit stimulus display time. Several studies applying biological motion tasks use a limited presentation time of the stimulus [126, 387, 127, 395, 415] and generally, shorter display times are associated with lower noise tolerance. When analysing the reaction times to stimulus presentation of a subset of ten healthy volunteers (median age: 13 years, age range: 7 - 26 years), no subject required more than 10 seconds to react (by button press) across trials and the mean reaction time for this group was 5 seconds. Lowering the stimulus presentation time from infinite, which was initially selected in order to allow sufficient time for subjects of all ages and visual abilities, to under 10 seconds could have the potential of making it more difficult for subjects to perform the task, preventing a ceiling effect. This way, the maximum density of 32 dots/deg$^2$ at 100% could be maintained throughout the *LumiTrack*$^{Tm}$ test battery. However, it might make the tasks significantly more difficult for very young children and patients.

[27] A satisfactory performance was defined as the subject carrying out the tests in a concentrated manner and finishing the tasks without interruption. Breaks were always allowed in between the individual tasks. Only n= 2 very young patients during early trials had difficulties with the fixed noise level of 25% and their data was not included in the analysis. The acceptability of the novel tests was therefore proven as 99% of participants showed a satisfactory performance.

[28] 5 pixel dot size

Naturally, a psychophysical test which exhibits a ceiling effect is not preferred, as this ”cuts short” the results and therefore does not give a complete assessment for a small part of the subject population. Importantly, however, this limitation only presented itself when testing healthy volunteers and was no issue in patients. Hence, for my study, the results obtained from the biological motion task are reliable and this ceiling effect is no limitation for the patient results or $LumiTrack^{Tm}$'s applicability in patient cohorts.

#### 5.7.2.2 Patients with ON-pathway dysfunction

The results portrayed in the previous sections suggest that the *LumiTrack*$^{Tm}$ psychophysical test battery was able to successfully assess motion perception and contrast sensitivity in subjects of a wide age range. Further, it was possible to delineate abnormalities in subgroups of patients. The finding of abnormal motion perception in the patient cohort suggests that the signalling disparity between ON-and OFF-pathways, originating at the level of the retinal bipolar cells and still evident at the level of the striate cortex, further continues to impact on visual performance which is subject to higher order visual processing.

Abnormal perception of motion is associated with impaired magnocellular function [360], further supported by the discovery that area MT gets a more profuse input from the parasol (i.e. magnocellular) than from midget (i.e. parvocellular) ganglion cell system [20]. In a study carried out by the Schiller research group, magnocellular lesions produced deficits in motion and flicker perception of primates [32]. The motion perception abnormalities detected in patients in this study therefore suggest an impact on magnocellular signalling by a retinal ON-pathway dysfunction. As information from magnocellular and parvocellular systems is pooled at a cortical level, such a disruption of a major visual pathway at an early stage could be expected to affect visual qualities transmitted by the parvocellular pathway as well. When introducing lesions into the parvocellular system, Schiller and colleagues observed deficits in the perception of form and texture in primates. The finding of abnormal perception of shape from motion, as well as biological motion in patients with ON-pathway dysfunction would agree with an impact of the disruption on magnocellular and parvocellular systems. Support for this suggestion comes from Alexander and colleagues (2004), as well as Wolf and Arden (1996), who found both systems to be affected in patients with Melanoma-associated retinopathy (MAR) who exhibit electrophysiological ERG evidence of a dysfunctional ON-pathway that is indistinguishable from cCSNB.

When assessed using *LumiTrack*$^{Tm}$, abnormalities in patients were most prevalent in the coherent motion task, where pure motion direction discrimination was

required. Here, the magnocellular system is thought to be primarily involved [416]. For the shape from motion task, the magnocellular and parvocellular systems are expected to be active in order to detect and distinguish the two shapes. Although more than half of the patients also experienced difficulties in this task, less patients overall showed a subnormal performance. As the biological motion task required input from both, magnocellular and parvocellular systems, an impact of ON-pathway dysfunction on performance was predicted. However, while most patients performed considerably below average, a wider normative data range meant that fewer patients performed at an abnormal level. One could speculate that the necessity of some social cognition for this task introduced a greater variability to results, as well as alleviating the effects of a retinal ON-pathway dysfunction on performance.

When assessing contrast sensitivity, patients experienced an decrease in performance with increasing test complexity, as was previously observed in healthy volunteers. While for motion perception, an age-based improvement of threshold values was observed in healthy subjects, a maturation of results with age in the patient cohort was more difficult to determine due to the relatively low amount of data points. A slight improvement in performance with age was visible, for example in the biological motion task; however, this was not consistent and some older patients performed worse than younger ones within the same subgroup. When regarding individual subgroups, results from $LumiTrack^{Tm}$ motion tasks matched the results obtained from VEP recordings, showing most abnormalities in both CSNB subgroups, as well as the PMM2-CDG subgroup. Again, most patients with DMD exhibited a relatively normal performance. This continuation of patterns of abnormality in the patient subgroups could indicate that the signalling asymmetry between ON-and OFF-pathways, previously detected at the level of the visual cortex via the VEP recordings, further continues into areas of higher cortical processing and is translated into subnormal motion perception and contrast sensitivity.

While the electrophysiological results matched the outcome of the complementary psychophysical tasks in terms of the distribution of abnormalities encountered across patient subgroups, the behaviour of results from ON-and OFF-pathways was

more complex in the psychophysical tasks. Motion perception values across tests and patient subgroups behaved relatively similar to positive and negative contrast stimulation. A slight tendency was exhibited by patients with cCSNB showing a poorer performance than patients with iCSNB across higher cortical Tests 2 and 3 in the positive contrast condition only. However, this trend was not consistent throughout the test battery.

When comparing contrast sensitivities in the positive and negative contrast spectra, a more persistent trend was observed among patients. Individuals with ON-pathway dysfunction consistently required a higher Michelson contrast in order to perceive stimuli under positive contrast conditions (i.e. when dots were brighter than the background). This was significant in the coherent motion task and agrees with the studies by Schiller, who found perceptual impairments to light increments / stimuli brighter than the background after blocking the ON-pathway with APB in primates [32, 281]. Upon analysing this finding within the individual subgroups this trend was found to be most prevalent within the iCSNB and cCSNB subgroups, matching their electrophysiological results of a greater disparity between ON and OFF signalling.

Based on the results obtained in this study, one could argue that a disparity of performance between ON and OFF systems in patients with retinal ON-pathway dysfunction, while present at the level of V1, is only perceptually distinguishable under lower contrast conditions. This notion would also agree with the greater ON/OFF response asymmetry detected recording VEPs under lower contrast, isolated check conditions. The motion perception tasks were always carried out at maximum Michelson contrast (100%, either positive or negative). The contrast sensitivity tasks, in order to capture finer contrast differences efficiently within one test, halved this maximum contrast value due to presentation of the black-or white-spectrum stimuli on a mid-grey background. While a disadvantage of the ON-system (or, a lower contrast sensitivity in the positive contrast spectrum) was observed in patients at lower contrast conditions, this asymmetry was not evident under maximum contrast conditions in the motion tests. A possible explanation

for this phenomenon could be that, while at low contrast conditions the parasol (M) system is active [417], at high contrast conditions, the midget (P) system also comes into play. As discussed earlier, the parasol ganglion cells provide input to the magnocellular pathway at the level of the LGN, which is responsible for motion and contrast vision. An impairment of the magnocellular pathway due to retinal ON-pathway dysfunction with only slight impact on the parvocellular pathway (as shape from motion and biological motion tasks also provided difficulties for patients) could explain the results obtained from patients using the $LumiTrack^{Tm}$ software. The outcome of a predominant impact on magnocellular processes would be primarily affecting perceptual tasks of lower complexity, as evident in the higher rate of abnormalities encountered in the coherent motion perception task (Test 1). Further, it explains the asymmetry of ON-and OFF-pathway results obtained in contrast sensitivity tests carried out at lower contrasts (with the disparity being significant for Test 1).

Having carried out the $LumiTrack^{Tm}$ tests in the patient cohort, a few unanswered questions remained, highlighting some limitations of the test battery. For one patient the fixed noise level during the contrast sensitivity assessments was still too difficult for the correct perception of the stimuli. During stimulus design and development, a fixed noise level of 25% was anticipated to be low enough, in order not to be an issue even when testing younger children. This assumption was further supported by none of the healthy volunteers having problems at this level in Tests 1 and 2. A few very young volunteers (n=2), however, showed some difficulties when using this noise level during early trials and their contrast sensitivity measures were therefore not included in the data analysis. Following from this, the idea arose to use a static noise mask for the biological motion task in such cases. This meant to maintain the same relative dot density as in the ”normal” animated condition but only presenting static noise dots. This made the detection of the point-light-walker in the field of dots easier, while still requiring the perception of a human figure in order to correctly decide on its facing direction. This method was subsequently trialled in those children who had problems perceiving the stimuli at a 25% noise level

and contrast sensitivity ranges were obtained successfully from them. Nonetheless, this data was excluded from the analysis as it was not strictly comparable to data obtained from subjects needing to detect the walker in a mask of moving dots.

Of course, when testing visual performance in young subjects and patients with visual impairments, chances are that one will encounter more subjects with problems at this noise level. Therefore, for future testing, it is suggested to lower the fixed noise level in the contrast sensitivity tasks even further to 15%, as at this level, retrospectively, no healthy volunteer had any issues perceiving the stimuli. The application of static masking noise dots can also be a good alternative for the biological motion task. While the necessity of application of static noise dots for a patient already indicates a poorer ability to detect biological motion from noise, this might, for example arise from issues with the perception of crowded displays. In such cases, a static noise mask can allow contrast sensitivity assessment of a biological motion stimulus. However, care must be taken in the subsequent comparison of results obtained this way across subjects.

Another limitation of result comparison across subjects can arise if an observer needs a bigger dot size. While all of the healthy volunteers, and almost all of the patients were able to carry out the test at a dot size of 5 px, one patient with iCSNB (Pat44) required a dot size of 10 px in order to easily perceive one single dot on the screen. While a comparison of motion perception and contrast sensitivity within a subject is not affected, the comparison to results obtained from tasks carried out with a 5 px dot might not be appropriate. Although no effect of a change in dot size on motion and contrast perception values was found in healthy observers, showing comparable motion thresholds, as well as contrast sensitivities (Figures 5.11 and 5.12), it is generally advised to be cautious when comparing results which were obtained using (even slightly) different parameters.

While the overall results obtained from patients give a relatively clear picture of abnormality in motion and contrast perception associated to retinal ON-pathway dysfunction, a more complex pattern emerges when trying to define individual impact in the different subgroups. Results on this level were by no means clearly

separated and varied within clinical conditions. While nonetheless test sensitivity to detect abnormalities in patients was relatively high, a few false negative results were obtained. These patients either exhibited normal motion perception or contrast sensitivity measures, or - in some cases - both. This variability of results within a patient subgroup is akin to the generally great fluctuation in visual performance encountered in patients with ON-pathway dysfunction. Of course, as mentioned previously when discussing the results of healthy observers, external factors such as the subject's attention and motivation to carry out the task could have influenced their performance. However, as with subjects in the cohort of healthy volunteers, great care was taken in order to ensure a good control over these external factors by monitoring each testing procedure, removing any distractions, as well as encouraging each child to complete the test. Further, if a satisfactory performance was not possible, the data from the tests was not included in the analysis.

Correlating the results obtained from the electrophysiological tests and the outcomes from the psychophysical tasks with the underlying genotypes of individual patients might give a more detailed insight into the causes of the distinct visual performances encountered in each subgroup. This genotype - phenotype correlation across patients is laid out in the following chapter.

Chapter 6

# Integration of phenotype and genotype data

## 6.1 Genotype - Phenotype comparison

The visual phenotypes of patients with ON-pathway dysfunction presented in the previous chapters showed a variability across, and sometimes even within, subgroups, despite more ON-pathway specific stimulation. While patients with cCSNB all showed marked ON system response delays in the isolated check VEP, their results obtained from psychophysical testing were less consistent. A similar picture was observed in patients with iCSNB and PMM2-CDG, displaying an even higher phenotypic variability. Hence, a correlation of the patients' visual phenotypes, as well as their genotypes was carried out in order to evaluate whether visual performance in conventional or novel vision tests was linked to underlying genetic make-up. The following sections display phenotypical data acquired by the novel electrophysiological and psychophysical tests, as well as conventional clinical measures of vision, together with the individual genotypes of patients.

### 6.1.1 Compiled performance analysis across patient subgroups

The following Figures 6.1 - 6.4 display the compiled and tabulated phenotype and genotype results obtained from individuals across the patient cohort, who had either carried out at least one of the novel ON-pathway dysfunction assessments, had a genetic diagnosis, or both. The total number of patients included in these charts are therefore as follows:

| Condition | n |
|---|---|
| cCSNB | 27 |
| iCSNB | 31 |
| DMD | 19 |
| PMM2-CDG | 15 |
| Total | 92 |

The performance of individual patients in the newly developed ON-pathway dysfunction test batteries, as well as the conventional pVEP was compared to the respective normative data sets obtained from healthy volunteers within this study and highlighted via a colour code:

- green: performance within normal limits

- orange: performance at the limit of normal
- red: performance abnormal
- black: test not carried out / no information available

The colour further indicated whether nystagmus was absent (green) or present (red) in individual patients.

Review of clinical patient data and the carrying out of the novel ON-pathway test batteries showed that most phenotypical information was available for patients with cCSNB and iCSNB. Out of the 27 patients with cCSNB, a genotype was obtained for 19[1]. Genetic analysis of patients within the cCSNB subgroup revealed predicted pathogenic mutations in the following four genes: *NYX* (n= 8), *TRPM1* (n= 6), *GRM6* (n= 3) and *GPR179* (n= 2). The protein products of all these genes are involved in the intracellular ON bipolar cell signalling cascade[166].

When assessing whether there was a difference in visual phenotype present between these genotypes, it emerged that the incidence of nystagmus was highest in patients with a mutation in *NYX* (4/8), whereas of the patients with affected *TRPM1* gene only two showed nystagmus (2/6). Such analysis became more speculative, as patient numbers within the genotype subgroups were small and out of the three patients with *GRM6* mutations, two showed nystagmus, compared to one out of the two patients with mutations affecting *GPR179*. In conclusion, mutations in all four genes can lead to nystagmus (Figure 6.1).

Patients with NYX mutations showed the largest group peak timing difference (TD) in the specialised ON-and OFF-pathway VEP (22ms, range: 14 - 28ms), and second highest group mean VA BEO (0.34 logMAR, range: 0.175 - 0.6 logMAR). Also, five out of eight patients with *NYX* mutations showed an abnormality in the conventional clinical pVEP. This may indicate a fairly severe phenotypical impact of NYX mutations on the visual physiological qualities assessed in this thesis.

The highest group mean VA was present in patients with *GRM6* mutations (0.43 logMAR, range: 0.175 - 0.8 logMAR), who all showed an abnormal clinical pVEP; however showed a group mean TD of only 11ms when recording the specialised isolated check VEPs[2]. A slightly lower group mean VA but higher VEP TD was present in patients with mutations in *GPR179* (0.26 logMAR, range: 0.2 - 0.325 logMAR; both patients with GPR179 mutations showed a TD of 17ms) and *TRPM1*

[1]The remaining eight patients are planned for investigation via the Oculome in the Sowden laboratory. DNA samples for these patients were collected during the course of this thesis but genetic analysis was not completed.

[2]Only two patients with GRM6 mutations carried out the novel electrophysiological tests. Both showed an ON-pathway peak delay of 11ms

(0.28 logMAR, range: -0.025 - 0.55 logMAR; 12ms, range: 10 - 15ms). None of the patients with *GPR179* mutation showed an abnormal conventional pVEP, and one out of six patients with variants in *TRPM1* did (Pat30). In conclusion, a greater ON / OFF system asymmetry does not seem to be linked to VA or the prevalence of abnormal pVEP waveforms in this small cohort of genotyped cCSNB patients.

Moreover, performance within the $LumiTrack^{Tm}$ test battery was variable across genotypes. However, the least abnormal performances were observed when carrying out the biological motion task. A more detailed assessment of the $LumiTrack^{Tm}$ results is provided in Section 6.2.2 of this chapter.

The biggest group of patients included in this genotype - phenotype analysis was the iCSNB subgroup (Figure 6.2). Out of these 31 patients, the DNA of 26 was sequenced[3]. While 24 out of 26 sequenced patients presented biallelic predicted pathogenic variants in *CACNA1f*, one showed a possible variant in *PDE6B*, indicating an autosomal dominant inheritance pattern (Pat8), and one did as of now not yield a possible pathogenic variant (Pat15).

Within the group of individuals with *CACNA1F* mutations, considerable variation in visual phenotype was found using conventional and novel assessments. Two thirds of patients with *CACNA1f* mutations exhibited nystagmus (16/24) and achieved an average group VA of 0.48 logMAR (0.125 - 0.8 logMAR). In stark contrast to the genotyped patients with cCSNB, iCSNB patients with confirmed genotype showed a lower ON / OFF VEP TD of only 2ms (range: -26 - 15ms), although 17/24 showed an abnormal clinical pVEP. Moreover, psychophysically, only three (out of 20) iCSNB patients showed abnormal biological motion perception, whereas this number was much higher in the cCSNB cohort (11/22). In conclusion, the phenotypical variation was present both within and between genotypes of patients with a subtype of CSNB.

[3]Out of the remaining five, three provided samples and consented to DNA analysis. These are planned for analysis on the Oculome in the Sowden laboratory (Pat 51, Pat98 and Pat124). There was no DNA available for two (Pat36 and Pat120).

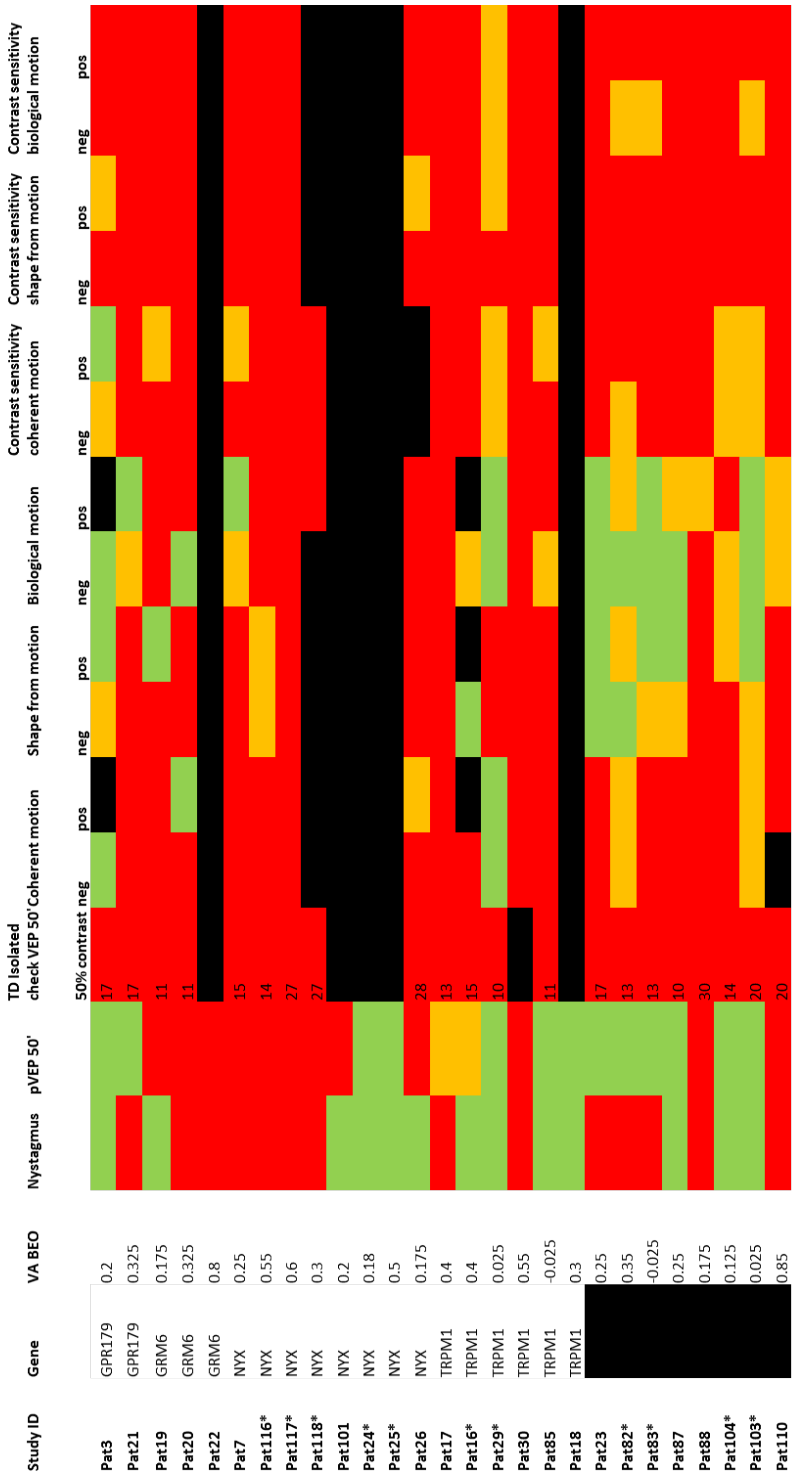


**Figure 6.1:** Overview over visual phenotypes, as well as genotypes of patients with cC-SNB. Abnormal performance is indicated by red cell colour, whereas green cell colour signifies normal performance. Highlighted in orange are cases in which the patient's performance lay just at the margin of normal. In the case of nystagmus, a red cell indicates the presence of nystagmus in the patient and a green cell its absence. A black cell indicates that a test was not carried out or a value not available. Related patients are displayed next to each other and indicated by an asterisk.

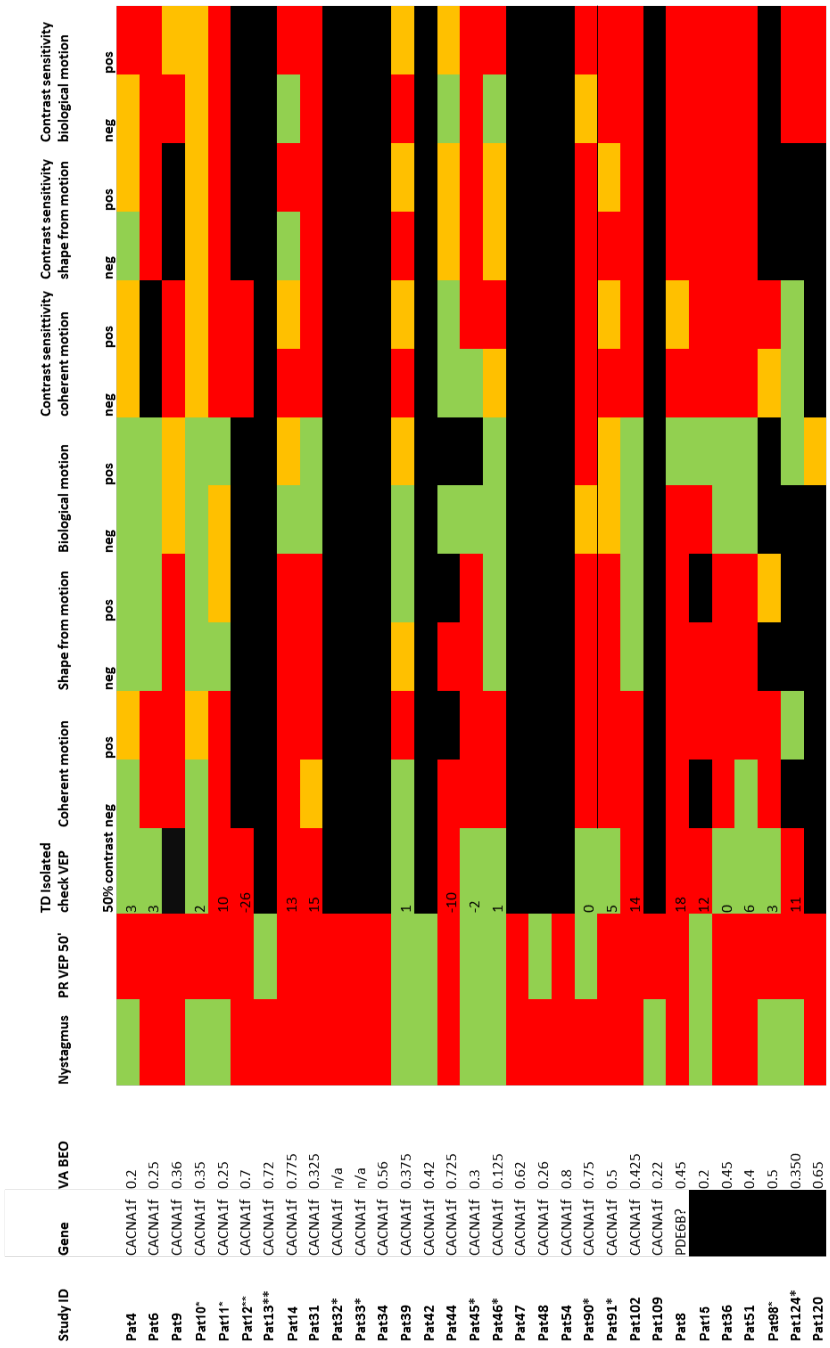


**Figure 6.2:** Overview over visual phenotypes, as well as genotypes of patients with iC-SNB. Abnormal performance is indicated by red cell colour, whereas green cell colour signifies normal performance. Highlighted in orange are cases in which the patient's performance lay just at the margin of normal. In the case of nystagmus, a red cell indicates the presence of nystagmus in the patient and a green cell its absence. A black cell indicates that a test was not carried out or a value not available. Related patients are displayed next to each other and indicated by an asterisk.

The DMD group correlations are shown in Figure 6.3. None of the patients with DMD showed nystagmus or an abnormal conventional pVEP, and also their respective group mean VA was comparable (pre exon 30: 0.003 logMAR, range: -0.15 - 0.4 logMAR; post exon 30: 0.004 logMAR, range: -0.175 - 0.5 logMAR). Further, motion perception was normal for all patients tested (n= 6) , except for one (Pat119) with a mutation pre exon 30, who showed abnormal biological motion perception. While patients with mutations post exon 30 showed a more abnormal ERG signature [163], as well as an ON system response delay, evident in a VEP TD difference of 6ms (range: -7 - 17ms) compared to -6ms (range: -20 - 3ms) for DMD pre exon 30 boys, patients with pre exon 30 mutations seemed to experience more contrast sensitivity abnormalities. Only two patients with *DMD* mutations pre exon 30 performed at the normative data margin for these assessment. In contrast, all three patients with pre exon 30 mutations who carried out the contrast sensitivity assessments, showed only marginally normal performance or even abnormality. In conclusion, the DMD patients assessed using conventional and novel measures of vision showed mostly normal performance for psychophysical and physiological tests. However, few patients within the DMD subgroups carried out the novel tests. Hence, the future investigation of further patients is important to validate and further investigate the slight visual abnormalities described in this thesis.

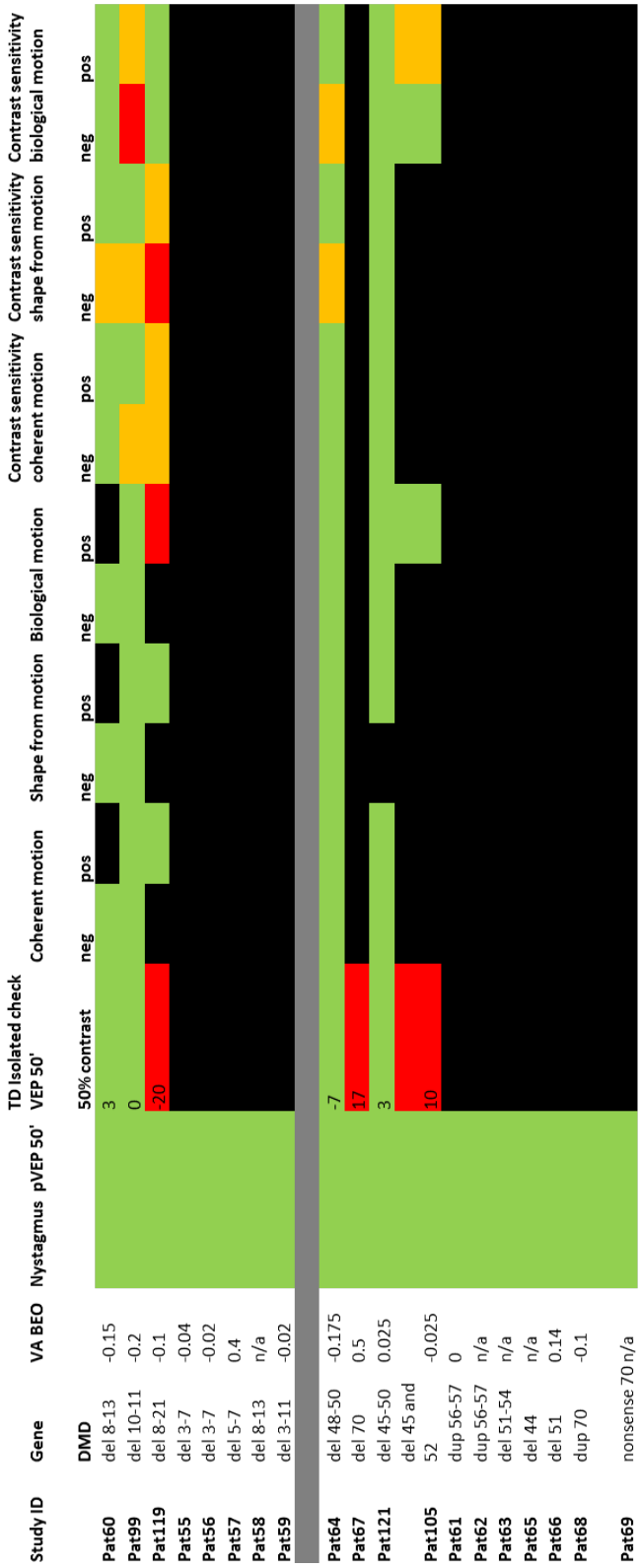


**Figure 6.3:** Overview over visual phenotypes, as well as genotypes of patients with DMD. Abnormal performance is indicated by red cell colour, whereas green cell colour signifies normal performance. Highlighted in orange are cases in which the patient's performance lay just at the margin of normal. In the case of nystagmus, a red cell indicates the presence of nystagmus in the patient and a green cell its absence. A black cell indicates that a test was not carried out or a value not available. Patients with mutations pre exon 30 and post exon 30 are separated by a grey line.

Within the PMM2-CDG subgroup, the incidence of nystagmus was five out of 13 patients (lacking information on two individuals). Curiously, however, there seemed to be an association of nystagmus and the presence of the heterozygous *p.Arg141His* variant. Out of eight patients with this variant, six had nystagmus, while there was no information on the other two available in the clinical records. It is noteworthy though that there were two further patients who exhibited nystagmus while not carrying the variant mentioned above (Pat73 and Pat75). The incidence of nystagmus in patients was not linked to performance in the pVEP, specialised VEP or psychophysical tasks.

While the group mean VA was not greatly abnormal (0.14 logMAR, range: 0.04 - 0.2 logMAR), six out of the 16 patients showed an abnormality in the conventional pVEP waveform. Only seven patients carried out the isolated check VEP recordings, resulting in a group mean TD of 7ms (range: 0 - 13ms), indicating an ON system response delay in all but one (Pat70) of assessed individuals. Psychophysically, all three patients who completed the novel tasks, showed abnormal motion perception and contrast sensitivity. An exception was Pat74, who performed at the margin of normal for negative contrast stimulation in three tasks. His performance was always abnormal under positive contrast conditions.

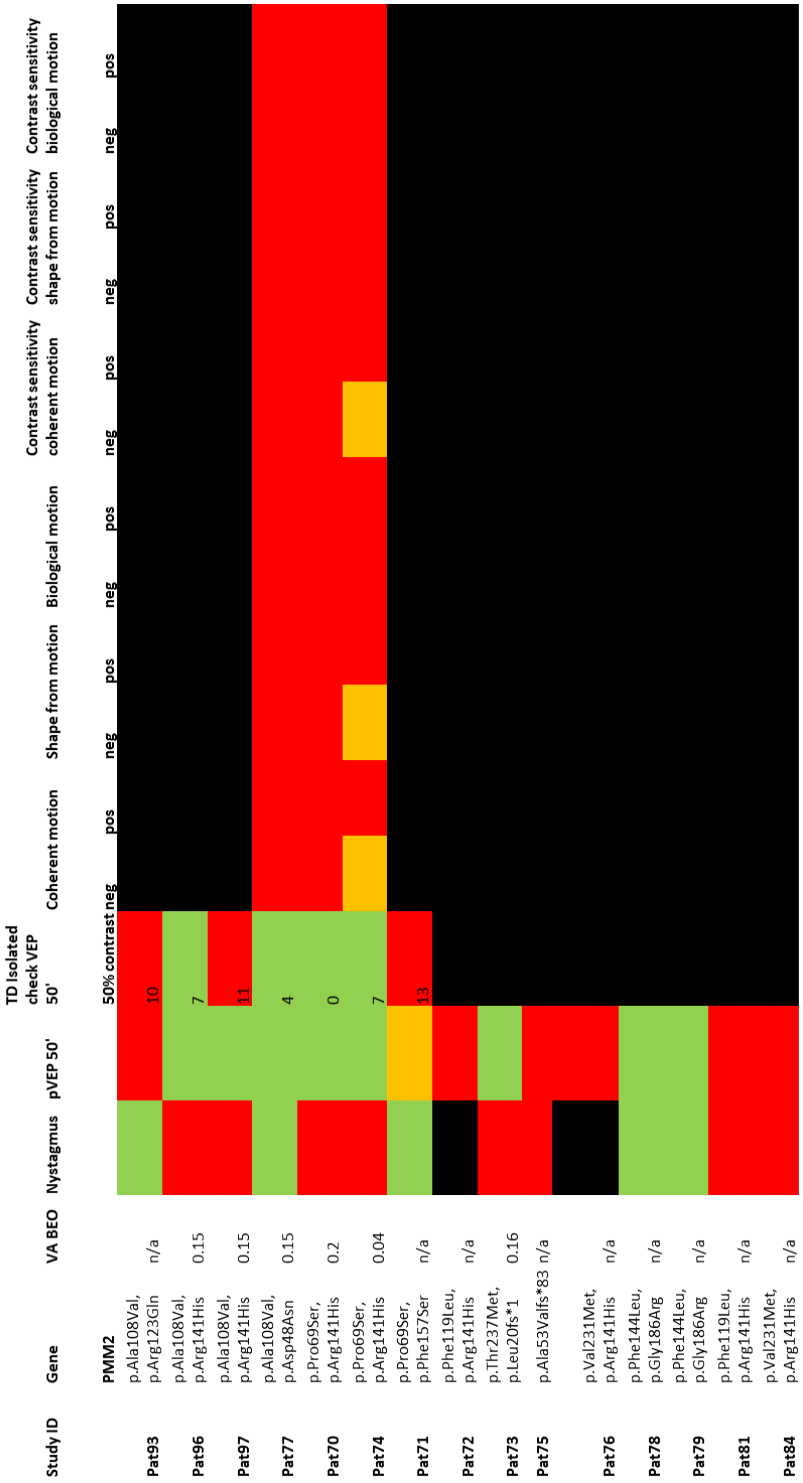


**Figure 6.4:** Overview over visual phenotypes, as well as genotypes of patients with PMM2-CDG. Abnormal performance is indicated by red cell colour, whereas green cell colour signifies normal performance. Highlighted in orange are cases in which the patient's performance lay just at the margin of normal. In the case of nystagmus, a red cell indicates the presence of nystagmus in the patient and a green cell its absence. A black cell indicates that a test was not carried out or a value not available.

## 6.2 Novel ON-pathway test batteries

In order to get a more detailed insight on patient performance linked to genotype in the novel ON-pathway dysfunction test batteries, these results are presented separately in the following sections. For reasons of comparability, the same presentation as utilised in the individual chapters was used whenever possible. As patients with iCSNB, DMD and PMM2-CDG were all affected by mutations of a single gene respectively, labels for individual patients were omitted in the figures for these subgroups. In contrast, patients with cCSNB showed a range of different genes involved and thus, the data of these patients was subdivided according to the patients' genotypes.

### 6.2.1 ON-and OFF-pathway VEPs

For presentation of the correlated VEP results, data from isolated check (i.e. positive and negative contrast) stimulation of 50% Michelson contrast was selected, as this condition revealed the most profound ON / OFF response timing differences (TD) across subgroups. The results are displayed in Figure 6.5.

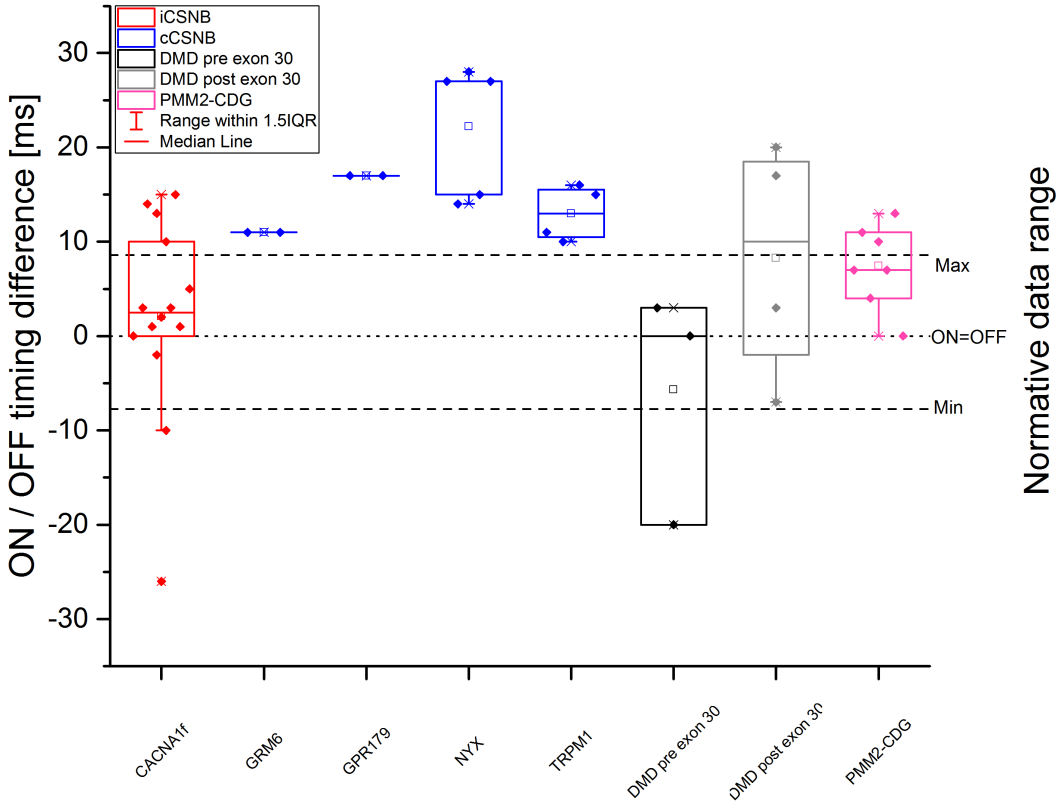


**Figure 6.5:** Overview over ON / OFF response timing differences in the specialised isolated check VEP to positive and negative contrast stimulation of 50% Michelson contrast across patient subgroups and genotypes. Different subgroups are shown by coloured boxes. All blue boxes show cCSNB patient values. Individual patient values are highlighted by diamond symbols. Dashed and dotted lines indicate the normative data range obtained from healthy volunteers.

As noted in Chapter 4, only one DMD patient with a mutation pre exon 30 showed an abnormal TD, whereas the overall TD difference for boys with a mutation post exon 30 was shifted towards an ON-delay (Mean TD: 6ms, range: -7 - 17ms). A similar picture was observed for PMM2-CDG patients (Mean TD: 7ms, range: 0 - 13ms). However, the subdivision of the cCSNB patient subgroup revealed a slight variation of the ON / OFF response TD across genotypes. Figure

6.5 displays the genes involved in subtypes of CSNB arranged in order of location in the photoreceptor / ON bipolar cell signalling cascade, with the protein product of *CACNA1f* (Mean TD: 2ms, range: -26 - 15ms) at the beginning (located in photoreceptor terminals), followed by *GRM6* (Both patients showed a TD of 11ms) - encoding the glutamate receptor specific to ON bipolar cells - and *GPR179* (Both patients showed a TD of 17ms), which is thought to play a role in the subsequently located G-protein complex. The protein products of *NYX* (Mean TD: 22ms, range: 14 - 28ms) and *TRPM1* stand at the end of this intracellular signalling cascade with nyctalopin thought to provide structural gating support for the cation channel TRPM1.

A trend was visible of increasing ON / OFF TD, an increasing ON system response delay, if the underlying genotype of a patient affected a protein located at later positions of the ON bipolar cell signalling cascade. Patients with iCSNB (and hence, a presynaptic disruption due to mutation in *CACNA1f*), showed variable values but an overall smaller group TD value than patients with cCSNB. In cCSNB, the signalling defect is located postsynaptically within the ON bipolar cell dendrites and patients with cCSNB showed higher ON / OFF TDs depending on the gene affected. The only exception to this modest tendency of TD increase provided patients with mutations in *TRPM1* (the apparent endpoint of the signalling cascade), who show a smaller TD than patients with *NYX* mutations.

### 6.2.2 *LumiTrack*$^{Tm}$

To assess whether this trend observed in the VEP data, reflecting the situation at the striate cortex, was still observable upon assessment of higher visual functions (presumably processed in subsequent cortical areas), the results obtained via the psychophysical software *LumiTrack*$^{Tm}$ were correlated to the patients' genotypes. The results for the motion perception assessments are shown in Figures 6.6 - 6.8, whereas those for the contrast sensitivity of motion tests are shown in Figures 6.9 - 6.11.

### 6.2.2.1 Motion perception

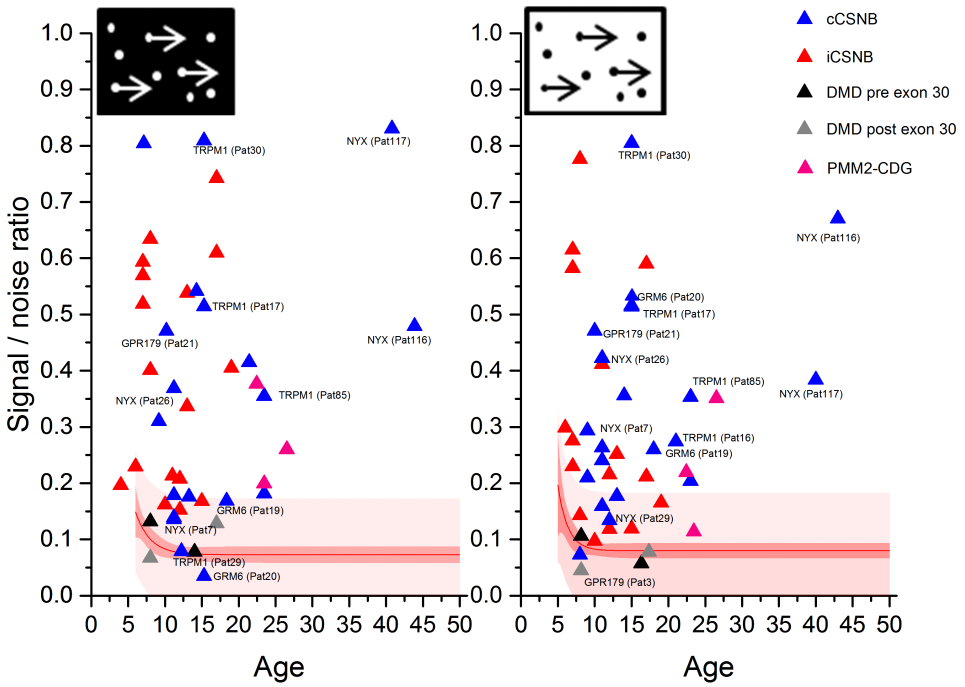


**Figure 6.6:** Overview over coherent motion thresholds obtained from patients across subgroups and genotypes to negative and positive contrast stimulation of 100% Michelson contrast. Individual patient values are highlighted by triangle symbols of different colours with genotypes of cCSNB patients given next to the respective symbols. The normative data range confidence interval (dark pink) and prediction interval (light pink) are indicated including the mean of data obtained from healthy volunteers (red line).

In contrast to the tendency observed in the specialised VEP results of patients with cCSNB, the performance of tasks associated with higher cortical areas did not yield a clear trend when motion perception phenotypes and genotypes were correlated in these patients. Individual cCSNB genotypes did not result in a clearly different performance across motion perception assessments. A similar picture emerged for patients with iCSNB and PMM2-CDG, who showed a wide range of values, albeit with the data of the PMM2-CDG subgroup showing a narrower spread. Patients within either DMD subgroup performed within the normal range across all three motion tests and a difference between either genotype was not apparent.

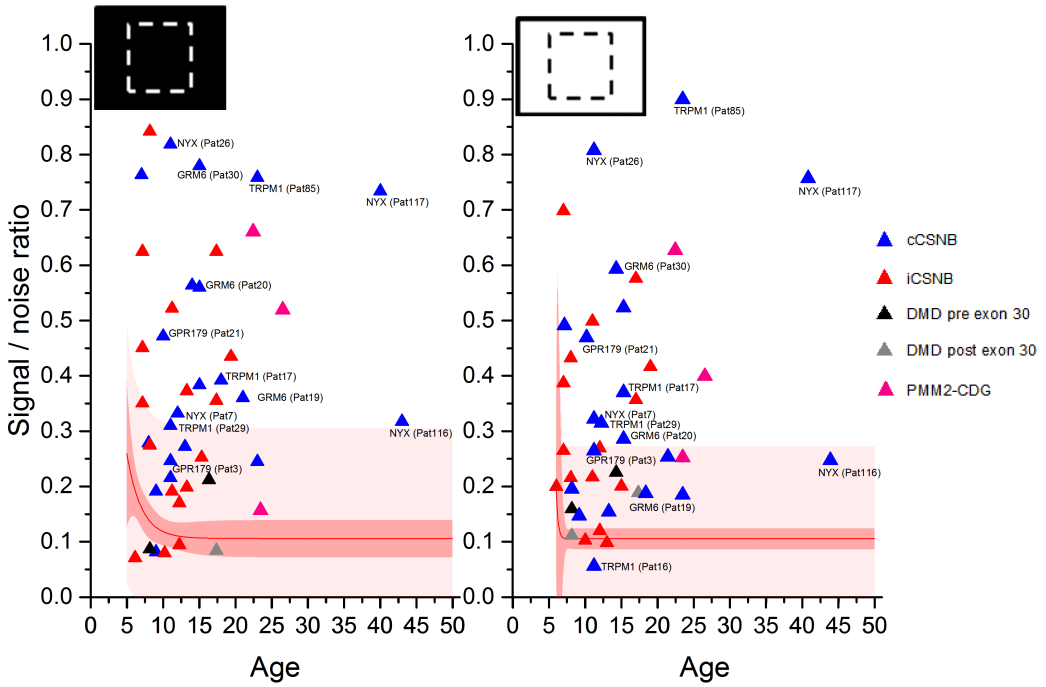


**Figure 6.7:** Overview over shape from motion thresholds obtained from patients across subgroups and genotypes to negative and positive contrast stimulation of 100% Michelson contrast. Individual patient values are highlighted by triangle symbols of different colours with genotypes of cCSNB patients given next to the respective symbols. The normative data range confidence interval (dark pink) and prediction interval (light pink) are indicated including the mean of data obtained from healthy volunteers (red line).

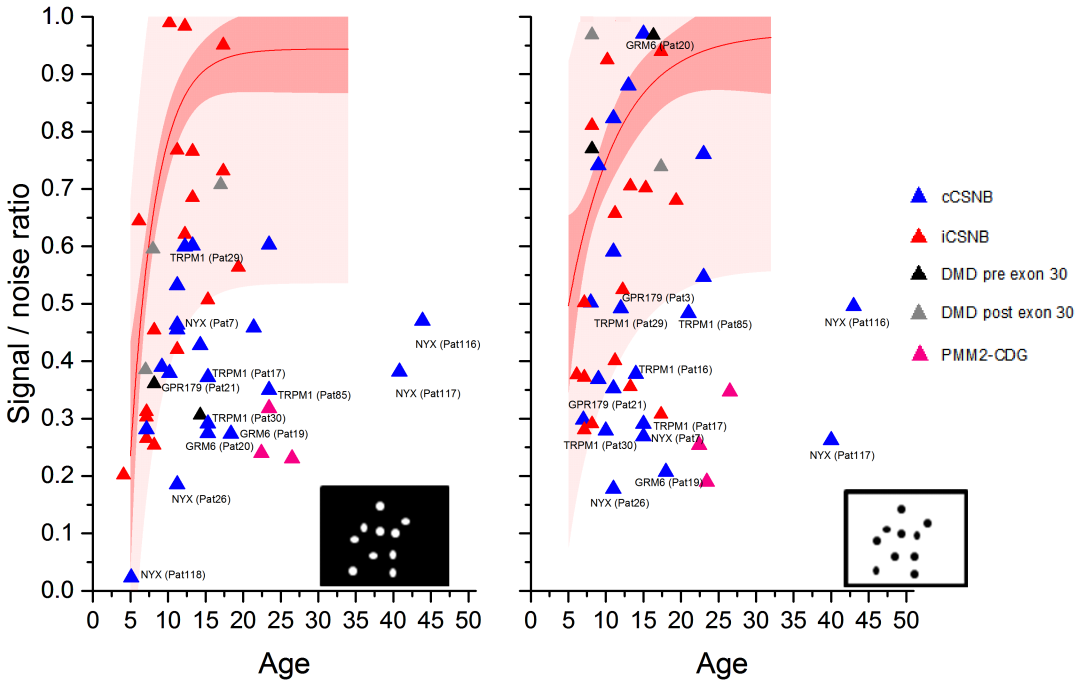


**Figure 6.8:** Overview over biological motion thresholds obtained from patients across subgroups and genotypes to negative and positive contrast stimulation of 100% Michelson contrast. Individual patient values are highlighted by triangle symbols of different colours with genotypes of cCSNB patients given next to the respective symbols. The normative data range confidence interval (dark pink) and prediction interval (light pink) are indicated including the mean of data obtained from healthy volunteers (red line).

### 6.2.2.2 Contrast sensitivity of motion

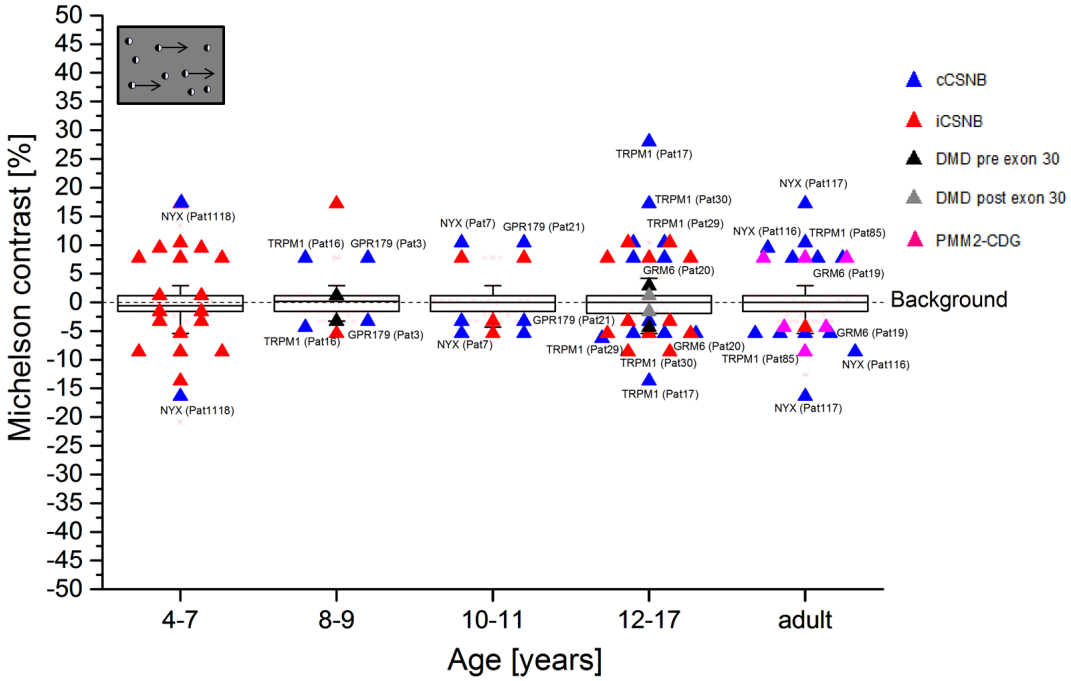


**Figure 6.9:** Overview over contrast sensitivity ranges of coherent motion perception obtained from patients across subgroups and genotypes to negative and positive contrast stimulation. Individual patient values are highlighted by triangle symbols of different colours with genotypes of cCSNB patients given next to the respective symbols. The normative data obtained from healthy volunteers is indicated by black boxes.

When regarding measures of contrast sensitivity, however, it appeared that patients with *NYX* mutations required the highest contrasts in order to perceive a stimulus across all three tests (see Figures 6.9 - 6.11). Performance of these patients was matched by that of Pat17 with a mutation in *TRPM1*, who always showed the broadest contrast sensitivity range within her age-group. Pat21 (*GPR179*) and both patients with mutations in *GRM6*, affecting the mGluR6 receptor specific to ON bipolar cells, showed a comparable performance in the contrast sensitivity assessments. Even though numbers for patients with the individual cCSNB genotypes were low, these results match the trend observed for the VEP data, with a poorer performance, the later the affected protein is located in the ON bipolar cell signalling cascade. Patients with iCSNB showed variable contrast sensitivity performances with some being highly abnormal and some falling within the normative data range for the

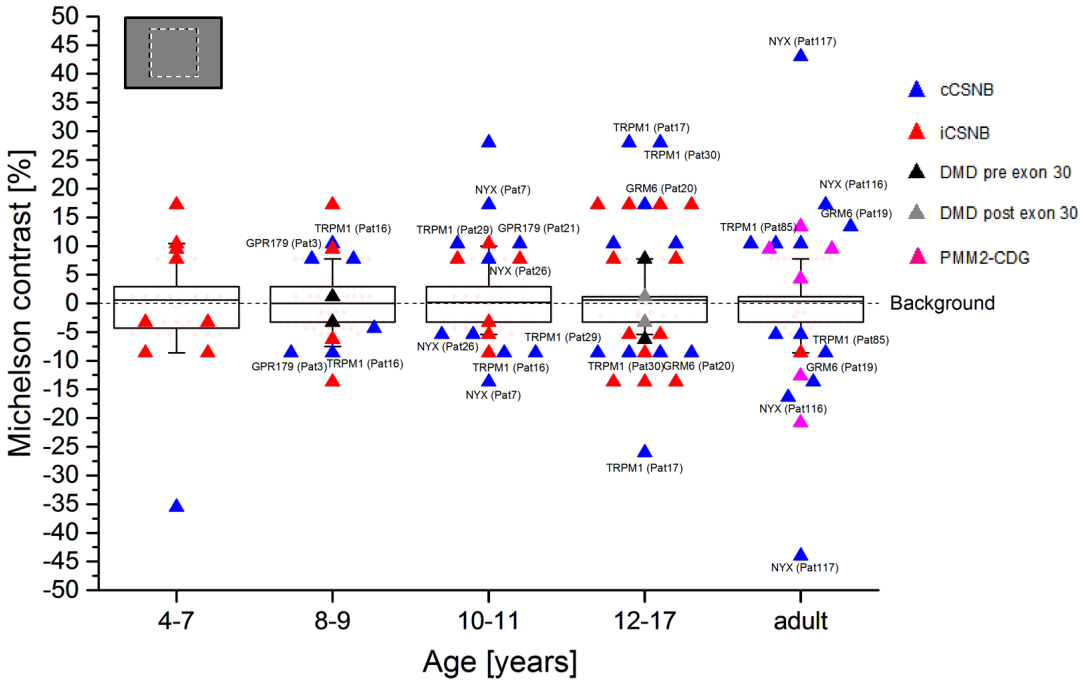


**Figure 6.10:** Overview over contrast sensitivity ranges of shape from motion perception obtained from patients across subgroups and genotypes to negative and positive contrast stimulation. Individual patient values are highlighted by triangle symbols of different colours with genotypes of cCSNB patients given next to the respective symbols. The normative data obtained from healthy volunteers is indicated by black boxes.

coherent motion contrast sensitivity assessment (Figure 6.9). The performance of patients with *DMD* mutations pre and post exon 30 never fell outside the normative data range and was comparable between both genotype subgroups. Patients with PMM2-CDG performed comparably to those with cCSNB.

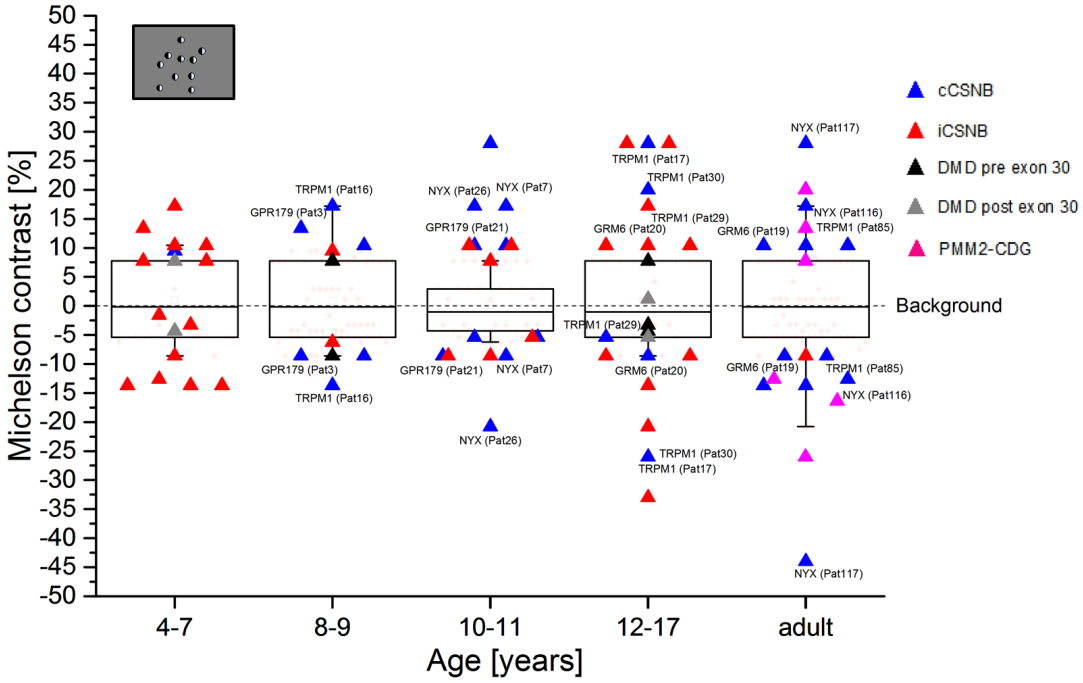


**Figure 6.11:** Overview over contrast sensitivity ranges of biological motion perception obtained from patients across subgroups and genotypes to negative and positive contrast stimulation. Individual patient values are highlighted by triangle symbols of different colours with genotypes of cCSNB patients given next to the respective symbols. The normative data obtained from healthy volunteers is indicated by black boxes.

## 6.3 Summary and conclusion

### 6.3.1 Summary

- A clear genotype - phenotype correlation did not not emerge when reviewing conventional clinical patient data. Nonetheless, it became clear that patients with mutations in *NYX* were more visually affected when compared to patients with variants in *GPR179* (when comparing VA, incidence of nystagmus and pVEP results). Patients with iCSNB experienced the poorest VA across patient subgroups. Further, patients with DMD did not show any abnormalities and the visual performance of both genotypes was comparable. Curiously, patients with PMM2-CDG showed an apparent link of the incidence of nystagmus and the presence of the heterozygous variant *p.Arg141His*.
- Among patients with a subtype of CSNB, a slight trend was apparent from electrophysiological data. Patients who exhibited a genetic variant affecting a protein placed later within the ON bipolar cell signalling cascade, showed a greater temporal ON/OFF VEP asymmetry. Following this trend and beginning with the genotype resulting in the least temporal asymmetry, the hierarchy presented as follows:
  *CACNA1f* (iCSNB) $<$*GRM6* $<$*GPR179 / TRPM1* $<$*NYX*.
- Behaviourally, such a trend was obscured by the within subgroup variability of the motion perception data. The only patients constantly performing at normal levels were boys with DMD. Upon contrast sensitivity assessment, however, it seemed that patients with *NYX* and *TRPM1* mutations required the highest contrasts for successful detection of the stimuli, whereas patients with *GPR179* and *GRM6* mutations needed less contrast. DMD patients with pre exon 30 mutations showed slightly poorer results for these assessments compared to DMD boys with mutations post exon 30. Patients with PMM2-CDG performed comparable to patients with cCSNB.

### 6.3.2 Conclusion

The study of the patient cohort presented in this thesis revealed a high variability in clinical visual phenotypes encountered across the patient subgroups; the observed ON-pathway dysfunction was shown to be induced by different molecular retinal defects. While the sites of defect in patients with iCSNB, cCSNB, as well as PMM2-CDG are relatively well known, the role of the different dystrophin isoforms expressed in the retina is still largely obscure [163]. Despite the different molecular irregularities in these distinct conditions, they all reveal an ERG signature indicative of ON-pathway dysfunction. Moreover, conventional clinical vision assessments did not deliver a satisfactory distinction between the ON-pathway dysfunction patient subgroups. Hence, in this thesis, more specific vision tests were developed in order to be able to distinguish and delineate further the differences between these. Apart from visual phenotype differences, a correlation of these with patient genotypes was of particular interest, in order to be able to better define whether a specific molecular deficit leads to a specific visual outcome. What does the genotype - phenotype correlation reveal about the impact a retinal ON-pathway dysfunction has on visual performance?

Looking at the correlation of the findings from conventional clinical tests, some separation could be achieved linking phenotypical results to the genotype. Within the cCSNB subgroup, presenting four different genotypes, a relatively clear distinction could only be made between patients with *NYX* mutations and those with *GPR179* mutations, who seemed to present a less severe visual phenotype when compared to NYX across all assessed visual functions and domains. Further, it was highlighted that patients with DMD showed no visual abnormalities, apart from their ERG signature suggesting ON-pathway dysfunction. The data obtained from the remaining patients remained highly variable within and across conditions, even in the face of the genotype being included in the analysis.

When regarding the novel ON-pathway test batteries developed, the cortical ON/OFF VEP measure gave the clearest distinction between different genotypes across all patient subgroups. The ON-response was delayed in the majority of pa-

tients when compared to healthy observers and between patient subgroups. These results indicate that the differences in electrophysiological signature present between conditions at the level of the ERG continues to be present at V1. Further, the trend observed in the VEP results of patients with a subtype of CSNB suggests that if proteins are affected, which are located later in the photoreceptor / ON bipolar cell signalling cascade, this might lead to a more severe effect on the ON-and OFF-pathway signal arrival symmetry at the level of the striate cortex. In accordance with this tendency, patients with PMM2-CDG showed comparable results to patients with cCSNB, most likely because the glycosylation defect in PMM2-CDG affects the same proteins which are affected by mutation in these patients, such as nyctalopin and mGluR6 [217].

An insight into higher cortical functions gained by psychophysical testing revealed more variable results. The trend observed previously at the level of the striate cortex, discerning the genotypes present in CSNB, was not obvious and no clear genotype advantage or disadvantage was present in tasks assessing motion perception. Again, patients with PMM2-CDG performed comparable to patients with CSNB. The individual molecular differences between patients with iCSNB, cCSNB and PMM2 observed at the retina and still at the striate cortex, are not markedly distinct and therefore lead to an almost indistinguishable perceptual outcome using the visual tests available. These results imply that, on the level of higher visual processing, a compensation mechanism might be at play.

The processing of visual tasks taking place in higher cortical areas is thought to experience significant interplay between different visual pathways [53, 54], which could have the potential of filtering out signals which are not sufficiently distinct. An increasing stimulus selectivity is known to be a property of many cortical cells [418]. The response behaviour of such cells is also becoming increasingly complex, the higher up in the visual pathway they are situated, allowing for greater robustness of the visual system [45, 46], as laid out in the introduction of this thesis. Following this line of thought, the minor differences observed in contrast sensitivities to perceive motion stimuli within the cCSNB subgroup, when linked to patient geno-

type, could suggest that the cortical stage influencing such contrast sensitivity might experience less integration of signals from different visual pathways and is therefore less ”robust” to differences in visual signals received. This could explain why it seemed that among the cCSNB patients, those with *NYX* and *TRPM1* mutations showed a slightly poorer contrast sensitivity of motion when compared to patients with *GPR179* and *GRM6* mutations[4].

In contrast, the performance of patients with DMD differs greatly to the one of the other patient subgroups. Thus, the functional role of dystrophin isoforms in the retina, while associated with the ON bipolar cell signalling cascade reflected in the ERG, must be distinct from the roles of proteins affected in CSNB and PMM2-CDG. In fact, so distinct that they not only lead to different VEP responses but also to a striking difference in perceptual visual performance between boys with DMD and the rest of the patient cohort. Differences between the two DMD genotypes, distinguishable at the retinal level and, to some extent, at the cortical level, were not apparent when assessing visual motion perception. This could indicate a relatively similar functional signature of the dystrophin isoforms affected by mutations pre and post exon 30.

Certainly, some intriguing questions remain from this analysis, such as the role of dystrophin in the retina with, or, in what way the different molecular defects could lead to the visual phenotypes observed. Further discussion of these results will therefore be presented in the subsequent General Conclusions and Discussion chapter.

[4]It is noteworthy that numbers within the individual genotype-subgroups were low, only allowing a speculative comparison between different genetic make-ups.

Chapter 7

# General Conclusions and Discussion

## 7.1 Summary of findings

- This thesis sought to elucidate the ways in which a disruption of the ON-pathway at the level of the retina might affect higher order visual signalling. Further, potential asymmetries between positive and negative contrast situations, thought to bias ON-and OFF-pathway contributions to the visual processes, were investigated. It was anticipated that such a disruption would be detectable in the VEP waveform and affect perceived vision. A cohort of n= 109 patients with ON-pathway dysfunction was included in this thesis for genetic analysis and assessment of physiological and psychophysical function.
- Patients showed recognisable patterns of ERG signatures across the ON-pathway dysfunction subgroups. Further, a range of visual impairments was present across subgroups. This was associated with the different molecular causes for this retinal signalling disruption across conditions and the importance of obtaining a complete phenotypical and genotypical picture of a patient for clinical diagnostics.
- The genotypes of patients with subtypes of CSNB were investigated via Next Generation Sequencing approaches ("The Oculome" gene panel or via Whole Exome Sequencing). Predicted pathogenic variants were detected and confirmed (via Sanger sequencing) in 92% of patients with ERG signatures of CSNB subtypes who had genetic testing carried out (n= 44/48). Patients with cCSNB showed mutations in genes associated with ON bipolar cell proteins *GRM6*, *TRPM1*, *GPR179* and *NYX*, whereas genetic testing in patients with iCSNB revealed mutations in *CACNA1f* only. Four CSNB patients (out of a total of 75 patients) remain unsolved and are recommended for further analysis via Whole Exome or Whole Genome Sequencing.
- A set of specialised electrophysiological stimuli, aiming to selectively elicit cortical responses from ON-and OFF-pathways was developed and applied across patient subgroups. Using these, an asymmetry of ON and OFF signal arrival at the striate cortex was detected in four out of five patient subgroups. Such an asymmetry was not detected in patients with DMD mutations

pre exon 30. VEP responses to ON-pathway stimulation were delayed up to 30ms in patients with cCSNB. This delay was more pronounced when stimuli were biased to highlight the magnocellular pathway (via isolated check VEPs). These findings suggest a delay in ON-pathway signalling, but not a complete blockade, at the retinal level.

- The behavioural impact of such an asymmetry of cortical signalling on visual qualities transmitted by ON-and OFF-pathways, was investigated using a novel psychophysical software. *LumiTrack*$^{Tm}$, a psychophysical software developed in this thesis, provided an easy and playful way to evaluate motion perception, as well as contrast sensitivity of motion, across several levels of complexity in young volunteers and patients from four years of age. A comparable software was not previously available for use in paediatric practice and these perceptual qualities have not been assessed in children with ON-pathway dysfunction before. Patients with cCSNB, iCSNB and PMM2-CDG showed subnormal motion perception thresholds, as well as a decrease in contrast sensitivity. With increasing text complexity, fewer patients showed motion perception abnormalities, yet contrast sensitivity abnormalities became more frequent in more complex tasks. These findings indicate an impact of a retinal ON-pathway dysfunction on higher cortical visual percepts which are crucial for everyday visual performance. Further, the results suggest an impact on functions mostly involving magnocellular function, however, a slight impairment of the parvocellular system could not be excluded.
- A genotype-phenotype correlation of the findings revealed a trend of increasing temporal ON/OFF VEP asymmetry in patients with cCSNB, associated with genetic defects affecting proteins placed later within the photoreceptor / ON bipolar cell signalling cascade. Here, patients with mutations in *NYX* were most severely affected. Such a genotypic distinction, detected at the level of the striate cortex, was less apparent when assessing visual functions associated with higher visual processing using psychophysical measures. Patients with mutations in genes *NYX* and *TRPM1*, whose protein products are

involved at the end of the intracellular signalling cascade in ON bipolar cells, seemed to require the highest stimulus/background contrast to perceive moving stimuli among patients with cCSNB. However, no clear distinction between genotype subgroups was apparent when regarding motion perception results at supra-threshold contrast level. Patients with CSNB and PMM2-CDG seemed to perform comparably across assessments, while an impact of an ON-pathway dysfunction in patients with *DMD* mutations post exon 30 was only observable at the level of the retina (ERG) and the striate cortex (VEP). DMD patients displayed almost completely normal visual perceptual performance, suggesting a molecular function of dystrophin in the signalling circuits of the retina which is distinct from that of the proteins involved in CSNB and PMM2-CDG.

## 7.2 Discussion

### 7.2.1 Visual impairment in the absence of ON-pathway signals?

In this thesis, I have presented evidence that patients with ON-pathway dysfunction show visual signalling abnormalities, not only at the retinal level, but also detectable at the level of the striate cortex, resulting in the perceptual impairment of important visual qualities transmitted by ON-and OFF-pathways, such as motion and contrast. These results are in agreement with my hypothesis that a retinal ON-pathway dysfunction at the level of the ON bipolar cells would disrupt visual signalling at the level of the striate cortex and in higher order visual areas[153, 154, 155].

ON-and OFF-pathways in the visual system are thought to have evolved in order to increase (contrast) sensitivity of the visual system, as well as to increase the dynamic range for detection of visual stimuli [419]. If light increments and decrements were signalled by a single pathway, the relatively low maintained activity of retinal ganglion cells and cortical neurons would make it difficult for the visual system to efficiently utilise a decrease in neuronal activity (as might be expected from OFF cells to a light increment). Hence, transmitting ON and OFF signals from eye to the brain via excitiatory connections, rather than by increases and decreases of firing rates within a single pathway, is an efficient and quick means of signal processing[1]. Further, as explained earlier[2], having parallel ON-and OFF-pathways also enables the visual system to efficiently enhance contrast sensitivity [326].

A disruption of ON-pathway ganglion cell firing was suspected to alter the arrival of visual signals at the striate cortex and this, in turn, to affect perceived vision. The delay of ON-pathway mediated signals detected in specialised ON/OFF VEPs of patients with cCSNB, iCSNB, as well as boys with *DMD* mutations post exon 30 and patients with PMM2-CDG, suggests a temporally altered signal transmission from the retinal level continuing until the striate cortex. Even though the VEP is a cortical measure, the notion of synaptic dysfunction due to receptor blockade

[1] Nonetheless, decreases of neuronal activity (in the OFF system in response to light increments or in the ON system in response to light decrements) are potentially still able to signal changes in ambient light to the cortex.

[2] Chapter 5, section 5.2

as a mechanism underlying VEP latency delays in humans was previously raised by Bodis-Wollner and colleagues [420]. In the past, disturbed ganglion cell and LGN ON-pathway signalling had only been suggested in the mouse and primate [156, 157, 158, 159, 327]. This thesis presents new insight into the pathology of human ON-pathway dysfunction.

While there was a clear difference in cortical VEP signature between the majority of patients and healthy observers, one observation was that a response could be recorded from VEP stimulation highlighting ON-pathway contribution. If the ON-pathway was completely blocked at the level of the bipolar cells, and thereby not transmitting any signals to the ganglion cells, one might expect a severely abnormal ON-pathway response at the cortical level. Instead, ON-and OFF-system responses were highly similar in appearance but the ON-pathway response was delayed in the VEP of most patients with ON-pathway dysfunction. This suggests that a signal is transmitted through the retinal layers and subsequently to the cortex, albeit with a temporal delay, even though signal transmission through ON bipolar cells is supposedly disrupted in patients. If this were the case, the question arises how such a temporal delay could be introduced at the retinal level.

My finding that a delayed response could be recorded from the ON-pathway to specialised ON/OFF VEP stimulation in subgroups of patients with a retinal ON-pathway dysfunction, signifies that the visual system could potentially have an alternative, route of transmitting ON-pathway signals from retina to visual cortex[3]. From this point, three alternatives are possible. Firstly, a partial preservation of the ON-pathway within the foveal region could explain the visual outcomes observed in patients. Secondly, the signal could be relayed via an alternative network of cell circuits, or, thirdly, the signal could be transferred via an alternative molecular signalling cascade, still resulting in the (delayed) depolarisation of ON bipolar cells.

[3] As mentioned earlier, decreases of neuronal activity within the intact OFF-pathway could potentially also signal changes in ambient light to the cortex. This could explain the relative preservation of the perception of light increments in patients with ON-pathway dysfunction (cCSNB specifically) in photopic conditions. In scotopic conditions, where rods are exclusively using the ON-pathway, a more severe impairment of vision can be observed clinically.

#### 7.2.1.1 Three hypotheses for ON-pathway signalling in retinal ON-pathway dysfunction

A partial preservation of healthy ON-and OFF-pathways within the fovea could explain the abnormal full field ERG results observed in patients with ON-pathway dysfunction, while allowing for relatively "mild" visual impairments under photopic light conditions reported in some cases. The full field ERG represents a whole-retina response and hence, if retinal abnormality was present but a healthy set of ON and OFF system terminals were confined to the macula or fovea, the contribution from the (healthy) foveal cells to the ERG waveform would most likely be overshadowed. Recently, at the 55th ISCEV symposium (2017), Dorfman and colleagues suggested this hypothesis as an explanation why patients with cCSNB appear to be photopically asymptomatic [421]. They indicated an ON-pathway deficit in the peripheral, but not the central retina of patients with cCSNB using the multifocal ERG.

While such a hypothesis could certainly explain the disparity between light adapted ERG findings and visual performance of cCSNB patients under photopic light conditions, the findings presented in this thesis suggest a different cause.

Firstly, the electrophysiological methods applied in this thesis were eliciting responses from the macula and were therefore ideal to investigate this hypothesis. The use of the VEP to selectively compare ON and OFF system contributions to cortical waveforms showed that a macula-driven ON system response can be recorded from the cortex, albeit with a delay compared to the OFF system response, in patients with ON-pathway dysfunction. These findings suggest that an ON-pathway signal is relayed through the macula/fovea in case of an ON-pathway dysfunction and it was hypothesised that the abnormalities in visual performance encountered by patients are caused by this ON and OFF system signal asymmetry[4].

Secondly, while patients with cCSNB are known to experience problems at low light levels, the results presented in this thesis show that a retinal ON-pathway

[4]Interestingly, Dorfman and colleagues did observe a delay in multifocal ERG waveform peak times for patients with cCSNB.

dysfunction can result in an impairment of visual behavioural qualities such as motion perception and contrast sensitivity under photopic light conditions. Further, the psychophysical assessments carried out using the LumiTrack$^{Tm}$ software, such as the biological motion detection or the contrast sensitivity assessments, relied on the use of foveal vision. The abnormal performance of patients in these tasks therefore suggests an ON-pathway abnormality also in the fovea. In summary, the results obtained in this thesis indicate a delay of the ON system, rather than a complete block or a healthy foveal ON system, resulting in the visual outcomes observed in patients with ON-pathway dysfunction. Hence, alternative pathways for ON system signals through the whole of the retina were considered more likely. Two ways of how this could be achieved are described below.

While there are are least three known pathways via which rod signals are transmitted across the retina under scotopic and mesopic light conditions [422, 423, 424, 24], only two major retinal pathways for cone signal transmission under photopic conditions are known: ON-and OFF-pathways. Rods never directly synapse onto ganglion cells but relay signals via ON bipolar cells to amacrine AII cells under scotopic conditions, which can make contacts with cone bipolar cells, OFF ganglion cells, as well as other amacrine cells [1]. In contrast, cone ON and OFF bipolar cells can transmit information about light increments and decrements directly onto ganglion cells. An extensive feedback and signalling network of amacrine cells is interleaved into these cone signal systems, with some bipolar cells connecting with retinal ganglion cells (for example [425, 426, 427, 428]). In the case of a disruption of the ON-pathway at the level of the cone ON-bipolar cells, the ON signal would need to be transmitted through another cell type, possibly OFF bipolar cells or the OFF surround of ON bipolar cells, at least initially, and could then be relayed by sign-inverting amacrine cells synapsing onto ON ganglion cells. Candidate amacrine cell populations which show synapses with ON ganglion cells exist and several could be candidates for such a task:

- A22, thought to be involved in visual coding of fast movements [425]
- ACh or Starburst amacrine cells, connecting to ON/OFF directionally selective ganglion cells [429, 428, 430, 431, 427, 432]
- A8, with a so far unknown role [426]
- Small diffuse amacrine cells of the midget system [433]

While all of these amacrine cells build connections linking cone bipolar cells and ON ganglion cells, it is difficult to highlight one of them as the most likely candidate, as knowledge about their exact function is sparse. The midget system is at its maximum density in the central retina [434] where cones outnumber rods. Thus, a large contribution of these cells to the VEP, which reflects the integrity of the macula, is a possibility. A pathway of ON signals from cones using the midget amacrine cell networks onto ON ganglion cells could provide a possible second route for ON signals through the retina under light adapted conditions and would affect a VEP response. Such a ”detour” from the original, direct photoreceptor-bipolar cell-ganglion cell route could introduce a temporal delay in ON signal transmission, which may be reflected in the observed ON/OFF VEP timing asymmetry. Under dark adapted conditions, if the rod ON bipolar-AII amacrine cell pathway is the only active route, the rod ON-pathway would still remain dysfunctional, agreeing with the night vision problems encountered in patients.

A logical draw-back of this hypothesis is that such an alternative, multicellular route for ON-pathway signals within the retina, involving the activation and input of several other cell types, would be inefficient in healthy individuals. Here, the direct original pathway would be activated by light. Further, a hypothetical alternative pathway would be activated by the same stimulus. This would result in several cellular signalling routes being active under healthy conditions, unless it is prevented by inhibitory signals. While inhibitory circuits are a common occurrence in the retina, in such a case, the cells involved in the ”alternative ON-pathway cell network” would need to be primed to be active under the circumstance that ON bipolar cell signalling fails. This presence of an additional cell network, requiring several levels of inhibitory feedback circuits to transfer ON-signals in the case of

dysfunction of the primary route, makes the "alternative ON-pathway cell network" a metabolically costly solution [435].

A more cost-effective explanation presents itself if an alternative molecular route exists within the ON bipolar cells. Such a pathway could provide an alternative regulatory mechanism, coming into play when the conventional signalling cascade is deregulated or disrupted by mutation. Alternative intracellular control mechanisms are common in the regulation of several important biological functions. An example for such a mechanism comes from cell apoptosis, where there are at least five different molecular pathways known to exist, leading to the same physiological outcome, programmed cell death [436, 437]. These range from having distinct starting points (i.e. membrane receptors) to several cascades involving different proteins. Another example for such a system can be found in the case of DMD. Here, the expression of utrophin, a protein with a highly similar molecular structure to dystrophin, was shown to prevent muscular dystrophy in dystrophin knock out mice [438, 439], almost completely taking over its function[5]. A similar situation within the molecular signalling cascade of ON bipolar cells, which carry out the important physiological function of transmitting light signals onto subsequent retinal cell types, is therefore a possibility.

The "negative ERG" detected in patients with ON-pathway dysfunction has classically been explained by functioning (hyperpolarising) photoreceptor cells, driving the a-wave. With the signal not depolarising the ON bipolar cells this results in an absence of the b-wave or a decrease in its size [441, 442]. However, Sieving (1993) conducted elegant experiments that suggested the electrophysiological phenotype observed in the light adapted ERG of patients with CSNB may also be explained by a signal delay of depolarising ON bipolar cells [161]. In his model, the more the signal from depolarising bipolar cells was delayed, the smaller the resulting b-wave was. His work suggests that an ON-pathway dysfunction might involve a slowing, rather than a complete block of signal transmission, at the photoreceptor / ON bipolar synapse[6]. This supports my second hypothesis of an alternative molec-

[5]Utrophin-based therapy is now in phase two clinical trials to treat patients with DMD [440].

[6]His experiments were initiated by the observation that patients with CSNB showed a slight

ular pathway within ON bipolar cells. Instead of a complete block of ON bipolar cell function, these cells are depolarised, albeit with a delay.

As an example, in the case of cCSNB patients with *GRM6* mutations (resulting in a loss of function of the mGluR6 glutamate receptor) such an alternative molecular route could be initiated by a different glutamate receptor present at ON bipolar cell dendrites. In addition to metabotropic glutamate receptors, ionotropic glutamate receptors were reported in cyprinid [443] and salamander [444] ON bipolar cells and rat retina [445]. While this shows that ON bipolar cells potentially express more than one glutamate receptor type on their membrane, ionotropic receptors are usually associated with OFF bipolar cells in humans [446] and present a rather fast mechanism. Hence, they are unlikely to play a major role in the delay of an ON signal in humans. The presence of several, slower, metabotropic glutamate receptors (mGluRs) was previously suggested and confirmed in the rodent inner nuclear layer [447, 448], as well as the outer plexiform layer [449]. Further, glutamate receptors with transporter-like pharmacology are known to exist on cone ON bipolar cell dendrites of basses [444][7]. Such alternative receptor proteins, by being slightly different functionally or in timing, could introduce a temporal delay, while still ensuring a signal relay via the depolarisation of the ON bipolar cell. For example, this could happen if an alternative receptor protein would require the recruitment of more downstream intermediary proteins to successfully complete the intracellular signalling cascade. Importantly, such a receptor could be blocked by a glutamate antagonist like APB, resulting in a complete disruption of the ON-pathway in the research setting, however, its function would not be disturbed by a mutation of *GRM6*.

Within this intracellular signalling network, the presence of several alternative proteins with similar functions within the molecular cascade would make for a relatively robust system. This could explain the abnormalities observed in patients with

delay of the light adapted b-wave. As discussed in Chapter 2, Section 2.3.2, this delayed peak might represent an OFF system response emerging due to abnormal ON system activity. Nonetheless, the hypothesis of a delayed signal transmission through depolarising bipolar cells as a cause for ON-pathway dysfunction in light of delayed cortical ON system responses is plausible.

[7] In primate ON bipolar cells, only the function of mGluR6 has been physiologically examined [450].

subtypes of CSNB, as well as PMM2-CDG, as in these cases similar proteins are affected by mutation or N-glycosylation defects (CACNA1f, CACNA2D4, GRM6, GPR179, LRIT3, NYX) [8]. Moreover, the slight distinction in results observed in the VEP data between patients with different genotypes could also be accounted for by this hypothesis. The temporal delay introduced into the ON signal might differ with the mutation type encountered in patients, depending on how much of an impairment of the original intracellular signalling cascade is caused by a certain mutation type. Following this hypothesis, the results obtained from the specialised ON/OFF VEP recordings indicate that the most severe intracellular impact would be caused by a lack of nyctalopin (encoded by *NYX*) as the compensation of its function might lead to the most severe temporal delays.

Of course, this hypothesis is highly speculative, but support for it could come from the discovery of further proteins involved in the ON bipolar cell signalling cascade leading to its depolarisation. Currently, there are no known candidate proteins, which could serve as alternatives to those mutated in patients with ON-pathway dysfunction, such as TRPM1, nyctalopin or GPR179. This highlights the importance of extensive genetic testing of patient cohorts and it emphasises the value NGS analysis can bring to the field, enabling the discovery of novel candidate genes in patients without a mutation in known ON-pathway dysfunction genes[9]. More importantly, such genetic analysis would benefit from research into protein function, alongside proteomic and transcriptomic analysis.

The lack of expression of certain proteins or their malfunction could potentially lead to the deregulation of others, delivering candidate proteins for the investigation of molecules involved in an alternative intracellular signalling pathway. A similar relationship was shown to exist in autism, where an upregulation of the mGluR5 receptor protein was linked to decreasing levels of the GABA A receptor beta 3 protein in patients [451]. Whether the expression of certain proteins is up-

[8] It is noteworthy that this statement relates to the ON-and OFF-pathway abnormalities observed in PMM2-CDG patients in this thesis. Clinically, a cone-rod dystrophy is common in this condition, which distinguishes it from the subtypes of CSNB [238, 216].

[9] For example, a further examination of the genotypes of the four CSNB patients without confirmed genotype in this thesis could lead to the discovery of such novel candidate genes and proteins.

regulated in patients with a mutation in an ON-pathway dysfunction gene, is not currently known. Such novel candidate proteins could perhaps initially be revealed by proteomic analysis in the nob CSNB mouse models. Observing the expression and activity levels of different proteins within the mutant retinae compared to the wild type could help to assess whether an alternative pathway is active in case of ON-pathway dysfunction, and give insight into potential proteins involved. Such analysis previously revealed TRPM1 as a candidate gene for CSNB [172, 203, 204].

Physiological support for either of the hypotheses presented here, could come from the recording of PERGs in human patients. If stimuli were designed to selectively bias waveform contribution from ON-and OFF-pathways, they could enable an insight into ON and OFF amacrine and ganglion cell circuits via electrophysiological methods. The stimuli utilised for the recording of specialised ON/OFF VEPs in this study could provide a starting point for such PERG recordings[10]. Specialised ON/OFF PERGs could give an insight into whether an ON signal is passed through the retinal ganglion cells with a delay.

[10]In fact, some light increment and decrement PERGs were simultaneously recorded from healthy volunteers during the validation phase of these stimuli. Reliable PERGs could be recorded from this stimulation and waveforms were akin to the conventional pattern reversal ERG waveforms obtained clinically. A manuscript including these data was accepted for publication in IOVS in December 2017: Fritsch, DM, Sowden, JC and Thompson, DA: "Pattern onset ERGs and VEPs produced by patterns arising from light increment and decrement", 2018. The manuscript can be found in the appendix.

### 7.2.2 Behavioural impact of a retinal ON-pathway dysfunction

Apart from the physiological impact of an ON-pathway dysfunction, it was important to investigate the visual perceptual impact of such a retinal signalling disruption. Psychophysical assessments of motion and contrast perception in patients with ON-pathway dysfunction revealed abnormalities in perceptual performance, which is heavily reliant on the accurate correlation of visual information (for example, the temporal integration of motion signals in the parietal cortex is crucial for decision making [452], whereas the importance for vision of correlated ganglion cell firing was highlighted in the salamander retina [155]), supporting the hypothesis that a retinal ON-pathway dysfunction likely results in visual impairment due to an abnormality of visual signalling.

Assuming that a complete ON-pathway signal block is present at the level of the bipolar cell level, some authors speculated that an ON signal could originate from the ON surrounds of OFF centre ganglion cells [288]. Theoretically, such surround input is gathered from bipolar cell signals, as well as from the interconnecting amacrine network (for example [453]). Schiller showed that the ON surround response of OFF cells in the LGN of rhesus monkeys was not affected by application of APB [327]. Further, Massey and colleagues reported that some OFF centre ganglion cells in the rabbit retina respond to light onset with a delayed response from the antagonistic surround [6]. Responses occurred around 90ms later than the ON centre response to the same stimulus, indicating a presence of ON-related visual signals even when ON-pathway glutamate receptors are blocked pharmacologically.

Such results, however, could also be explained by a delayed signal transmission through ON bipolar cells and do not exclude the possibility of a functional ON signal relay through the retina. Support comes from studies of nob mouse models lacking functional mGluR6 showing a response delay, rather than a response absence, to light onset in retinal ganglion and thalamus cells [158, 156, 454], resulting in receptive field abnormalities of these mice [157]. A signal delay from ON bipolar cells, as discussed in the previous section, could disturb the temporal structure of ganglion receptive fields, resulting in receptive fields with no clear sur-

round, as reported in nob3 mice by Maddox and colleagues. Subsequently, such ill-defined receptive fields could lead to ON-and OFF-pathway signals being out of sync temporally, impeding the ability of ganglion cell firing patterns to accurately develop.

Retinal activity is thought to be crucial for the correct wiring of the visual system during early development and a congenital abnormality affecting such firing patterns could logically have an impact on the visual circuitry. There is some evidence suggesting that ganglion cell firing specifically is needed for normal development of the visual system [455]. Blocking cat retinal ganglion cell activity with Tetrodotoxin (TTX), a blocker of voltage dependent sodium channels, was shown to prevent the segregation of ganglion cell axons into LGN layers, which is, in turn, important for the development of postsynaptic neurons [456]. Especially the directional tuning of direction sensitive retinal ganglion cells seems to be influenced by the integrity of the developing ON-pathway [457, 458]. In line with these results, it is likely that the development of receptive fields in these cells also relies on the temporal domain of signal input during development.

Signal firing patterns are crucial for the correct transmission and processing of motion and contrast signals within the visual pathways (for example [459, 460, 461]). Moreover, the importance of the temporal structure of such patterns was highlighted in a study from 2001, suggesting the magnitude of neuronal activation could depend on a specific ”ranking order” of a neuron's input [462]. If maximum activation of a neuron was dependent on the reception of synaptic input in an optimal order (or pattern), a temporal asymmetry between ON-and OFF-pathway signals may affect the activity of those cortical cells integrating signals from both pathways. Hence, an impact of such an abnormality on visual behavioural responses, such as observed in patients with ON-pathway dysfunction in this study, is feasible.

In this sense, a comparison might be drawn to vision under mesopic light conditions, where cone and rod photoreceptors are active simultaneously. The mesopic range has relatively ”soft” boundaries and reaches from the point where cones are

first active (cone threshold, at a light luminance of approximately 0.2 trolands) until the light level where rod saturation begins (at approximately 200 trolands) [463, 31]. At the dimmest light levels, rods first become active and are thought to transmit a signal via the slow rod pathway using the intermediary amacrine AII cells. In the healthy visual system, rod signals (i.e. ON-pathway signals) are delayed compared to cone signals [464, 465] and their delay at retinal ganglion cell level is estimated to be between 20 and 40ms in primates when measuring intracellular responses [463, 466], and between 8 and 20ms when measured psychophysically in human observers [463, 467, 468].

More recently, ON-pathway signalling delays of around 20ms were reported in mouse retinal parasol ganglion cells when presenting light targets under low mesopic light conditions [469]. These delays were non-existent once the background light was increased over the mesopic threshold. Importantly, such an asymmetry of ON-and OFF-pathway signalling was suggested to result in decreased VA under low light conditions [470, 31] in healthy individuals. Further, a deterioration of motion perception was observed under mesopic conditions in healthy observers, likely due to the incompleteness of integration of rod and cone signals in parasol ganglion cells which feed into the magnocellular system [471, 465, 472].

The ON system signal delay in retinal ganglion cells of 20ms described by Takeshita and colleagues [469], and also reported from detection tasks by Cao and colleagues [467, 463], resemble my findings of the cortical ON system signalling delay in patients with ON-pathway dysfunction[11] with an average ON delay of 18ms in patients with cCSNB. Additionally, the visual behavioural phenotypes of healthy individuals under mesopic conditions, such as subnormal VA and abnormalities in the perception of motion, are akin to those observed in patients with ON-pathway dysfunction under photopic conditions. This resemblance supports the proposal that retinal ON-pathway signalling delays could be the cause for the visual impairments experienced by patients. Following these findings, it could be concluded that an ON-pathway dysfunction, and therefore an ON and OFF system signalling asym-

[11]The ON/OFF VEP recordings in this study, however, were carried out under photopic conditions.

metry, may place a patient's visual system in a functionally mesopic state, at least to a certain extent.

#### 7.2.2.1 The curious case of patients with DMD

In this thesis, I have highlighted the similarities and differences between patient subgroups with ON-pathway dysfunction. While the hypotheses proposed in the previous section can explain the presence of delayed ON signals during vision testing and the visual impairments associated with it in patients with subtypes of CSNB and PMM2-CDG, they do not explain the striking difference in visual outcome between these patients and boys with DMD. Several studies investigated the unexpected link between *DMD* mutations and apparent abnormal retinal signalling, and most of these recorded the ocular phenotype of these patients alongside the ERG, but found generally no abnormalities (for example [258, 220, 473, 163]). Similarly, as described in Chapter 2, DMD patients showed clinically normal visual acuity, as well as normal fundi and retinal structure (OCT), alongside none of the visual perceptual deficits generally associated with a negative ERG, such as night blindness.

Ricotti and colleagues found electrophysiological differences between patients with *DMD* mutation pre and post exon 30 [163]. Boys with mutations upstream of exon 30, affecting expression of the long dystrophin isoform Dp427, showed normal dark adapted b:a-wave ratios. However, boys with mutations post exon 30 showed profoundly negative ERGs, with those mutations affecting shorter isoforms, such as Dp71, being associated with a more pronounced negative ERG waveform, as well as with autism spectrum disorder [163]. This suggests a differential effect of mutation location, and the dystrophin isoform affected, on retinal signalling and cognitive function. In my patient cohort, a distinction between these two groups also revealed some abnormalities of cortical ON/OFF VEP responses in patients with *DMD* mutations post exon 30, indicating a temporal signalling delay remaining detectable at the striate cortex. However, the asymmetry of DMD ON and OFF system signals was not as striking as in patients with subtypes of CSNB and PMM-CDG.

Only one recent study assessing visual function in boys with DMD detected abnormalities in visual perception. Costa and colleagues detected a high incidence of red-green vision defects in DMD patients with mutations post exon 30 using a bat-

tery of different assessments [474]. Such colour vision defects might be explained by the colour opponency of some ganglion cell receptive fields within the visual pathway receiving cone signal input [475, 15]. The existence of colour opponent receptive fields, receiving specific dichromatic input (red-green, or blue-yellow), was suggested in primate retina [476], LGN [477, 478] and cortex [479, 480]. All cone signals are relayed via ON or OFF bipolar cells and subsequently feed into ganglion cell receptive fields [481]. Hence, an ON-pathway dysfunction, impacting on the receptive fields of such red-green (or blue-yellow) colour opponent cells, underlying a subtle colour vision defect in patients is a possibility[12].

Nonetheless, if such defects are present to an extent, the question remains why these would not be detected in clinical practice. Costa and colleagues hypothesised that conventional colour vision assessments, such as the Ishihara Colour Vision test, are used to detect severe colour vision defects and therefore might not be sufficiently sensitive to expose the slight defects observed in these patients. In line with this thought, the psychophysical tests assessing motion perception might not have been sensitive enough to pick up the minor abnormalities in these subgroups. When evaluating contrast sensitivities of motion in more detail, however, some abnormality was detected in two DMD patients using $LumiTrack^{Tm}$. Consequently, this also means that the ERG and specialised VEPs provide more sensitive measures in this patient population, revealing slight physiological abnormalities.

Experiencing such ”subclinical” symptoms could explain why patients with DMD do generally not report any visual problems. An explanation could come from the presence of slight colour vision disadvantages within the general population, which is usually only revealed through specific colour vision testing and rarely through obstacles encountered in everyday life [474]. Unless individuals are faced with a task revealing a subtle impairment (such as a sensitive vision assessment), few are initially aware of such slight impairment, while an improvement in awareness often only comes with adult age [483, 484, 485, 486]. Due to patients

[12] Although patients with ON-pathway dysfunction are not usually described to experience colour vision deficits, one case report of mild defects for blue-yellow and red-green discrimination can be found in the literature [482].

with DMD often not surviving their second decade of life [487], such awareness of slight visual alterations might not be present in some. Moreover, due to the multitude of neuromuscular problems these patients experience, a possible minor visual impairment might not be immediately evident.

The question of the roles of different retinal dystrophin isoforms resulting in a negative ERG, yet allowing a normal visual phenotype, remains. Apart from the muscle, several dystrophin isoforms can be found in cells of the nervous system [488, 489], where they seem to localise to dendrites [490]. In the retina, four dystrophin isoforms (and their associated protein complexes) have been localised to the photoreceptor terminals and inner retinal synaptic layers (Dp427, Dp260 and Dp140) and Müller cells (Dp71) [491, 492, 225, 220, 493, 494, 495, 496]. ERG abnormalities have been detected in the absence of all these isoforms, with greater ERG abnormality and cognitive-neuropsychiatric disturbances linked to patients with mutations downstream of exon 30 [163].

In the retina, the lack of structural abnormalities in DMD patients, together with the physiological defect observed, suggests a role in neurotransmission for dystrophin isoforms. This could for example be through a role in the formation of an ion channel or an interaction with other signalling-related proteins. A functionally related protein, ankyrin, is present in the brain and associated with $Na^+$ channels [497], while dystrophin in the muscle is important for $Ca^{2+}$ homeostasis [498, 499] and hence the link to an ion channel regulating membrane potentials is possible. In the case of ON-pathway dysfunction, this could be the ($Ca^{2+}$ permeable) TRPM1 channel in ON bipolar cells or one of the $Ca^{2+}$ channels located in photoreceptor terminals.

Moreover, the fact that all dystrophin isoforms found in the retina contain similar protein binding regions [500], suggests that the isoforms have the capacity to overlap in function, at least to a certain extent. Abnormalities in the ERG in the disease context could therefore be caused by a disruption of dystrophin binding to its associated protein complexes or altered interaction with other proteins, influencing synaptic transmission indirectly [501, 502]. Taking the results obtained in this

study into account, a mutation of the shorter isoforms seems to lead to a more affected physiological phenotype, resulting in abnormal retinal and cortical signalling, which agrees with what is generally suggested in the literature [503, 163].

In summary, my findings show that patients with DMD show visual phenotypical abnormalities at the retinal and cortical level, which do not translate into obvious visual impairments. Hence, it would be of interest to evaluate perceptual visual function in these patients in further detail using more sensitive motion perception assessments, in order to detect possible subtle defects. Moreover, the DMD sample population carrying out the $LumiTrack^{Tm}$ psychophysical assessment was relatively small and any association between patient physiological and perceptual phenotypes would require further exploration on a larger cohort.

#### 7.2.2.2 Future work

The investigation of protein expression levels and function in ON-pathway dysfunction model organisms, alongside the genetic analysis of patient samples, can provide a first step to increase the knowledge on the key molecular processes important at the photoreceptor / ON bipolar cell synapse. Such future studies have the potential to discover key players within the ON bipolar cell signalling cascade. The exploration of potential alternative molecular pathways leading to depolarisation of these cells upon light stimulation further have the potential to initiate candidate gene sequencing approaches aiming to discover novel genes leading to ON-pathway dysfunction in patients and to identify possible molecular interventions.

Apart from the normal visual phenotypes observed in patients with DMD, other visual phenotypes encountered in patients could not be fully explained and require further investigation. Particularly some ocular and perceptual conditions seem to show a high incidence if the ON-pathway is disturbed. One example is the apparent increased susceptibility of some patients with CSNB to photo-aversion. An intriguing link exists to the recently described intrinsically photosensitive ganglion cells, which are thought to express the photopigment melanopsin [504] and mostly associated to the circadian rhythm [505]. However, recent research has revealed additional roles for those cells in conscious visual perception, including brightness discrimination in mice [506], as well as motion analysis [507]. These cells receive input from rod and cone ON bipolar cells [13] and have been linked to photo-aversion before [508]. Therefore, an abnormality of ON-pathway signalling could have an impact on these cells and their associated functions. Further study of these only very recently described cells will shed more light on their supposed role within visual perception and in a disease context[13].

A further factor contributing to visual impairment in some patients with ON-pathway dysfunction is the presence of nystagmus. Similarly to the incidence of photo-aversion in patients, the presence of nystagmus is variable in patients and

[13] As intrinsically photosensitive ganglion cells are thought to play a role in the circadian rhythm, some anecdotal evidence about patients with CSNB having trouble sleeping could reflect an impact on these visual processes. Such reports come from online support forums for people with CSNB, such as www.visionaware.org/forum/your-eye-condition/congenital-stationary-night-blindness.

a reason for its occurrence not known. A starting point for investigation in patients with PMM2-CDG might be provided by the apparent link of the occurrence of nystagmus in patients with the heterozygous variant *p.Arg141His* observed in this study.

Pieh and colleagues previously investigated nystagmus waveforms characteristics in patients with CSNB via eye-movement recordings and distinguished it from congenital idiopathic nystagmus [509]; however, no definite reason for its occurrence was suggested. The results presented in this thesis highlight a retinal signalling abnormality which is still detectable at the level of the visual cortex. It is therefore likely that such an abnormality is also present earlier at the level of the LGN. The primate LGN possesses connections to the cells of the superior colliculus [510], which plays an important role in the control of eye movements and saccades [511, 512]. Could an ON/OFF system signalling asymmetry disturb the execution of eve movements in the superior colliculus and hence explain the incidence of nystagmus in patients?

In line with this thought, is the suppression of the magnocellular system, which is thought to be initiated during a saccadic eye movement to dampen the sensation of retinal image motion [513], in some way linked to the magnocellular system deficits observed in patients in this thesis? Studies analysing the nystagmus waveforms observed in patients in detail (such as [509]) and comparing them with extensive genotypical information, alongside comparative studies investigating motion perception in patients with nystagmus and no other ocular conditions, could provide a starting point to answer these questions.

Another finding in this thesis was the slight difference in presence and absence of specific OPs across the patients subgroups. Especially striking were the contrasting results from dark adapted and light adapted OPs of patients with the complete and incomplete form of CSNB. Under dark adapted conditions, OPs of patients with cCSNB were almost completely abolished, whereas the same was true for patients with iCSNB under light adapted conditions. While dark adapted OPs are elicited to a relatively bright flash (3.0 cd*s*m$^{-2}$ according to ISCEV), potentially showing

some cone contribution, light adapted OPs are thought to reflect activity with the cone circuits only. Under dark adapted conditions, earlier OPs (OP2) seem to be linked to rod-mediated (ON) activity, whereas late OPs (OP4) are linked to the offset of a light stimulus, i.e. they likely stem from the cone system. OP3 in contrast seems to be evoked by an interplay from both systems [73, 81]. The absence of OP2 and OP3 in patients with cCSNB was linked to disturbed retinal ON-pathways before [78, 77]. The absence of all OPs in patients with iCSNB under cone-biased light conditions highlights this disorder's influence on ON-and OFF-pathways. As OPs are thought to mainly reflect spiking activity within the retinal amacrine cell feedback circuits, an alteration in ON-and OFF-pathway signal interplay within these circuits might result in the specific OP phenotypes encountered in this thesis.

In view of these results, it is curious why OP1 and OP4 were reduced in patients with DMD and mutations post exon 30 under light adapted conditions, indicating ON-and OFF-pathway impacts, without impacting significantly on behavioural visual performance of patients. In this sense, a further unanswered question is what OPs reveal generally about the functionality of vision in these patients. A detailed investigation of OPs under different light conditions across patient subgroups, aiming to link the presence or absence of specific OPs to individual genotypes and visual outcomes, may give an insight into the significance amacrine cell circuits have for the various visual behavioural phenotypes observed in this study.

### 7.2.3 Implications of findings for patients and clinical teams

This thesis presents a systematic study of visual phenotypes and genotypes in children with ON-pathway dysfunction. In order to evaluate the physiological impact such a dysfunction has on cortical signalling, a novel set of electrophysiological VEP stimuli, distinguishing contributions from ON-and OFF-pathways, was introduced. These novel stimuli outperformed the sensitivity and specificity of conventional cortical assessments in detecting abnormal ON-pathway function. Using the novel electrophysiological tests, physiological abnormalities were detected in 83% of patients with ON-pathway dysfunction, compared to only 37% when using conventional pVEP stimulation.

Results obtained from patients indicated an impact of a retinal ON-pathway disruption which was detectable at the level of the striate cortex, indicating a disruption of optic pathways originating in the retina, including the ganglion cells. Further, these specialised VEP recordings revealed a delay, rather than an absence, of ON-pathway signals at the striate cortex, implying that ERG phenotypes encountered in patients with ON-pathway dysfunction might be due to a signal delay, rather than a complete block of signal transmission at the level of the ON bipolar cells. The stimuli applied for cortical VEP recording in patients in this study, further provide a starting point for potential assessment of ganglion cell integrity of ON-and OFF-pathways via specialised PERG. These responses could be recorded simultaneously with VEPs, especially beneficial when recording from children where time efficiency is paramount.

Further, this thesis delivered the first quantifiable clinical assessment of motion perception and contrast sensitivity in such children, using a quick and playful psychophysical software called $LumiTrack^{Tm}$. This software compliments the novel electrophysiological test battery, which assesses the situation at the striate cortex, by combining higher cortical tasks assessing motion and contrast sensitivity within one, very mobile, test. Three domains of motion perception can be assessed under opposing contrast conditions, while contrast sensitivity within these tasks can be assessed in more depth. Further, these tasks are easy to carry out in children from at

least four years of age and take around 30min per subject, thereby providing an approachable way to assess visual function in a clinical paediatric setting. Designed with the variability of visual capabilities encountered in ophthalmological paediatric practice in mind, *LumiTrack*$^{Tm}$ allows the individual tailoring of the tasks by giving a flexibility of parameter choice, such as dot size and speed. At the same time importance was placed on maintaining constant test parameters across tasks, in order to ensure comparability of results obtained.

The physiological and perceptual results of these novel assessments allow a more realistic insight into a patient's visual capabilities. Firstly, this provides a more pragmatic link of conventional clinical vision assessments of ocular structure and physiology with visual qualities important in everyday life of patients. The objective assessment of such qualities was previously challenging in children and reliant on first-hand patient accounts. Being able to, for example, associate abnormalities in retinal structure with an objectively measurable and quantifiable perceptual defect, will provide a more complete clinical picture of a patient's visual phenotype. The large normative data set obtained from healthy volunteers of different ages in this study can aid in the determination of the perceptual abnormality in patients.

Consequently, clinical teams and carers might be able to better assess a patient's needs, optimising intervention to improve quality of life. In the face of difficulties perceiving low contrast, such an intervention could be to increase contrast of stairs and steps. Further, abnormal motion perception could lead to implications in the ability to carry out certain activities, such as some sports or driving a car. Secondly, being able to judge the visual capabilities and deficits a child has, in a more realistic way, aids parents, teachers and carers of patients to better understand their visual requirements. An adjustment and tailoring of the help a child with specific visual impairment receives at school can have significant benefit in his or her further cognitive and social development [123].

Further, the novel test batteries provide tools to investigate further and interpret better the patterns of visual loss which occur in children with visual impairment where testing was previously difficult. While they were developed with the

aim to investigate the ON-and OFF-pathways of vision, such tests, especially the psychophysical *LumiTrack*$^{Tm}$ software, are transferable to wider patients groups with visual impairments. Knowing how certain retinal or ocular defects translate into visual perception is an advantage for clinical care teams treating or assessing any visual condition. In the future, these tests may also be used to monitor interventions and the impact of treatments on perceptual visual function in children. These could include surgery for certain conditions but also monitoring the effectiveness of pharmacological treatments via clinical drug trials.

Ultimately, when combined with patient genotype, these novel vision assessments could further aid clinical teams and research teams in associating genetic make-ups with visual outcome. The molecular pathways involved in signal transmission at the photoreceptor / ON-bipolar cell synapse are largely unknown and several genetic key players are yet to be discovered. Obtaining a more detailed insight into the molecular processes at the retinal level especially with the potential of discovering novel genes involved - will inform translational studies that aim to restore function and influence connectivity in inherited retinal disease, for example through the development of gene-therapies.

In monogenic diseases, such as CSNB, a mutation in a specific gene can lead to a loss of protein function and result in a pathological phenotype. Gene therapy therefore aims to introduce functional cDNA for the affected gene into the cells. Such targeted cDNA is usually introduced using adeno associated viral vectors (AVV) in clinical studies attempting to treat eye conditions such as Lebers Congenital Amaurosis [144]. Evidently, such approaches are individually fitted and the exact cDNA introduced into a patient's cell depends on which gene is mutated in the individual. Thus, knowledge of the exact genotype of individual patients is crucial. Accordingly, studies linking genotype and phenotype of patients are an essential part leading to the development of gene therapy trials[14]. Moreover, the advent of gene editing, with the CRISPR-Cas9 system having received increased attention in recent years (for example [515, 516]), promises to directly target a patient's genome

[14]Recent advances in gene therapies for ocular disease are presented in a review by Petit and colleagues [514].

in order to treat inherited disease, making the knowledge of the exact variant present in a patient imperative.

## Appendix A

# Publications

Doc Ophthalmol (2017) 135:69–76
DOI 10.1007/s10633-017-9596-8

ORIGINAL RESEARCH ARTICLE

# The changing shape of the ISCEV standard pattern onset VEP

**Dorothy A. Thompson · Dennis M. Fritsch · Sharon E. Hardy · The POW Study Group**

Received: 23 March 2017 / Accepted: 25 May 2017 / Published online: 13 June 2017


**Abstract**
*Purpose* Pattern onset VEPs do not always show distinct C1–C2–C3 peaks and troughs. Our purpose was to study changes in pattern onset VEP with age to determine when the illustrated ISCEV standard onset VEP waveform can be reliably recorded.
*Methods* We recorded pattern onset VEPs from an Oz electrode referred to mid-frontal electrode according to ISCEV standards by presenting checks of 60′ and 15′ side length in a 15° field. Twenty-four adults aged 20–63 years participated. Amplitudes and latencies were collated. Pattern onset adult VEP shapes were compared to the waveform published in the ISCEV VEP standard and to paediatric pattern onset VEP waveforms recorded from 16 infants aged 7 months.
*Results* The shape of the pattern onset VEP changed gradually with age. The C1–C2–C3 morphology of the ISCEV standard pattern onset VEP becomes apparent consistently after 40 years to 60′ check stimulation. As age increases a negative trough, C2 is more frequently seen; however, the broad positive peak which characterises infant onset VEPs may still be recorded at 20 years. The group median measurements of onset VEPs to 60′ were C1 7 μV@ 88 ms (range 67–110 ms), C2 9 μV@109 ms (range 89–158 ms) and C3 13 μV@121–246 ms. To smaller 15′ checks, peak latencies were earlier and C2 became more obvious. The group median measures of onset VEPs to 15′ were C1 2 μV@69 ms (55–108 ms), C2 10 μV@90 ms (77–145 ms) and C3 14 μV@122 ms (99–200 ms).
*Conclusion* The ISCEV standard onset VEP best describes the waveform configuration and latency of the onset VEP produced by 60′ checks in adults of more than 40 years of age. The onset VEP waveform produced by 15′ checks is distinguished by more prominent negative C2 and earlier C1 and C2 latencies.

**Keywords** Pattern onset VEP · ISCEV standard VEP waveform · Waveform maturation · Check size · Age

D. A. Thompson (✉) · D. M. Fritsch · S. E. Hardy
The Tony Kriss Visual Electrophysiology Unit, Clinical and Academic Department of Ophthalmology, Great Ormond Street Hospital for Children, Great Ormond Street, London WC1N 3JH, UK
e-mail: dorothy.thompson@gosh.nhs.uk

D. A. Thompson · D. M. Fritsch
UCL Great Ormond Street Institute of Child Health , 30 Guilford Street, London WC1N 1EH, UK

## Introduction

Three visual stimuli are described in the 2016 ISCEV VEP standard; pattern reversal, pattern onset and flash [1]. Pattern reversal stimulation is the gold standard. A phase-reversing draughtboard produces a pattern

reversal VEP which is characterised by a positive peak at a latency of 100 ms. This is established by 7 months of age and is highly reproducible across individuals [2, 3]. Pattern onset and flash stimulation are recommended for patients with active defocus or nystagmus, or to identify chiasmal misrouting in albinism. VEPs produced by pattern onset and flash stimulation have complex polyphasic waveforms and show considerable inter-individual variation [1].

The pattern onset VEP waveform shown in the ISCEV VEP standards has well-described C1-positive–C2-negative–C3-positive peaks [1], but in practice these individual peaks are not always identifiable. Infants, for example, tend to show a single, simplified broad positive peak, which becomes more complex with maturation [4]. There are few published examples of pattern onset VEP waveforms. We sought to better describe and understand the waveform changes that may be expected in pattern onset VEPs produced by different check sizes at different ages when the ISCEV standard protocol is used.

## Methods and subjects

A cross-sectional observational study was carried out. Pattern onset VEPs were elicited from 24 adult subjects aged 20–63 years to the ISCEV standard VEP protocol which stipulates check side lengths 60′ and 15′ presented in a minimum 15° field recorded from Oz referred to Fz. The stimuli were presented for 200 ms onset/followed by 400 ms offset of mean luminance 82 cd/m$^2$ on a plasma display panel Michelson contrast 96% (max 170 cd/m$^2$/min 6 cd/m$^2$) viewed at 1 m. Pattern onset VEPs were additionally recorded from 5 adults who viewed the same stimuli in a larger 30° field and with a shorter onset period of 200 ms and from 10 teenagers to 60′ checks presented with an additional, longer inter-stimulus interval/offset interval of 1000 ms

Pattern onset VEPs recorded from Oz-mf 16 infants aged 7 months were retrospectively reviewed from a sample of more than 200 infants who were tested within the first year of life when laboratory reference data were compiled. The age 7 months was selected because it is the age at which pattern reversal p100 latencies fall within 10% of adult values. Onset VEPs in this infant reference study typically were recorded using a wider range of check sizes, 400′, 200′, 100′, 50′, 25′ and 12.5′ presented for 230 ms in a 30° field followed by a field of mean luminance for 330 ms. For this study, the stimuli had been displayed on a 74-cm NEC multi-synchronisation monitor (contrast 80% and luminance 50 cd/m$^2$).

The acquisition trigger timing, field size and check sizes presented on the plasma display panel were adjusted to match the NEC monitor. All data were recorded using the Espion system. The EEG was digitised using a sampling rate of 1 kHz and a band-pass filter of 0.312–100 Hz. The amplifiers had a fixed gain with an input range of ±0.5 V (Espion by Diagnosys, Cambridge, UK). The impedances of all electrodes were balanced and maintained below 5 kΩ throughout the recordings. In all cases, central fixation was monitored by CCTV.

The onset VEP waveforms were evaluated and the amplitude and latency of the main peaks and troughs measured. In cases where C1–C2–C3 morphology was not defined, the first main positive peak was taken as C1. In cases where C1 was not identified, but a negative C2 was prominent, the time point at the beginning of the C2 descent from baseline was taken as a C1 latency.

## Results

Pattern onset waveforms examples from healthy infants are shown in Fig. 1. Data from 16 infants aged 7 months, the age at which reversal VEPs are within 10% of adult latency [3], are shown in Fig. 2a, b.

At 7 months 13/16, infants showed an early positive peak mean C1 13 μV@94 ms (range 76–112 ms), seen in the top Fig. 2b. Of 13, 5 showed only the early positive peak, but 8/13 showed a positive peak at 138 ms as well (middle trace Fig. 2b). Of 16, 3 infants showed only a later positive peak (possibly C3), mean 135 ms (range 130–138 ms) bottom trace Fig. 2b.

Adult pattern onset VEP waveforms are arrayed in broad decade panels in Fig. 3. The ISCEV standard pattern onset VEP C1–C2–C3 configuration is seen more consistently after 45 years to 60′ checks (Fig. 3c). The C2 trough is more prominent in the pattern onset VEP waveform produced to smaller 15′ checks. C1 and C2 latencies are earlier to 15′ checks compared to 60′. The teenage pattern onset VEPs to 60′ were similar to those of the 20 year old shown in Fig. 3, a simple positive peak (Fig. 4).

The latency range of pattern onset VEP main peaks produced by 60′ and 15′ checks is detailed in Table 1.

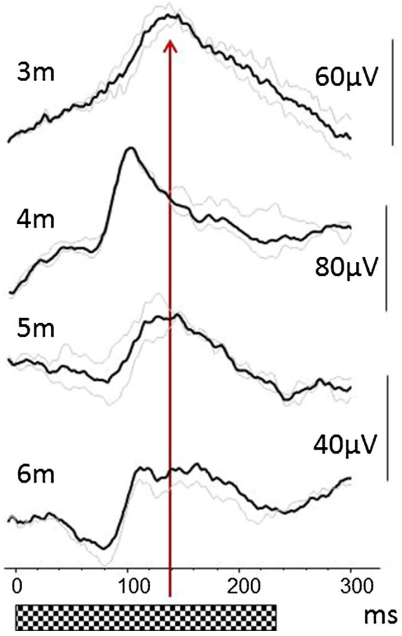


**Fig. 1** Example pattern onset VEPs waveforms from infants aged 3, 4, 5 and 6 months show a trend for the positive peak latency to reduce from 140 to 100 ms. The *solid line* is the average, repeated trials are shown in *grey*

When the latency ranges are translated onto the standard ISCEV onset VEP waveform in Fig. 5, there is good agreement with the 60′ check values.

We also compared the onset waveforms from the same adults produced by the ISCEV standard field size 15° with those from checks presented with a slightly longer onset period of 230 ms in a larger 30° field. Though waveforms differed within the same individual to 60′ or 15′, we did not observe an intra-individual difference between the onset VEP waveforms produced when either of these checks was presented in 15° or 30° field, nor did we observe any differences in the onset VEP waveform elicited to 200 ms compared to 230 ms onset, nor when the inter-stimulus interval/offset interval was 330 ms cf 1000 ms.

## Discussion

Pattern onset stimulation is an essential VEP stimulus for paediatric clinics where defocus and nystagmus are often encountered. The ISCEV VEP standard recognises that inter-individual variability of VEP waveforms produced by onset and flash stimulation is high [1], but the within individual concordance means that an inter-ocular comparison of onset and flash VEP waveforms can provide valuable clinical information, as can an inter-ocular comparison of the trans-occipital distribution of monocular responses. Indeed onset stimulation is required for detection of chiasmal misrouting of albinism in older subjects [4–7].

Published illustrations most often show onset VEP waveforms with C1:C2:C3 ratios that resemble the ISCEV standard waveform example [1]. Our findings caution that the composition of the onset VEP waveform is dependent upon age and check size. Our data suggest the onset VEP waveform illustrated in the ISCEV VEP standard [1] most likely represents the response produced by 60′ pattern onset in a 45 year old subject. The onset VEP waveform produced by smaller 15′ checks has a more prominent C2, compared to 60′, and has earlier C1 and C2 latencies. The range of latencies for each component described in our study of ISCEV standard onset VEPs agrees well with other published adult work, e.g. C1 65–80 ms, C2 90–110 ms, C3 150–200 ms [8] and C1 80–110 ms [9].

Although the C1 component is better seen in older subjects, it may also be enhanced by rapid onset periods (e.g. 25 ms onset [10] or 40 ms onset [11] compared to ISCEV standard 200 ms), use of lateral electrodes and large checks [12]. Indeed the spatial tuning of adult onset VEP components is complex; for example, Kriss et al. [8] reported that C1 is largest to 72′, C2 largest to 9′ and C3 bimodally larger to 9′ and 110′.

The three peaks of the onset VEP, C1, C2 and C3, appear to represent an interaction and temporal summation of activity from different cortical sources. These multiple, simultaneously active areas are very close together. Our data suggest ageing differentially alters the relative contribution of one or each component to the summated onset VEP waveform, but it is challenge to attribute a specific peak to a cortical source. Researchers have sought innovative ways to solve this inverse problem [13]. Parametric manipulations that include contrast adaptation, localising stimulation to small quadratic fields, which show the dependence of the waveform on retinal location, and principal component analyses and coregistration of fMRI, EEG and MEG have been used to infer cortical dipoles [10, 14–17].

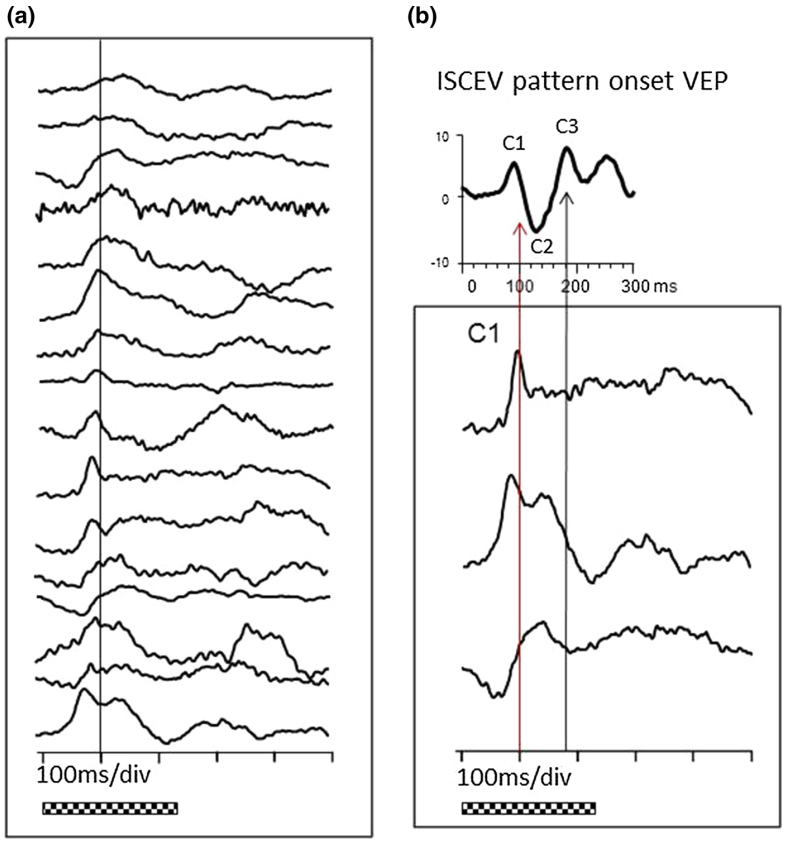


**Fig. 2** **a** Average onset waveforms from 16 individual infants all aged 7 months are arrayed. **b** Waveforms from 3 infants that exemplify the maximal waveform variation at 7 months are highlighted. The ISCEV standard waveform is shown on the same timescale in *black* for ease of comparison above

There is broad consensus that the onset VEP waveform has at least two overlapping time components: one from striate and the other from extra-striate areas [10, 14–17]. Classic studies from Jeffreys and Axford [10, 17] attributed C1 to striate cortex and C2 to extra-striate regions (for comparison C2 is P1 in di Russo et al. 2002 description [13]), whilst Spekreijse et al. [18] associated C1 with local luminance changes within the pattern arising from area 18 and C2, which is sensitive to contrast, defocus and pattern size, with striate areas [14]. This controversy is current some 50 years later [19, 20]. Mostly available data suggest C1 arises from multiple visual areas, but has a predominant contribution from V1 primary striate visual cortex in the early part of the waveform, whilst C2 reflects activity in dorsal and ventral extra-striate and C3 has also posterior parietal cortex contributions [21, 22].

During the early parametric studies two maturational phases for the onset VEP emerged: a rapid phase between birth and 8 months and followed by a slower phase ending at puberty with the C1–C2–C3 onset VEP morphology apparent at 16 years [11]. Published figures of paediatric pattern onset VEPs are very few. A population study of 214 children from 2 months to 12 years by De Vries-Khoe and Spekreijse [23] described how a negative peak (C2) became recognisable in the broad positive pattern onset VEP of children, with an incidence increasing continuously from 0% in the first five to ten months post-term to

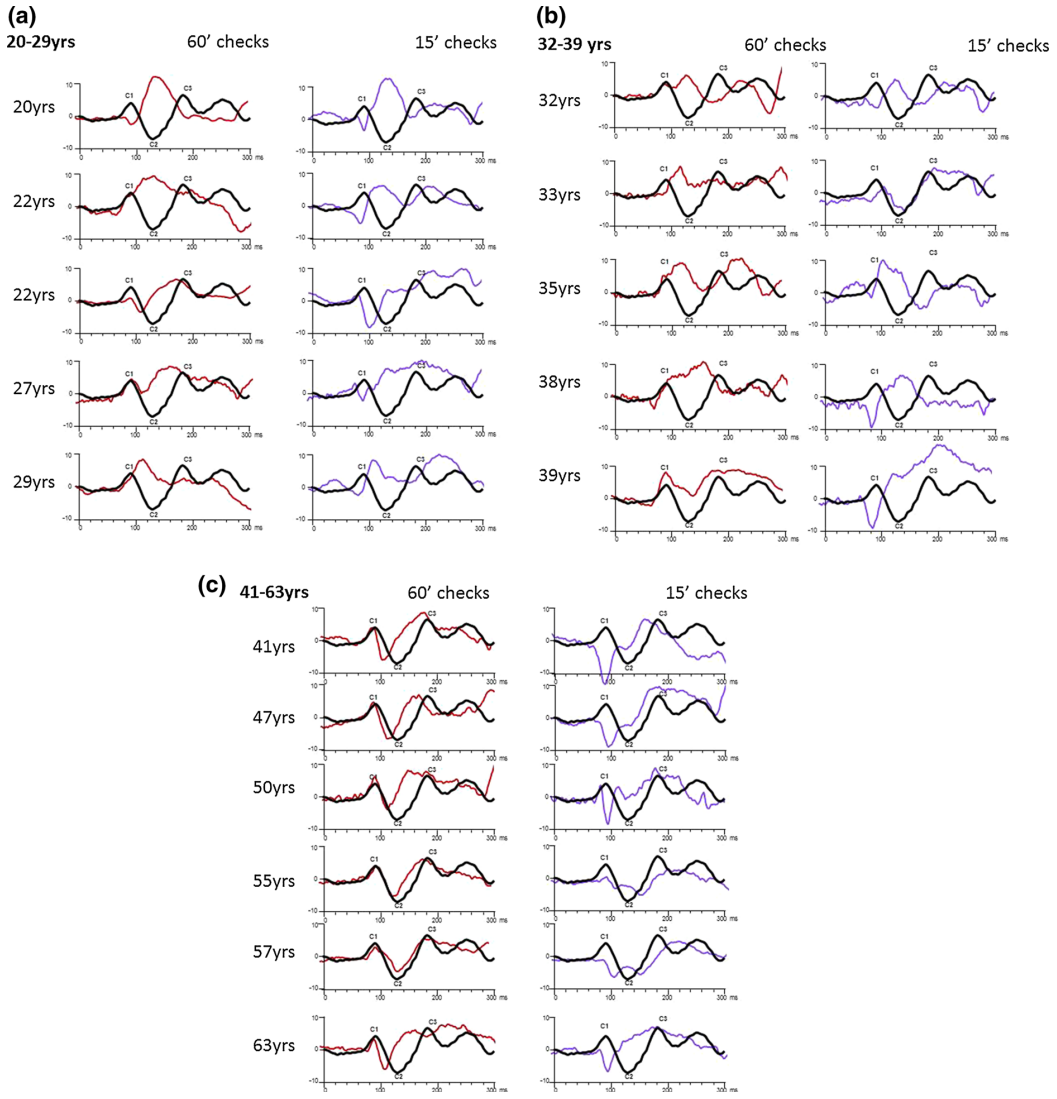


**Fig. 3** Three panels of adult pattern onset trace arrays are arranged in decades (**a**–**c**). Onset VEP waveforms produced by 60′ and 15′ checks in the same individual are displayed alongside each other, and each one is superimposed on the ISCEV template waveform in *black* for comparison. **a** Adult (aged 20–29 yrs), pattern onset waveforms overlaid on ISCEV standard waveform. **b** Adult (aged 32–39 yrs), pattern onset waveforms overlaid with ISCEV standard. **c** Adult (aged 41–63 yrs), pattern onset waveforms overlaid with ISCEV standard

about 40% at 20 months of age and to approximately 100% around 8 years of age. Ossenblok et al. [24] confirmed this in a detailed study of equivalent dipole source localisation of 10 children aged 6–16 years and described the evolved response as being a positive peak at 130 ms preceded by a negativity at 100 ms. These changes in onset VEP waveform from childhood to adulthood were attributed to changes in the activity profile of the striate cortex, which dominates in younger children whilst extra-striate activity

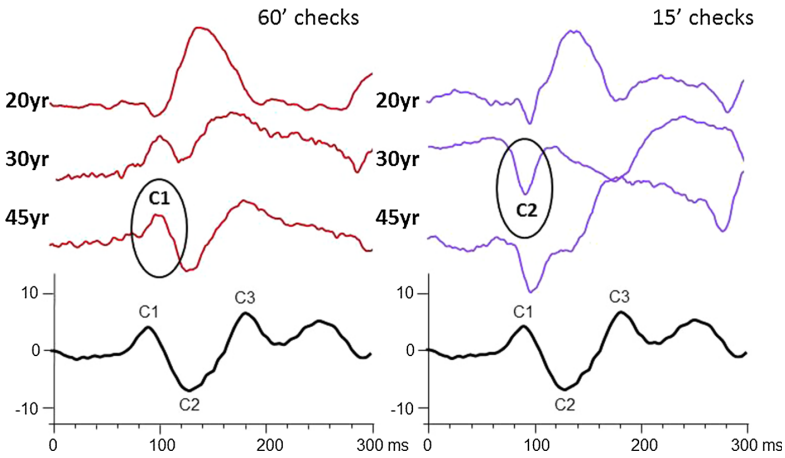


**Fig. 4** Example waveforms from 3 individuals are shown that summarise the main change in waveform features with check size and age during adulthood

**Table 1** The median and range of amplitude and latency of each peak of the pattern onset VEPs produced by 60′ and 15′ checks

| | 60′ median adult peaks (range) | | 15′ median adult peaks (range) | |
|---|---|---|---|---|
| C1 | 7uV@88 ms | (69–109 ms) | 2uV@69 ms | (60–95 ms) |
| C2 | 11uV@109 ms | (109–150 ms) | 14uV@90 ms | (79–143 ms) |
| C3 | 14uV@152 ms | (127–246 ms) | 14uV@122 ms | (100–167 ms) |

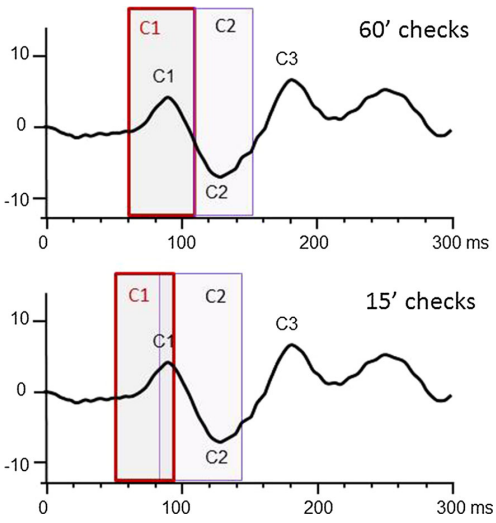


**Fig. 5** The latency range of the peaks C1 and C2 are displayed over the ISCEV waveform for 60′ and 15′ checks. The peaks to smaller checks are earlier than to larger checks. The ISCEV waveform peaks fall in the middle of the latency range of the adult C1 and C2 produced by 60′ check

dominates in later life [16]. Apkarian and Tijsson [9] describe the maturation of the albino trans-occipital asymmetry with some waveform illustrations of paediatric onset VEPs. They argued that C2 is not developed because of the immaturity of the sensitivity to fine elements in the striate cortex, but show C2 is developed by 20 years (using 12′ checks and 40 ms onset). They highlighted that reliable contra-lateral asymmetry in the pattern onset VEP is most consistently seen in the C1 peak—as this is not apparent or well developed in children it helps explain why the flash VEP is a preferred stimulus for checking for albino misrouting in young children under 3 years. Lenassi et al. [25] plotted onset VEP data from 13 children, aged 1 year and less, and suggested mean C1 latency becomes ~120 ms at 6 months, with a range 75–155 ms at 6 years. This agrees with the wide range of peak onset VEP latency in our study of 16 children at 7 months of 76–134 ms. Although there is a preponderance of an early first peak, some waveforms are dominated by later positive peaks.

Surprisingly our study shows a third ‘maturational’ or differential phase in the onset VEP waveform, or

rather continuous changes throughout adult life, with the emergence of a more prominent C1:C2 ratio with age. The underpinning physiological changes in the cortex between 40 and 60 years of age responsible for this are unclear and speculative. The occipital lobe is one of the brain areas most resilient to ageing. Myelination and synaptic pruning dominate the maturation changes in childhood whilst neuronal shrinkage and axonal fibre loss predominate ageing. Delineating a transition from maturation to degeneration associated with ageing is complicated to determine in vivo. Grey matter is fairly constant, but white matter volume increases until mid-40s, corresponding with a peak of myelination in some areas at 50 years, e.g. mesial temporal surface [26]. Brain weight is maximal around 20 years and does not reduce until after 50 years with a decline in brain volume starting around 45–50 years [26]. Age-related loss of grey matter is most prominent in the frontal and temporal lobes, with peak loss in dorsal brain areas around 50–70 years. The occipital lobes show least change, and although Good and colleagues [27] describe white matter loss in the occipital cortex, this occurs only towards the eighth and ninth decades. The network of higher-order regions that develop relatively late in adolescence shows accelerated degeneration in old age and heightened vulnerability to disorders that impact brain during adolescence and ageing [28, 29]. According to this 'last in first out' theory, we may speculate that that the onset components associated with extra-striate areas will be affected first by ageing and may underpin the waveform changes we have described.

In terms of VEP generation, these gradual anatomical and physiological changes in cortical tissue could alter extra-cellular or intra-cellular resistance, which in turn may change the relative amplitude and/or timing of one of the components contributing to the summated pattern onset VEP signal. A small latency difference in one component can have a substantial impact on the summated waveform shape, as seen when a 'negative' prolonged on flash ERG is modelled by delaying by 5 ms the depolarising bipolar contribution to the photopic prolonged on off macaque ERG a-wave [30, 31].

In summary, our data illustrate the changes in the ISCEV standard pattern onset VEP waveform throughout life and provide a template for clinical comparison. Further studies are needed to understand whether these changes may be exploited to explore ageing mechanisms and vulnerability to degenerative disease.

**Acknowledgements** The Pattern Onset Waveform (POW) study group members from the Clinical and Academic Department of Ophthalmology, Great Ormond Street Hospital London who contributed to this study are Katrina Prise, Victoria Reynolds, Dominique Versace, Sian Handley, Alki Liasis, Josie Evans, Ben Evans, Will Moore, Rob Henderson, Chris Lloyd, Richard Bowman, Lynne Speedwell, Clive Edelsten, Vasiliki Panteli, Jessica Gowing, Rosemary Wilson, Roopen Kuladia, Rachel Wells, Steph Figg, Joanna Randeree, Victoria Smith and Bronwen Walters.

**Funding** This study was supported by an Ulverscroft Vision Research Studentship awarded to Dennis Fritsch and the National Institute for Health Research Great Ormond Street Biomedical Research Centre (Grant No. 519201).

**Compliance with ethical standards**

**Conflict of interest** The authors declare that they have no conflict of interest. These data were first presented as an oral presentation at the ISCEV scientific meeting Singapore 2016.

**Ethical approval** All procedures performed in studies involving human participants were in accordance with the ethical standards of the institutional and/or national research committee and with the 1964 Helsinki Declaration and its later amendments or comparable ethical standards. Ethical approval for this registered study 14DS06 was obtained from the Great Ormond Street Hospital Institute of Child Health University College, London, 14/LP2136.

**Statement on the welfare of animals** This article does not contain any studies with animals performed by any of the authors.

**Informed consent** Informed consent was obtained from all individual participants included in the study.



## References

1. Odom JV, Bach M, Brigell M, Holder GE, McCulloch DL, Mizota A et al (2016) ISCEV standard for clinical visual evoked potentials: (2016 update). Doc Ophthalmol 133(1):1–9. doi:10.1007/s10633-016-9553-y
2. McCulloch DL, Skarf B (1991) Development of the human visual system: monocular and binocular pattern VEP latency. Invest Ophthalmol Vis Sci 32(8):2372–2381

3. Kriss A, Russell-Eggitt I (1992) Electrophysiological assessment of visual pathway function in infants. Eye 6(Pt 2):145–153. doi:10.1038/eye.1992.30
4. Kriss A, Russell-Eggitt I, Taylor D (1990) Childhood albinism. Visual electrophysiological features. Ophthalmic Paediatr Genet 11(3):185–192
5. Apkarian P, Reits D, Spekreijse H, Van Dorp D (1983) A decisive electrophysiological test for human albinism. Electroencephalogr Clin Neurophysiol 55(5):513–531
6. Creel D, Spekreijse H, Reits D (1981) Evoked potentials in albinos: efficacy of pattern stimuli in detecting misrouted optic fibers. Electroencephalogr Clin Neurophysiol 52(6):595–603
7. Brecelj J (2014) Visual electrophysiology in the clinical evaluation of optic neuritis, chiasmal tumours, achiasmia, and ocular albinism: an overview. Doc Ophthalmol 129(2):71–84. doi:10.1007/s10633-014-9448-8
8. Kriss A, Spekreijse H, Verduyn Lunel HFE, Braamhaar I, de Waal BJ, Barrett G (1984) A comparison of pattern onset, offset and reversal responses: effects of age, gender and check size. In: Nodar R, Barber C (eds) Evoked potentials ll. Butterworths, New york, pp 553–561
9. Apkarian P, Tijssen R (1992) Detection and maturation of VEP albino asymmetry: an overview and a longitudinal study from birth to 54 weeks. Behav Brain Res 49(1):57–67
10. Jeffreys DA, Axford JG (1972) Source locations of pattern-specific components of human visual evoked potentials. II. Component of extrastriate cortical origin. Exp Brain Res 16(1):22–40
11. Apkarian P, Reits D, Spekreijse H (1984) Component specificity in albino VEP asymmetry: maturation of the visual pathway anomaly. Exp Brain Res 53(2):285–294
12. Shawkat FS, Kriss A (1998) Sequential pattern-onset, -reversal and -offset VEPs: comparison of effects of checksize. Ophthalmic Physiol Opt 18(6):495–503
13. Fahle M, Bach M (2006) Origin of visual evoked potentials. In: Heckenlively JR, Arden GB (eds) Principles and practice of clinical electrophysiology of vision, 2nd edn. MIT Press, Cambridge, pp 207–234
14. Maier J, Dagnelie G, Spekreijse H, van Dijk BW (1987) Principal components analysis for source localization of VEPs in man. Vis Res 27(2):165–177
15. Manahilov V, Riemslag FC, Spekreijse H (1992) The Laplacian analysis of the pattern onset response in man. Electroencephalogr Clin Neurophysiol 82(3):220–224
16. Ossenblok P, Reits D, Spekreijse H (1994) Check size dependency of the sources of the hemifield-onset evoked potential. Doc Ophthalmol 88(1):77–88
17. Jeffreys DA, Axford JG (1972) Source locations of pattern-specific components of human visual evoked potentials. I. Component of striate cortical origin. Exp Brain Res 16(1):1–21
18. Spekreijse H, van der Tweel LH (1972) System analysis of linear and nonlinear processes in electrophysiology of the visual system II. Proc K Ned Akad Wet C 75(2):92–105
19. Kelly SP, Vanegas MI, Schroeder CE, Lalor EC (2013) The cruciform model of striate generation of the early VEP, re-illustrated, not revoked: a reply to Ales et al. (2013). Neuroimage 2013(82):154–159. doi:10.1016/j.neuroimage.2013.05.112
20. Ales JM, Yates JL, Norcia AM (2013) On determining the intracranial sources of visual evoked potentials from scalp topography: a reply to Kelly et al. (this issue). Neuroimage 64:703–711. doi:10.1016/j.neuroimage.2012.09.009
21. Di Russo F, Martinez A, Sereno MI, Pitzalis S, Hillyard SA (2002) Cortical sources of the early components of the visual evoked potential. Hum Brain Mapp 15(2):95–111
22. Vanni S, Warnking J, Dojat M, Delon-Martin C, Bullier J, Segebarth C (2004) Sequence of pattern onset responses in the human visual areas: an fMRI constrained VEP source analysis. Neuroimage 21(3):801–817. doi:10.1016/j.neuroimage.2003.10.047
23. De Vries-Khoe L, Spekreijse H (1982) Maturation of luminance and pattern EPs in man. Doc Ophthalmol Proc Ser 31:461–475
24. Ossenblok P, Reits D, Spekreijse H (1992) Analysis of striate activity underlying the pattern onset EP of children. Vis Res 32(10):1829–1835
25. Lenassi E, Likar K, Stirn-Kranjc B, Brecelj J (2008) VEP maturation and visual acuity in infants and preschool children. Doc Ophthalmol 117(2):111–120. doi:10.1007/s10633-007-9111-8
26. Sowell ER, Thompson PM, Toga AW (2004) Mapping changes in the human cortex throughout the span of life. Neuroscientist 10(4):372–392. doi:10.1177/1073858404063960
27. Good CD, Johnsrude IS, Ashburner J, Henson RN, Friston KJ, Frackowiak RS (2001) A voxel-based morphometric study of ageing in 465 normal adult human brains. Neuroimage 14(1 Pt 1):21–36. doi:10.1006/nimg.2001.0786
28. Raz N, Ghisletta P, Rodrigue KM, Kennedy KM, Lindenberger U (2010) Trajectories of brain aging in middle-aged and older adults: regional and individual differences. Neuroimage 51(2):501–511. doi:10.1016/j.neuroimage.2010.03.020
29. Douaud G, Groves AR, Tamnes CK, Westlye LT, Duff EP, Engvig A et al (2014) A common brain network links development, aging, and vulnerability to disease. Proc Natl Acad Sci U S A. 111(49):17648–17653. doi:10.1073/pnas.1410378111
30. Sieving PA, Murayama K, Naarendorp F (1994) Push–pull model of the primate photopic electroretinogram: a role for hyperpolarizing neurons in shaping the b-wave. Vis Neurosci 11(3):519–532
31. Sieving PA (1993) Photopic ON- and OFF-pathway abnormalities in retinal dystrophies. Trans Am Ophthalmol Soc. 91:701–773

Multidisciplinary Ophthalmic Imaging

# Pattern Onset ERGs and VEPs Produced by Patterns Arising From Light Increment and Decrement

Dennis Fritsch,[1,2] Jane C. Sowden,[1,2] and Dorothy A. Thompson[1,2]

[1]Clinical and Academic Department of Ophthalmology, Great Ormond Street Hospital London NHS Trust, London, United Kingdom
[2]University College London Great Ormond Street Institute of Child Health, London, United Kingdom

Correspondence: Dorothy Thompson;
dorothy.thompson@ucl.ac.uk.
Jane Sowden;
j.sowden@ucl.ac.uk.

Submitted: September 14, 2017
Accepted: November 20, 2017

Citation: Fritsch D, Sowden JC, Thompson DA. Pattern onset ERGs and VEPs produced by patterns arising from light increment and decrement. *Invest Ophthalmol Vis Sci*. 2017;58:XXX–XXX. DOI:10.1167/iovs.17-22984

**Purpose.** Our aim was to elaborate how on and off signals contribute to pattern ERGs and pattern visual evoked potentials (VEPs) by using pedestal patterns arising from incremental and decremental onset stimulation.

**Methods.** Pattern onset/offset ERGs and VEPs were produced by black and white checks of 60′ side length and 88% spatial contrast appearing in a 16° field for 200 ms from white (110 cd/m$^2$), black (7 cd/m$^2$), and gray (48 cd/m$^2$) backgrounds and disappeared for 1000 ms. Twenty healthy subjects participated in the study (median age 19.5, range, 5–31 years), 10 of whom also underwent pattern onset/offset ERG recordings to the same stimuli (median age 25.7, range, 22–31 years). VEPs were recorded from an occipital array referred to Fz. Pattern electroretinograms (PERGs) were recorded from DTL plus corneal electrodes referred to ipsilateral outer canthi.

**Results.** There was high correlation within subjects of the VEP waveform produced by patterns arising from light increment and decrement (group mean correlation coefficient of PVEPs to check appearance from black versus white: 87%). An average of increment and decrement PERGs simulated the onset PERG from a gray background. This waveform is akin to standard International Society for Clinical Electrophysiology of Vision (ISCEV) clinical PERGs to reversing checks.

**Conclusions.** In healthy individuals, the early components of the pattern onset/offset VEP waveforms are comparable to light increment and decrement pedestal stimulation. Pattern onset/offset ERGs to pedestal stimulation may be used to probe simultaneous recording of ERGs with VEPs in order to obtain an assessment of retinal ganglion cell and optic pathway function in patients with less stable fixation.

Keywords: ON-pathway, VEP, PERG, congenital nystagmus, OFF-pathway

ON- and OFF-pathways in the visual system convey the perceptions of light increment and decrement to the visual cortex.[1] In primates, a pharmacologic blockade of the ON-bipolar pathway using 2-amino-4-phosphonobutyric acid (APB) results in impairment of light increment perception, as well as loss of contrast sensitivity.[2] Patients with selective ON-pathway dysfunction are identified by flash electroretinograms (ERGs) that have reduced b-waves, so-called electronegative ERGs. This ERG phenotype localizes dysfunction to the synapse between photoreceptors and depolarizing bipolar cells and is a characteristic of the complete type of congenital stationary night blindness (cCSNB or CSNB1). Patients with CSNB1 often show visual problems in dim light conditions,[3–6] but the effects of this retinal dysfunction on subsequent neuronal pathways and cortical vision is not well understood at present.

In clinical electrophysiological practice the visual evoked potential (VEP) and the pattern electroretinogram (PERG) are used to assess visual pathway integrity and retinal ganglion cell function, respectively. Both responses, in accord with the International Society for Clinical Electrophysiology of Vision (ISCEV) standard recommendation, can be produced by phase reversing checkerboard stimuli made up of equal numbers of black and white checks.[7,8] This makes it feasible to assess retinal and optic nerve pathway function simultaneously in the same session.

Nystagmus is frequently seen in patients with a dysfunctional ON-pathway, which can make the electrophysiological recording to pattern reversal stimuli challenging. Although a pattern reversal VEP with normal time to peak can be recorded even in the presence of nystagmus,[9,10] the recording of a PERG—where good image quality and contrast is crucial to obtain a response[8]—can be difficult and results variable.[11]

In such cases, pattern onset stimulation can give insight into visual pathway function.[12,13] Here, we explore the potential of incremental and decremental "pedestal" pattern onset stimulation[14] with the aim of investigating and functionally distinguishing ON- and OFF-pathway contributions to ganglion cell and optic pathway function in healthy volunteers. These tests may present a viable electrodiagnostic alternative in patients with ON-pathway dysfunction who also have nystagmus.

## Methods

### Participants

Pattern onset VEP responses were recorded from 20 healthy subjects (median age 19.5 years; range, 5–31 years), of whom

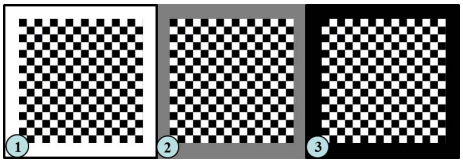


FIGURE 1. Overview of the stimuli used for the pedestal pattern onset VEPs and ERGs. Numbers 1 to 3 illustrate the different stimuli displaying a checkerboard of 88% Michelson spatial contrast appearing from three different backgrounds, with (1) presenting an overall light decrement upon appearance of the checkerboard and (3) an overall light increment; (2) shows the equivalent of a pattern onset VEP stimulus used in clinical practice with no luminance chance during stimulation.

10 were under 18 years of age (median age 10.5 years; range, 5–17 years) and 10 were over 18 years of age (median age 27 years; range, 22–31 years). The 10 adult subjects also consented to additional PERG recordings (visual acuity range with both eyes viewing: –0.275 to +0.15 logMAR). Onset PERGs were recorded separately from VEPs. For the recordings subjects were refracted as needed for best corrected vision outcome. The research followed the tenets of the Declaration of Helsinki. Informed consent was obtained from the subjects after explanation of the nature and possible consequences of the study. The research was approved by the Research Ethics Committee, NRES Committee London–South East (REC number 14/LO/2136).

### Electrode Placement

Pattern onset VEPs were recorded from an occipital array referred to Fz. An electroencephalogram (EEG) was recorded from the scalp overlaying the visual cortex (active electrode positions: O2, Oz, O1, P3, Pz, P4, inion, reference: Fz, ground: T3) following the international 10-20 EEG electrode placement system. Pattern onset ERGs were recorded from DTL plus corneal electrodes (Diagnosys LLC, Cambridge, UK) referred to outer canthi. Responses were recorded with both eyes viewing.

### Specifications

Pattern onset VEPs and pattern ERGs were recorded as continuous electroencephalography files using Neuroscan 4.2 software (Compumedics Ltd., Victoria, Australia). Amplifiers were set to an A/D rate of 1000 and had a band pass of 0.5 to 100 Hz. For stimulus generation, the Stim2 software was used (Compumedics Ltd.). The stimulus generation software sent out a trigger every time the stimulus was displayed to allow subsequent offline analysis of the continuous EEG file via epoching and averaging. One epoch was defined as the time range from 15 ms before stimulus/trigger until 400 ms after stimulus/trigger in order to capture all relevant components of VEP waveforms. An online artifact rejection was enabled for all responses outside of ±150-μV amplitude; responses with amplitudes falling outside of this range were rejected automatically. For each subject 150 accepted sweeps (2 × 75) were recorded for each VEP testing condition. PERG responses were averaged over 2 × 200 sweeps per condition in order to show repeatability. In order to distinguish the small-amplitude signals from noise, the mean noise level encountered in all subjects was retrieved by measuring the waveforms' mean deflection from zero over a period of 10 ms before stimulus. Subsequently, the 95% confidence interval (CI) of the noise was calculated. For the VEP recordings, the mean noise level was 0.93 μV with a 95% CI ranging from 0.55 to 1.29 μV; however, to obtain more robust values, we doubled the cutoff limit in order to achieve a supra-threshold level. The VEP components therefore needed to have an amplitude of at least 2.58 μV. For the PERG recordings, the mean noise level was 0.22 μV with a 95% CI ranging from 0.16 to 0.29 μV. At supra-threshold level, the PERG components needed to have an amplitude of at least 0.58 μV. Investigating the PERG offset response can be problematic due to the potential of blink artifacts at the end of the ISI (see, e.g., Fig. 5, traces 3 and 7). Choosing a poststimulus time window for the expected occurrence of the offset response is advised as highlighted in Figure 5. Here, we were looking for a defection from zero between 80 and 120 ms after stimulus offset.

### Stimuli

Electrophysiological stimuli were black and white checks of side length 60′ and 88% Michelson spatial contrast appearing in a 16° square stimulus field viewed at 1 m (within a bright 110 cd/m$^2$ surround of 87° × 62°). Stimuli were presented on a plasma display panel. Each stimulus was presented with one of three backgrounds—white background (mean luminance 110 cd/m$^2$), gray background (mean luminance 48 cd/m$^2$), black background (mean luminance 7 cd/m$^2$)—for 1000 ms, after which a checkerboard stimulus of the same size covered the same area for 200 ms. Representations of the pattern stimuli used in this study are displayed in Figure 1. These three stimuli were used to elicit pattern onset VEPs and ERGs.

## RESULTS

### VEP Results

In order to functionally distinguish ON- and OFF-pathways we recorded pattern onset VEPs to patterned stimuli arising from a

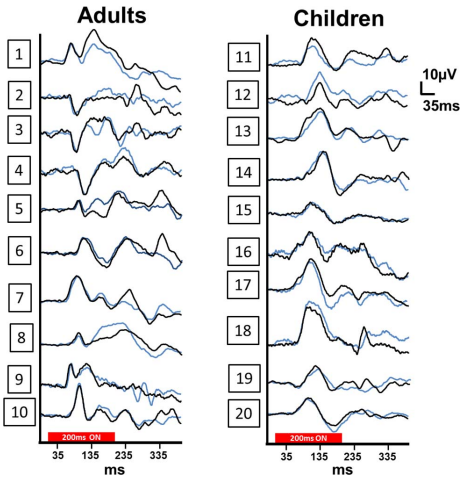


FIGURE 2. Pedestal pattern onset VEPs elicited with light increment (*blue*) and light decrement (*black*) stimulation overlaid for comparison. Each trace is an average of 150 sweeps recorded from Pz. Stimulus duration is displayed in *red*. Subjects arrayed in descending age order.

Investigative Ophthalmology & Visual Science

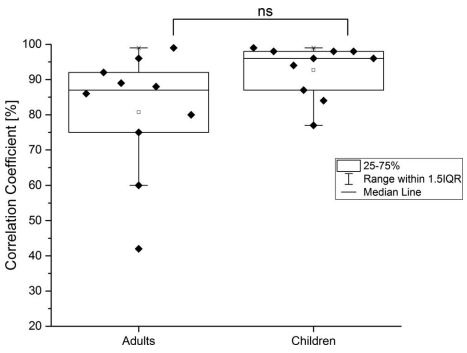


FIGURE 3. Comparison of the correlation coefficients obtained for each group from light increment and decrement VEP recordings. *Black diamonds* represent the individual subjects. *Boxes* give max and min (*x*), mean (*square*), and median (*border inside the boxes*), as well as 75% and 25% (*margins of the boxes*) percentiles. The children group displays an overall higher mean and median CC between the two conditions, as well as a narrower range of values. However, statistical analysis did not find a significant difference between the two groups (2-sample *t*-test: $P = 0.063$).

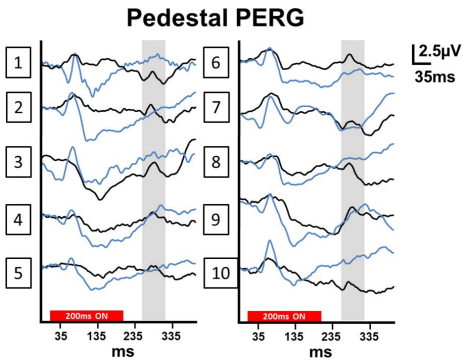


FIGURE 5. Pedestal pattern onset ERGs of adult subjects elicited with light increment (*blue*) and light decrement (*black*) stimulation are overlaid for comparison. Each trace is an average of 2 × 200 sweeps. Recordings were binocular; however, left eye is always displayed. No difference between right and left eye waveforms was observed. Stimulus duration is displayed in *red*. The time window used for investigation of the offset response is highlighted in *gray*.

black background (light increment) and a white background (light decrement), respectively. Reliable pattern onset VEP waveforms were recorded from all subjects to all three background conditions. Although the waveforms of the pattern onset VEPs varied across subjects and with age, within a healthy individual there was good concordance between waveforms produced by patterns appearing due to light increment and decrement (Fig. 2). In view of this variability, we chose to analyze the waveform shape and timing by calculating the correlation coefficient (CC) for each subject, rather than carrying out a simple component analysis. For this, we compared the waveform behavior and shape over a time period of 400 ms by comparing two corresponding points from the light increment and decrement conditions per millisecond. Hence, the similarity of both responses is calculated with a resolution of 400 points (1 point/ms). Resulting from this, the overall group mean CC was 87% with the smallest correlation within one subject being 42% and the highest 99% (Table).

Upon exploring the results empirically it seemed that in children the CC was higher than in adults; however, upon statistical analysis, this was not significant (2-sample *t*-test: $P = 0.063$; Fig. 3). Overall, the waveform shapes obtained from children were less variable than those from adults, with all of them showing a big positive first peak followed by a negativity. The waveform of the pattern onset VEP matures and becomes more complex with age and continues to differentiate into the three clear components, C1:C2:C3, by around 45 years.[15] Some young adult subjects showed similar-looking waveforms to children; others also displayed more complex responses. The

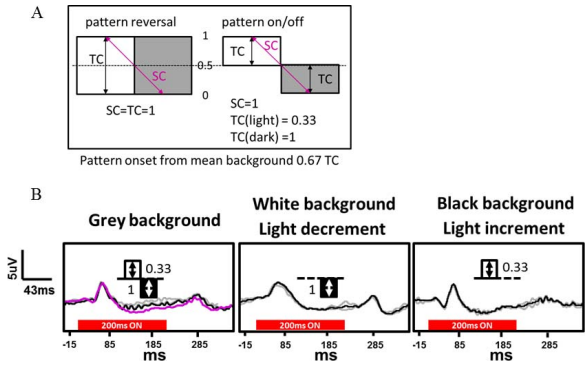


FIGURE 4. **(A)** A Reversal stimulus has equal spatial contrast (SC) and temporal contrast (TC), but a pedestal onset stimulus differs for light ON and light OFF and has a lower space-averaged temporal contrast of 67%.[22] **(B)** Representative pattern onset ERG traces of one subject for all three stimulations. *Gray traces* represent 200 averaged sweeps; *black traces* are averages of these. Offset PERGs are enhanced by light decrement. Onset PERGs have prominent N35 to light increment. An average of pedestal PERGs simulates the onset PERG from gray background (*purple overlay, column 1*).

Investigative Ophthalmology & Visual Science

**Table.** Correlation Coefficients of Pedestal Pattern Onset VEP Waveforms Across Subjects

| Subject | Correlation Coefficient, % | 95% CI Lower Limit, % | 95% CI Upper Limit, % | Subject | Correlation Coefficient, % | 95% CI Lower Limit, % | 95% CI Upper Limit, % |
|---|---|---|---|---|---|---|---|
| 1 | 75 | 66 | 82 | 11 | 96 | 95 | 97 |
| 2 | 96 | 95 | 98 | 12 | 94 | 91 | 96 |
| 3 | 60 | 47 | 70 | 13 | 98 | 97 | 99 |
| 4 | 88 | 83 | 91 | 14 | 98 | 97 | 99 |
| 5 | 42 | 26 | 56 | 15 | 84 | 78 | 87 |
| 6 | 89 | 85 | 93 | 16 | 87 | 82 | 91 |
| 7 | 92 | 88 | 94 | 17 | 98 | 97 | 99 |
| 8 | 99 | 98 | 99 | 18 | 99 | 98 | 99 |
| 9 | 80 | 73 | 86 | 19 | 77 | 69 | 84 |
| 10 | 86 | 80 | 90 | 20 | 96 | 93 | 97 |
| Mean CC > 18 y | | 80.7 ± 17.6 | | Mean CC < 18 y | | 92.7 ± 7.5 | |
| Total mean CC | | 87 | | Total MIN CC, % | 42 | Total MAX CC, % | 99 |

Values represent the percentage of correlation for waveforms obtained to light increment and decrement, as well as the 95% confidence interval. The closer this value is to 100, the more similar are the two waveforms. Mean CC is always given as percentage. Total mean CC is given with total minimum (MIN) and maximum (MAX) values, and mean CC of groups older and younger than 18 years is given with standard deviation (SD).

early peaks within 65 to 145 ms were the most similar when produced by light increment and decrement. This was supported by the finding that a higher group CC (90%) was achieved when analyzing only a duration of 200 ms from stimulus onset focusing on the timing of the first positive peak.

## PERG Results

Although pattern onset stimulation from a gray background displays less temporal contrast than reversal stimulation,[16] we were able to produce consistent onset PERGs in our cohort. These waveforms were akin to those obtained from clinical reversal stimulation when stimulation occurred from a gray background (Fig. 4B, first part of figure). The standard ISCEV PERG waveform is identified by three main components: N35, P50, and N95. When patterns appeared from a black background (light increment), a pronounced negativity with a timing matching the N35 could be observed immediately before the main positive peak (P50). Upon light decrement stimulation (pattern appearing from a white background), this negativity was not evident in any of the subjects, but a second prominent positive peak emerged at approximately 250 ms post stimulus, which most likely represents the stimulus offset response (Fig. 4B). Further, when averaging light increment and decrement responses together, the resulting waveform is almost identical to the one obtained from clinical pattern onset stimulation to a gray background (Fig. 4B, purple trace). An overview of all traces is given in Figure 5.

The amplitudes of the N35, P50, and N95 components were statistically different between the light increment, decrement, as well as gray background conditions with the light increment conditions giving consistently the biggest and best-defined responses (Fig. 6A). Responses elicited from light decrement stimulation were consistently smallest for these components, with the responses elicited to gray background condition being of intermediate amplitude. This picture was reversed when looking at the offset response, where the light decrement condition provoked the biggest responses and the light increment condition the smallest (1-way ANOVA with repeated measures and post hoc Bonferroni means comparison: P50: increment > decrement $P = 0.001$, increment > gray $P = 0.0055$; N95: increment > decrement $P < 0.001$, increment > gray $P < 0.001$; offset: decrement > increment $P = 0.0108$, offset decrement > gray $P = 0.0418$). When times to peak were compared across conditions and components, no statistically significant difference was found (Fig. 6B).

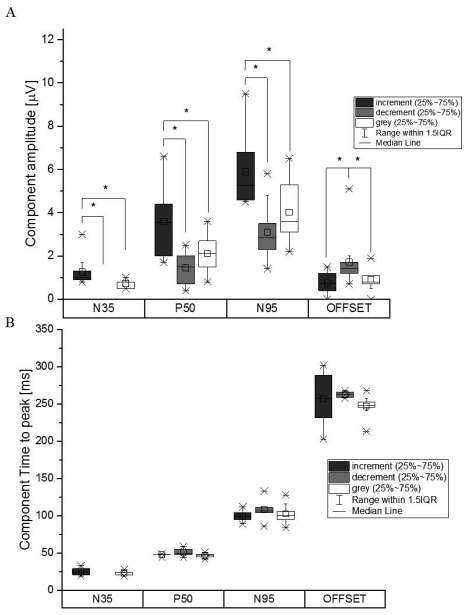


**Figure 6.** **(A)** P50 amplitude increased significantly in the light increment condition. ANOVA with repeated measures and post hoc Bonferroni means comparison: P50: increment > decrement $P < 0.001$, increment > gray $P = 0.006$; N95: increment > decrement $P < 0.001$, increment > gray $P < 0.001$; OFFSET: decrement > increment $P = 0.011$, offset decrement > gray $P = 0.042$. **(B)** P50 time to peak does not differ significantly across testing conditions. **(C)** Amplitudes of the offset responses to all three stimulation conditions were not significantly different. *Boxes* give max and min (*x*), mean (*square*), and median (*border inside the boxes*), as well as 75% and 25% (*margins of the boxes*) percentiles.



Allen Press, Inc. ■ 12 December 2017 ■ 11:09 am ■ Customer #IOVS-17-22984
//titan/production/i/iovs/live_jobs/iovs-58/iovs-58-14/iovs-58-14-28/layouts/iovs-58-14-28.3d

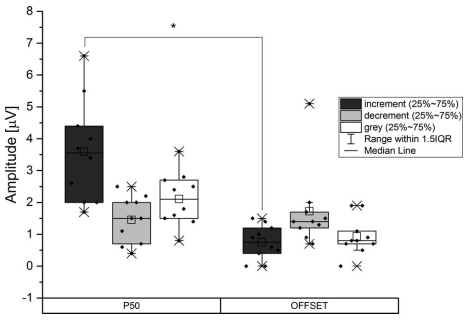


**Figure 7.** The P50 and offset amplitudes of corresponding testing conditions were similar for gray and white backgrounds (light decrement). P50 amplitude to light incremental stimulation was significantly higher in the cohort compared to the corresponding offset response (ANOVA with repeated measures and post hoc Bonferroni means comparison). *Boxes* give max and min (*x*), mean (*square*), and median (*border inside the boxes*), as well as 75% and 25% (*margins of the boxes*) percentiles.

Upon closer component analysis of the onset PERG waveforms obtained in our study group, we found that onset response (P50) amplitudes to 60′ checks across all conditions were constantly bigger than offset response amplitudes. Similar results were previously reported by Arden and Vaegan and others.[17–19] This difference was not found to be significant when patterns arose from gray or white backgrounds (light decrement); however, in response to a light increment, onset amplitudes were significantly higher than the corresponding offset response (Fig. 7).

## Discussion

In this study we have applied a set of electrophysiological tests assessing retinal ganglion cell, as well as visual pathway function, separately in the ON- and OFF-pathways of the visual system. This was achieved by utilizing conventional pattern onset stimulation and introducing a pedestal light increment and decrement component by presenting checkerboards arising from a black or white background, respectively. We were able to show that pattern onset VEPs are similar to incremental and decremental pedestal stimulation in healthy observers. Although there was waveform variation across the subject cohort, a good concordance within individual subjects was observed. Generally, the first positive peak seemed to be the most robust component when produced by light increment and decrement. These results suggest local spatial contrast changes rather than luminance changes (temporal contrast) to be the driver of these responses. This agrees with earlier work by Spekreijse, Estevez, and Van der Tweel and another group,[20,21] who found that cortical responses show a spatial contrast dependence. If it was temporal contrast, we may expect a bigger difference between incremental and decremental responses according to the inherent asymmetry in temporal contrast magnitude proposed by Drasdo and colleagues[22] (Fig. 4A).

In addition to VEPs, pattern onset ERGs were recorded to the same stimuli in order to capture inner retinal contributions of ON- and OFF-pathways. The summation of the increment and decrement PERGs showed great similarity to the waveforms obtained from a conventional clinical pattern reversal ERG with the main components being observed. Previous research established that there is no peak latency variation in the onset PERG with changing contrast.[23] We show here that the same is true when PERGs are elicited by patterns arising from light increments and decrements. In contrast, a marked difference in peak amplitude between onset PERGs produced by light increment and decrement was observed in this study. Not only were N35, P50, and N95 components significantly larger during light incremental stimulation, but the occurrence of an N35 was not observed in light decremental PERGs at all. A wealth of studies highlight an asymmetry in the processing and perception of darks and lights by the visual system. Initiated by Galilei's[24] irradiation illusion highlighting a higher visual spatial resolution for dark stimuli compared to light stimuli, this phenomenon was subsequently supported by more recent findings that OFF-center afferents dominate the cortical representation of central vision,[25] and that cortical neurons are more strongly driven by darks than by lights at low spatial frequencies.[26] These studies reveal a fundamental difference between ON-and OFF-pathway representation and processing in the cortex. Our results would agree with a larger retinal signal gain exhibited in the ON-pathway compared with a subsequently larger cortical signal gain in the OFF-pathway, as the subsequent cortical VEP waveforms to incremental and decremental stimulation were highly similar. At the retinal level, PERGs were bigger and better defined to light incremental stimulation, hinting at a potential advantage of the ON-system at this stage.

Pharmacologic studies have suggested that ON- and OFF-pathways contribute equally to the conventional pattern reversal ERG.[27] Interestingly, we found the pattern ERG offset response in our cohort to be of smaller amplitude than the pattern onset response. This was significant in the light increment condition. The check size used in this study (60′) might be the cause of this, as the amplitude of the offset response exhibits band-pass spatial tuning with larger amplitudes encountered using big check sizes.[18,19,23] Another possibility is that the offset response is driven more by temporal contrast than the onset response at this spatial frequency, resulting in different-sized components.[28] Furthermore, in this study, a substantial offset response was elicited only if the temporal contrast of the stimulus was higher than 33%, that is, in the light increment condition and when stimuli were appearing from a gray background.

In conclusion, our results show that pedestal pattern onset stimulation can be useful to assess ganglion cell as well as visual pathway integrity selectively in ON- and OFF-pathways. VEPs recorded from healthy volunteers show a high correlation when waveforms elicited to light incremental and decremental stimulation are compared. Pattern onset ERGs are of comparable morphology to conventional clinical pattern reversal ERG waveforms, displaying all major components. Pattern onset ERGs may be recorded simultaneously with onset VEPs.

These results suggest that these stimuli offer an effective means of investigating a dysfunctional ON-pathway and distinguishing ON and OFF signals from optic nerve and striate cortex. In particular, they can provide an alternative stimulus for assessing visual function in patients with ON-pathway dysfunction who can also have nystagmus.

### *Acknowledgments*

The authors thank the Ulverscroft Foundation and the National Institute of Health Research (NIHR) Biomedical Research Centre at Great Ormond Street Hospital and University College London, alongside the Great Ormond Street Hospital Children's Charity for the support of this study. All research at Great Ormond Street Hospital National Health Service (NHS) Foundation Trust and

University College London (UCL) Great Ormond Street Institute of Child Health is made possible by the NIHR Great Ormond Street Hospital Biomedical Research Centre. The views expressed are those of the author(s) and not necessarily those of the NHS, the NIHR, or the Department of Health.

Supported by an Ulverscroft Vision Research Studentship awarded to DF and the National Institute for Health Research Great Ormond Street Biomedical Research Centre (Grant No. 519201).

Disclosure: **D. Fritsch**, None; **J.C. Sowden**, None; **D.A. Thompson**, None

## *References*

1. Schiller PH, Sandell JH, Maunsell JHR. Functions of the ON and OFF channels of the visual system. *Nature*. 1986;322: 824–825.
2. Dolan RP, Schiller PH. Effects of ON channel blockade with 2-amino-4-phosphonobutyrate (APB) on brightness and contrast perception in monkeys. *Vis Neurosci*. 1994;11:23–32.
3. Bijveld MM, van Genderen MM, Hoeben FP, et al. Assessment of night vision problems in patients with congenital stationary night blindness. *PLoS One*. 2013;8:e62927.
4. Dryja TP, McGee TL, Berson EL, et al. Night blindness and abnormal cone electroretinogram ON responses in patients with mutations in the GRM6 gene encoding mGluR6. *Proc Natl Acad Sci U S A*. 2005;102:4884–4889.
5. Miyake Y, Yagasaki K, Horiguchi M, Kawase Y, Kanda T. Congenital stationary night blindness with negative electroretinogram: a new classification. *Arch Ophthalmol*. 1986;104: 1013–1020.
6. Audo I, Robson AG, Holder GE, Moore AT. The negative ERG: clinical phenotypes and disease mechanisms of inner retinal dysfunction. *Surv Ophthalmol*. 2008;53:16–40.
7. Odom JV, Bach M, Brigell M, et al. ISCEV standard for clinical visual evoked potentials (2016 update). *Doc Ophthalmol*. 2016;133:1–9.
8. Bach M, Brigell MG, Hawlina M, et al. ISCEV standard for clinical pattern electroretinography (PERG): 2012 update. *Doc Ophthalmol*. 2013;126:1–7.
9. Arlt A, Zangemeister WH. Influence of slow eye movements and nystagmus on pattern induced visual evoked potentials. *Neuro-Ophthalmology*. 1990;10:241–251.
10. Houston S, Fritsch D, Reynolds V, Liasis A, Thompson D. Pattern reversal VEP latency in children with nystagmus. *13th BrISCEV Symposium* 2015.
11. Sergouniotis PI, Robson AG, Li Z, et al. A phenotypic study of congenital stationary night blindness (CSNB) associated with mutations in the GRM6 gene. *Acta Ophthalmol*. 2012;90: e192–e197.
12. Hoffmann MB, Seufert PS, Bach M. Simulated nystagmus suppresses pattern-reversal but not pattern-onset visual evoked potentials. *Clin Neurophysiol*. 2004;115:2659–2665.
13. Saunders K, Brown G, McCulloch D. Pattern-onset visual evoked potentials: more useful than reversal for patients with nystagmus. *Doc Ophthalmol*. 1997;94:265–274.
14. Zemon V, Gordon J. Luminance-contrast mechanisms in humans: visual evoked potentials and a nonlinear model. *Vision Res*. 2006;46:4163–4180.
15. Thompson DA, Fritsch DM, Hardy SE. The changing shape of the ISCEV standard pattern onset VEP. *Doc Ophthalmol*. 2017. ?11
16. Thompson DA, Drasdo N. The origins of luminance and pattern responses of the pattern electroretinogram. *Int J Psychophysiol*. 1994;16:219–227.
17. Arden GB, Vaegan . Electroretinograms evoked in man by local uniform or patterned stimulation. *J Physiol*. 1983;341: 85–104.
18. Thompson DA, Drasdo N. Computation of the luminance and pattern components of the bar pattern electroretinogram. *Doc Ophthalmol*. 1987;66:233–244.
19. Török B, Meyer M, Wildberger H. The influence of pattern size on amplitude, latency and wave form of retinal and cortical potentials elicited by checkerboard pattern reversal and stimulus onset-offset. *Electroencephalogr Clin Neurophysiol*. 1992;84:13–19.
20. Spekreijse H, Estevez O, Van der Tweel LH. Luminance responses to pattern reversal. In: Pearlman JT, ed. *Xth I.S.C.E.R.G. Symposium*. Dordrecht: Springer Netherlands; 1973:205–211.
21. Riemslag FC, Ringo JL, Spekreijse H, Verduyn Lunel HF. The luminance origin of the pattern electroretinogram in man. *J Physiol*. 1985;363:191–209.
22. Drasdo N, Cox W, Thompson DA. The effects of image degradation on retinal illuminance and pattern responses to checkerboard stimuli. *Doc Ophthalmol*. 1987;66:267–275.
23. Thompson D, Drasdo N. The effect of stimulus contrast on the latency and amplitude of the pattern electroretinogram. *Vision Res*. 1989;29:309–313.
24. Galilei G. *Dialogo sopra i due massimi sistemi del mondo*. Florence: Landini; 1632.
25. Jin JZ, Weng C, Yeh C-I, et al. On and off domains of geniculate afferents in cat primary visual cortex. *Nat Neurosci*. 2008;11:88–94.
26. Kremkow J, Jin J, Komban SJ, et al. Neuronal nonlinearity explains greater visual spatial resolution for darks than lights. *Proc Natl Acad Sci U S A*. 2014;111:3170–3175.
27. Luo X, Frishman LJ. Retinal pathway origins of the pattern electroretinogram (PERG). *Invest Ophthalmol Vis Sci*. 2011; 52:8571–8584.
28. Thompson DA, Drasdo N. The origins of luminance and pattern responses of the pattern electroretinogram. *Int J Psychophysiol* 1994;16:219–227.

?10

**Appendix B**

# Patient Information Sheet used during recruitment of patients to the study

Great Ormond Street Hospital for Children NHS Foundation Trust

UCL INSTITUTE OF CHILD HEALTH

# *A study of how eye signals alter vision.*

INFORMATION FOR PARENTS OR GUARDIANS OF

**YOUNG PATIENTS PARTICIPATING**

Version 3.0, 28/01/2015

## Aim of this study

The eye uses different pathways to signal light (on path) and dark (off path). When the brain combines signals from on and off paths we are able to see different contrasts and patterns. We aim to find out how contrast vision is altered when ‘on-path’ signals from the retina in the eye are disrupted.

## Why are we doing this study?

If we identify aspects of visual impairment that are specific to disrupted ‘on-path’ connectors it could help us develop ways to compensate, e.g. by changing the lighting or reversing contrast of print. Eventually it may become possible to repair the ‘on path’ to restore visual function.

## The vision tests, (EEG, VEP, ERG).

We would like to record your child’s visual responses from the brain using an EEG and from the eye with an electroretinogram, ERG, and also to do some visual detection tests.

An EEG, or Electroencephalogram, measures all of the spontaneous brain activity going on at any time in our brains. Small electrodes placed on top of the scalp listen for the tiny electrical signals that the brain uses to send messages from one part of the brain to another. The signal we record is called a visual evoked potential or VEP. An electroretinogram or ERG is similar, but it records the signal from the retina, which is the light sensitive lining at the back of the eye.

Great Ormond Street Hospital for Children NHS Foundation Trust

UCL INSTITUTE OF CHILD HEALTH

## How are the vision tests done?

In the clinic rooms children may sit by themselves, or on your lap, on a chair in front of a large TV screen or in front of a flash globe. They may have a drink or eat a snack during the tests, & can enjoy some cartoons. Please do bring any favourite DVDs from home if your child wants.

## The EEG Test

Visually evoked potentials (VEPs) will be measured via the EEG. VEPs are evident when signals from the eye reach the vision areas of the brain. Small areas of scalp will be cleaned using a slightly gritty soap on a cotton wool bud, then electrodes will be positioned on your child’s head with a washable cream. A headband will be used to keep them in place. The lights in the room will be turned off and black and white patterns will be shown on the TV.

## The ERG test

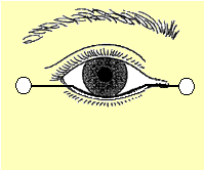

For the electroretinogram (ERG) test, sticker electrodes will be gently placed on your child’s cleaned temples and below the eye. An anaesthetic drop will then be put in the eye followed by a dilating drop to make the pupil big. This can make your child’s near vision blurry for a few hours, but takes away any sting from the dilating drops and stops a thin fibre electrode on the lower eyelid from tickling.

When the pupils are dilated we will show your child lights of different colours and brightness both in the dark and with the lights on. At the end of the test everything is easily removed and any cream is washed off with cotton wool and warm water. Both tests together take approximately 1.5 to 2 hours if done one after another.

## Visual detection test

This is a psychophysical assessment, where your child presses a button when they see a light on the TV. This simple test will not exceed 30 minutes.

Great Ormond Street Hospital for Children NHS Foundation Trust

UCL INSTITUTE OF CHILD HEALTH

## Genetic test DNA sample

If you and your child have not provided one before, we may ask for a small blood sample so that we can look for changes in your and your child’s genetic alphabet that may be associated with *known* genes and protein connectors in the ‘on-path’. The small blood sample will be taken from your and your child’s arm by an experienced practitioner. We can use spray or cream to numb the patch on the arm to minimise any discomfort. DNA will be extracted from these samples. Genes that may be involved in congenital eye defects that can alter the ‘on-path’ will be studied. This part of the study may take us up to 5 years before we get a result.

## Can I know the results obtained from the study samples?

It is not planned to routinely feedback the results from genetic or other tests obtained from the donated samples. However, if the research does identify a cause of the rare disease in your DNA, with your permission, we would let your doctor and your clinical care team know. All research results that are identified will need to be confirmed in an accredited diagnostic laboratory before being used in the clinical management of you and your family members.

## Are there any side effects or risks of the tests?

No risk is foreseen. The procedure of giving a blood sample may involve a momentary discomfort, from a needle prick, and may leave a small bruise. We use numbing cream or spray on the arm to lessen any discomfort.

The application of electrodes and types of vision tests used in this study have been carried out as a clinical routine on newborns and children at Great Ormond Street for over 20 years, and has never induced a seizure. There is, however, a very small risk that the flickering lights or patterns could induce a seizure. This risk is comparable to that of seizures being induced by video games on TV**.**

Great Ormond Street Hospital for Children NHS Foundation Trust

UCL INSTITUTE OF CHILD HEALTH

## Do I and my child have to take part in this study?

If you decide, now or at a later stage, that you and/or your child do not wish to take part in this study, that is entirely your right and it will in no way prejudice any future care your child or you may require.

## What are the potential benefits of the study?

The data that you’re and your child’s participation provide will help us better understand the role of ‘on path’ signals in children who have cortical visual impairment Also it will help our studies that aim to develop gene therapies for inherited retinal disease that may affect the ‘on path’.

Should we notice any unexpected vision difficulty that needs attention we will ask permission to tell your child’s GP for referral to an appropriate specialist.

## Who will have access to the case/research records?

All data and results will be kept confidential and will only be seen by the researchers involved in the study.

## Who do I speak to if problems arise?

If you have any concern or complaint about the way in which this research study has been, or is being conducted, please, as soon as possible discuss them with the researcher in the first instance. If the problems are not resolved, or you wish to comment in any other way, please contact the Patient Advice and Liaison Service (Pals) at GOSH:

By phone: 020 7829 7862 (direct line) By email: pals@gosh.nhs.uk

In person: The Pals office is located in the main hospital reception, on your right as you come through the entrance. It is open Monday to Friday from 10am to 5pm.

Great Ormond Street Hospital for Children NHS Foundation Trust

UCL INSTITUTE OF CHILD HEALTH

## Who has reviewed the study?

The Research Ethics Committee, NRES Committee London – South East has approved the study.

## Who do I contact if I want to know more about taking part in this study?

Mr Dennis Fritsch

Eye Department, Great Ormond Street Hospital for Children NHS Trust

Tel: 07842115138 Email: d.fritsch@ucl.ac.uk

## Appendix C

# Oculome NGS gene list

Genes associated with the Schubert-Bornschein types of CSNB are highlighted in **bold**.

ABCA4 ABCB6 ABCC6 ABHD12 ACBD5 ACTB ACTG1 ADAM9 ADAMTS10 ADAMTS18 ADAMTSL4 AGBL1 AGK AHI1 AIPL1 ALDH18A1 ALDH1A3 ALG3 ALMS1 AP3B1 ARL13B ARL2BP ARL6 ATF6 ATOH7 ATXN7 B3GALTL B9D1 B9D2 BBIP1 BBS1 BBS10 BBS12 BBS2 BBS4 BBS5 BBS7 BBS9 BCOR BEST1 BFSP1 BFSP2 BLOC1S3 BMP4 BMP7 C10orf2 C12ORF57 C12ORF65 C1QTNF5 C21orf2 C2orf71 C5ORF42 C8orf37 CA4 **CABP4 CACNA1F CACNA2D4** CAPN5 CBS CC2D2A CDH23 CDH3 CDHR1 CEP164 CEP250 CEP290 CEP41 CERKL CFH CHD7 CHM CHMP4B CHRDL1 CHST6 CIB2 CLDN19 CLN3 CLRN1 CNGA1 CNGA3 CNGB1 CNGB3 CNNM4 COG4 COG6 COL11A1 COL18A1 COL2A1 COL4A1 COL8A2 COL9A1 CRB1 CRIM1 CRX CRYAA CRYAA CRYAB CRYBA1 CRYBA4 CRYBB1 CRYBB2 CRYBB3 CRYGB CRYGC CRYGD CRYGS CSPP1 CTDP1 CYP1B1 CYP4V2 DCN DFNB31 DHDDS DHX38 DMD DPYD DTHD1 DTNBP1 EFEMP1 ELOVL4 EMC1 EPG5 EPHA2 ERCC1 ERCC5 ERCC6 EYA1 EYS FADD FAM111A FAM126A FAM161A FBN1 FBP1 FLVCR1 FNBP4 FOXC1 FOXC2 FOXE3 FOXL2 FRAS1 FREM1 FREM2 FSCN2 FTL FYCO1 FZD4 FZD5 GALE GALK1 GALT GCNT2 GDF3 GDF6 GFER GJA1 GJA3 GJA3 GJA8 GNAT1 GNAT2 **GNB3** GNPTG GPR125 GPR143 **GPR179** GPR98 GRIP1 GRK1 **GRM6** GSN GUCA1A GUCA1B GUCY2D HARS HCCS HESX1 HK1 HMCN1

HMGB3 HMX1 HPS1 HPS3 HPS4 HPS5 HPS6 HSF4 IDH3B IFT140 IFT172 IFT27 IGBP1 IKBKG IMPDH1 IMPG1 IMPG2 INPP5E INVS IQCB1 ITM2B JAG1 KAT2B KAT6B KCNJ13 KCNV2 KERA KIAA1549 KIF11 KIF7 KIZ KLHL7 KRT12 KRT3 LAMB2 LCA5 LCAT LCP1 LEPREL1 LIM2 LMX1B LRAT **LRIT3** LRP2 LRP5 LTBP2 LZTFL1 MAB21L2 MAF MAK MERTK MFN2 MFRP MIP MIR184 MIR204 MITF MKKS MKS1 MLL2 MTTP MVK MYO7A MYOC NAA10 NDP NEK2 NEUROD1 NHS NMNAT1 NOTCH2 NPHP1 NPHP3 NPHP4 NR2E3 NR2F1 NRL **NYX** OAT OCA2 OCRL ODZ3 OFD1 OPA1 OPA3 OPN1LW OPN1MW OPN1SW OPTN OTX2 PANK2 PAX2 PAX3 PAX6 PCDH15 PCYT1A PDE6A PDE6B PDE6C PDE6D PDE6G PDE6H PDZD7 PEX1 PEX2 PEX7 PGK1 PHOX2A PHYH PIGL PIKFYVE PITPNM3 PITX2 PITX3 PLA2G5 PLDN PLK4 PMM2 PNPLA6 POC1B POLG POLR1C POLR1D PORCN PQBP1 PRCD PRDM5 PROM1 PRPF3 PRPF31 PRPF4 PRPF6 PRPF8 PRPH2 PRSS56 PTCH1 PXDN RAB18 RAB28 RAB3GAP1 RAB3GAP2 RARB RASSF8 RAX RAX2 RB1 RBP3 RBP4 RD3 RDH11 RDH12 RDH5 RGR RGS9 RGS9BP RHO RIMS1 RLBP1 ROM1 RP1 RP1L1 RP2 RP9 RPE65 RPGR RPGRIP1 RPGRIP1L RS1 SAG SALL1 SALL2 SALL4 SCLT1 SDCCAG8 SEC23A SEMA3E SEMA4A SH3PXD2B SHH SIL1 SIPA1L3 SIX1 SIX3 SIX5 SIX6 SLC16A12 SLC24A1 SLC33A1 SLC38A8 SLC45A2 SLC4A11 SLC4A4 SLC7A14 SMOC1 SNRNP200 SOX2 SPATA7 SRD5A3 STRA6 TACSTD2 TBC1D20 TBC1D32 TBX22 TCOF1 TCTN1 TCTN2 TCTN3 TDRD7 TEAD1 TFAP2A TGFBI TIMM8A TIMP3 TMEM126A TMEM138 TMEM216 TMEM231 TMEM237 TMEM67 TMEM98 TMX3 TOPORS TREX1 TRIM32 **TRPM1** TSPAN12 TTC8 TTLL5 TTPA TUB TUBGCP4 TUBGCP6 TULP1 TWF1 TYR TYRP1 UBIAD1 UNC119 USH1C USH1G USH2A VAX1 VCAN VIM VPS13B VSX1 VSX2 WDR19 WDR36 WFS1 YAP1 ZEB1 ZEB2/ZFHX1B ZIC2 ZNF408 ZNF423 ZNF469 ZNF513

# Appendix D

# Influence of contrast condition on LumiTrack$^{Tm}$ motion threshold - omitting DMD patients

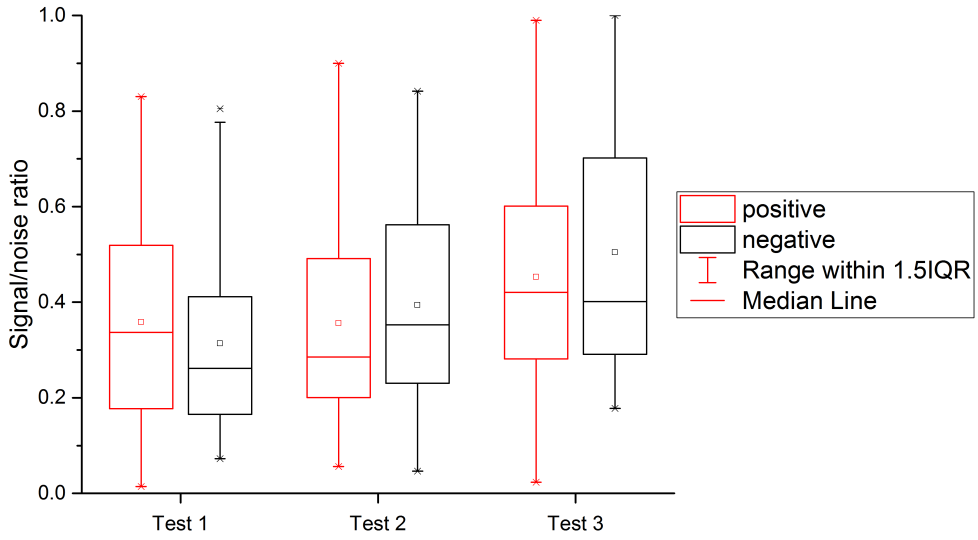


**Figure D.1:** The motion threshold values of all patients of the ON-pathway dysfunction cohort, except patients with DMD, for all three tests are shown. The values obtained from negative (black boxes) and positive (red boxes) contrast conditions are compared. Boxes give Max and Min (-), Mean (square), Median (line inside the boxes), 99% and 1% (x), as well as 75% and 25% (margins of the boxes) percentiles. Boxes give Max and Min (-), Mean (square), Median (line inside the boxes), 99% and 1% (x), as well as 75% and 25% (margins of the boxes) percentiles.

## Appendix E

# Comparing positive and negative contrast LumiTrack$^{Tm}$ motion threshold values - patients

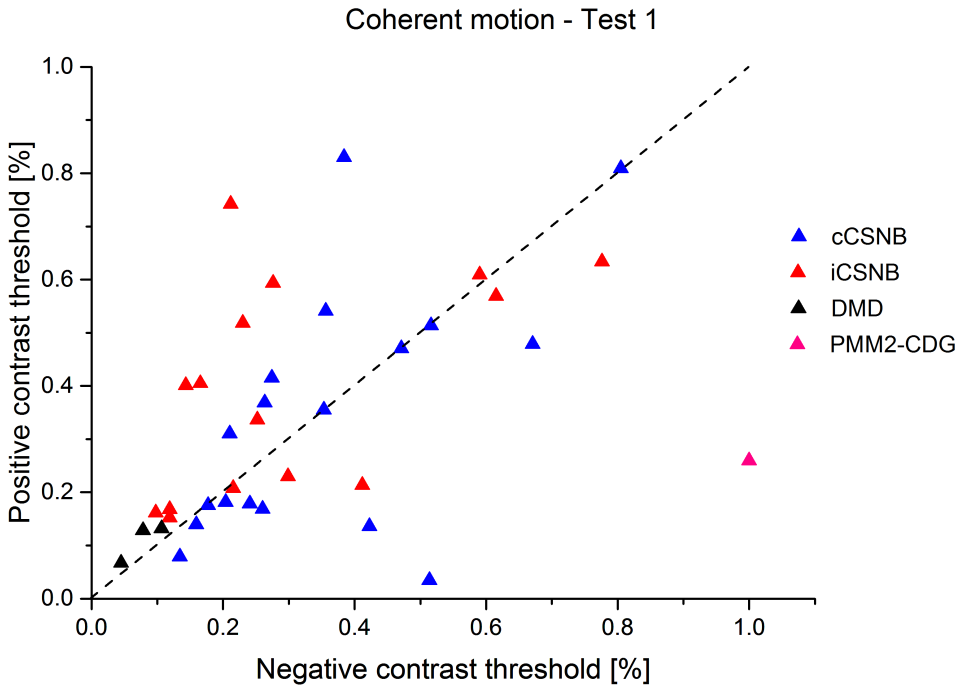


**Figure E.1**

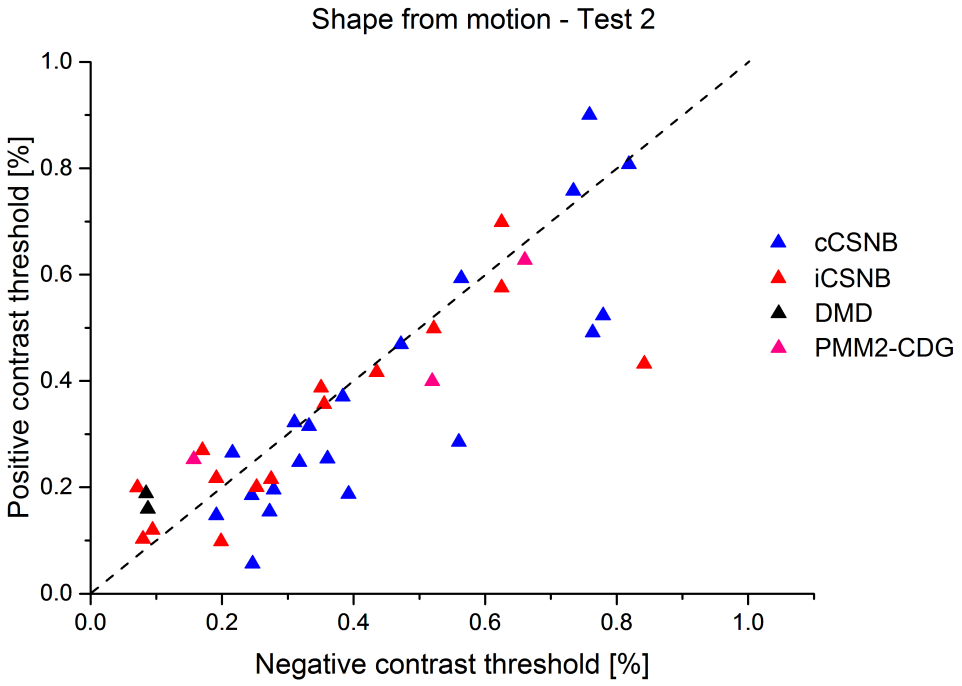


**Figure E.2**

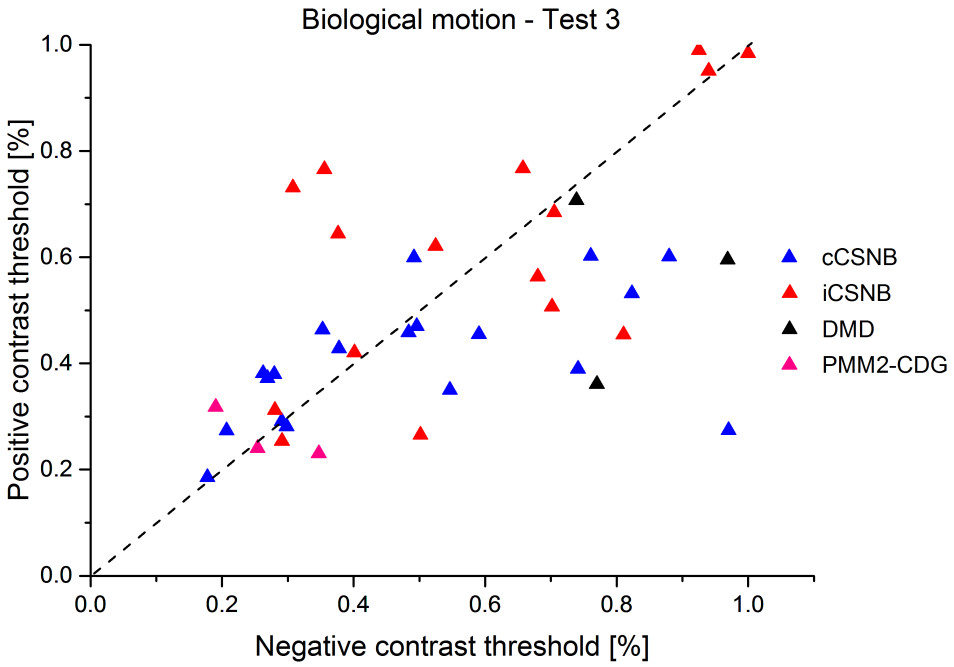


**Figure E.3**

**Appendix F**

# SureSelect Target Enrichment System Capture Process used for Oculome mutation screening

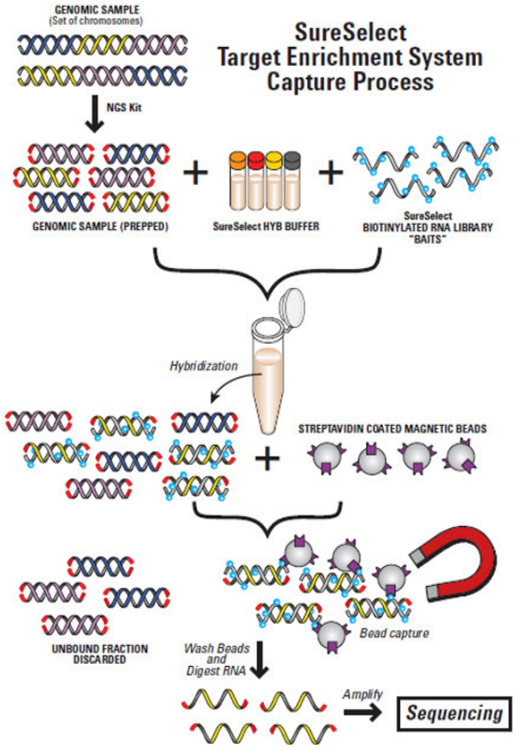


**Figure F.1:** An enzymatic shearing step simultaneously fragments DNA and ligates adapter-tags. Then samples are hybridized with 120-mer biotinylated cRNA library capture baits (436 genes, listed in Appendix C). Target regions are selected using magnetic streptavidin beads. Following this, a PCR amplifies and adds sample specific indices which are sequenced on MiSeq 2x150bp or HiSeq2500, using 2x100 bp reads. Taken from Agilent Technologies website: www.agilent.com

# Appendix G

# Primer list

| Primer name | sequence (5'to 3') |
|---|---|
| TRPM1 I1011NF | AGCATTGCATGGAGTAGGAA |
| TRPM1 I1011NR | GGAACTGATCATCTGCCTCA |
| GPR179 E1630QF | TCAACAGCAGGAGTCAGTTT |
| GPR179 E1630QR | TTTCCTCCACATCCAAAGGG |
| TRPM1 E1281KF | CCCAGTGAAAGGTGAAGACT |
| TRPM1 E1281KR | TGAAAACTTCCCTGCAGACT |
| TRPM1 L682PF | ACCTCTGACAGAAAGGGTTC |
| TRPM1 L682PR | TGAGAAGTACATTGGCCACC |
| GRM6 V243fsF | GGACCTCTTTGTTTTGGACG |
| GRM6 V243fsR | CAGGGAGAGTGTGTAAGGTG |
| GRM6 T177IF | CCTTCCATCTCCCATCTGTG |
| GRM6 T177IR | GCCCACACTATGTAGACTCC |
| GRM6 A738fs F | AGTGAATGAACAAGCAGCCA |
| GRM6 A738fs R | TGTCAGGGCTGGAATGGATT |
| GRM6 C522YF | TGGATGTGAGTGTGCAGAC |
| GRM6 C522YR | TGGCGTAGATGAGGAAGATG |
| GPR179 S329fsF | CCAGAGAAAGCCCCACATAA |
| GPR179 S329fsR | CCAGCCTTTTCCCTGATAGT |
| CAPN5 F32SF | CAGTCTATGGAGTCAGGCCG |
| CAPN5 F32SR | TACAGCCCATTCTCCAAGCT |
| CAPN5 D66GF | TCACCATGCTGATGATCACA |
| CAPN5 D66GR | TGAAAGTCTCATCTGCCACA |
| TRPM1 R941HF | CATGTCAGAACCAGGCAAAC |
| TRPM1 R941HR | ATACACAGTAGGCCCTCAAC |
| TRPM1 C954YF | CTGCCTGAGAAGAAGAGTGT |
| TRPM1 C954YR | AAATTGAAGGAAGCCATGCC |
| CACNA1F F | AGTGTTGCTCTGTCTGTTCA |
| CACNA1f R | GTAGACATTCTCCCCAGTGG |
| TRPM1 A1049TF | GAGTACAGTGGCTCGATCTC |
| TRPM1 A1049TR | ATTGGTATCTTGGGAGCGTT |
| CACNA1f Leu956Pro2 F | GTGAGATCTGAGGGCCTCTG |
| CACNA1f Leu956Pro2 R | CCACCCGGCAAACACTTATT |
| CACNA1f K875K F | GGGACAGGACAAGAGGCTAG |
| CACNA1f K875K R | AGGAGAAGAGCCCTAGGTGA |
| NYX Cys_Ala34del F | GTACAGGCAGGAGGGAGTTT |
| NYX Cys27_Ala34del F | GTTCCGGTCCAGGTCGATG |
| CAPN5Leu90Val F | CCCACAGGTTCTTCATCAGC |
| CAPN5Leu90Val R | CTGCCACAATCAGGTTCCG |

**Table G.1:** List of primers used for Sanger Sequencing

| Primer name | Oligo sequence (5'to 3') |
|---|---|
| LRIT3 Arg25Cys F | GATTTGAACCAAGGCCCTCC |
| LRIT3 Arg25Cys R | AGGGAAAGCAGCCAGAGAAT |
| GPR179Gly1991Glu F | ACAGACCCTTGCCATCTTGA |
| GPR179Gly1991Glu R | AGGTTCCTTCCCAGAACACA |
| GRM6Arg621Ter F | GAGGTGAGGCTGAAGGTGAT |
| GRM6Arg621Ter R | CTGTTGGCACTGCGAGGC |
| GPR179Pro1283Ser F | CCTTGGTGATGTCAGGGGTA |
| GPR179Pro1283Ser R | TCAAGCAATCAAAAGAAACCCC |
| GRM6Leu441Phe F | CCGGAACTTGTCTCATGTCT |
| GRM6Leu441Phe R | CGGGCACACTTTCTCTGGG |
| CACNA1f Arg454Gln F | AAGCTACAAGGTGGGATGGG |
| CACNA1f Arg454Gln R | GCCTCGATCTCAGTCCTTGA |
| NYX 2 F | CTGGAGCCTGCATTGTCTTG |
| NYX 2 R | TTGTCGTTGAGCAGCAGATG |
| NYXPat26 F | ACTCCCCACCACCCTGTC |
| NYXPat26 R | CAGATGCTCCAGGACGCC |
| CACNA1fPat4 F | CTGTGTTTGAGGCCCTTGTC |
| CACNA1fPat4 R | CCCCATGGTCCCTAGTTACC |
| NYXPat7 F | CCGCCTCTTCCTCTTCCG |
| NYXPat7 R | GAGAAACCAGGGCTGCCG |
| Cacna1fPat6 F | GGGGTTCAGAGCTAGGAGTG |
| Cacna1fPat6 R | CTATCACATGGCAAGGGTGG |
| Cacna1fPat14 F | CTCTTGAACCCTGGTGACCT |
| Cacna1fPat14 R | AGGTAGGAAGCAGCCACAAT |
| Cacna1fPat12 F | CTAGGGCTTGGTAGGGTGC |
| Cacna1fPat12 R | TCCCTAGTTACCTCCCCACA |
| TRPM1Pat26a F | TTTGTCCTGTCCATGTATCACA |
| TRPM1Pat26a R | GCAGACTGTTGACCTTCGAC |
| TRPM1Qdad R | ATTGCCTTTTCCACCTCTGC |
| TRPM1Qdad F | TGGAGTACAGTGGCTCGATC |
| Pat109 R | ACTGGGCTTCTCTGAGCAAT |
| Pat109 F | ATCTCCACTGGCCAGGTTG |
| Pat102 R | TTCCTATACATGGGTCCCGC |
| Pat102 F | GCTCTGATGAAATGAATGGGCT |
| Pat85 R | GGCAACAACAGAGAAGAAGCA |
| Pat85 F | ACTGCATTCATGTGACACGA |
| Pat46 R | GCCTCAGCCATTTTCTTTCTGA |
| Pat46 F | GGCGGGCTTATATGGTCATG |
| Pat90 R | CTAAGCCTTCCCTCAGCCAG |
| Pat90 F | AGGTTGAGGAAGGCAATGGA |
| Pat44 R | AGTTCGAGACCAACCTGACC |
| Pat44 F | GGACCCAAAGATGACAAGGC |
| Pat9 R | ACCCAGGGCAGTTCATACC |
| Pat9 F | CCGGTAATCCCAGCTACTCA |

**Table G.2:** List of primers used for Sanger Sequencing - continuation

| Primer name | Oligo sequence (5'to 3') |
|---|---|
| Pat101 R | GCGGAACAGGTTGTCGAAG |
| Pat101 F | ATCCTGCTGCCCGGACAG |
| Pat32 R | TTCTTGCAGCCCACCTCTC |
| Pat32 F | AGGGAGCTGGGTCTGAGA |
| Pat39 R | GAACCGTAATGTCTGACTTCACA |
| Pat39 F | TACATCCCTGACCCATCACC |
| Pat15 R | CCATAACGACCAGACCCTGT |
| Pat15 F | CCCACTCAAGTCAGCTCCTA |
| Pat3 R | TCCTGCAGCTGGAAGGTTG |
| Pat3 F | TTTAGGCCAGTGGAGAAGGG |
| Pat 16 and 29 R | CCATGGTACCAGGCATCTTTT |
| Pat 16 and 29 F | ATTAGGAAGCTCTTTGGGGAC |
| Pat8 R | GACCCCGATGTCCAGTGG |
| Pat8 F | GTCATGCTGTGTGTGGGATA |
| Pat111 R | CGGGATCTAAACTGCAGGGA |
| Pat111 F | CAGATGTGTGTCCAGACCCT |

**Table G.3:** List of primers used for Sanger Sequencing - continuation 2

# Bibliography


[1] H Kolb. The architecture of functional neural circuits in the vertebrate retina. The Proctor Lecture. *Invest Ophthalmol Vis Sci*, 35(5):2385–2404, 1994.

[2] Rita Rosenthal and Olaf Strauß. Ca2+-channels in the RPE. In *Photoreceptors and Calcium*, pages 225–235. Springer, 2002.

[3] Sönke Wimmers, Mike O Karl, and Olaf Strauss. Ion channels in the RPE. *Progress in retinal and eye research*, 26(3):263–301, 2007.

[4] E Zabala Aldunate. Role of microRNAs in cone photoreceptor development and during retinal degeneration. *PhD Thesis*, 2017.

[5] S Wang, C Sengel, M M Emerson, and C L Cepko. A gene regulatory network controls the binary fate decision of rod and bipolar cells in the vertebrate retina. *Developmental cell*, 30(5):513–527, 2014.

[6] S C Massey. Chapter 11 Cell types using glutamate as a neurotransmitter in the vertebrate retina. *Progress in Retinal Research*, 9(0):399–425, 1990.

[7] H Kolb. The neural organization of the human retina. *Principles and Practices of Clinical Electrophysiology of Vision*, pages 25–52, 1991.

[8] R A Shiells and G Falk. Glutamate receptors of rod bipolar cells are linked to a cyclic GMP cascade via a G-protein. *Proc Biol Sci*, 242(1304):91–94, 1990.

[9] S Nawy and C E Jahr. cGMP-gated conductance in retinal bipolar cells is suppressed by the photoreceptor transmitter. *Neuron*, 7(4):677–683, 1991.

[10] P de la Villa, T Kurahashi, and A Kaneko. L-glutamate-induced responses and cGMP-activated channels in three subtypes of retinal bipolar cells dissociated from the cat. *The Journal of neuroscience*, 15(5):3571–3582, 1995.

[11] John E Dowling. *The retina: an approachable part of the brain*. Harvard University Press, 1987.

[12] P V Sarthy and D M K Lam. Biochemical studies of isolated glial (muller) cells from the turtle retina. *The Journal of Cell Biology*, 78(3):675–684, sep 1978.

[13] Samer Hattar, H-W Liao, Motoharu Takao, David M Berson, and K-W Yau. Melanopsin-containing retinal ganglion cells: architecture, projections, and intrinsic photosensitivity. *Science*, 295(5557):1065–1070, 2002.

[14] P H Schiller and J G Malpeli. Functional specificity of lateral geniculate nucleus laminae of the rhesus monkey. *Journal of neurophysiology*, 41(3):788–797, 1978.

[15] Margaret Livingstone and David Hubel. Segregation of form, color, movement, and depth: anatomy, physiology, and perception. 1988.

[16] M J Hawken and A J Parker. Contrast sensitivity and orientation selectivity in lamina IV of the striate cortex of Old World monkeys. *Experimental Brain Research*, 54(2):367–372, 1984.

[17] R Shapley. Visual sensitivity and parallel retinocortical channels. *Annual review of psychology*, 41(1):635–658, 1990.

[18] David H Hubel and Margaret S Livingstone. Color and contrast sensitivity in the lateral geniculate body and primary visual cortex of the macaque monkey. *Journal of Neuroscience*, 10(7):2223–2237, 1990.

[19] Barry B Lee. Macaque ganglion cells and spatial vision. *Progress in brain research*, 95:33–43, 1993.

[20] J H Maunsell, Tara A Nealey, and Derryl D DePriest. Magnocellular and parvocellular contributions to responses in the middle temporal visual area (MT) of the macaque monkey. *Journal of Neuroscience*, 10(10):3323–3334, 1990.

[21] Natasha Barnard, Sheila Crewther, David Crewther, and Alexander Klistorner. Development Of Magnocellular Function In School Age Children: Poster# 33 (PO-321). *Optometry and Vision Science*, 72(12):207, 1995.

[22] David H Hubel, Janice Wensveen, and Bruce Wick. *Eye, brain, and vision*. Scientific American Library New York, 1995.

[23] Leo M Hurvich and Dorothea Jameson. *The perception of brightness and darkness*. 1966.

[24] M M Abd-El-Barr, M E Pennesi, S M Saszik, A J Barrow, J Lem, D E Bramblett, D L Paul, L J Frishman, and S M Wu. Genetic dissection of rod and cone pathways in the dark-adapted mouse retina. *J Neurophysiol*, 102(3):1945–1955, 2009.

[25] Stewart A Bloomfield and Ramon F Dacheux. Rod vision: pathways and processing in the mammalian retina. *Progress in retinal and eye research*, 20(3):351–384, 2001.

[26] EV Famiglietti and Helga Kolb. A bistratified amacrine cell and synaptic circuitry in the inner plexiform layer of the retina. *Brain research*, 84(2):293–300, 1975.

[27] Elio Raviola and Norton B Gilula. Gap junctions between photoreceptor cells in the vertebrate retina. *Proceedings of the National Academy of Sciences*, 70(6):1677–1681, 1973.

[28] Ed Soucy, Yanshu Wang, Sheila Nirenberg, Jeremy Nathans, and Markus Meister. A novel signaling pathway from rod photoreceptors to ganglion cells in mammalian retina. *Neuron*, 21(3):481–493, 1998.

[29] Shijun Weng, Wenzhi Sun, and Shigang He. Identification of ONOFF directionselective ganglion cells in the mouse retina. *J Physiol*, 562(3):915–923, 2005.

[30] Horace B Barlow and Richard M Hill. Selective Sensitivity to Direction of Movement in Ganglion Cells of the Rabbit Retina. *Science*, 139(3553):412, 1963.

[31] Andrew Stockman and Lindsay T Sharpe. Into the twilight zone: the complexities of mesopic vision and luminous efficiency. *Ophthalmic and physiological optics*, 26(3):225–239, 2006.

[32] Peter H Schiller, Julie H Sandell, and John H R Maunsell. Functions of the ON and OFF channels of the visual system. *Nature*, 322(6082):824–825, 1986.

[33] Shigetada Nakanishi. Second-order neurones and receptor mechanisms in visual- and olfactory-information processing. *Trends Neurosci*, 18(8):359–364, 1995.

[34] Stephen W Kuffler. Discharge patterns and functional organization of mammalian retina. *J Neurophysiol*, 16(1):37–68, 1953.

[35] Dennis Dacey, Orin S Packer, Lisa Diller, David Brainard, Beth Peterson, and Barry Lee. Center surround receptive field structure of cone bipolar cells in primate retina. *Vision Research*, 40(14):1801–1811, 2000.

[36] D H Hubel and T N Wiesel. Receptive fields of single neurones in the cat's striate cortex. *J Physiol*, 148(3):574–591, 1959.

[37] Shelley I Fried and Richard H Masland. Image processing: how the retina detects the direction of image motion. *Current Biology*, 17(2):R63–R66, 2007.

[38] Jonathan B Demb. Cellular mechanisms for direction selectivity in the retina. *Neuron*, 55(2):179–186, 2007.

[39] C W Oyster. The analysis of image motion by the rabbit retina. *The Journal of Physiology*, 199(3):613–635, 1968.

[40] W Rowland Taylor, Shigang He, William R Levick, and David I Vaney. Dendritic computation of direction selectivity by retinal ganglion cells. *Science*, 289(5488):2347–2350, 2000.

[41] Paul R Martin, Andrew J R White, Ann K Goodchild, Heath D Wilder, and Ann E Sefton. Evidence that Blueon Cells are Part of the Third Geniculocortical Pathway in Primates. *European Journal of Neuroscience*, 9(7):1536–1541, 1997.

[42] D H Hubel and T N Wiesel. Receptive fields of single neurones in the cat's striate cortex. *J Physiol*, 148(3):574–591, 1959.

[43] D H Hubel and T N Wiesel. Receptive fields, binocular interaction and functional architecture in the cat's visual cortex. *J Physiol*, 160(1):106–154.2, 1962.

[44] David H Hubel and Torsten N Wiesel. Receptive fields and functional architecture in two nonstriate visual areas (18 and 19) of the cat. *J Neurophysiol*, 28(2):229–289, 1965.

[45] B Dreher. Hypercomplex cells in the cat's striate cortex. *Invest Ophthalmol*, 11(5):355–356, 1972.

[46] Charles D Gilbert. Laminar differences in receptive field properties of cells in cat primary visual cortex. *J Physiol*, 268(2):391–421, 1977.

[47] Mortimer Mishkin and Leslie G Ungerleider. Contribution of striate inputs to the visuospatial functions of parieto-preoccipital cortex in monkeys. *Behavioural Brain Research*, 6(1):57–77, 1982.

[48] Melvyn A Goodale and A David Milner. Separate visual pathways for perception and action. *Trends Neurosci*, 15(1):20–25, 1992.

[49] Charles Cadieu, Minjoon Kouh, Anitha Pasupathy, Charles E Connor, Maximilian Riesenhuber, and Tomaso Poggio. A model of V4 shape selectivity and invariance. *Journal of neurophysiology*, 98(3):1733–1750, 2007.

[50] Leslie C Osborne, William Bialek, and Stephen G Lisberger. Time course of information about motion direction in visual area MT of macaque monkeys. *Journal of Neuroscience*, 24(13):3210–3222, 2004.

[51] Edward H F de Haan, Andy Young, and Freda Newcombe. Face recognition without awareness. *Cognitive Neuropsychology*, 4(4):385–415, 1987.

[52] James V Haxby, Barry Horwitz, Leslie G Ungerleider, Jose Ma Maisog, Pietro Pietrini, and Cheryl L Grady. The functional organization of human extrastriate cortex: a PET-rCBF study of selective attention to faces and locations. *Journal of Neuroscience*, 14(11):6336–6353, 1994.

[53] Guido Hesselmann and Rafael Malach. The link between fMRI-BOLD activation and perceptual awareness is stream-invariant in the human visual system. *Cerebral Cortex*, 21(12):2829–2837, 2011.

[54] Edward H F de Haan and Alan Cowey. On the usefulness of what'and where'pathways in vision. *Trends in cognitive sciences*, 15(10):460–466, 2011.

[55] Joel Norman. Two visual systems and two theories of perception: An attempt to reconcile the constructivist and ecological approaches. *Behavioral and brain sciences*, 25(1):73–96, 2002.

[56] H von Helmholtz. Beschreibung des Augenspiegels. In *Beschreibung Eines Augen-Spiegels*, pages 28–34. Springer, 1851.

[57] Yasir J Sepah, Abeer Akhtar, Mohammad Ali Sadiq, Yamama Hafeez, Humzah Nasir, Brian Perez, Narissa Mawji, Diana J Dean, Daniel Ferraz, and Quan Dong Nguyen. Fundus autofluorescence imaging: fundamentals and clinical relevance. *Saudi Journal of Ophthalmology*, 28(2):111–116, 2014.

[58] Karthikeyan Ganesan, Roshan Joy Martis, U Rajendra Acharya, Chua Kuang Chua, Lim Choo Min, E Y K Ng, and Augustinus Laude. Computer-aided diabetic retinopathy detection using trace transforms on digital fundus images. *Medical & biological engineering & computing*, 52(8):663–672, 2014.

[59] James G Fujimoto, Costas Pitris, Stephen A Boppart, and Mark E Brezinski. Optical coherence tomography: an emerging technology for biomedical imaging and optical biopsy. *Neoplasia*, 2(1-2):9–25, 2000.

[60] Rui Bernardes, Pedro Serranho, and Conceição Lobo. Digital ocular fundus imaging: a review. *Ophthalmologica*, 226(4):161–181, 2011.

[61] P J Saine. Fundus photography: What is a fundus camera. *Ophthalmic Photographers Society*, 2006.

[62] David Huang, Eric A Swanson, Charles P Lin, Joel S Schuman, William G Stinson, Warren Chang, Michael R Hee, Thomas Flotte, Kenton Gregory, and Carmen A Puliafito. Optical coherence tomography. *Science (New York, NY)*, 254(5035):1178, 1991.

[63] G Mizuo and B Nakamura. Das Wesen von Oguchischer Krankheit und eine Kenntnis iiber die Dunkeladaptation. *Acta Soc. ophthal. jap*, 18, 1914.

[64] Hugo F Mendes, Jacqueline van der Spuy, J Paul Chapple, and Michael E Cheetham. Mechanisms of cell death in rhodopsin retinitis pigmentosa: implications for therapy. *Trends in Molecular Medicine*, 11(4):177–185, 2005.

[65] Astrid Kafka-Lutzow, Tsuneo Tomita, and Takashi Yanagida. Origins of the erg waves. *Vision Research*, 21(11):1703–1707, 1981.

[66] C E Wright, D E Williams, N Drasdo, and G F A Harding. The influence of age on the electroretinogram and visual evoked potential. *Doc Ophthalmol*, 59(4):365–384, 1985.

[67] W W Dawson, G L Trick, and C A Litzkow. Improved electrode for electroretinography. *Invest Ophthalmol Vis Sci*, 18(9):988–991, 1979.

[68] Gösta Karpe. The basis of clinical electroretinography. *Acta Ophthalmol Suppl*, 24:1–118, 1945.

[69] Y Miyake, K Yagasaki, M Horiguchi, Y Kawase, and T Kanda. Congenital stationary night blindness with negative electroretinogram: A new classification. *Archives of ophthalmology*, 104(7):1013–1020, 1986.

[70] Lorrin A Riggs. Electroretinography in cases of night blindness. *American journal of ophthalmology*, 38(1):70–78, 1954.

[71] G Schubert and H Bornschein. Beitrag zur Analyse des menschlichen Elektroretinogramms. *Ophthalmologica*, 123(6):396–413, 1952.

[72] Lillemor Wachtmeister. Basic research and clinical aspects of the oscillatory potentials of the electroretinogram. *Doc Ophthalmol*, 66(3):187–194, 1987.

[73] Lillemor Wachtmeister. Oscillatory potentials in the retina: what do they reveal. *Progress in Retinal and Eye Research*, 17(4):485–521, 1998.

[74] Henny Heynen, Lillemor Wachtmeister, and Dirk van Norren. Origin of the oscillatory potentials in the primate retina. *Vision Research*, 25(10):1365–1373, 1985.

[75] Lillemor Wachtmeister and John E Dowling. The oscillatory potentials of the mudpuppy retina. *Invest Ophthalmol Vis Sci*, 17(12):1176–1188, 1978.

[76] Mathieu Gauvin, Allison L Dorfman, Nataly Trang, Mercedes Gauthier, John M Little, Jean-Marc Lina, and Pierre Lachapelle. Assessing the Contribution of the Oscillatory Potentials to the Genesis of the Photopic ERG with the Discrete Wavelet Transform. *BioMed research international*, 2016, 2016.

[77] John R Heckenlively, Deidre A Martin, and Arthur L Rosenbaum. Loss of electroretinographic oscillatory potentials, optic atrophy, and dysplasia in congenital stationary night blindness. *American Journal of Ophthalmology*, 96(4):526–534, 1983.

[78] Pierre Lachapelle, John M Little, and Robert C Polomeno. The photopic electroretinogram in congenital stationary night blindness with myopia. *Invest Ophthalmol Vis Sci*, 24(4):442–450, 1983.

[79] F Tremblay, I De Becker, C Cheung, and G R LaRoche. Visual evoked potentials with crossed asymmetry in incomplete congenital stationary night blindness. *Invest Ophthalmol Vis Sci*, 37(9):1783–1792, 1996.

[80] L Wachtmeister. Further studies of the chemical sensitivity of the oscillatory potentials of the electroretinogram (ERG). *Acta Ophthalmologica*, 58(5):712–725, 1980.

[81] M Kojima and E Zrenner. Off-components in response to brief light flashes in the oscillatory potential of the human electroretinogram. *Albrecht von Graefes Archiv für klinische und experimentelle Ophthalmologie*, 206(2):107–120, 1978.

[82] Pierre Guité and Pierre Lachapelle. The effect of 2-amino-4-phosphonobutyric acid on the oscillatory potentials of the electroretinogram. *Doc Ophthalmol*, 75(2):125–133, 1990.

[83] Daphne L McCulloch, Michael F Marmor, Mitchell G Brigell, Ruth Hamilton, Graham E Holder, Radouil Tzekov, and Michael Bach. ISCEV Standard for full-field clinical electroretinography (2015 update). *Doc Ophthalmol*, 130(1):1–12, 2015.

[84] Th Berninger and R P Schuurmans. Spatial tuning of the pattern ERG across temporal frequency. *Doc Ophthalmol*, 61(1):17–25, 1985.

[85] R P Schuurmans and T Berninger. Luminance and contrast responses recorded in man and cat. *Doc Ophthalmol*, 59(2):187–197, 1985.

[86] A Groneberg and C Teping. Topodiagnostik von Sehstörungen durch Ableitung retinaler und kortikaler Antworten auf Umkehr-Kontrastmuster. In

*Plastische Chirurgie der Lider und Chirurgie der Tränenwege*, pages 409–415. Springer, 1980.

[87] A Fiorentini, L Maffei, M Pirchio, D Spinelli, and V Porciatti. The ERG in response to alternating gratings in patients with diseases of the peripheral visual pathway. *Invest Ophthalmol Vis Sci*, 21(3):490–493, 1981.

[88] L Maffei and A Fiorentini. Electroretinographic responses to alternating gratings in the cat. *Experimental Brain Research*, 48(3):327–334, 1982.

[89] L Maffei, A Fiorentini, S Bisti, and H Holländer. Pattern ERG in the monkey after section of the optic nerve. *Experimental Brain Research*, 59(2):423–425, 1985.

[90] G E Holder. Significance of abnormal pattern electroretinography in anterior visual pathway dysfunction. *British Journal of Ophthalmology*, 71(3):166–171, 1987.

[91] T A Berninger and G B Arden. The pattern electroretinogram. *Eye*, 2:S257–S283, 1988.

[92] X Luo and L J Frishman. Retinal pathway origins of the pattern electroretinogram (PERG). *Invest Ophthalmol Vis Sci*, 52(12):8571–8584, 2011.

[93] Anthony G Robson, Ahmed El-Amir, Claire Bailey, Catherine A Egan, Frederick W Fitzke, Andrew R Webster, Alan C Bird, and Graham E Holder. Pattern ERG correlates of abnormal fundus autofluorescence in patients with retinitis pigmentosa and normal visual acuity. *Investigative ophthalmology & visual science*, 44(8):3544–3550, 2003.

[94] G E Holder. Pattern electroretinography (PERG) and an integrated approach to visual pathway diagnosis. *Prog Retin Eye Res*, 20(4):531–561, 2001.

[95] Francesco Di Russo, Wolfgang A Teder-Sälejärvi, and Steven A Hillyard. Steady-state VEP and attentional visual processing. *The cognitive electro-*

*physiology of mind and brain (Zani A, Proverbio AM, eds)*, pages 259–274, 2002.

[96] C E Schroeder, C E Tenke, and S J Givre. Subcortical contributions to the surface-recorded flash-VEP in the awake macaque. *Electroencephalography and Clinical Neurophysiology/Evoked Potentials Section*, 84(3):219–231, 1992.

[97] Béla Török, Manuel Meyer, and Hannes Wildberger. The influence of pattern size on amplitude, latency and wave form of retinal and cortical potentials elicited by checkerboard pattern reversal and stimulus onset-offset. *Electroencephalography and Clinical Neurophysiology/Evoked Potentials Section*, 84(1):13–19, 1992.

[98] Shozo Tobimatsu, Shizuka Kurita-Tashima, Miyuki Nakayama-Hiromatsu, Kohei Akazawa, and Motohiro Kato. Age-related changes in pattern visual evoked potentials: differential effects of luminance, contrast and check size. *Electroencephalography and Clinical Neurophysiology/Evoked Potentials Section*, 88(1):12–19, 1993.

[99] E Lenassi, K Likar, B Stirn-Kranjc, and J Brecelj. VEP maturation and visual acuity in infants and preschool children. *Doc Ophthalmol*, 117(2):111–120, 2008.

[100] D L McCulloch and B Skarf. Development of the human visual system: monocular and binocular pattern VEP latency. *Invest Ophthalmol Vis Sci*, 32(8):2372–2381, 1991.

[101] D A Thompson, D M Fritsch, and S E Hardy. The changing shape of the ISCEV standard pattern onset VEP. *Doc Ophthalmol*, 2017.

[102] S Rinalduzzi, A Brusa, and S Jones. Variation of visual evoked potential delay to stimulation of central, nasal, and temporal regions of the macula in optic neuritis. *Journal of Neurology, Neurosurgery, and Psychiatry*, 70(1):28–35, 2001.

[103] A M Halliday, W I McDonald, and Joan Mushin. Delayed Visual Evoked Response In Optic Neuritis. *The Lancet*, 299(7758):982–985, 1972.

[104] Maurice Wooldridge. Seeing Stars. *BMJ*, 310(6975):297, 1995.

[105] George M Bohigian. An Ancient Eye TestUsing the Stars. *Survey of Ophthalmology*, 53(5):536–539, 2008.

[106] August Colenbrander. The historical evolution of visual acuity measurement. *Visual impairment research*, 10(2-3):57–66, 2008.

[107] Peter K Kaiser. Prospective evaluation of visual acuity assessment: a comparison of snellen versus ETDRS charts in clinical practice (An AOS Thesis). *Transactions of the American Ophthalmological Society*, 107:311, 2009.

[108] Early Treatment Diabetic Retinopathy Study Research Group. Photocoagulation for diabetic macular edema: Early Treatment Diabetic Retinopathy Study report number 1. *Arch ophthalmol*, 103:1796–1806, 1985.

[109] S Kalpana, J Karthick, and S Jayarajini. Comparison of static visual acuity between Snellen and Early treatment diabetic retinopathy study charts. *International Journal of Educational Research and Development*, 12(3):82–88, 2013.

[110] Ian L Bailey and Jan E Lovie. New Design Principles for Visual Acuity Letter Charts*. *Optometry and Vision Science*, 53(11):740–745, 1976.

[111] Ian L Bailey and Jan E Lovie-Kitchin. Visual acuity testing. From the laboratory to the clinic. *Vision Research*, 90:2–9, 2013.

[112] R A Gibson and H F Sanderson. Observer variation in ophthalmology. *British Journal of Ophthalmology*, 64(6):457–460, 1980.

[113] Davida Y Teller. The development of visual acuity in human and monkey infants. *Trends in Neurosciences*, 4:21–24, 1981.

[114] Jane Gwiazda, Sarah Brill, Indra Mohindra, and Richard Held. Preferential looking acuity in infants from two to fifty-eight weeks of age. *Optometry and Vision Science*, 57(7):428–432, 1980.

[115] D L Mayer, A S Beiser, A F Warner, E M Pratt, K N Raye, and J M Lang. Monocular acuity norms for the Teller Acuity Cards between ages one month and four years. *Investigative ophthalmology & visual science*, 36(3):671–685, 1995.

[116] Y Pan, K Tarczy-Hornoch, S A Cotter, G Wen, M S Borchert, S P Azen, and R Varma. Visual acuity norms in pre-school children: the Multi-Ethnic Pediatric Eye Disease Study. *Optom Vis Sci*, 86(6):607–612, 2009.

[117] G B Arden and J J Jacobson. A simple grating test for contrast sensitivity: preliminary results indicate value in screening for glaucoma. *Invest Ophthalmol Vis Sci*, 17(1):23–32, 1978.

[118] Chris A Johnson and Robert P Scobey. Foveal and peripheral displacement thresholds as a function of stimulus luminance, line length and duration of movement. *Vision Research*, 20(8):709–715, 1980.

[119] Michael I Posner. Orienting of attention. *Quarterly journal of experimental psychology*, 32(1):3–25, 1980.

[120] Chris A Johnson, Michael Wall, and H Stanley Thompson. A history of perimetry and visual field testing. *Optometry & Vision Science*, 88(1):E8–E15, 2011.

[121] William M Hart and Bernard Becker. The onset and evolution of glaucomatous visual field defects. *Ophthalmology*, 89(3):268–279, 1982.

[122] Elliot B Werner and Stephen M Drance. Early visual field disturbances in glaucoma. *Archives of Ophthalmology*, 95(7):1173–1175, 1977.

[123] Jugnoo S Rahi and Noriko Cable. Severe visual impairment and blindness in children in the UK. *The Lancet*, 362(9393):1359–1365, 2003.

[124] Cari A Malcolm, Ruth Hamilton, Daphne L McCulloch, Colette Montgomery, and Lawrence T Weaver. Scotopic electroretinogram in term infants born of mothers supplemented with docosahexaenoic acid during pregnancy. *Invest Ophthalmol Vis Sci*, 44(8):3685–3691, 2003.

[125] Reut Parness-Yossifon and Marilyn Baird Mets. The electroretinogram in children. *Current opinion in ophthalmology*, 19(5):398–402, 2008.

[126] Piers Cornelissen, Alex Richardson, Alexandra Mason, Sue Fowler, and John Stein. Contrast sensitivity and coherent motion detection measured at photopic luminance levels in dyslexics and controls. *Vision Research*, 35(10):1483–1494, 1995.

[127] Dave Ellemberg, Terri L Lewis, Daphne Maurer, Sonia Brar, and Henry P Brent. Better perception of global motion after monocular than after binocular deprivation. *Vision Research*, 42(2):169–179, 2002.

[128] Elizabeth Milne, John Swettenham, and Ruth Campbell. Motion perception and autistic spectrum disorder: a review. *Current Psychology of Cognition*, 23(1/2):3, 2005.

[129] Robert K Koenekoop, Irma Lopez, Anneke I Den Hollander, Rando Allikmets, and Frans PM Cremers. Genetic testing for retinal dystrophies and dysfunctions: benefits, dilemmas and solutions. *Clinical & experimental ophthalmology*, 35(5):473–485, 2007.

[130] Frederick Sanger, Steven Nicklen, and Alan R Coulson. Dna sequencing with chain-terminating inhibitors. *Proceedings of the national academy of sciences*, 74(12):5463–5467, 1977.

[131] International Human Genome Sequencing Consortium et al. Finishing the euchromatic sequence of the human genome. *Nature*, 431(7011):931–945, 2004.

[132] Elaine R Mardis. The impact of next-generation sequencing technology on genetics. *Trends in genetics*, 24(3):133–141, 2008.

[133] Michael L Metzker. Sequencing technologies-the next generation. *Nature reviews genetics*, 11(1), 2010.

[134] Erwin L Van Dijk, Hélène Auger, Yan Jaszczyszyn, and Claude Thermes. Ten years of next-generation sequencing technology. *Trends in genetics*, 30(9):418–426, 2014.

[135] Sarah B Ng, Emily H Turner, Peggy D Robertson, Steven D Flygare, Abigail W Bigham, Choli Lee, Tristan Shaffer, Michelle Wong, Arindam Bhattacharjee, Evan E Eichler, et al. Targeted capture and massively parallel sequencing of 12 human exomes. *Nature*, 461(7261):272–276, 2009.

[136] J Craig Venter, Mark D Adams, Eugene W Myers, Peter W Li, Richard J Mural, Granger G Sutton, Hamilton O Smith, Mark Yandell, Cheryl A Evans, Robert A Holt, et al. The sequence of the human genome. *science*, 291(5507):1304–1351, 2001.

[137] Douglas F Easton, Paul DP Pharoah, Antonis C Antoniou, Marc Tischkowitz, Sean V Tavtigian, Katherine L Nathanson, Peter Devilee, Alfons Meindl, Fergus J Couch, Melissa Southey, et al. Gene-panel sequencing and the prediction of breast-cancer risk. *New England Journal of Medicine*, 372(23):2243–2257, 2015.

[138] Soo Hyun Nam, Young Bin Hong, Young Se Hyun, Da Eun Nam, Geon Kwak, Sun Hee Hwang, Byung-Ok Choi, and Ki Wha Chung. Identification of genetic causes of inherited peripheral neuropathies by targeted gene panel sequencing. *Molecules and cells*, 39(5):382, 2016.

[139] Arthur AB Bergen, Jacoline B ten Brink, Frans Riemslag, Ellen JM Schuurman, and Nel Tijmes. Localization of a novel x-linked congenital stationary night blindness locus: close linkage to the rp3 type retinitis pigmentosa gene region. *Human molecular genetics*, 4(5):931–935, 1995.

[140] Wylie Burke. Genetic testing. *New England Journal of Medicine*, 347(23):1867–1875, 2002.

[141] Jean Bennett, Teruyo Tanabe, Dexue Sun, Yong Zeng, Hlld Kjeldbye, Peter Gouras, and Albert M Maguire. Photoreceptor cell rescue in retinal degeneration (rd) mice by in vivo gene therapy. *Nature medicine*, 2(6):649–654, 1996.

[142] Gregory M Acland, Gustavo D Aguirre, Jharna Ray, Qi Zhang, Tomas S Aleman, Artur V Cideciyan, Susan E Pearce-Kelling, Vibha Anand, Yong Zeng, and Albert M Maguire. Gene therapy restores vision in a canine model of childhood blindness. *Nature genetics*, 28(1):92, 2001.

[143] Robert E MacLaren, Markus Groppe, Alun R Barnard, Charles L Cottriall, Tanya Tolmachova, Len Seymour, K Reed Clark, Matthew J During, Frans P M Cremers, and Graeme C M Black. Retinal gene therapy in patients with choroideremia: initial findings from a phase 1/2 clinical trial. *The Lancet*, 383(9923):1129–1137, 2014.

[144] Samuel G Jacobson, Artur V Cideciyan, Alejandro J Roman, Alexander Sumaroka, Sharon B Schwartz, Elise Heon, and William W Hauswirth. Improvement and decline in vision with gene therapy in childhood blindness. *New England Journal of Medicine*, 372(20):1920–1926, 2015.

[145] James W B Bainbridge, Alexander J Smith, Susie S Barker, Scott Robbie, Robert Henderson, Kamaljit Balaggan, Ananth Viswanathan, Graham E Holder, Andrew Stockman, and Nick Tyler. Effect of gene therapy on visual function in Leber's congenital amaurosis. *New England Journal of Medicine*, 358(21):2231–2239, 2008.

[146] Centers for Disease Control and Prevention. International classification of diseases. *Ninth Revision, Clinical Modification (ICD-9-CM) Internet address: http://www. cdc. gov/nchs/about/otheract/icd9/abticd9. htm.(Accessed 2004.)*, 2010.

[147] R Hewett and S Keil. Investigation of data relating to blind and partially sighted people in the Quarterly Labour Force Survey: October 2009September 2012. *Visual Impairment Centre for Teaching and Research (VICTAR), University of Birmingham. University of Birmingham, UK*, 2013.

[148] E Sakkalou, M O'reilly, H Sakki, M De Haan, A Salt, and N Dale. Investigation of infant development and mother-infant interactions in infants with visual impairment. *Developmental Medicine & Child Neurology*, 55:16, 2013.

[149] Dean Wyatte, David J Jilk, and Randall C O'Reilly. Early recurrent feedback facilitates visual object recognition under challenging conditions. *Frontiers in psychology*, 5, 2014.

[150] R E MacLaren, R A Pearson, A MacNeil, R H Douglas, T E Salt, M Akimoto, A Swaroop, J C Sowden, and R R Ali. Retinal repair by transplantation of photoreceptor precursors. *Nature*, 444(7116):203, 2006.

[151] Anai Gonzalez-Cordero, Emma L West, Rachael A Pearson, Yanai Duran, Livia S Carvalho, Colin J Chu, Arifa Naeem, Samuel JI Blackford, Anastasios Georgiadis, Jorn Lakowski, et al. Photoreceptor precursors derived from three-dimensional embryonic stem cell cultures integrate and mature within adult degenerate retina. *Nature biotechnology*, 31(8):741–747, 2013.

[152] Pierre Lachapelle, Sophie Rousseau, Michelle McKerral, Julie Benoit, R C Polomeno, R K Koenekoop, and John M Little. Evidence supportive of a functional discrimination between photopic oscillatory potentials as revealed with cone and rod mediated retinopathies. *Doc Ophthalmol*, 95(1):35–54, 1998.

[153] Michael J Berry, David K Warland, and Markus Meister. The structure and precision of retinal spiketrains. *Proceedings of the National Academy of Sciences*, 94(10):5411–5416, 1997.

[154] Jonathan D Victor and Keith P Purpura. Nature and precision of temporal

coding in visual cortex: a metric-space analysis. *J Neurophysiol*, 76(2):1310–1326, 1996.

[155] Markus Meister, Leon Lagnado, and Denis A Baylor. Concerted Signaling by Retinal Ganglion Cells. *Science*, 270(5239):1207–1210, 1995.

[156] Lawrence H Pinto, Martha H Vitaterna, Kazuhiro Shimomura, Sandra M Siepka, Victoria Balannik, Erin L Mcdearmon, Chiaki Omura, Stephen Lumayag, Brandon M Invergo, Brett Glawe, Donald R Cantrell, Samsoon Inayat, Marissa A Olvera, Kirstan A Vessey, Maureen A Mccall, Dennis Maddox, Catherine W Morgans, Brandon Young, Mathew T Pletcher, Robert F Mullins, John B Troy, and Joseph S Takahashi. Generation, identification and functional characterization of the nob4 mutation of Grm6 in the mouse. *Visual Neuroscience*, 24(01):111–123, 2007.

[157] Dennis M Maddox, Kirstan A Vessey, Gary L Yarbrough, Brandon M Invergo, Donald R Cantrell, Samsoon Inayat, Victoria Balannik, Wanda L Hicks, Norman L Hawes, Shannon Byers, Richard S Smith, Ron Hurd, Douglas Howell, Ronald G Gregg, Bo Chang, Jürgen K Naggert, John B Troy, Lawrence H Pinto, Patsy M Nishina, and Maureen A McCall. Allelic variance between GRM6 mutants, Grm6nob3 and Grm6nob4 results in differences in retinal ganglion cell visual responses. *J Physiol*, 586(18):4409–4424, 2008.

[158] Hiroki Sugihara, Tetsu Inoue, Shigetada Nakanishi, and Yutaka Fukuda. A late ON response remains in visual response of the mGluR6-deficient mouse. *Neuroscience Letters*, 233(23):137–140, 1997.

[159] Y Tao, T Chen, B Liu, J H Xue, L Zhang, F Xia, J J Pang, and Z M Zhang. Visual signal pathway reorganization in the Cacna1f mutant rat model. *Invest Ophthalmol Vis Sci*, 54(3):1988–1997, 2013.

[160] Isabelle Audo, Anthony G Robson, Graham E Holder, and Anthony T Moore.

The Negative ERG: Clinical Phenotypes and Disease Mechanisms of Inner Retinal Dysfunction. *Survey of Ophthalmology*, 53(1):16–40, 2008.

[161] P A Sieving. Photopic ON- and OFF-pathway abnormalities in retinal dystrophies. *Transactions of the American Ophthalmological Society*, 91:701–773, 1993.

[162] AHC Koh, CR Hogg, and GE Holder. The incidence of negative erg in clinical practice. *Doc Ophthalmol*, 102(1):19–30, 2001.

[163] Valeria Ricotti, Herbert Jagle, Maria Theodorou, Anthony T Moore, Francesco Muntoni, and Dorothy A Thompson. Ocular and neurodevelopmental features of Duchenne muscular dystrophy: a signature of dystrophin function in the central nervous system. *Eur J Hum Genet*, 2015.

[164] M M Bijveld, M M van Genderen, F P Hoeben, A A Katzin, R M van Nispen, F C Riemslag, and A M Kappers. Assessment of night vision problems in patients with congenital stationary night blindness. *PLoS ONE*, 8(5):e62927, 2013.

[165] Claire S Barnes, Kenneth R Alexander, and Gerald A Fishman. A distinctive form of congenital stationary night blindness with cone ON-pathway dysfunction. *Ophthalmology*, 109(3):575–583, 2002.

[166] Christina Zeitz, Anthony G Robson, and Isabelle Audo. Congenital stationary night blindness: An analysis and update of genotypephenotype correlations and pathogenic mechanisms. *Progress in Retinal and Eye Research*, 45:58–110, 2015.

[167] Chieko Koike, Takehisa Obara, Yoshitsugu Uriu, Tomohiro Numata, Rikako Sanuki, Kentarou Miyata, Toshiyuki Koyasu, Shinji Ueno, Kazuo Funabiki, Akiko Tani, Hiroshi Ueda, Mineo Kondo, Yasuo Mori, Masao Tachibana, and Takahisa Furukawa. TRPM1 is a component of the retinal ON bipolar cell transduction channel in the mGluR6 cascade. *Proceedings of the National Academy of Sciences*, 107(1):332–337, 2010.

[168] Catherine W Morgans, Ronald Lane Brown, and Robert M Duvoisin. TRPM1: The endpoint of the mGluR6 signal transduction cascade in retinal ON-bipolar cells. *Bioessays*, 32(7):609–614, 2010.

[169] Y Nakajima, H Iwakabe, C Akazawa, H Nawa, R Shigemoto, N Mizuno, and S Nakanishi. Molecular characterization of a novel retinal metabotropic glutamate receptor mGluR6 with a high agonist selectivity for L-2-amino-4-phosphonobutyrate. *Journal of Biological Chemistry*, 268(16):11868–11873, 1993.

[170] T P Dryja, T L McGee, E L Berson, G A Fishman, M A Sandberg, K R Alexander, D J Derlacki, and A S Rajagopalan. Night blindness and abnormal cone electroretinogram ON responses in patients with mutations in the GRM6 gene encoding mGluR6. *Proc Natl Acad Sci U S A*, 102(13):4884–4889, 2005.

[171] Rebecca R Bellone, Samantha A Brooks, Lynne Sandmeyer, Barbara A Murphy, George Forsyth, Sheila Archer, Ernest Bailey, and Bruce Grahn. Differential Gene Expression of TRPM1, the Potential Cause of Congenital Stationary Night Blindness and Coat Spotting Patterns (LP) in the Appaloosa Horse (Equus caballus). *Genetics*, 179(4):1861–1870, 2008.

[172] I Audo, S Kohl, B P Leroy, F L Munier, X Guillonneau, S Mohand-Said, K Bujakowska, E F Nandrot, B Lorenz, M Preising, U Kellner, A B Renner, A Bernd, A Antonio, V Moskova-Doumanova, M E Lancelot, C M Poloschek, I Drumare, S Defoort-Dhellemmes, B Wissinger, T Leveillard, C P Hamel, D F Schorderet, E De Baere, W Berger, S G Jacobson, E Zrenner, J A Sahel, S S Bhattacharya, and C Zeitz. TRPM1 is mutated in patients with autosomal-recessive complete congenital stationary night blindness. *Am J Hum Genet*, 85(5):720–729, 2009.

[173] M M van Genderen, M M Bijveld, Y B Claassen, R J Florijn, J N Pearring, F M Meire, M A McCall, F C Riemslag, R G Gregg, A A Bergen, and

M Kamermans. Mutations in TRPM1 are a common cause of complete congenital stationary night blindness. *Am J Hum Genet*, 85(5):730–736, 2009.

[174] Makoto Nakamura, Rikako Sanuki, Tetsuhiro R Yasuma, Akishi Onishi, Koji M Nishiguchi, Chieko Koike, Mikiko Kadowaki, Mineo Kondo, Yozo Miyake, and Takahisa Furukawa. TRPM1 mutations are associated with the complete form of congenital stationary night blindness. *Molecular vision*, 16:425, 2010.

[175] J Klooster, J Blokker, J B Ten Brink, U Unmehopa, K Fluiter, A A Bergen, and M Kamermans. Ultrastructural localization and expression of TRPM1 in the human retina. *Invest Ophthalmol Vis Sci*, 52(11):8356–8362, 2011.

[176] A Dhingra, M E Fina, A Neinstein, D J Ramsey, Y Xu, G A Fishman, K R Alexander, H Qian, N S Peachey, R G Gregg, and N Vardi. Autoantibodies in melanoma-associated retinopathy target TRPM1 cation channels of retinal ON bipolar cells. *J Neurosci*, 31(11):3962–3967, 2011.

[177] Cesare Orlandi, Ekaterina Posokhova, Ikuo Masuho, Thomas A Ray, Nazarul Hasan, Ronald G Gregg, and Kirill A Martemyanov. GPR158/179 regulate G protein signaling by controlling localization and activity of the RGS7 complexes. *The Journal of Cell Biology*, 197(6):711–719, 2012.

[178] E Orhan, L Prezeau, S El Shamieh, K M Bujakowska, C Michiels, Y Zagar, C Vol, S S Bhattacharya, J A Sahel, F Sennlaub, I Audo, and C Zeitz. Further insights into GPR179: expression, localization, and associated pathogenic mechanisms leading to complete congenital stationary night blindness. *Invest Ophthalmol Vis Sci*, 54(13):8041–8050, 2013.

[179] Yan Cao, Johan Pahlberg, Ignacio Sarria, Naomi Kamasawa, Alapakkam P Sampath, and Kirill A Martemyanov. Regulators of G protein signaling RGS7 and RGS11 determine the onset of the light response in ON bipolar neurons. *Proceedings of the National Academy of Sciences*, 109(20):7905–7910, 2012.

[180] Christina Zeitz, Harry Scherthan, Susanne Freier, Silke Feil, Vanessa Suckow, Susann Schweiger, and Wolfgang Berger. NYX (Nyctalopin on Chromosome X), the Gene Mutated in Congenital Stationary Night Blindness, Encodes a Cell Surface Protein. *Invest Ophthalmol Vis Sci*, 44(10):4184–4191, 2003.

[181] Yan Cao, Ekaterina Posokhova, and Kirill A Martemyanov. TRPM1 Forms Complexes with Nyctalopin In Vivo and Accumulates in Postsynaptic Compartment of ON-Bipolar Neurons in mGluR6-Dependent Manner. *The Journal of neuroscience*, 31(32):11521–11526, 2011.

[182] N Torben Bech-Hansen, Margaret J Naylor, Tracy A Maybaum, Rebecca L Sparkes, Ben Koop, David G Birch, Arthur A B Bergen, Clemens F M Prinsen, Robert C Polomeno, and Andreas Gal. Mutations in NYX, encoding the leucine-rich proteoglycan nyctalopin, cause X-linked complete congenital stationary night blindness. *Nature genetics*, 26(3):319–323, 2000.

[183] Christina Zeitz, SamuelG Jacobson, ChristianP Hamel, Kinga Bujakowska, Marion Neuillé, Elise Orhan, Xavier Zanlonghi, Marie-Elise Lancelot, Christelle Michiels, SharonB Schwartz, Béatrice Bocquet, Aline Antonio, Claire Audier, Mélanie Letexier, Jean-Paul Saraiva, TienD Luu, Florian Sennlaub, Hoan Nguyen, Olivier Poch, Hélène Dollfus, Odile Lecompte, Susanne Kohl, José-Alain Sahel, ShomiS Bhattacharya, and Isabelle Audo. Whole-Exome Sequencing Identifies LRIT3 Mutations as a Cause of Autosomal-Recessive Complete Congenital Stationary Night Blindness. *The American Journal of Human Genetics*, 92(1):67–75, 2013.

[184] Christina Zeitz, SamuelG Jacobson, ChristianP Hamel, Kinga Bujakowska, Marion Neuillé, Elise Orhan, Xavier Zanlonghi, Marie-Elise Lancelot, Christelle Michiels, SharonB Schwartz, Béatrice Bocquet, Aline Antonio, Claire Audier, Mélanie Letexier, Jean-Paul Saraiva, TienD Luu, Florian Sennlaub, Hoan Nguyen, Olivier Poch, Hélène Dollfus, Odile Lecompte, Susanne Kohl, José-Alain Sahel, ShomiS Bhattacharya, and Isabelle Audo. Whole-Exome

Sequencing Identifies LRIT3 Mutations as a Cause of Autosomal-Recessive Complete Congenital Stationary Night Blindness. *The American Journal of Human Genetics*, 92(1):67–75, 2013.

[185] F Mansergh, N C Orton, J P Vessey, M R Lalonde, W K Stell, F Tremblay, S Barnes, D E Rancourt, and N T Bech-Hansen. Mutation of the calcium channel gene Cacna1f disrupts calcium signaling, synaptic transmission and cellular organization in mouse retina. *Hum Mol Genet*, 14(20):3035–3046, 2005.

[186] N Torben Bech-Hansen, Margaret J Naylor, Tracy A Maybaum, William G Pearce, Ben Koop, Gerald A Fishman, Marilyn Mets, Maria A Musarella, and Kym M Boycott. Loss-of-function mutations in a calcium-channel $\alpha$1-subunit gene in Xp11. 23 cause incomplete X-linked congenital stationary night blindness. *Nature genetics*, 19(3):264–267, 1998.

[187] Bo Chang, John R Heckenlively, Philippa R Bayley, Nicholas C Brecha, Muriel T Davisson, Norm L Hawes, Arlene A Hirano, Ronald E Hurd, Akihiro Ikeda, Britt A Johnson, Maureen A Mccall, Catherine W Morgans, Steve Nusinowitz, Neal S Peachey, Dennis S Rice, Kirstan A Vessey, and Ronald G Gregg. The nob2 mouse, a null mutation in Cacna1f: Anatomical and functional abnormalities in the outer retina and their consequences on ganglion cell visual responses. *Visual Neuroscience*, 23(01):11–24, 2006.

[188] Christina Zeitz, Barbara Kloeckener-Gruissem, Ursula Forster, Susanne Kohl, István Magyar, Bernd Wissinger, Gábor Mátyás, François-Xavier Borruat, Daniel F Schorderet, Eberhart Zrenner, Francis L Munier, and Wolfgang Berger. Mutations in CABP4, the Gene Encoding the Ca2+-Binding Protein 4, Cause Autosomal Recessive Night Blindness. *The American Journal of Human Genetics*, 79(4):657–667, 2006.

[189] Katharina A Wycisk, Birgit Budde, Silke Feil, Sergej Skosyrski, Francesca Buzzi, John Neidhardt, Esther Glaus, Peter Nurnberg, Klaus Ruether, and

Wolfgang Berger. Structural and Functional Abnormalities of Retinal Ribbon Synapses due to Cacna2d4 Mutation. *Invest Ophthalmol Vis Sci*, 47(8):3523–3530, 2006.

[190] William A Catterall. Structure and Regulation of Voltage-Gated Ca2+ Channels. *Annual Review of Cell and Developmental Biology*, 16(1):521–555, 2000.

[191] Ajoy Vincent, Isabelle Audo, Erika Tavares, Jason T Maynes, Anupreet Tumber, Thomas Wright, Shuning Li, Christelle Michiels, Christel Condroyer, and Heather MacDonald. Biallelic mutations in GNB3 cause a unique form of autosomal-recessive congenital stationary night blindness. *The American Journal of Human Genetics*, 98(5):1011–1019, 2016.

[192] A Dhingra, H Ramakrishnan, A Neinstein, M E Fina, Y Xu, J Li, D C Chung, A Lyubarsky, and N Vardi. Gbeta3 is required for normal light ON responses and synaptic maintenance. *J Neurosci*, 32(33):11343–11355, 2012.

[193] M T Pardue, M A McCall, M M LaVail, R G Gregg, and N S Peachey. A naturally occurring mouse model of X-linked congenital stationary night blindness. *Invest Ophthalmol Vis Sci*, 39(12):2443–2449, 1998.

[194] Masayuki Masu, Hideki Iwakabe, Yoshiaki Tagawa, Tomomitsu Miyoshi, Masayuki Yamashita, Yutaka Fukuda, Hitoshi Sasaki, Kano Hiroi, Yasuhisa Nakamura, Ryuichi Shigemoto, Masahiko Takada, Kenji Nakamura, Kazuki Nakao, Motoya Katsuki, and Shigetada Nakanishi. Specific deficit of the ON response in visual transmission by targeted disruption of the mGIuR6 gene. *Cell*, 80(5):757–765, 1995.

[195] Haohua Qian, Rui Ji, Ronald G Gregg, and Neal S Peachey. Identification of a new mutant allele, Grm6 nob7, for complete congenital stationary night blindness. *Visual Neuroscience*, 32:null–null, 2015.

[196] Neal S Peachey, Nazarul Hasan, Bernard FitzMaurice, Samantha Burrill, Gobinda Pangeni, Son Yong Karst, Laura Reinholdt, Melissa L Berry, Marge

Strobel, and Ronald G Gregg. A missense mutation in Grm6 reduces but does not eliminate mGluR6 expression or rod depolarizing bipolar cell function. *Journal of Neurophysiology*, 118(2):845–854, 2017.

[197] Neal S Peachey, Thomas A Ray, Ralph Florijn, Lucy B Rowe, Trijntje Sjoerdsma, Susana Contreras-Alcantara, Kenkichi Baba, Gianluca Tosini, Nikita Pozdeyev, and P Michael Iuvone. GPR179 is required for depolarizing bipolar cell function and is mutated in autosomal-recessive complete congenital stationary night blindness. *The American Journal of Human Genetics*, 90(2):331–339, 2012.

[198] Marion Neuillé, Said El Shamieh, Elise Orhan, Christelle Michiels, Aline Antonio, Marie-Elise Lancelot, Christel Condroyer, Kinga Bujakowska, Olivier Poch, José-Alain Sahel, Isabelle Audo, and Christina Zeitz. Lrit3 Deficient Mouse (nob6): A Novel Model of Complete Congenital Stationary Night Blindness (cCSNB). *PLoS ONE*, 9(3):e90342, 2014.

[199] Clinton J Doering, Renata Rehak, Stephan Bonfield, Jean B Peloquin, William K Stell, Silvina C Mema, Yves Sauve, and John E McRory. Modified Cav1. 4 expression in the Cacna1fnob2 mouse due to alternative splicing of an ETn inserted in exon 2. *PLoS One*, 3(7):e2538, 2008.

[200] Dana Specht, Shu-Biao Wu, Paul Turner, Peter Dearden, Frank Koentgen, Uwe Wolfrum, Marion Maw, Johann Helmut Brandstatter, and Susanne tom Dieck. Effects of presynaptic mutations on a postsynaptic Cacna1s calcium channel colocalized with mGluR6 at mouse photoreceptor ribbon synapses. *Investigative ophthalmology & visual science*, 50(2):505–515, 2009.

[201] Nawal Zabouri and Silke Haverkamp. Calcium channel-dependent molecular maturation of photoreceptor synapses. *PLoS One*, 8(5):e63853, 2013.

[202] A Hemara-Wahanui, S Berjukow, C I Hope, P K Dearden, S B Wu, J Wilson-Wheeler, D M Sharp, P Lundon-Treweek, G M Clover, J C Hoda, J Striessnig, R Marksteiner, S Hering, and M A Maw. A CACNA1F mutation iden-

tified in an X-linked retinal disorder shifts the voltage dependence of Cav1.4 channel activation. *Proc Natl Acad Sci U S A*, 102(21):7553–7558, 2005.

[203] Zheng Li, Panagiotis I Sergouniotis, Michel Michaelides, Donna S Mackay, Genevieve A Wright, Sophie Devery, Anthony T Moore, Graham E Holder, Anthony G Robson, and Andrew R Webster. Recessive Mutations of the Gene TRPM1 Abrogate ON Bipolar Cell Function and Cause Complete Congenital Stationary Night Blindness in Humans. *The American Journal of Human Genetics*, 85(5):711–719, 2009.

[204] Maria M van Genderen, Mieke M C Bijveld, Yvonne B Claassen, Ralph J Florijn, Jillian N Pearring, Francoise M Meire, Maureen A McCall, Frans C C Riemslag, Ronald G Gregg, Arthur A B Bergen, and Maarten Kamermans. Mutations in TRPM1 Are a Common Cause of Complete Congenital Stationary Night Blindness. *The American Journal of Human Genetics*, 85(5):730–736, 2009.

[205] Françoise Haeseleer, Yoshikazu Imanishi, Tadao Maeda, Daniel E Possin, Akiko Maeda, Amy Lee, Fred Rieke, and Krzysztof Palczewski. Essential role of Ca2+-binding protein 4, a Cav1. 4 channel regulator, in photoreceptor synaptic function. *Nature neuroscience*, 7(10):1079, 2004.

[206] Klaus Ruether, Johannes Grosse, Eike Matthiessen, Kirstin Hoffmann, and Christian Hartmann. Abnormalities of the photoreceptor-bipolar cell synapse in a substrain of C57BL/10 mice. *Investigative ophthalmology & visual science*, 41(12):4039–4047, 2000.

[207] Katharina A Wycisk, Birgit Budde, Silke Feil, Sergej Skosyrski, Francesca Buzzi, John Neidhardt, Esther Glaus, Peter Nurnberg, Klaus Ruether, and Wolfgang Berger. Structural and Functional Abnormalities of Retinal Ribbon Synapses due to Cacna2d4 Mutation. *Invest Ophthalmol Vis Sci*, 47(8):3523–3530, 2006.

[208] Dagmar Knoflach, Vasily Kerov, Simone B Sartori, Gerald J Obermair, Claudia Schmuckermair, Xiaoni Liu, Vithiyanjali Sothilingam, Marina Garcia Garrido, Sheila A Baker, and Martin Glösmann. Cav1. 4 IT mouse as model for vision impairment in human congenital stationary night blindness type 2. *Channels*, 7(6):503–513, 2013.

[209] P de Lonlay, N Seta, S Barrot, B Chabrol, V Drouin, B M Gabriel, H Journel, M Kretz, J Laurent, M Le Merrer, A Leroy, D Pedespan, P Sarda, N Villeneuve, J Schmitz, E van Schaftingen, G Matthijs, J Jaeken, C Korner, A Munnich, J M Saudubray, and V Cormier-Daire. A broad spectrum of clinical presentations in congenital disorders of glycosylation I: a series of 26 cases. *Journal of Medical Genetics*, 38(1):14–19, 2001.

[210] J Jaeken. Congenital disorders of glycosylation (CDG): It's all in it! *J Inherit Metab Dis*, 26(2-3):99–118, 2003.

[211] P T Clayton and S Grunewald. Comprehensive description of the phenotype of the first case of congenital disorder of glycosylation due to RFT1 deficiency (CDG In). *J Inherit Metab Dis*, 32(1):137–139, 2009.

[212] Jaak Jaeken. Congenital disorders of glycosylation. pages 607–616, 2012.

[213] Leen Heykants, Els Schollen, Stephanie Grünewald, and Gert Matthijs. Identification and localization of two mouse phosphomannomutase genes, Pmm1 and Pmm2. *Gene*, 270(12):53–59, 2001.

[214] Hudson H Freeze. Towards a therapy for phosphomannomutase 2 deficiency, the defect in CDG-Ia patients. *Biochimica et Biophysica Acta (BBA)-Molecular Basis of Disease*, 1792(9):835–840, 2009.

[215] E Morava, H N Wosik, J Sykut-Cegielska, M Adamowicz, M Guillard, R A Wevers, D J Lefeber, and J R Cruysberg. Ophthalmological abnormalities in children with congenital disorders of glycosylation type I. *Br J Ophthalmol*, 93(3):350–354, 2009.

[216] D A Thompson, R J Lyons, I Russell-Eggitt, A Liasis, H Jagle, and S Grunewald. Retinal characteristics of the congenital disorder of glycosylation PMM2-CDG. *J Inherit Metab Dis*, 36(6):1039–1047, 2013.

[217] Isabelle Audo, Kinga Bujakowska, Elise Orhan, CharlotteM Poloschek, Sabine Defoort-Dhellemmes, Isabelle Drumare, Susanne Kohl, TienD Luu, Odile Lecompte, Eberhart Zrenner, Marie-Elise Lancelot, Aline Antonio, Aurore Germain, Christelle Michiels, Claire Audier, Mélanie Letexier, Jean-Paul Saraiva, BartP Leroy, FrancisL Munier, Saddek Mohand-Saïd, Birgit Lorenz, Christoph Friedburg, Markus Preising, Ulrich Kellner, AgnesB Renner, Veselina Moskova-Doumanova, Wolfgang Berger, Bernd Wissinger, ChristianP Hamel, DanielF Schorderet, Elfride DeBaere, Dror Sharon, Eyal Banin, SamuelG Jacobson, Dominique Bonneau, Xavier Zanlonghi, Guylene LeMeur, Ingele Casteels, Robert Koenekoop, VernonW Long, Francoise Meire, Katrina Prescott, Thomy deRavel, Ian Simmons, Hoan Nguyen, Hélène Dollfus, Olivier Poch, Thierry Léveillard, Kim Nguyen-Ba-Charvet, José-Alain Sahel, ShomiS Bhattacharya, and Christina Zeitz. Whole-Exome Sequencing Identifies Mutations in GPR179 Leading to Autosomal-Recessive Complete Congenital Stationary Night Blindness. *The American Journal of Human Genetics*, 90(2):321–330, 2012.

[218] Alan E H Emery. Population frequencies of inherited neuromuscular diseasesA world survey. *Neuromuscular Disorders*, 1(1):19–29, 1991.

[219] Michelle Eagle, Simon V Baudouin, Colin Chandler, David R Giddings, Robert Bullock, and Kate Bushby. Survival in Duchenne muscular dystrophy: improvements in life expectancy since 1967 and the impact of home nocturnal ventilation. *Neuromuscular disorders*, 12(10):926–929, 2002.

[220] De-Ann M Pillers, Dennis E Bulman, Richard G Weleber, Dayle A Sigesmund, Maria A Musarella, Berkley R Powell, William H Murphey, Carol Westall, Carole Panton, Laurence E Becker, Ronald G Worton, and Peter N

Ray. Dystrophin expression in the human retina is required for normal function as defined by electroretinography. *Nat Genet*, 4(1):82–86, 1993.

[221] Francesco Muntoni, Silvia Torelli, and Alessandra Ferlini. Dystrophin and mutations: one gene, several proteins, multiple phenotypes. *The Lancet Neurology*, 2(12):731–740, 2003.

[222] V N D'Souza, T M Nguyen, G E Morris, W Karges, D A Pillers, and P N Ray. A novel dystrophin isoform is required for normal retinal electrophysiology. *Hum Mol Genet*, 4(5):837–842, 1995.

[223] Ramin Tadayoni, Alvaro Rendon, L E Soria-Jasso, and Bulmaro Cisneros. Dystrophin Dp71: The Smallest but Multifunctional Product of the Duchenne Muscular Dystrophy Gene. *Molecular Neurobiology*, 45(1):43–60, 2012.

[224] K M Fitzgerald, G W Cibis, S A Giambrone, and D J Harris. Retinal signal transmission in Duchenne muscular dystrophy: evidence for dysfunction in the photoreceptor/depolarizing bipolar cell pathway. *Journal of Clinical Investigation*, 93(6):2425–2430, 1994.

[225] Eric Wersinger, Agnès Bordais, Yannick Schwab, Abdoulaye Sene, Romain Bénard, Violaine Alunni, José-Alain Sahel, Alvaro Rendon, and Michel J Roux. Reevaluation of Dystrophin Localization in the Mouse Retina. *Invest Ophthalmol Vis Sci*, 52(11):7901–7908, 2011.

[226] Vinita N D'Souza, Nguyen thi Man, Glenn E Morris, Wolfram Karges, De-Ann M Pillers, and Peter N Ray. A novel dystrophin isoform is required for normal retinal electrophysiology. *Hum Mol Genet*, 4(5):837–842, 1995.

[227] Jorge Aragón, Mayram González-Reyes, José Romo-Yáñez, Ophélie Vacca, Guadalupe Aguilar-González, Alvaro Rendón, Cyrille Vaillend, and Cecilia Montañez. Dystrophin Dp71 Isoforms Are Differentially Expressed in the Mouse Brain and Retina: Report of New Alternative Splicing and a Novel

Nomenclature for Dp71 Isoforms. *Molecular Neurobiology*, pages 1–11, 2017.

[228] Y Miyake. Establishment of the concept of new clinical entities–complete and incomplete form of congenital stationary night blindness. *Nippon Ganka Gakkai Zasshi*, 106(12):737–755, 2002.

[229] J Cammack, J Whight, V Cross, A T Rider, A R Webster, and A Stockman. Psychophysical measures of visual function and everyday perceptual experience in a case of congenital stationary night blindness. *Clin Ophthalmol*, 10:1593–1606, 2016.

[230] Panagiotis I Sergouniotis, Anthony G Robson, Zheng Li, Sophie Devery, Graham E Holder, Anthony T Moore, and Andrew R Webster. A phenotypic study of congenital stationary night blindness (CSNB) associated with mutations in the GRM6 gene. *Acta Ophthalmologica*, 90(3):e192–e197, 2012.

[231] Ranjay Chakraborty, Han na Park, Adam M Hanif, Curran S Sidhu, P Michael Iuvone, and Machelle T Pardue. ON pathway mutations increase susceptibility to form-deprivation myopia. *Experimental Eye Research*, 137:79–83, 2015.

[232] H Ali Vaghefi, W Richard Green, James S Kelley, Louise L Sloan, Richard E Hoover, and Arnall Patz. Correlation of clinicopathologic findings in a patient: congenital night blindness, branch retinal vein occlusion, cilioretinal artery, drusen of the optic nerve head, and intraretinal pigmented lesion. *Archives of Ophthalmology*, 96(11):2097–2104, 1978.

[233] I Watanabe, Y Taniguchi, K Morioka, and M Kato. Congenital stationary night blindness with myopia: a clinicopathologic study. *Doc Ophthalmol*, 63(1):55–62, 1986.

[234] Pooja Godara, Robert F Cooper, Panagiotis I Sergouniotis, Melissa A Diederichs, Megan R Streb, Mohamed A Genead, J Jason McAnany, An-

drew R Webster, Anthony T Moore, Adam M Dubis, Maureen Neitz, Alfredo Dubra, Edwin M Stone, Gerald A Fishman, Dennis P Han, Michel Michaelides, and Joseph Carroll. Assessing Retinal Structure in Complete Congenital Stationary Night Blindness and Oguchi Disease. *American Journal of Ophthalmology*, 154(6):987–1001.e1, 2012.

[235] M Sustar, D Perovšek, I Cima, B Stirn-Kranjc, M Hawlina, and J Brecelj. Electroretinography and optical coherence tomography reveal abnormal post-photoreceptoral activity and altered retinal lamination in patients with enhanced s-cone syndrome. *Doc Ophthalmol*, 130(3):165–177, 2015.

[236] Royce W S Chen, Jonathan P Greenberg, Margot A Lazow, Rithu Ramachandran, Luiz H Lima, John C Hwang, Carl Schubert, Alexandra Braunstein, Rando Allikmets, and Stephen H Tsang. Autofluorescence imaging and spectral-domain optical coherence tomography in incomplete congenital stationary night blindness and comparison with retinitis pigmentosa. *American journal of ophthalmology*, 153(1):143–154, 2012.

[237] Susan E Sparks and Donna M Krasnewich. PMM2-CDG (CDG-Ia). 2015.

[238] D A Thompson, R J Lyons, A Liasis, I Russell-Eggitt, H Jägle, and S Grünewald. REtinal on-pathway deficit in congenital disorder of glycosylation due to phosphomannomutase deficiency. *Archives of ophthalmology*, 130(6):712–719, 2012.

[239] Wyatt B Messenger, Paul Yang, and Mark E Pennesi. Ophthalmic findings in an infant with phosphomannomutase deficiency. *Doc Ophthalmol*, 128(2):149–153, 2014.

[240] Hanne Jensen, Susanne Kjaergaard, Flemming Klie, and H U Moller. Ophthalmic manifestations of congenital disorder of glycosylation type 1a. *Ophthalmic genetics*, 24(2):81–88, 2003.

[241] M Bach, M G Brigell, M Hawlina, G E Holder, M A Johnson, D L McCulloch, T Meigen, and S Viswanathan. ISCEV standard for clinical pattern

electroretinography (PERG): 2012 update. *Doc Ophthalmol*, 126(1):1–7, 2013.

[242] J Vernon Odom, Michael Bach, Mitchell Brigell, Graham E Holder, Daphne L McCulloch, Atsushi Mizota, and Alma Patrizia Tormene. ISCEV standard for clinical visual evoked potentials: (2016 update). *Doc Ophthalmol*, 133(1):1–9, 2016.

[243] William A Hare and Hau Ton. Effects of apb, pda, and ttx on erg responses recorded using both multifocal and conventional methods in monkey. *Doc Ophthalmol*, 105(2):189–222, 2002.

[244] John G Robson, Shannon M Saszik, Jameel Ahmed, and Laura J Frishman. Rod and cone contributions to the a-wave of the electroretinogram of the macaque. *The Journal of physiology*, 547(2):509–530, 2003.

[245] Audrey Chia, Wen Li, Donald Tan, and Chi D Luu. Full-field electroretinogram findings in children in the atropine treatment for myopia (atom2) study. *Doc Ophthalmol*, 126(3):177–186, 2013.

[246] Carol A Westall, Harjinder S Dhaliwal, Carole M Panton, Dayle Sigesmund, Alex V Levin, Ken K Nischal, and Elise Héon. Values of electroretinogram responses according to axial length. *Doc Ophthalmol*, 102(2):115–130, 2001.

[247] Paul Witkovsky, FE Dudek, and Harris Ripps. Slow piii component of the carp electroretinogram. *The Journal of general physiology*, 65(2):119–134, 1975.

[248] John G Robson and Laura J Frishman. The rod-driven a-wave of the dark-adapted mammalian electroretinogram. *Progress in retinal and eye research*, 39:1–22, 2014.

[249] Xijing Xu and Chester Karwoski. Current source density analysis of the electroretinographic d wave of frog retina. *Journal of neurophysiology*, 73(6):2459–2469, 1995.

[250] M Sustar, B Stirn-Kranjc, M Hawlina, and J Brecelj. Photopic ON- and OFF-responses in complete type of congenital stationary night blindness in relation to stimulus intensity. *Doc Ophthalmol*, 117(1):37–46, 2008.

[251] Ronald A Bush and Paul A Sieving. A proximal retinal component in the primate photopic ERG a-wave. *Investigative ophthalmology & visual science*, 35(2):635–645, 1994.

[252] Naheed Wali and Lawrence E Leguire. The photopic hill: a new phenomenon of the light adapted electroretinogram. *Doc Ophthalmol*, 80(4):335–342, 1992.

[253] R Hamilton, MA Bees, CA Chaplin, and DL McCulloch. The luminance–response function of the human photopic electroretinogram: A mathematical model. *Vision research*, 47(23):2968–2972, 2007.

[254] M-L Garon, AL Dorfman, J Racine, RK Koenekoop, JM Little, and P Lachapelle. Estimating on and off contributions to the photopic hill: normative data and clinical applications. *Doc Ophthalmol*, 129(1):9–16, 2014.

[255] Sophie Rousseau and Pierre Lachapelle. Transient enhancing of cone electroretinograms following exposure to brighter photopic backgrounds. *Vision research*, 40(8):1013–1018, 2000.

[256] Michael Bach, Mitchell G Brigell, Marko Hawlina, Graham E Holder, Mary A Johnson, Daphne L McCulloch, Thomas Meigen, and Suresh Viswanathan. Iscev standard for clinical pattern electroretinography (perg): 2012 update. *Doc Ophthalmol*, 126(1):1–7, 2013.

[257] Y Miyake, M Horiguchi, I Ota, and N Shiroyama. Characteristic ERG-flicker anomaly in incomplete congenital stationary night blindness. *Investigative ophthalmology & visual science*, 28(11):1816–1823, 1987.

[258] H Jensen, M Warburg, O Sjö, and M Schwartz. Duchenne muscular dystrophy: negative electroretinograms and normal dark adaptation. Reappraisal

of assignment of X linked incomplete congenital stationary night blindness. *Journal of Medical Genetics*, 32(5):348–351, 1995.

[259] Donald C Fletcher and Ronald A Schuchard. Preferred retinal loci relationship to macular scotomas in a low-vision population. *Ophthalmology*, 104(4):632–638, 1997.

[260] H Sakaue, O Katsumi, M Mehta, and T Hirose. Simultaneous pattern reversal erg and ver recordings. effect of stimulus field and central scotoma. *Investigative ophthalmology & visual science*, 31(3):506–511, 1990.

[261] H Masukagami, F Furuno, and H Matsuo. Blind spots of normal and high myopic eyes measured by fundus photo-perimetry. pages 489–493, 1987.

[262] Anita Haas, Josef Flammer, and Urs Schneider. Influence of age on the visual fields of normal subjects. *American journal of ophthalmology*, 101(2):199–203, 1986.

[263] Harry Moss Traquair and George Ian Scott. *Clinical perimetry*. Kimpton, 1957.

[264] Michael B Hoffmann, Petra S Seufert, and Michael Bach. Simulated nystagmus suppresses pattern-reversal but not pattern-onset visual evoked potentials. *Clinical Neurophysiology*, 115(11):2659–2665, 2004.

[265] Maria Michielde van Genderen. *Electrophysiology in visually impaired children*. Utrecht University, 2006.

[266] Clare Gilbert and Allen Foster. Childhood blindness in the context of VISION 2020: the right to sight. *Bulletin of the World Health Organization*, 79(3):227–232, 2001.

[267] Wolfgang Berger, Barbara Kloeckener-Gruissem, and John Neidhardt. The molecular basis of human retinal and vitreoretinal diseases. *Progress in retinal and eye research*, 29(5):335–375, 2010.

[268] Vincent Plagnol, James Curtis, Michael Epstein, Kin Y Mok, Emma Stebbings, Sofia Grigoriadou, Nicholas W Wood, Sophie Hambleton, Siobhan O Burns, Adrian J Thrasher, et al. A robust model for read count data in exome sequencing experiments and implications for copy number variant calling. *Bioinformatics*, 28(21):2747–2754, 2012.

[269] Sue Richards, Nazneen Aziz, Sherri Bale, David Bick, Soma Das, Julie Gastier-Foster, Wayne W Grody, Madhuri Hegde, Elaine Lyon, Elaine Spector, et al. Standards and guidelines for the interpretation of sequence variants: a joint consensus recommendation of the american college of medical genetics and genomics and the association for molecular pathology. *Genetics in medicine*, 17(5):405–423, 2015.

[270] Vinit B Mahajan, Jessica M Skeie, Alexander G Bassuk, John H Fingert, Terry A Braun, Heather T Daggett, James C Folk, Val C Sheffield, and Edwin M Stone. Calpain-5 Mutations Cause Autoimmune Uveitis, Retinal Neovascularization, and Photoreceptor Degeneration. *PLoS Genet*, 8(10):e1003001, 2012.

[271] Katherine J Wert, Jessica M Skeie, Alexander G Bassuk, Alicia K Olivier, Stephen H Tsang, and Vinit B Mahajan. Functional validation of a human CAPN5 exome variant by lentiviral transduction into mouse retina. *Hum Mol Genet*, 23(10):2665–2677, 2014.

[272] Graham F A Harding, James V Odom, Werner Spileers, Henk Spekreijse, and International Society for Clinical Electrophysiology of Vision. Standard for visual evoked potentials 1995. *Vision research*, 36(21):3567–3572, 1996.

[273] T Ung, L E Allen, A T Moore, D Trump, J Yates, and K Bradshaw. Is Optic Nerve Fibre Mis-Routing a Feature of Congenital Stationary Night Blindness? *Doc Ophthalmol*, 111(3):169–178, 2005.

[274] Zuzana Kubová, Jan Kremláček, Miroslav Kuba, Jana Chlubnová, and

Jaromír Svěrák. Photopic and scotopic VEPs in patients with congenital stationary night-blindness. *Doc Ophthalmol*, 109(1):9–15, 2004.

[275] P Feraco, M Mirabelli-Badenier, M Severino, M G Alpigiani, M Di Rocco, R Biancheri, and A Rossi. The Shrunken, Bright Cerebellum: A Characteristic MRI Finding in Congenital Disorders of Glycosylation Type 1a. *American Journal of Neuroradiology*, 33(11):2062–2067, 2012.

[276] Paolo Girlanda, Angelo Quartarone, Rosaria Buceti, Stefano Sinicropi, Vincenzo Macaione, Fawzy A Saad, Lorenzo Messina, Gian Antonio Danieli, Giuseppe Ferreri, and Giuseppe Vita. Extra-muscle involvement in dystrophinopathies: an electroretinography and evoked potential study. *Journal of the Neurological Sciences*, 146(2):127–132, 1997.

[277] Andreas Arlt and Wolfgang H Zangemeister. Influence of slow eye movements and nystagmus on pattern induced visual evoked potentials. *Neuro-Ophthalmology*, 10(5):241–251, 1990.

[278] KathrynJ Saunders, Graeme Brown, and DaphneL McCulloch. Pattern-onset visual evoked potentials: more useful than reversal for patients with nystagmus. *Doc Ophthalmol*, 94(3):265–274, 1997.

[279] S Houston, D M Fritsch, V Reynolds, A Liasis, and D A Thompson. Pattern reversal VEP latency in children with nystagmus. *BrISCEV conference Oxford 2015*, 2015.

[280] Robert P Dolan and Peter H Schiller. Effects of ON channel blockade with 2-amino-4-phosphonobutyrate (APB) on brightness and contrast perception in monkeys. *Visual Neuroscience*, 11(01):23–32, 1994.

[281] Peter H Schiller. The ON and OFF channels of the visual system. *Trends in neurosciences*, 15(3):86–92, 1992.

[282] E W Yund, D M Snodderly, N K Hepler, and R L DeValois. Brightness

contrast effects in monkey lateral geniculate nucleus. *Sensory Processes*, 1:260–271, 1977.

[283] Svein Magnussen and Alf Gland. Effects of steady surround illumination on the brightness and darkness enhancement of flickering lights. *Vision Research*, 15(12):1413–1416, 1975.

[284] Peter H Schiller. Central connections of the retinal ON and OFF pathways. *Nature*, 297(5867):580–583, 1982.

[285] Vance Zemon, James Gordon, and Janet Welch. Asymmetries in ON and OFF visual pathways of humans revealed using contrast-evoked cortical potentials. *Visual Neuroscience*, 1(01):145–150, 1988.

[286] Kenneth R Alexander, Aruna S Rajagopalan, William Seiple, Vance M Zemon, and Gerald A Fishman. Contrast response properties of magnocellular and parvocellular pathways in retinitis pigmentosa assessed by the visual evoked potential. *Investigative ophthalmology & visual science*, 46(8):2967–2973, 2005.

[287] V Zemon, J Gordon, and J Welch. Asymmetries in ON and OFF visual pathways of humans revealed using contrast-evoked cortical potentials. *Vis Neurosci*, 1(1):145–150, 1988.

[288] Claire S Barnes, Kenneth R Alexander, and Gerald A Fishman. A distinctive form of congenital stationary night blindness with cone ON-pathway dysfunction. *Ophthalmology*, 109(3):575–583, 2002.

[289] Kenneth R Alexander, Claire S Barnes, Gerald A Fishman, and Ann H Milam. Nature of the Cone ON-Pathway Dysfunction in Melanoma-Associated Retinopathy. *Invest Ophthalmol Vis Sci*, 43(4):1189–1197, 2002.

[290] H Spekreijse, O Estévez, and L H Van der Tweel. Luminance Responses to Pattern Reversal. In Jerome T Pearlman, editor, *Xth I.S.C.E.R.G. Symposium*, pages 205–211. Springer Netherlands, Dordrecht, 1973.

[291] Zuzana Kubová, Miroslav Kuba, Henk Spekreijse, and Colin Blakemore. Contrast dependence of motion-onset and pattern-reversal evoked potentials. *Vision research*, 35(2):197–205, 1995.

[292] A Kriss and I Russell-Eggitt. Electrophysiological assessment of visual pathway function in infants. *Eye*, 6(2):145–153, 1992.

[293] A Kriss. Skin ERGs: their effectiveness in paediatric visual assessment, confounding factors, and comparison with ERGs recorded using various types of corneal electrode. *International Journal of Psychophysiology*, 16(23):137–146, 1994.

[294] P Apkarian, D Reits, and H Spekreijse. Component specificity in albino VEP asymmetry: Maturation of the visual pathway anomaly. *Experimental Brain Research*, 53(2):285–294, 1984.

[295] A Kriss and I Russell-Eggitt. Electrophysiological assessment of visual pathway function in infants. *Eye*, 6(2):145–153, 1992.

[296] L H De Vries-Khoe and H Spekreijse. Maturation of luminance and pattern EPs in man. *Doc Ophthalmol Proc Ser*, 31:461–475, 1982.

[297] A Kriss and A M Halliday. A comparison of occipital potentials evoked by pattern onset, offset and reversal by movement. In *Evoked potentials*, pages 205–212. Springer, 1980.

[298] D A Jeffreys and J G Axford. Source locations of pattern-specific components of human visual evoked potentials. I. Component of striate cortical origin. *Experimental Brain Research*, 16(1):1–21, 1972.

[299] Vincent P Clark, Silu Fan, and Steven A Hillyard. Identification of early visual evoked potential generators by retinotopic and topographic analyses. *Human brain mapping*, 2(3):170–187, 1994.

[300] Francesco Di Russo, Antígona Martínez, Martin I Sereno, Sabrina Pitzalis, and Steven A Hillyard. Cortical sources of the early components of the visual evoked potential. *Human Brain Mapping*, 15(2):95–111, 2002.

[301] S R Butler, G A Georgiou, A Glass, R J Hancox, J M Hopper, and K R H Smith. Cortical generators of the CI component of the pattern-onset visual evoked potential. *Electroencephalography and Clinical Neurophysiology/Evoked Potentials Section*, 68(4):256–267, 1987.

[302] H Spekreijse and L H van der Tweel. System analysis of linear and nonlinear processes in electrophysiology of the visual system. I. *Proc K Ned Akad Wet C*, 75(2):77–91, 1972.

[303] N Drasdo, W Cox, and D A Thompson. The effects of image degradation on retinal illuminance and pattern responses to checkerboard stimuli. *Doc Ophthalmol*, 66(3):267–275, 1987.

[304] Simon P Kelly, M Isabel Vanegas, Charles E Schroeder, and Edmund C Lalor. The cruciform model of striate generation of the early VEP, re-illustrated, not revoked: A reply to Ales et al. (2013). *NeuroImage*, 82:154–159, 2013.

[305] Justin M Ales, Jacob L Yates, and Anthony M Norcia. On determining the intracranial sources of visual evoked potentials from scalp topography: A reply to Kelly et al. (this issue). *NeuroImage*, 64:703–711, 2013.

[306] A M Proverbio, A Zani, M S Gazzaniga, and G R Mangun. VEP evidence of hemispheric asymmetries for spatial frequency processing in a split-brain patient. In *Abstracts book of Cognitive Neuroscience Society. Second Annual Meeting*, volume 77, 1995.

[307] S Vanni, J Warnking, M Dojat, C Delon-Martin, J Bullier, and C Segebarth. Sequence of pattern onset responses in the human visual areas: an fMRI constrained VEP source analysis. *NeuroImage*, 21(3):801–817, 2004.

[308] Francesco Di Russo, Antigona Martínez, and Steven A Hillyard. Source Analysis of Event-related Cortical Activity during Visuo-spatial Attention. *Cerebral Cortex*, 13(5):486–499, 2003.

[309] Pauly Ossenblok, Dik Reits, and Henk Spekreijse. Check size dependency of the sources of the hemifield-onset evoked potential. *Doc Ophthalmol*, 88(1):77–88, 1994.

[310] Patricia Apkarian and Robert Tijssen. Detection and maturation of VEP albino asymmetry: an overview and a longitudinal study from birth to 54 weeks. *Behavioural Brain Research*, 49(1):57–67, 1992.

[311] Michael F Green, Pamela D Butler, Yue Chen, Mark A Geyer, Steven Silverstein, Jonathan K Wynn, Jong H Yoon, and Vance Zemon. Perception measurement in clinical trials of schizophrenia: promising paradigms from CNTRICS. *Schizophrenia bulletin*, 35(1):163–181, 2008.

[312] V Zemon and J Gordon. Luminance-contrast mechanisms in humans: visual evoked potentials and a nonlinear model. *Vision Res*, 46(24):4163–4180, 2006.

[313] L H Van der Tweel, D Regan, and H Spekreijse. Some aspects of potentials evoked by changes in spatial brightness contrast. In *Proceedings of seventh ISCERG symposium*, pages 1–12, 1969.

[314] A M Bloch. Experiences sur la vision. *Comptes Rendus de la Societé de Biologie*, 37:493–495, 1885.

[315] A Y Peters, K G Locke, and D G Birch. Comparison of the Goldmann-Weekers dark adaptometer and LKC technologies scotopic sensitivity tester-1. *Doc Ophthalmol*, 101(1):1–9, 2000.

[316] Sheila K West, Gary S Rubin, Aimee T Broman, Beatriz Munoz, Karen Bandeen-Roche, and Kathleen Turano. How does visual impairment affect

performance on tasks of everyday life?: The SEE Project. *Archives of Ophthalmology*, 120(6):774–780, 2002.

[317] James S Wolffsohn and Anthea L Cochrane. Design of the low vision quality-of-life questionnaire (LVQOL) and measuring the outcome of low-vision rehabilitation. *American journal of ophthalmology*, 130(6):793–802, 2000.

[318] Sima Shechter and Shaul Hochstein. On and off pathway contributions to apparent motion perception. *Vision research*, 30(8):1189–1204, 1990.

[319] Mark Edwards and David R Badcock. Global motion perception: interaction of the ON and OFF pathways. *Vision research*, 34(21):2849–2858, 1994.

[320] Christian Wehrhahn and Dietmar Rapf. ON-and OFF-pathways form separate neural substrates for motion perception: psychophysical evidence. *Journal of Neuroscience*, 12(6):2247–2250, 1992.

[321] Kareem A Zaghloul, Kwabena Boahen, and Jonathan B Demb. Different circuits for ON and OFF retinal ganglion cells cause different contrast sensitivities. *Journal of Neuroscience*, 23(7):2645–2654, 2003.

[322] P H Schiller, J H Sandell, and J H Maunsell. Functions of the ON and OFF channels of the visual system. *Nature*, 322(6082):824–825, 1986.

[323] Anita J Simmers, Tim Ledgeway, R F Hess, and Paul V McGraw. Deficits to global motion processing in human amblyopia. *Vision research*, 43(6):729–738, 2003.

[324] Cindy S Ho, Deborah E Giaschi, Catherine Boden, Robert Dougherty, Roy Cline, and Christopher Lyons. Deficient motion perception in the fellow eye of amblyopic children. *Vision research*, 45(12):1615–1627, 2005.

[325] Xiong-Li Yang and Samuel M Wu. Feedforward lateral inhibition in retinal bipolar cells: input-output relation of the horizontal cell-depolarizing bipolar cell synapse. *Proceedings of the National Academy of Sciences*, 88(8):3310–3313, 1991.

[326] Charles Chubb and George Sperling. Two motion perception mechanisms revealed through distance-driven reversal of apparent motion. *Proceedings of the National Academy of Sciences*, 86(8):2985–2989, 1989.

[327] Peter H Schiller. The connections of the retinal on and off pathways to the lateral geniculate nucleus of the monkey. *Vision Research*, 24(9):923–932, 1984.

[328] A F Dean and D J Tolhurst. On the distinctness of simple and complex cells in the visual cortex of the cat. *The Journal of Physiology*, 344(1):305–325, 1983.

[329] M J Hawken, A J Parker, and C Blakemore. Detection and discrimination mechanisms in the striate cortex of the old-world monkey. *Vision: Coding and efficiency*, pages 103–116, 1990.

[330] Sunil P Gandhi, David J Heeger, and Geoffrey M Boynton. Spatial attention affects brain activity in human primary visual cortex. *Proceedings of the National Academy of Sciences*, 96(6):3314–3319, 1999.

[331] M Concetta Morrone and D C Burr. Feature detection in human vision: A phase-dependent energy model. *Proceedings of the Royal Society of London B: Biological Sciences*, 235(1280):221–245, 1988.

[332] Adriana Fiorentini, Günter Baumgartner, Svein Magnussen, Peter H Schiller, and James P Thomas. The perception of brightness and darkness: Relations to neuronal receptive fields. 1990.

[333] Lothar Spillmann and John S Werner. *Visual perception: The neurophysiological foundations*. Elsevier, 2012.

[334] R Shapley and V Hugh Perry. Cat and monkey retinal ganglion cells and their visual functional roles. *Trends in Neurosciences*, 9:229–235, 1986.

[335] R B Tootell, Susan L Hamilton, and Eugene Switkes. Functional anatomy of macaque striate cortex. IV. Contrast and magno-parvo streams. *Journal of Neuroscience*, 8(5):1594–1609, 1988.

[336] R J Howard, M Brammer, I Wright, P W Woodruff, E T Bullmore, and S Zeki. A direct demonstration of functional specialization within motion-related visual and auditory cortex of the human brain. *Current Biology*, 6(8):1015–1019, 1996.

[337] H B Barlow, R M Hill, and W R Levick. Retinal ganglion cells responding selectively to direction and speed of image motion in the rabbit. *J Physiol*, 173(3):377–407, 1964.

[338] Hiroshi Ishikane, Mie Gangi, Shoko Honda, and Masao Tachibana. Synchronized retinal oscillations encode essential information for escape behavior in frogs. *Nat Neurosci*, 8(8):1087–1095, 2005.

[339] Thomas A Munch, Rava Azeredo da Silveira, Sandra Siegert, Tim James Viney, Gautam B Awatramani, and Botond Roska. Approach sensitivity in the retina processed by a multifunctional neural circuit. *Nat Neurosci*, 12(10):1308–1316, 2009.

[340] Reinhold Thiel, Paul Clark, Richard B Wheeler, Paul W Jones, Marcel Rivecccie, and Jean-Fabien Dupont. Assessment of image quality in digital cinema using the motion quality ruler method. *SMPTE motion imaging journal*, 116(2-3):61–73, 2007.

[341] H B Barlow and W R Levick. The mechanism of directionally selective units in rabbit's retina. *J Physiol*, 178(3):477–504, 1965.

[342] Bence P Olveczky, Stephen A Baccus, and Markus Meister. Segregation of object and background motion in the retina. *Nature*, 423(6938):401–408, 2003.

[343] Bernhard Hassenstein and Werner Reichardt. Systemtheoretische analyse der zeit-, reihenfolgen-und vorzeichenauswertung bei der bewegungsperzeption des rüsselkäfers chlorophanus. *Zeitschrift für Naturforschung B*, 11(9-10):513–524, 1956.

[344] Jonathan B Demb, Kareem Zaghloul, and Peter Sterling. Cellular Basis for the Response to Second-Order Motion Cues in Y Retinal Ganglion Cells. *Neuron*, 32(4):711–721, 2001.

[345] Thomas Euler, Peter B Detwiler, and Winfried Denk. Directionally selective calcium signals in dendrites of starburst amacrine cells. *Nature*, 418(6900):845–852, 2002.

[346] Frank Werblin, Greg Maguire, Peter Lukasiewicz, Scott Eliasof, and Samuel M Wu. Neural interactions mediating the detection of motion in the retina of the tiger salamander. *Visual Neuroscience*, 1(03):317–329, 1988.

[347] Hubert Eichner, Maximilian Joesch, Bettina Schnell, Dierk F Reiff, and Alexander Borst. Internal structure of the fly elementary motion detector. *Neuron*, 70(6):1155–1164, 2011.

[348] Matthew S Maisak, Juergen Haag, Georg Ammer, Etienne Serbe, Matthias Meier, Aljoscha Leonhardt, Tabea Schilling, Armin Bahl, Gerald M Rubin, Aljoscha Nern, Barry J Dickson, Dierk F Reiff, Elisabeth Hopp, and Alexander Borst. A directional tuning map of Drosophila elementary motion detectors. *Nature*, 500(7461):212–216, 2013.

[349] E J Chichilnisky and R S Kalmar. Temporal Resolution of Ensemble Visual Motion Signals in Primate Retina. *The Journal of neuroscience*, 23(17):6681–6689, 2003.

[350] Hubert Eichner, Maximilian Joesch, Bettina Schnell, Dierk F Reiff, and Alexander Borst. Internal structure of the fly elementary motion detector. *Neuron*, 70(6):1155–1164, 2011.

[351] Andrew J Anderson, Julie Jiao, and Bang V Bui. Efficiently Measuring Magnocellular and Parvocellular Function in Human Clinical Studies. *Translational vision science & technology*, 4(5):1, 2015.

[352] Jonathan J Nassi and Edward M Callaway. Parallel processing strategies of the primate visual system. *Nature reviews. Neuroscience*, 10(5):360, 2009.

[353] Alicia Cheng, Ulf T Eysel, and Trichur R Vidyasagar. The role of the magnocellular pathway in serial deployment of visual attention. *European Journal of Neuroscience*, 20(8):2188–2192, 2004.

[354] Edward M Callaway. Structure and function of parallel pathways in the primate early visual system. *The Journal of physiology*, 566(1):13–19, 2005.

[355] Lawrence C Sincich and Jonathan C Horton. The circuitry of V1 and V2: integration of color, form, and motion. *Annu. Rev. Neurosci.*, 28:303–326, 2005.

[356] D Ferster. Spatially opponent excitation and inhibition in simple cells of the cat visual cortex. *The Journal of neuroscience*, 8(4):1172–1180, 1988.

[357] Zheng Liu, James P Gaska, Lowell D Jacobson, and Daniel A Pollen. Interneuronal interaction between members of quadrature phase and anti-phase pairs in the cat's visual cortex. *Vision Research*, 32(7):1193–1198, 1992.

[358] S Zeki. Cerebral akinetopsia (visual motion blindness). *Brain*, 114(2):811–824, 1991.

[359] Roger B H Tootell, John B Reppas, Kenneth K Kwong, Rafael Malach, Richard T Born, Thomas J Brady, Bruce R Rosen, and John W Belliveau. Functional analysis of human MT and related visual cortical areas using magnetic resonance imaging. *Journal of Neuroscience*, 15(4):3215, 1995.

[360] Bela Julesz. Foundations of cyclopean perception. 1971.

[361] Hans Wallach and D N O'connell. The kinetic depth effect. *Journal of experimental psychology*, 45(4):205, 1953.

[362] Stefan Treue, Masud Husain, and Richard A Andersen. Human perception of structure from motion. *Vision Research*, 31(1):59–75, 1991.

[363] J J Koenderink and A J van Doorn. Dynamic shape. *Biological Cybernetics*, 53(6):383–396, 1986.

[364] M Oram and D Perrett. Responses of Anterior Superior Temporal Polysensory (STPa) Neurons to “Biological Motion” Stimuli. *Cognitive Neuroscience, Journal of*, 6(2):99–116, 1994.

[365] M W Oram and D I Perrett. Integration of form and motion in the anterior superior temporal polysensory area (STPa) of the macaque monkey. *J Neurophysiol*, 76(1):109–129, 1996.

[366] Gunnar Johansson. Visual perception of biological motion and a model for its analysis. *Perception & Psychophysics*, 14(2):201–211, 1973.

[367] LynnT Kozlowski and JamesE Cutting. Recognizing the sex of a walker from a dynamic point-light display. *Perception & Psychophysics*, 21(6):575–580, 1977.

[368] Ian M Thornton. The Visual Perception Of Human Locomotion. *Cognitive Neuropsychology*, 15(6-8):535–552, 1998.

[369] Lucia M Vaina, Marjorie Lemay, Don C Bienfang, Albert Y Choi, and Ken Nakayama. Intact biological motion and structure from motion perception in a patient with impaired motion mechanisms: A case study. *Visual Neuroscience*, 5(04):353–369, 1990.

[370] Michael S Beauchamp, Kathryn E Lee, James V Haxby, and Alex Martin. Parallel Visual Motion Processing Streams for Manipulable Objects and Human Movements. *Neuron*, 34(1):149–159, 2002.

[371] Emily D Grossman and Randolph Blake. Brain Areas Active during Visual Perception of Biological Motion. *Neuron*, 35(6):1167–1175, 2002.

[372] David I Perrett, M H Harris, A J Mistlin, Jari K Hietanen, Philip J Benson, R Bevan, S Thomas, Mike W Oram, Juan Ortega, and Kirsty Brierly. Social Signals Analyzed at the Single Cell Level: Someone is Looking at Me, Something Moved! *International Journal of Comparative Psychology*, 4(1), 1990.

[373] William T Newsome, AIUCHIKA Mikami, and Robert H Wurtz. Motion selectivity in macaque visual cortex. III. Psychophysics and physiology of apparent motion. *Journal of Neurophysiology*, 55(6):1340–1351, 1986.

[374] Lars Muckli, Axel Kohler, Nikolaus Kriegeskorte, and Wolf Singer. Primary visual cortex activity along the apparent-motion trace reflects illusory perception. *PLoS biology*, 3(8):e265, 2005.

[375] Suzanne P McKee and Scott NJ Watamaniuk. The psychophysics of motion perception. *Visual detection of motion*, pages 85–114, 1994.

[376] Praveen K Pilly and Aaron R Seitz. What a Difference a Parameter Makes: a Psychophysical Comparison of Random Dot Motion Algorithms. *Vision Research*, 49(13):1599–1612, 2009.

[377] Cheryl K Hiscock, Janet Dry Branham, and Merrill Hiscock. Detection of feigned cognitive impairment: The two-alternative forced-choice method compared with selected conventional tests. *Journal of Psychopathology and Behavioral Assessment*, 16(2):95–110, 1994.

[378] Janine Spencer, Justin O'Brien, Kevin Riggs, Oliver Braddick, Janette Atkinson, and John Wattam-Bell. Motion processing in autism: evidence for a dorsal stream deficiency. *NeuroReport*, 11(12):2765–2767, 2000.

[379] Oliver Braddick. A short-range process in apparent motion. *Vision Research*, 14(7):519–527, 1974.

[380] Alan Cowey, Gianluca Campana, Vincent Walsh, and Lucia M Vaina. The role of human extra-striate visual areas v5/mt and v2/v3 in the perception of the direction of global motion: a transcranial magnetic stimulation study. *Experimental brain research*, 171(4):558, 2006.

[381] Emily Grossman, M Donnelly, R Price, D Pickens, V Morgan, G Neighbor, and Randolph Blake. Brain areas involved in perception of biological motion. *Brain*, 12(5), 2006.

[382] Lucia M Vaina, Jeffrey Solomon, Sanjida Chowdhury, Pawan Sinha, and John W Belliveau. Functional neuroanatomy of biological motion perception in humans. *Proceedings of the National Academy of Sciences*, 98(20):11656–11661, 2001.

[383] Martin A Giese and Tomaso Poggio. Neural mechanisms for the recognition of biological movements. *Nat Rev Neurosci*, 4(3):179–192, 2003.

[384] Peter Neri, M Concetta Morrone, and David C Burr. Seeing biological motion. *Nature*, 395(6705):894–896, 1998.

[385] HCCH Levitt. Transformed updown methods in psychoacoustics. *The Journal of the Acoustical society of America*, 49(2B):467–477, 1971.

[386] Elizabeth Milne, John Swettenham, Peter Hansen, Ruth Campbell, Helen Jeffries, and Kate Plaisted. High motion coherence thresholds in children with autism. *Journal of Child Psychology and Psychiatry*, 43(2):255–263, 2002.

[387] Joel B Talcott, Peter C Hansen, Charles Willis-Owen, Iain W McKinnell, Alex J Richardson, and John F Stein. Visual magnocellular impairment in adult developmental dyslexics. *Neuro-Ophthalmology*, 20(4):187–201, 1998.

[388] Miguel A Garca-Pérez. Forced-choice staircases with fixed step sizes: asymptotic and small-sample properties. *Vision research*, 38(12):1861–1881, 1998.

[389] Birger Kollmeier, R H Gilkey, and Ulrich K Sieben. Adaptive staircase techniques in psychoacoustics: A comparison of human data and a mathematical model. *The journal of the Acoustical Society of America*, 83(5):1852–1862, 1988.

[390] David M Green, Virginia M Richards, and T G Forrest. Stimulus step size and heterogeneous stimulus conditions in adaptive psychophysics. *The Journal of the Acoustical Society of America*, 86(2):629–636, 1989.

[391] R S Schlauch and Richard M Rose. Two, three, and fourinterval forced-choice staircase procedures: Estimator bias and efficiency. *The Journal of the Acoustical Society of America*, 88(2):732–740, 1990.

[392] Terri-Lynn MacKay, L S Jakobson, D Ellemberg, T L Lewis, D Maurer, and O Casiro. Deficits in the processing of local and global motion in very low birthweight children. *Neuropsychologia*, 43(12):1738–1748, 2005.

[393] Brent W Edwards and Gregory H Wakefield. Smallsample statistical analysis of Levitt's psychophysical procedure. *The Journal of the Acoustical Society of America*, 83(S1):S17–S17, 1988.

[394] John Wattam-Bell. Coherence thresholds for discrimination of motion direction in infants. *Vision Research*, 34(7):877–883, 1994.

[395] N M Taylor, L S Jakobson, D Maurer, and T L Lewis. Differential vulnerability of global motion, global form, and biological motion processing in full-term and preterm children. *Neuropsychologia*, 47(13):2766–2778, 2009.

[396] Kara S Hanson, Harold E Bedell, Janis M White, and Michael T Ukwade. Distance and near visual acuity in infantile nystagmus. *Optometry & Vision Science*, 83(11):823–829, 2006.

[397] Richard V Abadi and Christine M Dickinson. Waveform characteristics in congenital nystagmus. *Doc Ophthalmol*, 64(2):153–167, 1987.

[398] Joseph S Lappin, Duje Tadin, Jeffrey B Nyquist, and Anne L Corn. Spatial and temporal limits of motion perception across variations in speed, eccentricity, and low vision. *Journal of Vision*, 9(1):30, 2009.

[399] E E Parrish, D E Giaschi, C Boden, and R Dougherty. The maturation of form and motion perception in school age children. *Vision research*, 45(7):827–837, 2005.

[400] Batsheva Hadad, Sivan Schwartz, Daphne Maurer, and Terri L Lewis. Motion perception: a review of developmental changes and the role of early visual experience. *Frontiers in integrative neuroscience*, 9, 2015.

[401] Curtis L Baker and Oliver J Braddick. The basis of area and dot number effects in random dot motion perception. *Vision Research*, 22(10):1253–1259, 1982.

[402] R J Snowden and O J Braddick. The combination of motion signals over time. *Vision Research*, 29(11):1621–1630, 1989.

[403] Oliver Braddick, Janette Atkinson, and John Wattam-Bell. Normal and anomalous development of visual motion processing: motion coherence and dorsal-stream vulnerability'. *Neuropsychologia*, 41(13):1769–1784, 2003.

[404] D Ellemberg, T L Lewis, M Dirks, D Maurer, T Ledgeway, J-P Guillemot, and F Lepore. Putting order into the development of sensitivity to global motion. *Vision research*, 44(20):2403–2411, 2004.

[405] Jason E Reiss, James E Hoffman, and Barbara Landau. Motion processing specialization in Williams syndrome. *Vision research*, 45(27):3379–3390, 2005.

[406] BatSheva Hadad, Daphne Maurer, and Terri L Lewis. Long trajectory for the development of sensitivity to global and biological motion. *Developmental science*, 14(6):1330–1339, 2011.

[407] Robert Fox and Cynthia McDaniel. The perception of biological motion by human infants. *Science*, 218(4571):486–487, 1982.

[408] Ilona Kovács, Petra Kozma, Ákos Fehér, and György Benedek. Late maturation of visual spatial integration in humans. *Proceedings of the National Academy of Sciences*, 96(21):12204–12209, 1999.

[409] Marina Pavlova, Ingeborg Krägeloh-Mann, Alexander Sokolov, and Niels Birbaumer. Recognition of Point-Light Biological Motion Displays by Young Children. *Perception*, 30(8):925–933, 2001.

[410] Peter R Huttenlocher. Synaptic density in human frontal cortex-developmental changes and effects of aging. *Brain Res*, 163(2):195–205, 1979.

[411] Nitin Gogtay, Jay N Giedd, Leslie Lusk, Kiralee M Hayashi, Deanna Greenstein, A Catherine Vaituzis, Tom F Nugent, David H Herman, Liv S Clasen, and Arthur W Toga. Dynamic mapping of human cortical development during childhood through early adulthood. *Proceedings of the National academy of Sciences of the United States of America*, 101(21):8174–8179, 2004.

[412] Dave Ellemberg, Terri L Lewis, Chang Hong Liu, and Daphne Maurer. Development of spatial and temporal vision during childhood. *Vision research*, 39(14):2325–2333, 1999.

[413] Jani Mantyjarvi, Johan Himberg, and Tapio Seppanen. Recognizing human motion with multiple acceleration sensors. In *Systems, Man, and Cybernetics, 2001 IEEE International Conference on*, volume 2, pages 747–752. IEEE, 2001.

[414] Susan J Leat, Naveen K Yadav, and Elizabeth L Irving. Development of visual acuity and contrast sensitivity in children. *Journal of Optometry*, 2(1):19–26, 2009.

[415] Davide Bottari, Nikolaus F Troje, Pia Ley, Marlene Hense, Ramesh Kekunnaya, and Brigitte Röder. The neural development of the biological motion processing system does not rely on early visual input. *Cortex*, 71:359–367, 2015.

[416] JH Maunsell and DC van Essen. The connections of the middle temporal visual area (mt) and their relationship to a cortical hierarchy in the macaque monkey. *Journal of Neuroscience*, 3(12):2563–2586, 1983.

[417] Bernt Christian Skottun. The magnocellular deficit theory of dyslexia: the evidence from contrast sensitivity. *Vision Research*, 40(1):111–127, 2000.

[418] D H Hubel and T N Wiesel. Receptive fields of single neurones in the cat's striate cortex. *J Physiol*, 148(3):574–591, 1959.

[419] Peter H Schiller, Julie H Sandell, and John H R Maunsell. Functions of the ON and OFF channels of the visual system. *Nature*, 322(6082):824–825, 1986.

[420] Ivan Bodis-Wollner, Melvin D Yahr, Leland Mylin, and J Thornton. Dopaminergic deficiency and delayed visual evoked potentials in humans. *Annals of Neurology*, 11(5):478–483, 1982.

[421] A. L. Dorfman, M. Gauvin, J. M. Little, R. C. Polomeno, and P. Lachapelle. Dwt analysis of mfergs explains lack of cone on-pathway complaints in csnb. *ISCEV symposium 2017, published abstract*, 2017.

[422] Iris Hack, Leo Peichl, and Johann Helmut Brandstätter. An alternative pathway for rod signals in the rodent retina: rod photoreceptors, cone bipolar cells, and the localization of glutamate receptors. *Proceedings of the National Academy of Sciences*, 96(24):14130–14135, 1999.

[423] Yoshihiko Tsukamoto, Katsuko Morigiwa, Mika Ueda, and Peter Sterling. Microcircuits for night vision in mouse retina. *Journal of Neuroscience*, 21(21):8616–8623, 2001.

[424] Yoshihiko Tsukamoto and Naoko Omi. Functional allocation of synaptic contacts in microcircuits from rods via rod bipolar to AII amacrine cells in the mouse retina. *Journal of Comparative Neurology*, 521(15):3541–3555, 2013.

[425] N Cuenca, L DeKorver, H Kolb, and J DeJuan. Neurocircuitry Of Substance-P Containing Amacrine Cells In The Human Retina. In *Investigative Ophthalmology & Visual Science*, volume 35, page 1492. Lippincott-Raven Publ 227 East Washington Sq, Philadelphia, PA 19106, 1994.

[426] Sammy Lee, Arndt Meyer, Timm Schubert, Laura Hüser, Karin Dedek, and Silke Haverkamp. Morphology and connectivity of the small bistratified A8 amacrine cell in the mouse retina. *Journal of Comparative Neurology*, 523(10):1529–1547, 2015.

[427] David I Vaney. The mosaic of amacrine cells in the mammalian retina. *Progress in retinal research*, 9:49–100, 1990.

[428] E V Famiglietti and N Tumosa. Immunocytochemical staining of cholinergic amacrine cells in rabbit retina. *Brain research*, 413(2):398–403, 1987.

[429] Franklin R Amthor, Clyde W Oyster, and Ellen S Takahashi. Morphology of on-off direction-selective ganglion cells in the rabbit retina. *Brain research*, 298(1):187–190, 1984.

[430] Edward V Famiglietti. Synaptic organization of starburst amacrine cells in rabbit retina: analysis of serial thin sections by electron microscopy and graphic reconstruction. *Journal of Comparative Neurology*, 309(1):40–70, 1991.

[431] M Tauchi and R H Masland. The shape and arrangement of the cholinergic neurons in the rabbit retina. *Proceedings of the Royal Society of London B: Biological Sciences*, 223(1230):101–119, 1984.

[432] David I Vaney. Territorial organization of direction-selective ganglion cells in rabbit retina. *Journal of Neuroscience*, 14(11):6301–6316, 1994.

[433] Helga Kolb, LI Zhang, Laura Dekorver, and Nicolas Cuenca. A new look at calretinin-immunoreactive amacrine cell types in the monkey retina. *Journal of Comparative Neurology*, 453(2):168–184, 2002.

[434] H Kolb. Photoreceptors. 2012.

[435] Simon B Laughlin, Rob R de Ruyter van Steveninck, and John C Anderson. The metabolic cost of neural information. *Nature neuroscience*, 1(1):36–41, 1998.

[436] Klaus-Michael Debatin. Apoptosis pathways in cancer and cancer therapy. *Cancer Immunology, Immunotherapy*, 53(3):153–159, 2004.

[437] Katja C Zimmermann and Douglas R Green. How cells die: apoptosis pathways. *Journal of Allergy and Clinical Immunology*, 108(4):S99–S103, 2001.

[438] Nicolas Deconinck, Jonathon Tinsley, Fabienne De Backer, Rosie Fisher, David Kahn, Steve Phelps, Kay Davies, and Jean-Marie Gillis. Expression of truncated utrophin leads to major functional improvements in dystrophin-deficient muscles of mice. *Nature medicine*, 3(11):1216–1221, 1997.

[439] Jonathon Tinsley, Nicolas Deconinck, Rosie Fisher, David Kahn, Steve Phelps, Jean-Marie Gillis, and Kay Davies. Expression of full-length utrophin prevents muscular dystrophy in mdx mice. *Nature medicine*, 4(12):1441–1444, 1998.

[440] F Muntoni, K Maresh, K Davies, S Harriman, G Layton, R Rosskamp, A Russell, B Tejura, and J Tinsley. Phaseout dmd: a phase 2, proof of concept, clinical study of utrophin modulation with ezutromid. *Neuromuscular Disorders*, 27:S217, 2017.

[441] Ronald E Carr. Congenital stationary nightblindness. *Transactions of the American Ophthalmological Society*, 72:448, 1974.

[442] H Ripps. Night blindness revisited: from man to molecules. Proctor lecture. *Investigative ophthalmology & visual science*, 23(5):588–609, 1982.

[443] V P Connaughton and R Nelson. Axonal stratification patterns and glutamategated conductance mechanisms in zebrafish retinal bipolar cells. *The Journal of physiology*, 524(1):135–146, 2000.

[444] S A Picaud, H P Larsson, G B Grant, H Lecar, and F S Werblin. Glutamate-gated chloride channel with glutamate-transporter-like properties in cone photoreceptors of the tiger salamander. *Journal of Neurophysiology*, 74(4):1760–1771, 1995.

[445] Thomas S Otis and Craig E Jahr. Anion currents and predicted glutamate flux through a neuronal glutamate transporter. *Journal of Neuroscience*, 18(18):7099–7110, 1998.

[446] Katsuko Morigiwa and Noga Vardi. Differential expression of ionotropic glutamate receptor subunits in the outer retina. *Journal of Comparative Neurology*, 405(2):173–184, 1999.

[447] Robert M Duvoisin, Congxiao Zhang, and K Ramonell. A novel metabotropic glutamate receptor expressed in the retina and olfactory bulb. *Journal of Neuroscience*, 15(4):3075–3083, 1995.

[448] E Hartveit, J H Brandstätter, R Enz, and H Wässle. Expression of the mRNA of seven metabotropic glutamate receptors (mGluR1 to 7) in the rat retina. An in situ hybridization study on tissue sections and isolated cells. *European Journal of Neuroscience*, 7(7):1472–1483, 1995.

[449] Peter Koulen, Rainer Kuhn, Heinz Wässle, and Johann Helmut Brandstätter. Group I metabotropic glutamate receptors mGluR1$\alpha$ and mGluR5a: localization in both synaptic layers of the rat retina. *Journal of Neuroscience*, 17(6):2200–2211, 1997.

[450] M M Slaughter and R F Miller. 2-amino-4-phosphonobutyric acid: a new pharmacological tool for retina research. *Science*, 211(4478):182–185, 1981.

[451] S Hossein Fatemi, Timothy D Folsom, Rachel E Kneeland, and Stephanie B Liesch. Metabotropic glutamate receptor 5 upregulation in children with autism is associated with underexpression of both fragile x mental retardation protein and gabaa receptor beta 3 in adults with autism. *The Anatomical Record*, 294(10):1635–1645, 2011.

[452] Michael N Shadlen and William T Newsome. The variable discharge of cortical neurons: implications for connectivity, computation, and information coding. *Journal of neuroscience*, 18(10):3870–3896, 1998.

[453] Botir T Sagdullaev and Maureen A Mccall. Stimulus size and intensity alter fundamental receptive-field properties of mouse retinal ganglion cells in vivo. *Visual neuroscience*, 22(5):649–659, 2005.

[454] René C Rentería, Ning Tian, Jianhua Cang, Shigetada Nakanishi, Michael P Stryker, and David R Copenhagen. Intrinsic ON Responses of the Retinal OFF Pathway Are Suppressed by the ON Pathway. *The Journal of neuroscience*, 26(46):11857–11869, 2006.

[455] Jay Demas, Botir T Sagdullaev, Erick Green, Lisa Jaubert-Miazza, Maureen A McCall, Ronald G Gregg, Rachel O L Wong, and William Guido. Failure to Maintain Eye-Specific Segregation in nob, a Mutant with Abnormally Patterned Retinal Activity. *Neuron*, 50(2):247–259, 2006.

[456] C J Shatz and M P Stryker. Prenatal tetrodotoxin infusion blocks segregation of retinogeniculate afferents. *Science*, 242(4875):87–89, 1988.

[457] Michal Rivlin-Etzion, Kaili Zhou, Wei Wei, Justin Elstrott, Phong L Nguyen, Ben A Barres, Andrew D Huberman, and Marla B Feller. Transgenic mice reveal unexpected diversity of on-off direction-selective retinal ganglion cell subtypes and brain structures involved in motion processing. *Journal of Neuroscience*, 31(24):8760–8769, 2011.

[458] Silvia J H Park, In-Jung Kim, Loren L Looger, Jonathan B Demb, and Bart G Borghuis. Excitatory synaptic inputs to mouse on-off direction-selective retinal ganglion cells lack direction tuning. *Journal of Neuroscience*, 34(11):3976–3981, 2014.

[459] Daniel S Reich, Jonathan D Victor, Bruce W Knight, Tsuyoshi Ozaki, and Ehud Kaplan. Response Variability and Timing Precision of Neuronal Spike Trains In Vivo. *J Neurophysiol*, 77(5):2836–2841, 1997.

[460] Yang Dan, Jose-Manuel Alonso, W Martin Usrey, and R Clay Reid. Coding of visual information by precisely correlated spikes in the lateral geniculate nucleus. *Nature neuroscience*, 1(6), 1998.

[461] Juliana M Rosa, Sabine Ruehle, Huayu Ding, and Leon Lagnado. Crossover inhibition generates sustained visual responses in the inner retina. *Neuron*, 90(2):308–319, 2016.

[462] Simon Thorpe, Arnaud Delorme, and Rufin Van Rullen. Spike-based strategies for rapid processing. *Neural networks*, 14(6):715–725, 2001.

[463] Dingcai Cao, Barry B Lee, and Hao Sun. Combination of rod and cone inputs in parasol ganglion cells of the magnocellular pathway. *Journal of Vision*, 10(11):4, sep 2010.

[464] Donald IA MacLeod. Rods cancel cones in flicker. *Nature*, 235(5334):173–174, 1972.

[465] Sanae Yoshimoto and Tatsuto Takeuchi. Visual motion priming reveals why motion perception deteriorates during mesopic vision. *Journal of vision*, 13(8):8, 2013.

[466] Barry B Lee, Vivianne C Smith, Joel Pokorny, and Jan Kremers. Rod inputs to macaque ganglion cells. *Vision research*, 37(20):2813–2828, 1997.

[467] Dingcai Cao, Andrew J Zele, and Joel Pokorny. Linking impulse response functions to reaction time: Rod and cone reaction time data and a computational model. *Vision Research*, 47(8):1060–1074, 2007.

[468] Hao Sun, Joel Pokorny, and Vivianne C Smith. Brightness induction from rods. *Journal of Vision*, 1(1):4–4, 2001.

[469] Daisuke Takeshita, Lina Smeds, and Petri Ala-Laurila. Processing of single-photon responses in the mammalian On and Off retinal pathways at the sensitivity limit of vision. *Philosophical Transactions of the Royal Society B: Biological Sciences*, 372(1717), feb 2017.

[470] Adriana Fiorentini, Mario Pirchio, and Donatella Spinelli. Scotopic contrast sensitivity in infants evaluated by evoked potentials. *Investigative ophthalmology & visual science*, 19(8):950–955, 1980.

[471] Jutta Billino, Frank Bremmer, and Karl R Gegenfurtner. Motion processing at low light levels: Differential effects on the perception of specific motion types. *Journal of Vision*, 8(3):14–14, 2008.

[472] E D Grossman and R Blake. Perception of coherent motion, biological motion and form-from-motion under dim-light conditions. *Vision Research*, 39(22):3721–3727, 1999.

[473] I De Becker, D Christine Riddell, Joseph M Dooley, and Francoise Tremblay. Correlation between electroretinogram findings and molecular analysis in the Duchenne muscular dystrophy phenotype. *British journal of ophthalmology*, 78(9):719–722, 1994.

[474] Marcelo Fernandes Costa, Andre Gustavo Fernandes Oliveira, Claudia Feitosa-Santana, Mayana Zatz, and Dora Fix Ventura. Red-green color vision impairment in Duchenne muscular dystrophy. *The American Journal of Human Genetics*, 80(6):1064–1075, 2007.

[475] Peter H Schiller. The color-opponent and broad-band channels of the primate visual system. In *From pigments to perception*, pages 127–132. Springer, 1991.

[476] Peter Gouras. Identification of cone mechanisms in monkey ganglion cells. *The Journal of physiology*, 199(3):533–547, 1968.

[477] Russell L De Valois. Central mechanisms of color vision. In *Central Processing of Visual Information A: Integrative Functions and Comparative Data*, pages 209–253. Springer, 1973.

[478] Torsten N Wiesel and David H Hubel. Spatial and chromatic interactions in the lateral geniculate body of the rhesus monkey. *Journal of neurophysiology*, 29(6):1115–1156, 1966.

[479] Bruce M Dow and Peter Gouras. Color and spatial specificity of single units in Rhesus monkey foveal striate cortex. *Journal of Neurophysiology*, 1973.

[480] Charles R Michael. Color vision mechanisms in monkey striate cortex: simple cells with dual opponent-color receptive fields. *Journal of Neurophysiology*, 1978.

[481] H Kolb. The architecture of functional neural circuits in the vertebrate retina. The Proctor Lecture. *Invest Ophthalmol Vis Sci*, 35(5):2385–2404, 1994.

[482] Xue Tan, Aya Aoki, and Yasuo Yanagi. Color vision abnormality as an initial presentation of the complete type of congenital stationary night blindness. *Clinical Ophthalmology (Auckland, N.Z.)*, 7:1587–1590, aug 2013.

[483] D F Ventura, L C L Silveira, A R Rodrigues, J M De Souza, M Gualtieri, D Bonci, and M F Costa. Preliminary norms for the Cambridge colour test. *Normal and defective colour vision*, pages 331–339, 2003.

[484] Dora F Ventura, Marcelo T V Costa, Marcelo F Costa, Adriana Berezovsky, Solange R SalomÃo, Ana LUÍZA SimÕes, Marcos Lago, Luiz Hm CANTO

Pereira, MarcÍlia A M Faria, and John M De Souza. Multifocal and full-field electroretinogram changes associated with color-vision loss in mercury vapor exposure. *Visual Neuroscience*, 21(3):421–429, 2004.

[485] Marcelo Fernandes Costa, Dora Fix Ventura, Felipe Perazzolo, Marcio Murakoshi, and Luiz Carlos De LIMA Silveira. Absence of binocular summation, eye dominance, and learning effects in color discrimination. *Visual Neuroscience*, 23(3-4):461–469, 2006.

[486] Dora Fix Ventura, Mirella Gualtieri, André G F Oliveira, Marcelo F Costa, Peter Quiros, Federico Sadun, Anna Maria de Negri, Solange R Salomao, Adriana Berezovsky, and Jerome Sherman. Male prevalence of acquired color vision defects in asymptomatic carriers of Leber's hereditary optic neuropathy. *Investigative Ophthalmology & Visual Science*, 48(5):2362–2370, 2007.

[487] Katharine Bushby, Richard Finkel, David J Birnkrant, Laura E Case, Paula R Clemens, Linda Cripe, Ajay Kaul, Kathi Kinnett, Craig McDonald, and Shree Pandya. Diagnosis and management of Duchenne muscular dystrophy, part 1: diagnosis, and pharmacological and psychosocial management. *The Lancet Neurology*, 9(1):77–93, 2010.

[488] Frederick M Boyce, Alan H Beggs, Chris Feener, and Louis M Kunkel. Dystrophin is transcribed in brain from a distant upstream promoter. *Proceedings of the National Academy of Sciences*, 88(4):1276–1280, 1991.

[489] Jamel Chelly, Hélène Gilgenkrantz, Martine Lambert, Ghislaine Hamard, Philippe Chafey, Dominique Récan, Pierre Katz, Albert de la Chapelle, Michel Koenig, and Ieke B Ginjaar. Effect of dystrophin gene deletions on mRNA levels and processing in Duchenne and Becker muscular dystrophies. *Cell*, 63(6):1239–1248, 1990.

[490] Hart G W Lidov, Timothy J Byers, Simon C Watkins, and Louis M Kunkel.

Localization of dystrophin to postsynaptic regions of central nervous system cortical neurons. *Nature*, 348(6303):725–728, 1990.

[491] H Ueda, Takeshi Baba, Nobuo Terada, Yasuko Kato, Shigeo Tsukahara, and Shinichi Ohno. Dystrophin in rod spherules; submembranous dense regions facing bipolar cell processes. *Histochemistry and cell biology*, 108(3):243–248, 1997.

[492] Françcois Rodius, Thomas Claudepierre, Haydee Rosas-Vargas, Bulmaro Cisneros, Cecilia Montanez, Henri Dreyfus, Dominique Mornet, and Alvaro Rendon. Dystrophins in developing retina: Dp260 expression correlates with synaptic maturation. *Neuroreport*, 8(9):2383–2387, 1997.

[493] Teruhisa Miike, Masahiko Miyatake, Jien Zhao, Kowashi Yoshioka, and Makoto Uchino. Immunohistochemical dystrophin reaction in synaptic regions. *Brain and Development*, 11(5):344–346, 1989.

[494] Frank Schmitz, Marion Holbach, and Detlev Drenckhahn. Colocalization of retinal dystrophin and actin in postsynaptic dendrites of rod and cone photoreceptor synapses. *Histochemistry and Cell Biology*, 100(6):473–479, 1993.

[495] F Schmitz and D Drenckhahn. Dystrophin in the retina. *Prog Neurobiol*, 53(5):547–560, 1997.

[496] Toshiya Tamura, Kowashi Yoshioka, Yoshihiro Jinno, Norio Niikawa, and Teruhisa Miike. Dystrophin isoforms expressed in the mouse retina. *Journal of the neurological sciences*, 115(2):214–218, 1993.

[497] B E Flucher and M P Daniels. Distribution of Na+ channels and ankyrin in neuromuscular junctions is complementary to that of acetylcholine receptors and the 43 kd protein. *Neuron*, 3(2):163–175, 1989.

[498] Jean-Marie Gillis. Membrane abnormalities and Ca homeostasis in muscles

of the mdx mouse, an animal model of the Duchenne muscular dystrophy: a review. *Acta Physiologica*, 156(3):397–406, 1996.

[499] C George Carlson. The dystrophinopathies: an alternative to the structural hypothesis. *Neurobiology of disease*, 5(1):3–15, 1998.

[500] Yoshihide Sunada and Kevin P Campbell. Dystrophin-glycoprotein complex: molecular organization and critical roles in skeletal muscle. *Current opinion in neurology*, 8(5):379–384, 1995.

[501] Martina Blank, Peter Koulen, and Stephan Kröger. Subcellular concentration of $\beta$dystroglycan in photoreceptors and glial cells of the chick retina. *Journal of Comparative Neurology*, 389(4):668–678, 1997.

[502] Hideho Ueda, Takashi Gohdo, and Shinichi Ohno. $\beta$-Dystroglycan localization in the photoreceptor and Müller cells in the rat retina revealed by immunoelectron microscopy. *Journal of Histochemistry & Cytochemistry*, 46(2):185–191, 1998.

[503] D A Pillers, K M Fitzgerald, N M Duncan, S M Rash, R A White, S J Dwinnell, B R Powell, R E Schnur, P N Ray, G W Cibis, and R G Weleber. Duchenne/Becker muscular dystrophy: correlation of phenotype by electroretinography with sites of dystrophin mutations. *Hum Genet*, 105(1-2):2–9, 1999.

[504] Ignacio Provencio and Daniel M Warthen. Melanopsin, the photopigment of intrinsically photosensitive retinal ganglion cells. *Wiley Interdisciplinary Reviews: Membrane Transport and Signaling*, 1(2):228–237, 2012.

[505] David M Berson, Felice A Dunn, and Motoharu Takao. Phototransduction by retinal ganglion cells that set the circadian clock. *Science*, 295(5557):1070–1073, 2002.

[506] Tiffany M Schmidt, Nazia M Alam, Shan Chen, Paulo Kofuji, Wei Li, Glen T

Prusky, and Samer Hattar. A role for melanopsin in alpha retinal ganglion cells and contrast detection. *Neuron*, 82(4):781–788, 2014.

[507] Xiwu Zhao, Ben K Stafford, Ashley L Godin, W Michael King, and Kwoon Y Wong. Photoresponse diversity among the five types of intrinsically photosensitive retinal ganglion cells. *The Journal of physiology*, 592(7):1619–1636, 2014.

[508] Kathleen B Digre and K C Brennan. Shedding light on photophobia. *Journal of neuro-ophthalmology: the official journal of the North American Neuro-Ophthalmology Society*, 32(1):68, 2012.

[509] C Pieh, B Simonsz-Toth, and I Gottlob. Nystagmus characteristics in congenital stationary night blindness (CSNB). *British Journal of Ophthalmology*, 92(2):236–240, 2008.

[510] Peter H Schiller, Joe G Malpeli, and Stan J Schein. Composition of geniculostriate input ot superior colliculus of the rhesus monkey. *Journal of Neurophysiology*, 42(4):1124–1133, 1979.

[511] Choongkil Lee, William H Rohrer, and David L Sparks. Population coding of saccadic eye movements by neurons in the superior colliculus. *Nature*, 332(6162):357–360, 1988.

[512] Peter H Schiller, Julie H Sandell, and John H Maunsell. The effect of frontal eye field and superior colliculus lesions on saccadic latencies in the rhesus monkey. *Journal of neurophysiology*, 57(4):1033–1049, 1987.

[513] David C Burr, M Concetta Morrone, and John Ross. Selective suppression of the magnocellular visual pathway during saccadic eye movements. *Nature*, 371(6497):511, 1994.

[514] Lolita Petit, Hemant Khanna, and Claudio Punzo. Advances in gene therapy for diseases of the eye. *Human gene therapy*, 27(8):563–579, 2016.

[515] Le Cong, F Ann Ran, David Cox, Shuailiang Lin, Robert Barretto, Naomi Habib, Patrick D Hsu, Xuebing Wu, Wenyan Jiang, and Luciano A Marraffini. Multiplex genome engineering using CRISPR/Cas systems. *Science*, 339(6121):819–823, 2013.

[516] Ophir Shalem, Neville E Sanjana, Ella Hartenian, Xi Shi, David A Scott, Tarjei S Mikkelsen, Dirk Heckl, Benjamin L Ebert, David E Root, and John G Doench. Genome-scale CRISPR-Cas9 knockout screening in human cells. *Science*, 343(6166):84–87, 2014.